Developments in Sedimentology 51

Diagenesis, IV

K. H. Wolf and G.V. Chilingarian
(Editors)

Elsevier

DEVELOPMENTS IN SEDIMENTOLOGY 51

Diagenesis, IV

FURTHER TITLES IN THIS SERIES
VOLUMES 1-11, 13-15, 17, 21-25A, 27, 28, 31, 32 and 39 are out of print

12 *R.G.C. BATHURST*
CARBONATE SEDIMENTS AND THEIR DIAGENESIS
16 *H.H. RIEKE III and G.V. CHILINGARIAN*
COMPACTION OF ARGILLACEOUS SEDIMENTS
18A *G.V. CHILINGARIAN and K.H. WOLF, Editors*
COMPACTION OF COARSE-GRAINED SEDIMENTS, I
18B *G.V. CHILINGARIAN and K.H. WOLF, Editors*
COMPACTION OF COARSE-GRAINED SEDIMENTS, II
19 *W. SCHARZACHER*
SEDIMENTATION MODELS AND QUANTITATIVE STRATIGRAPHY
20 *M.R. WALTER, Editor*
STROMATOLITES
25B *G. LARSEN and G.V. CHILINGAR, Editors*
DIAGENESIS IN SEDIMENTS AND SEDIMENTARY ROCKS
26 *T. SUDO and S. SHIMODA, Editors*
CLAYS AND CLAY MINERALS OF JAPAN
29 *P. TURNER*
CONTINENTAL RED BEDS
30 *J.R.L. ALLEN*
SEDIMENTARY STRUCTURES
33 *G.N. BATURIN*
PHOSPHORITES ON THE SEA FLOOR
34 *J.J. FRIPIAT, Editor*
ADVANCED TECHNIQUES FOR CLAY MINERAL ANALYSIS
35 *H. VAN OLPHEN and F.VENIALE, Editors*
INTERNATIONAL CLAY CONFERENCE 1981
36 *A. IIJIMA, J.R. HEIN and R. SIEVER, Editors*
SILICEOUS DEPOSITS IN THE PACIFIC REGION
37 *A. SINGER and E. GALAN, Editors*
PALYGORSKITE-SEPIOLITE: OCCURRENCES, GENESIS AND USES
38 *M.E. BROOKFIELD and T.S. AHLBRANDT, Editors*
EOLIAN SEDIMENTS AND PROCESSES
40 *B. VELDE*
CLAY MINERALS—A PHYSICO-CHEMICAL EXPLANATION OF THEIR OCCURENCE
41 *G.V. CHILINGARIAN and K.H. WOLF, Editors*
DIAGENESIS, I
42 *L.J. DOYLE and H.H. ROBERTS, Editors*
CARBONATE-CLASTIC TRANSITIONS
43 *G.V. CHILINGARIAN and K.H. WOLF, Editors*
DIAGENESIS, II
44 *C.E. WEAVER*
CLAYS, MUDS, AND SHALES
45 *G.S. ODIN, Editor*
GREEN MARINE CLAYS
46 *C.H. MOORE*
CARBONATE DIAGENESIS AND POROSITY
47 *K.H. WOLF and G.V. CHILINGARIAN, Editors*
DIAGENESIS, III
48 *J.W. MORSE and F.F. MACKENZIE*
GEOCHEMISTRY OF SEDIMENTARY CARBONATES
49 *K. BRODZIKOWSKI and A.J. VAN LOON*
GLACIGENIC SEDIMENTS
50 *J.L. MELVIN*
EVAPORITES
52 *W. SCHWARZACHER*
CYCLOSTRATIGRAPHY AND THE MILANKOVITCH THEORY

DEVELOPMENTS IN SEDIMENTOLOGY 51

Diagenesis, IV

Edited by

K.H. Wolf
18, Acacia Street, Eastwood, Sydney, N.S.W. 2122 (Australia)

and

G.V. Chilingarian
Civil Engineering Department, University of Southern
California, Los Angeles, CA 90089 - 1211 (USA)

ELSEVIER
Amsterdam — London — New York — Tokyo 1994

ELSEVIER SCIENCE B.V.
Sara Burgerhartstraat 25
P.O. Box 211, 1000 AE Amsterdam, The Netherlands

Library of Congress Cataloging-in-Publication Data

Diagenesis, IV / edited by K.H. Wolf and G.V. Chilingarian.
p. cm. -- (Developments in sedimentology ; 51)
Includes bibliographical references and index.
ISBN 0-444-88517-X
1. Diagenesis. I. Wolf, K. H. (Karl H.) II. Chilingarian, George V., 1929- . III. Title: Diagenesis, 4. IV. Title: Diagenesis, four. V. Series.
QE571.D5 1993
552'.03--dc20 93-1987
CIP

ISBN: 0-444-88517-X

© 1994 Elsevier Science B.V. All rights reserved.

No part of this publication may be reproduced, stored in a retrieval system or transmitted in any form or by any means, electronic, mechanical, photocopying, recording or otherwise, without the prior written permission of the publisher, Elsevier Science B.V., Copyright & Permissions Department, P.O. Box 521, 1000 AM Amsterdam, The Netherlands.

Special regulations for readers in the USA - This publication has been registered with the Copyright Clearance Center Inc. (CCC). Salem. Massachusetts. Information can be obtained from the CCC about conditions under which photocopies of parts of this publication may be made in the USA. All other copyright questions, including photocopying outside of the USA, should be referred to the publisher.

No responsibility is assumed by the publisher for any injury and/or damage to persons or property as a matter of products liability, negligence or otherwise, or from any use or operation of any methods, products, instructions or ideas contained in the material herein.

This book is printed on acid-free paper.

Printed in The Netherlands

DEDICATION

This book is dedicated to the following scientists who made fundamental contributions to sedimentology and diagenesis:

Koichi Aoyagi (zeolites, carbonates)
R.G.C. Bathurst (carbonates)
C.C. von der Borch (dolomites)
Robert E. Garrison (silica–carbonate rocks; cyclicity of sedimentary rocks; and phosphates)
James R. Hein (marine diagenesis)
Miriam Kastner (mineralogy; petrology; and stable isotope geochemistry)
S.G. Kossovskaya (clays)
C.L.V. Monty (carbonates)
L.L. Sloss (fundamentals of sedimentology)
N.M. Strakhov (diagenesis of sediments)
Bruce Velde (clays)
E. Weaver (clays)
and **D.H. Zenger** (dolomitization)

and to our inspirer

Dr. S. GOLOMB

one of the foremost mathematicians in the world

This Page Intentionally Left Blank

LIST OF CONTRIBUTORS

BJÖRN BAHRIG, Baugrundinstitut Smoltczyk und Partner, Untere Waldplätze 14, D-7000 Stuttgart 80, Germany. *Present address:* Arbeitsgemeinschaft Boden- und Grundwasserschutz, Winterbergstraße 14, D-7750 Konstanz 19, Germany

DEBA P. BHATTACHARYYA, Earth Sciences and Resources Institute, University of South Carolina, Columbia, SC 29208, USA

UWE BRAND, Geological Sciences, Brock University, St. Catharines, Ontario, L2S 3A1, Canada

K. BRODZIKOWSKI, Zakład Geologii, Instytut Geografii Fizycznej i Kształtowania Środowiska, Uniwersytetu Łódzkiego, Al. T. Kościuszki 21, 90-418 Łódź, Poland

GEORGE V. CHILINGARIAN, Civil Engineering Department, University of Southern California, Los Angeles, CA 90089-1211, USA

JANET DEHMER, Lehrstuhl für Erdöl und Kohle, Rheinisch-Westfälische Technische Hochschule, Aachen, Germany

THOMAS DEWERS, Department of Geological Sciences, Indiana University, Bloomington, IN 47405, USA. *Present address:* Center for Tectonophysics, Texas A&M University, College Station, TX 77843, USA

J. DUPLAY, Centre National de la Recherche Scientifique, Centre de Géochimie de la Surface, 1 Rue Blessig, 67084 Strasbourg Cedex, France. *Present address:* Universidade de São Paulo, Campus de Piracicaba, Centro de Energia Nuclear na Agricultura, São Paulo, Brazil

ALFRED HOLLERBACH, Bundesanstalt für Geowissenschaften und Rohstoffe, 3000 Hannover 51, Germany

BRIAN JONES, Department of Geology, University of Alberta, Edmonton, Alberta, T6G 2E3, Canada

ARNO MÜCKE, Mineralogisch-Petrologisches Institut der Georg-August-Universität Göttingen, Goldschmidtstraße 1, 3400 Göttingen, Germany

P. ORTOLEVA, Department of Chemistry, Indiana University, Bloomington, IN 47405; and Geo-Chemical Research Association, Bloomington, IN 47401, USA

MARK R. SEELY, Kerr-McGee Corporation, 3 North Point, Suite 100 Houston, TX 77060, USA

P.L. SMART, Department of Geography, University of Bristol, Bristol BS8 1SS, UK

ICHIRO SUNAGAWA, Kashiwa-cho 3-54-2, Tachikawa, Tokyo 190, Japan (*Formerly:* Institue of Mineralogy, Petrology and Economic Geology, Tohoku University, Aoba, Sendai 980, Japan)

Y. TARDY, Centre National de la Recherche Scientifique, Centre de Géochimie de la Surface, 1 rue Blessig, 67084 Strasbourg Cedex, France. *Present address:* Universidade de São Paulo, Campus de Piracicaba, Centro de Energia Nuclear na Agricultura, São Paulo, Brazil

A.J. VAN LOON, P.O. Box 1254, 6801 BG Arnhem, The Netherlands

KARL H. WOLF, 18 Acacia Street, Eastwood, Sydney, NSW 2122, Australia

V.P. WRIGHT, Postgraduate Research Institute for Sedimentology, The University, P.O. Box 227, Whiteknights, Reading, RG6 2AB, UK

CONTENTS

Chapter 3. EARLY-DIAGENETIC DEFORMATION STRUCTURES IN THE OVERBURDEN OF THE BEŁCHATÓW BROWN-COAL MINE (CENTRAL POLAND): A PREDICTIVE TOOL REGARDING ENGINEERING-GEOLOGICAL CONDITIONS DURING EXPLOITATION

Chapter 4. DEVELOPMENT OF DIAGENETIC DIFFERENTIATED STRUCTURE THROUGH REACTION–TRANSPORT FEEDBACK

PART II. POSTDIAGENETIC FERRUGINIZATION OF PHANEROZOIC (OOLITIC) IRONSTONES: A CONTRIBUTION TO THEIR GENESES

This Page Intentionally Left Blank

Diagenesis, IV. Developments in Sedimentology 51
edited by K.H. Wolf and G.V. Chilingarian
© 1994 Elsevier Science B.V., Amsterdam. All rights reserved.

Chapter 1

INTRODUCTION

KARL H. WOLF and GEORGE V. CHILINGARIAN

Putting the present volume into context with earlier publications; successes and open-ended diagenetic problems; and overview of present chapters.

INTRODUCTORY REMARKS

The present volume continues the philosophy of gathering contributions on diagenesis in behalf of those directly utilizing such periodic literary surveys, namely, academics and practitioners (teachers, researchers, and oil and ore explorationists). Thus, Volume IV is a logical successor of the previous three volumes — indeed of the whole series of *Developments in Sedimentology* (hereafter D.I.S.).

The scope, or application, of diagenesis has broadened gradually over the past few decades, so that there is hardly any low-temperature/low-pressure geologic topic or environment that has not been touched by the "diageneticists'" scrutiny. Of course, accompanying the widening of scope was an increase in the depth of study (i.e., more details by many more investigators) employing increasingly complex and precise instruments. Abstract concepts/hypotheses/theories likewise have developed from — sometimes — trial-and-error to sophisticated approaches. Collectively, then, these developments have resulted in diagenesis being today a speciality encompassing classical and modern petrography/petrology, geochemistry, geophysics (particularly certain techniques and concepts), geobiology, and, of course, for large-scale sedimentation, depositional–environmental reconstructions and tectonics. Certain types of diagenetic phenomena and products are so widespread and important from both the theoretical and practical/economic viewpoints that numerous volumes have been dedicated to them, exemplified, for example, by three volumes on compaction (i.e., D.I.S. Nos. 16, and 18A plus 18B). Numerous other volumes cover carbonates, dolomites, stromatolites, silica, phosphorites, clays, bentonites, evaporites, etc.

The combination of concepts and techniques required in research depends on the particular problem and the specific preferences of the researchers — there are "innumerable" potential combinations. The scale alone will compel one to meticulously choose a philosophy that promises the best results. For example, laboratory studies to explain field observations will require a different methodology in contrast to regional diagenetic-variation studies needed to demonstrate the influence of tectonism which, in turn, influenced the sedimentary depositional–diagenetic system over a larger area. Considering also that the approach changes with the types of lithologies encountered (e.g., carbonates vs. siliciclastics vs. clay-rich deposits vs. evaporites vs. volcanics vs. ore minerals, etc.), it is relatively easy to visualize many possible variations in the study of diagenesis. These methodological differences ought to be carefully investigated in the future — perhaps one should develop a "Philosophy of Diagenesis"?

The diageneticists' broad coverage of just about all geo-environments may suggest that no new frontiers are left — only increasingly more detailed studies can be performed on the same material in the same environments. On first sight, this might be the case, but geoscientists have only begun regional (macro-/mega-scale) three-dimensional reconstructions, which offer new comparative/contrastive-type challenges in all earth-science disciplines. In the context of uniformitarianism, there are certainly tremendous problems in separating the anthropological pollution-type diagenetic phenomena from the "natural, purer" ones! If a distinction is impossible, then any diagenetic data from a neoenvironment (say, a bay, fjord, inland sea, ...) cannot be utilized to understand the paleosetting. Perhaps in some cases one has to use data of the latter to be able to identify the ancient conditions?!

Not withstanding the successes in diagenetic investigations (i.e., numerous problems seem to have been solved — until the same problems are re-opened by new conceptual or instrumental approaches, for example, or by some intellectual radical who doubts the status quo!), there ARE some open-ended unresolved enigmas. The dolomite and phosphorite deposits are familiarly still problematic (see Fowles, 1991; McKenzie, 1991; Föllmi, 1991).

In spite of the broad worldwide coverage of diagenetic studies, there are a few topics that have attracted only cursory attention. Some years ago, one of the editors (K.H.W.) has suggested that much could be learned through "*cryological diagenetic*" studies. A second problem is diagenesis of material in suspension, e.g., material brought into the sea or a large lake undergoing chemical, biological, and physical changes before accumulating at the bottom, when other types of processes may take over. One may start by discussing the cryological diagenetic phenomena on land — this would be part of pedological, terrestrial diagenesis.

It is well-known that in permafrost regions in the northern hemisphere (Canada, Alaska, Siberia, Scandinavia) the ground or soil contains a large amount of subsurface frozen water, and that this ice forms numerous types of textures, fabrics, and structures ranging in scale or size from microscopic particles, through nodular or lens-like accumulations to larger massive concentrations. The latter can form pingos, i.e., huge underground ice masses that "flow" (creep?) towards one locality or several preferential localities, lift the top part of the ground/soil, and then "creepingly (= in slow motion) erupt" through a vent or vents to flow down the sides of these volcano-like pingos. See geomorphology books dealing with arctic regions; for example, Washburn, 1980 and Krantz et al., 1988.) What is the significance of this to diageneticists?

The various styles of micro–meso–macroscale textures-to-structures of ice in permafrost grounds are equivalent to (as already suggested by the above-used terms like nodular and lens-like) similar carbonate and silica (chert) concentrations in the stratigraphic or lithologic record. These latter concentrations also occur as intergranular cement (and "matrix") and as larger nodules/concentrations and lenses as well as beds. The comparison of these concentrations in the permafrost ground and within the stratigraphic record stops here, however, because there are no carbonate or silica pingos in the neo- or paleoenvironments (although many mud-volcanoes have been discovered, which may be the result of another phenomenon or other phenomena).

In both the above-outlined cryological ice-rich and geochemical (e.g., carbonate and silica-comprising) systems, the materials had to be derived from somewhere and to migrate towards a specific locality to form the variously textured and structured concentrations. Investigation of the water–ice system may well result in information that offers better understanding of the geochemical complexes. There appears to be a micro- to macroscaled continuum/spectrum among or between the neopermafrost textures and structures, indicating that the process or processes involved in the water–ice movements operate(s) over a large range of scales. Question: Inasmuch as carbonate and silica do not form the larger-scale pingo-like structures (in contrast to ice), what precisely are the differences between the two systems? There may be, however, a close phenomenological relationship between the formation of *ice*-pingos and *evaporite-mineral* intrusions (for example, salt domes).

There is no doubt that the study of cryological, permafrost, glacial or ice diagenesis will be of both theoretical and practical/applied importance — the latter in the context of civil engineering soil problems, for instance! Even in oil exploration, the study of the behavior of ice may be important (see the important discussions by Ridley and Dominic, 1988). Those, interested in investigating fluid inclusions' composition and isotopic variations, perhaps in context of environmental reconstructions and age determination, must read the paper by Alley et al. (1988).

Just one more problem that requires continued attention (many papers have already discussed this): an increase in precision/accuracy/reliability in dating or age determination of diagenetic processes and their products (aside from refining the related boundary-setting enigma to differentiate between syngenesis, diagenesis, burial metamorphism, catagenesis and their specific phenomena like maturation of organic matter, among others). The study of cyclicity, periodicity, laminations/bedding features, etc., in diagenetic paleosystems must often rely on less-precise techniques today. Age-determination methods, despite great advances made, still have — and always will have — certain limitations, but the utmost limit has as yet not been reached so that further refinements are possible. The plus/minus range attached to all absolute ages can be narrowed, bur certainly never reduced to nil. Also, errors may have been introduced into the published literature based on the unproven assumption that a specific dating technique *is* reliable. In some instances, it was later discovered — by "unexpected errors affecting dating techniques" (see under this title the article by A. Coghlan, 1989) — that radiocarbon dating provided misleading information. How careful does one have to be in regard to all other age-determination methods? Especially, if one attempts very precise dating with a minimum plus/minus range?!

Related to age-determination problems, are the difficulties in precise correlation of, for instance, laminated sediments that may reflect sea-level changes, climatic variations, or some other cyclic/periodic phenomena. Seismic reflections in pelagic sediments exemplifies these difficulties, compounded by diagenetic dissolution facies!

According to Winterer (1991), dissolution (diagenetic) facies in pelagic sediments were first systemized and exploited — controversially — in 1969, when stratigraphers incorporated theses secondary-alteration facies into the large-scale frameworks of plate tectonics stratigraphy and sequence stratigraphy. Thus they were considered in the context of problems of local and regional paleoceanography as well as in the global enigmas related to eustatic sea-level changes. Consequently, depending on the presence or absence, or the degree and style, of development of these diagenetic dissolution surfaces, seismic-reflector-based correlations may be reliable or unreliable. New concepts must be developed, therefore, to resolve the long-standing controversies over the origin and significance of seismic reflectors in pelagic sediments, where diagenetic influences are prominent and widespread.

Many more open-ended problems in diagenesis have been outlined by Wolf and Chilingarian in the Introduction and Chapter 1 of Volume 41, *Diagenenis I*, pages 1–23 and 25–553, respectively.

The next question is: are there any new *conceptual* methods which can be applied to the modern challenges? The numerous *instrumental* methods or techniques, including computerization during information synthesis and analysis are well known. The affirmative reply leads one into integration/holistics, fractal and chaos theories.

The diagenetic–epigenetic–catagenetic dolomite-forming systems (several types) offer one unresolved enigma (see above-cited references) that unequivocally needs a holistic or systems analysis approach; it has been partly attempted, but not fully successful. In this context, it is obvious that the problems of fluid/solution movements still need to be addressed: are there any textural, isotopic, elemental, geophysical, etc., properties that can be used as fluid movement-direction criteria?

Whatever one's personal preferential/selective philosophy may be, an intellectual thread tying all concepts and techniques together is offered by systems synthesis/analysis (used here as a collective term that includes holistics, synectics, Gaia, cybernetics, etc.). One must attempt to INTEGRATE all data, theories, methods and techniques to ascertain REAL PROGRESS on both the micro- and macroscales in the study of neo- and paleodiagenetic complexes.

The relatively new concepts–hypotheses–theories–natural laws (not quite yet laws?) of fractals and chaos have definitely been adopted by earth scientists to study both neo- and paleophenomena, as demonstrated by an increase in articles and books on the subject. There are a few new bandwagons! Fractals and chaos theories are part of the systems synthesis and analysis and can be applied to the whole range of micro- and macroproblems; the latter on a worldwide scale. In the context of diagenesis, these two phenomena have also been applied already; however, space does not permit discussion here. The FPVs (the abbreviation coined by the senior editor, K.H.W., for "factors–parameters–variables") involved with these two phenomena are all complexly interrelated with many more of the over 300 FPVs identified during the past two decades (K.H.W., in progress since about 1970).

In a general way, diagenesis *en toto* during its earlier history was perhaps more of an academic, curiosity-driven, theoretical subdiscipline of sedimentary petrology, although it did find soon some practical applications in determinations, for example, of reservoir properties. Increasingly, however, diagenesis became more inclined to solve practical/applied problems. Thus, more practitioners and researchers unfamiliar with the basics of petrography/petrology, even highly specialized geologists, have had to become involved in diagenetic studies, even if only marginally. Consequently, it is advisable to provide here a brief guide to at least some of the other publications on diagenesis to put the present volume in a broader context/perspective.

In many of the books, a *number of definitions of diagenesis* have been discussed. The controversies surrounding this seemingly simple matter continue because of different nomenclatural requirements by different groups of researchers. Perhaps the definitional thicket can never be levelled to everyone's satisfaction, so that in any study one must provide an unequivocal definition-cum-explanation of terms and classifications used. What is a researcher — like an engineer or organic chemist — supposed to deduce from the variable definitions, nomenclatures/terminologies, and classifications involved in the study of syngenesis–diagenesis–catagenesis–burial metamorphism, etc.?! The whole problem cannot be redigested here — several books in the D.I.S. series have done that. See especially Volume 8, Chapter 2 by R.W. Fairbridge; Volume 18A, Chapter 1 by G.V. Chilingar, K.H. Wolf and D.R. Allen; Volume 18B, Chapter 1 by K.H. Wolf, G.V. Chilingar and D.F. Branagan; Volume 25A, Chapter 1 by G. Larsen and G.V. Chilingar; Volume 25B, Chapter 2 by R.W. Fairbridge; and Volume 41, Chapter 1 by K.H. Wolf and G.V. Chilingarian (refer to the footnotes of Table 1-1 for information on the volumes.

Those non-geologists who require a very brief introduction to sedimentology and sedimentary petrography–petrology can consult the two introduction chapters in the D.I.S. volumes 18A and 18B.

Although each of the topics dealt with in Chapters 2 to 13 in the present volume are self-contained, all of the subject matters have been under investigation for several decades; however, some unique approaches are evident in some instances. Thus, to obtain some introductory and/or supplementary information, Table 1-1 is a guide to the earlier material — as based on the D.I.S. volumes only.

SUMMARY

The present Diagenesis Volume IV consists of 12 chapters, in addition to the introduction, which are briefly discussed here.

Chapter 2 — Nucleation, growth and dissolution of crystals during sedimentogenesis and diagenesis, by Ichiro Sunagawa

On the basis of recent understandings of the crystal growth mechanism in simple aqueous systems taking place at ordinary temperatures and pressures, Sunagawa discusses nucleation, growth, dissolution kinetics, morphology, and formation of texture during sedimentogenesis and diagenesis. Reference was made to examples of systems in natural sedimentogenetic–diagenetic environments. Sunagawa summarizes essential points which must be considered in any analysis, based on the results obtained recently from the in-situ investigations of simple aqueous systems.

TABLE 1-1

Volumes in Elsevier's *Developments in Sedimentology* (= D.I.S.) (horizontal, top-axis) (see footnotes) offering introductory and/or supplementary information to chapters in the present Volume IV (vertical, left-hand axis)

Volume IV Chapter No.	D.I.S. Volume																			
	2	8	9A+B	12	14	15	16	18A+B	21	24	25A+B	29	40	41	43	44	45	46	47	48
2. Nucleation, growth and dissolution		×	×	×				×			×			×					×	×
3. Diagenetic deformation structures		×	×				×	×			×			×					×	
4. Diagenetic differential feedback		×	×					×			×			×				×	×	×
5. Smectites, illites, glauconite	×	×	×			×	×		×	×	×		×	×	×	×	×			
6. Chalk-siderite, climatic control	×	×	×		×						×	×		×				×	×	×
7. Stylolites, limestone compaction		×	×	×			×	×			×			×				×	×	×
8. Chemical, replacement, biogenic limestones		×	×	×				×			×			×				×	×	×
9. Dolomitization, trace elements, isotopes		×	×					×			×			×				×		×
10. Organic matter		×	×				×				×			×					×	
11. Ferruginization, red beds	×	×			×			×			×	×		×	×				×	
12. Plants, microorganisms, karst			×								×			×				×	×	×
13. Karst — hydrocarbons			×								×			×				×	×	×

The following D.I.S. volumes have been listed to contain material that offer introductory and/or supplementary information in support to the chapters of the present volume.

2. G.C. Amstutz (Editor) — Sedimentology and Ore Genesis.
8. G. Larsen and G.V. Chilingar (Editors) — Diagenesis in Sediments.
9A+B. G.V. Chilingar, H.J. Bissell and R.W. Fairbridge (Editors) — Carbonate Rocks, I and II.
12. R.G.C. Bathurst — Carbonate Sediments and Their Diagenesis.
14. K.W. Glennie — Desert Sedimentary Environments.
15. C.E. Weaver and L.D. Pollard — The Chemistry of Clay Minerals.
16. H.H. Rieke III and G.V. Chilingarian — Compaction of Argillaceous Sediments.
18A+B. G.V. Chilingarian and K.H. Wolf (Editors) — Compaction of Coarse-grained Sediments, I and II.
21. B. Velde — Clays and Clay Minerals in Natural and Synthetic Systems.
24. R.E. Grim and N. Güven (Editors) — Bentonites.
25A+B. G. Larsen and G.V. Chilingar (Editors) — Diagenesis in Sediments and Sedimentary Rocks, I and II.
29. P. Turner — Continental Red Beds.
40. B. Velde — Clay Minerals — A Physico-chemical Explanation of Their Occurrence.
41. G.V. Chilingarian and K.H. Wolf (Editors) — Diagenesis, I.
43. G.V. Chilingarian and K.H. Wolf (Editors) — Diagenesis, II.
44. C.E. Weaver — Clays, Muds and Shales.
45. G.S. Odin (Editor) — Green Marine Clays.
46. C.H. Moore — Carbonate Diagenesis and Porosity.
47. K.H. Wolf and G.V. Chilingarian (Editors) — Diagenesis, III.
48. J.W. Morse and F.F. Mackenzie — Geochemistry of Sedimentary Carbonates.

This chapter comprises eleven sections. Following the introduction, differences among crystal growths from different phases are described in Section 2. Sunagawa showed that crystal growth in sedimentogenetic–diagenetic environments should be treated as those from an aqeous solution phase. In section 3, problems to be solved in verifying the growth mechanism of crystals from aqeous solution are pointed out. In the following Sections 4 to 6, these problems are discussed mainly based on the results obtained by the in-situ observation methods. In Section 4, after describing essential concepts in classical nucleation theory, importance of secondary nucleation and metastable nucleation in the analysis of natural systems is pointed out. In Section 5, the mode of transportation of solute components to the surface of a growing crystal and how they are incorporated into the crystal are described. Effect of Earth's gravity and solution flow upon growth and dissolution of crystals are discussed in this section. In Section 6, structures of solid–liquid interfaces (interface roughness) and growth mechanism are described. In Section 7, external and internal morphologies of single crystals are analyzed on the basis of the relation between driving force and growth rate, as well as growth mechanisms. Section 8 offers a discussion on textural features of mineral aggregates. Theses two sections provide the information necessary to analyze the growth mechanisms and growth histories of mineral crystals. In Section 9, growth of crystals in diagenetic environments is discussed. It is suggested that dissolution-and-precipitation process, and not the solid-state recrystallization, operates in these environments. In section 10, similarities and differences of growth and dissolution of crystals are presented.

Chapter 3 — Early diagenetic deformation structure in the overburden of Bełchatów Brown Coal Mine (Central Poland), by A.J. Van Loon and K. Brodzikowski

According to Van Loon and Brodzikowski, the early-diagenetic deformation structures found in the still unconsolidated Quaternary overburden of the open-cast brown-coal mine near Bełchatów (SW of Łódź) pose interesting problems from both purely scientific and applied mining–engineering points of view. The analysis of these structures, resulting in an improved insight into their genesis, has contributed to a better understanding of the geological history of the graben area in which the mine is situated. A more reliable prediction of the mining conditions to be expected during ongoing exploitation was thus achieved.

Analysis of the various types of deformations showed that there are genetically (sedimentologically) related groups, each of which is characterized by a specific combination of features. This finding greatly helped to identify complex deformations. Recognition of their structural style made it possible to include such structures in the set of data used for prediction of zones where mining problems might be encountered. Data relating to the lateral and vertical extent and the intensity of the deformation were among the information used by Van Loon and Brodzikowski. Such predictions appeared to be a great contribution to improvement of mining efficiency (e.g., fewer non-operational hours for the excavators) and to the optimization of mining safety conditions (e.g., less manned equipment being threatened by burial under slumping masses of sediment).

The most important group of deformation, related to mining problems, appeared to result from endogenic activity, which is, of course, an important parameter because of the large-scale structures produced. To a lesser extent, mining problems are caused by structures resulting from exogenic processes, such as glaciotectonism and overburden-induced diapirism. These processes gave rise to somewhat less abrupt and/or smaller lithological changes in horizontal directions. Most penecontemporaneous and other early-diagenetic deformational processes (among which there are bioturbation and cryoturbation) are of only minor importance to the engineering and mining conditions, because the resulting structures are small as compared to the size of the excavators. These relatively small deformations are nevertheless important, because their analysis allows a reconstruction of the depositional environment and of the geological (including the deformational) history of the sediments.

Chapter 4 — Development of diagenetic differential structure through reaction–transport feedback, by P. Ortoleva

As pointed out by Ortoleva, patterns of mineralization may develop during diagenesis, that are not a direct reflection of sedimentary features or stresses and fluids imposed on the boundaries of a basin. The amplification of omnipresent nonuniformities of textural or compositional variables result in the development of these patterns. This arises through feedback involving the coupling of diagenetic reaction, transport, and mechanical processes.

The spatial scale of these patterns varies from microns to kilometers. Ortoleva discusses examples which include intracrystalline oscillatory zoning, millimeter- to meter-scale differentiated layering and stylolites, banded patterns of the Liesegang type, scalloping or fingering of reaction fronts, pulsatile fluid release from overpressurized zones in deep basins, reaction-driven advection, and kilometer-scale basin compartmentation. Qualitative mechanisms for the development of these phenomena and their implications for interpreting the physicochemical dynamics of a sedimentary basin are suggested by Ortoleva.

The implications of the above-cited phenomena is that such variations can occur spontaneously through the coupling of operating diagenetic processes. This could have very profound implications for the interpretation of many features in a sedimentary basin. These phenomena can underlie important aspects of the localization of concentrations of petroleum and valuable mineral reserves. Ortoleva concludes that the study of self-organization and other non-linear dynamic phenomena in a sedimentary basin is an important area of future academic and applied research. This chapter demonstrates a new trend by utilizing numerous modern concepts in the study of petrology in the context of diagenesis.

Chapter 5 — Stability fields of smectites and illites including glauconites as a function of temperature and chemical composition, by Y. Tardy and J. Duplay

According to Tardy and Duplay, besides arguments which suggest that clay minerals are metastable phases at the Earth's surface, indications exist also that the chemical compositions of smectites and illites approximately reflect the temperatures of formation as well as the different chemical environments in which they may approximately equilibrate. The thermodynamic properties of clay minerals are also explored.

Almost all the standard XRD-determined pure clay phases appear to be mixtures of particles of highly variable chemical compositions. Furthermore, within an *apparent* monomineralic population of particles, correlations among the chemical variables clearly reflect the temperatures at which these populations are supposed to have been formed: (1) The $(Fe^{3+})^{VI}$ content in the octahedral position correlates positively with the tetrahedral charge (glauconites) at low temperature and with the octahedral charge (celadonite) at high temperature. (2) The $(Al^{3+})^{VI}$ content correlates negatively with the tetrahedral charge at low temperatures (montmorillonite) and positively with the tetrahedral charge (illite) at higher temperatures. (3) The $(Mg^{2+})^{VI}$ content correlates negatively with the tetrahedral charge (stevensite) at low temperatures, whereas it correlates positively with the tetrahedral charge at high temperature (saponite).

A thermodynamic ideal solid-solution analogue is proposed by the authors which accounts for these correlations. The solid-solution is considered, at a particle scale, as an ideal mixture of individual layers, weakly attached to each other. Each layer presents the chemical composition of a given end-member, so that the proportions of different end-members change from one particle to another. Inasmuch as the solid-solution theory requires that several ideal solid-solutions cannot be in equilibrium in the same environment, one must conclude that each particle with its surrounding solutions is an independent microsystem.

Considering one particle of a given chemical composition, the multiple solid-solution theory allows the calculation of the weight contribution of each end-member into the ideal clay solid-solution, along with the chemical composition of the aqueous solutions in equilibrium with this particle in its independent microenvironment.

This model is able to predict the nature of the chemical correlations which are expected, at a given temperature, within a given population. This model is also applied to the prediction of the temperature required for the conversion of smectite to illite during diagenesis (≈200°C).

Chapter 6 — Formation of alternating chalk–siderite units during the Neogene in the Black Sea — an example of climatic control of early diagenetic processes,
by Björn Bahrig

The Plio-Pleistocene chemical sediments of the Black Sea, cored during the Leg 42B cruise, are characterized by alternating chalk and siderite units. They were analyzed by Bahrig with respect to the distribution and chemical and stable isotope composition of calcite and siderite. The results allowed a reconstruction of the early diagenetic history of both units. The siderite was precipitated from an anoxic pore water enriched in iron, during an early diagenetic phase of intensive microbial destruction of organic matter. During the chalk formation periods, the low Fe/Ca ratio in the pore water prohibited any siderite genesis. Thus, using the planktogenic calcite content, the pore-water chemistry was coupled to the climate-dependent chemical and ecological evolution of the whole basin.

According to Bahrig, the siderite formation periods were characterized by a low nutrient input, low productivity, and precipitation of only minor amounts of calcite. The resulting high Fe/Ca ratio in the pore water promoted the siderite genesis. In contrast, during chalk formation a higher nutrient input promoted a higher plankton (calcite) productivity, thus producing the laminated chalks. Because of a low Fe/Ca ratio, only pyrite instead of siderite was precipitated from the pore water during this period.

Chapter 7 — Formation of stylolites, marl/limestone alterations, and dissolution (clay) seams by unstable chemical compaction of argillaceous carbonates,

by T. Dewers and P. Ortoleva

In this chapter, the authors present reaction–transport models for fine-grained argillaceous carbonates, which account for the coupled diagenetic processes of "chemical" compaction (pressure solution), cementation, solute transport, texture-dependent poro-elasticity, and kinetic inhibition of calcite–water reaction due both to solute inhibition and clay (or other) grain coatings. The models evolve the spatial distribution of descriptive variables in time. According the Wanless (1979)*, variations in the relative rates of reaction at grain contacts versus that at free grain faces lead to three basic manifestations of pressure solution in rocks: "non-seam solution" (intergranular pressure solution), "sutured-seam solution" (stylolites), and "non-sutured-seam solution" (dissolution seams). Also, within a distinct range of the ratio between contact and free-face reaction rates, the formation of decimeter-scale marl–limestone alternations is predicted to occur.

As Dewers and Ortoleva point out, different behaviors manifest themselves according to such factors as depositional lithology, initial porosity, thermal and burial history, pore-fluid chemistry, and clay content, because of the direct relationship of these factors to calcite–water reaction kinetics.

In fine-grained limestones ($\approx$1–5 μm apart), when buried sufficiently deep, small-scale laminations (spaced $\approx$20–100 μm) or stylolites result if the rock contains little or no clay. For rocks with greater amounts of clay, clay segregations in zones of relatively greater amounts of compaction alternate with layers containing relatively more cement on the centimeter-to-decimeter scale. In the case of low-porosity clay-rich rocks, the spacing between dissolution seams is shown to decrease with increasing clay content owing to clay-enhanced grain-boundary diffusion.

The authors show that the modeling provides a unified picture in which diagenetic features in limestones, attributable to pressure solution, can be understood in terms of the interaction of reaction and transport in a closed system, both during and after decrease in porosity owing to compaction.

---

*See Chapter 7 for this reference.

Chapter 8 — Morphochemical and replacement diagenesis of biogenic carbonates, by U. Brand

As pointed out by Brand, morphochemical and replacement diagenesis of sedimentary minerals, particularly inorganic and organic carbonates, deals with the complex alteration processes, reactions, and their products. This occurs in the near-surface environment under changing or constant conditions. The author offers a comprehensive evaluation of the water/rock ratio, and nature and type of diagenetic fluids involved in the transformation processes of biogenic carbonates.

In the construction of their endo- and exoskeletons, many marine organisms use low-Mg calcite, intermediate-Mg calcite, high-Mg calcite and/or aragonite, in various proportions responding to ecological pressures. Structural features — such as shell layering, ornamentation, porosity, and individual crystal morphology and orientation — may greatly influence the degree of postdepositional alterations. These intrinsic parameters in conjunction with extrinsic ones, such as the physicochemical nature of the diagenetic fluid(s) and water/rock ratio system(s), may provide sufficient driving force to bring about the transformation for biogenic carbonates within set chronologic (time) constraints. Three major steps in the transformation process have been mentioned to explain the stabilization of the carbonate allochems. The end-product of this process is usually the low-Mg calcite, and biogeochemical information about the original carbonate allochem is greatly dependent on the degree of transformation. Within the system, several parameters (such as original carbonate mineralogy, physicochemical character of the diagenetic fluid(s), water/rock ratio of the microenvironment, and general thermodynamic properties of the solid phase) may be rate-limiting factors, with the slowest one being the controlling one. In the transition process, three members of the low, intermediate, and high water/rock ratio stand out with distinguishable morphochemical end-product characteristics. Allochems altered in systems having low water/rock ratio may retain much of their original morphochemical precursor characteristics despite the change of the mineralogic framework. On the other end of the transition spectrum are allochems altered in systems with high water/rock ratio, with little or no information retained by the diagenetic end-product. Brand states that the important transitional products are common and are readily definable within the context of water/rock ratios.

The degree of replacement of carbonate allochems strongly depends on the availability and amount of material, relative saturation state between liquid and solid phases, and, probably just as important, the stress-induced force of crystallization to drive the process to completion. Major replacement minerals are pyrite, silica, dolomite and phosphate minerals, with replacement taking place almost simultaneously with (or subsequent to) dissolution of the host carbonate. Differences between the host material and the replacement minerals usually lead to significant loss of original morphochemical information, which is especially true at the microscopic level(s). In conclusion, Brand states that replacement of biogenetic carbonate allochems is a relatively early diagenetic process proceeding across thin-film fronts driven by the force of crystallization stresses.

Chapter 9 — Multiple dolomitization of the Warsaw and Salem formations (Middle Mississippian), western flank of the Illinois Basin: textural, trace elemental and isotopic signatures of four types of dolomite — a case study, by D.P. Bhattacharyya and M.R. Seely

Bhattacharyya and Seely describe multiple dolomitization processes and episodes, which produce four texturally and chemically distinct types of dolomite (T1 to T4) in the Warsaw and Salem formations (Mississippian), along the western flank of the Illinois Basin. Three types (T1–T3) were produced in specific facies in response to processes inherited from the earlier depositional environments. The all-pervasive type T4 was formed during burial diagenesis.

The Salem Formation represents a restricted marine depositional setting; during and in which the earliest, matrix-replacive dolomite of type T1 was formed by evaporation-modified seawater. Subsequently, the fresh-water influx into the sediments produced the T2 dolomite cement through partial dissolution of the early-formed T1 dolomite. The matrix-replacive T3 dolomite in the open-marine Warsaw Formation, on the other hand, originated concurrently with T1–T2 episodes in the nearshore milieu, from the interstitial seawater modified by early organic matter degradation and methanogenesis. Finally, large rhombs of a strongly ferroan T4 dolomite cement were precipitated late in all the lithofacies of both Salem and Warsaw formations from a highly evolved pore fluid during burial and upward migration of the fluid through the sequence.

The superposition of multiple dolomitization processes, especially the T1–T2 processes in the near-shore association, caused partial to total cannibalization and/or reequilibration of the preexisting phase(s), the extents of which were primarily controlled by the permeability of the host facies during a specific dolomitization episode. Although the elemental compositions of the coexisting dolomites in both formations show parallel evolutionary trend when combined together on the basis of regime, the unaffected relicts of each dolomite type retained the elemental and isotopic signatures characteristic of their modes of formation.

Bhattacharyya and Seely believe that the pore fluid responsible for the latest dolomitization episode (T4) probably originated in the deeper part of the basin. Dolomite of a similar type is associated with the Mississippi Valley-type Pb–Zn mineralization in the Paleozoic sequence of the area, and is considered the "ore-stage" dolomite. Thus, the chemistry of these dolomites may provide further constraints on the genesis of the associated sulfide ores.

Chapter 10 — Diagenesis of organic matter, by A. Hollerbach and J. Dehmer

Hollerbach and Dehmer deal with the diagenesis of organic matter in Recent sediments, where diagenesis took place under low temperature conditions (below 50°C) and is mainly controlled by biochemical, physical, and chemical transformation mechanisms. Biochemical processes are mainly enzymatic carried out predominantly by fungi and microorganisms, whereas physical and chemical transformation is dependent on the temperature, pH, and Eh conditions during deposition. Organic matter in the biosphere is mainly plant-derived, including the following substance groups: lignin, carbohydrates, proteins, and lipophilic substances. As pointed out by Hollerbach and Dehmer, these lipophilic substances (especially the hydrocarbons and NSO-compounds), when isolated from Recent sediments, provide the organic geochemist with information on (1) the origin of the organic matter present and (2) the depositional environment.

The chemistry and distribution of numerous groups of compounds were examined by Hollerbach and Dehmer. These include long-chained *n*-alkanes, carboxylic acids, and alcohols, which are often components of fats and waxes. Their distribution in sediments can provide information on whether terrestrial or aquatic (marine or lacustrine) material has been deposited. Furthermore, the abundance and chemistry of cyclic compounds were discussed, including the terpenoid compounds (diterpenoids, triterpenoids and hopanoids), which have special regulatory or protective functions, mainly in higher plants and microorganisms. Also examined were distribution and early diagenesis of the steroids. Aromatic compounds are seldom found in living organisms; however, their occurrence in Recent sediments may point to the presence of bacterial or photochemical activity (picene compounds) or to the anthropogenic pollution caused by human activity (e.g., fossil fuel combustion). Some of the anthropogenically derived aromatic compounds may be carcinogenic.

Hollerbach and Dehmer also give a brief account on chlorophyll and its products during diagenesis: pristane, phytane, and the porphyrins. The distribution and chemistry of lignin, carbohydrates, proteins, and amino acids are also discussed, as well as the formation of humic substances.

Chapter 11 — Postdiagenetic ferruginization of sedimentary rocks (sandstones, oolitic ironstones, kaolins and bauxites), including a comparative study of the reddening of red beds, by Arno Mücke

In the first part of Chapter 11, Mücke reviews the known models of red-bed formation, whereas, in the second, he presents a new model and compares it with the earlier ones.

The main models in red-bed formation are: (1) the *detrital* one of Folk, (2) the *detrital/postdepositional* one of van Houten, and (3) the *diagenetic* one of Walker. Whereas Folk discussed petrologic observations on a microscopic scale, van Houten considered the stability of minerals and sedimentological aspects of red beds and their associated drab deposits. On the other hand, Walker showed that the decomposition of detrital hornblende and biotite took place during diagenesis leading to the formation of clay and ferric hydroxide, which subsequently dehydrated to hematite.

In the second part, an additional model for red beds is introduced by Mücke. This so-called *ferruginization model* was observed in iron-rich sandstones of the Bahariya Formation of the Bahariya Oasis, Western Desert, Egypt. The origin and distribution of the coloring material is postdiagenetic, resulting from iron-rich solutions, which penetrated the rocks and replaced the original cement. Mobilization of iron is enhanced under reducing conditions, whereas precipitation takes place in an oxidizing environment.

Postdiagenetic ferruginization is not restricted to the red beds, but is a common feature to many oolitic ironstones. Mücke demonstrated this in the last part of Chapter 11. Ferruginization results in a marked enrichment in iron of the original sediment (= protore) owing to the replacement by ferric hydroxide.

Ferruginization is not identical with laterization and is caused by oxidizing meteoric waters which percolate the protore. The decomposition of pyrite and marcasite, which are abundant in all these deposits, produces an acidic environment resulting in the mobilization of iron. Descending acid solutions of this nature obtain their iron from the upper sequences of the sediments that are bleached by this process. As these solutions penetrate into deeper parts of the sediments, dissolving chamosite, an alkaline environment is created, resulting in precipitation of iron. Ferruginization advances through the permeable sediment in a rollfront-like manner.

In all deposits investigated, the ooids were reworked, retransported and redeposited at least once. This led many authors to the assumption that ooids consisting of ferric hydroxide and/or hematite are of primary origin. Instead, it is demonstrated that these ooids are redeposited in their ferruginized state and are surviving diagenesis in a metastable state in this environment.

Ferruginization is also observed in kaolins. Primary kaolin deposits can contain peloids also consisting of kaolinite. Such deposits, in which ferruginization was strongly developed, can resemble oolitic ironstones. All the investigated deposits of this type were previously known as oolitic ironstones. Ferruginization, which occurs in bauxites also, is less developed.

Chapter 12 — Diagenetic processes associated with plant roots and microorganisms in karst terrains of the Cayman Islands, British West Indies, by Brian Jones

Jones discusses the experimental results of the role of microorganisms (lichens, algae, cyanobacteria, fungi) in carbonate diagenesis. He examined the contributions of microorganisms to diagenesis of carbonates (both dolostones and limestones) exposed on the Cayman Islands, British West Indies.

The occurrence of microorganisms throughout the karst terrains of the Cayman Islands demonstrated that they are capable of inhabiting numerous different settings, which are under the influence of many different environmental parameters. The identification of microorganisms is difficult, however, especially in the presence of mineralization.

According to Jones, microorganisms mediate numerous destructive and constructive processes. The former include: (1) etching that produces angular to almond-shaped etch pits; (2) boring which may lead to sparmicritization; (3) etching that produces spiky calcite; and (4) irregular etching, leading to sparmicritization. These processes result in the liberation of $CaCO_3$ into the surrounding pore fluids.

Constructive processes comprise: (1) calcification of filaments and fruiting bodies; (2) selective fixing of elements, such as Mn, Fe and Al; (3) trapping and binding of loose sediment particles to form microstromatolites; and (4) precipitation of calcite or aragonite cements with changes in the physicochemical properties of the pore fluids.

Calcification of filaments and bodies (occurring while the organism is alive, shortly after its death, or considerable time after its death) can involve: (1) crystals that show a preferred orientation relative to the filament; (2) crystals that are randomly oriented; (3) dendritic crystals; (4) needle-like crystals; and (5) small, irregular, anhedral crystals.

Rare examples of filaments coated with crystals also occur.

Chapter 13 — Paleokarst (dissolution diagenesis): its occurrence and hydrocarbon exploration significance, by V.P. Wright and P.L. Smart

A variety of groundwaters are responsible for dissolution of carbonate rocks. Karst features, including caves, are a prominent feature of carbonate terrains today and have formed in many carbonate buildups through geologic time. As pointed out by Wright and Smart, the importance of karstic porosity formation is only now becoming appreciated by sedimentologists and explorationists.

Fluids responsible for karstic porosity formation include meteoric waters, mixed seawater–meteoric waters, thermal waters, and basin-derived fluids enriched in H_2S and CO_2. Many extensive cave systems today are the products of either thermal or basin-derived fluids. Three broad karst systems are defined: the meteoric, the marine-mixing, and the burial systems (thermal and basin-derived fluids). Each one of the karst types has a distinctive "facies" signature.

Although palaeokarsts are common in the geologic record, they are typically polyphase, making interpretation difficult. Palaeokarst development can be fitted into a broad sequence stratigraphic framework. Sequence boundaries influenced by fourth- and fifth-order sea-level falls are influenced by meteoric and mixing-type karst processes, affecting unconsolidated and unstable carbonate sediments. During relatively short exposure periods, karstic porosity development is typically small-scale, whereas during ice-house global climates with enhanced fourth-order sea-level falls, porosity development is large-scale. During the third-order falls more extensive karstic porosity can develop in more cemented and mineralogically stabilized carbonates.

According to Wright and Smart, the lower-order sequence unconformities are associated with more prolonged exposure and tectonic activity. Basin-derived fluids, related to tectonic activity, can create extensive porosity. Prolonged periods of karst development, however, can lead to loss of porosity unless base-level changes lead to rejuvenation.

A range of palaeokarst associations can be recognized. Distinctive fracture-related palaeokarst systems are found around many ancient platform margins, commonly associated with neptunian dykes. This type of palaeokarst can be compared with the cave systems found around the Bahamian platform margins. Extensional tectonic regimes with half-graben "tilt-block" systems have similar fracture-related palaeokarsts. Characteristically, the degree of palaeokarst development decreases down the hanging walls of carbonate platforms developed in such systems. Many major palaeokarsts are associated with foreland basins, with the phase of karst development corresponding to the migration of the foreland bulge.

The authors reviewed several common types of palaeokarsts, with poorly documented modern analogues.

REFERENCES

Alley, R.B., Perepezko, J.H. and Bentley, C.R., 1988. Long-term climate changes from crystals growth. *Nature*, 332: 592–593.

Coghlan, A., 1989. Unexpected errors affect dating techniques. *New Sci.*, 123 (1684): 10.

Föllmi, K.B., 1991. Phosphatic sediments — ordinary or extraordinary deposits? In: D.W. Müller, J.A. McKenzie and H. Weissert (Editors), *Controversies in Modern Geology — Evolution of Geological Theories*. Academic Press, London, pp. 55–84.

Fowles, J., 1991. Dolomite: the mineral that shouldn't exist. *New Sci.*, 132 (1792): 38–42.

Krantz, W.B., Gleason, K.J. and Caine, N., 1988. Patterned ground-permafrost regions. *Sci. Am.*, Dec., pp. 44–50.

Matthews, S.A., 1987. Ice on the World. *Natl. Geogr.*, 171 (1): 78–103.

McKenzie, J.A., 1991. The dolomite problem: an outstanding controversy. In: D.W. Müller, J.A. McKenzie and H. Weissert (Editors), *Controversies in Modern Geology — Evolution of Geological Theories*. Academic Press, London, pp. 37–54.

Ridley, I. and Dominic, K., 1988. Gas hydrates keep energy in ice in ocean sediments. *New Sci.*, 117 (1601): 53–58.

Washburn, A.L., 1980. *Geocryology*. John Wiley and Sons, New York, N.Y., 406 pp.

Winterer, E.L., 1991. Pelagic sediments, seismic reflectors, and changes in sealevel. In: D.W. Müller, J.A. McKenzie and H. Weissert (Editors), *Controversies in Modern Geology — Evolution of Geological Theories*. Academic Press, London, pp. 211–230.

This Page Intentionally Left Blank

Diagenesis, IV. Developments in Sedimentology 51
edited by K.H. Wolf and G.V. Chilingarian
© 1994 Elsevier Science B.V., Amsterdam. All rights reserved.

Chapter 2

NUCLEATION, GROWTH AND DISSOLUTION OF CRYSTALS DURING SEDIMENTOGENESIS AND DIAGENESIS

ICHIRO SUNAGAWA

INTRODUCTION

The purpose of this chapter is to summarize essential points to be considered in analyzing the mineral crystal-growth phenomena in sedimentogenetic, including diagenetic, environments, namely nucleation, growth, dissolution kinetics, morphology, and texture formation. The arguments are based on recent understandings of the crystal growth mechanisms in simple aqueous systems taking place at ordinary temperatures and pressures. It is not intended to deal with examples of systems in natural sedimentogenetic–diagenetic environments, although reference will be made where this is appropriate. Some of the terms used in this chapter may be uncommon among, or different from, those used by the geological community. The writer believes, however, that the present treatment provides a useful background to analyze the geochemical, mineralogical and petrological problems, as the knowledge of simple systems is applicable to more complicated and impure natural systems, either directly or after some modifications.

This contribution consists of 11 sections. Following the introduction, differences among crystal growths from different phases are described in the second section. It is shown that crystal growth in sedimentogenetic and diagenetic environments should be treated as those from an aqueous solution phase. In the third section, problems to be solved in verifying the growth mechanism of crystals from aqueous solution are pointed out. Sections 4 to 6 cover nucleation, mass-transfer phenomena, structures of solid–liquid interfaces and growth mechanisms. In sections 7 and 8, necessary information is given to analyze the growth mechanisms and growth histories of mineral crystals based on the results of their characterization, i.e., external and internal morphologies of crystals and crystal aggregates. Growth of crystals in diagenetic environments is discussed in section 9, whereas in section 10, similarity and difference between growth and dissolution of crystals are presented. The last section constitutes conclusions. A list of suggested books and review papers, in addition to the list of references, completes this chapter.

CRYSTAL GROWTH IN DIFFERENT PHASES

Crystal growth can be divided into (a) solid-state crystallization and (b) crystallization from disordered mother phases. Solid-state crystallization is termed recrystallization in physics and metallurgy (in chemistry this term is used differently; in mineralogy/petrography and petrology, various definitions have been offered — e.g., see Flügel, 1982, among many others) and refers to the coarsening of grain size starting from compact aggregates of much smaller grains of the same crystalline phase. The coarsening occurs because the strains in the grain boundaries are released by the thermal energy applied to the system. The fluxes or solvents, such as H_2O, Cl_2 or CO_2, are not assumed to be present at the grain boundaries. If crystallization proceeds through dissolution of one grain by the flux and precipitation of another grain, it should be treated as solution growth, and not solid-state crystallization. Equilibrium state is achieved when all grains attain equal size and the grain boundary meets at 120°. If further thermal energy is applied, a few grains start to grow much larger. This is called secondary recrystallization. The coarsening of particular grains in this stage is not due to the so-called "Ostwald ripenig" (e.g., see Baronnet, 1982), in which coarsening of grains takes place through dissolution of smaller grains and growth of larger grains at the expense of the former owing to the surface energy term. In the secondary recrystallization, grain growth occurs because the effect of impurities upon the grain boundary movement is suppressed. In geological systems, pure solid-state crystallization is not common. The formation of marble from limestone or quartzite from quartz grains may be regarded as belonging to this category.

Crystallization from a disordered mother phase is further divided into (1) melt growth, (2) solution growth, and (3) vapor growth. Melt growth refers to the solidification of a crystalline phase from its own melt, as in the case of Czhochralski growth of silicon crystals from the melt of silicon (e.g., see Chernov, 1984). If other components are present in the system, they can act as solvents (or fluxes), and reduce the melting point. This should be considered as solution growth, even if the viscosity and temperature of the liquid are high. Geologists often assume only crystal growth from aqueous solutions in terms of solution growth and regard magmatic crystallization as melt growth, simply because the latter takes place at elevated temperatures and from highly viscous liquid. There can be a variety of solvents, and if solvents and solute–solvent interactions are present, the crystallization should be regarded as solution growth, irrespective of the temperature or viscosity of the liquid phase.

Essential differences among melt growth, solution growth, and vapor growth are summarized in Table 2-1. Melt growth takes place in a condensed system, where the density difference between melt and solid is very small. Inasmuch as simple condensation process cannot cause rearrangement of the structure in the solidification of melt, heat transfer from the system plays the most important role in this crystallization. Mass transfer plays only negligible role, probably less than a few percent.

Solution growth and vapor growth constitute crystallization from diluted phases. Thus, mass-transfer (mass transportation and condensation processes) plays the essential role, probably more than 95%. In addition to this difference, growth temperatures are different among the three cases. The presence of solute–solvent interaction, which is absent in melt growth and PVT, characterizes solution growth and CVT. In vapor growth, two categories may be distinguished (Table 2-1): One refers to vaporization and condensation of the same compound (PVD or PVT:

TABLE 2-1

Characteristics of crystal growths in melt, solution and vapor phases

	Melt	Solution		Vapor	
		high-temperature solution (flux)	low-temperature aqueous solution	CVT (involving chemical reaction)	PVT (pure vapor phase)
State	Very condensed		→		Very diluted
Driving	Heat transfer Supercooling (ΔT)	Mass transfer (mass transportation and condensation) Supersaturation (σ)			
Growth temperature	High	Medium	Low	Medium to Low	
Solute–solvent interaction	None	Strong	Strongest	Strong	None
α	Small	Medium	Medium	Large	Largest
Interface roughness	Rough	Smooth	Smooth	Smooth	Smooth
Principal growth mechanism	Continuous	Two-dimensional nucleation growth to spiral mechanism growth			

physical vapor deposition or transportation), whereas the other involves chemical reaction (CVD or CVT: chemical vapor deposition or transportation). PVD is close to the melt growth, except for the big difference in the condensation states. CVD is closer to the solution growth, because solute–solvent interaction is involved.

Based on the above classification, it is understood that crystallizations, taking place in nature to form minerals, rocks and ore deposits, can be principally treated as solution growth. Magmatic crystallization is a type of high-temperature solution-growth with silicates and volatile components acting as solvents. In both regional and contact metamorphism, inasmuch as intergranular volatile components play an important role as solvents, the crystallization should essentially be regarded as solution growth. Thus, the process is dissolution-and-precipitation via an intergranular thin film of solution phase. In sedimentogenetic and diagenetic environments, the crystallization takes place principally in an aqueous solution phase at ordinary temperature and pressure conditions. For further discussion of the characteristics of natural crystallization, the reader may refer to Sunagawa (1984).

In the present chapter, the arguments are mainly based on the results of theoretical and experimental investigations on aqueous solution growth of simple systems. The writer tried to relate these to the problems involved in impure, complicated real systems in sedimentogenetic–diagenetic environments.

The sedimentogenetic–diagenetic processes can be classified as follows:

(1) crystallization under surficial conditions, like precipitation of evaporites, etc.;

(2) precipitation of authigenic minerals in intergranular spaces of allogenic mineral fragments in sediments; and

(3) crystallization and transformation of minerals during diagenesis, catagenesis, or low-grade metamorphism.

In all these processes, precipitation of minerals occurs in an aqueous solution phase at ordinary temperature and pressure. Proceeding from (1) to (3), the volume of aqueous solution diminishes and crystallization takes place in a more confined environment. In (1), crystallization takes place in a large volume of aqueous solution when a supersaturated state is achieved principally by evaporation. In (2), crystallization occurs in the intergranular aqueous solution of allogenic mineral fragments, whereas in (3) crystallization proceeds through thin film of aqueous solution. Temperature and pressure also increase from (1) to (3).

Extensive experimental and theoretical investigations have been undertaken to verify the mechanism of crystal growth in an aqueous solution phase in simple and pure systems. These include investigations on (1) mass-transport phenomena from bulk solution to the surface of growing crystals, (2) the effect of solution flow and convections of various types upon mass-transport process, (3) diffusion boundary layer, (4) growth or dissolution rates versus driving force (supersaturation) relations of a bulk crystal and individual growth pyramid, (5) growth or dissolution mechanism, and (6) morphological variations in relation to the driving force. Measurements of kinetic parameters have been made by both ex-situ and in-situ methods. In the ex-situ methods, the growth rates versus driving force relations are measured experimentally under well-controlled internal conditions, but indirectly from the outside. Based on these relations, the mechanisms of crystal growth are analyzed on the basis of theoretically predicted relations. Although experiments of this type are undertaken under very precisely controlled growth conditions, the results are indirect ones, because the process is not directly observed or recorded.

In recent years, in-situ observation methods have been developed, in which a complete process is observable with a very high degree of "visibility" and can be, thus, recorded — the growth conditions are as precisely controlled as in the case of ex-situ experiments. In-situ observations and measurements of (1) advancing rates of growth or dissolution layers with a height of the order of a nanometer, (2) behavior of individual growth hillocks and dislocations, (3) mass-transport behavior, and (4) not only bulk but also surface supersaturations (now possible in these investigations) (e.g., refer to Maiwa et al., 1989; Onuma et al., 1989a, b; Tsukamoto, 1989; Sunagawa, 1990). In Table 2-2, the in-situ observation methods (A) and the phenomena so far investigated (B), in the author's former group, to verify the mechanism of crystal growth and dissolution in aqueous solutions, are summarized, together with references. Similar in-situ observation methods have been developed for vapor growth and growth in silicate or oxide systems at high temperatures, which are not included in the table (see Tsukamoto, 1989 and Sunagawa, 1990). By summarizing the data and concepts obtained through recent in-situ investigations, the writer tried to analyze how mineral crystals nucleate, grow, and dissolve (or transform) in sedimentogenetic–diagenetic environments. Main differences between experimental simple system and natural complicated system are (1) natural crystallization takes

TABLE 2-2

Recently developed in-situ observation methods for the verification of the mechanism of nucleation, growth and dissolution of crystals

---

A. *In-situ observation methods:*

(1) Purpose: To perform kinetic measurements under well-controlled conditions and with a very high visibility, while the whole process is observed in-situ and recorded. This is achieved by a combination of an improved observation system, a system to control growth parameters,and a recording system (Tsukamoto, 1983).

(2) Temperature control at fluctuation much lower than 1/100°C is achieved by means of personal computers. Experiments are performed in a thermostated room or in a clean-air room (Tsukamoto, 1989; Sunagawa, 1990).

(3) Various optical microscopies of both transmission and reflection types (including phase contrast, interference contrast microscopies) are used for in-situ direct observation of kinetic processes at a very high visibility, in combination with CCD video system. Aberration corrected objective lens with a long working distance is used to improve visibility (Tsukamoto and Sunagawa, 1985). Michelson-type interferometer attached to an objective lens is used for the measurement of advancing rates of spiral growth layers, slopes of a growth hillock, etc. (Maiwa, 1987; Onuma, 1988).

(4) Schlieren technique and Mach-Zhender interferometry are used to visualize or measure concentration gradient in diffusion boundary layer, surface supersaturation, or buoyancy-driven convection (Onuma, 1988).

(5) Two-baths flow system is adopted in order to investigate the effect of solution flow or to obtain uniform surface supersaturation. A system to control the temperature of the growth cell by circulating thermostated water was also adopted, depending on the purpose of experiments.

(6) Laser light scattering method and Raman spectroscopy are applied to investigate clustering or nucleation phenomena.

B. *Phenomena so far investigated:*

(1) Formation of clusters, embryonic particles and nuclei in a solution and secondary nucleation phenomenon by means of laser light scattering technique and Raman spectroscopy (Azuma et al., 1989, on lysozyme; Onuma, 1988, on barium nitrate).

(2) Mass transport phenomena, like diffusion boundary layer, buoyancy-driven convection, effect of flow, etc. by means of Schlieren technique and Mach-Zhender interferometry (Onuma et al., 1988, on barium nitrate; Onuma et al., 1989a, b, on K-alum).

(3) Measurement of driving force at a growing interface (surface super- and under-saturation) by means of Mach-Zhender interferometry (Onuma et al., 1989a, on K-alum).

(4) Effect of buoyancy-driven convection upon surface microtopography (Onuma et al., 1989b, on barium nitrate and cadmium iodide).

(5) Identification of dislocation characters in a growing crystal by polarization microscopy (Maiwa, 1989; Maiwa et al., 1990, on barium nitrate) and by etch pit method (Onuma et al., 1990, on K-alum).

(6) Investigation of behavior of dislocations in relation to bulk supersaturation, σ_b, by a combination of X-ray topography and in-situ observation (Maiwa, 1987; Maiwa et al., 1987; on barium nitrate).

(7) Observation of monomolecular growth layers on a growing face (Tsukamoto, 1983, 1989, on cadmium iodide and barium nitrate; also Tsukamoto and Sunagawa, 1985).

(8) Growth or dissolution rates of a face and advancing rates of spiral layers versus bulk supersaturation, σ_b, relations, by direct measurements on TV screen (Tsukamoto, 1983, on cadmium iodide, and barium nitrate; also on KAP: $C_6H_4 \cdot COOH \cdot COOK$).

(9) Normal growth rates, slopes of individual growth hillocks and advancing rates of growth spiral layers versus bulk supersaturation σ_b, or surface supersaturation, σ_s, relations (Maiwa, 1987; Maiwa et al., 1989, on barium nitrate; Onuma, 1988 and Onuma et al., 1989a, b, 1990, on K-alum).

(10) Effect of impurities upon surface microtopography of crystal faces and crystal morphology (Li et al., 1990; on KCl).

place in impure, multicomponent aqueous solutions; (2) that more complicated movements of mother aqueous solution and fluctuations in growth parameters are expected; and (3) that perhaps the time factor is different, although this can be substituted by the driving force factor.*

PROBLEMS IN VERIFYING THE GROWTH MECHANISM OF CRYSTALS

As schematically illustrated in Fig. 2-1, growth of crystals proceeds in the following sequence: (1) achievement of driving force for crystallization by attaining supersaturated state, either through changing temperature or pressure (depending on the dependence of solubility on the temperature and pressure), or through evaporation or diffusion; (2) appearance of embryonic particles owing to the concentration fluctuation in the system, some of which may grow to a critical size (may be regarded

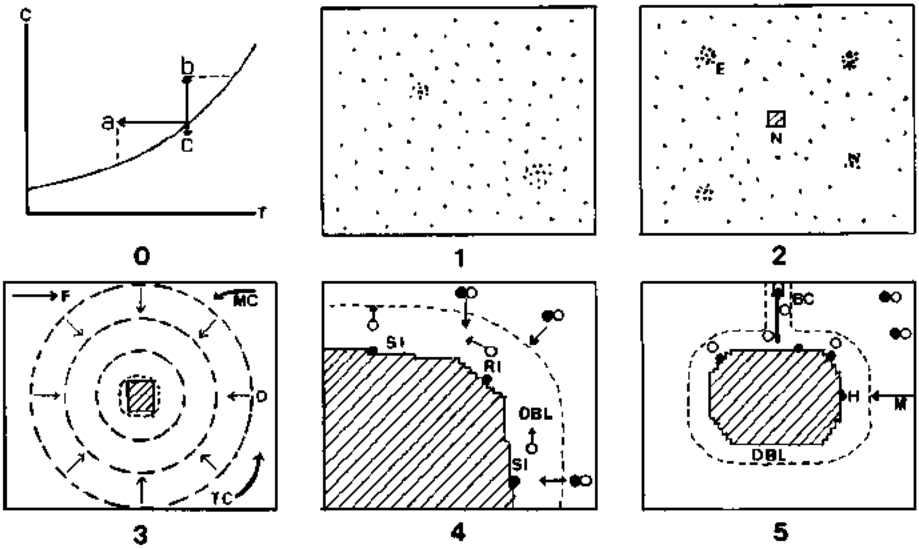

Fig. 2-1. Schematic illustration of the process of growth of crystals from solution phase, and the problems involved at each step. (0) Solubility curve; C = concentration, T = temperature. Supersaturated state is attained by changing temperature (a), or by evaporation (b), or by diffusion (c). (1) Supersaturated solution. There is a fluctuation in concentration, which leads to the appearance of embryonic particles. (2) Appearance of embryonic particles (E) and critical nucleus (N). (3) Mass transportation from the bulk to the surface of a growing crystal by diffusion (D), thermal (TC), or Marangonian (MC) convection and solution flow (F). (4) Transportation of solute–solvent complexes (○●) to diffusion boundary layer (DBL), incorporation of solute component (●) at kinks on rough (RI) and smooth (SI) interfaces and escape of solvent component (○). (5) Mass transport (M) and heat transfer (H) involved in solution growth, and buoyancy-driven convection (BC).

Driving force can be expressed by supersaturation, σ, supercooling, ΔT; however in this chapter it is expressed in a more generalized form: $\Delta\mu/kT$, where $\Delta\mu$ is the chemical potential difference between solid and fluid phases, k is the Boltzmann constant, and T is the growth temperature in absolute scale.

as the nucleation stage up to this point); (3) mass transport from the bulk solution to the surface of a growing crystal through diffusion, convection of various types, or solution flow; (4) incorporation of solute component into the crystal at kinks on the solid–liquid interface, via several desolvation steps (see later explanation) (this may be called the stage of crystal growth in narrower sense); and (5) concurrent escape of crystallization heat and desolvated solvent component from the interface to the bulk solution. It is necessary, therefore, to understand (1) the states of solute components in bulk solution; (2) how they are transported to the growing surface of a crystal; (3) how they are incorporated into the crystal; (4) how the rate and mechanism of incorporation vary depending on the interface structure; and (5) what kind of effect the Earth gravity and the flow of solution may have on the mass-transport behavior. In the in-situ experiments of simple systems, these problems have been investigated at visibilities of nanometer order under precisely controlled growth parameters.

In real system, the growth conditions may fluctuate or abruptly change during the process of growth, which leads to the variation of growth rates, morphology and degree of perfection of crystals. Even if a constant growth condition is maintained, the growth rate of a crystal may fluctuate owing to unbalanced diffusion and growth rate. Also growth rates are anisotropic, i.e., they are different depending on crystallographic orientations. As a result, various micro-textures, like growth sectors, growth banding, etc., will appear in single crystals owing to the variation in physical perfection and chemical homogeneity. The internal morphology of a single crystal records the growth history. The external morphology of a crystal represents one — i.e., the final stage — of these processes, but is influenced by the growth history. The textures of crystal aggregates appear due to the nucleation and growth processes of multiple crystals. Inasmuch as these morphological and textural features are the only key features preserved ("message of ancient processes"), it is important to understand the factors that control them.

In a solution system, solute component is always armoured (bound) by the solvent component. Both solute and solvent components are transported together in a form of solute–solvent complexes to the growing surface of a crystal, where desolvation takes place. Desolvation occurs at several steps as schematically illustrated in Fig. 2-2. At each step, the corresponding energy barrier has to be overcome. Thus,in solution growth, the desolvation steps control the growth rates to a great extent.

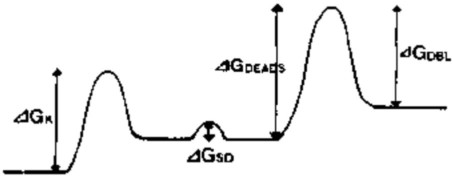

Fig. 2-2. Desolvation steps and associated energy barrier that solute–solvent complex must overcome before the solute component incorporates into a crystal at a kink. ΔG_{DBL} is the energy barrier required when solute–solvent complex enters the diffusion boundary layer; ΔG_{DEADS}, when it arrives and gets adsorbed on the interface: ΔG_{SD}, for surface diffusion; ΔG_K, when it incorporates at a kink.

The solute–solvent interaction energy, $\oint_{sf}$, is one of the most important variables in analyzing the mechanism of crystal growth. It varies with the chemistry of the system.

NUCLEATION

In classical nucleation theory, three important concepts were established: critical nucleus, homogeneous nucleation, and heterogeneous nucleation. As shown in Fig. 2-3, inasmuch as the nucleation energy is determined by the surface energy term (a gain) and the volume energy term (a loss), there is a critical size, r_c, below which an embryonic particle may easily dissociate or coagulate again, and above which it can grow steadily. The embryonic particle which attains this size is called the critical nucleus. The size decreases as the driving force increases.

Homogeneous nucleation is a process taking place without any help other than the energy required to form a nucleus. This process needs much higher activation energy (in driving force, or in ΔT, one order of magnitude higher) than the heterogeneous nucleation. Heterogeneous nucleation refers to the nucleation on the substrate (or other materials including ionic entities) and requires less activation energy, because the interfacial energy between the newly appearing phase and the substrate reduces the surface energy value. Epitaxial growth, nucleation on the wall of a crucible, nucleation in the presence of other solid particles or impurity components in a system, etc., belong to this category. If a seed crystal (of the same compound) is present, on the other hand, no extra energy is required, because growth commences immediately on the seed surface. In natural crystallization, homogeneous nucleation is hardly expected to occur. The nucleation is principally a heterogeneous one, owing to the presence of other components and phases.

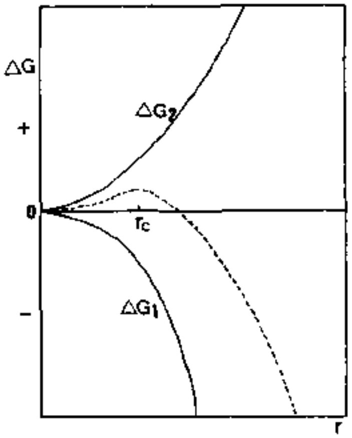

Fig. 2-3. Schematic illustration of the presence of a critical size r_c in homogeneous nucleation. The volume enery term (ΔG_1) is a loss, whereas the surface energy term (ΔG_2) is a gain. Dotted line indicates the total energy change (ΔG) for nucleation with increasing size of the nucleus r.

In the sedimentogenetic–diagenetic environments listed as surficial condition (1), a supersaturated state is achieved principally by evaporation. Thus, the free surface of aqueous solution attains the highest supersaturation state and nucleation preferentially takes place on the surface of solution. In the environments listed as precipitation of authigenic minerals (2) and diagenetic (3), the surface of other solid particles will provide sites for heterogeneous nucleation.

Inasmuch as it is necessary to overcome the activation energy which consumes the driving force in any nucleation process, the probability of further nucleation decreases drastically once nucleation occurs, unless new conditions are attained. Depending on how nucleation occurs, various rock textures appear, e.g., holocrystalline, hypidiomorphic, granular, or porphyritic textures, when the system is in a more or less static state. When there is a dynamic movement, one has to take another factor into consideration, i.e., secondary nucleation.

This concept of secondary nucleation has been used for a long time in the practical industrial crystallization field, where production of a large number of tiny crystal grains of equal size is the ultimate aim. If growth conditions are precisely controlled so that nucleation occurs only once and no coagulation of once nucleated particles takes place during the growth process, this aim may be achieved. But, this is practically impossible to achieve. Thus, in the industrial crystallization practice, seed crystals are added to a supersaturated solution when appropriate conditions are attained. After agitating this solution, a huge number of tiny crystals suddenly form simultaneously. This is called secondary nucleation, although the phenomenon has no relation to the primary nucleation described above. Secondary nucleation occurs because as a result of agitation mechanically detached particles from the seeds act as self-seeding sources.

In spite of its potential importance in the analysis of crystallization of various geological materials where dynamic movements are expected to occur frequently, not enough attention has been paid to this concept in analyzing the textures of geological samples. An exceptional experiment which demonstrated the importance of this phenomenon, although the experiment is not directly related to sedimentogenetic–diagenetic processes, is the work of Kouchi et al. (1986). They demonstrated that nucleation rates increased by one order of magnitude when dynamic movement was applied in mixing two basaltic magmas. Hyalopyritic texture, commonly observed in basalts, could be experimentally reproduced for the first time by this experiment when a magma contains phenocrysts. In static experiments, these textures could not be reproduced, even if conditions allowed nucleation to take place at two distinct stages.

Secondary nucleation phenomenon is expected to occur more commonly and frequently in sedimentary environments, because turbulence in solution flow and detachment and destruction of pre-existing crystallites should be ubiquitous in these environments.

Finally, it is necessary to discuss the metastable nucleation. The activation energy, A_N, for nucleation is defined by the following equation:

$$A_N = \eta \frac{\gamma^3}{\Delta\mu^2} \tag{2-1}$$

where η is the viscosity (controlling the mass transfer rate), γ is the interfacial energy, $\Delta\mu$ is the driving force. Due to the competition between the surface energy and the driving force, it is likely that thermodynamically labile phases nucleate prior to the appearance of a stable phase. Upon appearance of the structure of a labile phase in the system, further growth occurs, and the phase may grow steadily as if it is a stable phase. Such a phenomenon may be called metastable nucleation and is encountered in real systems more commonly than usually assumed. Formation of aragonite in living shell fish is a popular example of metastable nucleation. Synthesis of diamond from vapor phase at 1 atm pressure is a recently-achieved exciting new technology utilizing this phenomenon. Metastable nucleation is also commonly encountered in silicate systems (e.g., see Abe et al., 1987, 1990; Sunagawa, 1989, 1990; Tsukamoto, 1989; Nakamura et al., 1990). If formation of stable phase is suppressed for some reasons, crystals of metastably nucleated phase can grow steadily, as in the case of aragonite in shells. Geologic time may be required to transform the metastably nucleated phase to the stable phase in some cases. In many cases, however, metastably nucleated phases may dissolve or transform to the stable phase once the latter appears (Abe et al., 1991).

MASS TRANSFER AND THE EFFECT OF GRAVITY AND SOLUTION FLOW

In solution growth, mass transfer plays an essential role. The solute component is transported from the bulk solution to the surface of a critical nucleus, and growth of the crystal proceeds through the incorporation of solute components into the crystal at kinks and steps on the interface. Mass transfer occurs (1) by diffusion as a result of the presence of concentration gradient between the bulk solution and the surface of a growing crystal; (2) by convection as a result of temperature difference (thermal convection), surface tension of the solution (Marangonian convection), or gravity effect; and (3) by various types of solution flow.

Around a growing crystal, there is a diffusion boundary layer with a thickness of the order of a few tens to a few hundreds of microns in which concentration gradient is much sharper than that between the bulk solution and the growing surface. The concentration at the growing surface is not zero, i.e., there is a supersaturation of solution adjacent to a growing surface, which is lower than the supersaturation of a bulk solution but higher than the equilibrium value. Supersaturation of a bulk solution apart from the surface and that of a solution adjacent to the surface are respectively denoted bulk supersaturation and surface supersaturation. The difference in concentration between the bulk and surface supersaturations, namely, the concentration gradient within the diffusion boundary layer, defines the driving force for growth. The thickness of a diffusion boundary layer increases as bulk supersaturation increases, but stabilizes at a few tens to a few hundreds of microns in a stagnant system. When flow is present, the thickness decreases, but never to absolute zero. Figure 2-4 schematically illustrates the concept of diffusion boundary layer in growth of crystals in solution.

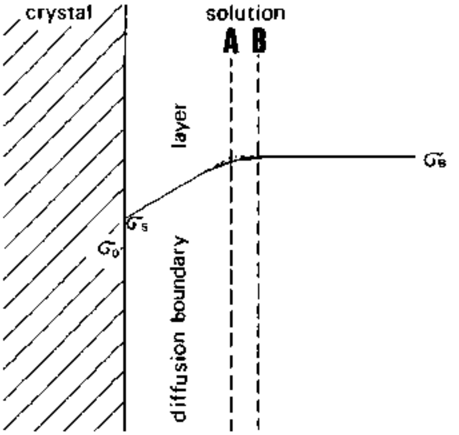

Fig. 2-4. Schematic illustration of diffusion boundary layer and the concentration change. The width of a diffusion boundary layer may be taken either as a line *A* or *B*. σ_B = bulk supersaturation, σ_S = surface supersaturation, σ_0 = equilibrium concentration.

In recent experimental works using the Mach-Zhender interferometry, Onuma (1988) and Onuma et al. (1989a, b) demonstrated that the surface supersaturation was about 6 to 20% lower, depending on the rate of flow of the solution (0 ~ 40 cm/s), than the bulk supersaturation in the case of growth of K-alum crystals from aqueous solution. Undersaturation was more than 40% lower than the bulk undersaturation in the case of dissolution. The bulk and surface supersaturations are not linearly related when flow velocity is small.

The Earth gravity, in particular, has an important effect on solution growth, because desolvation takes place in solution growth and the desolvated solvent components try to escape from the surface of a growing crystal. The diffusion boundary layer becomes diluted and lighter during crystal growth, or condensed and heavier as dissolution proceeds. Thus, a positive (i.e., rising) buoyancy-driven convection plume is expected to occur from the top surface in the case of crystal growth, and a negative (i.e., downward) convection plume from the bottom surface in the case of dissolution. Inasmuch as there is a continuous inflow from the bulk solution in the case of crystal growth, the behavior of buoyancy-driven convection will vary depending on the competition between the inflow and outflow, i.e., depending on the bulk supersaturation. According to a recent investigation on the growth of $Ba(NO_3)_2$ crystals from the aqueous solution (Onuma, 1988; Onuma et al., 1988), only the thickness of diffusion boundary layer expands at lower bulk supersaturation ($\sigma_b < 0.5\%$). Unstable and intermittent buoyancy-driven convection appears in the intermediate bulk supersaturation range (from 0.5% to 3.0%), whereas a sharp upward-rising plume appears perpendicularly from the top surface in the higher supersaturation range (from 3% to above 10%). Figure 2-5 shows this change observed around a $Ba(NO_3)_2$ crystal growing in a stagnant solution. At bulk supersaturation higher than 8%, several buoyancy-driven convection plumes appear in a bundle.

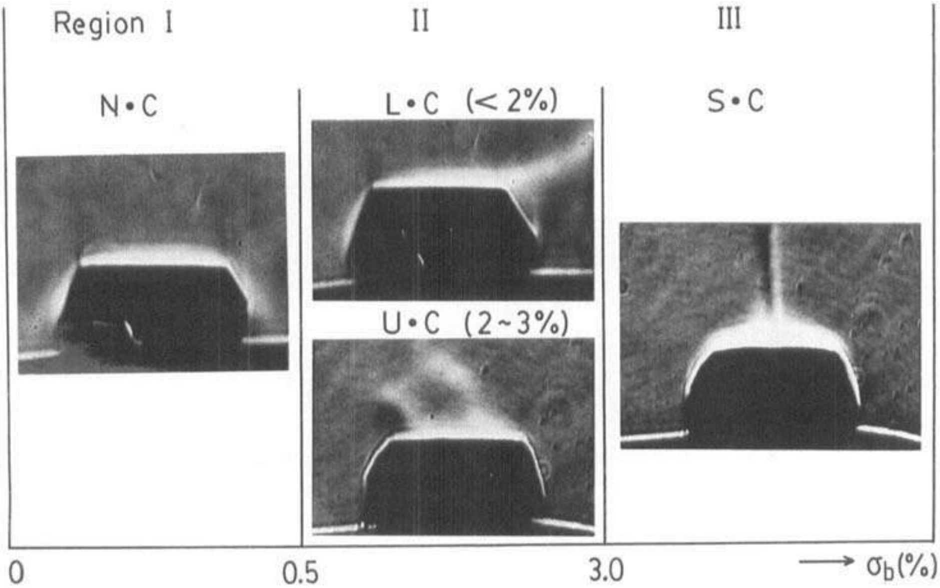

Fig. 2-5. The observed changes of the behavior of buoyancy-driven convection plumes in relation to the bulk supersaturation. In *Region I* ($N \times C$), no convection appears; in *Region II*, either lateral convection ($L \times C$) or unstable ($U \times C$) convection are seen; in *Region III*, upward-rising convection plume ($S \times C$) appears steadily. $Ba(NO_3)_2$. (After Onuma et al., 1988.)

The most exciting observation at higher bulk supersaturation was that a high-density lenticular layer appeared on the top surface. Upon agitation of the system, an avalanche of numerous tiny crystallites appeared in the bulk solution in a few tens of seconds (Fig. 2-6). It was suggested that embryonic particles were present in the high-density lenticular layer and they acted as self-seeding centers when dispersed into the bulk solution. It is highly possible that at greater driving force, particularly in the impure real systems, clustered (or polymerized) embryonic particles will form from the solution. When there is a flow of solution over a growing surface, both the thickness of diffusion-boundary layer and the behavior of buoyancy-driven convection plume are modified depending on the flow velocity. Figure 2-7 exemplifies the change of the thickness of diffusion boundary layer (closed triangles) and of the surface supersaturation (closed circles), and of Berg effect (surface supersaturation is higher along the edges of a growing interface of a polyhedral crystal than at the center of the face, to which this term is applied; Berg, 1938), on changing the flow velocity from 3 to 40 cm/s. By increasing the flow velocity, the thickness of diffusion boundary layer decreases, the surface supersaturation at the center of a face increases, the Berg effect is less enhanced and the area of uniform surface supersaturation expands. Also, the point of origin of buoyancy-driven convection plume on the surface moves from the center of a face to the rear edge, from where it escapes obliquely at higher flow velocity.

Due to the presence of a rising plume, a depleted area appears at the root of the plume. This reduces the growth rate and has a definitive effect upon the

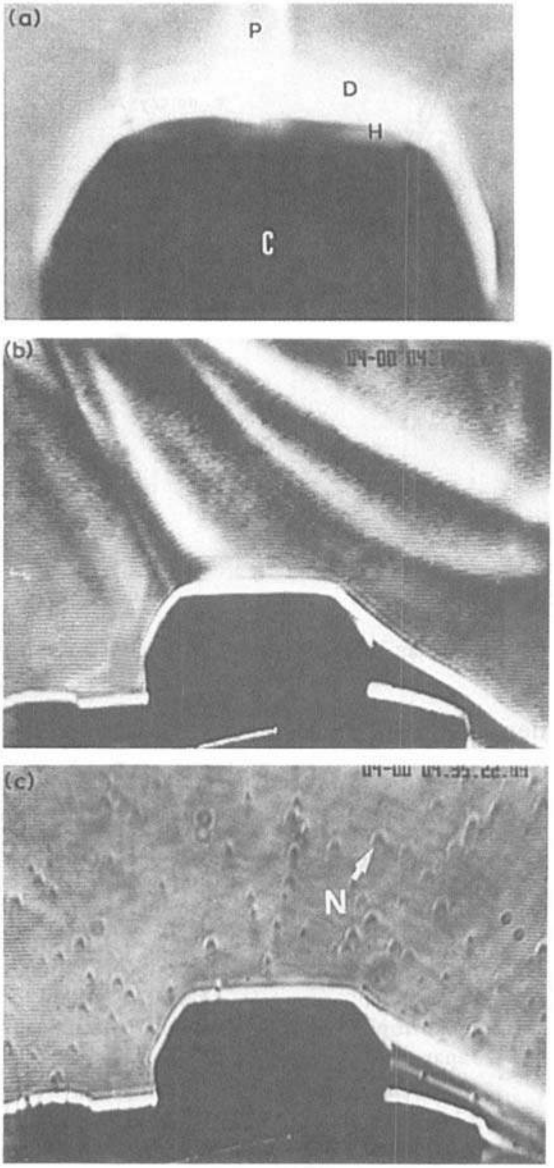

Fig. 2-6. Due to the presence of lenticular layer with high density (*H*) within the diffusion boundary layer (*D*) on a growing top (111) surface of a $Ba(NO_3)_2$ crystal (*C*) at a high bulk supersaturation (a), an avalanche of tiny crystallites (*N*) appears after a few tens of seconds (c) when the solution is agitated (b). *P* = buoyancy-driven convection plume. (After Onuma, 1988; and Tsukamoto, 1989.)

surface microtopography (growth spirals and other step patterns) and the perfection (dislocations, hollow cores, bunched growth steps and associated entrapment of inclusions, and other defects) of the crystal. In Fig. 2-8, a good example of the effect

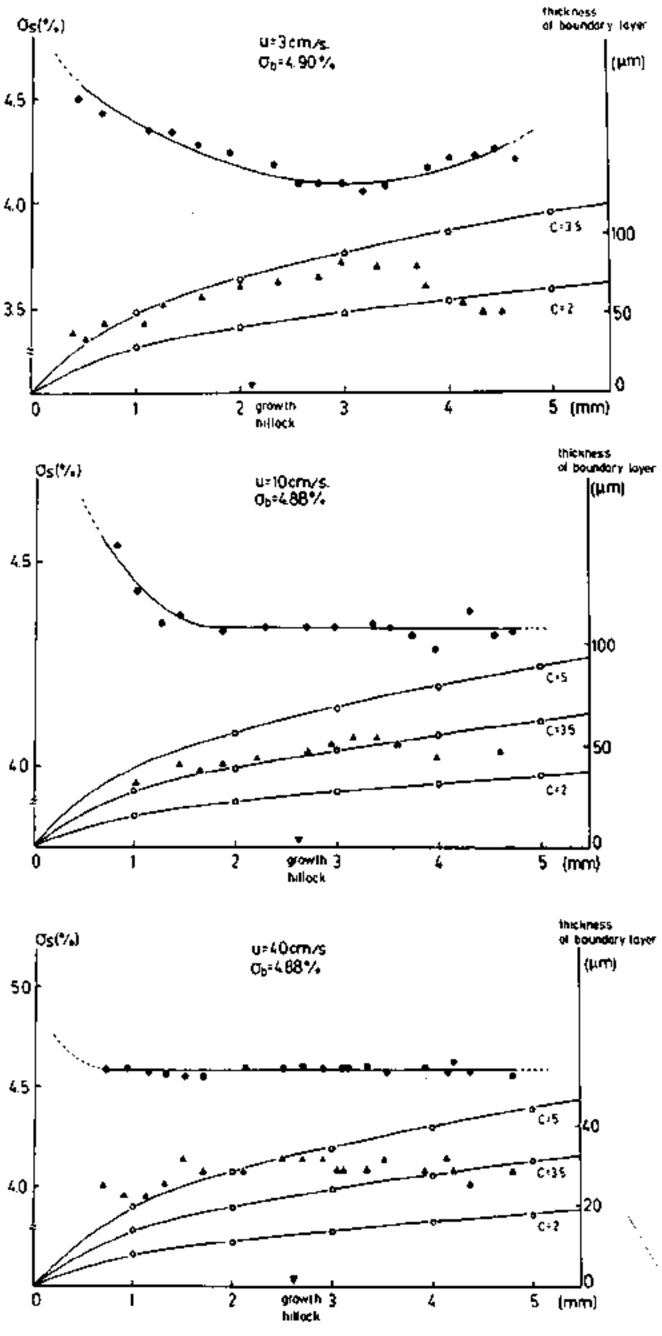

Fig. 2-7. Change in the thickness of diffusion boundary layer (solid triangle) and the surface supersaturation σ_s (solid circle) on the top (111) face of a K-alum crystal with increasing rates of solution flow, u, under a constant bulk supersaturation σ_b. Horizontal axis indicates the distance from the front edge of an octahedral crystal to the rear edge against the direction of flow and the position of the growth hillock (▽). Curves with open circles are theoretical curves at different constants. (After Onuma et al., 1989a.)

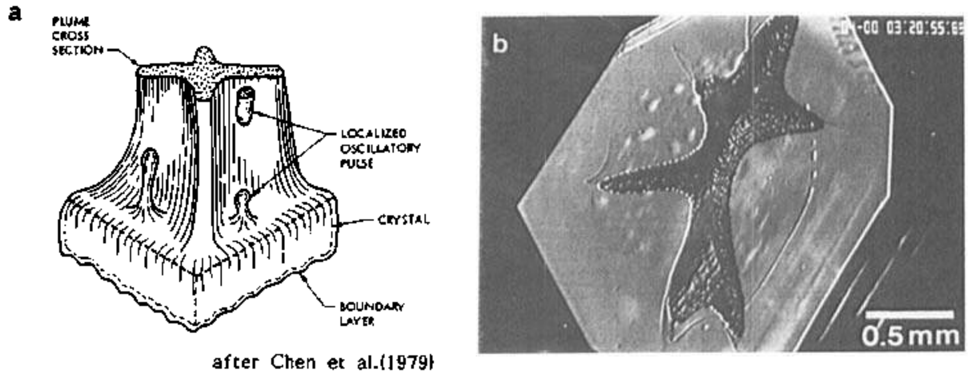

after Chen et al.(1979)

Fig. 2-8. (a) Three-dimensional shape and cross-section of buoyancy-driven convection. (After Chen et al., 1979.) (b) The observed amoeboid depression on a (111) face of K-alum. (After Onuma et al., 1989b.)

of buoyancy-driven convection plume is shown (Onuma et al., 1989b). Amoeboid central depression in Fig. 2-8b is due to the presence of depleted area at the root of buoyancy-driven convection plume, which matches well the cross-section (Fig. 2-8a) of a buoyancy-driven convection plume reported by Chen et al. (1979).

The buoyancy-driven convection plume originates from the top surface in growth and from the bottom surface in dissolution, but not from the side surfaces. Desolvated solvent components move along the side surface to the top surface (growth) or to the bottom surface (dissolution) and escape from there. As a result, a distinct anisotropy in the surface supersaturation and the resultant growth or dissolution rates appears even among crystallographically equivalent faces (Onuma et al., 1990). Inasmuch as a large number of crystals grow concurrently and side-by-side and turbulent flow is present in real systems particularly in sedimentogenetic environments of category (1) and (2) (see section "Crystal growth in different phases", p. 19), interference and overlapping of diffusion boundary layers and buoyancy-driven convection plumes should be ubiquitous. This leads to an expectation that detachments of already-formed crystals and the secondary nucleation phenomenon due to this should be an universally encountered phenomenon in sedimentogenetic environments.

INTERFACE ROUGHNESS AND GROWTH MECHANISM

A crystal grows through incorporation of solute components at kinks and steps on the interface. Before complete desolvation occurs, several desolvation stages take place: (a) when an armoured (i.e., bound with solvent component) solute component (solute–solvent complex) enters into the diffusion boundary layer; (b) when solute component reaches the interface and during its surface diffusion along the interface; and (c) when solute component enters into a step or a kink position, as schematically illustrated in Fig. 2-2. At each stage it should overcome the corresponding activation energy barrier.

The modes of incorporation of solute component into a crystal should be different depending on the kink density, i.e., atomic structure, of an interface. If an interface is composed of only kink sites, i.e., is atomically rough, the desolvated solute components can immediately find sites to be incorporated into the crystal as soon as they arrive at kink sites. If an interface is atomically smooth, principally consisting of a flat surface with a low density of kinks and steps, the solute component has to wander on the smooth surface for a while until it finds an appropriate kink site or before it escapes from the surface.

Depending on the roughness of the interface, the growth mechanisms are different. Continuous growth or an adhesive-type growth mechanism is expected on a rough interface, and the interface advances perpendicularly to the original interface. On an atomically smooth interface, growth can proceed via the advancement of the steps of growth layers of monomolecular height or of bunched growth layers. The growth layers are parallel to the interface, because incorporation of the solute component occurs at kink sites and then step sites, and not on the flat surface. Two-dimensional layer growth is the principal growth process on a smooth interface. There are two ways in which growth layers can originate on such an interface: (1) by two-dimensional nucleation on the surface to form an island or (2) from steps provided by screw or mixed-type dislocations. Either two-dimensional nucleation growth mechanism or spiral growth mechanism will operate in this case. The growth rates versus driving force relations are different, depending on the growth mechanism and the roughness of interfaces. They are schematically shown in Fig. 2-9.

The roughness of an interface in solution system may be evaluated using the Jackson's α factor (Jackson, 1958) generalized by Bennema and Gilmer (1973), as expressed by the following equation:

$$\alpha = \xi \, \frac{\oint_{\mathrm{sf}} - \frac{1}{2}\left(\oint_{\mathrm{ss}} + \oint_{\mathrm{ff}}\right)}{k\, T_{\mathrm{G}}} \tag{2-2}$$

where $\oint_{\mathrm{ss}}$ is the bonding energy in the solid phase, $\oint_{\mathrm{ff}}$ is the fluid–fluid interaction energy, $\oint_{\mathrm{sf}}$ is the solid–fluid (or solute–solvent) interaction energy, k is the Boltzmann

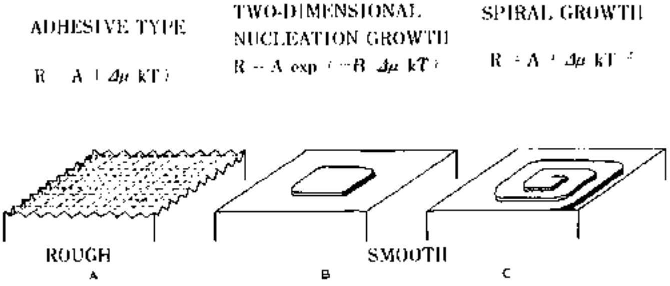

Fig. 2-9. Diagrams explaining growth mechanisms on rough and smooth interfaces and the corresponding relations between the growth rate, R, and the driving force $\Delta\mu/kT$. A and B are constants, k is the Boltzmann constant, T is the growth temperature, and $\Delta\mu$ is the chemical potential difference between crystal and solution.

constant, T_G is the growth temperature, and ξ is the orientational factor. The following facts have been well established as to the interface roughness in Jackson's (1958) original treatment and by the extensive computer simulations (e.g., Gilmer and Jackson, 1977): (a) there is a critical value above which an interface becomes smooth and below which it is rough (in Jackson's equation, an interface with $\alpha > 3$ is smooth and that with $\alpha < 3$ is rough); and (b) with increasing temperatures, a smooth interface transforms to a rough interface above a critical temperature. This temperature is called the roughening transition temperature.

In Jackson's original theory, the α value was a constant to characterize a material, because the equilibrium temperature and not growth temperature is used in the formula. The α values of metals are usually smaller than 3 and, thus, tend to grow on rough interfaces, whereas crystals with complicated structure usually have α values larger than 3 and grow on smooth interfaces. The α values depend on crystallographic orientation. Depending on such orientation, both smooth and rough interfaces may be present in the case of materials with α values higher than 3.

In the generalized formula, the α values can be different depending on the phase type (melt, solution or vapor) from which crystals grow and type of solvent, or the strength of solute–solvent interaction energy in the case of crystal growth from solution phase. The α values decrease with increasing growth temperature and solute–solvent interaction energy. The interface roughness also increases with increasing driving force (Temkin, 1971a, b). A smooth interface transforms into a rough interface at higher driving force. In this case, it is called kinetic roughening transition.

Inasmuch as growth temperatures are much lower in solution than in melt for the same material, the interfaces are in general smoother for the crystal growth in solution than in melt. The smoothest interface may be expected in the case of vapor growth (see Table 2-1).

MORPHOLOGY

Based on the discussion given in the preceding three sections, growth rate versus driving force relation can be schematically expressed as shown in Fig. 2-10. There are two boundaries in this figure as indicated by * and **. Under driving force higher than $\Delta\mu/kT^{**}$, the interface is expected to be rough, whereas below this driving force it is smooth. Hence, in the region above $\Delta\mu/kT^{**}$, growth occurs principally on the rough interfaces. This implies that the outline of a growing crystal is rounded or parabolic. As growth proceeds, particularly in impure systems, the outline becomes morphologically unstable. The morphological instability (refer to, for example, Sekerka, 1972) may take place mainly due to the constitutional supercooling in impure real system. The morphology of crystals to be expected under this condition is, thus, dendritic. At higher driving force, spherulitic or bow-tie morphology consisting of crystals radiating from a center is expected. Further increasing the driving force, fractal pattern will appear by coagulation of tiny crystals which are nucleated independently. Within the region below $\Delta\mu/kT^{**}$, where

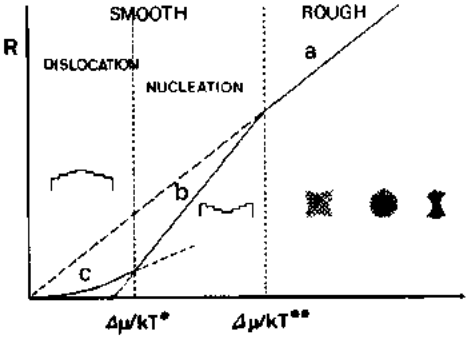

Fig. 2-10. Growth rate versus driving force relation for adhesive type growth (curve *a*), two-dimensional nucleation growth (curve *b*), and spiral growth (curve *c*) mechanisms. Morphological variations from polyhedral, hopper, dendritic, spherulitic, and bow-tie form are explained on this diagram. The diagram shows only one section. The boundaries of $\Delta\mu/kT^*$ and $\Delta\mu/kT^{**}$ change depending on crystallographic orientation, phase, type of solvent, and the size of crystal. (After Sunagawa, 1984.)

growth on the smooth interface is expected, two regions are distinguished: (a) below $\Delta\mu/kT^*$, and (b) between $\Delta\mu/kT^*$ and $\Delta\mu/kT^{**}$. In the region below $\Delta\mu/kT^*$, the growth is mainly governed by the spiral growth mechanism, resulting in a polyhedral crystal bounded by flat faces. Inasmuch as the dependence of growth rates upon the growth parameters is orientational, there are various morphologies of polyhedral crystals, i.e., habit variations. Also surface microtopographs of crystal faces (spiral morphologies) vary depending on growth conditions.

The major factors causing habit variation of polyhedral crystals and surface microtopographs were identified to be temperature, supersaturation, type of solvent and solubility, and impurity elements (see Sunagawa, 1988a, b; Sunagawa and Bennema, 1982).

Between $\Delta\mu/kT^*$ and $\Delta\mu/kT^{**}$, there is a two-dimensional nucleation growth mechanism. A hopper morphology is expected, because growth layers preferentially originate from the edges of a face and advance inwards due to the Berg effect.

The actual values of $\Delta\mu/kT^*$ and $\Delta\mu/kT^{**}$ differ depending on the phase type, solid-fluid interaction energy ϕ_{sf}, crystallographic orientation of the material, and crystal sizes (Kuroda et al., 1987). They are all, except for the size, related to the generalized α value. Results of a computer simulation by Kuroda et al. (1977) on the stability fields of polyhedral, hopper, and dendritic morphologies in relation to the crystal size and supersaturation are presented in Fig. 2-11.

The $\Delta\mu/kT^{**}$ is much smaller in the growth of crystals from the melt than from the solution or vapor. This implies that a dendritic morphology is more likely expected to occur in growth of crystals from the melt than from the solution or vapor for the same material. On the other hand, a polyhedral morphology is more likely to appear in the case of crystal growth from the vapor or solution. Some of the empirically known facts on crystal morphology, which are presented below, are based on the difference in values of $\Delta\mu/kT^*$ and $\Delta\mu/kT^{**}$. In spite of the fact that growth takes place in similar aqueous solutions, it has been empirically shown that

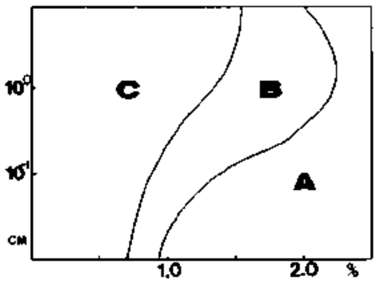

Fig. 2-11. Stability fields of polyhedral, hopper and dendritic morphology in relation to crystal size and bulk supersaturation. Horizontal axis indicates bulk supersaturation (in %), whereas vertical axis shows crystal size (in cm). Region *A* dendritic morphology, *B* hopper morphology, and *C* polyhedral morphology. (Modified after Kuroda et al., 1977.)

$NaClO_3$ polyhedral crystals are easily obtained, whereas NaCl and NH_4Cl crystals usually adopt hopper and dendritic morphologies, respectively. The measured σ^{**} ($\Delta\mu/kT^{**}$) values are ca. 3.0% for $NaClO_3$, 0.5% for NaCl, and less than 0.1% for NH_4Cl.

Interfacial roughness is orientation dependent. Interfaces with different degrees of roughness coexist on one growing crystal. The normal growth rates at the rougher interfaces are higher than those at smoother interfaces, resulting in an anisotropic external form. The anisotropy increases with increasing driving force, because roughening transition of rougher interfaces occurs at smaller driving force than that in the case of smoother interfaces.

Orientational dependence of interfacial roughness can be correlated with Hartman and Perdok's (1955) PBC theory. The F-face in the PBC theory corresponds to a smooth interface, whereas the K-face corresponds to a rough interface. The S-face is inbetween these two types. The structurally deduced morphology on the basis of PBC analysis is a kind of abstract morphology and has no relation with the thermodynamic parameters. Yet it is useful as a criterion to evaluate deviations of growth morphology from its ideal state (structural morphology, i.e., the morphology expected from the structural factor alone), and to deduce the factors which caused the deviation. The PBC analysis has been improved in recent years (Hartman, 1987; Bennema, 1989).

During the growth process, the growth rates, the resulting surface microtopography of crystal faces, and external morphology of crystals may change due to the fluctuation in growth parameters and to the unbalanced growth and diffusion rates. Due to the fluctuation of growth parameters, growth banding appears. Inasmuch as the interface roughness and growth rates are different depending on the crystallographic orientation, growth sector boundaries appear. As growth proceeds, the concentration of solute components in the diffusion boundary layer is depleted, resulting in slowing down of the growth rate. Mass transportation of solute components from the bulk solution to the growing surface by diffusion is in general slower than that necessary to compensate concurrently the depletion in the diffusion boundary layer due to growth. Crystal growth is like breathing or pulsation. This is another reason for the appearance of growth banding. Inasmuch as morphology of crystals

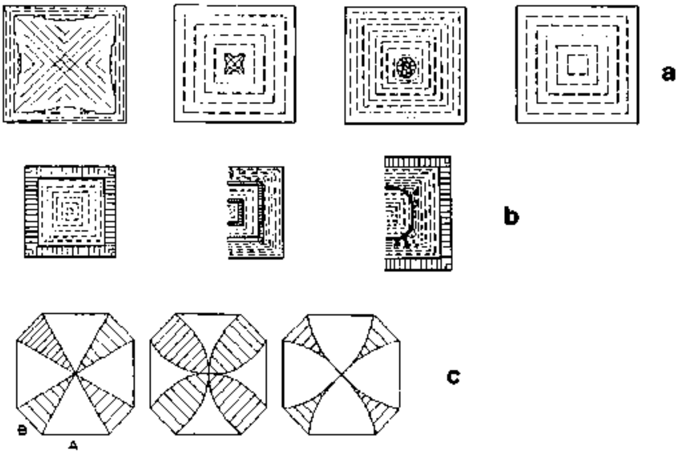

Fig. 2-12. Expected various internal morphologies (heterogeneities) in single crystals. (a) Top row indicates various morphologies expected when the driving force diminishes monotonously; (b) middle row shows the case when growth parameters change abruptly during growth; and (c) the bottom row indicates a variety of growth sector boundaries, depending on the relative growth rates of the two faces.

varies (from spherulitic, dendritic, and hopper to polyhedral) with decreasing driving force, various internal morphologies should be detected (if appropriate characterization techniques are applied) in the final single crystals, even if they appear to be perfectly homogeneous and exhibit good polyhedral external forms. Figure 2-12 shows various internal morphologies. There are no homogeneous and perfect single crystals in natural minerals. If inhomogeneity and imperfection are not detected in natural single crystals, one should take it as an indication that the characterization techniques were not sensitive enough.

Depending on growth environments, distribution of dislocations in a single crystal may be different. If a crystal grows in a non-confined (where open space is available) and isotropic environment, it will show dislocation bundles radiating from a point in the center of the crystal. If anisotropy is present in the environment, such as solution flow, off-centered dislocation bundles will appear. This leads to an anisotropic development of crystallographically equivalent faces. Needle or thin platy habit of cubic crystals or whiskers are representative examples of such a case. Another cause for anisotropic development of crystallographically equivalent faces is the presence of a preferential active growth site, such as seen in whiskers due to VLS (vapor–liquid–solid) mechanism (Wagner and Ellis, 1964). When a crystal grows in a confined environment, where not much space is available, there will be a number of points of origin of dislocation bundles. These are schematically illustrated in Fig. 2-13.

All these morphological features recorded in mineral crystals should be utilized as key criteria to deduce the growth histories of mineral crystals formed in sedimentogenetic and diagenetic environments.

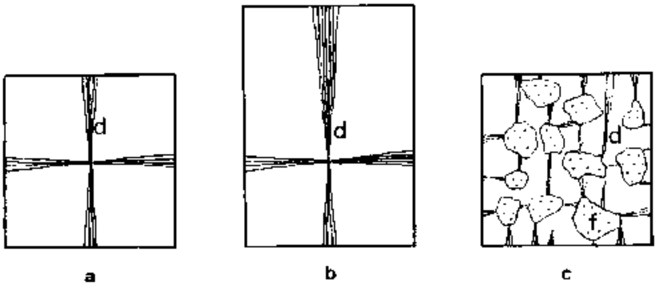

Fig. 2-13. Expected distribution of growth-induced dislocations in a single crystal, depending on environmental conditions. (a) Non-confined and isotropic environment, (b) non-confined but anisotropic environment, and (c) confined environment.

AGGREGATION OF CRYSTALS; TEXTURE FORMATION

In the preceding sections, growth of single crystals was mainly discussed. In this section, factors which control the modes of aggregation of crystals, namely, texture formation, are briefly considered.

When nucleation takes place on a substrate surface, crystals with different orientations meet as growth proceeds. Depending on their relative orientations to the substrate surface, only those perpendicularly oriented can survive and continue to grow, whereas others terminate their growth when they meet the former. Depending upon relative orientations to the substrate surface, a selection process takes place as schematically illustrated in Fig. 2-14. This is called geometrical selection (Grigoriev, 1965). Depending on the form of substrate surface, various textures, such as spherical, reniform, botryoidal, and oolitic will appear. The surfaces of allogenic mineral fragments provide various forms of substrate surfaces, giving rise to a variety of textures. In Fig. 2-15, a variety of substrate surfaces and textures are schematically illustrated.

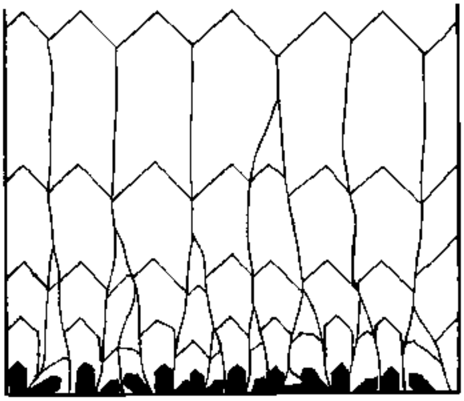

Fig. 2-14. Schematic illustration of the principle of geometrical selection.

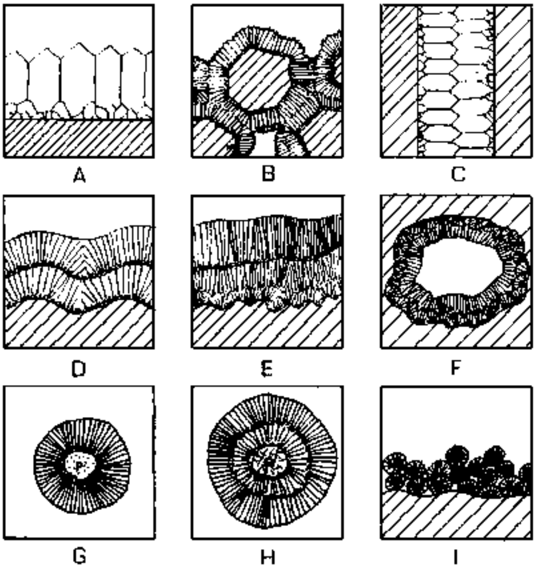

Fig. 2-15. Schematic illustration of various types of crystal aggregates (textures) depending on the form of substrate surface. Solid substrate is indicated by inclined lines sloping to the left. *P* in G is a foreign solid particle, and *R* in H is an aggregate of the same crystals having random orientation.

Agitation applied to a solution containing a large number of tiny crystals, or rolling of crystals on an inclined bed floor in a salt lake, may often result in the coalescence of tiny crystals to form a spherical aggregate, in which crystals are randomly oriented. The aggregates act as core substrate for further growth, and spherulitic aggregate with core and rim portion appears through geometric selection process. In the rim portion, crystals appear in a tangentially radiating form from the core surface.

GROWTH OF CRYSTALS IN DIAGENETIC ENVIRONMENT

Whether diagenesis, catagenesis, and low-grade metamorphism proceed through a solid-state transformation or through a dissolution-and-precipitation process, is still a controversial subject. As already pointed out in the introduction and the second section, the present author is in favor of the latter model, based on the investigation of sheet silicate minerals formed by hydrothermal metasomatism and regional metamorphism, although these processes occur at higher temperatures and pressures than those existing during the diagenesis.

Based on the observations made by means of electron microscopic decoration technique (also called atomic replication technique) of surface microtopographs of these sheet silicate minerals, the following conclusions are possible:

(1) Kaolin-group minerals, sericite, and chlorite of hydrothermal metasomatic origin universally exhibit typical growth spirals with the height of unit cell order (10 Å). Coalescence of crystals is less commonly encountered among these crystals than

those formed in hydrothermal vein-type deposits. The observations indicate that the crystallization proceeded by the spiral growth mechanism in a static solution at a low supersaturation. This implies that the growth took place in thin film of dilute solution phase, which appeared through dissolution of original rocks by the hydrothermal solution at the reaction front of metasomatism. Dissolution-and-precipitation process was thus suggested (Sunagawa and Koshino, 1975).

(2) The surface microtopographs of sericite and porphyroblastic white mica (in different metamorphic grades of regional metamorphic rocks of Sambagawa Belt, Shikoku, Japan) indicated absence of spiral patterns and presence of concentric smooth and rugged step patterns with unit cell heights. Smooth steps are growth steps, whereas rugged steps are dissolution steps. Depending on the metamorphic grade and location in one metamorphic zone, and on the difference of sericite and porphyroblastic white mica, the two patterns are different. Based on these observations, it was suggested that the interstitial volatile components played an important role in regional metamorphism, with dissolution-and-precipitation process taking place, and that Ostwald ripening was responsible for the formation of porphyroblastic white mica (Tomura et al., 1979).

In Fig. 2-16, representative examples of surface microtopographs observed on sheet silicates by the decoration technique are shown.

Diagenesis takes place at much lower pressures and temperatures and in the presence of larger volume of interstitial solutions than in the case of regional metamorphism. It is reasonable to assume that a dissolution-and-precipitation process operates similarly in the mineral formation during diagenesis. Ostwald ripening is likely to take place in such environments. The reader may refer to a review paper by Baronnet (1982).

DISSOLUTION

Although growth and dissolution processes appear to be in a symmetrical relation, in reality both are asymmetrical. Growth rate versus driving force (supersaturation) relations are in most cases different from dissolution rate versus driving force (undersaturation) relations. The asymmetry is caused by the difference of the role of lattice defects and the associated strain fields in the two processes. Screw and mixed-type dislocations provide steps which are active sites for spiral growth. Pure edge dislocations may provide sites for repeated two-dimensional nucleation, which may occur only under a higher driving force condition than that required for the spiral growth. Point defects are ineffective for growth.

Inasmuch as strain fields are associated with any type of dislocations, point defects, and inclusions, they can act as active sites for dissolution. Also edges and corners of a polyhedral crystal, and steps of growth layers on a flat face are easier sites to initiate dissolution than the flat surface. Dissolution from edges, corners and strain fields associated with outcrops of lattice defects on the surface, transforms a polyhedral crystal to a rounded one. Finally, this leads to a complete dissolution.

When dissolution proceeds, a solute component dissolved from the top surface

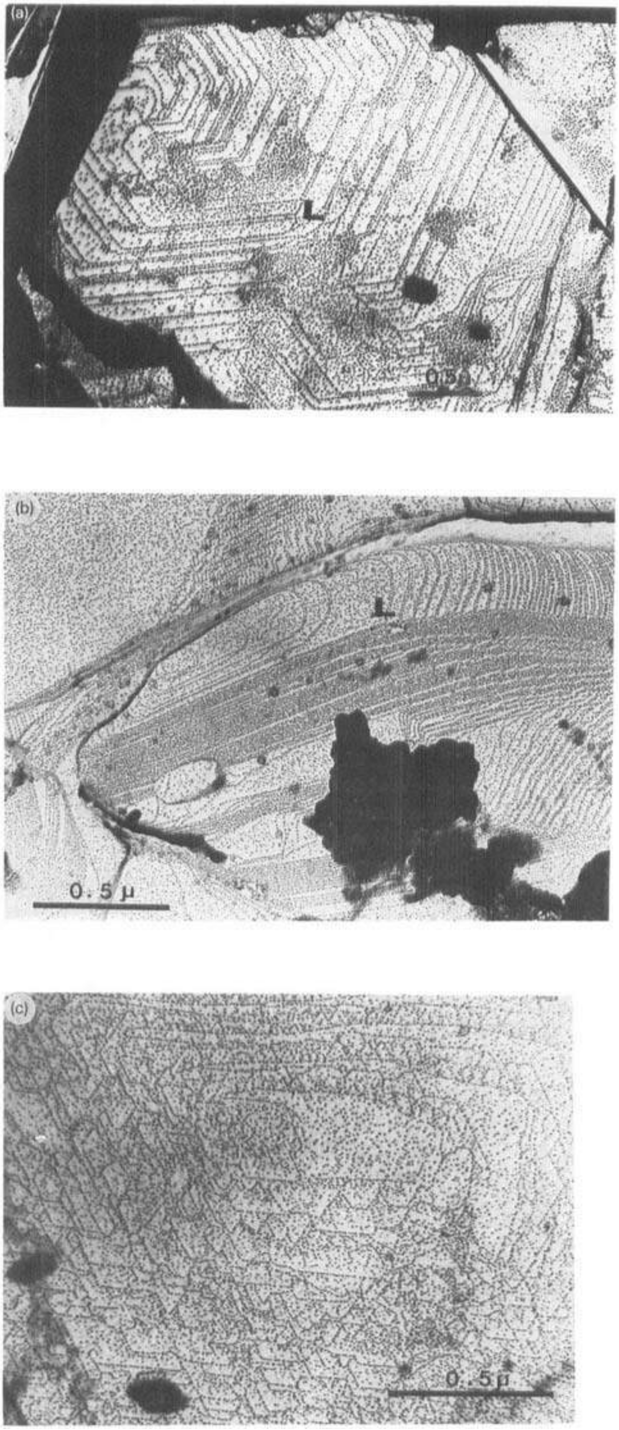
(a)
L
0.5µ
(b)
L
0. 5 µ
(c)
0. 5µ

of a crystal can not easily escape from the diffusion boundary layer due to gravity. As a result, the deviation of surface undersaturation from the bulk undersaturation becomes greater than in the case of growth. When the rate of solution flow is small, the discrepancy increases as dissolution proceeds and can become as much as 40% (Onuma et al., 1990).

Elemental process of dissolution is a layer-by-layer process on the flat surface similar to the case of growth. At first, the steps of a spiral start to recede two-dimensionally, and original smooth growth steps become rugged. The rugged dissolution steps are due to the strain fields around adsorbed impurities along the original steps. After a short period of this process, an etch pit appears at the spiral center. Further progress of dissolution leads to the appearance of a large number of both point-bottomed and flat-bottomed etch pits at sites on the surface other than the spiral center. The etch pits, which originated from the outcrops of dislocations, show point-bottomed form, whereas those which originated from the point defects or inclusions show flat-bottomed form. The morphology and orientation of etch pits vary depending on the conditions. Sometimes dislocation-hollows or tunnels are formed when the strain field around a dislocation (or a dislocation bundle) and the driving force are higher than the respective critical values. Dislocation-hollows may appear both as a result of growth and dissolution. The thermodynamic stability conditions for the occurrence of dislocation-hollows were analyzed by Van der Hoek et al. (1982). Dissolution also proceeds from edges or corners of a polyhedral crystal, because they constitute rough interfaces having innumerable kink sites. A rounded morphology with curved surfaces appears as a result. Natural diamond crystals are a representative example (Sunagawa, 1984).

Dissolution is also orientation- and structure-dependent. Crystals with an hourglass structure (growth sectors with different solid solution components), compositional zoning due to solid solution, etc., behave differently from the chemically homogeneous crystals formed by dissolution process. Dissolution will proceed selectively.

CONCLUSIONS

In most of the geological processes, it is not possible to observe directly the process of crystallization and texture formation. Only indirect methods are available, namely, the theoretical or conceptional (but abstract) deductive approach based on the in-

---

Fig. 2-16. Representative examples of surface microtopographs observed on sheet silicate minerals, taken by the decoration technique of electron microscopy. (a) Dickite from a hydrothermal metasomatic deposit. (Interlaced spiral steps of 10 Å in height are seen. The interlacing is due to zigzag stacking in the dickite structure, the unit cell of which consists of two kaolinite sheets, each having a height of 10 Å.) (After Sunagawa and Koshino, 1975.) (b) Porphyroblastic white mica, showing closed smooth step pattern (coupled steps are indicative of 2M structure). (c) Sericite showing rugged step pattern. Both (b) and (c) are observed on mica occurring in regional metamorphic rocks. *L* indicates interlaced or coupled steps. (After Tomura et al., 1979.)

terpretation of mineral crystal and textural characteristics. Through characterization, one can attempt to reconstruct the deviations of various physical and chemical properties from their ideal states, because these provide the record of growth histories and changes in growth parameters. These include external and internal morphologies, surface microtopography, various lattice defects and chemical heterogeneities in single crystals, and textures of crystal aggregates. Increasingly, more sophisticated methods have been used to observe imperfections and inhomogeneities in single crystals and textures, such as various optical microscopy, scanning and transmission electron microscopy, X-ray topography, cathode luminescence topography, scanning tunnel microscopy, and electron probe microanalyzer.

These abstract, conceptional deduction of growth histories based on the results of characterization of mineral crystals should naturally be backed by theoretical and experimental verifications. The results of investigations of simple systems offer useful data for this purpose, owing to the recent progress in experimental verification of crystal-growth mechanism by means of in-situ observation methods.

The present author has been involved in verification of crystal-growth mechanism of simple laboratory systems, but also is interested in real systems of geological interest. He is willing to cooperate with geologists to solve these problems.

ACKNOWLEDGEMENTS

The author expresses his sincere thanks to his former colleagues and students at the Institute of Mineralogy, Petrology and Economic Geology, Tohoku University, who co-operated with him in developing the in-situ observation methods to verify the mechanism of crystal growth. Particular thanks are due to Drs. K. Tsukamoto, K. Maiwa and K. Onuma, among others.

The help extended by Drs. George V. Chilingarian and Karl H. Wolf is also greatly appreciated.

BIBLIOGRAPHY AND REFERENCES

Books

Berner, R.A., 1980. *Early Diagenesis, A Theoretical Approach.* Princeton University Press, N.J., 241 pp.

Chernov, A.A., 1984. *Modern Crystallography, III, Crystal Growth.* Springer-Verlag, Heidelberg, 517 pp.

Grigoriev, D.P., 1965. *Ontogeny of Minerals.* Israel Programme for Scientific Translations, Jerusalem, 284 pp.

Hartman, P. (Editor), 1972. *Crystal Growth: An Introduction.* North-Holland, Amsterdam, 531 pp.

Sunagawa, I. (Editor), 1988. *Morphology of Crystals, Part A, B.* Terra Sci. Publ., Tokyo/D. Reidel, Dordrecht, 743 pp.

Sunagawa, I. (Editor), 1989. *Morphology and Growth Unit of Crystals.* Terra Sci. Publ., Tokyo, 690 pp.

Review articles

Baronnet, A., 1982. Ostwald ripening in solution growth, the case of calcite and mica. *Estud. Geol. (Madrid)*, 38: 185–198

Sunagawa, I., 1984. Growth of crystals in nature. In: I. Sunagawa (Editor), *Materials Science of The Earth's Interior.* Terra Sci. Publ., Tokyo/D. Reidel, Dordrecht, pp. 63–105.

Sunagawa, I., 1988a. Morphology of minerals. In: I. Sunagawa (Editor), *Morphology of Crystals, Part B.* Terra Sci. Publ., Tokyo/D. Reidel, Dordrecht, pp. 509–587.

Sunagawa, I., 1988b. Surface microtopography of crystal faces. In: I. Sunagawa (Editor), *Morphology of Crystals, Part A.* Terra Sci. Publ., Tokyo/D. Reidel, Dordrecht, pp. 323–365.

Sunagawa, I., 1989. Crystal growth and geosciences. In: H. Arend and J. Huiliger (Editors), *Crystal Growth in Science and Technology.* Plenum, New York, N.Y., pp. 253–266.

Sunagawa, I., 1990. In-situ observation of nucleation, growth and dissolution of crystals in ordinary temperature aqueous solutions and high temperature silicate solutions. In: F. Marumo (Editor), *Dynamic Processes of Material Transport and Transformation in the Earth's Interior.* Terra Sci. Publ., Tokyo, pp. 141–170.

Sunagawa, I. and Bennema, P., 1982. Morphology of growth spirals, theoretical and experimental. In: W.A. Wilcox (Editor), *Preparation and Properties of Solid State Materials, Vol. 7.* Marcel Dekker, New York, N.Y., pp. 1–129.

Tsukamoto, K., 1989. In-situ direct observation of a crystal surface and its surroundings. In: I. Sunagawa (Editor), *Morphology and Growth Unit of Crystals.* Terra Sci. Publ., Tokyo, pp. 451–478.

Cited references

Abe, T., Tsukamoto, K. and Sunagawa, I., 1987. Instrumentation for in-situ observation of growth and dissolution processes of crystals in high temperature solutions at 1600°C. *Mineral. J.*, 13: 479–489.

Abe, T, Tsukamoto, K. and Sunagawa, I., 1991. Nucleation, growth and stability of $CaAl_2Si_2O_8$ polymorphs. *Phys. Chem. Miner.*, pp. 473–484.

Azuma, T., Tsukamoto, K. and Sunagawa, I., 1989. Clustering phenomenon and growth units in lysozyme aqueous solution as revealed by laser light scattering method. *J. Crystal Growth*, 98: 371–376.

Baronnet, A., 1982. Ostwald ripening in solution growth, the case of calcite and mica. *Estud. Geol. (Madrid)*, 38: 185–198.

Bennema, P., 1989. Crystallographic rules to determine connected nets from crystallographs based on theories of roughening: crystallographic and physical implications. In: I. Sunagawa (Editor), *Morphology and Growth Unit of Crystals.* Terra Sci. Publ., Tokyo, pp. 219–245.

Bennema, P. and Gilmer, G.H., 1973. Kinetics of crystal growth. In: P. Hartman (Editor), *Crystal Growth, An Introduction.* North-Holland, Amsterdam, pp. 263–327.

Berg, W.F., 1938. Crystal growth from solutions. *Proc. R. Soc. London, Ser. A*, 164: 79–95.

Chen, P.S., Shlichta, P.J., Wilcox, W.R. and Lefever, R.A., 1979. Convection phenomena during the growth of sodium chlorate crystals from solution. *J. Crystal Growth*, 47: 43–60.

Chernov, A.A., 1984. *Modern Crystallography, III. Crystal Growth.* Springer-Verlag, Heidelberg, 517 pp.

Flügel, E., 1982. *Microfacies Analysis of Limestones.* Springer-Verlag, Berlin, 2nd ed., 633 pp.

Gilmer, G.H. and Jackson, K. A., 1977. Computer simulation of crystal growth. In: E. Kaldis and H.J. Scheel (Editors), *Current Topics in Materials Science, Vol. 2.* North-Holland, Amsterdam, pp. 80–114.

Grigoriev, D.P., 1965. *Ontogeny of Minerals.* Israel Programme for Scientific Translations, Jerusalem, 284 pp.

Hartman, P., 1987. Modern PBC theory. In: I. Sunagawa (Editor), *Morphology of Crystals, Part A.* Terra Sci. Publ., Tokyo/D. Reidel, Dordrecht, pp. 271–319.

Hartman, P. and Perdok, W.G., 1955. On the relation between structure and morphology of crystals. *Acta Crystallogr.*, 8: 49–52, 521–524, 525–529.

Jackson, K.A., 1958. Mechanism of growth. In: *Liquid Metals and Solidification.* Am. Soc. Metals, Cleveland, Ohio, pp. 174–186.

Kouchi, A., Tsuchiyama, A. and Sunagawa, I., 1986. Effect of stirring on crystallization kinetics of basalt: texture and element partitioning. *Contrib. Mineral. Petrol.*, 93: 429–438.

Kuroda, T., Irisawa, T. and Ookawa, A., 1977. Growth of a polyhedral crystal and its morphological stability. *J. Crystal Growth*, 42: 41–46.

Kuroda, T., Irisawa, T. and Ookawa, A., 1987. Transition from polyhedral to dendritic morphology. In: I. Sunagawa (Editor), *Morphology of Crystals, Part B.* Terra Sci. Publ., Tokyo/D. Reidel, Dordrecht, pp. 589–612.

Li Lian, Tsukamoto, K. and Sunagawa, I., 1990. Impurity adsoption and habit changes in aqueous solution grown KCl crystals. *J. Crystal Growth*, 99: 150–155.

Maiwa, K., 1987. *Role of Lattice Defects in Aqueous Solution Growth of $Ba(NO_3)_2$ Crystals.* Ph.D. Thesis, Tohoku Univ., Sendai, 130 pp.

Maiwa, K. Tsukamoto, K. and Sunagawa, I., 1987. Growth induced lattice defects in $Ba(NO_3)_2$ crystals. *J. Crystal Growth*, 82: 611–620.

Maiwa, K., Tsukamoto, K., Sunagawa, I., Chuan-zhen Ge and Nai-ben Ming, 1989. Observation of screw and mixed dislocations in barium nitrate crystals by means of birefringence and X-ray topography. *J. Crystal Growth*, 99: 590–594.

Maiwa, K., Tsukamoto, K. and Sunagawa, I., 1990. Activities of spiral growth hillocks on the (111) faces of barium nitrate crystals growing in an aqueous solution. *J. Crystal Growth*, 102: 43–53.

Nakamura, H., Tsukamoto, K. and Sunagawa, I., 1990. In-situ observation of high temperature silicate solutions. *J. Crystal Growth*, 99: 1227–1231.

Onuma, K., 1988. *A Combined Investigations of Interface Kinetics and Environmental Phase in Aqueous Solution Growth.* Ph.D Thesis, Tohoku Univ., Sendai, 195 pp.

Onuma, K., Tsukamoto, K. and Sunagawa, I., 1988. Role of buoyancy driven convection in aqueous solution growth; a case study of $Ba(NO_3)_2$ crystal. *J. Crystal Growth*, 89: 177–188.

Onuma, K., Tsukamoto, K. and Sunagawa, I., 1989a. Measurements of surface supersaturations around a growing K-alum crystal in aqueous solution. *J. Crystal Growth*, 98: 377–383.

Onuma, K., Tsukamoto, K. and Sunagawa, I., 1989b. Effect of buoyancy driven convection upon the surface microtopographs of $Ba(NO_3)_2$ and CdI_2 crystals. *J. Crystal Growth*, 98: 384–390.

Onuma, K., Tsukamoto, K. and Sunagawa, I., 1991. Dissolution kinetics of K-alum crystals in relation to the surface undersaturations. *J. Crystal Growth*, 110: 724–732.

Sekerka, R.F., 1972. Morphological stability. In: P. Hartman (Editor), *Crystal Growth: An Introduction.* North-Holland, Amsterdam, pp. 403–443.

Sunagawa, I., 1984. Morphology of natural and synthetic diamonds. In: I. Sunagawa (Editor), *Materials Science of The Earth's Interior.* Terra Sci. Publ., Tokyo/D. Reidel, Dordrecht, pp. 303–330.

Sunagawa, I., 1988a. Morphology of minerals. In: I Sunagawa (Editor), *Morphology of Crystals, Part B.* Terra Sci. Publ., Tokyo/D. Reidel, Dordrecht, pp. 509–587.

Sunagawa, I. 1988b. Surface microtopography of crystal faces. In: I. Sunagawa (Editor), *Morphology of Crystals, Part A.* Terra Sci. Publ., Tokyo/D. Reidel, Dordrecht, pp. 323–365.

Sunagawa, I., 1989. Crystal growth and geosciences. In: H. Arend and J. Huiliger (Editors), *Crystal Growth in Science and Technology.* Plenum, New York, N.Y., pp. 253–266.

Sunagawa, I. 1990. In-situ observation of nucleation, growth and dissolution of crystals in ordinary temperature aqueous solutions and high temperature silicate solutions. In: F. Marumo (Editor), *Dynamic Processes of Material Transport and Transformation in the Earth's Interior.* Terra Sci. Publ., Tokyo, pp. 141–170.

Sunagawa, I. and Bennema, P., 1982. Morphology of growth spirals, theoretical and experimental. In: W.A. Wilcox (Editor), *Preparation and Properties of Solid State Materials, Vol. 7,* Marcel Dekker, New York, N.Y., pp. 1–129.

Sunagawa, I. and Koshino, Y., 1975. Growth spirals on kaolin group minerals. *Am. Mineral.*, 60: 407–412.

Temkin, O.E., 1971a. Phenomenological kinetics of the motion of a phase boundary. *Sov. Phys.–Crystallogr.*, 15: 767–772.

Temkin, O.E., 1971b. Kinetic phase transition during a phase conversion in a binary alloy, *Sov. Phys.–Crystallogr.*, 15: 773–780.

Tomura, S., Kitamura, M. and Sunagawa, I., 1979. Surface microtopography of metamorphic white mica. *Phys. Chem. Miner.*, 4: 1–17.

Tsukamoto, K., 1983. In situ observation of mono-molecular growth steps on crystals growing in aqueous solution, I. *J. Crystal Growth*, 61: 199–209.

Tsukamoto, K., 1989. *In-situ Observation Methods Developed for the Verification of Crystal Growth Mechanisms.* Ph.D. Thesis, Tohoku Univ., Sendai, 189 pp.

Tsukamoto, K. and Sunagawa, I., 1985. In situ observation of mono-molecular growth steps on crystals growing in aqueous solution, II. Specially designed objective lens and Nomarski prism for in situ observation by reflected light. *J. Crystal Growth*, 71: 183–190.

Tsukamoto, K., Abe, T. and Sunagawa, I., 1983. In situ observation of crystals growing in high temperature melts or solutions. *J. Crystal Growth*, 63: 215–218.

Van der Hoek, B., Van der Eerden, J.P. and Bennema, P., 1982. Thermodynamical stability conditions for the occurrence of hollow cores caused by stress of line and planar defects. *J. Crystal Growth*, 56: 621–632.

Wagner, R.S. and Ellis, W.C., 1964. Vapour–liquid–solid mechanism of single crystal growth. *Appl. Phys. Lett.*, 4: 89–90.

This Page Intentionally Left Blank

Diagenesis, IV. Developments in Sedimentology 51
edited by K.H. Wolf and G.V. Chilingarian
© 1994 Elsevier Science B.V., Amsterdam. All rights reserved.

Chapter 3

EARLY-DIAGENETIC DEFORMATION STRUCTURES IN THE OVERBURDEN OF THE BEŁCHATÓW BROWN-COAL MINE (CENTRAL POLAND): A PREDICTIVE TOOL REGARDING ENGINEERING-GEOLOGICAL CONDITIONS DURING EXPLOITATION

A.J. VAN LOON and K. BRODZIKOWSKI

INTRODUCTION

The Kleszczów Graben (Fig. 3-1), separating the Łodź depression in the north from the Radomsko elevation in the south, has an E–W direction. Its length is 40–50 km and its width is 1–3 km (Biernat, 1968; Pożaryski, 1971; Pożaryski and Brochwicz-Lewiński, 1978; Ciuk and Piwocki, 1980; Brodzikowski et al., 1987b). The existence of some tectonic discontinuity in the area was long known, but the graben structure was discovered only during the sixties, when a drilling program was initiated to explore a thick brown-coal occurrence (Baraniecka, 1971; Kossowski, 1974).

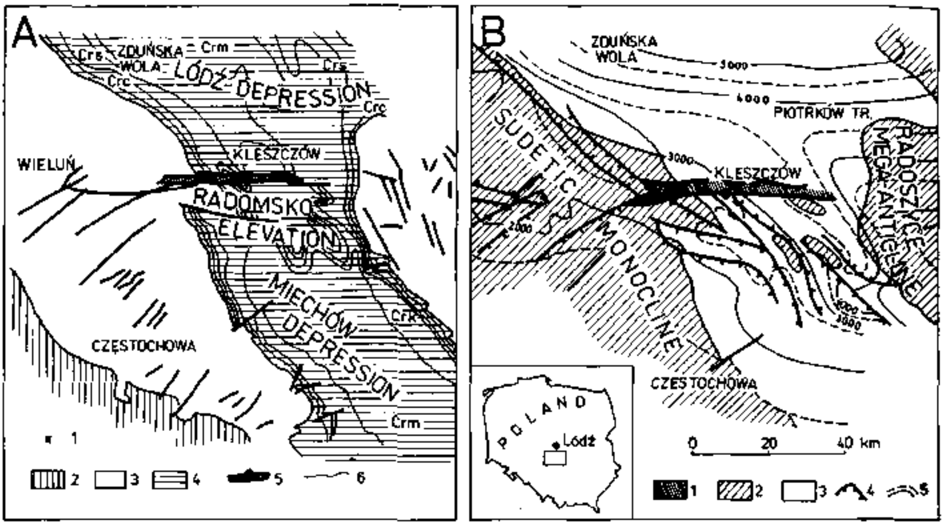

Fig. 3-1. Location of the Kleszczów Graben and the open-cast brown-coal mine near Bełchatów. (A) Main structural elements. *1* = Permian Dębina diapir; *2* = Sudetic monocline; *3* = Silesia–Cracow monocline; *4* = depressions filled with Cretaceous deposits, covered by Cenozoic deposits; *5* = Kleszczów Graben; *6* = stratigraphic boundaries within the Cretaceous (*Crc* = Cenomanian and Turonian; *Crs* = Santonian and Coniacian; *Crk* = Campanian; and *Crm* = Maestrichtian). (B) Principal tectonic elements of the Radomsko High and position of the Kleszczów Graben (simplified after Pożaryski, 1971). *1* = Kleszczów Graben; *2* = Jurassic covered by Cenozoic; *3* = Cretaceous covered by Cenozoic; *4* = faults; and *5* = depth of Zechstein base.

The beginning of the graben's history probably dates from either the late Variscan or the early Alpine orogeny. Evidence for this presumed age is the frequent occurrence of fault zones in the pre-Mesozoic substratum. These zones are interpreted as post-Variscan relaxation phenomena. Horizontal displacement along these discontinuities led, probably during the Laramide phase of the Alpine orogeny, to SE–NW trending folds. These folds are now expressed topographically as the Radomsko elevation (Pożaryski, 1971).

In a more strict sense, the Kleszczów Graben was presumably formed almost simultaneously with the latest folding stages (that formed the Radomsko elevation) and as a result of tensional fracturing and faulting of the anticlinal hinge zones at the transition from the Radomsko elevation to the Łódź depression. This most probably happened during the Laramide phase and, thus, in the earliest Tertiary.

The actual (E–W) graben direction follows the structural trend in the Carboniferous (and older) substratum. Whereas the influence is obvious, it is quite complex, because the graben blocks are positioned in an *en échelon* pattern that is related to the Laramide fold direction.

Together, the data make it most probable that the Kleszczów Graben represents a zone of local weakness, along which tensional fractures formed in the anticlines of the Radomsko folds (Fig. 3-2). The variations in the direction of the faults in the marginal zones of the graben particularly support this view (cf. Brodzikowski et al., 1987b).

The graben contains a thick succession of (predominantly Early and Middle) Miocene brown-coal, which is being exploited near the town of Bełchatów in an open-cast mine (Fig. 3-3) with a current surface area of some 15 km^2. More than 100 m of Quaternary and Tertiary overburden (Fig. 3-4) are being removed and exploitation of the brown-coal will proceed locally, in a secondary graben, to at least 350 m below surface.

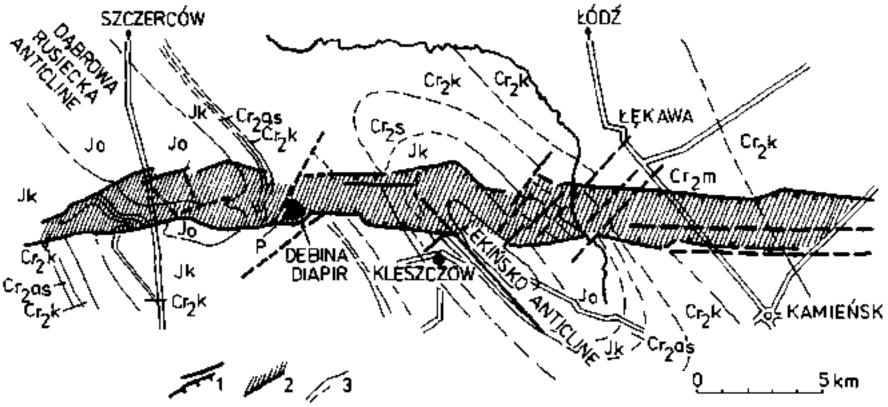

Fig. 3-2. Schematic tectonic setting of the Kleszczów graben. *1* = faults; *2* = graben boundary; *3* = stratigraphic boundary; *Cr$_2$m* = Maestrichtian; *Cr$_2$t* = Turonian; *Cr$_2$a-s* = Albanian and Santonian; *Jk* = Kimmeridgian; *J$_o$* = Oxfordian; and *P* = Permian.

Fig. 3-3. Overview of the Bełchatów brown-coal mine in exploitation.

Removal of the overburden in particular, but also excavation of the brown-coal, poses problems because the mining equipment works at more or less horizontal levels (Fig. 3-5). The lithology of these levels shows rapid variations as a consequence of several types of soft-sediment deformations that range from less than a millimeter (Fig. 3-6) to tens of meters in diameter. Studies were, therefore, carried out to predict the workability of the lithological units that would be encountered. Analysis of the individual deformation structures and their tectonic styles (which are distinctly different in the various parts of the graben) proved to be particularly helpful in predicting the location, size, and frequency of deformation structures that might pose problems to the mining equipment, or that might affect the safety of the workers.

TYPES OF DEFORMATION STRUCTURES

Deformation structures and the processes that cause them can be classified on the basis of various criteria (Nagtegaal, 1965; Van Loon, 1978). Time is one of them (Table 3-1): the process may take place during sedimentation, during several stages of early diagenesis (when the sediment is not yet lithified) or later. Nature of forces and agents (Table 3-2) and size (Table 3-3) are also criteria that can be used for the purpose, but the best insight into the deformational history is obtained by classifying the structures according to their genesis (Table 3-4). This approach seems also preferable from a geological–engineering point of view, because a regional survey on this basis will commonly yield the data that are necessary to take timely adequate measures to prevent damage to mining equipment.

A genetic classification can also be based on a number of criteria (cf. Van Loon, 1992). The choice of the most appropriate system depends on the specific purpose of the investigation and on the geological characteristics of the study area. In the case of the Bełchatów mine, the classification should, obviously, be aimed at a system that would be helpful for developing measures to solve (or, if possible, prevent) engineering–geological and mining problems.

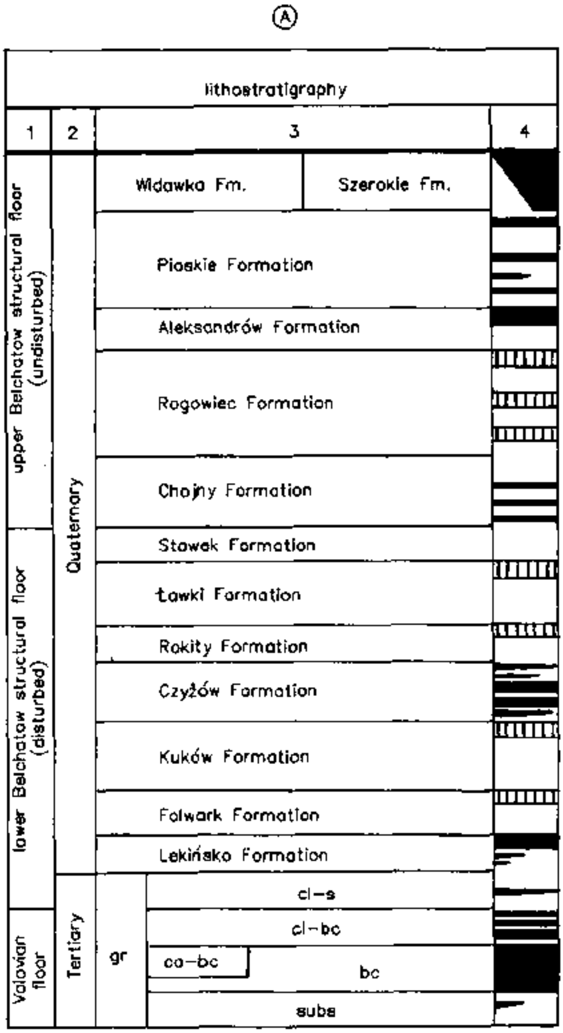

Fig. 3-4. Composite stratigraphic sections for zones Q and T of the graben. (A) Theoretical profile. *1* = structural units; *2* = age; *3* = formations; and *4* = lithology (black = organic; vertical lines = diamicts; white = other glacigenic and interglacial non-organic deposits).

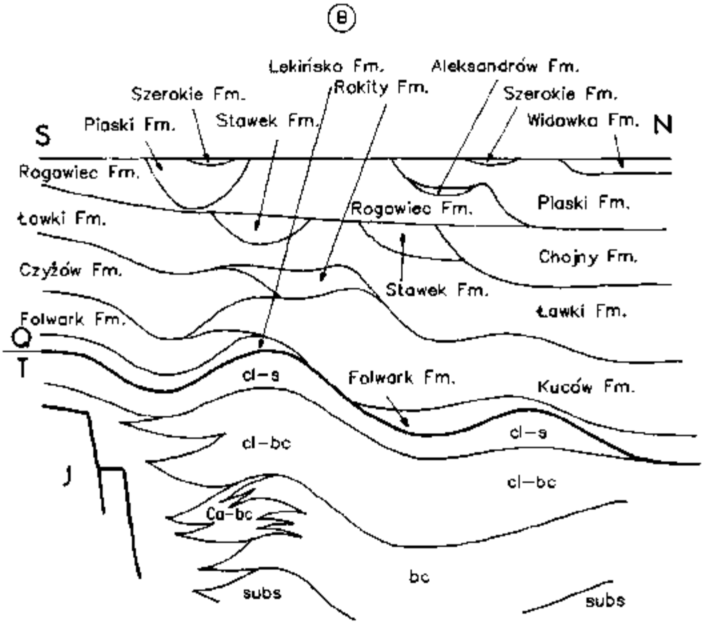

Fig. 3-4 (continued). (B) Schematic cross-section. *cl* = clay; *s* = sand; *bc* = brown-coal; *ca* = calcareous; *subs* = mainly sandy substratum.

The following categories of exogenic soft-sediment deformation structures were distinguished in the Bełchatów area (also see Table 3-4): synsedimentary and metasedimentary structures, cryogenic structures, glaciotectonic structures, biogenic structures (bioturbations), structures formed by gravity-induced surficial mass movements and temperature-induced deformations. In addition, there are soft-sediment deformation structures induced by endogenic activity (tectonic structures sensu stricto). Many structures, however, are due to a combination of two or more (sometimes both endogenic and exogenic) deformational processes. Thus, the exact positioning of structures within a terminological framework may, therefore, be difficult. This problem must also be faced in the Bełchatów brown-coal mine, because a major category of the deformations present here is constituted of structures that developed due to a combination of processes; such structures are termed "polygenetic structures".

All the above categories occur frequently in the area of study (Brodzikowski and Gotowała, 1980; Brodzikowski, 1982a, b, 1983, 1985; Gotowała and Hałuszczak, 1982a; Brodzikowski and Van Loon, 1987; Brodzikowski et al., 1987a, c, d). The various groups of soft-sediment deformation structures mentioned above are discussed successively in the following subsections.

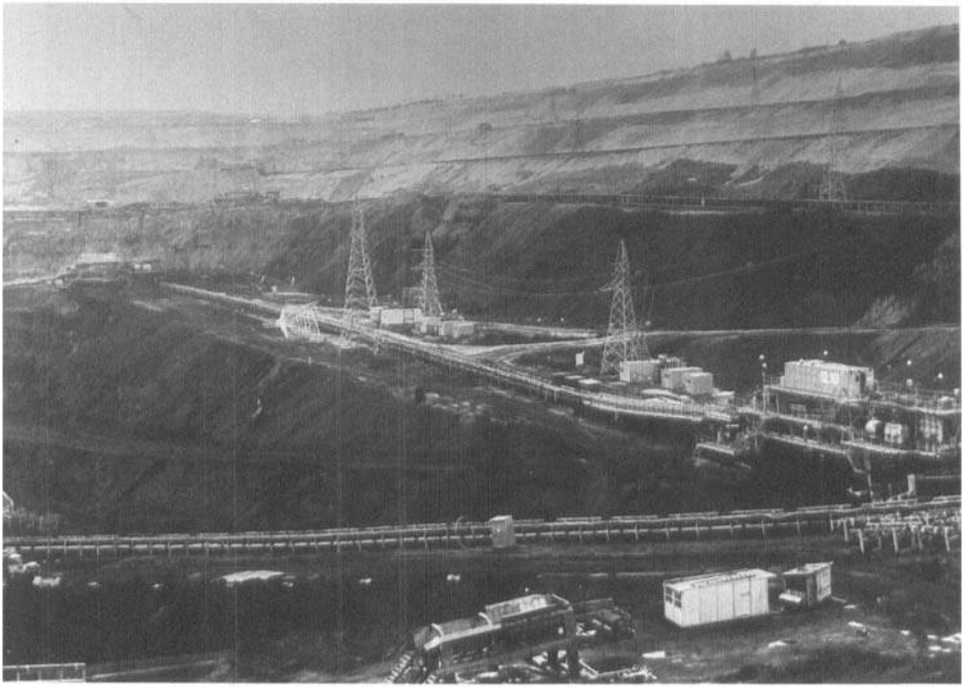

Fig. 3-5. Buildings and equipment at a "terrace" in the upper part of the brown-coal mine. Note the horizontal character of the "terraces"; this is a prerequisite for both stabilization of the scarps and proper functioning of the excavators. Also note the height difference between the successive "terraces", being a measure for the capacity of the excavators.

TABLE 3-1

Classification of sedimentary and diagenetic structures according to their time of development

Name		Time of genesis	Example	Reference
Presedimentary		Before deposition of the sediment layer involved	Flute cast	Allen, 1982
Formation of soft-sediment deformation structures	Synsedimentary	During deposition of the sediment layer involved	Current ripple	Allen, 1982
	Metasedimentary	After deposition of the sediment layer involved but before deposition of the next layer	Gravifossum	Nagtegaal, 1965; Van Loon and Wiggers, 1976
	Postsedimentary (early diagenetic)	After burying of the sediment layer involved but before lithification	Vertical burrow	Seilacher, 1953
Postsedimentary (post-early diagenetic)		After lithification	Pressure solution	Bathurst, 1976

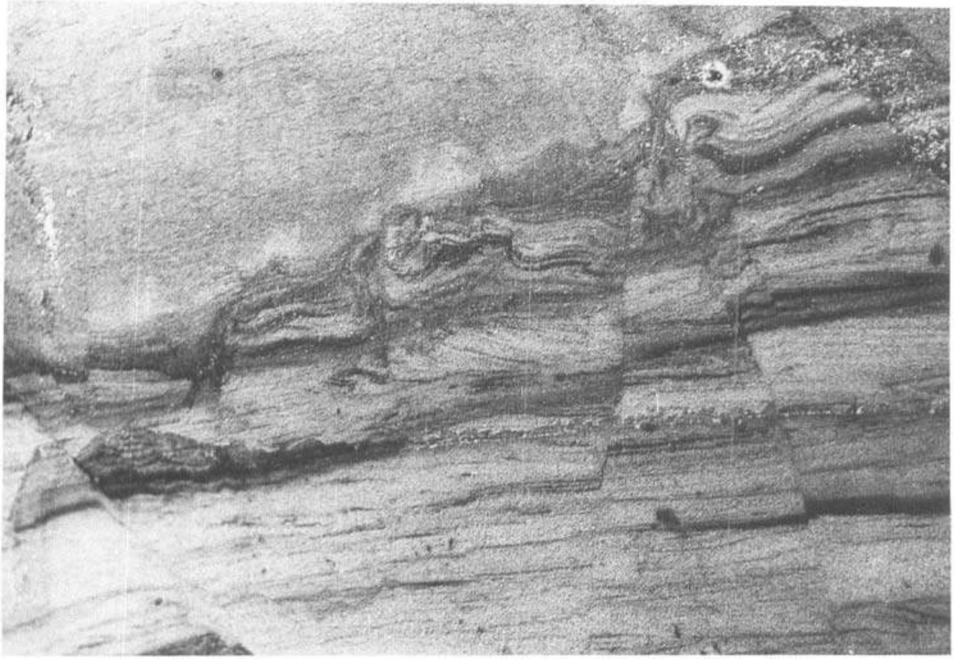

Fig. 3-6. Microscale deformations in the Pleistocene overburden (width of photograph is about 10 cm).

Synsedimentary and metasedimentary deformation structures

Synsedimentary and metasedimentary deformation structures include those that were formed as a result of the sedimentary process itself (the synsedimentary deformations, such as convolutions in the c-unit of turbidites: Fig. 3-7), or due to either physical (e.g., thixotropic) or chemical characteristics (e.g., solubility, possibility to

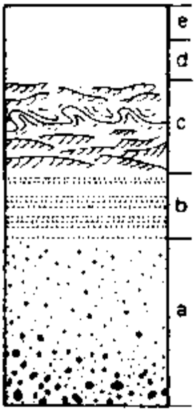

Fig. 3-7. Idealized turbidite sequence (after Bouma, 1962) with convolutions in the c-unit.

TABLE 3-2

General classification scheme of soft-sediment deformation structures according to the nature of the forces and agents involved

Name	Nature	Example[a]
Exogenic structures	Due to processes in the atmosphere, hydrosphere or surficial layers of lithosphere	
a. Fault structure	Due to movement of sediment masses along a plane	Dead-ice structure (Brodzikowski and Van Loon, 1980) (Fig. 3-6)
b. Fold structure	Due to relative movement of sediment particles without losing mutual contacts	Load cast (Brodzikowski and Van Loon, 1980) (Fig. 3-8)
c. Breccia	Due to movement of small masses of unconsolidated material, with loss of mutual contact	Slide breccia (Brodzikowski and Van Loon, 1985) (Fig. 3-6)
Endogenic structure	Due to processes in the interior of the Earth	
a. Fault structure	Due to movement of sediment masses along a plane	Graben plane (Brodzikowski et al., 1987d) (Fig. 3-22)
b. Fold structure	Due to relative movement of sediment particles without losing mutual contacts	Tectonics-related drag folds (Brodzikowski et al., 1987d) (Fig. 3-19)
c. Breccia	Due to movement of small masses of unconsolidated material, with loss of mutual contact	Fault breccia (Fig. 3-17)

[a] Between parentheses: example of an illustration of the pertinent structure.

TABLE 3-3

Size-related aspects of deformation structures in the Bełchatów brown-coal mine

Name	Amplitude	Example	Illustration
Large-scale structure	>10 m	Diapir	Fig. 3-21
Meso-scale structure	1–10 m	Slump	Fig. 3-16
Small-scale structure	1 cm–1 m	Load cast	Fig. 3-11
Micro-scale structure	<1 cm	Kink structure	Fig. 3-6

bind and loose crystal water) of the sediment itself (the metasedimentary deformations, which are also called "penecontemporaneous" or "early-diagenetic sensu stricto" in the literature on soft-sediment deformations; see, among others, Reineck and Singh, 1980 and Van Loon, 1992). Structures of this category are those most commonly exposed in the scarps of the Bełchatów open-cast mine.

TABLE 3-4

Genetic classification of deformational processes (after Van Loon, 1992)

Name	Deformational agent	Examples of structures
Bioturbation [a]	Organisms	Root-induced fissures; burrows
Cryoturbation [a]	Freezing/melting alternation	Dead-ice faults; pingos
Glaciturbation [a]	Moving ice	Glacial folds; ice-push-induced kinks
Thermoturbation [a]	Temperature-induced stress	Heat-induced cracks; cold-induced cracks
Graviturbation [a]	Gravity-induced processes	Slumps; gravifossum
Hydroturbation [a]	Water	Desiccation cracks; wave-induced breccias
Chemoturbation	Chemical reaction(s)	Crystal-growth imprints; solution infilling
Atmoturbation	Weather	Rain-drop imprints; imprints made by wind-blown fragments
Endoturbation [a]	Endogenic activity	Fault breccias; convolutions
Astroturbation	Processes in the universe	Meteorite crater; meteorite imprint

[a] These processes have been recognized with certainty to have played a role in the genesis of deformation structures in the overburden of the Belchatow brown-coal mine.

Many of these structures are due to gravitation: they commonly developed as a result of reversed density gradients (cf. Anketell et al., 1970). Synsedimentary or — more commonly — metasedimentary rearrangement of the density distribution, in order to obtain a more stable condition, sometimes resulted in more or less horizontal changes within a previously unstable succession of layers or laminae (cf. Anketell and Dżułyński, 1968), giving rise to convolutions. A more stable density distribution also could be obtained by the downward movement of relatively "heavy" material, which gave rise to structures such as load casts (Fig. 3-8) and pseudonodules. A third possibility was the upward movement of "light" material, resulting in structures such as diapirs (Fig. 3-9) and clastic dykes. Deformations as a result of rearrangement of density are always particularly frequent in successions that show rapid vertical alternations of fine- and coarse-grained layers, because of the subtle (but nevertheless most effective) difference in specific weight between water-rich (or water-saturated) sand and clay. The size of these structures commonly ranges from a few millimeters up to 2.5 m. Strongly deformed units (Fig. 3-10) may occupy several thousands of square meters (as revealed by the gradual removal of sediment during ongoing exploitation).

Metasedimentary deformations that are not due to an unstable density distribution within the sedimentary succession are also very frequent. They may occur as a result of differential compaction, fluidization (Fig. 3-11), dilatation, desiccation, etc. The amplitude of the deformations (here taken to be determined by the maximum vertical displacement of material belonging to one specific deformation structure) usually does not exceed the thickness of the layer (or set of layers) involved, which

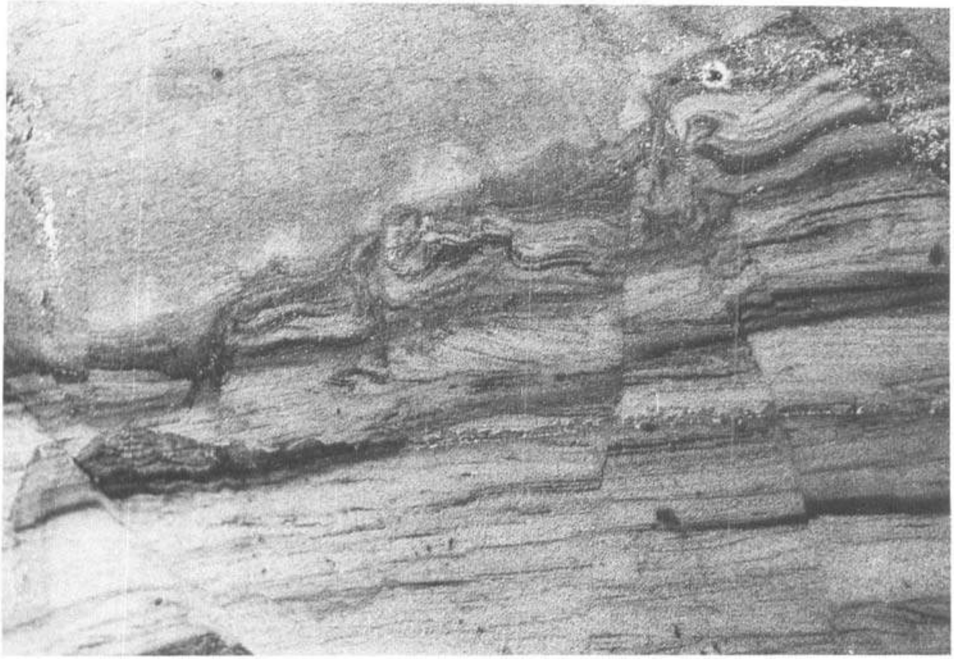

Fig. 3-8. Horizon of fluvial deposits with abundant load casts. The sediments were formed during the Wartanian/Odranian interstadial time.

Fig. 3-9. Example of a diapir as encountered frequently in the overburden of the Bełchatów brown-coal mine.

Fig. 3-10. Horizon of Vistulian fluviolacustrine deposits with several types of early-diagenetic deformations, among others load casts and cryoturbations (including cryogenically deformed load casts). Photograph by A. Haluszczak.

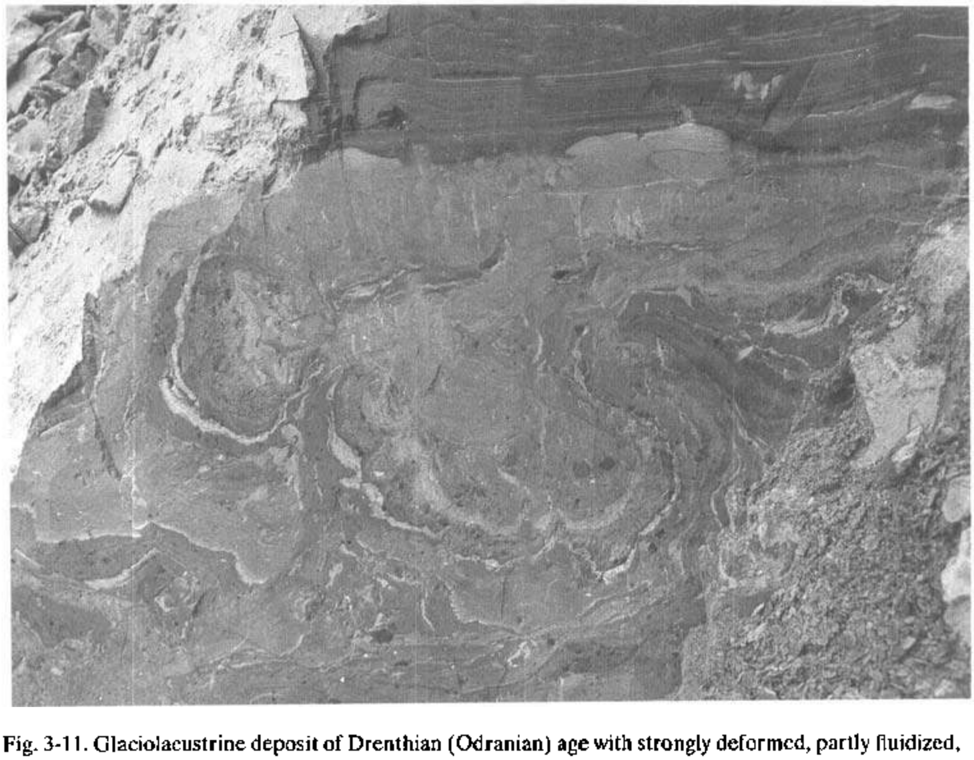

Fig. 3-11. Glaciolacustrine deposit of Drenthian (Odranian) age with strongly deformed, partly fluidized, structures. Photograph by A. Haluszczak.

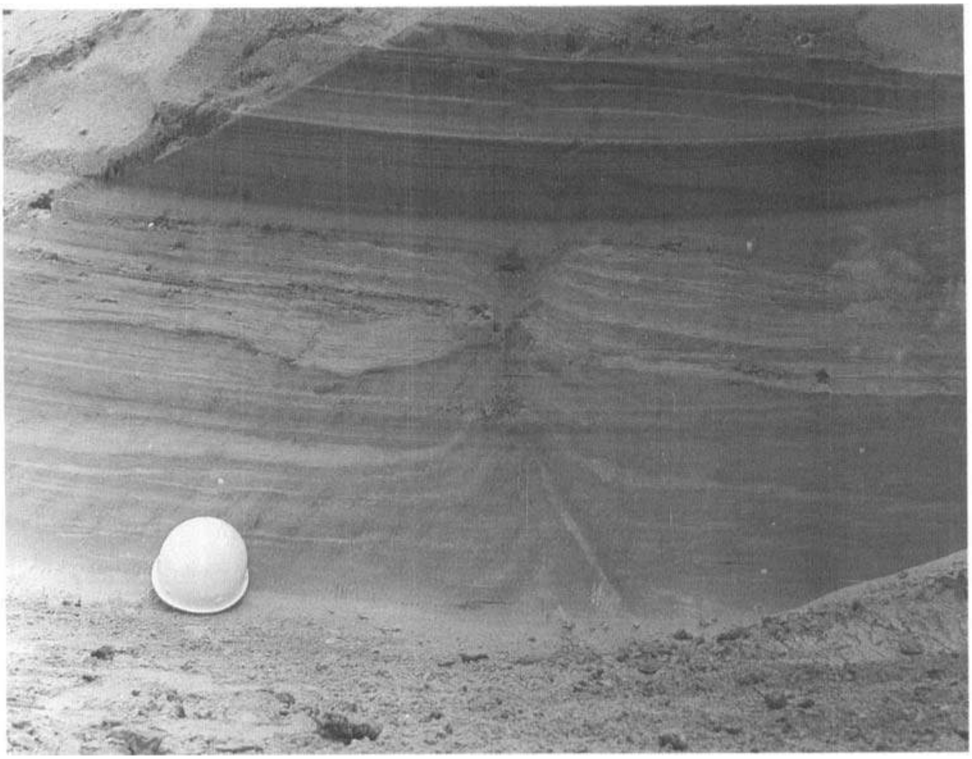

Fig. 3-12. Characteristic water-escape structure in fine-grained Vistulian glaciolacustrine sediments. Photograph by R. Gotowala.

implies that the amplitude is commonly less than 1 m, and most frequently in the millimeter to centimeter range. Flexures and small faults formed during compaction are the most common specimens. Sets of small-scale water-escape structures and related deformations (cf. Liszkowski, 1971) are frequently present in muddy/sandy and muddy/clayey sediments (Fig. 3-12).

The size of the structures in this category with a relatively large amplitude allows to observe them in the scarps of the mine from rather far away. This makes it easy to trace levels with such structures over a fairly large distance (up to several kilometers). Except for one type, however (see the subsection headed "Polygenetic diapirism"), they are small enough not to pose problems for exploitation activities. The microscale and small-scale structures (with sizes in the order of millimeters and centimeters, sometimes also decimeters) cannot be seen from a distance and their lateral extent cannot be determined accurately. It is known from detailed observations, however, that such small-scale structures occur throughout the sediment, although their frequency depends on the stratigraphic unit. As expected, the ratio between the various types of small-scale deformations of this category also depends on the stratigraphic unit (Fig. 3-13). It is obvious that deformations of this size, even though

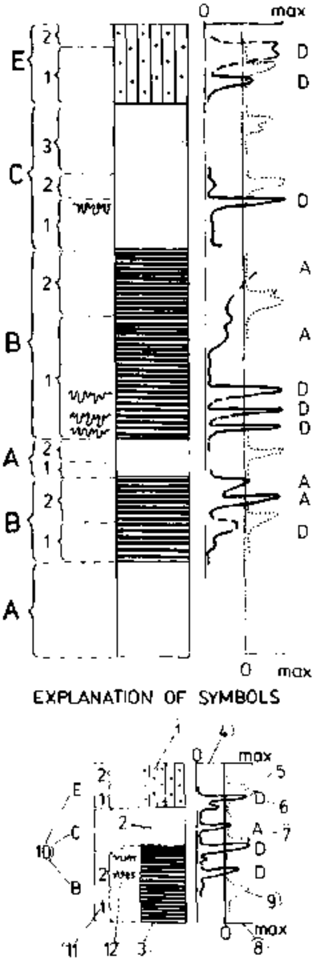

Fig. 3-13. Schematic section of Odranian deposits with deformation horizons that are related to momentary endogenic processes (after Brodzikowski, 1982a). *1* = glacial till; *2* = fluvioglacial deposit; *3* = glaciodeltaic and glaciolacustrine deposits; *4* = relative scale indicating the intensity of endogenic activity; *5* = endogenic activity; *6* = horizon with early-diagenetic (penecontemporaneous) deformations; *7* = sudden change in sedimentary conditions; *8* = relative scale indicating abruptness of facies changes; *9* = facies changes; *10* = sedimentary cycle; *11* = sedimentary subcycle; *12* = large-scale early-diagenetic deformations.

they may occur in large numbers, cannot affect the activity of the big excavators ad other mining equipment.

Cryogenic structures

Cryogenic deformations (Fig. 3-14), which are a (cold) climate-induced type of early-diagenetic deformations, are very common in the Bełchatów area (Goździk, 1980) and usually have amplitudes of less than one meter. Fissure networks, present

Fig. 3-14. Frost fissure in a sandy glaciofluvial succession of the Czyżów Series (middle Elsterian?).

in particular in layers with thicknesses of less than 60 cm, are the most common.

This group includes micro- to small-scale deformations (see Table 3-3) that do not influence the macroscale structure. They are, therefore, not important from a mining or an engineering–geological point of view.

Glaciotectonic structures

Glaciotectonic deformations (formed by forces exerted by a moving ice mass) are present primarily in the upper part of the outcrop. They were formed subglacially, i.e., as a result of ice affecting its substratum. No indications were found in the Bełchatów area for glaciotectonic deformations as a result of ice pushing away the material alongside or in front of the extending ice mass. The glaciotectonic deformations present in the open-cast mine have amplitudes up to 15 m and occur in parallel zones with a horizontal extent in the order of some 300 m (Brodzikowski, 1982b, 1985).

Glaciotectonic forces did not cause significant vertical displacements, so that the deformations are mainly restricted to a few levels (the area underwent several Pleistocene glaciations) in the upper part of the succession (Gotowała and Haluszczak, 1982a). Such deformed horizons most frequently consist of lumps of glacial till, alternating irregularly with lumps of glaciofluvial (sometimes glaciolacustrine) material (Fig. 3-15). The horizontal alternations of material with largely different mechanical characteristics may pose problems for the mining equipment, but the restricted size of the irregularities (commonly not more than 2 m) usually makes these problems of only minor importance. The few larger irregularities (see above) may, however, pose major problems. Moreover, it is known from exposures in the direct neighborhood (gravel pits, etc.) that considerably larger glaciotectonic deformations could be encountered in the future (Klatkowa, 1972, 1980).

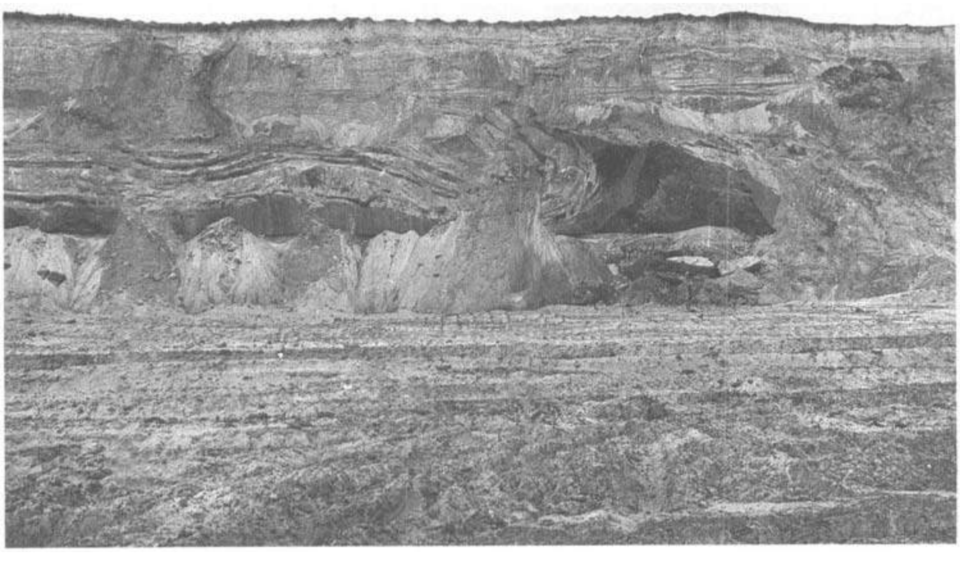

Fig. 3-15. Overturned fold in varved glaciolacustrine deposits of Wartanian age. The folding is a result of glaciotectonic push. Photograph by R. Gotowała.

Bioturbations

Deformations due to the mechanical or physicochemical activity by organisms can be caused by both plants and animals (mainly *Exichnia*, according to the nomenclature by Martinsson, 1970; or *Domichia*, according to the nomenclature by Seilacher, 1953).

The deformations caused by plants (such as irregular deformations caused by the growth of roots) and animals (mainly burrows) represent microscale to small-scale phenomena that have no influence on the general geological structure. The bioturbations may be accompanied by changes in mechanical characteristics (e.g., presence of iron oxides and hydroxides precipitated around roots), but the small size of such mechanical irregularities makes their influence on the workability of the deposits untraceably small.

Deformations resulting from gravity-induced surficial mass movements

Deformation structures resulting from surficial mass movements are seen especially in the northern part of the mining area. They are represented by gravitation-induced mudflow deposits and slumps developed on the surfaces of "fossilized" slopes (Fig. 3-16).

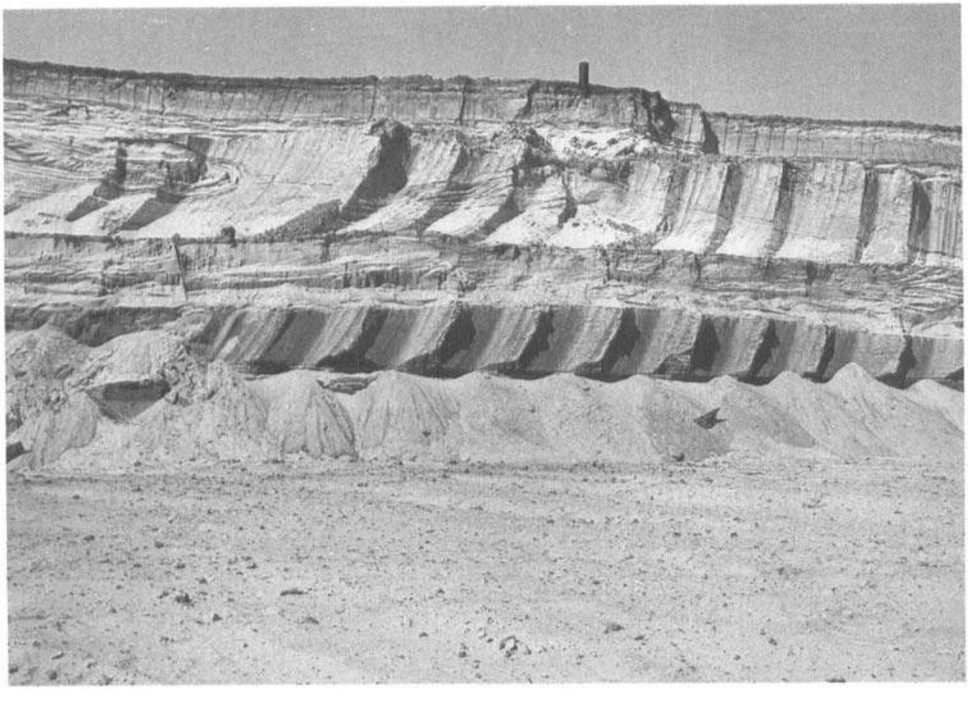

Fig. 3-16. Horizon with Drenthian (Odranian) sediments showing clear indications of gravity-induced mass transport along a fossil slope. Photograph by A. Haluszczak.

Complex disharmonic folds and whole sliding zones have been observed as a cover of slopes that once existed along a Wartanian (late Weichselian) interphase (or interstadial) valley. The folds are developed in fluviolacustrine Vistulian (Weichselian) sands and silts. Their formation was probably triggered by earthquakes or by (tectonically induced) subsidence of the substratum. The amplitude of the structures amounts locally to 10–15 m, so that they are distinctly visible in the mine's scarps. Lithological contrasts, however, are not very strong, because the material involved in the mass transport was not significantly different from the sediments on top of which the masses came to rest (short-distance, intrabasinal transport over a slightly inclined slope). The resulting grain-size differences and other characteristics are consequently so small that they do not pose engineering–geological problems (Kasza et al., 1978, 1980).

Early-diagenetic deformations induced by endogenic activity

The last group of "single origin" deformation structures is a result of the direct effect of endogenic processes (horizontal and vertical displacements within the substratum, and seismic activity). Structures of this type occur frequently, on all scales, particularly in the lower part of the overburden. The upper part was also affected, but with less intensity (Brodzikowski et al., 1980; Brodzikowski and Kasza, 1982).

The structures consist of folds, faults, overthrusts, fault breccias, slickensides along the fault planes, and slide zones, often of a very complicated nature and complex geometry. The amplitude of these deformations ranges from a few millimeters to some 50 m. The larger structures have a strong influence on the overall structural picture (Figs. 3-17, 3-18, 3-19). Block movements related to graben formation have resulted in sudden lateral changes in lithology, thus affecting workability.

Polygenetic deformations

The early-diagenetic structures with the greatest impact on working conditions in the open-cast mine (see the section headed "Conclusions with respect to the mining conditions in the graben"), particularly regarding the removal of the overburden by big excavators, are large-scale diapirs and diapir-like folds. These structures may have amplitudes of several tens of meters (Fig. 3-20), although much smaller ones are present (Fig. 3-21) and, indeed, are much more common. The structures formed as a response to non-uniform pressure exerted by the weight of the overlying sediments (and/or ice during a glacierization), but it is most likely that endogenic forces — now reflected in faults and in earthquake-induced deformation horizons — triggered the process.

The combination of endogenic forces (with varying directions of the largest stress) and "normal" early-diagenetic processes (commonly a vertical orientation of the largest stress) is the reason for applying the term "polygenetic" to these structures. It is probable that glaciotectonism also played a role in the development of these structures, but it is almost impossible to deal with the local consequences of this

Fig. 3-17. Dislocation of unconsolidated glaciolacustrine sediments of the overburden located above a fault zone in the hard-rock substratum of the graben. Photograph by R. Gotowala.

Fig. 3-18. Large-scale folds in glacigenic deposits of Drenthian (Odranian) age. The height of the wall is about 20 m.

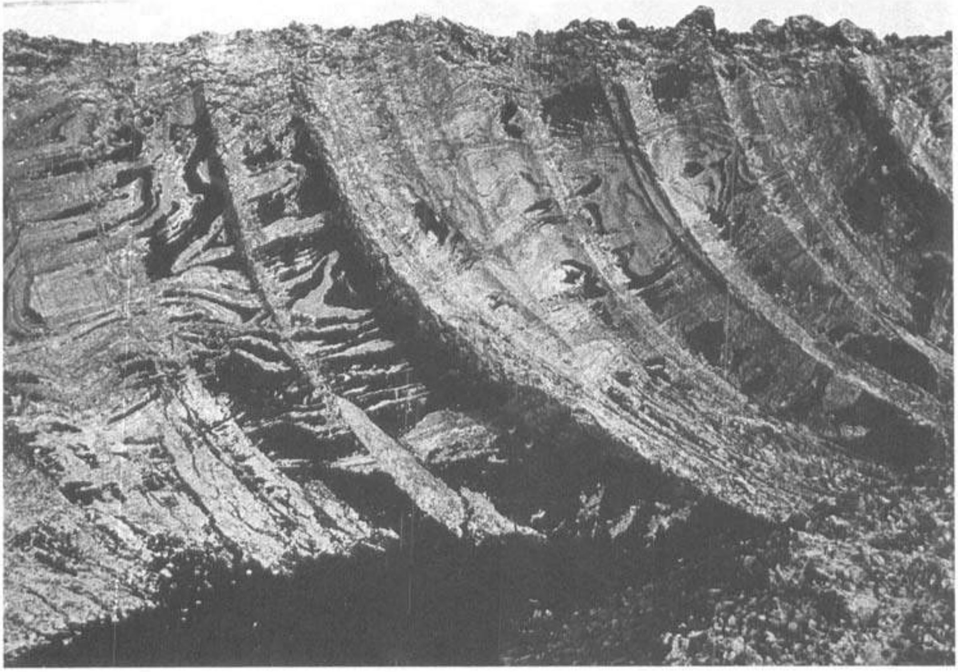

Fig. 3-19. Detail of the interior of a large-scale fold in Drenthian (Odranian) glaciolacustrine deposits. This part of the early-diagenetic structure is characterised by disharmonic folding. Photograph by R. Gotowała.

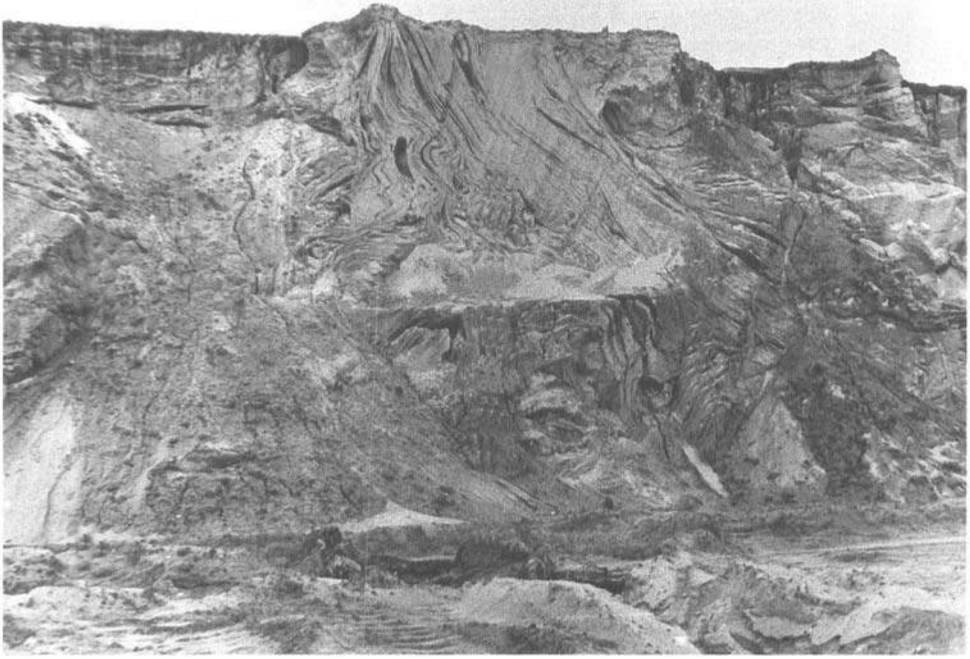

Fig. 3-20. Complex diapir-like fold in glaciolacustrine sediments. The height of the wall is about 20 m.

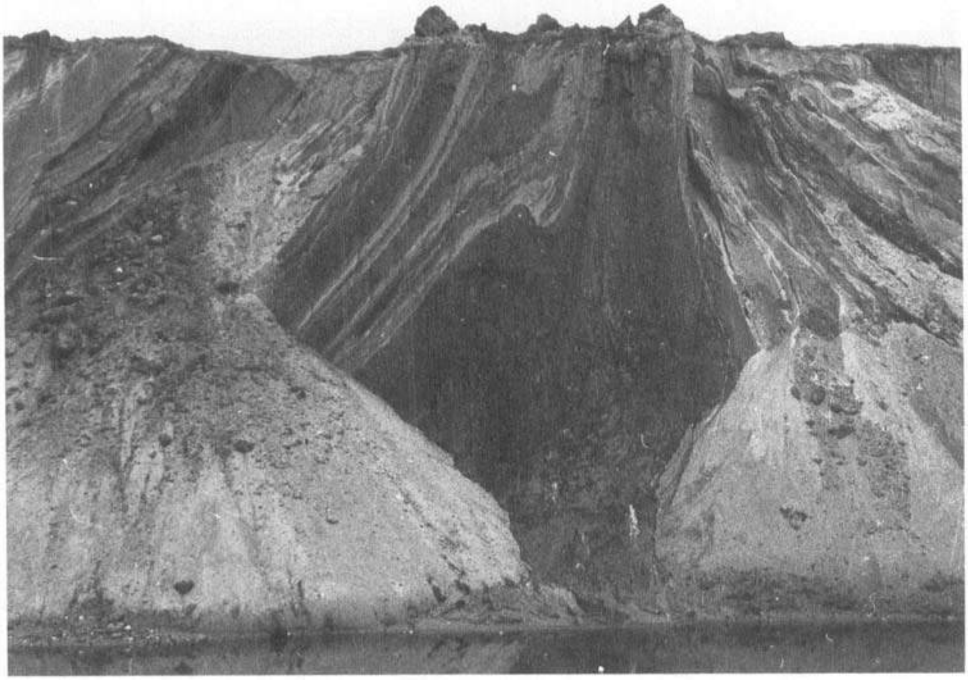

Fig. 3-21. Characteristic part of a 30-m-high diapir-like fold penetrating glacigenic deposits.

factor, if one is predicting the deformation structures to be encountered during a next phase of exploitation. Nevertheless, the polygenetic structures are most important for the effectivity of the procedure for removal of the overburden. The structures, therefore, are discussed in more detail in the subsection "Polygenetic diapirism".

DEVELOPMENT OF THE STRUCTURES INFLUENCING MINING CONDITIONS

Three of the above-mentioned categories of early-diagenetic deformation structures appear to influence mining conditions, mainly through sudden transitions in the horizontal direction of the mechanical properties of the sediment. These three categories of structures result from endogenic forces, glaciotectonism and polygenetic diapirism.

Endogenic activity

Endogenic forces have resulted (and still result) in block-wise subsidence (sometimes upheaval) of the Mesozoic substratum of the graben. A result is the large-scale vertical displacement of the unlithified sediments: both the Tertiary brown-coal and the overburden. The vertical displacements in the substratum become gradually less

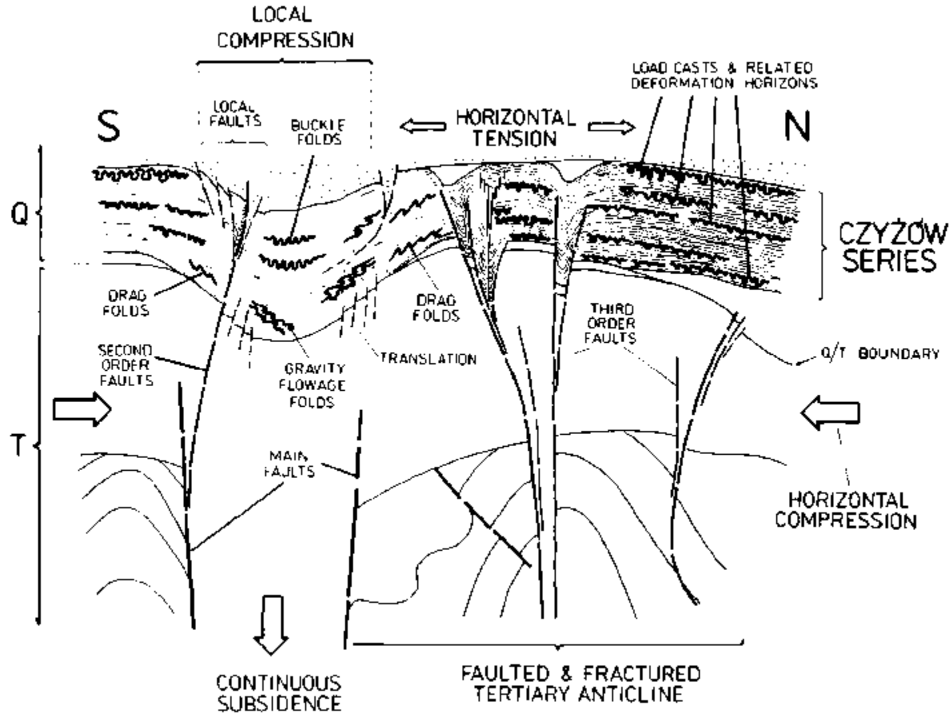

Fig. 3-22. Part of a stratigraphic profile, showing early-diagenetic faults in the Czyżów Series due to endogenic activity and relationships with the structural elements within the Tertiary.

distinct in the brown-coal infilling of the graben and in the overburden. Nevertheless, the tectonic movements are, indeed, clearly reflected in the Tertiary brown-coal and in the overburden, particularly in the form of faults (Fig. 3-22). Vertical displacements may amount to tens of meters, thus strongly affecting the "terrace-bound" workability (especially at sudden horizontal transitions between brown-coal and siliciclastic sediments with strongly cohesive tills as a most problematic type of deposit). The endogenic processes are still active, as shown by the frequent displacements that still take place along fault planes that reach the surface (Gotowała and Pilecki, 1982).

Passing through a fault zone with a considerable change in mechanical properties (especially cohesiveness) may pose severe problems for the equipment involved. As a rule, lithological changes due to processes other than this graben-related faulting tend to give fewer large-scale or less distinct contrasts in the Bełchatów area. Consequently, these truly tectonic early-diagenetic deformations belong to the most troublesome category from a mining point of view.

Glaciotectonism

Preliminary investigations of the graben area, carried out before the start of the first mining activities, gave the impression that the most troublesome type of deformation would be the glaciotectonic structures. Some geologists even suggested that only glaciotectonic structures would have to be taken into account in the Quaternary part of the overburden. This view was abandoned only after it had become clear from the exposures formed during the mining activities that the deformations owing to endogenic activity were the most significant from an engineering–geological point of view, whereas glaciotectonics had only little influence on the overall structure of the Quaternary deposits (Brodzikowski and Kasza, 1982).

The minor role of glaciotectonism is now explained by the more or less continuous subsidence of the sediments in the graben. The advancing ice masses affected the graben sediments less than their equivalents outside, because the graben area formed a topographic depression that yielded relatively little resistance to the continental glaciers. The soft-sediment substratum of the ice in the graben, characterized by ongoing subsidence, was therefore only (relatively) slightly affected by the ice. Thus, large glaciotectonic deformations at the ice/sediment interface were formed only rarely (Brodzikowski, 1985).

This hypothesis is confirmed by all observations made in the mine's scarps: the glaciotectonic deformations described above are concentrated in the upper part of the succession. It cannot be fully excluded, however, that ongoing exploitation will reveal the presence of glaciotectonic structures in the lower part of the overburden also (Gotowała and Hałuszczak, 1982a, b), although recognizing these structures will certainly be very difficult because of the intense endogenic–tectonic deformation of all these deposits.

Polygenetic diapirism

Three types of polygenetic deformation structures that result in some part from diapiric processes are encountered in the Kleszczów Graben.

The first type is represented by bodies of an extremely large size and a complex internal structure that intruded the overlying material. The intrusive bodies consist in most cases of reworked (Tertiary) brown-coal fragments mixed with sand. This mixture was probably formed during the intrusion process when both water-rich types of sediments had already passed the liquid limit (Fig. 3-23). The fluidized material intruded the overlying Quaternary deposits to a very high level: the largest structures of this type show vertical displacements of 50–80 m. The central "stem" of the intrusive bodies commonly has an elliptical shape with a smaller (horizontal) axis of 10–20 m, but much smaller stems (0.5–2 m) have also been encountered. The top part of the structures, which always has an irregular shape (partly due to erosional processes) and is always distinctly flattened, is much larger (up to 50 m in diameter), implying that the structures have a shape that is more or less comparable to that of a mushroom.

The second type, of which only one distinct representative has so far been encountered during exploitation of the brown-coal mine, might be called a "diapir-like fold". This fold was more than 70 m high and comprised Tertiary and Quaternary sediments of different lithologies. The width at the base of the structure was about 300 m, whereas the top part had a diameter of only about 20 m. Detailed field

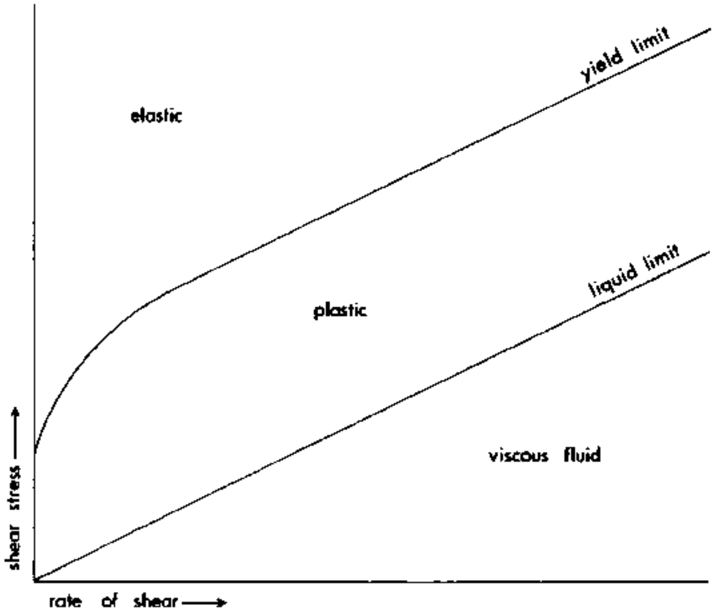

Fig. 3-23. Idealized relation between plastic and viscous fluid flow. (After Dott, 1963; Van Loon, 1970.)

studies revealed that the structure was located on top of a "high" in the substratum, which suggests a genesis induced by endogenic forces. In addition, the position and extension of the structure seemed to indicate a shaping by glaciotectonic pressure. Finally, the interior of the structure showed many irregularities that could be explained satisfactorily only by assuming an internal rearrangement of material in response to an unstable density distribution. The diapir thus constitutes a characteristic example of a polygenetic structure. Although this type of diapir is rare in the mining area (the specimen described may be unique), it had a great impact on the mining process, because the fold structure induced instability of the scarps that it intersected.

The third type consists of folds that underwent fluidization and diapirism in their top parts, after the folds had been formed. The intruded parts consist of coaly/sandy detritus of Tertiary age and of Quaternary fine-grained deposits. The largest structures of this type show signs of slight diapirism in their central parts as well. The genesis of the structures is not yet fully clear, but endogenic activity and diagenetic conditions certainly played a role. It is remarkable that these structures are found only along the south-marginal fault system of the graben. The structures obviously were formed during a number of subsequent stages. They have amplitudes up to 60–70 m.

The Tertiary and Quaternary overburden of the brown-coal area was formed in a period of rapid changes of climate and environmental conditions. Periods of glacierization in particular were characterized by irregular topography, basins of restricted size, rapid fluctuations in water and sediment supply, etc. The consequence was a complex sedimentary pattern with rapid lithofacies transitions, both vertically and horizontally. This provides highly suitable conditions for continued diapirism, because of common vertical pressure gradients, due to the irregular depositional and erosional patterns. Most important for the diapirism was that the graben area has been covered several times by continental glaciers. It is well known that unconsolidated sediments of "suitable" lithology (especially a high content of silt-sized material: Boswell, 1949, 1950, 1952, 1961; Van Loon and Wiggers, 1975; Allen, 1982; Mills, 1983; Van Loon and Brodzikowski, 1987) greatly facilitate the formation of diapirs along the ice margin, where the pressure gradients are largest (e.g., Schwan et al., 1980). This factor may also have been responsible for at least part of the giant diapirs. All diapirs investigated in the Kleszczów Graben were, however, at least partially induced by endogenic forces. This tectonism may also have accelerated the diapiric process.

Diapirs pierce, by definition, through material of different lithology. This explains why a horizontally working excavator meets severe problems due to this diapirism: soft brown-coal deposits may suddenly be followed by overconsolidated subglacial tills, etc. It is, therefore, most important that the preferential locations of large diapirs could be inventoried, thus providing a tool for the prediction of the locations where excavators might be confronted with these structures. The predictive value of the models established for the purpose has proven to be reasonably accurate, but new data obtained during ongoing exploitation of the brown-coal mine allow the model to be further refined continuously.

CONCLUSIONS WITH RESPECT TO THE MINING CONDITIONS IN THE GRABEN

Optimization of open-cast mining, including removal of the overburden, requires good planning that should be based on, among others, reliable prediction of the working conditions. Investigations made in this framework, in connection with open-cast mining of unconsolidated sediments, tend to focus on the characteristics of the sediments with respect to:

(1) their workability by mining equipment (excavators, conveyor belts, etc.);

(2) the dewatering of the material; and

(3) the stability of the mine's slopes.

Such analyses are traditionally based on lithology, the vertical succession of layers with different lithology, and the physical mechanical parameters of all lithological units. The study carried out in the Bełchatów open-cast mine confirms, however, as did similar studies carried out by the authors in other brown-coal outcrops (e.g., Brodzikowski and Van Loon, 1983), that the units' relative positions and early-diagenetic deformation, rather than the mechanical features of the units, play the most important role with respect to mining conditions (see also Brodzikowski and Kasza, 1982; Kasza, 1982, 1987a, b).

It was found, for instance, that dewatering problems in the brown-coal levels are very frequently due to mesoscale structural traps. Large-scale structures do not commonly form effective traps because their surface area is so large that there are sufficient pathways for water to escape. On the other hand, small-scale structures do not contain enough water to pose real dewatering problems. It was also found that loss of scarp stability in the form of slumps occurs mainly where the unit involved dips towards the center of the mine. Slumping masses need not only a good detachment plane (which is commonly provided by clay-rich brown-coal layers), but also an inclination (which is commonly present in the Bełchatów mining area as a result of previous deformational processes), and an "empty space" where the sediment masses can move to. Such empty spaces, not present earlier, are now provided as a result of the ongoing exploitation.

Removal of the overburden poses even more complex problems than does excavation of the brown-coal itself. Dewatering problems and slumps occur under the same conditions as in the brown-coal but additional problems arise. These are most frequently related to horizontal changes in strength of the material, owing to rapid lateral and vertical facies changes within the Quaternary glacigenic units, and to the presence of large deformation structures (mainly of truly tectonic origin, but also due to polygenetic diapirism and glaciotectonism).

For example, locations with a high fault frequency generally show a distinct increase of strength-parameter values, possibly because the forces finally resulting in fault structures did exert pressures that led to increased compaction and/or consolidation (expulsion of pore water, decreasing porosity, better orientated particles, etc.). This implies that such zones of geological weakness are, in contrast to what might be expected, more difficult to work than zones which have not been affected by fault movements. Moreover, faults commonly form part of structural traps which may contain water masses that may be set free suddenly if affected by an excavator. Fault planes, if developed in a "suitable" direction, may also favor the occurrence of slumps by providing detachment planes.

Glaciotectonic deformations and structures resulting from surficial mass movements are generally smaller and consequently less important from a mining point of view, although these types of early-diagenetic deformation structures tend to be much more complex. These complex structures, however, are usually small enough to have no, or almost no, effect on the scale of the mining equipment. Obviously, still smaller early-diagenetic deformation structures, such as cryogenic structures and bioturbations, have no influence at all on the excavation process.

Thus, it is obvious that the detailed analysis of the early-diagenetic deformation structures in the overburden increased the insight into the rapid lateral lithological changes that occur. The reconstruction of the genesis of the various types of structures makes it possible to predict the locations and the nature of such lateral lithological changes with reasonable accuracy. This is done by establishing the levels and zones where such structures appear to be concentrated. Economic and safe removal of the overburden is, thus, greatly enhanced.

ACKNOWLEDGEMENTS

The field studies were carried out in close cooperation with Docent Dr. L. Kasza (University of Wrocław) who initiated the investigation of the major mining problems. Discussions with him were most fruitful. Thanks are due to our colleagues Roman Gotowała, M.Sc., and Andrzej Hałuszczak (both from the University of Wrocław) for discussions and permission to reproduce some of their photographs.

The project was supported by the Bełchatów open-cast mine and by the Geological Survey (Wrocław Section). Many thanks are also due to the Director of the Bełchatów open-cast mine, Stanisław Drozdowski.

Dr. M.-L. Schönbaum-Desbarats (SBS Science Consultancy, Venhorst, The Netherlands) kindly corrected the English of the manuscript.

REFERENCES

Allen, J.R.L., 1982. *Sedimentary Structures, Their Character and Physical Basis, Vol. 2. Developments in Sedimentology 30B.* Elsevier, Amsterdam, 663 pp.

Anketell, J.M. and Dżułyński, S., 1968. Patterns of density-controlled convolutions involving statistically homogeneous and heterogeneous layers. *Rocz. Polsk. Towarz. Geol.*, 38: 401–409.

Anketell, J.M., Cegła, J. and Dżułyński, S., 1970. On the deformational structures in systems with reversed density gradients. *Rocz. Polsk. Towarz. Geol.*, 40: 3–30.

Baraniecka, M.D., 1971. Dorzecze Widawki na tle obszaru marginalnego stadiału Mazowiecko-Podlaskiego (Warty) w Polsce (with English summary: The Widawka drainage basin as a part of the marginal area of the Masovian–Podlasie (Warta) stadial in Poland). *Bull. Inst. Geol. Warsawa*, 254: 11–36.

Bathurst, R.G.C., 1976. *Carbonate Sediments and Their Diagenesis.* Elsevier, Amsterdam, 2nd ed., 658 pp.

Biernat, S., 1968. Problemy tektoniki i morfologii stropu mezozoiku między Bełchatowem a Działoszynem (with English summary: Tectonical and morphological problems of the Mesozoic top between Bełchatów and Działoszyn). *Kwart. Geol.*, 12: 296–307.

Boswell, P.H.G., 1949. A preliminary examination of the thixotropy of some sedimentary rocks. *Q.J. Geol. Soc. London*, 104: 499–526.

Boswell, P.H.G., 1950. Thixotropic and allied phenomena in geological deposits. *Proc. Liverpool Geol. Soc.*, 20: 86–105.

Boswell, P.H.G., 1952. The determination of the thixotropic limits of sediments. *Liverpool Manchester Geol. J.*, 1: 1–22.

Boswell, P.H.G., 1961. *Muddy Sediments.* W. Heffer and Sons, Cambridge, 140 pp.

Bouma, A.H., 1962. *Sedimentology of Some Flysch Deposits.* Elsevier, Amsterdam, 168 pp.

Brodzikowski, K., 1982a. Problemy wykształcenia modelu sedymentacyjnego okresów glacjalnych w rowie tektonicznym (Problems with respect to the development of a sedimentation model for the tectonic graben). In: M.D. Baraniecka, K. Brodzikowski and L. Kasza (Editors), *Czwartorzęd Rejonu Bełchatowa. Przew. I Sympozjum: Główne Kierunki i Wstępne Wyniki Badań w Zakresie Stratygrafii i Struktur Osadów. Wyd. Geol.*, Wrocław/Warszawa, pp. 66–103.

Brodzikowski, K., 1982b. Przejawy subglacitektonizmu okresu warciańskiego w przekroju Chojny (Subglacitectonic features of Wartanian age in the Chojny section). In: M.D. Baraniecka, K. Brodzikowski and L. Kasza (Editors), *Czwartorzęd Rejonu Bełchatowa. Przew. I Sympozjum: Główne Kierunki i Wstępne Wyniki Badań w Zakresie Stratygrafii i Struktur Osadów. Wyd. Geol.*, Wrocław/Warszawa, pp. 212–223.

Brodzikowski, K., 1983. Metasedimentary deformational processes and structures induced by endogene tectonic agents. *Abstr. 4th I.A.S. European Regional Meet.*, Split, pp. 34–35.

Brodzikowski, K., 1985. Glacial deformation environment in the subsiding zone with special references to the Kleszczów tectonic graben. *Quat. Stud. Poland*, 6: 5–22.

Brodzikowski, K. and Gotowała, R., 1980. Struktury deformacyjne osadów czwartorzędowych (Deformational structures in the Quaternary deposits). *Przew. 52 Zjazdu Pol. Tow. Geol.*, Bełchatów, pp. 309–314.

Brodzikowski, K. and Kasza, L., 1982. Geneza struktur deformacyjnych osadów czwartorzędowych w rowie Kleszczowa i ich znaczenie w prognozie geologiczno-górniczej (Genesis of the Quaternary deformation structures and their role in geological-mining forecasting). In: M.D. Baraniecka, K. Brodzikowski and L. Kasza (Editors), *Czwartorzęd Rejonu Bełchatowa. Przew. I Sympozjum: Główne Kierunki i Wstępne Wyniki Badań w Zakresie Stratygrafii i Struktur Osadów. Wyd. Geol.*, Wrocław/Warszawa, pp. 204–211.

Brodzikowski, K. and Van Loon, A.J., 1980. Sedimentary deformations in Saalian glaciolimnic deposits near Włostów (Żary area, western Poland). *Geol. Mijnbouw*, 59: 251–272.

Brodzikowski, K. and Van Loon, A.J., 1983. Sedimentology and deformational history of unconsolidated Quaternary sediments in the Jaroszów Zone (Sudetic Foreland). *Geol. Sudetica*, 18: 121–196.

Brodzikowski, K. and Van Loon, A.J., 1985. Penecontemporaneous non-tectonic brecciation of unconsolidated silts and muds. In: R. Hesse (Editor), *Sedimentology of Siltstone and Mudstone. Sediment. Geol.*, 41: 269–282.

Brodzikowski, K. and Van Loon, A.J., 1987. A systematic classification of glacial and periglacial environments, facies and deposits. *Earth-Sci. Rev.*, 24: 297–381.

Brodzikowski, K., Gotowała, R. and Hałuszczak, A., 1980. Kompleksy osadowe odsłoniętej części nadkładu czwartorzędowego (Depositional complexes of the Quaternary overburden). *Przew. 52 Zjazdu Pol. Tow. Geol.*, Bełchatów, pp. 305–308.

Brodzikowski, K., Gotowała, R., Hałuszczak, A., Krzyszkowski, D. and Van Loon, A.J., 1987a. Soft-sediment deformations from glaciodeltaic, glaciolacustrine and fluviolacustrine sediments in the Kleszczów Graben (central Poland). In: M.E. Jones and R.M.F. Preston (Editors): Deformation of sediments and sedimentary rocks. *Geol. Soc. London, Spec. Publ.*, 29: 255–267.

Brodzikowski, K., Gotowała, R., Kasza, L. and Van Loon, A.J., 1987b. The Kleszczów Graben (central Poland): reconstruction of the deformational history and inventory of the resulting soft-sediment deformational structures. In: M.E. Jones and R.M.F. Preston (Editors): *Deformation of Sediments and Sedimentary Rocks. Geol. Soc. London, Spec. Publ.*, 29: 241–254.

Brodzikowski, K., Hałuszczak, A., Krzyszkowski, D. and Van Loon, A.J., 1987c. Genesis and diagnostic value of large-scale gravity-induced penecontemporaneous deformation horizons in Quaternary sediments of the Kleszczów Graben (central Poland). In: M.E. Jones and R.M.F. Preston (Editors), *Deformation of Sediments and Sedimentary Rocks. Geol. Soc. London, Spec. Publ.*, 29: 287–298.

Brodzikowski, K., Krzyszkowski, D. and Van Loon, A.J., 1987d. Endogenic processes as a cause of penecontemporaneous soft-sediment deformations in the fluviolacustrine Czyżów Series (Kleszczów Graben, central Poland). In: M.E. Jones and R.M.F. Preston, R.M.F. (Editors), *Deformation of Sediments and Sedimentary Rocks. Geol. Soc. London, Spec. Publ.*, 29: 269–278.

Ciuk, E. and Piwocki, M., 1980. Geologia trzeciorzędu w rowie Kleszczowa i jego otoczeniu (Tertiary geology of the Kleszczów Graben and its surroundings). *Przew. 52 Zjazdu Pol. Tow. Geol.*, Bełchatów, pp. 56–70.

Dott, R.H., 1963. Dynamics of subaqueous gravity depositional processes. *Am. Assoc. Pet. Geol. Bull.*, 47: 104–128.

Gotowała, R., 1980. Tektonika i wykształcenie strukturalne czwartorzędu w rejonach Piaski i Buczyna-Chojny (Tectonics and structural development of the Quaternary in the Piaski and Buczyna-Chojny zones). In: M.D. Baraniecka, K. Brodzikowski and L. Kasza (Editors), *Czwartorzęd Rejonu Bełchatowa. Przew. I Sympozjum: Główne Kierunki i Wstępne Wyniki Badań w Zakresie Stratygrafii i Struktur Osadów. Wyd. Geol.*, Wrocław/Warszawa, pp. 41–65.

Gotowała, R. and Hałuszczak, A., 1982a. Rozwoj strukturalny zaburzeń w poziomie górnych iłów warwowych (Development of deformation structures within the upper varved clays). In: M.D. Baraniecka, K. Brodzikowski and L. Kasza (Editors), *Czwartorzęd Rejonu Bełchatowa. Przew. I Sympozjum: Główne Kierunki i Wstępne Wyniki Badań w Zakresie Stratygrafii i Struktur Osadów. Wyd. Geol.*, Wroctław/Warszawa, pp. 199–203.

Gotowała, R. and Hałuszczak, A., 1982b. Struktury glacitektoniczne rejonu "Piaski" (Glacitectonic structures in the Piaski zone). In: M.D. Baraniecka, K. Brodzikowski and L. Kasza (Editors), *Czwartorzęd Rejonu Bełchatowa. Przew. I Sympozjum: Główne Kierunki i Wstępne Wyniki Badań w Zakresie Stratygrafii i Struktur Osadów. Wyd. Geol.*, Wrocław/Warszawa: 224–228.

Gotowała, R. and Pilecki, K., 1982. Geologiczno gornicze uwarunkowanie procesów odkształceń górotworu w rejonach Piaski i Buczyna–Choiny (Geological and mining conditions due to strain in the overburden in the Piaski and Buczyna–Chojny zones). In: M.D. Baraniecka, K. Brodzikowski and L. Kasza (Editors), *Czwartorzęd Rejonu Bełchatowa. Przew. I Sympozjum: Główne Kierunki i Wstępne Wyniki Badań w Zakresie Stratygrafii i Struktur Osadów. Wyd. Geol.*, Wrocław/Warszawa, pp. 234–242.

Goździk, J. 1980 Osady i struktury peryglacjalne z plejstocenu okolic Bełchatowa (Pleistocene periglacial sediments and structures in the surroundings of Bełchatów). *Przew. 52 Zjazdu Pol. Tow. Geol.*, Bełchatów, pp. 322–325.

Kasza, L., 1982. Znaczenie podstawowych badań czwartorzędu dla rozpoznania środowiska geologiczno-górnicznego (The role of routine studies of the Quaternary in determining the characteristics of the mining-geological environment). In: M.D. Baraniecka, K. Brodzikowski and L. Kasza (Editors), *Czwartorzęd Rejonu Bełchatowa. Przew. I Sympozjum: Główne Kierunki i Wstępne Wyniki Badań w Zakresie Stratygrafii i Struktur Osadów. Wyd. Geol.*, Wrocław/Warszawa, pp. 104–118.

Kasza, L., 1987a. Przyklady rozwoju procesów geologiczno–inzynierskich w strefie zbocza pólnocnego (Examples of geological–engineering processes in the zone of the northern slope). In: M.D. Baraniecka, K. Brodzikowski and L. Kasza (Editors), *Czwartorzęd Rejonu Bełchatowa. Przew. II Sympozjum. Wyd. Geol.*, Wrocław/Warszawa, pp. 213–214.

Kasza, L., 1987b. Problematyka badań aplikacyjnych z zakresu geologii czwartorzędu dla potrzeb KWB Bełchatów (Applied studies of Quaternary geology for the Bełchatów mine). In: M.D. Baraniecka, K. Brodzikowski and L. Kasza (Editors), *Czwartorzęd Rejonu Bełchatowa, Przew. II Sympozjum, Wyd. Geol.*, Wrocław/Warszawa, pp. 81–86.

Kasza, L., Gotowała, R., Hałuszczak, A. and Olszewski, B., 1978. Wpływ określonych powierzchni strukturalnych na stateczność górotworu i charakter procesów osuwiskowych na czynnych kopalniach odkrywkowych (The influence of structural surfaces on the stability of the overburden, and characteristics of slumping processes in open-cast mines). *Arch. Zakładu Geologii Stosowanej, Inst. Nauk Geol., Uniw. Wrocławskiego*, 35 pp.

Kasza, L., Olszewski, A.N., Lorenc, T. and Olszewski, B., 1980. Problemy geologii inzynierskiej w rejonie kopalni Bełchatów (Geological–engineering problems in the area of the Bełchatów mine). *Przew. 52 Zjazdu Pol. Tow. Geol.*, Bełchatów, pp. 344–363.

Klatkowa, H., 1972. Paleogeografia Wyżyny Łodzkiej i obszarów sasiednich podczas zlodowacenia warciańskiego (Avec résumé: Paléogéographie du Plateau de Łódź et du terrain avoisinant pendant la glaciation de la Warta). *Acta Geogr. Lodziensa*, 28: 220 pp.

Klatkowa, H., 1980. Boryszów-pagórki szczelinowe strefy brzeżnej Lądolodu Warciańskiego (The Boryszów Hills, formed as infillings of marginal crevasses of the Warta ice sheet). *Przew. 52 Zjazdu Pol. Tow. Geol.*, Bełchatów, pp. 269–273.

Kossowski, L., 1974. Budowa geologiczna złoża węgla brunatnego Bełchatów ze szczególnym uwzględnieniem tektoniki podłoża (with English summary: The geological structure of Bełchatów brown coal deposit considering the tectonics of the underlayer). *Górn. Odkrywk.*, 10/11: 336–344.

Liszkowski, J., 1971. Filtracyjne deformacje utworów lessowych (with English summary: Filtrational deformations of loess sediments). *Bull. Inst. Geol.*, 13: 87–132.

Martinsson, A., 1970. Toponomy of trace fossils. In: T.P. Crimes and J.C. Harper (Editors): *Trace Fossils*. Seel House, Liverpool, pp. 323–330.

Mills, P.C., 1983. Genesis and diagnostic value of soft-sediment deformation structures — a review. *Sediment. Geol.*, 35: 83–104.

Nagtegaal, P.J.C., 1965. An approximation to the genetic classification of non-organic sedimentary structures. *Geol. Mijnbouw*, 44: 347–352.

Pożaryski, W., 1971. Tektonika elewacji radomskowskiej (with English summary: Tectonics of Radomsko elevation). *Ann. Geol. Soc. Poland*, 41 (1): 169–179.

Pożaryski, W. and Brochwicz-Lewiński, W., 1978. On the Polish Trough. In: A.J. van Loon (Editor), *Key-notes of the MEGS-II, Amsterdam. Geol. Mijnbouw*, 57: 545–558.

Reineck, H.-E. and Singh, I.B., 1980. *Depositional Sedimentary Environments*. Springer-Verlag, Berlin, 2nd ed., 549 pp.

Schwan, J., Van Loon, A.J., Steenbeek, R. and Van der Gaauw, P., 1980. Intraformational clay diapirism and extrusion in Weichselian sediments at Ormehøj (Funen, Denmark). *Geol. Mijnbouw*, 59: 241–250.

Seilacher, A., 1953. Studien zur Palichnologie. I. Ueber die Methoden der Palichnologie. *Neues Jahrb. Geol. Paläontol., Abh.*, 96: 421–452.

Van Loon, A.J., 1970. Grading of matrix and pebble characteristics in syntectonic pebbly mudstones and associated conglomerates, with examples from the Carboniferous of northern Spain. *Geol. Mijnbouw*, 49: 41–56.

Van Loon, A.J., 1978. Sedimentaire structuren. In: *Grote Spectrum Encyclopedie*. Spectrum, Utrecht, 16: 472–475.

Van Loon, A.J., 1992. The recognition of soft-sediment deformations as early-diagenetic features — a literature review. In: K.H. Wolf and G.V. Chilingarian (Editors), *Diagenesis III. Developments in Sedimentology, Vol 47*. Elsevier, Amsterdam, pp. 135–189.

Van Loon, A.J. and Brodzikowski, K., 1987. Problems and progress in the research on soft-sediment deformations. *Sediment. Geol.*, 50: 167–193.

Van Loon, A.J. and Wiggers, A.J., 1975. Holocene lagoonal silts (formerly called "sloef" from the Zuiderzee. *Sediment. Geol.*, 13: 47–55.

Van Loon, A.J. and Wiggers, A.J., 1976. Metasedimentary "graben" and associated structures in the lagoonal Almere Member (Groningen Formation, The Netherlands). *Sediment. Geol.*, 16: 237–254.

This Page Intentionally Left Blank

Diagenesis, IV. Developments in Sedimentology 51
edited by K.H. Wolf and G.V. Chilingarian
© 1994 Elsevier Science B.V., Amsterdam. All rights reserved.

Chapter 4

DEVELOPMENT OF DIAGENETIC DIFFERENTIATED STRUCTURE THROUGH REACTION–TRANSPORT FEEDBACK

P. ORTOLEVA

INTRODUCTION: SELF-ORGANIZATION AND REACTION–TRANSPORT FEEDBACK

The predominant view of repetitive mineralogic patterns in sedimentary rocks, such as limestone/marl alternations, is that they are depositional in origin. Researchers as far back as Liesegang (1913) have suggested, however, that banded or other patterns can result from the interplay of mineral reactions and solute transport. In this chapter it is suggested that such phenomena are widespread during diagenesis and that they can appear at a range of length scales (from microns to kilometers) and via a wider variety of mechanisms than was heretofore recognized. Furthermore, such phenomena underlie key processes that are of fundamental and practical importance, such as the preservation or destruction of porosity and permeability, the migration and trapping of petroleum, and the distribution and properties of ore bodies.

Recent advances in our understanding of the role of fluctuation and instability in the development of organized repetitive compositional patterns in reaction–transport systems (Nicolis and Prigogine, 1977) have greatly aided in the modeling of repetitive mineral patterns in geological systems, which may develop in the absence of initial repetitive structure (such as sedimentary bedding) (Ortoleva et al., 1987a, 1990; Ortoleva, 1993). Inasmuch as such patterns can organize themselves from an initially undifferentiated or weakly differentiated medium, and because they involve a role for grain growth and dissolution reactions, it is suggested that they are examples of "geochemical self-organization" and they are termed "diagenetic differentiated structures" in the context of diagenesis as follows.

Self-organization in geochemical or other systems proceeds via the amplification of omnipresent non-uniformity. An example of non-uniformity of interest here can be bedding or other variations in mineralogy or texture introduced during deposition or prior to lithification. General conditions necessary for these effects to be manifested are discussed in the concluding section. Future chapters will be dedicated to the development of quantitative mathematical reaction–transport models. The author first reviews some of the amplification mechanisms, and qualitatively describes their consequences and suggests situations in which they may lead to important diagenetic phenomena. The discussion starts with the smallest scale patterning involving intracrystalline repetitive zoning variations in solid solutions and ends with the patterns of basin-scale pressure compartmentation.

OSCILLATORY INTRACRYSTAL ZONING

Calcite grown from aqueous solution under diagenetic conditions may incorporate impurities in a zoning pattern consisting of concentric alternations of impurity content. Such oscillatory zoning in the case of Mn impurity has been demonstrated in the laboratory by Reeder et al. (1990) to involve a role for diffusion in the aqueous medium from which the crystals grow. Whereas a mechanism for oscillatory zoning is still being investigated, the view of the author is as follows (Ortoleva, 1990).

Surface-attachment kinetic mediated growth from aqueous solution

The growth of solid solution crystals involving complex endmember units may proceed via an attachment limited process involving the construction of endmember units at the crystal surface. To illustrate how attachment limited kinetics can allow for the creation of crystals with oscillatory compositional zoning, one can consider the growth of a binary crystal composed of A and B endmember units from an aqueous solution involving solutes X and Y such that X ↔ A and Y ↔ B. On considering the "autocatalytic" case where the rate of creation of A units increases with f, the fraction of A units at the surface, a cyclic growth can occur as shown in Fig. 4-1. Suppose the crystal starts with an A-rich nucleus. Then the volume fraction f of A units is large at the surface. Because the rate coefficient for the A production process X → A increases with f, A-rich growth can persist even after the concentration of X in the growth medium near the crystal rim is significantly depleted in X. As Y is not being consumed rapidly during this phase, it tends to build up near the crystal surface. Ultimately X can become so depleted that B growth tends to dominate with the resulting drop in f. Then X can build up in the growth medium near the crystal surface until A-rich growth again commences and A-autocatalysis can again take

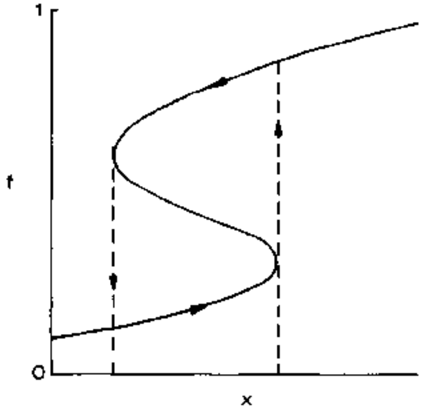

Fig. 4-1. Folded nonequilibrium fractionation curve showing mole fraction f of one endmember of a binary solid solution as a function of the concentration of a pore fluid, x, at the grain–melt interface, from which that endmember is constructed. The indicated cycle suggests the possibility of periodic zoning when the non-equilibrium fractionation curve is multiple-valued.

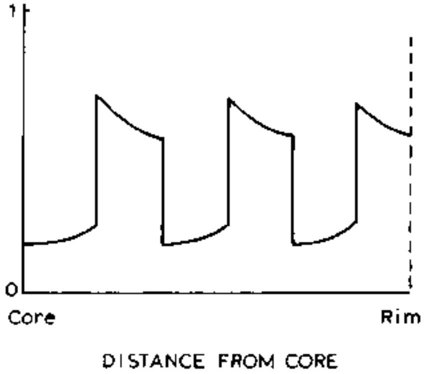

Fig. 4-2. Profile of periodic zoning that would result from the cycle indicated in Fig. 4-1.

place. This process would produce a periodic zoning from crystal core to rim, with a profile indicated in Fig. 4-2.

The above oscillatory scenario requires the essential A-autocatalytic feedback coupled to diffusion in the growth medium. Therefore, stirring the fluid from which the crystal is growing can repress oscillation. Also, growth must be sufficiently rapid, i.e., the system must be sufficiently far from equilibrium; otherwise equilibrium fractionation between the growth medium and the crystal would be obtained. Under near-equilibrium conditions, gradients cannot build up in the growth medium and hence oscillation is prevented.

Unstable solid–solid replacement fronts

A second mechanism for the development of oscillatory zoning may operate when a higher free energy phase is replaced via a transition front into one of lower free energy. If the lower free energy phase is less accepting of an impurity than the higher free energy one, the impurity will tend to accumulate at the interface. Thus, impurity may reach such high levels that it is forced into the lower free energy phase, so distorting the latter that it accepts the buildup of impurity precipitously, depleting the interface of it and switching the lower free-energy phase back into a more pure growth mode. Consequently, the impurity could become incorporated in a series of localized pulses similar to that in Fig. 4-2, but the maxima would be narrow. In a sense this mechanism is based on an autocatalytic rate of impurity incorporation.

In order for the lower free energy phase to keep growing, overcoming the lattice strains due to high impurity content, it is clear that the driving force for reaction (the free energy difference between the two phases) must be sufficiently large. Thus, this form of oscillatory zoning also can only be generated sufficiently far from equilibrium.

PATTERNING THROUGH NUCLEATION AND RIPENING PROCESSES

Liesegang banding: Ostwald–Prager theory

Banding arising from the interdiffusion of coprecipitates was suggested by Liesegang (1913) as a mechanism for the generation of certain types of banded mineralization patterns. The Ostwald (1925)–Prager (1956) model of Liesegang banding has been discussed extensively in the chemical and geologic literature. The O-P model is based on a repetitive cycle of supersaturation, nucleation and depletion. It is perhaps most easily understood in terms of a flow problem analogous to the situation of a redox front as in Fig. 4-3, involving aqueous species X and Y and

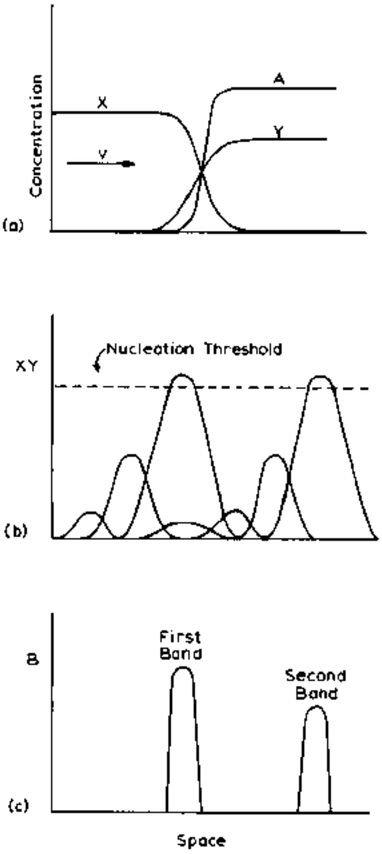

Fig. 4-3. Ostwald supersaturation–nucleation–depletion cycle for a system under imposed flow from the left. (a) The X-bearing fluid imposed from the left reacts with mineral A to form aqueous species Y, producing the A dissolution front that propagates to the right at a speed much lower than the imposed fluid flow velocity *v*. (b) Evolution of the profile of the XY concentration product. When XY exceeds the nucleation threshold, a first B precipitate band is formed (shown in c). After precipitation takes place, the system becomes locally depleted in X and Y; with subsequent buildup of XY downstream, a second B-band forms when the nucleation threshold is again exceeded.

minerals A and B in the following reactions:

$$X + A \rightarrow Y$$

$$X + Y \leftrightarrow B.$$

Here X and Y play roles analogous to O_2 and Fe^{2+}, whereas A and B are analogs of pyrite and an iron oxide mineral. The overall situation is the replacement of A by B. Nucleation and growth of B, however, tends to lower the concentration product XY in solution. This then tends to repress further B nucleation until the A-dissolution front advances sufficiently far downflow that upstream diffusion of Y to the region of B growth is no longer effective. The product of X and Y concentrations resulting from incoming X and upstream diffusion of Y can again reach the threshold for B-nucleation and a second B band is created, completing the O-P cycle.

In order to continue to operate, the O-P mechanism requires a continuous influx of reactant X. Furthermore, B growth kinetics must be sufficiently fast so that downstream B nucleation can be periodically repressed. The combination of continuous maintenance out of equilibrium and the B-nucleation inhibition effect are requisites for O-P Liesegang banding.

Unstable coarsening

The genesis of banded precipitation patterns may also proceed via a spatial instability of the Ostwald coarsening process (Lovett et al., 1978; Ortoleva, 1979; Feeney et al., 1983). Next, one can consider a spatially uniform distribution of spherical precipitate particles the radius of which is greater than that of the critical nucleus. Because of surface tension, the solubility of such particles decreases with increasing radius. Thus if the particles in one region of space are slightly larger than those in its surroundings, the former will grow at the expense of the latter, increasing the amplitude of the original non-uniformity. This is a self-enhancing process that makes the uniform precipitate unstable to the formation of patterning as suggested in Fig. 4-4.

In order for this process to operate, the system must initially be far from equilibrium as follows. The lowest free energy state to which any precipitate tends to evolve is that of a very few large particles — the Ostwald ripening process (Lifshitz and Slyouzov, 1961). The larger the particle size the weaker the dependence of solubility on the particle radius. In order for the feedback leading to patterning to operate, the initial sol must be very fine and hence far from equilibrium.

The essence of the above patterning mechanism is the involvement of solute diffusion and the dependence of grain solubility on a "textural" variable — here grain radius. In the next section, it is shown how the generalization of this theme allows for mechanochemical feedback in stressed rocks.

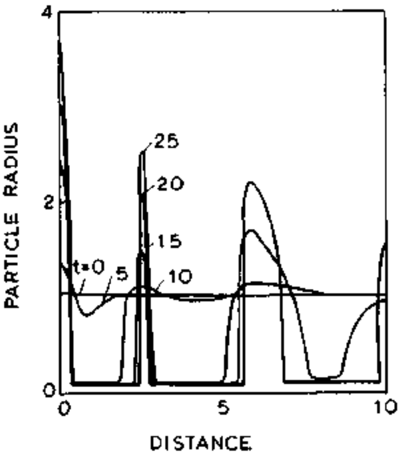

Fig. 4-4. Simulation of a coarsening instability in one spatial dimension driven by the dependence of particle solubility on particle radius. Note the induction of a number of satellite bands by the initial ($t = 0$) small-amplitude disturbance at the left.

MECHANOCHEMICAL FEEDBACK

At sufficient depth a number of possible feedbacks exist that involve the effective dependence of a grain's solubility on the mineral volume fractions and other textural variables in the volume element in which the grain resides. Such feedbacks can lead to the generation of sub-meter scale repetitive textural patterns that arise during diagenesis. Examples of these may include:

- roughly evenly spaced arrays of stylolites in limestones and sandstones (Heald, 1955; Tada and Siever, 1988);
- small-scale (microstylolite) laminations in chalk (Ekdale and Bromley, 1988);
- diagenetic bedding in alternating marl/limestone sequences (Barrett, 1964; Simpson, 1985; Bathurst, 1986; Ricken, 1986);
- layers of enhanced intergranular pressure solution alternating with domains of cementation in sandstones (Thomson, 1959; Heald and Anderegg, 1960);
- bands of authigenic muscovite in very fine-grained sandstones (Z. Al-Shaieb, private communication, 1988);
- spaced cleavage in argillaceous rocks (Alvarez et al., 1978; Engelder and Marshak, 1985); and
- pressure seals of meter scale (or greater) thickness composed of layered cements and/or arrays of stylolites (Tigert and Al-Shaieb, 1990).

To illustrate how mechanochemical feedback can lead to such features, two simple cases are considered here: one of a bimineralic rock of low porosity, and the other of a monomineralic porous rock.

Low-porosity rocks

On considering a grain in a small volume of rock, the stress experienced by the grain depends on the mechanical properties of the grains in that volume as well as the stress σ^m applied at the boundaries of that volume. The mechanical properties of the surrounding medium depend on the mineral identity, grain size, number of grains per unit volume, and grain shape and crystallographic orientation, i.e., on the "texture" of the surrounding medium. Thus, in a sense, the stress on the selected grain depends on texture. But the stress applied to the selected grain will modify its free energy and hence its solubility. As grain dissolution affects texture and texture affects solubility, there is the potential for a mechanochemical feedback capable of destabilizing the state of uniform texture and generating diagenetic differentiated structure.

More precisely, consider the case of a rock the mechanical response of which is elastic. Then the selected grain, if roughly spherical, can be considered as an inclusion (in the sense of Eshelby, 1957) in a matrix the mechanical properties of which are the statistical average of the mechanical properties of all grain types as weighted consistently with the local texture (in the simplest case, via a volume fraction average, for example). Using the results of Eshelby's matrix-inclusion calculations, the properties of the statistically weighted average medium and Kamb's (1959) formulae for the free energy of stressed solids, one can develop explicit formulae for the dependence of the free energy of the selected grain on the texture within and the stress applied to the volume element containing the grain of interest (Dewers and Ortoleva, 1989). A result of such a MFEK (mean field Eshelby–Kamb) model is seen in Fig. 4-5. In this model a deviatoric free energy of a calcite grain is given as a function of calcite volume fraction in a calcite–illite rock. As the calcite free energy decreases with increasing calcite content, one can see the potential for the segregation of calcite from illite. This relationship between calcite free energy and

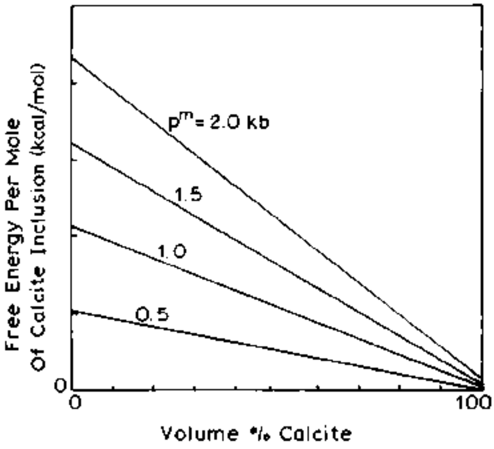

Fig. 4-5. Calcite free energy in a micaceous, low-porosity limestone showing the tendency for calcite segregation. Contoured for stress. p^m = hydrostatic pressure.

surrounding texture is a mechanism for differentiation between calcite and clay, and is explored in Chapter 7 in this volume.

An analogous situation exists in the quartz plus muscovite system, with muscovite exhibiting the tendency towards segregation. Whether or not muscovite segregation does occur in this system is actually a more subtle question. Using the MFEK approach, one can show that the free energy of a quartz grain in the same rock also decreases with muscovite volume fraction. Thus, in a sense, muscovite kinetics must be faster than that of quartz, as can occur with very fine muscovite grains, so that the active muscovite surface area is much greater than that of quartz. Otherwise, the tendency toward muscovite segregation from quartz will be overcome by the tendency of quartz to grow in muscovite-rich regions. Furthermore, chemical coupling between muscovite and quartz via SiO_2 in the intergranular fluid film also plays a role. For example, decreased quartz solubility lowers the concentration of aqueous silica and, hence, promotes muscovite dissolution. Thus, segregation depends strongly on the chemical as well as the mechanical nature of the system. The above, and related models, have been used to describe metamorphic layering (Dewers and Ortoleva, 1990a) and arrays of clay seams (see Chapter 7 in this volume).

Porous rocks

If mechanochemical coupling can lead to self-organization in low-porosity rocks due to contrasting mechanical properties between minerals, it seems likely that contrasts between matrix and pore fluid properties can also lead to self-organization. The non-uniform distribution of stresses along a grain's surface in a porous rock necessitates a more detailed description of grain geometry. Furthermore, porous rocks at depth tend to compact, so that any potential feedback operating in them must progress over a background of ambient compaction.

The notion of a pattern-forming feedback in porous rocks is quite straightforwardly understood. The author and coworkers originally formulated a simple reaction–transport model based on the assumption that the average stress on a grain increases with porosity (Merino et al., 1983). Thus, dissolution would occur in higher porosity domains and grain growth would occur in lower porosity domains, thereby intensifying the initial textural contrast. This model had a weakness in that it did not account for compaction. Ricken (1986) suggested that a feedback could exist wherein increased local grain contact area relieves stress, which in turn induces overgrowth and hence larger contact area, completing a feedback loop. In order to obtain a quantitative reaction–transport model that accounts for grain reaction at contacts and at free faces, compaction and the temporal evolution of the supra-grain scale distribution of stresses, a model was constructed based on Weyl's (1959) simple grain packing geometry, Kamb's (1959) expression for the free energy of a stressed grain and effective stress theory for elastic, fluid-pressured porous media. The result is a quantitative model of stylolites, layered compaction/overgrowth alternations, marl/limestone differentiated layering and a host of related submeter scale structures as mentioned above. The model is presented in Chapter 7 of this volume.

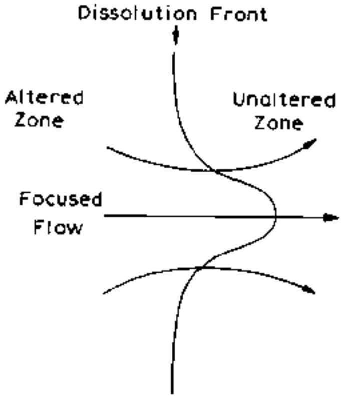

Fig. 4-6. Flow self-focusing results when the altered zone upstream from a reaction front has higher porosity/permeability than that in the unaltered zone. This can lead to the instability of a planar reaction front to the formation of bumps or scallops.

REACTION FRONT MORPHOLOGICAL INSTABILITY

Self-focusing flow

When a fluid flows through a rock, reaction fronts are created across which at least one mineral in the rock is dissolved (if the fluid is undersaturated with respect to one or more of the minerals in the rock). If permeability increases as a result of the passage of a reaction front, a planar front can be destabilized as a result of flow self-focusing as suggested in Fig. 4-6. A small bump in the reaction front focuses the flow to its tip because of the increase in permeability within the bump. The increased flow-through raises the rate of dissolution at the bump and, therefore, tends to speed up the local velocity of front advancement and thereby elongate the bump. Ultimately the bump becomes long enough that the fluid reaching its tip becomes saturated due to solute diffusion from the sides. In this way, any further bump elongation becomes arrested, and the bump can reach a steady state. Flow self-focusing can lead to the creation of scalloped or fingered reaction fronts of a variety of morphologies (Chadam et al., 1986, 1988; Ortoleva et al., 1987b; Chen and Ortoleva, 1990a, b, 1992, 1993).

Diagenetic reaction fronts

Natural examples of such patterned reaction fronts are reviewed in Ortoleva et al. (1987b). Reaction fronts play an important role in diagenesis. Notable examples are redox fronts (such as those leading to role-type uranium deposits), dissolution of carbonate cements from sandstones, dolomitization fronts in limestones, and feldspar dissolution fronts in sandstones (often leading to the creation of clay minerals). In the latter case, the clay may actually cause a decrease in permeability and, hence, the stabilization of the planar front. In extreme cases, where the matrix is completely dissolved out, dissolution holes may be created leading to karst terrains.

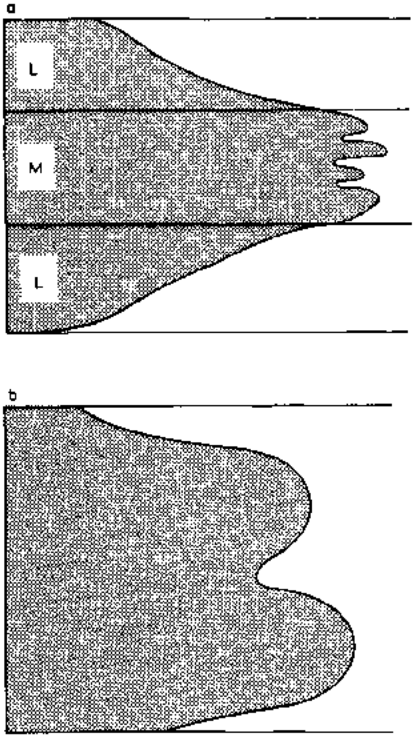

Fig. 4-7. (a) Cross-section of a dolomitization front (shaded) intruding into limestone (unshaded), showing fingering developing due to flow self-focusing of Mg^{2+}-bearing fluids within a more-permeable bed (*L* and *M* indicate less and more permeable beds). (b) Plan view illustrates the possibility of the scalloping of a dolomitization front.

Even in the presence of rock non-uniformity of depositional origin (beds or lenses), the self-focusing flow instability can play an important role as suggested in Fig. 4-7. The front can be scalloped within a given bed (as seen in the vertical cross-section of Fig. 4-7a) or in the horizontal dimension within a bed (as seen in the plan view of Fig. 4-7b).

REACTION MEDIATED, BUOYANCY DRIVEN ADVECTION

The dependence of pore fluid mass density on temperature and composition can lead to density inversions (heavier fluids overlying lighter fluids) that can drive spatially and temporally ordered patterns of advective fluid flow. The classic theoretical work in this area was on the genesis of advection cell patterns driven by the geothermal gradient analogous to the free fluid Bénard convection cells (Combarnous and Bories, 1975; Wood and Hewett, 1982). The possibility that such flow patterns can be driven by reaction due to the composition dependence of fluid mass density, makes such phenomena relevant to a discussion of diagenetic differentiated structures.

If saline waters overlie fresh waters, a large density inversion results that can drive flows as apparently occurs near salt domes (Ranganathan and Hanor, 1988). From the present point of view, this could be of interest in that it could lead to a breaking of the rotational symmetry around the dome. Instead of a flow pattern with downward velocity along the flanks of the dome that is independent of angle around the dome, the flow breaks up into an array of plumes of higher downward velocity alternating with slower downward velocity domains.

A second example of patterned reaction-driven advection is that associated with the genesis of petroleum. For example, the mass density of an aqueous solution of methane decreases with increasing methane content. Thus, methane generated from kerogen at depth can cause a pattern of cellular advection involving methane-rich updrafts alternating with relatively methane poor downdrafts (Park et al., 1990). The flow can even be oscillatory in time. When organic components separate into distinct liquid or gas phases, density inversions may lead to upward migration in the form of finger-like structures of the Saffman-Taylor type (Douglas, 1959; Glimm et al., 1985).

In principle, a sedimentary basin may exhibit a variety of buoyancy-driven advection patterns when chemical reaction and thermal expansion (in light of the geothermal gradient) overcome fluid compressibility (and the resulting increase of density with depth). An interesting case is that of carbonate minerals the solubility of which tends to decrease with temperature. This effect could lead to the redeposition of carbonate minerals from overlying beds into deeper lying patterns associated with the carbonate mineral dissolution-driven flow. Such a flow can be sustained for long times because there is a source of ions (say calcite dissolution) underlain by a sink (calcite precipitation) (Dewers and Ortoleva, 1989). This distinguishes this system from the case of halite, the solubility of which increases with temperature (and hence depth). Although carbonate-dissolution-driven flow provides a gentler driving force for convection than halite, it can persist over greater times.

Reaction-driven convection can combine with flow self-focusing (see previous section) to produce large enhancement of fluid velocities. For example, the updraft of hot fluids can increase permeability which, in turn, increases updraft velocity and local temperature. Thus mineral reactions can enhance and lock-in flow patterns via the accompanying change of permeability. Such effects can also play a role by enhancing or sealing-off fault-associated flow pathways.

BASIN COMPARTMENTS AND THEIR NON-LINEAR DYNAMICS

According to Bradley (1975) and Powley (1975 and later) sedimentary basins are typically divided into kilometer-scale compartments. These compartments are defined by vertical and horizontal bounding "seals" consisting of very low-permeability rock of roughly 10–100 m thickness. Across the seals, relatively large pore fluid pressure differences can be sustained. Pressures within the compartments may be

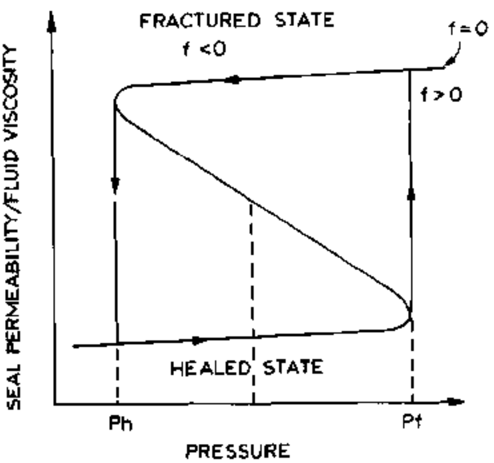

Fig. 4-8. Plane of seal permeability and compartment pressure illustrating oscillatory fluid release. p_h is the healing pressure, and p_f is the fracturing pressure. The S-shaped curve, similar in form to that seen in Fig. 4-1, suggests a repetitive cycle of fracturing, depressurizing, healing, and pressurizing.

abnormal, in that they differ from their hydrostatic value, being either over- or under-pressured. A number of properties of compartments suggest that they may be an example of kilometer-scale geochemical self-organization (Dewers and Ortoleva, 1988, 1993; Ortoleva, 1990; Ortoleva and Al-Shaieb, 1993), although the question of compartment genesis is not pursued here.

Next, the writer considers the phenomenon of oscillatory fluid release from overpressured compartments via a mechanism of seal puncture and healing as suggested by Bradley (1975) and Powley (1975 and later) and formulated as a quantitative reaction–transport problem by Ghaith et al. (1990) and Dewers and Ortoleva (1993). An interaction of fluid pressurizing effects and rock fracturing can lead to oscillatory fluid release from overpressured compartments as follows. If k is the permeability of the seal and p_c is the compartment fluid pressure (assumed spatially constant here for simplicity), the basic oscillation can be illustrated as shown in Fig. 4-8. When the seal is in the healed state, its permeability is low and a pressurization mechanism (see below) can raise p_c. If p_c exceeds the value p_f, the seal is fractured and, as the fracturing process is relatively fast, seal permeability jumps to its value in the fractured state. In this state, fluid loss dominates the overpressurization mechanism and p_c drops. If it drops below a value denoted p_h, the seal heals and seal permeability decreases. Once in the healed state, p_c can again rise due to pressurizing mechanisms.

Increases in pore fluid pressure in regions of rock surrounded by relatively low-permeability barriers can be from three sources: thermal expansion, reactions resulting in increases in volume, and compaction. All of these sources for abnormal fluid pressure may act simultaneously.

Clearly, oscillation can exist only in an intermediate range of overpressurizing rate. If the latter is too small, then leakage from the seal in the healed state will always keep p_c below p_f, whereas if the rate of overpressure development is too large, p_c will always stay above p_f.

CONCLUSIONS

All of the above mechanisms may be understood in the more general context of non-equilibrium phenomena in reaction–transport systems (see Nicolis and Prigogine, 1977). In that view there are two necessary conditions for self-organization, temporal oscillation and other non-linear phenomena:

(1) the system must be displaced sufficiently far from equilibrium and

(2) the dynamics must be non-linear.

By definition, diagenesis is mainly a process of rock chemical transformation and, hence, the first criterion may be satisfied under some conditions. Furthermore, the rates of the active diagenetic processes are often quadratic or other non-linear functions of solute concentrations, texture, fluid pressure and other descriptive variables.

Even if the above necessary conditions are typically satisfied, self-organization or oscillatory or other complex temporal dynamics do not necessarily occur. Rather, one can observe from the examples of the previous sections that some type of feedback arising from the active processes must be imbedded in the overall reaction–transport mechanical network. With this, one concludes that in principle, self-organization and other non-linear phenomena should be expected in a wide range of diagenetic contexts. Delineating quantitative criteria for their realization requires more detailed examination of active processes.

Three approaches to the study of non-linear diagenetic phenomena suggest themselves. An exemplary petrologic and field study is that of Ricken (1986) who demonstrated quite convincingly that there is a mechanism of amplification of textural contrast operating in the development of many marl/limestone sequences. Attempts to reproduce certain mineral banding phenomena in the laboratory date back to Liesegang (1913). The third approach compliments the first two; it proceeds via the development and analysis of quantitative reaction–transport models. This is the approach taken in the set of articles to appear in this and later volumes in this series.

The first companion article in the series is on stylolites, clay seams, diagenetic bedding and related mechanochemical phenomena (see Chapter 7). Chapters in the next volume will focus on the reaction front fingering and other flow self-focusing phenomena. Chapters on other self-organization and non-linear temporal dynamical phenomena as outlined above are also planned.

In conclusion, the purpose of the present and companion chapter is to make the suggestion that self-organization and other non-linear phenomena can play key roles in diagenesis. The objective is to set forth these ideas to complement more classical approaches — i.e., presenting them as alternatives when classical explanations do not seem to be adequate. To be sure, the list of possible mechanisms of self-organization and other non-linear phenomena set forth above is not meant to be complete, nor is it suggested that they are all definitely operating in sedimentary basins. Rather, the list is meant to suggest the types of things that can happen. It is expected, however, that as this field of research in diagenesis develops, new insights into heretofore perplexing occurrences will emerge.

ACKNOWLEDGEMENTS

Research supported by grants from the Basic Energy Sciences Program of the US Department of Energy, the Gas Research Institute, and the National Science Foundation.

REFERENCES

Alvarez, W., Engelder, T. and Geiser, P.A., 1978. Classification of solution cleavage in pelagic limestones. *Geology*, 6: 263–266.

Barrett, P.J., 1964. Residual seams and cementation in Oligocene shell calcarenites, Te Kuiti Group. *J. Sediment. Petrol.*, 34: 524–531.

Bathurst, R.G.C., 1986. Diagenetically enhanced bedding in argillaceous platform limestones: stratified cementation and selective compaction. *Sedimentology*, 34: 740–778.

Bradley, J.S., 1975. Abnormal formation pressure. *Bull. Am. Assoc. Pet. Geol.*, 59: 957–973.

Chadam, J., Sen, A. and Ortoleva, P., 1986. Reactive infiltration instabilities. *I.M.A. J. Appl. Math.*, 36: 207–221.

Chadam, J., Sen, A. and Ortoleva, P., 1988. A weakly nonlinear stability analysis of the reactive infiltration interface. *SIAM, J. Appl. Math.*, 48: 1362–1378.

Chen, W. and Ortoleva, P., 1990a. Reaction front fingering in carbonate cemented sandstones. In: P. Ortoleva, B. Hallet, A. McBirney, I. Meshri, R. Reeder and P. Williams (Editors), *Self-Organization in Geological Systems: Proceedings of a Workshop held 26–30 June 1988, University of California, Santa Barbara. Earth-Sci. Rev.*, 29: 183–198.

Chen, W. and Ortoleva, P., 1990b. Self-organization in far-from-equilibrium reactive porous media subject to reaction front fingering. In: D. Walgraef and N.M. Ghoniem (Editors), *Patterns, Defects and Materials Instabilities*. NATO ASI Series, 183: 203–220.

Chen, W. and Ortoleva, P., 1992. Development of complex reaction–infiltration morphologies through nonlinear fluid–rock interaction: Modeling asymptotic and numerical studies. In: W.E. Fitzgibbon and M.F. Wheeler (Editors), *Modeling and Analysis of Diffusive and Advective Processes in Geosciences*, SIAM, 52–70.

Chen, W. and Ortoleva, P., 1993. Development of complex reaction front morphologies through nonlinear fluid–rock interaction. In: J. Chadam (Editor), *Free Boundary Conference Proceedings, Montreal, 1990* (in press).

Combarnous, M.A. and Bories, S.A., 1975. Hydrothermal convection in saturated porous media. *Adv. Hydrosci.*, 10: 231–306.

Dewers, T. and Ortoleva, P., 1988. The role of geochemical self-organization in the migration and trapping of hydrocarbons. *Appl. Geochem.*, 3: 287–316.

Dewers, T. and Ortoleva, P., 1989. Mechano-chemical coupling in stressed rocks. *Geochim. Cosmochim. Acta*, 53: 1243–1258.

Dewers, T. and Ortoleva, P., 1990a. Geochemical self-organization, III. A mean field, pressure solution model of spaced cleavage and metamorphic segregational layering. *Am. J. Sci.*, 290: 473–521.

Dewers, T. and Ortoleva, P., 1990b. A coupled reaction/transport/mechanical model for intergranular pressure solution, stylolites, and differentiated compaction and cementation in clean sandstones. *Geochim. Cosmochim. Acta*, 54: 1609–1625.

Dewers, T. and Ortoleva, P., 1993. Nonlinear dynamical aspects of deep basin hydrology: fluid compartment formation and episodic fluid release. *Am. J. Sci.* (submitted).

Douglas, J., Peaceman, D. and Rachford, H., 1959. A method for calculating multi-dimensional immiscible displacement. *AIME Trans.*, 216: 297.

Ekdale, A.A. and Bromley, R.G., 1988. Diagenetic microlamination in chalk. *J. Sediment. Petrol.*, 58: 857–861.

Engelder, T. and Marshak, S., 1985. Disjunctive cleavage formed at shallow depths in sedimentary rocks. *J. Struct. Geol.*, 7: 327–343.

Eshelby, J.D., 1957. The determination of the elastic field of an ellipsoidal inclusion and related problems. *Proc. R. Soc. London, Ser. A*, 241: 376–396.

Feeney, R., Schmidt, S.L., Strickholm, P., Chadam, J. and Ortoleva, P., 1983. Periodic precipitation and coarsening waves: applications of the competitive particle growth model. *J. Chem. Phys.*, 78: 1293.

Ghaith, A.Y., Chen, W. and Ortoleva, P., 1990. Oscillatory methane release from shale source rocks. In: P. Ortoleva, B. Hallet, A. McBirney, I. Meshri, R. Reeder and P. Williams (Editors), *Self-Organization in Geological Systems: Proceedings of a Workshop held 26–30 June 1988, University of California, Santa Barbara. Earth-Sci. Rev.*, 29: 241–248.

Glimm, J., Lindquist, B., McBryan, O. and Tryggvason, G., 1985. Sharp and diffuse fronts in oil reservoirs: front tracking and capillarity. *SIAM, Proc. Math. and Comp. Methods in Seismic Exploration and Reservoir Modeling,* Houston, Texas, January 1985.

Heald, M.T., 1955. Stylolites in sandstones. *J. Geol.*, 63: 101–114.

Heald, M.T. and Anderegg, R.C., 1960. Differential cementation in the Tuscarora sandstone. *J. Sediment. Petrol.*, 30: 568–577.

Kamb, W.B., 1959. The theory of preferred crystal orientation developed by crystallization under stress. *J. Geol.*, 67: 153–60.

Liesegang, R.E., 1913. *Geologische Diffusionen.* Steinkopff, Dresden.

Lifshitz, I.M. and Slyouzov, V.V., 1961. The kinetics of precipitation from supersaturated solid solutions. *J. Phys. Chem. Solids*, 19: 35–50.

Lovett, R., Ross, J. and Ortoleva, P., 1978. Kinetic instabilities in first order phase transitions. *J. Chem. Phys.*, 69: 947.

Merino, E., Strickholm, P. and Ortoleva, P., 1983. Generation of evenly spaced pressure solution seams during late diagenesis: a kinetic theory. *Contrib. Mineral. Petrol.*, 83: 360–370.

Nicolis, G. and Prigogine, I., 1977. *Self-Organization in Non-Equilibrium Systems.* Wiley, New York, N.Y., 491 pp.

Ortoleva, P., 1979. Selected topics from the theory of nonlinear physico-chemical phenomena. In: H. Eyring (Editor), *Theoretical Chemistry, Periodicities in Chemistry and Biology, Vol. IV.* Academic Press, New York, N.Y., pp. 235–286.

Ortoleva, P., 1990. Role of attachment kinetic feedback in the oscillatory zoning of crystals grown from melts. In: P. Ortoleva, B. Hallet, A. McBirney, I. Meshri, R. Reeder and P. Williams (Editors), *Self-Organization in Geological Systems: Proceedings of a Workshop held 26–30 June 1988, University of California, Santa Barbara. Earth-Sci. Rev.*, 29: 3–8.

Ortoleva, P., 1993. *Geochemical Self-Organization.* Oxford University Press (in press).

Ortoleva, P. and Al-Shaieb, Z., 1993. Genesis and dynamics of basin compartments and seals. *Am. J. Sci.* (submitted).

Ortoleva, P., Merino, E., Chadam, J. and Moore, C.H., 1987a. Geochemical self-organization, I. Reaction–transport feedbacks and modeling approach. *Am. J. Sci.*, 287: 979–1007.

Ortoleva, P., Merino, E., Chadam, J. and Sen, A., 1987b. Geochemical self-organization, II. The reactive-infiltration instability. *Am. J. Sci.*, 287: 1008–1040.

Ortoleva, P., Hallet, B., McBirney, A., Meshri, I., Reeder, R. and Williams, P. (Editors), 1990. *Self-Organization in Geological Systems: Proceedings of a Workshop held 26–30 June 1988, University of California, Santa Barbara. Earth-Sci. Rev.*, 29: 417 pp.

Ostwald, W.Z., 1925. Über die Geschwindigkeitsfunktion der Viskosität Disperser Systeme, I. *Kolloid-Z.*, 36: 99.

Park, A., Dewers, T. and Ortoleva, P., 1990. Cellular and oscillatory self-induced methane migration. In: P. Ortoleva, B. Hallet, A. McBirney, I. Meshri, R. Reeder and P. Williams (Editors), *Self-*

Organization in Geological Systems: Proceedings of a Workshop held 26–30 June 1988, University of California, Santa Barbara. Earth-Sci. Rev., 29: 249–265.

Powley, D.E., 1975 and later. Course notes used in AAPG Petroleum Exploration Schools.

Powley, D. and Bradley, J.J., 1987. Pressure compartments (unpublished manuscript).

Prager, S., 1956. Periodic precipitation. *J. Chem. Phys.*, 25: 279.

Ranganathan, V. and Hanor, J.S., 1988. Density driven groundwater flow near salt domes. *Chem. Geol.*, 74: 173–188.

Reeder, R.J., Fagioli, R.O. and Meyers, W.J., 1990. Oscillatory zoning of Mn in solution-grown calcite crystals. In: P. Ortoleva, B. Hallet, A. McBirney, I. Meshri, R. Reeder and P. Williams (Editors), *Self-Organization in Geological Systems: Proceedings of a Workshop held 26–30 June 1988, University of California, Santa Barbara. Earth-Sci. Rev.*, 29: 39–46.

Ricken, W., 1986. *Diagenetic Bedding.* Springer-Verlag, Berlin, 210 pp.

Simpson, J., 1985. Stylolite-controlled layering in homogeneous limestones: pseudo-bedding produced by burial diagenesis. *Sedimentology*, 32: 495–505.

Tada, R. and Siever, R., 1989. Pressure solution during diagenesis: a review. *Annu. Rev. Earth Planet. Sci.*, 17: 89–118.

Thomson, A., 1959. Pressure solution and porosity. In: H.A. Ireland (Editor), *Silica in Sediments. Soc. Econ. Paleontol. Mineral., Spec. Publ.*, 7: 92–110.

Tigert, V. and Al-Shaieb, Z., 1990. Pressure seals: their diagenetic banding patterns. In: P. Ortoleva, B. Hallet, A. McBirney, I. Meshri, R. Reeder and P. Williams (Editors), *Self-Organization in Geological Systems: Proceedings of a Workshop held 26–30 June, 1988, University of California at Santa Barbara. Earth-Sci. Rev.*, 29: 227–240.

Weyl, P.K., 1959. Pressure solution and the force of crystallization. *J. Geophys. Res.*, 64: 2001–2025.

Wood, J.R. and Hewett, T.A., 1982. Fluid convection and mass transfer in porous sandstones — a theoretical model. *Geochim. Cosmochim. Acta*, 46: 1707–1713.

Diagenesis, IV. Developments in Sedimentology 51
edited by K.H. Wolf and G.V. Chilingarian
© 1994 Elsevier Science B.V., Amsterdam. All rights reserved.

Chapter 5

STABILITY FIELDS OF SMECTITES AND ILLITES INCLUDING GLAUCONITES AS A FUNCTION OF TEMPERATURE AND CHEMICAL COMPOSITION

Y. TARDY and J. DUPLAY

INTRODUCTION

In the last few years, a large number of studies have been devoted to clay mineral geochemistry and to clay stability fields under natural conditions. The present-day knowledge has been considerably improved by additional natural observations, mineralogical data, crystallographic measurements, and conceptual models.

Among the different families of clay minerals, smectites and illites have received particular attention, probably because, apart from chlorites, they offer a large variety of compositions, and they cover, in nature, a large range of stability fields. In fact, at and near the surface of the Earth, they form or survive over a wide range of temperature, pressure and solution concentration conditions. Smectites and illites are particularly interesting in the scope of the clay mineral geochemistry.

Furthermore, clay minerals are now introduced in computer models which simulate the mass transfers occurring in nature (Fritz, 1975, 1981, 1985). These computations are based on thermodynamic equilibria between a large number of chemical variables: simple and complex aqueous species, solid-solutions and minerals of complex chemical compositions, so that mass transfer simulations are now supposed to work not only as idealized but also as realistic models. This chapter is an attempt to analyze the difficulties and the possibilities to treat clay minerals as phases in thermodynamic equilibrium in their environment, and to be able to interpret their chemical composition as indicator of salinities and temperatures of solutions in which they may form or equilibrate.

DIFFICULTIES OF DEFINING CLAY MINERAL STABILITIES

The abundance and the diversity of smectites and illites at the surface of the Earth suggest that these clay minerals can reflect differences among the chemical conditions in which they form and can exert control on their chemical environments. As perfectly pointed out by May et al. (1986), however, all of the experimentally determined solubilities or stabilities appear uncertain due to complications arising in part from the experimental techniques employed and in part from the nature of the minerals. Furthermore, both the accuracy of the selected free energy values and the validity of assumptions involved in their use are suspect in many instances for both technical and theoretical reasons. If gibbsite and kaolinite are simple and nearly ideal minerals, smectites appear, on the other hand, to be very complex with regard to their stability field evaluation. The difficulties arise for several reasons: (1) variations in mineral crystallinity (May et al., 1979b; Tsuzuki and Kawabe, 1983), (2) variations in particle size (Bassett et al., 1979), (3) uncertainty about mineral purity which may skew both the dissolution chemistry and the formula determination, and (4) compositional heterogeneity of the minerals themselves.

The second problem, which unfortunately cannot be entirely solved before the first questions will be completely answered, concerns the possibility for smectites, illites or interstratified minerals to survive as metastable phases in weathering profiles or in sedimentary columns. Lippmann (1977, 1979a, 1979b, 1982) developed several arguments which suggest that "only metastable systems are capable of carying information. By virtue of their metastability, clay minerals are useful as stratigraphic markers, as indicators of diagenesis as distinct from metamorphism. If silicates would readily equilibrate at ordinary temperature, neither soils nor clays would exist and Earth would be covered by a shell of barren rocks to be classified near the greenschist facies" (Lippmann, 1982, p. 485).

It is clear that the metamorphic minerals, such as muscovite, pyrophyllite or dickite, have true stability fields in stability diagrams, although they do not readily form at 25°C (Lippmann, 1982). It would be useful, however, to be able to predict the domains of formation of clay minerals as function of their chemical composition, assumed to be exactly known.

If direct solubility measurements, and the concept of clay minerals as single phases, fail as the base of the prediction of their stability fields (May et al., 1986), one must search for a new approach, based on the thermodynamics of metastable phases applied to inhomogeneous systems, and to be able to reproduce the large variety of mineral associations, observed in natural environments and persisting during a relatively short period of geological time.

STABILITY FIELD OF SMECTITES

Three important steps have marked the progressive recognition of the great variety of smectite stability fields in nature.

Aluminous montmorillonite

In the 1950's, soil scientists first clearly described the mineral succession: gibbsite–kaolinite–montmorillonite, in soils as function of climate, topography and nature of the parent rock (Jackson et al., 1948; Leneuf, 1959; Millot, 1964; Barshad, 1966). Gibbsite appears in leached conditions in the upper parts of the profiles, in the topographic highs and under humid tropical climates, when the percolating solutions are diluted. Montmorillonite appears in confined conditions, in the lower parts of the profiles, downstream in landscapes and under semi-arid climates, when the percolating solutions are concentrated by evaporation or by a long advance through the weathering zone.

TABLE 5-1

Equilibrium reactions and solubility product constants for gibbsite, kaolinite and an idealized Ca-beidellite, at 25°C (after Fritz and Tardy, 1973; Droubi et al., 1976)

Gibbsite:

$$Al(OH)_3 + 3\,H^+ = Al^{3+} + 3\,H_2O$$

with: $\log[Al^{3+}]/[H^+]^3 + 3\log[H_2O] = \log K_{sp} = 8.205$

Kaolinite:

$$0.5\,Al_2Si_2O_5(OH)_4 + 3\,H^+ = Al^{3+} + SiO_2 + 2.5\,H_2O$$

with: $\log[Al^{3+}]/[H^+]^3 + \log[SiO_2] + 2.5\log[H_2O] = \log K_{sp} = 3.205$

Smectite:

$$3\,[Ca_{0.167}\,(Al_2)\,(Si_{3.67}Al_{0.33})\,O_{10}(OH)_2] + 22\,H^+ = 2.5\,H_2O + 11\,SiO_2 + 7\,Al^{3+} + 0.5\,Ca^{2+}$$

with: $7\log[Al^{3+}]/[H^+]^3 + 11\log[SiO_2] + 0.5\log[Ca^{2+}]/[H^+]^2 + 14\log[H^2O] = \log K_{sp} = 18.60$

or: $\log[Al^{3+}]/[H^+]^3 + 1.57\log[SiO_2] + 0.071\log[Ca^{2+}]/[H^+]^2 + 4.667\log[H_2O] = \log K_{sp} = 2.66$

Square brackets ([ ]) designate activity of aqueous species in solution.

At the same time, thermodynamic models and calculations based on natural observations or experiments in laboratory were undertaken. The first studies are probably those of Garrels (1957) and Hemley (1959) cited by Garrels and Christ (1965). They were followed by those of Wollast (1961, 1963), Hemley et al. (1961), Frink and Peech (1962), Orville (1963), Helgeson (1964), De Keyser (1964), Feth et al. (1964), Kittrick (1966, 1969), Kramer (1968), and Tardy (1969).

In weathering profiles, gibbsite, kaolinite and montmorillonite may form successively from humid to semi-arid tropical climates (Lelong et al., 1976). The solubility products and equilibrium reactions concerning the aluminous minerals are presented in Table 5-1.

The kaolonite–gibbsite boundary is defined by:

$$\log[SiO_2] - 0.5\log[H_2O] = -4.5$$

The smectite–kaolinite boundary is defined for an idealized smectite stoichiometry by the following equation:

$$0.57\log[SiO_2] + 0.071\log[Ca^{2+}]/[H^+] + 2.167\log[H_2O] = -1.042$$

The equilibrium diagrams of Fig. 5-1 show clearly that gibbsite is stable in dilute and acid waters, whereas montmorillonite or beidellite is stable in more concentrated solutions of higher pH and higher-soluble silica activities. Waters collected in different temperate or tropical regions are positioned as function of $\log[Na^+]/[H^+]$, $\log[Ca^{2+}]/[H^+]^2$ and $\log[SiO_2]$. Concentrated waters from arid

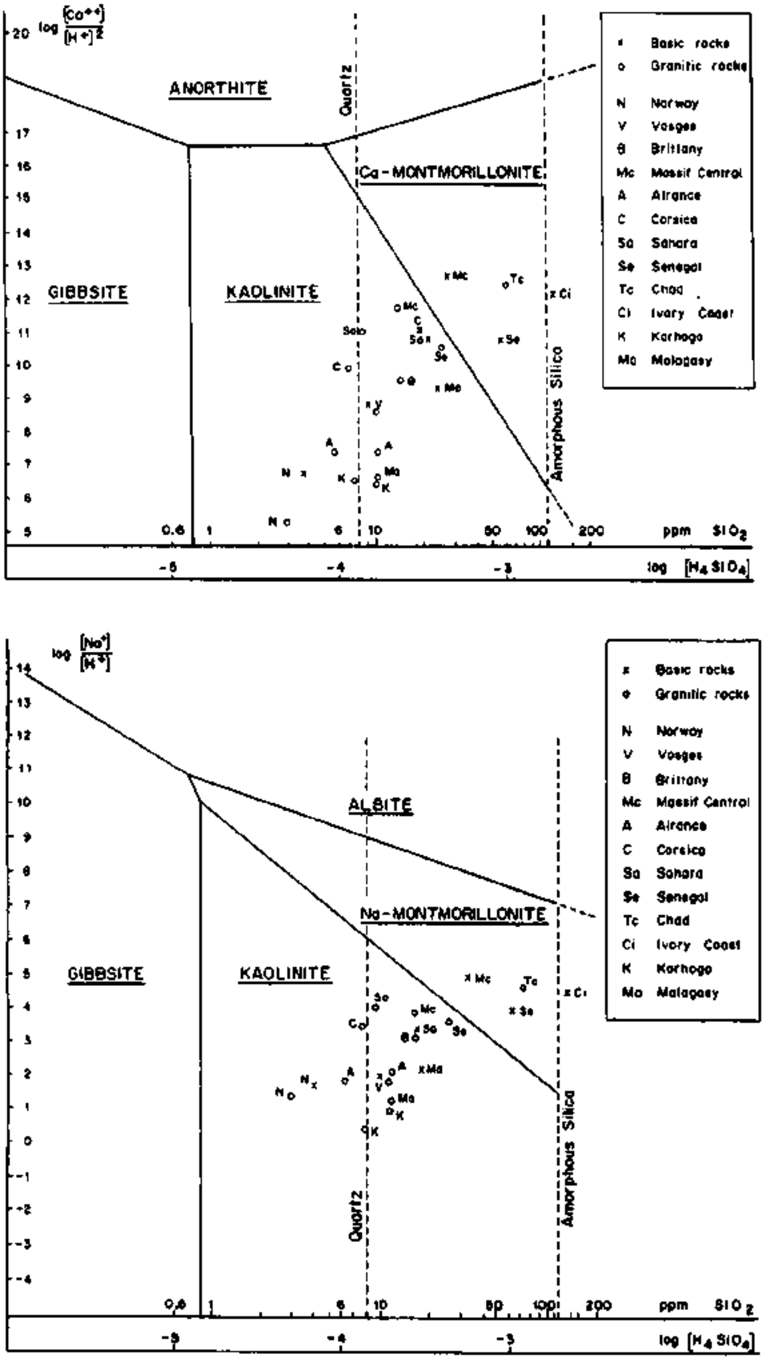

Fig. 5-1. Stability field diagram of gibbsite, kaolinite and montmorillonite, and position of drainage water collected in different climatic environments (solubility data at 25°C). (From Tardy, 1971.)

countries fall in the montmorillonitic domain. Dilute waters collected in humid areas fall in the domain of kaolinite, close to the gibbsite boundary (Tardy, 1971).

At that stage of investigation, it has been clearly recognized that montmorillonite is more "soluble" than kaolinite, i.e., forms in solutions of higher pH and is characterized by higher concentrations of cations and silica. The systems studied, however, were supposed to be exclusively aluminous and the influence of smectite compositions on their stability fields was, at that moment, not yet very well discerned.

Four major smectite stages of weathering and sedimentation: nontronite, beidellite, montmorillonite, and stevensite

In sediments, a clear distinction between the aluminous montmorillonite and the magnesian stevensite was recognized quite early (Millot, 1949, 1964; Millot et al., 1960; Grim and Kulbicki, 1961; Bradley and Fahey, 1962).

The distribution of smectites in sedimentary environments was extensively examined by Huertas et al. (1970). Later on, Trauth (1977) studied in detail the sediments of the Paris Basin and clearly showed that the chemical composition of smectites changes progressively from paleosoils and moderately leached continental material to marine evaporites deposited in confined areas. A comprehensive sequence was established (Table 5-2). The chemical composition of the most frequent and widespread smectite, found in the continental deposits and in the detrital fraction of the coastal marine sediments, is close to that of the soil ferri-beidellite described by Paquet (1970).

Furthermore, in most of the facies deposited near the shorelines, the continental influence is marked by the formation of an aluminous montmorillonite, whereas in the evaporitic facies stevensite and sepiolite are predominant. In the intermediate stages, smectites are progressively enriched in magnesium and depleted in aluminium and iron. The bulk structural formulas indicate compositions somewhat in the middle between dioctahedral and trioctahedral minerals and also indicate some important tetrahedral substitutions, which may localize these smectites within the group of saponites.

Similar sequences were described in some weathering profiles and in the Lake Chad sediments. Wildman et al. (1968, 1971) have stated that in weathering profiles located on basic and ultramafic rocks, nontronite appears in dilute environments and stevensite or saponite in more concentrated ones.

TABLE 5-2

Sequence from detrital (mostly beidellite) to evaporitic (mostly stevensite) sediments in Paris Basin. Structural formulas and octahedral occupancies (after Trauth, 1977)

Beidellite:	$Ca_{0.133}(Al_{1.327}Fe^{3+}_{0.5}Mg_{0.26})(Al_{0.267}Si_{3.733})O_{10}(OH)_2$	2.09
Smectite, Wyoming:	$Ca_{0.06}K_{0.5}(Al_{1.44}Fe^{3+}_{0.30}Mg_{0.30})(Si_4)O_{10}(OH)_2$	2.04
Smectite, Cheto:	$Ca_{0.12}K_{0.16}(Al_{1.18}Fe^{3+}_{0.24}Mg_{0.60})(Si_4)O_{10}(OH)_2$	2.02
Saponite:	$Ca_{0.12}K_{0.13}(Al_{0.80}Fe^{3+}_{0.24}Mg_{1.35})(Al_{0.21}Si_{3.79})O_{10}(OH)_2$	2.39
Stevensite:	$Ca_{0.08}Na_{0.08}K_{0.16}(Al_{0.21}Fe^{3+}_{0.07}Mg_{2.40})((Si_4)O_{10}(OH)_2$	2.68

TABLE 5-3

Chemical composition (millimoles/kg H_2O) of waters of the Lake Chad system (Gac, 1980). The most stable clay minerals are, respectively, kaolinite for water A (Chari River), nontronite for B (delta), beidellite for C and D (lake), and saponite or stevensite for E and F (interdune salines)

	Na	K	Ca	Mg	HCO_3	SO_4	Cl	SiO_2	TDS (mg/l)	pH	f_{CO_2} calculated
A	0.123	0.242	0.091	0.47	0.478	–	–	0.329	61.0	6.8	$10^{-2.3}$
B	0.141	0.060	0.126	0.099	0.626	0.010	0.020	0.385	76.0	7.4	$10^{-2.8}$
C	0.353	0.111	0.206	0.152	1.150	0.010	0.020	0.385	76.0	7.4	$10^{-2.8}$
D	2.060	0.605	0.625	0.480	3.950	0.090	0.150	0.879	548.3	8.8	$10^{-3.3}$
E	16.039	2.294	0.409	0.845	13.380	0.887	0.730	0.496	1759.2	8.9	$10^{-2.9}$

The Lake Chad system was extensively studied by Lemoalle and Dupont (1973), Carmouze (1976), Gac (1980) and Gac and Tardy (1980). It was demonstrated that the nature and the composition of the smectites, formed in lake sediments, change from nontronite to beidellite or montmorillonite and to stevensite, when waters are progressively concentrated by evaporation (Table 5-3). Nontronite is formed within the ferruginous oolites (Carmouze et al., 1977; Pedro et al., 1978) and in the very dilute waters of the Chari river delta. Beidellite and montmorillonite were found stable together with calcite in the moderately concentrated waters of the northern part of the lake. Stevensite is formed in the sodium carbonate brines of the salines of Kanem, Chad.

Equilibria in magnesian systems were experimentally studied by Hostetler (1963), Hostetler and Christ (1965), Hostetler et al. (1971), Bricker et al. (1973), Christ et al. (1973) and Hemley et al. (1977a, b). Stability fields of talc, sepiolite and other magnesium minerals were, since that time, precisely determined.

During the same period of time, the concepts of clay solubility and clay stability field have shown considerable progress. Attempts to measure the smectite and illite solubilities were performed by Kittrick (1971a, b; 1973), Routson and Kittrick (1971) and Weaver et al. (1971). At about the same time, attempts to estimate the thermodynamic properties of minerals were proposed by Karpov and Kashik (1968) and Eugster and Chou (1973). Tardy and Garrels (1974), therefore, presented an empirical method for estimating ΔG_f°, the Gibbs free energies of formation of illites, vermiculites and smectites. This method has been generalized and applied to minerals of discrete chemical compositions. Other methods of estimation proposed later by Nriagu (1975), Chen (1975), Mattigod and Sposito (1978), Tardy (1979), Tardy and Fritz (1981) and Sposito (1986) have confirmed the consistency of the original approach. Tardy et al. (1974a, b) estimated the stability fields of nontronite, beidellite and stevensite by using the Tardy and Garrels (1974) method. Their results have been used to calculate the equilibrium reaction constants (Table 5-4) between kaolinite, goethite, nontronite, beidellite, and saponite. Tardy and Gac (1979), Gac (1980) and Tardy (1981) showed (Fig. 5-2) the excellent agreement between the calculated stability fields and the observed sequence of smectites stable in the waters of the Lake Chad system.

TABLE 5-4

Variations of the equilibrium constant at 25°C for the reaction: smectite (nontronite, beidellite, or stevensite) = kaolinite +goethite (after Gac, 1980)

Nontronite = kaolinite + goethite:

$$Ca_{0.22}(Fe_{1.77}Mg_{0.21})(Al_{0.17}Si_{3.83})O_{10}(OH)_2 + 0.86\,H^+$$
$$= 1.77\,FeO(OH) + 0.085\,Al_2Si_2O_5(OH)_4 + 0.22\,Ca^{2+} 0.21\,Mg^{2+} + 3.66\,SiO_2 + 0.375\,H_2O$$

with: $\log K_R = 0.22 \log[Ca^{2+}]/[H^+]^2 + 0.21 \log[Mg^{2+}]/[H^+]^2 + 3.6 \log[SiO_2] + 0.375 \log[H_2O]$
$= -487.636$

Beidellite = kaolinite + goethite:

$$Ca_{0.133}(Al_{1.327}Fe_{0.5}Mg_{0.26})(Al_{0.267}Si_{3.733})O_{10}(OH)_2 + 0.451\,H_2O + 0.786\,H^+$$
$$= 0.50\,FeO(OH) + 0.797\,Al_2Si_2O_5(OH)_4 + 0.133\,Ca^{2+} + 0.26\,Mg^{2+} + 2.139\,SiO_2$$

with: $\log K_R = 0.133 \log[Ca^{2+}]/[H^+]^2 + 0.26 \log[Mg^{2+}]/[H^+]^2 + 2.139 \log[SiO_2] - 0.451 \log[H_2]$
$= -2.18$

Stevensite = kaolinite + goethite:

$$Na_{0.19}(Al_{0.51}Fe_{0.16}Mg_{1.90})(Si_4)O_{10}(OH)_2 + 3.99\,H^+$$
$$= 0.16\,FeO(OH) + 0.255\,Al_2Si_2O_5(OH)_4 + 0.19\,Na^+ + 1.90\,Mg^{2+} + 3.49\,SiO_2 + 2.405\,H_2O$$

with: $\log K_R = 0.19 \log[Na^+]/[H^+] + 1.90 \log[Mg^{2+}]/[H^+]^2 + 3.49 \log[SiO_2] + 2.405 \log[H_2O]$
$= 14.731$

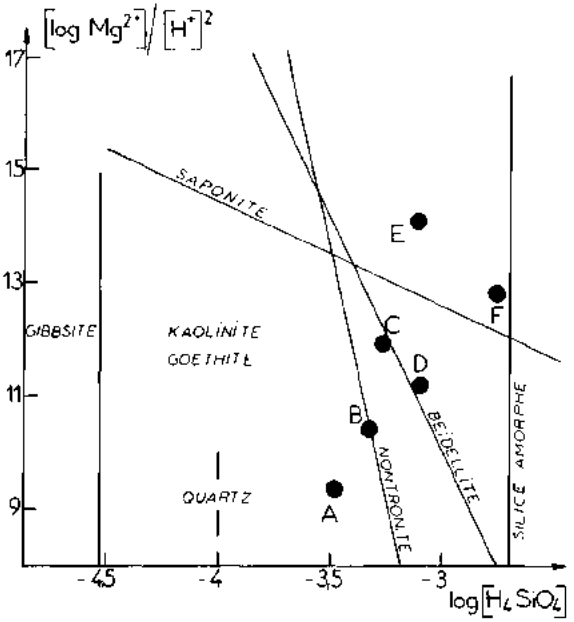

Fig. 5-2. Stability fields (at 25°C) of nontronite, beidellite and saponite and characteristics of different waters of the Lake Chad system. (From Gac, 1980.)

Obviously, nontronite is the most stable and the least soluble is smectite. In contrast, stevensite appears as the least stable and the most soluble clay mineral, whereas beidellite and montmorillonite occupy intermediate positions:

Nontronite < beidellite or montmorillonite < stevensite.

The dioctahedral iron-rich smectites presenting a high tetrahedral charge can form in very dilute environments. The trioctahedral magnesium-rich stevensite, presenting a very low tetrahedral charge can form in very saline and concentrated environments. The existence and the stability of beidellite, montmorillonite and saponite are perhaps more questionable.

In fact, the most typical smectites, found in soils, i.e., in low-temperature weathering conditions, generally show chemical compositions of ferri-beidellites (Trauth et al., 1967; Paquet, 1970). In iron-rich environments, nontronite, characterized by a large tetrahedral charge, may form instead of beidellite. In the nontronite–beidellite dioctahedral series, therefore: higher the iron $((Fe^{3+})^{VI})$ content in octahedral position, higher the tetrahedral substitution of $(Si^{4+})^{IV}$ by $(Al^{3+})^{IV}$ ions (Paquet, 1970). Weaver and Pollard (1975) have also found, in this mineral series, a good positive correlation between $(Fe^{3+})^{VI}$ and $(Al^{3+})^{IV}$.

Furthermore, as pointed out by Robert (1973), the neoformed soil smectites are probably closer to the true montmorillonites, characterized by a low tetrahedral charge, than to the beidellites. Barshad (1966) and Barshad and Kishk (1969), however, have also described neoformed vermiculites, characterized by low tetrahedral charges, or mica-degraded vermiculites characterized by high tetrahedral charges. Soil smectites, called ferri-beidellites, probably differ from the beidellite *sensu stricto* which is a very rare mineral of hydrothermal origin (Weaver and Pollard, 1975). These smectites are probably mixtures of nontronites, Al- and Fe-vermiculites (degraded micas with high tetrahedral charges), and neoformed Al-montmorillonites (with low tetrahedral charges).

Similar considerations can be drawn for the sedimentary saponites. According to Weaver and Pollard (1975), most of the saponites described in the literature are of hydrothermal origin. A metamorphic origin is even proposed by Wilson et al. (1968) for a saponite in the Dalradian metalimestones of Scotland. Thus, it is probable that "saponites", described by Trauth (1977) in sediments, are in fact intermediate stages between detrital beidellites and neoformed stevensites, both probably characteristic of low-temperature smectites. As for soil beidellites, sedimentary saponites are probably mixtures. They may differ from the true saponites of hydrothermal origin.

Thus, in the conditions of weathering and sedimentation, each smectite type characterized by a given bulk composition also appears to be characterized by a specific field of stability. In iron-rich environments and in dilute solutions, nontronite (with high tetrahedral charge) is stable. In aluminium-rich environments and in moderately concentrated solutions Al-vermiculite, beidellite and montmorillonite are formed or preserved together. In evaporitic and confined environments, where solutions are concentrated, stevensite (with low tetrahedral charge) appears as the most stable trioctahedral smectite.

The sequence ranging from nontronite, stable in diluted environments, to stevensite, formed in concentrated brines, is the result of a progressive increase of Mg^{2+}in octahedral and Si^{4+}in tetrahedral sites, and a decrease of Fe^{3+}or Al^{3+}in tetrahedral and octahedral positions.

Field observations suggest that the bulk composition of smectitic materials changes when the chemical composition of solutions, in which they form or reequilibrate, also changes. Thus, in thermodynamic models applied at a field scale, smectites can be considered as phases of variable chemical compositions, even if they may appear, at a crystal scale, as mixtures of apparently separate components.

STABILITY FIELDS OF ILLITES

The specific nature of illite is still an unresolved problem (Weaver and Pollard, 1975). In fact, pure monomineralic samples are difficult to find and, consequently, the mineral species characteristics and properties are not easy to define. Illite is, in fact, the dominantly potassic, dioctahedral, aluminous, mica-like fraction of clay size materials in alteration products, sedimentary rocks and metasediments (Velde, 1977). Illitic minerals include also dioctahedral ferric minerals, such as glauconite and celadonite.

Near the Earth's surface, two majors situations seem to have provided most of the *sensu lato* aluminous illite materials: (1) the hydrothermal alteration of feldspars or other aluminosilicates into illites or sericites, and (2) the conversion by diagenesis or low-grade metamorphism of smectitic or other detrital micaceous and feldspatic materials into illite, phengite or mica-like minerals.

The ferri-illites, glauconites and celadonites are also formed in two different environments: (1) neoformation in slightly oxidizing or slightly reducing marine sedimentary environments, and (2) hydrothermal alteration of oceanic basalts.

Illite forms as a result of alteration, at a given temperature, of an original material, which was previously deposited either at a higher or at a lower temperature. This material, therefore, reacts with a given solution at the temperature of illite formation. Thus, illite chemical composition should reflect the bulk chemical composition of the original material, the chemical composition of the solution and the temperature of formation. Two mechanisms for the illite formation by transformation or by neoformation have been classically proposed. The layer-by-layer transformation of smectites as suggested by Lucas (1962), Millot (1964), Dunoyer de Segonzac (1969, 1970a, b) and Hower et al. (1976) is a solid state transformation theory. It was successfully applied to the clay-rich sediments, such as shales for example, and has drawn the attention to the fact that smectites provide most of the chemical material required for the illite formation. The neoformation of filamentous diagenetic illite, precipitated from pore waters in sandstone reservoirs, was observed by Wilson and Pittman (1977) and by McHardy et al. (1982). The neoformation theory is now adopted by several authors, such as Lynch (1985), Nadeau et al. (1985) and Nadeau and Bain (1986), as the fundamental mechanism for illite formation even when smectites are abundant and when interstratified I/S are present as intermediate stages. Therefore, the term *conversion* of smectite to illite will be used instead of *transformation* which, for historical reasons, involves a solid state mechanism (Nadeau et al., 1985).

Conversion of smectites during compaction and diagenesis or low-grade metamorphism occurs along at least three geochemical and mineralogical pathways:

beidellites or montmorillonites → illites,
saponites or stevensites → corrensites or chlorites,
nontronites → glauconites or celadonites.

These conversions occur at different temperatures as discussed below.

In a recent paper, Chang and Mackenzie (1986) reviewed the conditions of clay diagenesis and compared the evolution of dioctahedral and trioctahedral smectites subjected to burial diagenesis. As temperature increases, dioctahedral smectites (beidellites or montmorillonites) convert into illites, whereas trioctahedral smectites (saponites or stevensites) convert into corrensite or chlorite.

The compositional changes accompanying the smectite-to-illite conversion as deduced from published chemical analyses, were summarized by Hower and Mowatt (1966), Garrels and Mackenzie (1974), Hower (1981), and Lynch (1985). The main chemical changes, with increasing number of illite layers, are a gain of interlayer potassium, increasing substitution of aluminum for silicon in the tetrahedral layer, loss of water, and losses of octahedral magnesium or iron (Dunoyer de Segonzac, 1970a, b).

The compositional changes accompanying the saponite-to-chlorite conversion are a loss of interlayer cations, increasing substitution of aluminum for silicon in tetrahedral layer, and an overall increase of the total iron and magnesium content, followed by a fixation of magnesium in the brucitic layer. Chang and Mackenzie (1986) concluded that the ordering of illite/smectite takes place within a temperature range of 90–115°C, whereas the ordering of chlorite/saponite (corrensite) occurs at a temperature of 60–70°C. These authors also showed that the two different conversions may occur in the same sediment, that is, in the same chemical environment.

Glauconite commonly forms in slightly compacted iron-bearing marine sediments at low temperature and during the earliest stage of diagenesis. In such environments, glauconite may form directly, but the dioctahedral iron-rich smectite (nontronite) may also convert into mixed-layered nontronite/glauconite (Lamboy, 1967; Porrenga, 1967; Giresse and Odin, 1973). The compositional changes accompanying these conversions result in a gain of aluminum substituting for tetrahedral silicon, and a loss of water (Burst, 1958; Thompson and Hower, 1975).

Celadonite is commonly found in vesicular cavities, formed during the hydrothermal alteration of basalts. Volcanic clastic rocks upon diagenetic alteration or low-grade metamorphism (zeolite facies) often develop celadonite-bearing assemblages (Wise and Eugster, 1964; Weaver and Pollard, 1975). In the iron-bearing series, celadonites tend to form at higher temperatures and glauconite at lower.

Trioctahedral illites were described by Walker (1950) and by Weiss et al. (1956), but they are very rare minerals and do not form commonly in nature. This is probably because the trioctahedral Mg-illite would be stable at a temperature higher than the

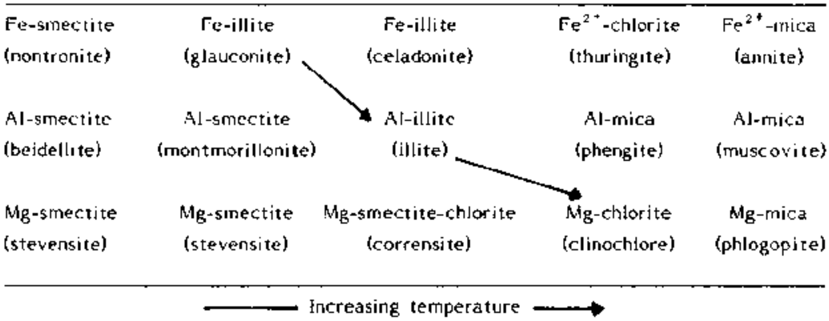

Fe-smectite (nontronite)	Fe-illite (glauconite)	Fe-illite (celadonite)	Fe^{2+}-chlorite (thuringite)	Fe^{2+}-mica (annite)
Al-smectite (beidellite)	Al-smectite (montmorillonite)	Al-illite (illite)	Al-mica (phengite)	Al-mica (muscovite)
Mg-smectite (stevensite)	Mg-smectite (stevensite)	Mg-smectite-chlorite (corrensite)	Mg-chlorite (clinochlore)	Mg-mica (phlogopite)

Fig. 5-3. Schematic evolution of the smectites, chlorites and micas as a function of temperature.

one required to form a Mg-chlorite phase: phlogopite, the magnesian mica, may form at very high temperatures. During the burial diagenesis of a Mg-rich sedimentary facies, an increase in temperature and pressure will act in favor of the conversion of stevensite into corrensite and chlorite and not into the trioctahedral illites, which are generally absent (Fig. 5-3).

It can be concluded that in environments which differ in their chemistry, the temperature of illite formation increases from iron-rich, to aluminum-rich, to magnesium-rich environments. Iron-rich illite (glauconite) forms at very low temperature (room temperature). Magnesium-rich trioctahedral illite should form at a temperature so high that chlorite forms before. Magnesium-rich illite is not found in nature.

Fe-illite	Al-illite	Mg-illite
(glauconite)	(illite)	(trioctahedral illite)

—— *temperature increase* ⟶

The micaceous minerals, such as mixed-layer illite–smectite, illite, and celadonite, and the chloritic minerals such as corrensite or chlorite, form at elevated temperature and pressure. The trioctahedral Mg-rich illite would form at even higher temperature, but appears near the surface of the Earth. It is less stable than chlorite. Glauconite is the unique mica that forms directly at low temperature and pressure.

The temperature of mica formation is the lowest for the iron-bearing mineral sequence, intermediate for the aluminous series, and the highest for the Mg-rich minerals.

Many recent studies have been devoted to the problems of the conditions of formation of clay minerals and to their stability in natural environments. Solutions to these problems, however, are not yet satisfactory and the conclusions generally turn around the same questions: (1) did the clay minerals form in near-equilibrium conditions, (2) do the thermodynamic principles apply to clay minerals? The answer to these two questions may be yes, but only if one admits that their mineralogical and chemical compositions reflect the macro- or the micro-environments of their formation or the temperature at which they equilibrate. However, the procedure of experimental measurements, the way to investigate the extreme imbrication of natural systems or microsystems, and the appropriate thermodynamic approach to treat the natural complexity (previously supposed to have been understood) have not yet been clearly defined.

In the particular case of the smectite/illite layers, thermodynamics seem to be so difficult to apply, that many researchers are inclined to believe that equilibrium cannot truly exist in clay mineral systems.

SMECTITE/ILLITE MIXED LAYERS CONSIDERED AS TWO SEPARATE SMECTITE AND ILLITE PHASES

One of the most interesting and debated questions regarding stabilities of clay minerals concerns the transformation of smectites into illites through the intermediate stages of mixed-layers illite/smectite, occurring in the course of the sediment burial diagenesis. The question was initiated by Zen (1972), discussed by Lippmann (1979b) and clearly rediscussed by Garrels (1984) as follows: should the mixed-layers smectite/illite be considered as single phases or as mixtures of two separate phases, i.e., illite and smectite?

It is commonly accepted that illite/smectite interlayered particles are composed of two discrete species:(1) montmorillonite with low interlayer charge, and (2) illite with high interlayer charge. The illite layers are formed by diagenetic alteration of original montmorillonite layers. The conversion of a single isolated montmorillonite layer to an illite layer would clearly be a phase change, because there are marked structural differences between them. The question arises, however, as to whether, in an intimate mixture, there are enough interactions between the constituent phases so that their properties may be modified. Two types of recently reported results may suggest that mixed-layers are not continuous solid-solutions, but mixtures of two separate phases.

Physical mixtures of smectite and illite particles

In a series of papers, McHardy et al. (1982), Nadeau et al. (1984a, b, c), Nadeau (1985), and Wilson and Nadeau (1985) have apparently resolved the question of the interaction between particles of different nature, within interstratified clay minerals of different types. Transmission electron microscopic (TEM) examination of the <0.1 μm fractions of different smectites and interstratified smectite/illite show that these clays, when dried from suspension, consist primarily of both 10 Å and 20 Å thick particles, respectively (one or two individual layers). The X-ray diffraction (XRD) examination of sedimented aggregates of such smectite or mixed-layer clays, on the other hand, indicate that the effective number of coherently diffracting unit cells is systematically higher. The authors reconcile this discrepancy by postulating interparticle diffraction effects from the sedimented aggregates of oriented particles and conclude that standard XRD data from sedimented aggregates may not be able to distinguish between true interstratification and interparticle diffraction effects of intimate physical mixtures. As a consequence of this postulate, the naturally occurring smectite/illite or chlorite/illite mixed-layers may be physical mixtures of

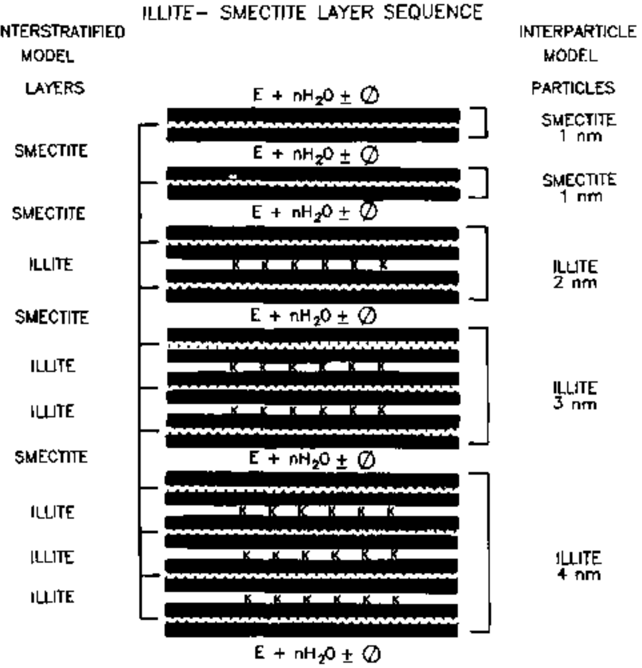

Fig. 5-4. Diagrammatic representation of illite particles cross-section. (From Nadeau and Bain, 1986, fig. 1, p. 456.)

thin particles, which exhibit interparticle, intra-aggregate diffraction phenomena. Large particles are almost always aggregates of smaller particles and yield rotational turbostratic electron diffraction patterns rather than single crystal patterns (Fig. 5-4).

Montmorillonite/illite stability diagrams

The second argument in favor of the two independent phase systems is provided by Garrels (1984). There are two different ways to consider the montmorillonite/illite stability changes during diagenesis: either (1) smectite and illite constitute one solid-solution phase of variable composition, as proposed by Aagaard and Helgeson (1983), or (2) smectite and illite are two discrete separate phases. The solution compositions shown on Fig. 5-5 fit the two-phase systems better than they fit a solid-solution model. Aagaard and Helgeson (1983) stated that no compositions are available in the literature for waters that are known to coexist with illite. Garrels (1984) considered that data on coexisting aqueous solutions apparently are more nearly consistent with the interpretations of Nadeau et al. (1984c), stating that in smectite/illite mixed-layers the two mineral species can be considered as two separate phases.

Nadeau et al. (1984c) concluded that "randomly interstratified smectite/illite would be composed of populations of illite and smectite particles. During diagenesis, smectite particles become unstable and dissolve, while illite particles are neoformed.

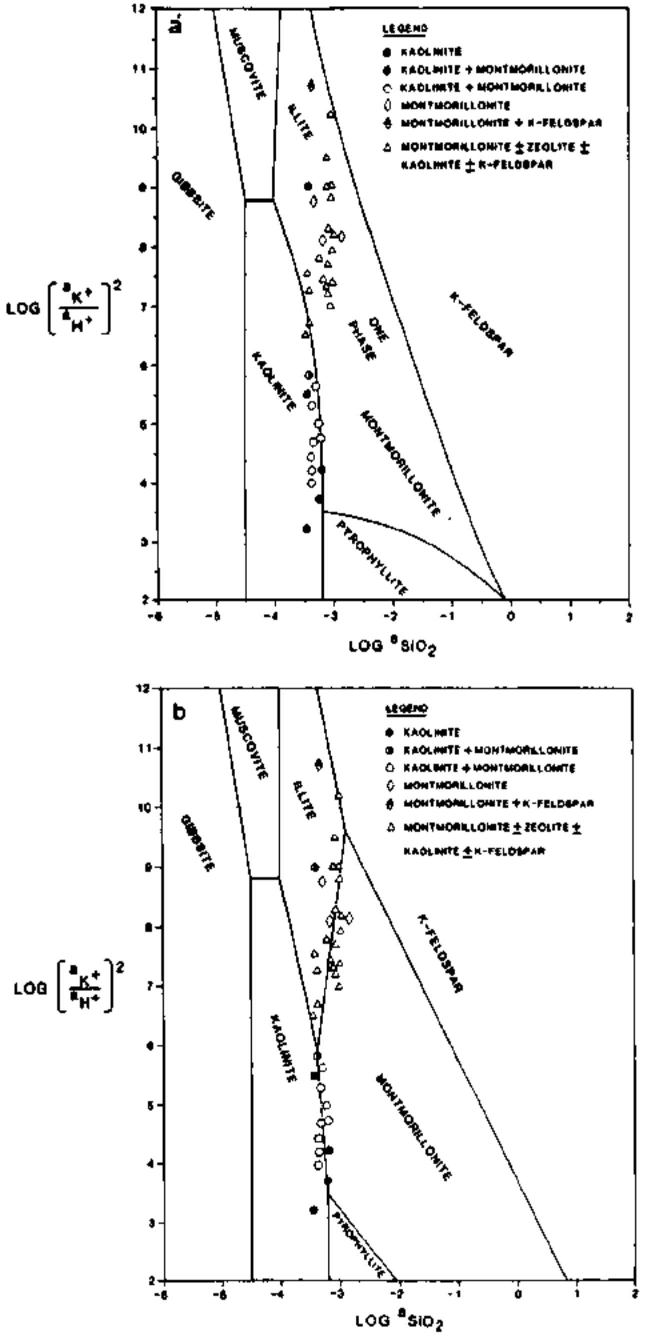

Fig. 5-5. Ion activity diagrams illustrating the relations to be expected if montmorillonite and illite behave (a) as a solid-solution, or (b) as two discrete phases. (From Garrels, 1984, figs. 3 and 4, p. 164.)

As diagenesis continues, the thickness of the fundamental illite particle increases within the population. When the particles become sufficiently thick to produce diffraction maxima with 10 Å series, the clay material is identified by XRD as conventional illite."

Although these conclusions are fairly convincing, it seems that there are still some points, i.e., energetic relationships between smectite and illite layers, which may be subject to discussion.

INTERLAYER ENERGIES

Among the two types of elementary 10 Å layers, only the illitic layers are capable to organize into particles of different thickness (20 Å, 30 Å, 40 Å and 50 Å, for example), whereas the smectite elementary layers are only present as particles having thickness of about 10 Å. In the model of Nadeau and his coworkers, the illitic layers are strongly organized in a face-to-face system, involving important interlayer energies. On the other hand, in a face-to-face system of two elementary smectitic layers (or between smectite and illite layers), the ordering is poor, the arrangement is turbostratic, and the resulting interlayer energy may be low or at least negligible compared to the total energy of illite.

The turbostratic disordering due to the rotation or to the displacement of the individual layers, is a general phenomenon within the smectite group and is understood as a necessity for two layers to adapt and to fit the structure of the hydration water in the interlayers (Mering and Oberlin, 1967, 1971). The existence of some turbostratic disordering among the smectite layers does not necessarily mean that the energy of attraction between two adjacent layers is very low. Neither does it mean that there is no energetic binding between two individual layers of smectite, or between the smectitic and the illitic layers separated by an interlayer of hydrated ions.

The existence of individual particles of illite of various thickness as a function of the temperature during diagenesis, perhaps may not definitely prove (1) that no energetic relationships exist between illite and smectite individual particles, and (2) that a particle-scale solid-solution concept may not explain the chemical correlations observed within clay particle populations, as discussed in the next section.

STABILITY OF MONOMINERALIC CLAY PARTICLE POPULATIONS

What is called a pure clay mineral phase generally appears to be a population of individual clay particles of different chemical compositions. This is true for vermiculites (Ildefonse et al., 1979), for talcs (Noack and Duplay, 1983), for smectites and illites (Duplay, 1982, 1984; Paquet et al., 1981, 1983; Tardy et al., 1981; Duplay et al., 1986), and for many kinds of clay minerals encountered in nature, as clearly shown in many recently published papers. The range of chemical compositions may be considerable as demonstrated, for example, by Nahon et al. (1982) for a nontronite, in which the number of octahedral atoms of Fe^{3+} and Mg^{2+} may,

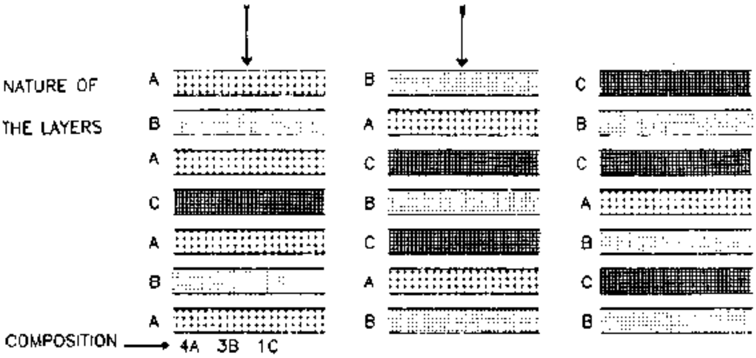

Fig. 5-6. Schematic representation of particle microprobe chemical analysis. The differences in compositions are due to the various possibilities to stack and arrange individual layers of specific compositions.

respectively, vary from 0.5 to 1.2 and 0.7 to 1.7, whereas the tetrahedral aluminum may change from 0.1 to 0.6 (per 22 negative charges in the formula). Then, if one recognizes that the solubility product of a clay mineral is significantly dependent on its chemical composition, the question which arises is to decide whether or not such a population can present a precisely delineated field of stability. In other words, can the stability field of a given clay population, apparently monomineralic, be evaluated from the calculated solubility product of the average chemical composition of such a population made of millions of individual particles covering a large range of chemical formulas? This is not only particularly true for smectites, but also for illites and interstratified illite–smectites.

Within an apparently monomineralic population of particles, chemical microprobe analyses of individual particles are performed perpendicularly to the layer surfaces (Fig. 5-6). The diversity of the particle chemical compositions depends on the variety of the individual layers, which are stacked and perhaps organized as random interstratified layers. Correlations among chemical variables allow one to reconstitute the composition of the individual end-members and to speculate on their temperature of formation.

The alteration of basalts generally yields a series of clay minerals formed at the same place, in the same chemical environment, but at different temperatures. The first stages may be typically hydrothermal, whereas the last ones may be formed at low temperature after the cooling of the basalts and the circulating fluids. A large number of examples are given in the literature.

The first example presented here concerns a celadonite found in the small cavities of the upper Cretaceous basalt in the Troodos Massif of Cyprus and described by Duplay et al. (1986). The chemical formula, calculated from the bulk analysis of 100 mg of separated material, is characteristic of a typical celadonite, as defined by Buckley et al. (1978), Wiewiora et al. (1979), Köster (1982), Bailey et al. (1984), Bailey (1985), and AIPEA Nomenclature Committee:

TABLE 5-5

Extreme compositions in the particle population of the Cyprus celadonite

(1) $Ca_{0.00}K_{1.00}(Al_{0.28}Fe^{3+}_{0.75}Mg^{2+}_{0.955})(Al_{0.00}Si_{4.00})O_{10}(OH)_2$
(2) $Ca_{0.002}K_{0.88}(Al_{0.017}Fe^{3+}_{1.210}Mg^{2+}_{0.920})(Al_{0.405}Si_{3.595})O_{10}(OH)_2$
(3) $Ca_{0.12}K_{0.67}(Al_{0.10}Fe^{3+}_{0.79}Mg^{2+}_{1.31})(Al_{0.19}Si_{3.81})O_{10}(OH)_2$
(4) $Ca_{0.00}K_{0.78}(Al_{0.40}Fe^{3+}_{0.88}Mg^{2+}_{0.74})(Al_{0.10}Si_{3.90})O_{10}(OH)_2$

TABLE 5-6

Average composition of celadonites (1) and glauconites (2) within the particle population of the Cyprus celadonite

(1) $Ca_{0.04}K_{0.835}(Al_{0.275}Fe^{3+}_{0.800}Mg_{0.980})(Al_{0.10}Si_{3.90})O_{10}(OH)_2$
(2) $Ca_{0.02}K_{0.840}(Al_{0.14}Fe^{3+}_{1.00}Mg_{0.985})(Al_{0.22}Fe_{0.05}Si_{3.73})O_{10}(OH)_2$

$$Ca_{0.01}K_{0.82}(Al_{0.27}Fe^{3+}_{0.89}Fe^{2+}_{0.12}Mg_{0.72})(Al_{0.02}Si_{3.98})O_{10}(OH)_2$$

A fraction of the powder was examined by TEM and microprobe, and 42 individual particles were analyzed by the method of Duplay (1984). Selected data, shown in Table 5-5, indicate that particle compositions range from a true magnesian celadonite (1) to a true glauconite (2); some intermediate compositions mark some slight tendencies towards trioctahedral (3) or dioctahedral (4) K-vermiculite, K-saponite, or K-montmorillonite.

Correlation diagrams (Fig. 5-7) show two clearly identified populations. Both have about the same layer charge and the same Mg content (Table 5-6), but celadonite (1), characterized by a low tetrahedral and a high octahedral charge, contains less octahedral aluminum and less octahedral iron than glauconite (2). Furthermore, glauconite (2) is characterized by higher tetrahedral and lower octahedral charges than in celadonite.

The second example presented here concerns a celadonite and three smectites formed during the hydrothermal alteration of basalts under submarine conditions, collected in the Reykjanes Ridge (SW Iceland, DSDP Leg 49, hole 407) (celadonite 2V, saponite 2V, nontronite 2R, nontronite K2) or within the hydrothermal mounts of Galapagos (DSDP Leg 70, hole 506, section 2) (nontronite V2). Three of these minerals have been formed under hydrothermal conditions, whereas the nontronite K2 seems to have been formed at low temperature (Duplay, 1989) (Table 5-7).

In each of these samples, about fifteen particles were analyzed. The correlation coefficients between the three types of charges, [tetrahedral negative charge (CHT), octahedral negative charge (CHO), and total layer charge (CHF)] and the amounts of octahedral cations (Fe, Al, Mg) were calculated and are given in Table 5-8. Two groups of correlation appear, depending on the estimated temperature of mineral formation (low and hydrothermal temperatures) (Table 5-9, Fig. 5-8). The following conclusion can be drawn in the framework of a solid-solution theory as already described by Fritz (1981, 1985), Tardy et al. (1981) and Duplay (1982):

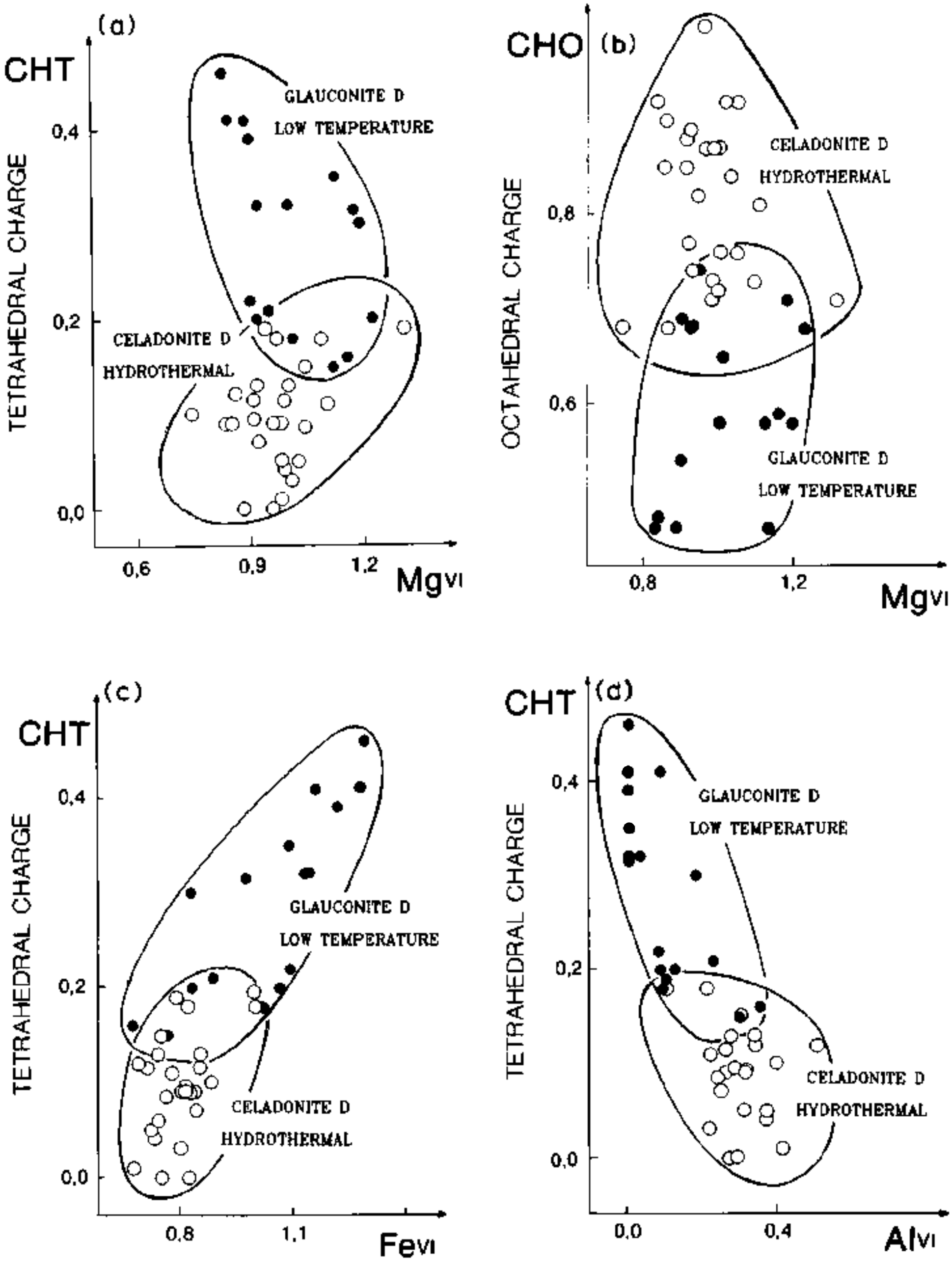

Fig. 5-7. Correlation diagrams: (a) between tetrahedral charge (CHT) and octahedral magnesium (Mg^{VI}), (b) octahedral charge (CHO) and octahedral magnesium (Mg^{VI}), (c) tetrahedral charge (CHT) and octahedral iron (Fe^{VI}), (d) tetrahedral charge and octahedral aluminium (Al^{VI}), for a low-temperature glauconite (D) and an hydrothermal celadonite (D) (open circles) from an altered basalt of the Troodos Massif (solid circles) of Cyprus.

TABLE 5-7

Chemical formulas of a hydrothermal celadonite (1), a low-temperature glauconite (2), a hydrothermal nontronite (3) and a low-temperature nontronite (4)

(1) Celadonite 2V	$Ca_{0.008}K_{0.770}(Al_{0.10}Fe^{3+}_{1.135}Mg_{0.785})(Al_{0.06}Si_{3.94})O_{10}(OH)_2$
(2) Glauconite D	$Ca_{0.020}K_{0.850}(Al_{0.10}Fe^{3+}_{1.030}Mg_{1.010})(Al_{0.22}Fe_{0.05}Si_{3.71})O_{10}(OH)_2$
(3) Nontronite V2	$Ca_{0.007}K_{0.345}(Al_{0.315}Fe^{3+}_{1.235}Mg_{0.585})(Al_{0.18}Si_{3.82})O_{10}(OH)_2$
(4) Nontronite K2	$Ca_{0.02}K_{0.54}(Al_{0.11}Fe^{3+}_{1.555}Mg_{0.30})(Al_{0.205}Si_{3.795})O_{10}(OH)_2$

TABLE 5-8

Correlation coefficients between the type of charge [tetrahedral charge (CHT), octahedral charge (CHO), and total layer (CHF)] and the content of octahedral cations (Fe, Al, or Mg) within particle populations of an hydrothermal celadonite (2V), an hydrothermal nontronite (V2), a low-temperature glauconite (D) and a low-temperature nontronite (K2)

	Celadonite 2V	Glauconite D	Nontronite V2	Nontronite K2
Tetrahedral charge				
CHT-Fe	−0.41	+0.80	−0.57	+0.57
CHT-Al	−0.59	−0.72	+0.28	−0.31
CHT-Mg	+0.76	−0.49	+0.77	−0.50
Octahedral charge				
CHO-Fe	+0.92	−0.44	+0.40	0.00
CHO-Al	−0.20	+0.25	−0.34	−0.37
CHO-Mg	−0.96	+0.24	−0.62	+0.22
Layer charge				
CHF-Fe	+0.89	+0.50	+0.26	+0.54
CHF-Al	−0.75	−0.61	−0.47	−0.74
CHF-Mg	−0.67	−0.37	−0.34	0.00

(1) At low temperatures, the tetrahedral charge (CHT) is well correlated with octahedral iron $(Fe^{3+})^{VI}$. This can be called the glauconite effect, which may correspond to an important contribution of the ferri-muscovite end-member to the solid-solution.

(2) At low temperatures, layer charge (CHF) is negatively correlated with the octahedral aluminum $(Al^{3+})^{VI}$ and to a lesser extend with octahedral magnesium (Mg^{VI}). This can be called the pyrophyllite and the talc effects, which may correspond to important contributions of such end-members to the presumed solid-solutions.

(3) At low temperatures, octahedral charge (CHO) is not very well correlated with the contents of any of the octahedral ions. It seems, however, that the Fe^{3+}-celadonite $[K(Fe^{3+}_{1.667})(Si_4)O_{10}(OH)_2]$ is the less important celadonite end-member. On the other hand, the Mg-celadonite $[K(Mg_{2.5})(Si_4)O_{10}(OH)_2]$ or the Al-celadonite $[K(Al_{1.667})(Si_4)O_{10}(OH)_2]$ end-members may compete for the octahedral charge.

(4) At higher temperatures, the tetrahedral charge (CHT) is correlated with octahedral magnesium $(Mg^{2+})^{VI}$. This can be called the phlogopite effect, which

TABLE 5-9

Correlation between the type of charge [tetrahedral charge (CHT), octahedral charge (CHO), and total layer (CHF)] and the content of octahedral cations (Fe, Al, or Mg) in low-temperature and hydrothermal iron-rich clay mineral populations

Low-temperature clay mineral population	Hydrothermal clay mineral population
The higher the octahedral iron $(Fe^{3+})^{VI}$,	*The higher the octahedral iron* $(Fe^{3+})^{VI}$,
the higher the tetrahedral charge	the lower the tetrahedral charge
the lower the octahedral charge	the higher the octahedral charge
the higher the total layer charge	the higher the total layer charge
The higher the octahedral aluminum $(Al^{3+})^{VI}$,	*The higher the octahedral aluminum* $(Al^{3+})^{VI}$,
the lower the tetrahedral charge	the lower the tetrahedral charge
the higher the octahedral charge	the lower the octahedral charge
the higher the total layer charge	the lower the total layer charge
The higher the octahedral magnesium $(Mg^{2+})^{VI}$,	*The higher the octahedral magnesium* $(Mg^{2+})^{VI}$,
the lower the tetrahedral charge	the higher the tetrahedral charge
the lower the octahedral charge	the lower the octahedral charge
the lower the total layer charge	the lower the total layer charge

may correspond to an important contribution of the $[K(Mg_3)(AlSi_3)O_{10}(OH)_2]$ end-member to the supposed solid-solution.

(5) At high temperature, layer charge (CHF) is negatively correlated with octahedral aluminum $(Al^{3+})^{VI}$ and almost equally to octahedral magnesium $(Mg^{2+})^{VI}$. This can be due to a similar, but important, contribution of the pyrophyllite $[Al_2Si_4O_{10}(OH)_2]$ and of the talc $[Mg_3Si_4O_{10}(OH)_2]$ end-members for lowering the layer charge. By contrast, the octahedral iron $(Fe^{3+})^{VI}$ tends to act in favor of an increase of the total layer charge.

(6) At high temperatures, octahedral charge (CHO) is mostly due to iron content $(Fe^{3+})^{VI}$, only partly due to octahedral aluminum content $(Al^{3+})^{VI}$, but not at all due to octahedral magnesium $(Mg^{2+})^{VI}$.

Then, in these series of minerals the same considerations can be presented differently.

(1) Octahedral iron $(Fe^{3+})^{VI}$ seems above all to be introduced as $[KFe_2^{3+}AlSi_3O_{10}(OH)_2]$ at higher temperatures, whereas the weight of $[Fe_2^{3+}Si_4O_{10}(OH)_2]$ as end-member is low in all cases.

(2) Octahedral aluminum $(Al^{3+})^{VI}$ at any temperature seems to be introduced more as $[Al_2Si_4O_{10}(OH)_2]$ than as $[KAl_{1.667}Si_4O_{10}(OH)_2]$, and to a lesser extent as the muscovite $[KAl_2Si_3O_{10}(OH)_2]$ end-member.

(3) Octahedral magnesium $(Mg^{2+})^{VI}$ seems to be better explained by the talc $[(Mg_3Si_4O_{10}(OH)_2]$ than by the phlogopite end-member $[KMg_3AlSi_3O_{10}(OH)_2]$ at low temperatures, whereas the situation is reverse at high temperatures. In both cases, but especially at high temperatures, the Mg-celadonite end-member contribution is relatively small.

These observations seem to support the idea that clay minerals are not physical

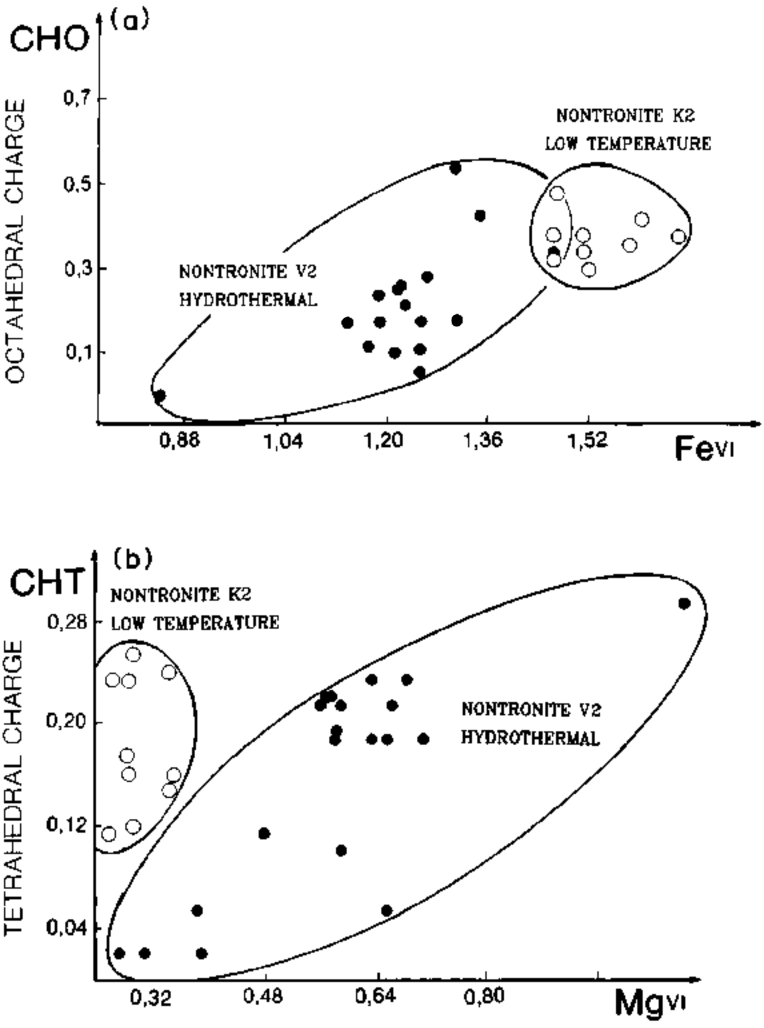

Fig. 5-8. Correlation diagrams: (a) between octahedral charge (CHO) and octahedral iron (Fe^{VI}), (b) tetrahedral charge (CHT) and octahedral magnesium (Mg^{VI}), for a low-temperature nontronite (K2) (Reykjanes Ridge, Iceland) and an hydrothermal nontronite (V2) (Galapagos), in altered submarine basalts. CHO and CHT stand, respectively, for octahedral and tetrahedral charges.

mixtures, in various proportions, of separate phases of discrete compositions which coexist independently. The temperature dependence of the solubility products of the end-members and the temperature dependence of the weight of each of these defined end-members within clay mineral populations indicate clearly that some thermodynamic relationships may exist to regulate these highly complex systems. Within a given population, the extreme diversity of the clay particle compositions, however, indicates also that any overall equilibrium could not at all have been attained and suggests that equilibria may have been reached only locally in a large variety of aqueous microsystems.

IDEAL SOLID-SOLUTION MODEL OF A LARGE NUMBER OF END-MEMBERS

The tests of equilibrium in clay mineral systems may be performed only if the variety and the complexity of clay mineral compositions are taken into consideration.

Clay minerals and especially smectites and illites always have a large number of sites and cation substitutions. The interlayer sites may be occupied by Na^+, K^+, Mg^{2+}, and Ca^{2+} at different hydration stages as functions of temperature, solution salinity, and degree of compaction of the sediment. The interlayer charge is balanced by variable tetrahedral and octahedral charge deficiencies. The octahedral sites may be occupied by at least four different cations: Fe^{3+}, Al^{3+}, Fe^{2+}, and Mg^{2+}. Then the number of individual components, which define a clay mineral composition and determine — if admitted — clay mineral stability, is very high:

(a) 4 pyrophyllite–talc components,

(b) 4 muscovite–phlogopite components, with 4 possible interlayer cations, and

(c) 4 celadonite components, with 4 possible interlayer cations.

The number of possible end-members, therefore, ranges between 12, if only potassium mica components are involved, and 36, if the four interlayer cations (Na^+, K^+, Mg^{2+}, and Ca^{2+}) are taken into consideration (for the mica and celadonite components).

Thermodynamics of equilibrium between multicomponent solid-solutions and aqueous solution is extremely complex and a general model is not yet entirely available. The solubility products of many end-members (celadonites, for example) are not known. Data for the mixing energies of several cations in different structural sites are not available. Measured Gibbs free-energy changes as functions of crystallinity and grain size are also not available.

Despite these intrinsic difficulties, it seems interesting to explore what conditions clay minerals would have to satisfy in order to form solid-solutions of a large number of end-members. Truesdell and Christ (1968) and Stoessel (1979, 1981) adopted regular solid-solution models to calculate the thermodynamic consequences of compositional variation in montmorillonites and illites. Helgeson and Mackenzie (1970) have adopted an ideal solid-solution model, whereas Aagaard and Helgeson (1983) proposed an ideal mixing of atoms on homological sites in montmorillonites and illites. All of these models have been applied to a rather small number of components and, for that reason, fail to simulate the reality (see Merino and Ransom, 1982). In contrast, and for a very large number of end-members, Fritz (1981, 1985) and Tardy and Fritz (1981) proposed an ideal multicomponent mixing model which simulates the variability of clay mineral compositions as they appear in nature.

In this model, it is supposed that end-members can mix ideally either among the different sites of individual layers or among the different layers of individual particles. If one believes, for example, that dioctahedral and trioctahedral end-members cannot mix ideally and in all proportions, at a molecular scale, one may admit that they can be interlayered and mixed at a scale to form particles without involving large interlayer energies.

The equilibrium condition between a solid-solution and an aqueous solution is described by the Mass Action Law applied to each of the j end-members which contribute to the solid-solution (Fritz, 1981, 1985). For each of the j end-members, one has:

$$K_j = (Q_j/A_j) = (Q_j/X_j\lambda_j)$$

where K_j = the solubility product, Q_j = the corresponding ion activity product in solution, λ_j = the activity coefficient, X_j = the mole fraction, and A_j = the activity of the jth end-member, in the solid-solution.

On considering, for example, a simplified illite or smectite formula with no octahedral charge, the interlayer being saturated with only one cation (K^+):

$$nK_x(Al_{2-y-0.67z}Fe^{3+}_yMg_z)(Al_xSi_{4-x})O_{10}(OH)_2$$

This formula is obtained by combining two sites of substitution (one tetrahedral and one octahedral site). Six end-members define this solid-solution:

3 micas	muscovite:	$K(Al_2)(Si_3Al)O_{10}(OH)_2$
	Fe^{3+}-muscovite:	$K(Fe_2)(Si_3Al)O_{10}(OH)_2$
	phlogopite:	$K(Mg_3)(Si_3Al)O_{10}(OH)_2$
3 pyrophyllites	pyrophyllite:	$(Al_2)(Si_4)O_{10}(OH)_2$
	Fe^{3+}-pyrophyllite:	$(Fe_2)(Si_4)O_{10}(OH)_2$
	talc:	$(Mg_3)(Si_4)O_{10}(OH)_2$

Solid-solution composition is completely defined by only three variables (x, y, z) for the quantity of solid-solutions defined by one additional variable n (n = number of moles of solid-solution per kilogram of water). Thus, one needs 4 relationships between the solid-solution phase and the aqueous phase in order to define both the amount and chemical composition of the clay solid-solution in equilibrium with a given aqueous solution, for any geochemical process.

The relationships required depend on the type of solid-solution involved. For a simple pure mineral, the equilibrium condition is written by using only one equation, which is the classical Mass Action Law equation. This condition allows to calculate the unique unknown, which defines completely the solid phase, that is, the quantity (n) of solid phase in equilibrium with the aqueous solution (one unknown, one equation per pure phase).

For a binary solid-solution, the Mass Action Law is applied for two end-members. This allows to calculate the two unknowns: the total amount of solid-solution (n) and one substitution or composition parameter (x), which corresponds to the mole fraction X_1 or X_2 of one of the two end-members. The second mole fraction is calculated from the relation $X_1 + X_2 = 1$.

If one considers now a generalized multipole solid-solution, the problem becomes much more complex. There are two types of possible generalization: (1) a solid-solution of j end-members due to only one type of substitution; and (2) the general case involving several types of substitutions, which is the case for real clay minerals such a smectites, illites and chlorites.

The first case (one type of site or substitution) is only an extension of the binary solid-solution to j end-members, with j Mass Action Law equations (one per theoretical end-member). The unknowns are (n) and ($j - 1$) substitution or composition parameters: x, y, $z\ldots$ which correspond also to ($j - 1$) mole fraction X_j, the last being defined by the rule of conservation ($\sum X_j = 1$). In that case, the number of independent unknowns is equal to the number of end-members.

The general case (two or more types of sites or substitutions) is characterized by linked relations among the solid-solution parameters (K_j, X_j), as shown by Fritz (1981). It can be summarized, as follows: for the illite formula given above and formed by the mixing of 6 end-members. The corresponding aqueous ionic activity products Q_j obey the following interrelations:

$$\frac{[\mathrm{Al}^{3+}]^2}{[\mathrm{Fe}^{3+}]^2} = \frac{Q(\text{Al-pyrophyllite})}{Q(\text{Fe-pyrophyllite})} = \frac{Q(\text{Al-muscovite})}{Q(\text{Fe-muscovite})}$$

$$\frac{[\mathrm{Al}^{3+}]^2}{[\mathrm{Mg}^{2+}]^3} = \frac{Q(\text{Al-pyrophyllite})}{Q(\text{talc})} = \frac{Q(\text{Al-muscovite})}{Q(\text{phlogopite})}$$

They correspond to relations between solubility products and mole fractions of the end-members in the solid-solution, in accordance with the Mass Action Law (Tardy and Fritz, 1981). For each end-member j:

$$Q_j = K_j X_j \lambda_j \tag{1}$$

or for an ideal solid-solution ($\lambda_j = 1$):

$$Q_j = K_j X_j \tag{2}$$

Thus it follows:

$$\frac{X(\text{Al-pyrophyllite})\,K(\text{Al-pyrophyllite})}{X(\text{Fe-pyrophyllite})\,K(\text{Fe-pyrophyllite})} = \frac{X(\text{Al-muscovite})\,K(\text{Al-muscovite})}{X(\text{Fe-muscovite})\,K(\text{Fe-muscovite})}$$

and

$$\frac{X(\text{Al-pyrophyllite})\,K(\text{Al-pyrophyllite})}{X(\text{talc})\,K(\text{talc})} = \frac{X(\text{Al-muscovite})\,K(\text{Al-muscovite})}{X(\text{phlogopite})\,K(\text{phlogopite})}$$

These Mass Action Law relations are linked by relationships (1) and (2) among K_j and X_j values, whatever the chemistry of the aqueous solution in equilibrium could be. Finally, for the example chosen, the seven apparent unknowns ($6X_j$ plus n) are linked by two relations due to the Mass Action Law and one conservative relation ($\sum X_j = 1$). Thus, four independent unknowns and four independent equations remain. The resolution of the system gives the total number of moles of solid-solution (n) and three composition parameters (x, y, z) if the solution chemistry is known (Q_j and, consequently, X_j). On the contrary, if the composition of the clay is known (n, x, y, z), the mole fraction distribution for the solid-solution (X_j)

and the ion-activity products (Q_j) in the solution can be calculated and estimated, respectively.

In conclusion, one may notice that, in an ideal model, the contribution of each end-member to the solid-solution phase (X_j) is directly proportional to the saturation index of the end-member in the aqueous solution ($X_j = Q_j/K_j$). Considering a given aqueous solution chemistry (Q_j = constant), therefore, the contribution of an end-member is taken inversely proportional to its selected solubility product: the lower the solubility product of an end-member (the higher its stability) the higher its contribution to the solid-solution.

CONTRIBUTION OF DIFFERENT END-MEMBERS DEPENDING ON TEMPERATURE AND CHEMICAL COMPOSITION

Recently, the solubility product of the clay mineral end-member have been refined in order to allow simulations of clay mineral formation during weathering, diagenesis, and hydrothermal alteration. In such research, one tends to model real chemical compositions and distribution of charges of clay minerals as they appear in natural conditions (Fritz, 1981; Tardy and Fritz, 1981; Tardy, 1982).

The solubility products of eight clay mineral end-members are given in Table 5-10 (Fritz, 1981). They do not correspond to the values of the pyrophyllite or muscovite solubility products, but to clay mineral end-members having the chemical composition of pyrophyllite or muscovite. These values are used to estimate the

TABLE 5-10

Solubility products of some clay mineral endmembers as a function of temperature (after Fritz, 1981; Duplay, 1989)

Mineral formula	Logarithm of solubility products (log K_{sp})			
	0°C	25°C	100°C	200°C
Pyrophyllite–talc				
$Al_2Si_4O_{10}(OH)_2$	2.613	1.061	2.801	−6.116
$Fe_2Si_4O_{10}(OH)_2$	−13.162	−13.700	−15.459	−17.126
$Fe_3Si_4O_{10}(OH)_2$	8.894	7.235	3.118	−0.141
$Mg_3Si_4O_{10}(OH)_2$	27.671	25.162	19.063	14.030
Mica				
$KAl_2AlSi_3O_{10}(OH)_2$	20.361	16.656	8.459	1.777
$KFe_2AlSi_3O_{10}(OH)_2$	4.321	1.088	−4.542	−9.187
$KFe_3AlSi_3O_{10}(OH)_2$	27.309	23.373	14.324	7.282
$KMg_3AlSi_3O_{10}(OH)_2$	46.907	41.91	30.749	21.736
Celadonites				
$KAl_{1.667}Si_4O_{10}(OH)_2$	7.907	6.345	0.681	−4.128
$KFe^{3+}_{1.667}Si_4O_{10}(OH)_2$	−6.169	−6.956	−11.087	−14.803
$KFe^{2+}_{2.5}Si_4O_{10}(OH)_2$	13.392	11.740	5.860	1.101
$KMg_{2.5}Si_4O_{10}(OH)_2$	29.289	26.929	19.401	13.160

temperature and the composition dependence of the smectite-to-illite conversion.

Fe^{3+}-, Al^{3+}-, Fe^{2+}-, or Mg^{2+}-smectites are represented here, respectively, by clay minerals with the composition of Fe^{3+}-pyrophyllite, pyrophyllite, minnesotaite and talc.

Fe^{3+}-, Al^{3+}-, Fe^{2+}-, or Mg^{2+}-illites are represented here, respectively, by clay minerals having the composition of Fe^{3+}-muscovite, muscovite, annite, and phlogopite.

One may consider, for example, the equilibrium of talc and phlogopite:

$$\underset{\text{(talc)}}{Mg_3Si_4O_{10}(OH)_2} + K^+ + Al^{3+} + 2H_2O = \underset{\text{(phlogopite)}}{KMg_3AlSi_3O_{10}(OH)_2} + 4H^+ + SiO_2$$

and, more generally, the equilibrium of an $(Y)Si_4O_{10}(OH)_2$ end-member with the corresponding $K(Y)AlSi_3O_{10}(OH)_2$ mica is as follows:

$$(Y)Si_4O_{10}(OH)_2 + K^+ + Al^{3+} + 2H_2O = K(Y)AlSi_3O_{10}(OH)_2 + 4H^+ + SiO_2$$

where (Y) may represent Fe_2^{3+}, Al_2^{3+}, or Mg_3^{2+}.

If $\log K_R$, is the difference between the $\log K_{sp}$, i.e., the solubility product of the micaceous end-member and the solubility product of the corresponding pyrophyllite–talc-like end-member, then:

$$\log K_R = \log K_{sp}[K(Y)AlSi_3O_{10}(OH)_2] - \log K_{sp}[(Y)Si_4O_{10}(OH)_2]$$

The data of Table 5-11 were calculated from the $\log K_{sp}$ in Table 5-5 (Fritz, 1981). They are shown in Fig. 5-9 and Table 5-10.

It appears that:

(1) $\log K_R$ increases from the ferric (Fe^{3+}) to the aluminous (Al^{3+}), to the ferrous (Fe^{2+}) and, finally, to the magnesian (Mg^{2+}) series both at 25°C and at 200°C;

(2) the difference between the $\log K_R$ (200°C) and the $\log K_R$ (25°C) decreases from the ferric (Fe^{3+}), to the aluminous (Al^{3+}), to the ferrous (Fe^{2+}) and, finally, to the magnesian (Mg^{2+}) series;

(3) at 25°C, the relative stability of the micaceous end-member compared to the pyrophyllite–talc-like end-member decreases in the following order:

Fe^{3+}-muscovite > muscovite > annite > phlogopite; and

(4) an increase in temperature will tend to reverse this sequence, becoming:

phlogopite > annite > muscovite > Fe^{3+}-muscovite.

In other words, at low temperatures, the conversion of Fe^{3+}-pyrophyllite into Fe^{3+}-muscovite would tend to be much easier than the transformation of talc into phlogopite-like mineral. At high temperature, this advantage would be attenuated and the transformation of minnesotaite or a talc-like mineral into a ferrous or a magnesian trioctahedral mica would be preferred. In conclusion, these data suggest that the temperature required for the transformation of a smectite into an illite would be low if the Fe^{3+}content is high or if the Mg^{2+}content is low. The temperature of the transformation would be high if the Fe^{3+}content is low or if the Mg^{2+}content is

TABLE 5-11

Equilibrium constants for the conversion of smectites into illites

---

Fe^{3+}-pyrophyllite = Fe^{3+}-muscovite:

$$Fe_2Si_4O_{10}(OH)_2 + K^+ + Al^{3+} + 2\,H_2O = KFe_2AlSi_3O_{10}(OH)_2 + 4\,H^+ + SiO_2$$

$$\begin{aligned}\log K_R &= \log K_{sp}(KFe_2AlSi_3O_{10}(OH)_2 - \log K_{sp}(Fe_2Si_4O_{10}(OH)_2)\\ &= 1.088 + 13.700 = 14.788 \text{ at } 25°C\\ &= -9.187 + 17.126 = 7.939 \text{ at } 200°C\end{aligned}$$

$$\log K_R(200°C) - \log K_R(25°C) = -6.849$$

Pyrophyllite = muscovite:

$$Al_2Si_4O_{10}(OH)_2 + K^+ + Al^{3+} + 2\,H_2O = KAl_2AlSi_3O_{10}(OH)_2 + 4\,H^+ + SiO_2$$

$$\begin{aligned}\log K_R &= \log K_{sp}(KAl_2AlSi_3O_{10}(OH)_2 - \log K_{sp}(Al_2Si_4O_{10}(OH)_2)\\ &= 16.656 - 1.061 = 15.595 \text{ at } 25°C\\ &= 1.777 + 6.116 = 7.893 \text{ at } 200°C\end{aligned}$$

$$\log K_R(200°C) - \log K_R(25°C) = -7.702$$

Minnesotaite = annite:

$$Fe_3Si_4O_{10}(OH)_2 + K^+ + Al^{3+} + 2\,H_2O = KFe_3AlSi_3O_{10}(OH)_2 + 4\,H^+ + SiO_2$$

$$\begin{aligned}\log K_R &= \log K_{sp}(KFe_3AlSi_3O_{10}(OH)_2 - \log K_{sp}(Fe_3Si_4O_{10}(OH)_2)\\ &= 23.273 - 7.235 = 16.038 \text{ at } 25°C\\ &= 7.282 + 0.141 = 7.423 \text{ at } 200°C\end{aligned}$$

$$\log K_R\ (200°C) - \log K_R\ (25°C) = -8.615$$

Talc = phlogopite:

$$Mg_3Si_4O_{10}(OH)_2 + K^+ + Al^{3+} + 2\,H_2O = KMg_3AlSi_3O_{10}(OH)_2 + 4\,H^+ + SiO_2$$

$$\begin{aligned}\log K_R &= \log K_{sp}(KMg_3AlSi_3O_{10}(OH)_2 - \log K_{sp}(Mg_3Si_4O_{10}(OH)_2)\\ &= 41.913 - 25.162 = 16.751 \text{ at } 25°C\\ &= 21.736 - 14.030 = 7.706 \text{ at } 200°C\end{aligned}$$

$$\log K_R\ (200°C) - \log K_R\ (25°C) = -9.045$$

---

high. In all cases, $Al^{3+}$and $Fe^{2+}$are in an intermediate position. These calculations confirm natural observations (Fig. 5-3).

When temperature changes, the solubility products also change (Table 5-10 and Fig. 5-9). If the model is correct, one may expect that in a given clay mineral, with a given chemical composition, the relative contribution (X_j) of the end-members also changes. Data of Table 5-10 represented on Fig. 5-9 shows, for example, that the solubility product of phlogopite is the highest at low temperatures and the lowest at high temperatures. Thus, one may expect that the contribution of the phlogopitic end-member would be smaller at low temperatures and more important at high temperatures. Furthermore, for similar reasons, one can expect that the contribution of Fe^{3+}-muscovite would be more important at low temperature and negligible in

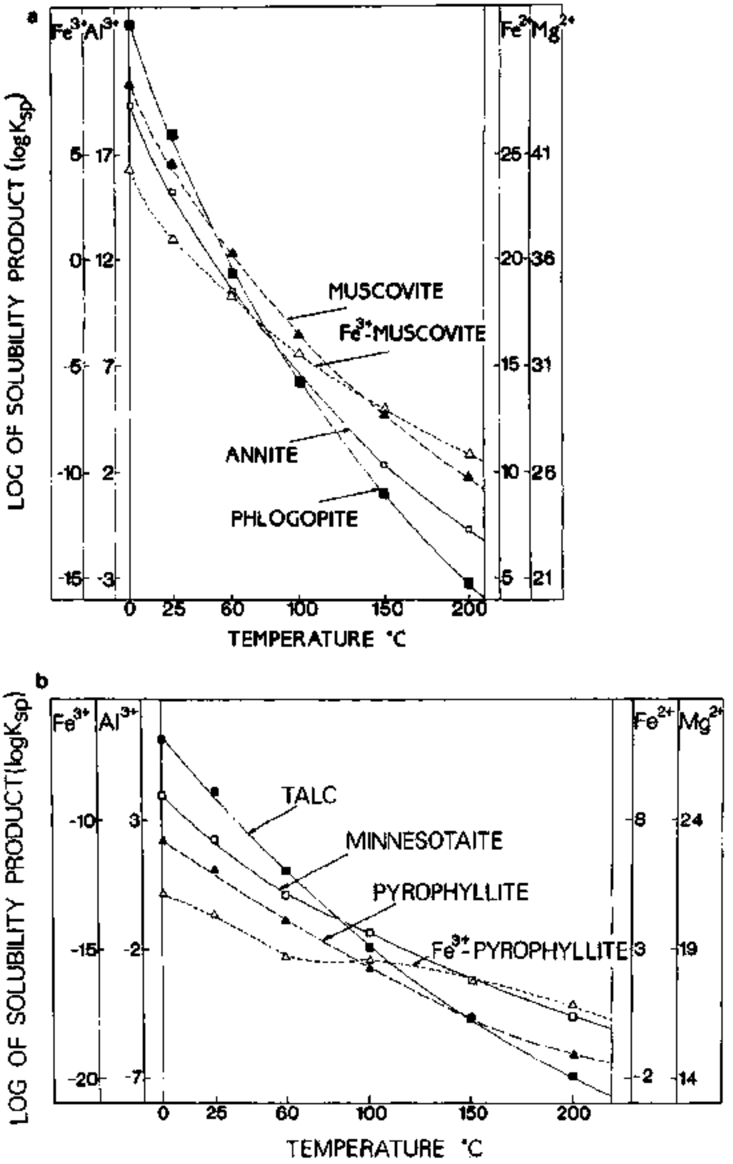

Fig. 5-9. Variation of the solubility product (K_{sp}) of (a) mica-type clay mineral components and (b) pyrophyllite–talc-type clay mineral components, as a function of temperature.

hydrothermal environment. These contributions were calculated (program CISSFIT) for the glauconite D, the celadonite 2V and the two nontronites given in Table 5-7. The diagrams of Fig. 5-10 show the relative contribution of the three types of end-members: pyrophyllite, muscovite, and celadonite for the three octahedral cations: Al^{3+}, Fe^{3+}, and Mg^{2+} at 25°C and at 200°C.

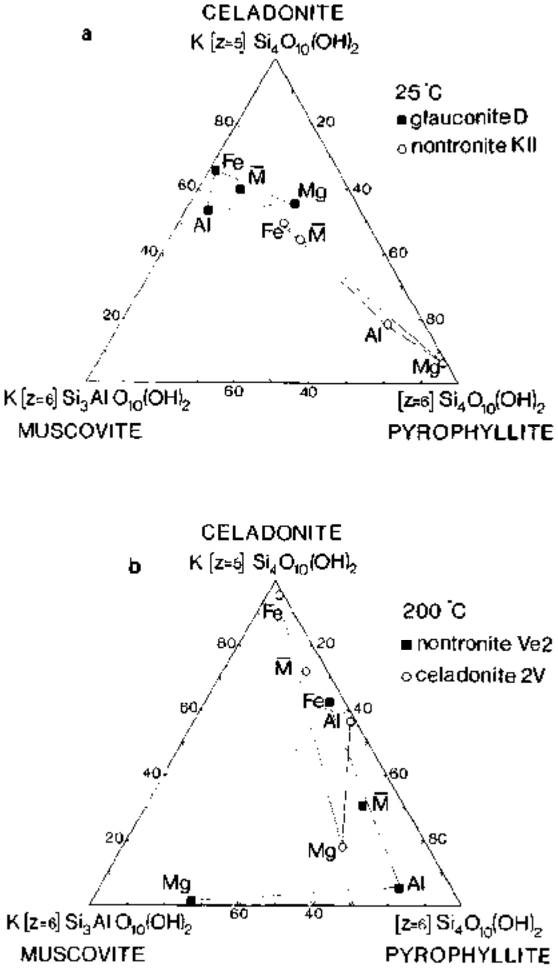

Fig. 5-10. Triangular diagram showing the weighted contribution of the three types of end-members (pyrophyllite, muscovite, and celadonite) in the three Al^{3+}-, Fe^{3+}- and Mg^{2+}-clay minerals at 25°C (a) and 200°C (b).

It is interesting to note that the correlation coefficients (Table 5-8), which are also supposed to reflect the contribution of the end-members, confirm (almost perfect correlation) the distribution based on the multicomponent ideal solid-solution model, i.e.:

(1) at low temperatures, the tetrahedral charge is mostly due to the important contribution of the Fe^{3+}-muscovite (glauconite effect), and Mg^{2+} is mostly related to the talc, whereas Al^{3+} to the pyrophyllite, and

(2) at high temperatures, the tetrahedral charge is mostly due to an important contribution of Mg^{2+}-mica (phlogopite effect), whereas the octahedral charge is particularly due to Fe^{3+} content (celadonite effect).

These data confirm the fact that the celadonite 2V and the nontronite 2V are of hydrothermal origin and that glauconite D and nontronite K2 are of low-temperature origin, so that specific compositional correlations obtained for a population of clay particles in fact characterize its temperature of formation.

LOCAL EQUILIBRIA IN POPULATIONS OF MICROSYSTEMS

Chemical analyses of populations of clay particles within different clay samples have shown important variations of composition from one particle to another. If one tries to interpret these variations of composition through equilibrium conditions of multicomponent solid-solutions with aqueous solutions, it appears that a true equilibrium condition can only be obtained in a microsystem of one particle and its surrounding solution. Equilibrium cannot be reached between the overall population of particles and the bulk solution. The multicomponent solid-solution theory is able to predict, for each individual clay particle, the composition of the solution in which this particle has been equilibrated. One uses the general expression for ideal behavior:

$$Q_j = K_j X_j$$

The determination of X_j allows also the calculation of the different Q_j (the ionic activity product in solution) and consequently the calculation of the following aqueous activity ratios or activities:

$$[K^+]/[H^+], \quad [Mg^{2+}]/[H^+]^2, \quad [Al^{3+}]/[H^+]^3, \quad [Fe^{3+}]/[H^+]^3, \text{etc.}$$

in the corresponding equilibrium solution.

These calculated activity characteristics of the solutions in equilibrium with the different particles of the same clay samples (glauconite D and celadonite 2V) appear in Table 5-12. In this table, only four particles of celadonite and five particles of glauconite (extreme compositions) were represented among large numbers detected by analyses. The differences in activities of silica and in cation-to-proton activity ratios are more than significant and would correspond to important differences in element molalities (factors varying between 1 and 10).These values give an idea of the dispersion that would represent the real population of aqueous solutions corresponding to all the particles of a sample.

The next question is: what may be the origin of these differences in the activities and activity ratios from one aqueous microsystem to another? Two major reasons may be found:

(1) One must remember that clays are built using about 7 to 10 major elements. Some of these elements, major in the solid-solutions are nearly always traces in the solution, because of their very low "solubility" (like Al, Fe^{3+}, and Fe^{2+}). The formation of any clay microsample will then have a drastic effect on the aqueous molalities of these elements and will strictly depend on their availability not only in the aqueous solution, but also in the solid phase being destroyed.

TABLE 5-12

Calculated chemical composition of the solutions supposed to be in equilibrium with several clay particles of different compositions selected within the glauconite D population (at 25°C) and the celadonite 2V population (at 200°C)

	Temperature (°C)	1*	2	3	4	5	6	7	8
Glauconite D 32	25	−3.35	5.08	−1.94	12.18	9.25	2.08	17.60	7.51
Glauconite D 31	25	−3.15	5.45	−1.79	12.23	8.14	1.00	2.45	7.55
Glauconite D 4	25	−2.82	5.40	−2.31	11.92	7.65	0.58	1.61	10.00
Glauconite D 28	25	−3.01	5.27	−2.16	12.07	8.18	1.08	15.57	10.37
Glauconite D 9	25	−2.80	5.39	−2.25	11.91	7.54	0.49	1.43	8.76
Glauconite D mean	25	−3.07	5.35	−1.96	12.14	8.13	6.61	14.98	8.11
Celadonite 2V 5N	200	−2.60	1.37	−4.24	7.89	2.40	-	9.72	−5.42
Celadonite 2V 6N	200	−2.61	1.23	−4.30	7.86	2.62	-	9.46	−6.83
Celadonite 2V 5B	200	−2.43	1.03	−4.66	7.65	2.49	-	-	−7.27
Celadonite 2V 6B	200	−2.53	1.19	−4.41	7.77	2.50	-	-	−7.53
Celadonite 2V mean	200	−2.55	1.23	−4.39	7.81	2.51	-	8.96	−6.75

* 1 = $\log[SiO]_2$; 2 = $\log[Al^{3+}]/[H^+]^3$; 3 = $\log[Fe^{3+}]/[H^+]^3$; 4 = $[Mg^{2+}]/[H^+]^2$; 5 = $\log[K^+]/[H^+]$; 6 = $\log[Na^+]/[H^+]$; 7 = $\log[Ca^{2+}]/[H^+]^2$; 8 = $\log K_{sp}$ of the solid solution.

(2) The mobilities of the different elements in the solution, from one of these microsystems to another, could also explain part of such chemical differences.

CONCLUSIONS

Many natural occurrences, chemical experimental data, crystallographic observations and theoretical reasons together suggest that clay minerals are metastable phases at the surface of the Earth. This is also true for some other kinds of minerals, such as Mg-calcites, iron and aluminum oxides and hydroxides, and minerals which present crystal defects, cationic substitutions and grain-size variability.

The abundance, diversity and environmental specificity of different smectites and illites, found in various sediment facies, weathering products and hydrothermal alteration products suggest, however, that these clay minerals and their chemical composition variations reflect to some extent (1) the temperature at which they form and (2) the differences in the chemical conditions in which they tend to equilibrate. Thus, the thermodynamic stability of clay minerals merits further investigation.

Almost all the XRD-determined pure clay phases are in fact mixtures of particles having highly varied chemical compositions. Furthermore, within a monomineralic population of particles, chemical variables are intercorrelated in such a way that the signs of the correlations clearly reflect the temperature at which that population has been formed.

A thermodynamic ideal solid-solution analogue has been proposed to explain such particle population behavior:

(1) Each particle is assumed to be — at a particle scale — an ideal solid-solution of several end-members (mineral components).

(2) There are no counter-indications to consider that each particle is a solid-solution of discrete layers of various chemical compositions. The validity of the solid-solution concept is unaffected by the scale at which the end-member mixing is organized: at a molecular scale, at a layer scale or at any intermediate scale (domains).

(3) Each individual particle is assumed to be in equilibrium, in its own microenvironment, with an aqueous solution, differing in composition from one particle to another.

(4) The chemical composition of each particle treated separately can be expressed as the weighted contribution of all end-members, which is a function of temperature and of the chemical composition of the microsite aqueous solution.

(5) According to the definition of the equilibrium condition ($X_j = Q_j/K_j$), the higher the solubility product of a given end-member, the lower is its weighted contribution to the solid-solution; the lower the solubility product of a given end-member, the higher is its weighted contribution to the solid-solution. At low temperatures, the dominant end-members are:

(a) for iron, the Fe^{3+}-muscovite, so that glauconite is the only mica stable at room temperature;

(b) for aluminum, both pyrophyllite and Al^{3+}-celadonite, so that montmorillonite is the most stable aluminous clay mineral at room-temperature conditions; and

(c) for magnesium, the talc and the Mg-celadonite end-members, so that stevensites are stable.

In hydrothermal conditions:

(a) for iron, the Fe^{3+}-celadonites are more stable;

(b) for aluminum, the Al^{3+}-mica is dominant, so that illite is stable; and

(c) for the magnesium, the phlogopite end-member is dominant, so that saponites are the hydrothermal smectites.

Glauconites (Fe^{3+}-mica) form at low temperatures, whereas illites (Al^{3+}-mica) form at higher temperatures. Mg-illite would form at much higher temperatures. Chlorite is stable at lower temperature and becomes the most stable phase involving magnesium.

Thus, it can be imagined that a stock of individual smectite layers of different compositions, organized in particles, would be progressively used as temperature increases, to form illitic layers. At low temperatures, the first illitic layers formed are the Fe^{3+}-rich layers. When temperature increases, the illitic layers which form are aluminous. At the same time, the Mg-rich layers are progressively converted into saponite, then into corrensite, and finally into chlorite.

In this schematic model, smectite may dissolve and be replaced by illitic layers at any temperature ranging from the lowest to the highest. When temperature increases, illites of different compositions form continuously and the number of illitic layers increases. Finally, smectites disappear and illite becomes predominant, together with chlorite, in the clay fraction.

Thus, the model presented by the writers accounts for the compositional variabilities and for the observed correlations among chemical components within a population of individual particles constituting a given XRD-determined clay mineral phase.

ACKNOWLEDGEMENTS

This work was supported by the Swedish Nuclear Fuel Supply (SKB) at Stockholm, Sweden, contract 85/907/180 and the Commissariat à l'Energie Atomique (CEA) at Fontenay aux Roses, France, contract No. BC-3133.

The authors thank Prof. Enrique Merino from the University of Bloomington, Indiana, U.S.A.; Dr. Paul H. Nadeau from the MacAulay Institute for Soil Research at Aberdeen, Scotland; Dr. Howard M. May, from the U.S. Geological Survey at Menlo Park, California, U.S.A.; and Prof. Charles D. Curtis from the University of Sheffield, U.K.; for their very helpful comments and criticisms of the manuscript. The help extended by Drs. G.V. Chilingarian and K.H. Wolf is also appreciated.

REFERENCES

Aagaard, P. and Helgeson, H.C., 1983. Activity/composition relations among silicates and aqueous solutions: II. Chemical and thermodynamic consequences of ideal mixing of atoms on homological sites in montmorillonites, illites and mixed layer clays. *Clays Clay Miner.*, 31(3): 207–217.

Bailey, S.W., 1985. Structural studies of clay minerals during 1981–1985. *Proc. 8th Inter. Clay Conf.*, Denver, Colo., pp. 3–8.

Bailey, S.W., Brindley, G.W., Fanning, D.S., Kodama, H. and Martin, R.T., 1984. Report of the Clay Minerals Society nomenclature committee for 1982 and 1983. *Clays Clay Miner.*, 32(3): 239–240.

Barshad, I., 1966. The effect of variation in precipitation on the nature of clay mineral formation in soils from acid and basic igneous rocks. *Int. Clay Conf.*, Jerusalem, 1: 167–173.

Barshad, I. and Kishk, F.M., 1969. Chemical composition of soil vermiculite clays as related to their genesis. *Contrib. Mineral. Petrol.*, 24: 136–155.

Bassett, R.L., Kharaka, Y.K. and Langmuir, D., 1979. Critical review of the equilibrium constants for kaolinite and sepiolite. In: E.A. Jenne (Editor), *Chemical Modeling of Aqueous Systems. Am. Chem. Soc. Symp. Ser.*, 93: 389–400.

Bradley, W.F. and Fahey, J.J., 1962. Occurrence of stevensite in the Green River Formation of Wyoming. *Am. Mineral.*, 47: 996–998.

Bricker, O.P., Nesbitt, H.W. and Gunter, W.D., 1973. The stability of talc. *Am. Mineral.*, 58: 64–72.

Buckley, H.A., Bevan, J.C., Brown, K.M., Johnson, L.R. and Farmer, V.C., 1978. Glauconite and celadonite: two separate mineral species. *Mineral. Mag.*, 42: 373–382.

Burst, J.F., 1958. Mineral heterogeneity in "glauconite pellets". *Am. Mineral.*, 43: 481–497.

Carmouze, J.P., 1976. La régulation hydrogéochimique du Lac Tchad. Contribution à l'analyse biodynamique d'un système endoréique en milieu continental. *Trav. Doc. ORSTOM*, 58: 458 pp.

Carmouze, J.P., Pedro, G. and Berrier, J., 1977. Sur la nature des smectites de néoformation du Lac Tchad et leur distribution spatiale en fonction des conditions hydrogéochimiques. *C. R. Acad. Sci. Paris, Sér. D*: 615–618.

Chang, H.K. and Mackenzie, F.T., 1986. Comparisons between dioctahedral and trioctahedral diagenesis, Brazilian offshore basins. *Clays Clay Miner.*, 34: 407–423.

Chen, C.H., 1975. A method of estimation of standard free energies of formation of silicate minerals at 298, 15°K. *Am. J. Sci.*, 275: 801–817.

Christ, C.L., Hostetler, P.B. and Siebert, R.M., 1973. Studies in the system $MgO-SiO_2-CO_2-H_2O$. III. The activity product constant of sepiolite. *Am. J. Sci.*, 273: 65–83.

De Keyser, W.L., 1964. Contribution à l'étude du système silice alumine. *Bull. Soc. Fr. Céram.*, 62: 19–33.

Droubi, A., Vieillard, P., Bourrie, G., Fritz, B. and Tardy, Y., 1976. Etude théorique de l'altération des plagioclases. Bilans et conditions de stabilité des minéraux secondaires en fonction de la pression partielle de CO_2 et de la température (0°C à 100°C). *Sci. Géol. Bull.*, 29(1): 45–62.

Dunoyer de Segonzac, G., 1969. Les minéraux argileux dans la diagenèse. Passage au métamorphisme. *Mém. Serv. Carte Géol. Alsace-Lorraine*, 29: 320 pp.

Dunoyer de Segonzac, G., 1970a. The birth and development of the concept of diagenesis (1866–1966). *Earth-Sci. Rev.*, 4: 153–201.

Dunoyer de Segonzac, G., 1970b. The transformation of clay minerals during diagenesis and low-grade metamorphism: a review. *Sedimentology*, 15: 281–346.

Duplay, J., 1982. *Analyses Chimiques de Populations de Particules Argileuses*. Thèse Sci., Univ. of Poitiers, Poitiers, 110 pp.

Duplay, J., 1984. Analyses chimiques ponctuelles de particules d'argiles. Relations entre variations de compositions dans une population de particules et température de formation. *Sci. Géol. Bull.*, 37(4): 307–317.

Duplay, J., 1989. Géochimie des argiles et géothermométrie des populations monominérales de particules. *Sci. Géol., Mém., Strasbourg*, 82: 190 pp.

Duplay, J., Desprairies A., Paquet H. and Millot G., 1986. Céladonites et glauconites. Double population de particules dans la céladonite de Chypre. Essai sur les températures de formation. *C. R. Acad Sci. Paris*, 305 (4): 181–186.

Eugster, H.P. and Chou, I.M., 1973. The depositional environments of Precambrian banded iron-formations. *Econ. Geol.*, 68: 1144–1168.

Feth, J.H., Roberson, C.E. and Polzer, W.L., 1964. Sources of mineral constituents in water from granitic rocks Sierra Nevada, California and Nevada. *U.S. Geol. Surv., Water Supply Pap.*, 1 535-I: 70 pp.

Frink, C.R. and Peech, M., 1962. The solubility of gibbsite in aqueous solutions and soil extracts. *Soil Sci. Soc. Am. Proc.*, 26: 346–347.

Fritz, B., 1975. Etude thermodynamique et simulation des réactions entre minéraux et solutions. Applications à la géochimie des altérations et des eaux continentales. *Sci. Géol. Mém., Strasbourg*, 41: 152 pp.

Fritz, B., 1981. Etude thermodynamique et modélisation des réactions hydrothermales et diagénétiques. *Sci. Géol. Mém., Strasbourg*, 65: 197 pp.

Fritz, B., 1985. Multicomponents solid-solutions for clay minerals and computer modeling of weathering processes. In: J.L. Drever (Editor), *The Chemistry of Weathering. NATO ASI Ser.*, 149: pp. 19–34.

Fritz, B. and Tardy, Y., 1973. Etude thermodynamique du système gibbsite, quartz, kaolinite, gaz carbonique. *Sci. Géol. Bull.*, 26(4): 339–367.

Gac, Y., 1980. Géochimie du Bassin du Lac Tchad. Bilan de l'altération de l'érosion et de la sédimentation. *Trav. Doc. ORSTOM*, 123: 251 pp.

Gac, Y. and Tardy, Y., 1980. Géochimie d'un paysage tropical: le Bassin du Lac Tchad. In: Y. Tardy (Editor), *Géochimie des Interactions Entre les Eaux, les Minéraux et les Roches*. Eléments, Tarbes, 239 pp.

Garrels, R.M., 1957. Some free energy values from geologic relations. *Am. Mineral.*, 42: 780–791.

Garrels, R.M., 1984. Montmorillonite/illite stability diagram. *Clays Clay Miner.*, 32: 161–166.

Garrels, R.M. and Christ, C.L., 1965. *Solutions, Minerals and Equilibria.* Harper and Row, New York, N.Y., 450 pp.

Garrels, R.M. and Mackenzie, F.T., 1974. Chemical history of the oceans deduced from post-depositional changes in sedimentary rocks. In: *Studies in Paleo-oceanography. Soc. Econ. Paleontol., Spec. Publ.*, 20: 193–204.

Giresse, P. and Odin, G.S., 1973. Nature minéralogique et origine des glauconites du plateau continental du Gabon et du Congo. *Sedimentology*, 20: 457–488.

Grim, R.E. and Kulbicki, G., 1961. Montmorillonite: high temperature reactions and classification. *Am. Mineral.*, 46: 1329–1369.

Helgeson, H.C., 1964. *Complexing and Hydrothermal Ore Deposition.* Pergamon, New York, N.Y., 128 pp.

Helgeson, H.C. and Mackenzie, F.T., 1970. Silicate–sea water equilibria in the ocean system. *Deep-Sea Res.*, 17: 877–892.

Hemley, J.J., 1959. Some mineralogical equilibria in the system K_2O–Al_2O_3–SiO_2–H_2O. *Am. J. Sci.*, 257: 241–270.

Hemley, J.J., Meyer, C. and Richter, D.H., 1961. Some alteration reactions in the system Na_2O–Al_2O_3–SiO_2. *U.S. Geol. Surv., Prof. Pap.*, 424-D: 338–340.

Hemley, J.J., Montoya, J.W., Christ, C.L. and Hostetler, P.B., 1977a. Mineral equilibria in the MgO–SiO_2–H_2O, I. Talc–chrysotile–forsterite–brucite stability relations. *Am. J. Sci.*, 277: 322–351.

Hemley, J.J., Montoya, J.W., Shaw, D.R. and Luce, R.W., 1977b. Mineral equilibria in the MgO–SiO_2–H_2O, II. Talc–antigorite–forsterite–anthophyllite–enstatite stability relations and some geologic implications in the system. *Am. J. Sci.*, 277: 353–383.

Hostetler, P.B., 1963. The stability and surface energy of brucite in water at 25°C. *Am. J. Sci.*, 251: 238–258.

Hostetler, P.B. and Christ, C.L., 1968. Studies in the system MgO–SiO_2–CO_2–H_2O, I. The activity-product constant of chrysotile. *Geochim. Cosmochim. Acta*, 32: 485–497.

Hostetler, P.B., Hemley, J.J., Christ, C.L. and Montoya, J.W., 1971. Talc chrysotile equilibrium in aqueous solutions. *Geol. Soc. Am., Abstr.*, 3: 305.

Hower, J., 1981. X-ray diffraction identification of mixed-layer clay minerals. In: F.J. Longstaffe (Editor), *Clays and Resource Geologist. Mineral. Assoc. Can., Short Course Handbook*, 7: 39–59.

Hower, J. and Mowatt, T.C., 1966. The mineralogy of illites and mixed-layer illite–montmorillonite. *Am. Mineral.*, 51: 825–854.

Hower, J., Eslinger, E.V., Hower, M.E. and Perry, E.A., 1976. Mechanism of burial metamorphism of argillaceous sediment, 1. Mineralogical and chemical evidence. *Geol. Soc. Am. Bull.*, 87: 725–737.

Huertas, F., Linares, J. and Martin-Vivaldi, J.L., 1970. Clay mineral geochemistry in basic sedimentary environments. *Reun. Hispano-Belge de Minerals de la Arcilla, C.S.I.C.*, Madrid, 211–214.

Ildefonse, P., Copin, E. and Velde, B., 1979. A soil vermiculite formed from a metagabbro, Loire Atlantique, France. *Clay Miner.*, 14: 201–210.

Jackson, M.L., Tyler, S.A., Willis, A.L., Bourbeau, G.A. and Pennington, R.P., 1948. Weathering sequence of clay-size minerals in soils and sediments. *J. Phys. Colloid Chem.*, 52(7): 1237–1260.

Karpov, I.K. and Kashik, S.A., 1968. Computer calculation of standard isobaric–isothermal potentials of silicates by multiple regression from a crystallo-chemical classification. *Geochim. Int.*, 5: 706–713.

Kittrick, J.A., 1966. Free energy of formation of kaolinite, from solubility measurements. *Am. Mineral.*, 51: 1457–1466.

Kittrick, J.A., 1969. Soil minerals in the Al_2O_3–SiO_2–H_2O system and theory of their formation. *Clays Clay Miner.*, 17: 157–167.

Kittrick, J.A., 1971a. Montmorillonite ezquilibria and the weathering environment. *Soil Sci. Soc. Am. Proc.*, 35: 815–820.

Kittrick, J.A., 1971b. Stability of montmorillonites, I. Belle Fourche and clay spur montmorillonites. *Soil Sci. Soc. Am. Proc.*, 35: 140–145.

Kittrick, J.A., 1973. Mica-derived vermiculites as unstable intermediates. *Clays Clay Miner.*, 21: 479–488.

Köster, H.M., 1982. The crystal structure of 2:1 layer silicates. In: H. Van Olphen and F. Veniale (Editors), *Proc. Int. Clay Conf., Bologna, Pavia, 1981.* Elsevier, Amsterdam, pp. 41–71.

Kramer, J.R., 1968. Mineral–water equilibria in silicate weathering. *23rd Int. Geol. Congr., Prague*, 6: 149–160.

Lamboy, M., 1967. Répartition de la glauconie sur le plateau continental de la Galia et des Asturies (Espagne). *C. R. Acad. Sci. Paris*, 265: 855–857.

Lelong, F., Tardy, Y., Grandin, G., Trescases, J.J. and Boulange, B., 1976. Pedogenesis, chemical weathering and processes of formation of some supergene ore deposits. In: K.H. Wolf (Editor), *Handbook of Stratabound and Stratiform Ore Deposits, Vol. 3.* Elsevier, Amsterdam, pp. 93–174.

Lemoalle, J. and Dupont, B., 1973. Iron bearing oolites and the present conditions of iron sedimentation in lake Chad (Africa). In: G.C. Amstutz and A.J. Bernard (Editors), *Ores Sediments.* Springer-Verlag, Berlin, pp. 167–178

Leneuf, N., 1959. *L'Altération des Granites Calco-alcalins et des Granodiorites en Côte-d'Ivoire Forestière et des Sols qui en sont Dérivés.* Thèse Sci., Univ. of Paris, Paris, 210 pp.

Lippmann, F., 1977. The solubility products of complex minerals, mixed crystals, and three-layer clay minerals. *Neues Jahrb. Mineral., Abh.*, 130: 243–263.

Lippmann, F., 1979a. Stabilitätsbeziehungen der Tonminerale. *Neues Jahrb. Mineral., Abh.*, 136: 287–309.

Lippmann, F., 1979b. Stability diagrams involving clay minerals. *8th Conf. on Clay Mineralogy and Petrology, Teplice, Prague*, pp. 153–171.

Lippmann, F., 1982. The thermodynamic status of clay minerals. In: H. Van Olphen and F. Veniale (Editors), *Proc. Int. Clay Conf., Bologna, Pavia, 1981.* Elsevier, Amsterdam, pp. 475–485.

Lynch, F.L., 1985. *The Stoichiometry of Smectite to Illite Reaction in a Contact Metamorphic Environment.* M.A. Thesis, Dartmouth College, Hanover, N.H., 93 pp.

Lucas, J., 1962. La transformation des minéraux argileux dans la sédimentation. Etude sur les argiles du Trias. *Mém. Serv. Carte Géol. Alsace-Lorraine*, 18(4): 217–242.

Mattigod, S.V. and Sposito, G., 1978. Improved method for estimating the standard free energies of formation of smectites. *Geochim. Cosmochim. Acta*, 42: 1753–1762.

May, H., Helmke, P.A. and Jackson, M.L., 1979a. Determination of mononuclear dissolved aluminum in near neutral waters. *Chem. Geol.*, 24: 259–269.

May, H., Helmke, P.A. and Jackson, M.L., 1979b. Gibbsite solubility and thermodynamic properties of hydroxy-aluminum ions in aqueous solution at 25°C. *Geochim. Cosmochim. Acta*, 43: 861–868.

May, H., Kinninburgh, D.G., Helmke, P.A. and Jackson, M.L., 1986. Aqueous dissolution, solubilities and thermodynamic stabilities of common aluminosilicate clay minerals: kaolinite and smectite. *Geochim. Cosmochim. Acta*, 50: 1667–1677.

McHardy, W.J., Wilson, M.J and Tait, J.M., 1982. Electron microscope and X-ray diffraction studies of filamentous illitic clay from sandstones of the Magnus field. *Clay Miner.*, 17: 23–39.

Mering, J. and Oberlin, A., 1967. Electron optical study of smectites. *15th Natl. Conf. Proc., Clays Clay Miner.*, 3–25.

Mering, J. and Oberlin, A., 1971. The smectites. In: J.A. Gard (Editor), *Electron Optical Investigation of Clays.* Mineral. Soc., London, pp. 193–229.

Merino, E. and Ransom, B., 1982. Free energies of formation of illite solid solutions and their compositional dependence. *Clays Clay Miner.*, 30: 29–39.

Millot, G., 1949. Relations entre la constitution et la genèse des roches sédimentaires argileuses. *Géologie Appliquée et Prospection Minières*, Nancy, 2: 352 pp.

Millot, G., 1964. *Géologie des Argiles.* Masson, Paris, 499 pp.

Millot, G., Elouard, P., Lucas, J. and Slansky, M., 1960. Une séquence sédimentaire et géochimique des minéraux argileux: montmorillonite, attapulgite, sépiolite. *Bull. Groupe Fr. Argiles*, 12: 77–82.

Nadeau, P.H., 1985. The physical dimensions of fundamental particles. *Clay Miner.*, 20: 499–514.

Nadeau, P.H. and Bain, D.C., 1986. The composition of some smectite and diagenetic illitic clays and implications for their origin. *Clays Clay Miner.*, 34: 455–4464.

Nadeau, P.H., Tait, J.M., McHardy, W.J. and Wilson, M.J., 1984a. Interstratified XRD characteristics of physical mixtures of elementary clay particles. *Clay Miner.*, 19: 67–76.

Nadeau, P.H., Wilson, M.J., McHardy, W.J. and Tait, J.M., 1984b. Interparticle diffraction: a new concept for interstratified clays. *Clay Miner.*, 19: 757–769.

Nadeau, P.H., Wilson, M.J., McHardy, W.J. and Tait, J.M., 1984c. Interstratified clays as fundamental particles. *Science*, 225: 923–925.

Nadeau, P.H., Wilson, M.J., McHardy, W.J. and Tait, J.M., 1985. The conversion of smectite to illite during diagenesis: evidence from some illitic clays from bentonites and sandstones. *Mineral. Mag.*, 49: 393–400.

Nahon, D., Colin, F. and Tardy, Y., 1982. Formation and distribution of Mg, Fe, Mn-smectites in the first stages of lateritic weathering of forsterite and tephroite. *Clay Miner.*, 17: 339–348.

Noack, Y. and Duplay, J., 1983. Talc and the weathering-hydrothermal alteration boundary. *Int. Colloq. CNRS, Petrology of Weathering and Soils, Paris. Sci. Géol. Mem.*, 72: 121–130.

Nriagu, J., 1975. Thermochemical approximations for clay minerals. *Am. Mineral.*, 60: 834–839.

Orville, P.M., 1963. Alkali ion exchange between vapor and feldspar phases. *Am. J. Sci.*, 261: 201–237.

Paquet, H., 1970. Evolution géochimique des minéraux dans les altérations et les sols des climats méditerranéens et tropicaux à saisons contrastées. *Mém. Serv. Carte Géol. Alsace-Lorraine*, 30: 212 pp.

Paquet, H. Duplay, J. and Nahon, D., 1981. Variation in the composition of phyllosilicates monoparticles in a weathering profile of ultrabasic rock. In: H. Van Olphen and F. Veniale (Editors), *Proc. Int. Clay Conf., Bologna, Pavia 1981*. Elsevier, Amsterdam, pp. 595–603.

Paquet, H. Duplay, J., Nahon, D., Tardy, Y. and Millot, G. 1983. Analyses chimiques de particules isolées dans les populations de minéraux argileux. Passage de smectites magnésiennes trioctaédriques aux smectites ferrifères dioctaédriques au cours de l'altération des roches ultrabasiques. *C. R. Acad. Sci. Paris*, 296: 699–704.

Pedro, G., Carmouze, J.P. and Velde, B., 1978. Peloidal nontronite formation in recent sediments of Lake Chad. *Chem. Geol.*, 23: 139–149.

Porrenga, D.H., 1967. Glauconite and chamosite as depth indicators in the marine environmrnt. *Mar. Geol.*, 5: 495–501.

Robert, M., 1973. The experimental transformation of mica towards smectite. Relative importance of total charge and tetrahedral substitution. *Clays Clay Miner.*, 21(3): 167–174.

Routson, R.C. and Kittrick, J.A., 1971. Illite solubility. *Soil Sci. Soc. Am. Proc.*, 35: 715–718.

Sposito, G., 1986. On the polymer model of thermochemical clay mineral stability. *Clays Clay Miner.*, 34(2): 198–203.

Stoessel, R.K., 1979. A regular solution site mixing model for illites. *Geochim. Cosmochim. Acta*, 43: 1151–1159.

Stoessel, R.K., 1981. Refinements in a site mixing model for illites: local electrostatic balance at the quasi chemical approximation. *Geochim. Cosmochim. Acta*, 45: 1733–1741.

Tardy, Y., 1969. Géochimie des altérations. Etude des arènes et des eaux de quelques massifs cristallins d'Europe et d'Afrique. *Mém. Serv. Carte Géol. Alsace-Lorraine*, 31: 199 pp.

Tardy, Y., 1971. Characterization of the principal weathering types by the geochemistry of waters from some european and african crystalline massifs. *Chem. Geol.*, 7: 253–271.

Tardy, Y., 1979. Relationships among Gibbs energies of formation of compounds. *Am. J. Sci.*, 279: 217–224.

Tardy, Y., 1981. Silice, silicates magnésiens, silicates sodiques et géochimie des paysages arides. *Bull. Soc. Géol. Fr.*, 7(23): 325–334.

Tardy, Y., 1982. Kaolinite and smectite stability in weathering conditions. *Estud. Geol.*, 38: 295–312.

Tardy, Y. and Fritz, B., 1981. An ideal solid-solution model for calculating solubilbity of clay minerals. *Clay Miner.*, 16: 361–373.

Tardy, Y. and Gac, Y., 1979. Contrôle de la composition chimique des solutions par la précipitation des minéraux dans les sols. *Sci. Soc.*, 2(3): 107–123.

Tardy, Y. and Garrels, R.M., 1974. A method of estimating the Gibbs energy of formation of layer silicates. *Geochim. Cosmochim. Acta*, 38: 1101–1116.

Tardy, Y., Cheverry, C. and Fritz, B., 1974a. Néoformation d'une argile magnésienne dans les dépressions interdunaires du Lac Tchad. Application au domaines de stabilité des phyllosilicates alumineux, magnésiens et ferrifères. *C. R. Acad. Sci. Paris*, 278: 1999–2002.

Tardy, Y., Trescases, J.J. and Fritz, B., 1974b. Evaluation de l'enthalpie libre de formation de montmorillonites ferrifères. *C. R. Acad. Sci. Paris*, 278: 1665–1668.

Tardy, Y., Duplay, J. and Fritz, B., 1981. Chemical composition of individual clay particles: an ideal solid-solution model. In: H. Van Olphen and F. Veniale (Editors), *Proc. Int. Clay Conf., Bologna, Pavia 1981*. Elsevier, Amsterdam, pp. 441–450.

Thompson, G.R. and Hower, J., 1975. The mineralogy of glauconite. *Clays Clay Miner.*, 23: 289–300.

Trauth, N., 1977. Argiles évaporitiques dans la sédimentation carbonatée continentale et épicontinentale tertiaire. Bassin de Paris, de Mormoiron et de Salinelle (France), Jbel Ghassoul (Maroc). *Sci. Géol. Mém.*, 49: 195 pp.

Trauth, N., Paquet, H., Lucas, J. and Millot, G., 1967. Les montmorillonites des vertisols lithomorphes sont ferrifères: conséquences géochimiques et sédimentologiques. *C. R. Acad. Sci. Paris*, 264: 1577–1579.

Truesdell, A.H. and Christ, C.L., 1968. Cation exchange in clays interpreted by regular solution theory. *Am. J. Sci.*, 266: 402–412.

Tsuzuki, Y. and Kawabe, I., 1983. Polymorphic transformations of kaolin minerals in aqueous solution. *Geochim. Cosmochim. Acta*, 47: 59–66.

Velde, B., 1977. A proposed phase diagram for illites, expanding chlorite, corrensite and illite/montmorillonite mixed-layered minerals. *Clays Clay Miner.*, 25: 264–270.

Walker, G.F., 1950. Trioctahedral minerals in the soil clays of northeast Scotland. *Mineral. Mag.*, 29: 72–84.

Weaver, R.M. and Pollard, L.D., 1975. *The Chemistry of Clay Minerals. Developments in Sedimentology, Vol. 15.* Elsevier, Amsterdam, 213 pp.

Weaver, R.M., Jackson, M.L. and Syers, J.K., 1971. Magnesium and silicon activities in matrix solutions of montmorillonite-containing soils in relation to clay mineral stability. *Soil Sci. Soc. Am. Proc.*, 35: 823–830.

Weiss, A., Koch, G. and Hoffman, N.U., 1956. Zur Kenntnis von trioctaedrischem Illit. *Z. Naturforsch.*, 11b: 429–430.

Wiewiora, A., Lacka, B. and Szczyrba, J., 1979. Celadonite, glauconite and skolite: nomenclature and identification problems. *8th Conf. on Clay Mineralogy and Petrology, Teplice, Prague*, pp. 47–58.

Wildman, W.E., Jackson, M.L. and Whittig, L.D., 1968. Iron-rich montmorillonite formations in soils derived from serpentinite. *Soil Sci. Soc. Am. Proc.*, 32: 787–794.

Wildman, W.E., Whittig, L.D. and Jackson, M.L., 1971. Serpentine stability in relation to formation of iron-rich montmorillonite in some California soils. *Am. Mineral.*, 56(3): 587–602.

Wilson, M.D. and Pittman, E.D., 1977. Authigenic clays in sandstones: recognition and influence on reservoir properties and paleoenvironments analysis. *J. Sediment. Petrol.*, 47: 3–31.

Wilson, M.J. and Nadeau, P.H., 1985. Interstratified clay minerals and weathering processes. In: J.I. Drever (Editor), *The Chemistry of Weathering.* Reidel, Dordrecht, pp. 97–118.

Wilson, M.J., Bain, D.C. and Mitchell, W.A., 1968. Saponite from the Dalradian meta-limestones of northeast Scotland. *Clay Miner.*, 7: 343–349.

Wise, W.S. and Eugster, H.P., 1964. Celadonite: synthesis, thermal stability and occurences. *Am. Mineral.*, 49: 1031–1083.

Wollast, R., 1961. Aspect chimique du mode de formation des bauxites dans le Bas-Congo. *Bull. Séanc. Acad. R. Sci., O.M. Bruxelles*, 7(3): 468–489.

Wollast, R., 1963. Aspect chimique du mode de formation des bauxites dans le Bas-Congo, II. *Bull. Acad. R. Sci., O.M. Bruxelles*, 9: 392–412.

Zen, E.A., 1972. Gibbs free energy, enthalpy and entropy of ten rock forming minerals. Calculations, discrepancies and implications. *Am. Mineral.*, 57: 524–553.

Diagenesis, IV. Developments in Sedimentology 51
edited by K.H. Wolf and G.V. Chilingarian
© 1994 Elsevier Science B.V., Amsterdam. All rights reserved.

Chapter 6

THE FORMATION OF ALTERNATING CHALK/SIDERITE UNITS DURING THE NEOGENE IN THE BLACK SEA — AN EXAMPLE OF CLIMATIC CONTROL OF EARLY DIAGENETIC PROCESSES

BJÖRN BAHRIG

INTRODUCTION

The formation of siderite in lacustrine and marine sediments has been discussed in the literature (e.g., Irion, 1977; Hsü and Kelts, 1978; Gautier, 1982; Bahrig, 1988). Generally, the precipitation of siderite is restricted to environments characterized by the following conditions (Curtis and Spears, 1968; Stumm and Morgan, 1981; Fig. 6-1):

(1) a low redox potential (+100 mV at pH 7), which provides a sufficient availability of Fe^{2+} and stabilizes siderite as a thermodynamic phase;

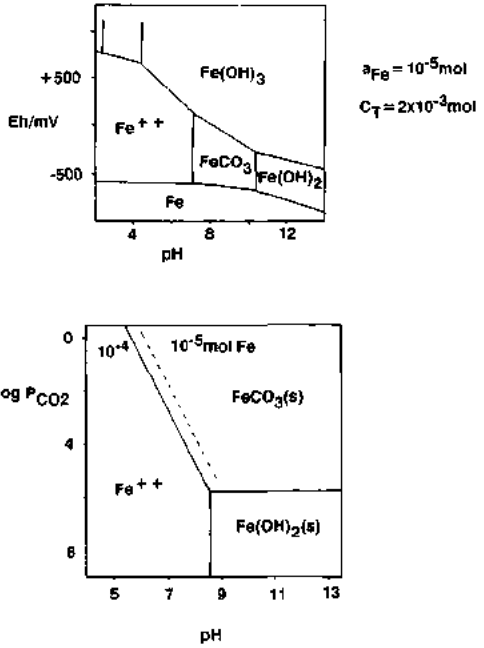

Fig. 6-1. Stability diagrams of siderite: The upper diagram shows that in sedimentary environments the stability field of siderite is limited by dissolution and oxidation reaction to pH < 7.0 and Eh > +100 mV. The lower diagram stresses the stabilization of siderite by high activities of iron and carbonate ions. (After Stumm and Morgan, 1981.)

(2) a low sulfide concentration ($<10^{-7}$ mol/l HS^-), because at higher concentrations any iron is precipitated as Fe-monosulfide or pyrite; and

(3) a partial pressure of CO_2 of $>10^{-6}$ atm, which is achieved in natural environments either by microbial activity (Irwin et al., 1977; Hangari et al., 1980), by volcanic exhalations (Bahrig, 1988), or by dissolution of less stable carbonates (Einsele and von Rad, 1979).

The siderite in sediments can be used as an indicator of Berner's (1981) "post-oxic" environment, characterized by strong anoxia coupled to a low sulfate reduction. Thus, in marine pore water, characterized by a high availability of reducible sulfate, siderite can be precipitated only under very special conditions. Papers about marine siderite-bearing sequences have been published by Weber et al. (1964); Timofeyeva et al. (1976); and Mozley (1989).

Different approaches have been adopted in the interpretation of the chemical and stable isotope composition of siderite:

(1) Carbon and oxygen stable isotope data from siderite have been used as tracers of the salinity of pore solutions (Weber et al., 1964; Timofeyeva et al., 1976), but these attempts were found to be not generally applicable.

(2) The $\delta^{13}C$ often exhibits a strong signature of a methanogenic environment, where the precipitation of siderite was coupled to processes of methane formation (Gautier, 1982; Matsumoto, 1989).

(3) Bahrig and Conze (1986) and Bahrig (1988, 1989) made an attempt to distinguish between purely diagenetic signatures and those that may yield some information about the depositional environment, as in some oil shale lakes or during the late glacial/post glacial climatic development of German crater lakes, for example.

(4) Summarizing the chemical data published about siderite, Fe/Mn-siderites may be distinguished from Ca/Mg-siderites:

(a) Fe/Mn-siderite seems to be formed preferably during very early diagenetic phases at the sediment/water boundary (Pearson, 1979; Talbot et al., 1984; Bahrig, 1989).

(b) Ca/Mg-siderites indicate additional Ca/Mg-sources like silicates (Matsumoto and Iijima, 1981; Bahrig, 1989), carbonates (Postma, 1981), or marine pore solutions (Mozley, 1989).

The present contribution links geochemical information from early diagenetic processes to the general, climate-dependent development of the water and sediments of the Black Sea Basin. A new model for the formation of the cyclic chalk/siderite change in the Neogene chemical sediments is presented.

METHODS

The samples were taken from DSDP cores 380/380A that were obtained during the Leg 42B cruise in the Black Sea in 1975 (Supko et al., 1978).

A petrographic examination was undertaken by means of thin-sections, smear slides, and XRD (Philips XRD, Cu-Kα, Ni-filter). The siderite samples were cleaned from organic matter by a 24-h reaction with a 1% sodium-hypochloride solution. Various tests with a siderite standard showed that this treatment had almost no effect on the stable isotope data ($< 0.1‰$), as long as both reaction time and hypochlorite concentration were sufficient for a total oxidation. In contrast to samples from other localities (Bahrig, 1988, 1989), the Black Sea samples did not allow a complete removal of organic matter by a simple heating to 400°C.

The separation of C- and O-isotopes from calcite and siderite was performed during the normal CO_2-preparation with 100% H_3PO_4 (McCrea, 1950), using a modification of the calcite/dolomite separation as suggested by McKenzie (1976).

(1) First, the sample is allowed to react at 25°C for 2.5 hours in a water bath.

(2) The calcite-CO_2 is removed (siderite/calcite ratio < 5.0).

(3) The reaction then is continued at 60°C for 8 hours in a water bath.

(4) The siderite-CO_2 is removed.

Test runs with different mixtures of calcite and siderite standards with $\delta^{13}C$ and $\delta^{18}O$ differences of $>20‰$ exhibited a perturbation of $<0.5‰$ of this treatment in comparison to the pure 1-phase samples.

In the case of a siderite/calcite ratio of 5.0, however, the calcite gas should be removed after 0.5 h and only the siderite signal should be used.

The siderite data were corrected to 25°C according to the calibration curve of Bahrig (1989).

To avoid contamination from the detrital dolomite in the Upper Siderite sequence, only those samples were used that showed no XRD signal of dolomite.

The stable isotope determinations were carried out with a VG micromass 903 at the ETH Zürich. All data were corrected to PDB at 25°C.

SEDIMENTS AND PALEOENVIRONMENTAL DATA

General

The whole sedimentary sequence cored in holes 379–381 documents the history of the Black Sea Basin from the Miocene to the present (Hsü, 1978; Figs. 6-2 and 6-3). The sequence starts with Miocene black shales and laminated Ca/Mg-carbonates. The early phase of the basin development ended with the sedimentation of pebbly dolomite-bearing muds, thus marking a regressive period. According to Hsü and Giovanoli (1979), this period may correspond to the Messinian event of the Mediterranean Sea.

The following, approximately 450 m thick chemical sediments are characterized by two alternating chalk units, with typical planktogenic calcite grains, and two diatomaceous siderite units (Hsü and Kelts, 1978). A comparison between the sedimentary and palynological data (Fig. 6-3) reveals that the formation of the siderite units corresponds to periods of a more arid climate; in contrast, the chalk units were formed during more humid climatic periods.

The interpretation of the stratigraphy of this sequence has been the subject of some controversy. According to Hsü (1978) and Hsü and Giovanoli (1979), the

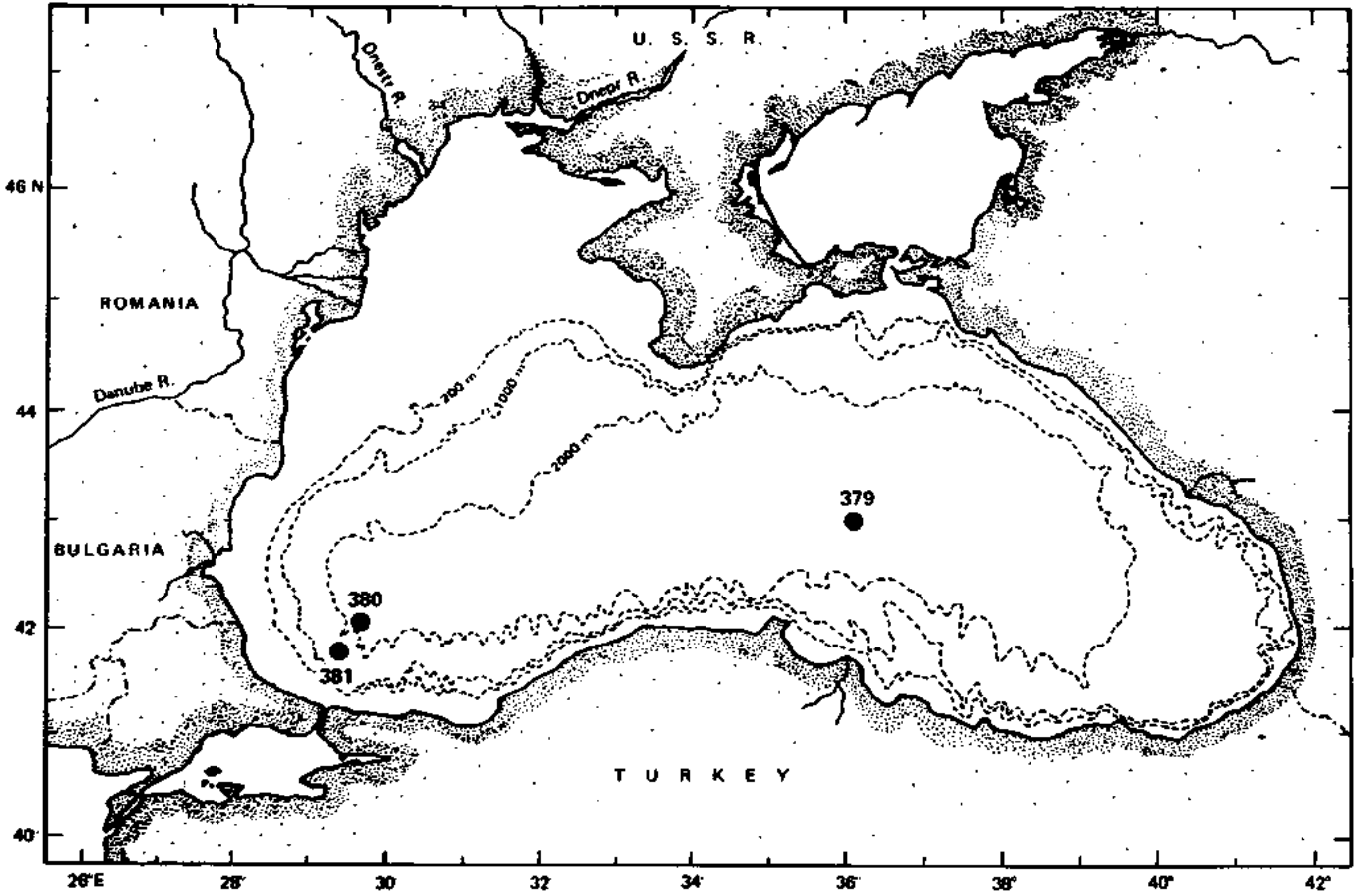

Fig. 6-2. Map of the Black Sea with position of holes 379 and 380/380A. (After Ross et al., 1978.)

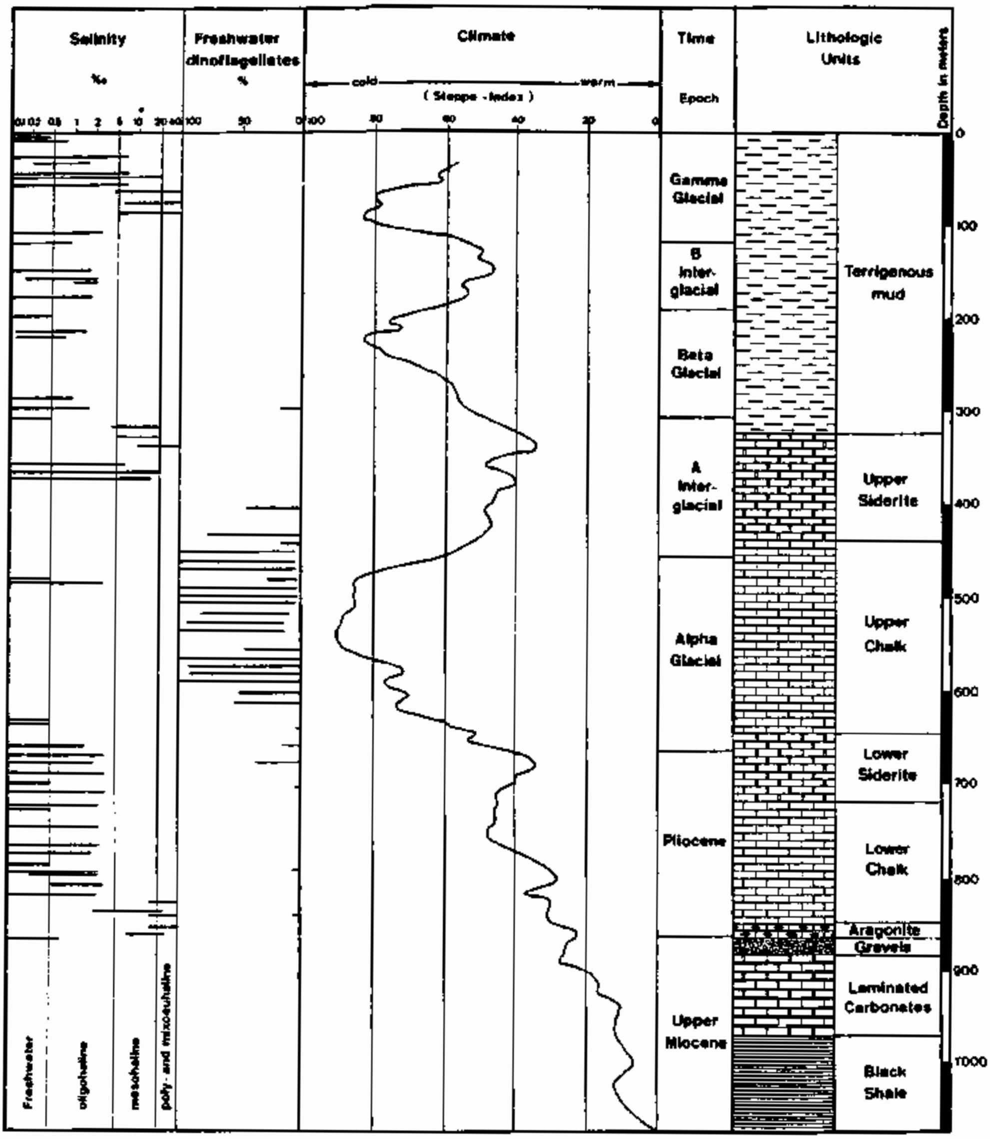

Fig. 6-3. Stratigraphy of core 380/380A including main climatic and salinity data. The cyclic change of chalk and siderite units correlates with climatic fluctuations between arid and humid periods. (After Hsü, 1978.)

transition from clastic to chemical sedimentation took place during the Pliocene. In contrast, Schrader (1978) presented arguments for a Pleistocene age of the whole sequence of chemical sediments, based on micropaleontological data.

At about 320 m depth, siliciclastic sediments occur again, coinciding with the beginning of the Beta-glacial period (Fig. 6-3). From that time on, the sedimentation

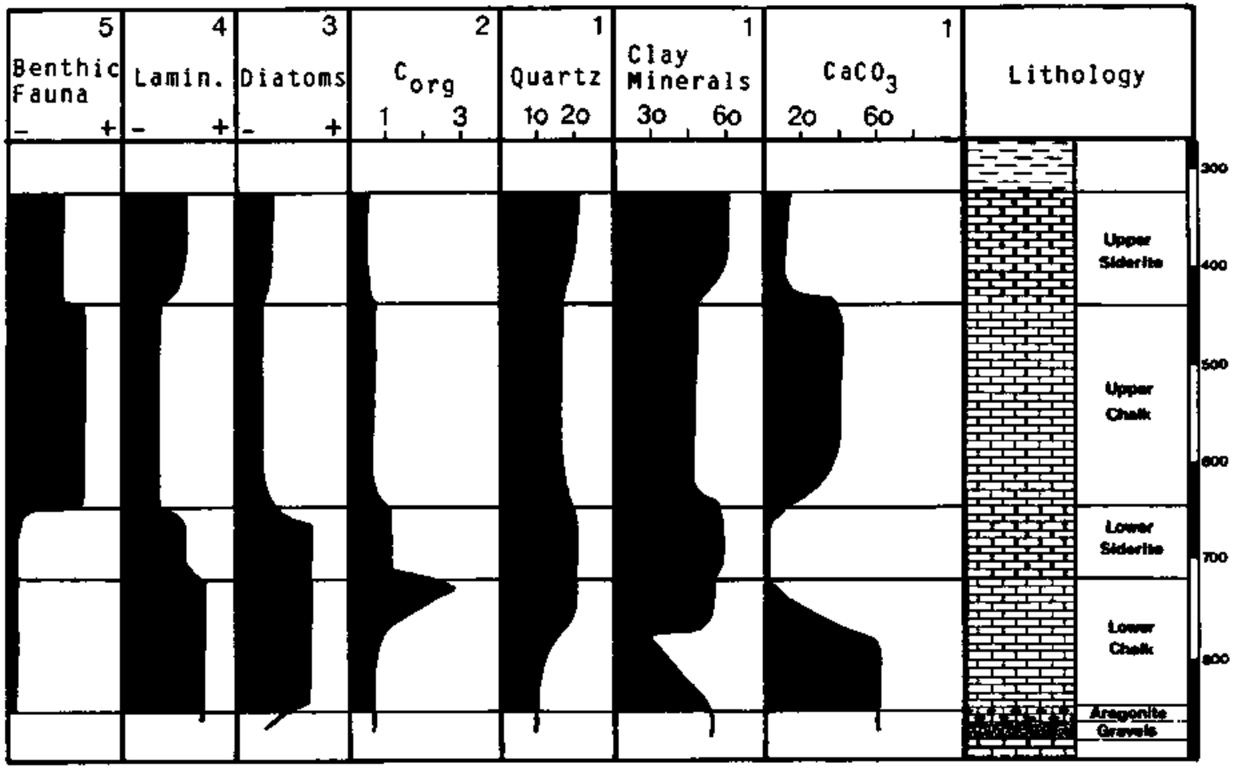

Fig. 6-4. Schematic diagram of important petrographic data from the Black Sea chemical sediments. Cyclic variations of the mineral composition are superposed by a more general development of the fauna and the organic chemistry. (Data from: *1* = Trimonis et al., 1978; *2* = Emelyanov et al., 1978; *3* = Traverse, 1978; *4* = Hsü and Kelts, 1978, Stoffers and Müller, 1978; *5* = Hsü and Kelts, 1978; Olteanu, 1978.)

was dominated by clastic input from the River Danube (Popp, 1968; Shimkus and Trimonis, 1974; Hsü, 1978).

Chemical sediments

The twofold repetition of the chalk and siderite units characterizes a period when the Black Sea was a closed basin without a permanent connection to the Mediterranean Sea.

Hsü and Kelts (1978) suggested that a low detritus input was the main condition for the concentration of precipitated carbonates in the sediments. Figure 6-4 summarizes some of the most important sedimentological data of this sequence.

Most of the sediments are laminated clays and silts, with small grains of typical planktogenic calcite, constituting about 40–60% by weight in the chalk units and about 5–18% by weight in the siderite units. In contrast to the light-grey chalk sediments, the green-grey to olive-grey siderite-bearing muds have the typical odor of "protopetroleum" (Stoffers and Müller, 1978).

Additionally, Fig. 6-4 shows that cyclic changes of some main sedimentary characteristics are superposed by a more steady, climate-governed variation of both fauna and flora:

(1) At the transition of the Pliocene to the Alpha glacial period, both diatoms and C_{org} diminish, thus indicating a reduction of the phytoplankton.

(2) At the same time, less frequently laminated core sections and the existence of a benthic fauna indicate that an oxygenated deep-water mass developed at least periodically during the Alpha glacial period (Olteanu, 1978).

(3) The third important feature of the chemical sedimentary sequence is a decrease in the salinity from brackish to fresh water during the Lower Chalk and Lower Siderite periods (Schrader, 1978).

(4) A brackish water chemistry again developed during the Upper Siderite period, when a rising water level in the Mediterranean Sea promoted an episodic introduction of saline water into the Black Sea basin.

OCCURRENCE AND CHARACTERISTICS OF SIDERITE

In both siderite units, three types of siderite can be distinguished macroscopically: disseminated crystals, layers of millimeter to centimeter thickness and concretions of millimeter to 5 cm in diameter. In the Lower Siderite period, these types are more or less evenly distributed; whereas the siderite layers predominate in the lower part of the Upper Siderite, from section 380A/9 to 380/40. The upper part of the Upper Siderite consists mostly of concretions and disseminated crystals.

The shapes of the individual crystals vary independently from the macroscopic types. They are equant, rounded and anhedral in the Upper Siderite sequence and anhedral, wheat-grain- or dumb-bell-shaped in the Lower Siderite deposits. These are in good agreement with the observations of Hsü and Kelts (1978), who published SEM pictures of different Black Sea siderites.

TABLE 6-1

Chemistry of Black Sea siderites from the chemical sediments. In contrast to the Mn-rich carbonates from the Lower Siderite Unit, the siderites from the Upper Siderite Unit exhibit a significant rise of earth-alkaline ions (after Stoffers and Müller, 1978)

Sample (interval in cm)	Fe (%)	Mn (%)	Ca (%)	Mg (%)
Hole 380				
21-4, 45–46	12.0	0.30	6.7	1.9
37-1, 60–63	22.0	0.54	6.6	1.43
37-2, 41–43	16.3	0.29	7.4	1.55
38-2, 24–26	13.96	0.25	5.6	1.72
40-1, 80–82	15.5	0.28	5.9	1.67
Hole 380A				
1-3, 111–113	13.3	0.36	7.0	1.74
4-4, 122–123	22.0	0.43	5.7	1.34
8-2, 117–119	13.38	0.51	6.0	1.5
8-5, 148–150	25	0.71	4.6	0.97
9-1, 126–128	18.22	0.76	3.8	1.36
10-1, 148–150	12.38	0.58	5.6	1.62
12-1, 68–70	25.0	1.93	4.9	1.13
12-4, 93–95	13.0	0.63	9.0	1.47
34, CC	30.0	1.93	4.6	0.62
36-2, 80–82	28.2	2.90	4.2	0.52
36-6, 134–136	31.6	1.70	2.3	0.67
39-3, 102–104	23.6	1.48	3.1	0.94
39-3, 109–110	23.25	1.44	2.4	0.94
40-5, 60–63	31.6	7.00	1.8	0.26
42-1, 5–7	30.0	2.59	2.2	0.84
42-2, 40–42	19.24	0.98	5.6	1.1

The size of the crystals and crystal aggregates ranges from 5 μm to 20 μm and rarely reaches 30 μm.

In addition to the crystal shape, the chemistry of the siderites from both units exhibits characteristic differences (Stoffers and Müller, 1978; Table 6-1):

(1) iron carbonate from the Upper Siderite sequence is enriched with Ca and Mg, whereas the Mn content is low; and

(2) Fe-carbonate from the Lower Siderite deposits contains less Ca and Mg, but up to 7 wt.% Mn. In the case of earth-alkaline ions, the Mg content drops from >1 wt.% in the Upper Siderite sequence to <1 wt.% in the Lower Siderite deposits.

STABLE ISOTOPE DATA OF SIDERITE AND CALCITE

Figure 6-5 shows two cumulative plots of δ^{13}C and δ^{18}O data (Table 6-2) from both calcite and siderite samples.

The diagram for Lower Siderite deposits exhibits a strong variation of the siderite

TABLE 6-2

Stable isotope data of calcite and siderite samples from the Black Sea chemical sediments

Sample Hole/Core/Section/Sample	Siderite		Calcite	
	$\delta^{13}C$	$\delta^{18}O$	$\delta^{13}C$	$\delta^{18}O$
Hole 380				
380/37/1/60–61	−0.84	−4.71		
380/37/2/35–37	+0.87	−2.62	+0.32	−4.55
380/37/2/85–87	+1.02	−2.26	−0.24	−4.84
380/38/2/95–97			+1.53	−4.24
380/40/1/142–143	+0.01	−0.22	−0.50	−3.29
Hole 38A				
380A/4/3/126–128	+0.01	−0.80	−0.70	−3.78
380A/4/4/18–20			+0.22	−3.79
380A/4/4/23–24	−1.02	−2.93	+2.51	−4.20
380A/4/4/82–84	+0.84	−0.33	+0.70	−3.89
380A/6/3/63–65	+2.02	−4.57		
380A/6/3/124–126	+0.90	−3.18	+1.58	−6.17
380A/8/2/140–142			+0.99	−3.89
380A/9/3/133–135	+1.82	−2.45	+0.58	−5.17
380A/9/3/135–137	+1.26	−2.01		
380A/9/4/78–80	+2.86	−2.52	+0.54	−7.11
380A/9/5/29–31			−0.20	−4.89
380A/9/5/47–49			+0.40	−7.05
380A/9/6/88–89			+2.61	−3.84
380A/9/6/106–167	+2.51	−3.24	+2.58	−5.20
380A/9/6/116–118	+2.34	−5.10	+2.51	−5.64
380A/35/2/135–139	+4.27	−4.71	+1.94	−7.28
380A/36/2/77–79			+1.75	−4.92
380A/37/2/35–37			−0.49	−4.19
380A/39/3/102–104	−0.83	−6.73		
380A/41/1/55–57	+11.22	−1.47		
380A/42/4/14–16			+1.09	−2.16
380A/42/4/20–22	+10.35	−1.28		
380A/42/4/23–25	+8.90	+0.12	+1.88	−5.94
380A/42/4/53–55	+1.50	−4.48	+1.49	−6.71
380A/42/4/110–112	+2.26	−1.57	+1.13	−4.36
380A/42/6/24–26	+5.45	−3.50		

$\delta^{13}C$, which rises from between −1‰ and +2‰ PDB for the disseminated type to >+10‰ for the concretions. The layered type siderite seems to vary between these extreme values. The planktogenic calcite is characterized by a stable isotope composition similar to that of the disseminated siderite.

The diagram of the Upper Siderite carbonates seems to reflect similar environmental conditions in the $\delta^{18}O$ data. The contents of ^{13}C of calcite and all three siderite types, however, plot in the same interval of −2‰ to +4‰.

A stratigraphic plot of the siderite stable isotope data exhibits no systematic variation of $\delta^{13}C$ and $\delta^{18}O$. In contrast, the stable isotopes of the planktogenic calcite vary systematically between the different stratigraphic units (Fig. 6-6). The mean values of $\delta^{18}O$ drop from about −4‰ in the Lower Chalk to −5‰ in the Lower Siderite and −6.4‰ in the Upper Chalk. In the Upper Siderite they rise again to −4.7‰. This curve is covariant with the development of the Steppe Index of Traverse (1978; Fig. 6-3), as well as with the development of the salinity (Schrader, 1978; Fig. 6-6).

The $\delta^{13}C$ data suggest a general difference in the CO_2 budget of siderite and calcite units. The $CaCO_3$ of calcite units exhibits $\delta^{13}C$ mean values of +0.75‰ to +1.2‰. In contrast, in the siderite units the analyses of $CaCO_3$ give mean values of +2.8‰ to +3.6‰.

SIDERITE FORMATION AND EARLY DIAGENETIC CONDITIONS

The varieties of crystal habit, chemistry, and stable isotope data clearly reflect differences of the early diagenetic environment for both siderite units.

Varying siderite types and crystal habits and a high Fe/Mn content are typical

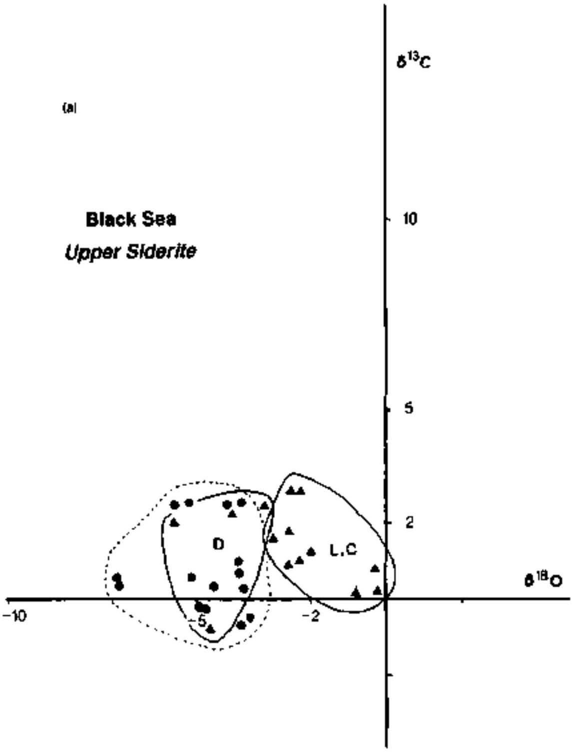

Fig. 6-5. Stable isotope diagrams for calcite (dots) and siderite (triangles) of both siderite units. The Lower Siderite exhibits a wide variety of $\delta^{13}C$-values, the concretions showing a strong signal of methanogenesis. Siderite types: C = concretions, L = layers, D = disseminated siderite. (Including data from Deuser et al., 1978.)

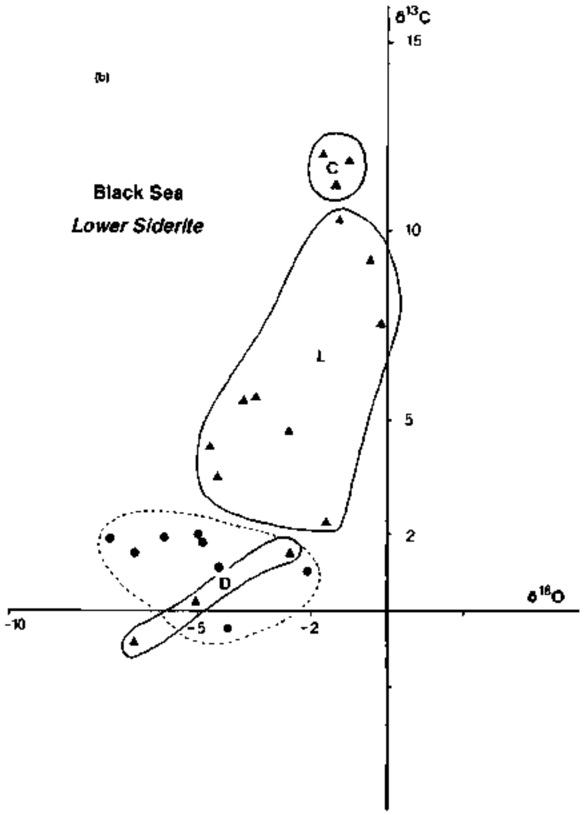

Fig. 6-5 (continued).

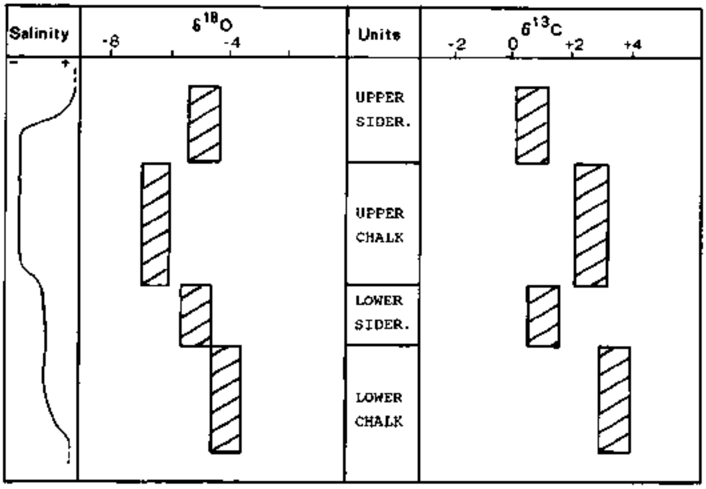

Fig. 6-6. Mean stable isotope values of calcites from the different units of the chemical sediments, including data from Deuser et al. (1978). The $\delta^{13}C$ is characterized by a cyclic variation of the mean values; the $\delta^{18}O$ seems to reflect the salinity changes.

of the Lower Siderite deposits, where the stable isotope data indicate a siderite formation during different stages of early diagenesis, including methanogenesis.

In contrast, the Upper Siderite $FeCO_3$ exhibits a more uniform crystal shape, an almost constant $\delta^{13}C$ and a high Ca/Mg content, suggesting a higher earth-alkali/iron content of the pore solutions.

Both manganese and iron are generally transported to the lake bottom as particles of oxides or oxide–hydroxides (Wetzel, 1975). When the redox conditions become anoxic at the sediment/water boundary due to O_2 consumption by microbial organic matter decomposition, both metals are remobilized as Fe^{2+}- and Mn^{2+}-ions (Stumm and Morgan, 1981; Fig. 6-1). If at the same time, the CO_2 partial pressure exceeds 10^{-6} atm and the sulfide concentration is below 10^{-7} mol/l, a siderite characterized by a high Fe/Mn content may be precipitated.

Thus, a siderite with substantial amounts of earth-alkali ions indicates additional sources of these elements within the formation, e.g., unstable carbonates (Einsele and von Rad, 1979; Matsumoto and Iijima, 1981) or silicates. Bahrig (1988) found a significant rise in the Ca/Mg content of siderite in sediments of the Eocene Messel oil shale lake during a phase of higher clastic input, which later dropped substantially with the reduction in the coarse clastic layers.

In the Black Sea, Hsü and Kelts (1978) found that strong corrosion of the planktogenic calcite is characteristic of the Upper Siderite deposits, where the high Ca/Mg content of the siderite seems to reflect the high calcite content of the sediments.

A mobilization of both Ca/Mg and CO_2 from this calcite could furthermore explain the almost constant $\delta^{13}C$ of the Upper Siderite carbonates.

In general, the siderite stable isotope data show that the disseminated siderite type of the Lower Siderite sequence and all three types of the Upper Siderite sequence plot in the field of "normal" lacustrine carbonates (e.g., Clayton and Degens, 1959; Hoefs, 1980). In the Lower Siderite sequence, a part of the siderite layers and all concretionary siderites exhibit a strong $\delta^{13}C$ signal of methanogenesis.

In contrast to the earlier diagenetic phases, during which the negative $\delta^{13}C$ signal of the organic substance is transferred to the pore-water CO_2 by microbial destruction, in a methanogenic environment the C-pool of the organic matter is divided into isotopically extremely light CH_4 ($\delta^{13}C$ of -60 to -110‰; Whiticar et al., 1986) and a CO_2 that is enriched in ^{13}C. These conditions are reflected by extremely positive $\delta^{13}C$ values of carbonates formed during this diagenetic phase (Irwin et al., 1977; Kelts and McKenzie, 1982; Henderson et al., 1984).

For a further interpretation of these data, the question is raised as to which type of siderite was precipitated first: the concretions or the disseminated crystals? This question can be answered by a careful interpretation of the oxygen isotope data:

The $\delta^{18}O$ difference between planktogenic calcite and concretionary siderite is $+3.0$ to $+3.5$‰ PDB in both siderite units. About 1.5‰ of this difference can be explained by the different fractionation factors of calcite and siderite (Fig. 6-7), using the data of Becker and Clayton (1976) and Golyshev et al. (1981). Another 0.75‰ is caused by the different fractionation of oxygen during the H_3PO_4 preparation (Bahrig, 1988). The remaining 0.75 to 1.3‰ point to a temperature difference of

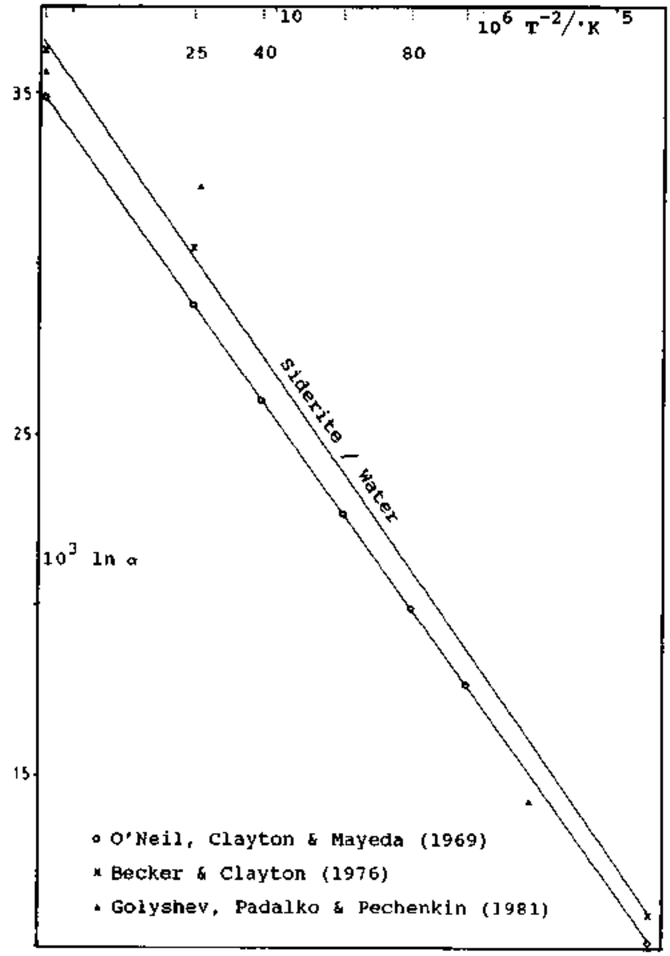

Fig. 6-7. Calculated curves for the temperature dependence of the oxygen stable isotope fractionation of calcite and siderite. The difference of the oxygen fractionation between both carbonates is about 1.5‰ for sedimentary environments.

4–6°C during the formation of both carbonates (O'Neil et al., 1969), if they were precipitated from the same solution.

Thus, if the whole water mass of the Black Sea exhibited a constant $\delta^{18}O$ at the time of calcite precipitation, surface water temperature of only 8–10°C can be deduced.

The paleoenvironment data, however, suggest the existence of an at least periodically stagnant water mass with an anoxic hypolimnion. Thus, a proposed $\delta^{18}O$ gradient of +1 to +2‰ from hypolimnion to epilimnion, owing to evaporation from the surface water, yields a more realistic water temperature of 15 to 20°C for the epilimnion, where the calcite was precipitated during the summer algal blooms (Hsü and Kelts, 1978).

If a similar calculation is performed for the disseminated siderite type, no realistic temperatures can be obtained, because no $\delta^{18}O$ difference exits between this siderite and calcite. As a consequence, the formation of siderite must have started with the concretions and finished with the precipitation of disseminated siderite crystals. Siderite layers seem to have been formed during the entire duration of $FeCO_3$ precipitation.

The evolution of the pore-water chemistry reflected by the $\delta^{13}C$ and $\delta^{18}O$ variations of the Lower Siderite $FeCO_3$ types is quite similar to the formation of dolomite in the Quaternary sediments of the Gulf of California (Kelts and McKenzie, 1982) and in the diatomaceous Sisquoc Formation in California (Henderson et al., 1984). In both sequences, the dolomite formation started during an early diagenetic phase with strong methanogenesis. Younger generations of dolomite reflect a continuous depletion of ^{13}C and ^{18}O in the pore water due to decreasing methanogenesis and a reduction of isotopically heavy CO_2 by carbonate precipitation.

The Upper Siderite unit shows no $\delta^{13}C$ gradient of different siderite types, though the $\delta^{18}O$ data suggest a similar chronology of their formation. Two factors may explain this observation:

(1) a less-intensive microbial destruction of organic matter without methanogenesis, because the C_{org} content is substantially lower in comparison to the Lower Siderite unit (Fig. 6-4); and

(2) a dissolution of calcite, which could buffer the ^{13}C content of the CO_2 and mobilize Ca and Mg.

Although both factors seem to carry equal importance, the second one may offer an answer to the question as to why siderite could be precipitated only during the formation of siderite units. Results of an experimental study by Füchtbauer (1980) showed that the formation of Ca-rich siderite is limited to an Fe/Ca of >0.2 in the precipitating solution, so that higher Ca concentrations led to the formation of only (Fe)-calcite.

During his work on the early diagenesis in Swiss lakes, Emerson (1976) found that in the sediment/water boundary layer the mobilization of Fe^{2+} and Mn^{2+} and rising CO_2 partial pressure as a result of microbial activity is accompanied by a release of Ca and Mg to the pore water from unstable Ca/Mg-carbonates. Moreover, a replacement of calcite by siderite has been observed by Einsele and von Rad (1979) in deep-sea sediments from Leg 47. One of the reasons for this phenomenon may be the lower solubility of siderite than that of calcite by a factor of about 10^2.

If these observations and experimental data are used to interpret the difference between the siderite and the chalk units, the calcite content seems to be the controlling factor for the siderite formation. Only during the formation of siderite units, the content of calcite/iron oxides and hydroxides was low enough to permit the precipitation of siderite in a pore solution with a Fe/Ca ratio > 0.2. During the chalk formation periods, the calcite content of the sediments was high and the Fe/Ca of the pore solution < 0.2; as a consequence no siderite could be precipitated.

The hypothesis of the Fe/Ca ratio to be the controlling factor was also favored by Hsü and Kelts (1978). These authors tried to explain the restriction of the siderite formation to warmer periods by a rise of the Fe/Ca ratio of the whole water mass due to a climate-dependent variation of the river-water chemistry in the catchment area. Additional arguments for this change of both river water and Black Sea chemistry, however, cannot be found in the sedimentary sequence.

The diagenetic model proposed here needs no additional hypothetical factors aside from the sediment composition. The different chemistry at the sediment/water boundary and in the early diagenetic pore solutions, which is governed by the calcite content, adequately explains the formation of siderite only during certain periods of the sedimentary history of the Black Sea.

GENERAL MODEL FOR THE FORMATION OF THE CHALK AND SIDERITE UNITS

Table 6-3 summarizes the most important characteristics of chalk and siderite units of the Black Sea sedimentary sequence. Concerning the C-budget, the following observations must be included in a general model:

(1) the $\delta^{13}C$ of the planktogenic calcite is about 2‰ higher in the chalk units;

(2) the H/C ratio drops below 1.0 in the Lower Siderite unit but rises to > 1.0 in both chalk units (Huc et al., 1978); and

(3) the glucose/ribose ratio is <20 in both chalk units, and >20 in the Lower Siderite (Mopper et al., 1978).

Both the low H/C ratio and the high glucose/ribose ratio are interpreted by the above authors as indicators of a higher amount of terrigenous organic detritus in the organic matter. In contrast, the chalk units are characterized by a higher input of autochthonous, algal organic carbon to the sediments.

The $\delta^{13}C$ data may be interpreted to represent two general phenomena:

(1) McKenzie (1982) observed a rise of $\delta^{13}C$ in planktogenic calcite during periods of high productivity in Swiss lakes. This effect is explained by the concentration of ^{12}C in algae and macrophytes (Osmond and Ziegler, 1975). Thus, with rising productivity the epilimnion of lakes is enriched in isotopically heavy CO_2, which is incorporated into planktogenic calcite.

TABLE 6-3

Some main characteristics of the two phases of chalk and siderite formation during the history of the Black Sea

	Siderite Unit	Chalk Unit
Precipitation of calcite	low	high
Precipitation of siderite	high	low
Lamination of sediments	dominant	dominant
Fe/Ca ratio in pore solutions	high	low
Organic substance	detritic	planktogenic
Nutrient input	low	high
Productivity	moderate	high
Steppe Index	forest	steppe
Climate	more humid	more arid
Stage	interglacial	glacial interstadial

(2) A high input of ^{12}C-enriched terrigenous organic detritus leads to a lower $\delta^{13}C$ of the lake water, should enough C from this material be released to the lake water by microbial processes.

The examination of the organic chemistry data of the sediments reveals a close correspondence with the interpretation of isotope data. Both a high phytoplankton productivity during the chalk formation periods and a higher input of organic detritus during the more humid siderite formation periods (Traverse, 1978) may provide a further explanation for the trend in the chemical and isotopic data.

Generally, the siderite and chalk units represent two different stages of the chemical and ecological system of the Black Sea lake. Based on the climatic conditions, these two stages may be characterized as follows (Table 6-3, Fig. 6-8):

During *siderite periods* the climate was more humid, resulting in a higher input of terrigenous organic detritus.

This material was largely composed of chemically stable humic substances (Huc et al., 1978): as a consequence, the nutrient level of the epilimnion was low, resulting in a moderate plankton productivity. This was furthermore promoted by a strong fixation of nutrients in the land plants, documented in the pollen flora as a "forest vegetation". Only small amounts of calcite were precipitated during the summer months, and were additionally reduced in the lower water column before reaching the lake bottom.

The lamination of the sediments suggests at least a periodically stagnant, oxygen-free deep-water mass (Hsü and Kelts, 1978). The Fe and Mn were mobilized at the sediment/water interface by microbial oxygen consumption and precipitated as carbonates in a reducing but sulfide-poor pore-water environment.

During the Lower Siderite period, the higher organic matter content additionally favored an early diagenetic methanogenesis (Lovley and Klug, 1986).

In contrast, the *chalk periods* were characterized by a high phytoplankton productivity. Periodically, high amounts of calcite were precipitated and reached the lake

Fig. 6-8. General model for the origin of the Black Sea chemical sediments, stressing the strong interaction of climate, flora and fauna, sediment composition, and diagenesis. Supplementary data are given in Table 6-3.

During the Lower Chalk period, the vegetation was of steppe-type and the input of nutrients into the Black Sea Basin was high. This resulted in a high biological productivity and precipitation of planktogenic calcite. An anoxic hypolimnion is indicated by laminated sediments. During the following Lower Siderite period, the forest vegetation fixed more nutrients, a reduced nutrient input allowed only a low plankton productivity, and only a small amount of calcite was precipitated. In the anoxic sediment a high Fe/Ca ratio and methanogenesis promoted the formation of siderite.

In the following chalk period, a reduced vegetation cover again allowed an increase of the nutrient transport into the lake basin. More planktogenic calcite could precipitate. In the deep water mass, periods of anoxia alternated with times of oxic conditions. In the sediments, the low Fe/Ca ratio prevented siderite formation.

During the Upper Siderite period, the climatic conditions again promoted the fixation of nutrients in the land plants. A low productivity resulted. Additionally, the high water level in the Mediterranean Sea led to the spill-over events, during which saline water was introduced into the Black Sea Basin. A brackish water mass developed in the lower part of the anoxic deep water. Thus, in the central basin pyrite was precipitated; the siderite formation was limited to the marginal part of the deep water facies.

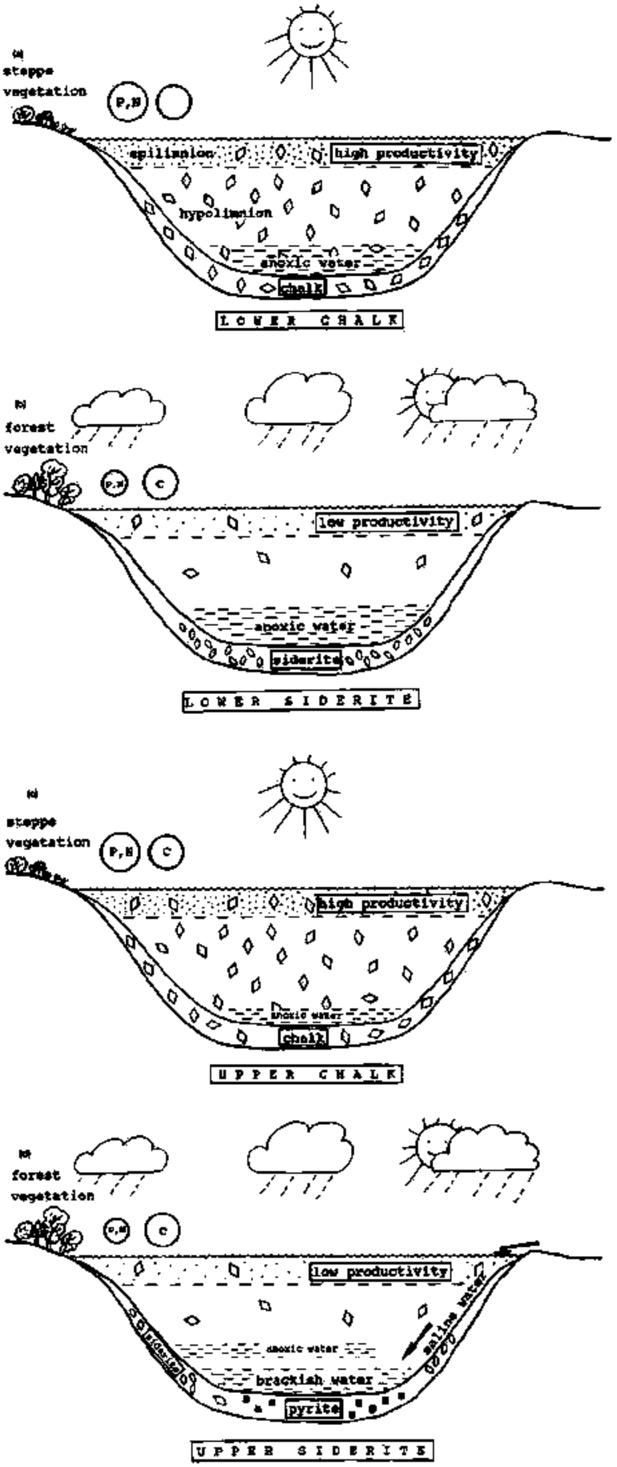
(a)
steppe vegetation
P,N
epilimnion
high productivity
hypolimnion
anoxic water
chalk
LOWER CHALK
(b)
forest vegetation
P,N
C
low productivity
anoxic water
siderite
LOWER SIDERITE
(c)
steppe vegetation
P,N
C
high productivity
anoxic water
chalk
UPPER CHALK
(d)
forest vegetation
P,N
C
low productivity
saline water
anoxic water
brackish water
siderite
pyrite
UPPER SIDERITE

bottom. The sedimentary organic matter shows a predominance of autochthonous algal material.

During a more arid climate (Traverse, 1978), the vegetation changed to a "steppe"-like flora, so that the input of organic detritus was low. Moreover, less nutrients were fixed by the land vegetation resulting in a higher nutrient input to the lake water, which lead to a high biological productivity. A periodic stratification of the water mass is suggested by the laminated sediments. A benthic ostracod fauna was established during the Upper Chalk time (Olteanu, 1978), indicating an oxygenated hypolimnion.

In the sediments, the high calcite content resulted in a high Ca/Fe ratio of the pore water so that no siderite could precipitate.

This cyclic succession of the siderite and chalk periods is superposed on a more general development of the lake, governed by long-term variations of climate and salinity.

Figure 6-4 shows that during the Pliocene to lower Pleistocene time a cooling of the lake water was accompanied by a reduction of the diatom flora and of the organic matter flux to the sediments. The $\delta^{18}O$ of the planktogenic calcite varies parallel to both steppe index and salinity.

This trend may theoretically be explained by a climate-dependent variation of the evaporation. If this alone were the controlling factor, however, a more cyclic variation parallel to the twofold climatic change between warm/humid and cool/arid would be expected.

Thus, the change from isotopically-heavy brackish water in the Pliocene to an isotopically-light fresh water in the Pleistocene provides the most likely explanation for this observation. In contrast to the interpretation of the diatom flora by Schrader (1978), who proposed that in the Lower Siderite period the Black Sea was already a fresh-water lake, the isotopes indicate that the lake did not reach this stage before the Upper Chalk period. This interpretation is further supported by the development of a rich fresh-water dinoflagellate flora during this period.

The rise of the $\delta^{18}O$ in the Upper Siderite period reflects a rising salinity of the lake water as a result of spill-over events, when saline water from the Mediterranean Sea entered the Black Sea. During this period, a stratification of the water mass is clearly reflected in the diagenetic pattern of the sediments. The Upper Siderite unit of the marginal facies is substituted by a pyrite unit in hole 379 within the central part of the Black Sea Basin, where the sulfide was precipitated from a brackish, sulfate-rich water.

ACKNOWLEDGEMENTS

These investigations were carried out at the ETH Zürich with the help of a post-doctoral grant of the Deutsche Forschungsgemeinschaft. H. Füchtbauer and K. Hsü offered technical support and advice. Additional valuable suggestions were made by K. Kelts, J. McKenzie, F. Niessen, and H. Oberhänsli, whose help is gratefully acknowledged. The help extended by Drs. George V. Chilingarian and K.H. Wolf is also greatly appreciated.

REFERENCES

Bahrig, B., 1985. Diagenese und Sedimentation in Laacher Seebecken. *Bochumer Geol. Geotechn. Arb.*, 19: 239 pp.

Bahrig, B., 1988. Paleoenvironment information from deep water siderite (Lake of Laach, W. Germany). In: A. Fleet, K. Kelts, M. Talbot (Editors), *Lacustrine Petroleum Source Rocks. Geol. Soc. London, Spec. Publ.*, 40: 153–158.

Bahrig, B., 1989. Stable isotope composition of siderite as an indicator of the paleoenvironment history of oil shale lakes. *Palaeogeogr., Palaeoclimatol., Palaeoecol.*, 70: 139–151.

Bahrig, B. and Conze, R., 1986. Siderit als Tracer frühdiagenetischer Prozesse. *1. Treffen deutschsprachiger Sedimentologen, 7–8 March 1986, Abstr.*, pp. 8–11.

Baur, M.E., Hayes, J.M, Studley, S.A. and Walter, M.R., 1985. Millimeter-scale variations of stable isotope abundances in carbonates from banded iron-formations in the Hamersley Group of Western Australia. *Econ. Geol.*, 80: 270–282.

Becker, R.H. and Clayton, R.N., 1976. Oxygen isotope study of a Precambrian banded iron-formation, Hamersley Range, Western Australia. *Geochim. Cosmochim. Acta*, 40: 1153–1165.

Berner, R.A., 1981. A new geochemical classification of sedimentary environment. *J. Sediment. Petrol.*, 51: 359–365.

Clayton, R.N. and Degens, E.T., 1959. Use of carbon isotope analysis of carbonates for differentiating fresh-water and marine sediments. *Bull. Am. Assoc. Pet. Geol.*, 43: 890–897.

Curtis, C.D. and Spears, D.A., 1968. The formation of sedimentary iron minerals. *Econ. Geol.*, 63: 257–270.

Deuser, W.G., Degens, E.T. and Stoffers, P., 1978. O-18 and C-13 contents of carbonates from Deep Sea Drilling Sites in the Black Sea. *Init. Rep. DSDP*, 42, 2: 617–624.

Einsele, G. and von Rad, U., 1979. Facies and paleoenvironment of Lower Cretaceous sediments at DSDP site 397 and in the Aaiun Basin (northwest Africa). *Init. Rep. DSDP*, 47(1): 559–577.

Emelyanov, E. et al., 1978. Geochemistry of Late Cenozoic sediments of the Black Sea, Leg 42B. *Init. Rep. DSDP*, 42, 2: 543–606.

Emerson, S., 1976. Early diagenesis in anaerobic lake sediments: chemical equilibria in interstitial waters. *Geochim. Cosmochim. Acta*, 40: 925–934.

Füchtbauer, H., 1980. Experimental precipitation of ferroan calcites. *IAS 1st Europ. Meet., Bochum, 1980, Abstr.*, pp. 170–171.

Gautier, D.L., 1982. Siderite concretions: indicators of early diagenesis in the Gammon Shale (Cretaceous). *J. Sediment. Petrol.*, 52: 859–871.

Golyshev, S.I., Padalko, N.L. and Pechenkin, S.A., 1981. Fractionation of stable oxygen and carbon isotopes in carbonate systems. *Geokhimiya*, 10: 1427–1441.

Hangari, K.M., Ahmad, S.N. and Perry, E.C., Jr., 1980. Carbon and oxygen isotope ratios in diagenetic siderite and magnetite from Upper Devonian Ironstone, Wadi Shatti District, Libya. *Econ. Geol.*, 75: 538–545.

Henderson, N.C., Jr., Crawford, G.A., Dunham, J.B. and Osborne, R.H., 1984. Relationship of diagenetic dolomite to depositional facies in diatomaceous strata, Upper Sisquoc Fm., Casmalia Hills, Santa Barbara Co., California. In: R.E. Garrison, M. Kastner and D.H. Zenger (Editors), *Dolomites of the Monterey Formation and Other Organic-rich Units. Pacific Sect., Soc. Econ. Paleontol. Mineral.*, 41: 119–140.

Hoefs, J., 1980. *Stable Isotope Geochemistry*. Springer, Berlin, 208 pp.

Hsü, K.J., 1978. Stratigraphy of the lacustrine sedimentation in the Black Sea. *Init. Rep. DSDP*, 42, 2: 509–524.

Hsü, K.J. and Giovanoli, F., 1979. Messinian Event in the Black Sea. *Palaeogeogr., Palaeoclimatol., Palaeoecol.*, 29: 75–93.

Hsü, K.J. and Kelts, K., 1978. Late Neogene sedimentation in the Black Sea. In: A. Matter and M.E. Tucker (Editors), *Modern and Ancient Lake Sediments. IAS Spec. Publ.*, 2: 127–144

Huc, A.Y., Durand, B. and Monin, J.C., 1978. Humic compounds and kerogens in cores from Black Sea sediments, Leg 42B — Holes 379A,B, and 380A. *Init. Rep. DSDP*, 42: 737–748.

Irion, G., 1977. Der eozäne See von Messel. *Nat. Mus.*, 107: 214–218.

Irwin, H., Curtis, C. and Coleman, M., 1977. Isotopic evidence for source of diagenetic carbonates formed during burial of organic-rich sediments. *Nature*, 269: 209–213.

Kelts, K. and McKenzie, J.A., 1982. Diagenetic dolomite formation in Quaternary anoxic diatomaceous muds of Deep Sea Drilling Project Leg 64, Gulf of California. *Init. Rep. DSDP*, 64: 553–570.

Lovley, D.R. and Klug, M.J., 1986. Model for the distribution of sulfate reduction and methanogenesis in freshwater sediments. *Geochim. Cosmochim. Acta*, 50: 11–18.

Matsumoto, R., 1989. Isotopically heavy oxygen-containing siderite derived from the decomposition of methane hydrate. *Geology*, 17: 707–710.

Matsumoto, R. and Iijima, A., 1981. Origin and diagenetic evolution of Ca/Mg/Fe carbonates in some coalfields of Japan. *Sedimentology*, 28: 239–259.

McCrea, J.M., 1950. On the isotope chemistry of carbonates and a paleotemperature scale. *J. Chem. Phys.*, 18: 849–857.

McKenzie, J.A., 1976. *Isotope Study of the Hydrology and the Coexisting Carbonate Phases from Site of Recent Dolomitization of the Coastal Sabkha of Abu Dhabi.* Dissertation, ETH Zürich No. 5778: 164 pp.

McKenzie, J.A., 1982. Carbon-13 cycle in Lake Greifen: A Model for restricted ocean basins. In: S.O. Schlanger and M.B. Cita (Editors), *Nature and Origin of Cretaceous Carbon-rich Facies.* Academic Press, London, pp. 197–207.

Mopper, K., Michaelis, W., Garrasi, C. and Degens, E.T., 1978. Sugars, amino acids, and hydrocarbons in Black Sea sediment from DSDP Leg 42B cores. *Init. Rep. DSDP*, 42, 2: 697–706.

Mozley, P.S., 1989. Relation between depositional environment and the elemental composition of early diagenetic siderite. *Geology*, 17: 704–706.

Olteanu, R., 1978. Ostracoda from DSDP Leg 42B. *Init. Rep. DSDP*, 42, 2: 1017–1038.

O'Neil, J.R., Clayton, R.N. and Mayeda, T.K., 1969. Oxygen isotope fractionation in divalent metal carbonates. *J. Chem. Phys.*, 51: 5547–5558.

Osmond, C.B. and Ziegler, H., 1975. Schwere Pflanzen und leichte Pflanzen: Stabile Isotope im Photosynthesestoffwechsel und in der Biochemischen Ökologie. *Naturwiss. Rundsch.*, 28: 323–328.

Pearson, M.J., 1979. Geochemistry of the Hepworth Carboniferous sediment sequence and origin of the diagenetic iron minerals and concretions. *Geochim. Cosmochim. Acta*, 43: 927–941.

Popp, N., 1968. Quaternary deposit in the Danube valley. *Rev. Roumaine Geol., Geophys. Geogr., Ser. Geogr.*, 12: 67–72.

Postma, D., 1981. Formation of siderite and vivianite and the porewater composition of a recent bog sediment in Denmark. *Chem. Geol.*, 31: 225–244.

Postma, D., 1982. Pyrite and siderite formation in brackish and freshwater swamp sediments. *Am. J. Sci.*, 282: 1151–1183.

Ross, D.A., Neprochnov, Y.P. et al., 1978. *Initial Reports of the Deep Sea Drilling Project, Vol. 42, Part 2.* U.S. Government Printing Office, Washington, D.C., 1244 pp.

Schrader, H.-J., 1978. Quaternary through Neogene history of the Black Sea, deduced from the paleoecology of diatoms, silicoflagellates, ebridians, and chrysomonads. *Init. Rep. DSDP*, 42, 2: 789–902.

Shimkus, K.M. and Trimonis, S., 1974. Modern sedimentation in the Black Sea. In: E.T. Degens and D.A. Ross (Editors), *The Black Sea; Geology, Chemistry, and Biology. Am. Assoc. Pet. Geol., Mem.*, 20: 249–278.

Stoffers, P. and Müller, G., 1978. Mineralogy and lithofacies of Black Sea sediments, Leg 42B, Deep Sea Drilling Project. *Init. Rep. DSDP*, 42, 2: 373–412.

Stumm, W. and Morgan, J.J., 1981. *Aquatic Chemistry.* Wiley, New York, N.Y., 2nd ed., 780 pp.

Supko, P., Ross, D.A. and Neprochnov, Y.P., 1978. Introduction and explanatory notes, Leg 42B, Deep Sea Drilling Project. *Init. Rep. DSDP*, 42, 2: 3–15.

Talbot, M.R., Livingstone, D.A., Palmer, P.G., Maley, J., Melack, J.M., Delibrias, G. and Gullikson, S., 1984. Preliminary results from sediment cores from Lake Bosumtwi, Ghana. In: *Paleoecology of Africa and the Surrounding Islands*, 16: 173–192.

Timofeyeva, Z.V., Kuznetsova, L.D. and Dontsova, Y.I., 1976. Oxygen isotopes and siderite formation. *Geokhimiya*, 10: 1462–1475.

Traverse, A., 1978. Palynological analysis of DSDP Leg 42B (1975) cores from Black Sea. *Init. Rep. DSDP*, 42, 2: 993–1016.

Trimonis, E.S. et al., 1978. X-ray mineralogy studies Leg 42B. *Init. Rep. DSDP*, 42, 2: 451–468.

Weber, J.N., Williams, E.G. and Keith, M.L., 1964. Paleoenvironmental significance of carbon isotopic composition of sideritic nodules in some shales of Pennsylvanian age. *J. Sediment. Petrol.*, 34: 814–818.

Wetzel, R.G., 1975. *Limnology*. Saunders, Philadelphia, Pa., 743 pp.

Whiticar, M.J., Faber, E. and Schoell, M., 1986. Biogenic methane formation in marine and freshwater environments: CO_2 reduction vs. acetate fermentation — isotope evidence. *Geochim. Cosmochim. Acta*, 50: 693–709.

This Page Intentionally Left Blank

Diagenesis, IV. Developments in Sedimentology 51
edited by K.H. Wolf and G.V. Chilingarian
© 1994 Elsevier Science B.V., Amsterdam. All rights reserved.

Chapter 7

FORMATION OF STYLOLITES, MARL/LIMESTONE ALTERNATIONS, AND DISSOLUTION (CLAY) SEAMS BY UNSTABLE CHEMICAL COMPACTION OF ARGILLACEOUS CARBONATES

THOMAS DEWERS and PETER ORTOLEVA

INTRODUCTION AND EXAMPLES

Stress-induced reaction and mass transfer, often termed "pressure solution" or "solution transfer", has been implicated as a means for compactional loss of porosity in limestones (Neugebauer, 1974; Meyers, 1980; Meyers and Hill, 1983), as well as in the genesis of several types of banded, laminated, or other planar features in limestones during diagenesis. Examples of these include stylolites (Stockdale, 1922; Tada and Siever, 1988; termed sutured seam solution by Wanless, 1979), clay seams and spaced cleavage (Marshak and Engelder, 1985; termed non-sutured seam solution by Wanless, 1979), microlaminations with respect to porosity (Ekdale and Bromley, 1988), marl/limestone alternations (Ricken, 1986; Bathurst, 1987) and flaser or nodular bedding (Garrison and Kennedy, 1977). These structures are similar in that in most cases they appear to involve regions of heightened dissolution alternating with zones of cementation. However, the dramatic differences in the spacing and morphology of the dissolution zones that characterize these phenomena pose the question as to how a single diagenetic process can produce such a variety of responses.

In this chapter, using reaction–transport modeling, the writers attempt to describe the evolution of clay seams, stylolites, and marl/limestone alternations during chemical compaction in terms of a few coupled diagenetic processes. The model discussed herein accounts for diffusional mass transport, texture-dependent effective stress distribution, different reaction rates and driving forces for reaction at grain contacts and at grain "free" faces, and rate inhibition due both to solute inhibitors and clay coatings. The premise is that four manifestations of "pressure solution" in argillaceous carbonates (intergranular pressure solution or fitted fabric, marl/limestone alternations, stylolites, dissolution or clay seams) all arise from the same set of coupled processes under different limiting situations. In particular, it is shown that the reaction rate at grain–grain contacts relative to that at free grain faces is one deciding factor between behaviors in porous rocks. As the rates vary with, for example, pore fluid chemistry, temperature, clay content, and amount of overgrowth cement at grain contacts, the response of a porous rock to pressure solution will vary widely with different conditions. The case is examined in which calcite grains form the load-supporting framework, with an insoluble material (e.g., clay minerals or organic residue) residing in the pore space between the supporting grains but not necessarily filling them.

In addition, an example of clay seam formation in a low-porosity calcite–clay rock is examined using a model developed in an earlier study (Dewers and Ortoleva, 1989). This model incorporates results on the elastic matrix-inclusion problem (Eshelby, 1957) into a reaction–transport formalism. The effect of enhanced diffusion at phyllosilicate–calcite grain boundaries on the length scale and timing of clay seam formation is explored in this limit of low porosity.

The textural detail contained within the present model as well as its quantitative nature allows for rigorous comparison with observation. As an example, the case of diagenetic bedding (marl/limestone alternations) as studied by Ricken (1986) is considered. Observations place constraints on initial lithology, burial history, genesis time, and the characteristic length (or repeat distance) for the alternation. Furthermore, the nature of the repetitive lithologic pattern is quite well defined and "universal" — bands of enhanced compaction, porosity and clay content alternate with bands of calcite overgrowth. Finally, a wealth of calcite kinetic and thermodynamic data as well as mechanical and transport data strongly constrain the parameters of the model. Thus, it is held that this modeling approach will be of great value in interpreting the observations on these phenomena by placing them within a unified mechanochemical framework.

Figure 7-1 shows a burial scenario linking the evolution of what may be termed "self-organization" phenomena or "diagenetically differentiated structures" (see Chapter 4) — stylolites, centimeter-to-decimeter-scale marl/limestone alternations,

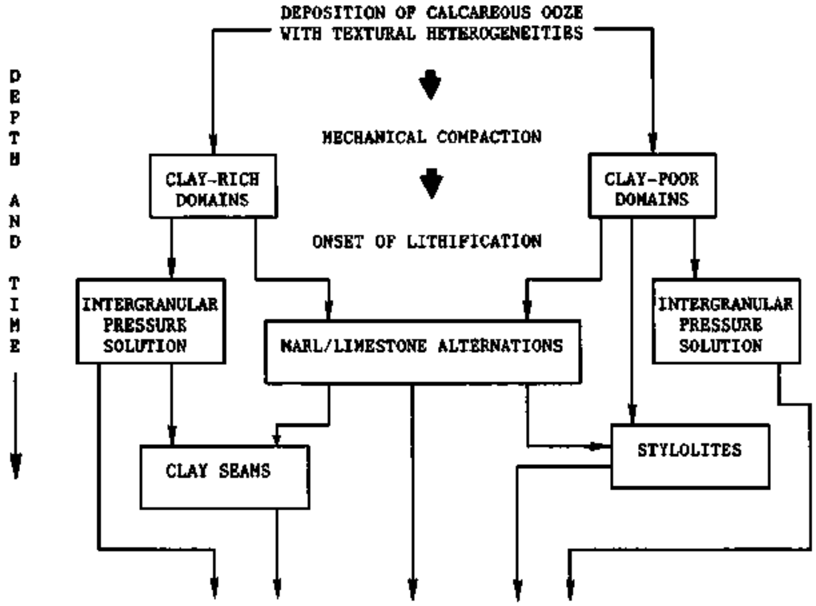

Fig. 7-1. Flow chart linking the postdepositional evolution of calcareous ooze with depth, as a function of burial. Depending on the initial lithology, the sediment can develop into stylolites, clay seams, marl/limestone alternations, or some combination thereof, during diagenesis.

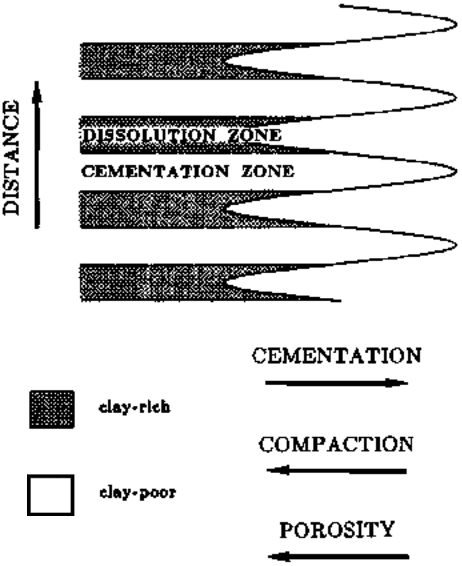

Fig. 7-2. Schematic cross-section of diagenetic marl–limestone alternations. Zones of greater compaction, clay, and porosity alternate with zones of greater cementation. (After Ricken, 1986, fig. 17.)

and millimeter-to-submillimeter-scale clay seams. Observations on pelagic calcareous sediments (Matter, 1974) and rocks derived from calcareous oozes (Schlanger and Douglas, 1974; Scholle, 1977; Ricken, 1986) suggest that the sequence of events in the ooze–chalk–limestone transition involves an initial stage of mechanical compaction (say, to 200 m below the sediment–water interface) followed by the initiation of cementation at grain contacts (Matter, 1974), and a shift in the dominant compaction mechanism from mechanical to chemical (Ricken, 1986; Schlanger and Douglas, 1974). Subsequently, zones of slightly enhanced cementation alternating with non-cemented zones are seen to arise, seemingly as a result of the processes involved in lithification (Matter, 1974; Baker et al., 1980). In clay-bearing limestones, these alternating zones may be the precursor to some examples of marl/limestone alternations, in which zones of greater compaction alternate with zones of greater cementation as shown in Fig. 7-2 (Hallam, 1986; Ricken, 1986; Bathurst, 1987; Beaudoin et al., 1989). Presumably, carbonate is lost in the strongly compacting (and clay-rich) domains and gained at the cemented (carbonate-rich) zones as depicted in Fig. 7-2. In some examples of marl/limestone alternations, the carbonate-rich "beds" contain stylolites, whereas adjacent clay-rich ones contain closely spaced clay seams. Thus, the formation of stylolites, clay seams, and marl/limestone alternations, generally attributable to pressure solution, seemingly come about according to differences in clay content at different times in the burial history of the sediment.

An abundance in clay, however, may cause a rock to respond to burial by pervasive chemical compaction, or intergranular pressure solution, rather than by localized dissolution along clay seams. Figure 7-3 shows boundary lines separating the domain

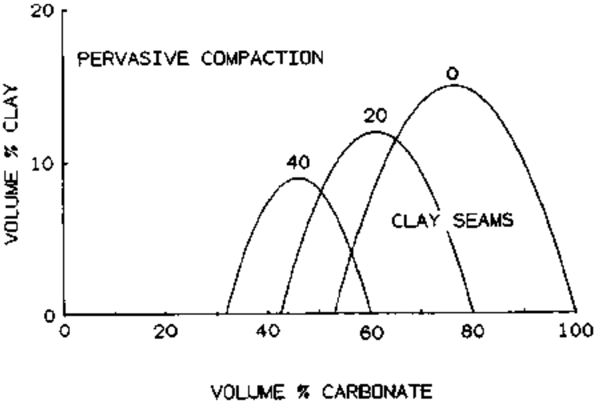

Fig. 7-3. Domains in the space of carbonate volume % vs. clay volume %, contoured for porosity, in which compaction was localized at clay seams, or remained pervasive throughout the rock. The development of clay seams is confined to argillaceous carbonates relatively poor in clay. (After Barrett, 1964, fig. 4.)

of clay seam formation from pervasive (chemical) compaction in shallow limestones as determined by Barrett (1964). He showed that rocks with or without regularly spaced dissolution seams differed in the amounts of clay and silt in the non-carbonate fraction. Barrett's (1964; see fig. 4) data are replotted in Fig. 7-3 in terms of whole rock average volume fractions of calcite and clay, for a constant porosity. Although Barrett did not report the porosities of his rocks, it is likely that the range in porosity extended from 0 to 20%. Clearly, limestones of a given porosity with greater than a critical clay content do not contain clay seams but respond to stress by pervasive pressure solution.

The question arises as to the exact role of clay in pressure solution processes. Clay was apparently first linked to pressure solution by Heald (1956). He recognized a substantial increase in the amount of pressure solution in clay versus non-clay bearing sandstone beds and attributed it to permeability differences. Since then, enhanced pressure solution by clay has been attributed to clay-influenced solution chemistry (Thomson, 1959), enhanced diffusion within and along clay mineral surfaces lining grain contacts (Weyl, 1959), and the preservation of relatively smaller grain contacts by the inhibition of overgrowth (Buxton and Sibley, 1980; Heald and Anderegg, 1960).

Clay inhibition of overgrowth formation has been recognized in both sandstones (Heald and Anderegg, 1960; Buxton and Sibley, 1981; Tillman and Almon, 1979, figs. 24–27 and 33) and in limestones (Bausch, 1968; Marschner, 1968; Matter, 1974, plate 9, fig. 4; Baker et al., 1980; Buxton and Sibley, 1981). Figure 7-4 shows data from Bausch (1968) in terms of grain size in Jurassic limestones versus the inverse of volume % clay. A straight line connecting four of the data points passes through the origin, suggesting a linear relationship between grain size and inverse of clay content. It is conjectured that the interface detachment kinetics at grain–fluid interfaces is

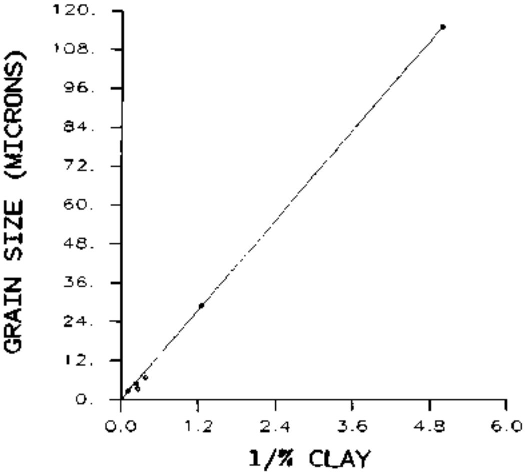

Fig. 7-4. Grain size of calcite in Jurassic limestones as a function of the inverse of clay content (volume %) lies on a straight line that passes through the origin. This relationship is consistent with a calcite free-face reaction rate that is limited by diffusion through a thin coating of clay. (Data from Bausch, 1968, table 1.)

impeded by a layer of clay that coats the otherwise free grain surface. Reaction at these faces may be limited by diffusion through the coating if it is sufficiently thick. In a later section, it is demonstrated that the linear relation in Fig. 7-4 can be explained by such a clay coating model.

Compaction may proceed relatively homogeneously throughout a sediment, or may become localized. In this chapter, localized compaction is considered "unstable", whereas pervasive compaction or intergranular pressure solution (IPS) is termed "stable". This chapter addresses three pathways for such an instability by which small non-uniformities in texture, e.g., porosity, size, and shape of grains, become amplified during burial diagenesis and accompanying overall porosity loss. In the first two, compaction may become spatially localized during porosity loss accompanying burial, whereas the third addresses differentiation between calcite and clay after porosity loss. Because pressure solution at grain contacts and cementation both result in a net increase in contact area, the normal stress acting across horizontal contacts may actually decrease, even during burial with the attendant increase in overburden loading. This is a stabilizing effect or negative feedback, because any textural heterogeneity resulting in a local decrease in contact area would be smoothed out because of a local increase in the rate of pressure solution there. If, on the other hand, the contact area is prevented from increasing, either due to dissolution at free-faces or by inhibition of overgrowth cementation by, e.g., a clay coating, compaction may proceed at some localities at a higher than average rate. Because heterogeneities will not under such circumstances necessarily be dampened, non-uniformities in texture can become enhanced. One can equate the unstable behavior resulting from dissolution at free faces with a mechanism for stylolitization, and that resulting from the presence of clay to a mechanism leading to the formation of marl/limestone alternations and centimeter-scale clay seams. It will become evident from our simulations that development of unstable behavior not only depends on the operation of a mechanism for instability, but also on the nature of initial textural heterogeneities.

This demonstrates an underlying universality to the dynamics which lead to the formation of stylolites, marl/limestone alternations, and clay seams. Spatially separate regions of rock may undergo chemical compaction and cementation at different rates due to slight initial lithological differences. With transport down chemical potential gradients existing between regions undergoing diagenesis at different rates, the spatially separate zones of dissolution and cementation can be self-enhancing.

More precisely, one of the self-enhancing or "positive feedback" mechanisms operates as follows. Overgrowth cementation increases grain contact areas, which in turn decreases the force per area across contacts, and increases the length of the diffusion path. This decreases the driving force for contact dissolution and may decrease reaction rates if grain boundary diffusion is the limiting step in reaction, having the net effect of favoring further cementation.

Positive feedback mechanisms of this type, which one may term "mechanochemical" feedback (Ortoleva et al., 1987; Dewers and Ortoleva, 1989; Ortoleva, 1994, see Chapter 4 this volume) have been implicated in the genesis of phenomena ranging from metamorphic layering (Ortoleva et al., 1982; Dewers and Ortoleva, 1990a), stylolites (Merino et al., 1983; Dewers and Ortoleva, 1990b), the growth of concretions in a host rock by constant volume replacement (Dewers and Ortoleva, 1990c), and the formation of marl/limestone alternations (Ricken, 1986). Differentiation between mineral constituents by mechanochemical means during diagenesis was apparently first referred to by Sujkowski (1958).

In argillaceous carbonates at diagenetic conditions, the length scale and the precise rate determining step (i.e., dissolution or precipitation) involved in the genesis of the banded patterns depends on grain size, amount of clay, porosity, and other factors which affect relative reaction rates at grain contacts and free faces. The way in which pressure solution is manifested, and the type of phenomena which emerges, depends on the rate determining step. This is demonstrated in Fig. 7-5. Specifically, we have found that intergranular pressure solution occurs when grain-contact reaction is rate determining. Stylolites occur when dissolution at grain contact peripheries is faster than within contacts themselves, and marl/limestone alternations and centimeter-scale clay seams result when free-face reaction is the rate limiting process, due to the inhibition of precipitation there by clay. The localization of dissolution can either be due to the amplification of an inherited depositional layering, or can arise spontaneously by the amplification of omnipresent textural non-uniformities through the interaction of dissolution, diffusional solute transport, and cementation.

To obtain an accurate description of carbonate diagenesis, some observations which are key in formulating the model are listed below:

(1) The chief means for lithification of calcareous oozes is seen by many authors to be cements derived from pressure solution and from the dissolution of small, very soluble grains (<1 μm in size) (Neugebauer, 1974; Schlanger and Douglas, 1974).

G^c = reaction rate at grain contacts

G^f = reaction rate at free faces

IPS

$G^c > G^f$; REACTION AT FREE FACES IS RATE LIMITING; MAY OR MAY NOT INVOLVE CLAY

STYLOLITIZATION

$G^c < G^f$; CONTACT REACTION IS RATE LIMITING; DOES NOT INVOLVE CLAY

MARL/LIMESTONE ALTERNATIONS

$G^c > G^f$; G^f LESS THAN A CRITICAL G^c; INVOLVES CLAY

LOW-POROSITY CLAY SEAMS

$G^c \simeq G^f$

Fig. 7-5. Differences in the relative rate of reaction at grain–grain contacts versus that at grain-free faces determines whether chemical compaction will act pervasively throughout a rock or will localize at textural perturbations. Stylolites can result in relatively clean limestones if contact rates are comparable to or less than free-face rates. Marl/limestone alternations can develop from argillaceous carbonate sediment if free-face rates are sufficiently less than contact rates in the nascent marl layers. In both clean limestones and limestones containing greater than a critical clay content, intergranular pressure solution, or pervasive chemical compaction will result if contact rates are faster than free-face rates.

The small particles may be derived from "disaggregation" of planktonic fossils by dissolution (Schlanger and Douglas, 1974). In either case, the bulk of the cement is seen as locally derived, in a process termed "auto-lithification". Ricken (1986), using mass balance calculations and compaction estimates derived from shape changes in burrows, showed that a closed-system redistribution of carbonate was sufficient to account for observed volume losses and gains at dissolution and cementation sites. The spatial profiles of cementation patterns around stylolites and examples of diagenetic bedding are consistent with a diffusion-dominated solute transport mechanism (Merino et al., 1983; Ricken, 1986).

(2) Wanless (1979) attributed the different behaviors of non-seam solution (pervasive intergranular pressure solution), sutured seam solution (stylolites), and non-sutured seam solution (clay seams) to a contrast in "competency". Competency in this context is referred to cementation and clay content. Buxton and Sibley (1981) carried this further, showing that grain size, amount of cement, and clay content influenced the style of pressure solution in rocks that experienced the same burial history.

(3) A direct causal relationship between stylolites or spaced cleavage and applied stress is straightforwardly made, as the foliation defined by the cleavage and, in the case of stylolites, the direction of suturing, correlates to directions of maximum principle compressive stress (Alvarez et al., 1978; Marshak and Engelder, 1985) or

along planes of shear (Spang et al., 1979). This relationship may be extended to the banding characteristic of marl/limestone alternations (Ricken, 1986).

(4) Diagenesis of the clay-mineral fraction of argillaceous carbonates takes place at deeper depths and longer time scales than does diagenesis of the carbonate fraction (Matter, 1974). The diagenesis of carbonates and clay minerals may, therefore, proceed relatively independently at low temperature.

In summary, to describe the genesis of pressure solution structures in argillaceous carbonates, one needs to account for closed system diagenesis, variations in stress with lithology and depth of burial, and effects of clay on calcite reaction rates. In addition, it appears that much of carbonate diagenesis involves a reactively inert non-carbonate fraction consisting of mostly silt and clay. The present model does not, however, account for the presence of very-fine, supersoluble particles.

REACTION–TRANSPORT–MECHANICAL MODELS

Quantitative modeling of mechanochemical diagenesis requires a description of several coupled processes in terms of the partial differential equations that describe their dynamics. In this chapter, these are

(1) the interaction between calcite and pore fluid and complexing between various aqueous species;

(2) solid and fluid transport;

(3) mechanics of stress distribution as a function of rock textural change and changes in fluid and lithostatic pressures accompanying burial; and

(4) the effect of applied stress, the nature of the solid–fluid interface, and grain geometry on the rate of grain reaction.

In the following section, the authors present a set of equations which incorporate these factors into a unified reaction–transport–mechanical model.

Textural model and conservation of mass equations

Weyl (1959) and others (Angevine and Turcotte, 1983; Palciauskas and Domenico, 1989) have quantified chemical compaction in terms of truncated spheres in a simple rectangular packing. Dewers and Ortoleva (1990b) showed that this grain geometry could be included in a reaction–transport model by accounting for reaction at both grain-to-grain contacts and free faces. Figure 7-6 depicts both free faces and contacts for a grain in this packing, and defines the geometrical variables required for its quantification. The textural variables of porosity (ϕ), number density (n), grain volume (V), and surface areas for the different contact sites (A_x, A_y, A_z and A_f) are determinable from the four variables accounting for height (L_z), width (L_y and L_x), and radius (L_f) of the truncated spheres; Table 7-1 gives the necessary formulas.

For the above textural model, conservation of mass for solute species α takes the form

$$\frac{\partial \phi c_\alpha}{\partial t} = \nabla \cdot J_\alpha - n\rho v_\alpha \sum_i \tilde{A}_i G_i + \phi W_\alpha, \quad \alpha = 1, 2, \ldots N \tag{7-1}$$

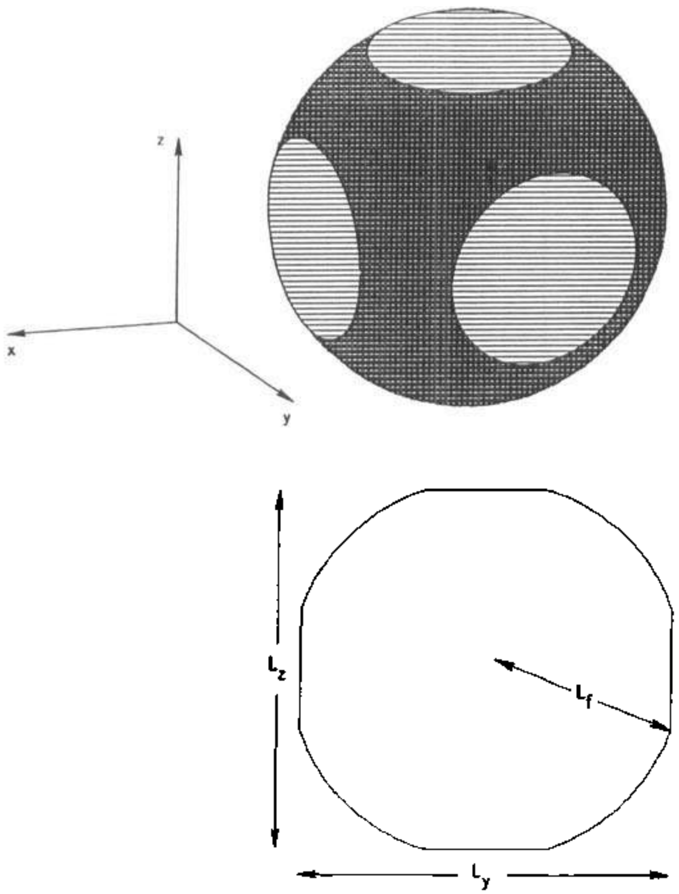

Fig. 7-6. Spherical grains truncated at contacts are placed in simple rectangular packing for the textural model used in the quantitative reaction–transport model. Grain texture is quantified in terms of L_f, the radius of the truncated sphere, L_z, the height of the vertical grain truncation and L_x and L_y, the horizontal dimensions of the box that truncates the grain. Surface areas of the free faces and contacts, porosity, and grain number density are found from these four basic variables.

where c_α is the concentration of α in moles per pore volume, ϕ is porosity, J_α is the flux of species α, W_α is the net rate for aqueous reactions affecting α, n is the number of calcite grains per unit volume, ρ is the solid molar density of calcite, N is the number of aqueous species in the system, and ν_α is the stoichiometric coefficient relating species α to the reaction taking place at site i on the calcite grain (assuming that reaction is unique at a given site and the same at all sites, for simplicity). The area factor $\tilde{A}_i$ for an i-type site is defined as follows: if G_i is the rate of change of L_i due to reaction, then $A_i G_i$ is the total rate of change of grain volume due to reactions at the i site. Letting A_z be the area of a single z-type contact then $\tilde{A}_z$ is A_z

TABLE 7-1

Geometrical parameters for spheres in simple cubic packing

V	$= -\frac{8\pi}{3}L_f^3 + \pi L_z \left\{L_f^2 - \frac{L_z^2}{12}\right\} + 2\pi L_x \left\{L_f^2 - \frac{L_x^2}{12}\right\}$	(grain volume)
n	$= \frac{1}{L_z L_x^2}$	(grain number density)
A_f	$= 4\pi L_f \left\{\frac{L_z}{2} + L_x - 2L_f\right\}$	(area of free face)
A_x	$= 4\pi \left\{L_f^2 - \frac{L_x^2}{4}\right\}$	(total area of x-contact)
A_z	$= 2\pi \left\{L_f^2 - \frac{L_z^2}{4}\right\}$	(total area of z-contact)
ϕ_{ca}	$= \frac{V}{L_z L_x^2}$	(volume fraction of calcite)
ϕ	$= 1 - \phi_{ca} - \phi_{cl}$	(porosity)

(= 1/2 total z-type contact area) (and similarly for $\tilde{A}_x$ and $\tilde{A}_y$) where $\tilde{A}_f = A_f$ (= total free face area). Each variable represents the typical or average quantity over a region of space containing many (e.g., 100) grains, termed a macrovolume element. In the case of supra-grain-scale diffusional and advective transport, $\boldsymbol{J}_\alpha$ takes the form:

$$\boldsymbol{J}_\alpha = -\phi D_\alpha \tau_\alpha \nabla c + (\boldsymbol{v} + \boldsymbol{u})\phi c_\alpha, \tag{7-2}$$

where $\boldsymbol{v}$ is the advective velocity relative to $\boldsymbol{u}$; $\boldsymbol{u}$ is the velocity of rock (compaction) flow; D_α is the diffusion coefficient in bulk water at the appropriate temperature T and fluid pressure p, and τ is tortuosity. Ortoleva et al. (1987) demonstrated that, because solid molar densities exceed pore fluid concentrations by several orders of magnitude, Eq. 7-1 may give a good approximation to be evaluated at steady state:

$$-\nabla \cdot \boldsymbol{J}_\alpha - n\rho\nu_\alpha \sum_i \tilde{A}_i G_i + \phi W_\alpha = 0. \tag{7-3}$$

For the case of the reaction:

$$\text{calcite} \rightleftharpoons \text{Ca}^{2+} + \text{CO}_3^{2-} \tag{7-4}$$

Equation 7-3 for Ca^{2+} may be written as follows:

$$-\nabla \cdot \boldsymbol{J}_{\text{Ca}^{2+}} = n\rho \sum_i \tilde{A}_i G_i - \phi W_{\text{Ca}^{2+}}. \tag{7-5}$$

The rate of change of grain dimensions includes contributions from reaction as well as from compaction-related rock flow (Dewers and Ortoleva, 1990b):

$$\frac{\partial L_i}{\partial t} = \boldsymbol{u} \cdot \nabla L_i + G_i, \quad i = x, y, z, \text{f}. \tag{7-6}$$

In the case of uniaxial compaction (the dominant compaction component during burial in the absence of imposed tectonic forces), the change in rock flow velocity due to dissolution at horizontal contacts is found from:

$$\frac{\partial u_z}{\partial z} = G_z/L_z \tag{7-7}$$

When subject to boundary conditions on u_z, this equation allows the incorporation of effects of both burial and chemical compaction.

Variables which are "conserved" quantities, i.e., those expressed per volume as in number densities or volume fractions, follow a different conservation law than grain sizes. For clay or any other material which lines the pores but does not react, conservation of mass yields:

$$\frac{\partial \phi_{\mathrm{cl}}}{\partial t} = -\boldsymbol{\nabla} \cdot (u\phi_{\mathrm{cl}}), \tag{7-8}$$

where ϕ_{cl} is the volume fraction of clay or pore-lining material.

The porosity in the presence of non-supporting, pore-lining clay minerals is found from:

$$\phi = 1 - \phi_{\mathrm{cl}} - \phi_{\mathrm{ca}}, \tag{7-9}$$

where ϕ_{ca} is the volume fraction of calcite as found in Table 7-1.

Equation 7-9 is a restatement of Ricken's (1987) compaction equation, which takes the form

$$N_c = (100 - \bar{K})(1 - \phi)(100 - C)/100 \tag{7-10}$$

where N_c = non-carbonate volume normalized by the primary (uncompacted) sediment volume; $\bar{K}$ = percent compaction of the primary sediment volume; and C = carbonate volume normalized by the volume of pore-free solids.

These variables can be recast in terms of textural variables introduced earlier. If V^{T} represents a volume of sediment (solid plus pores), V^{I} is the initial, uncompacted volume, V_{f} is the pore volume, V_{cl} is the volume of clay, and V_{ca} is the volume of calcite within the sediment volume, then N_c, C, and $\bar{K}$ by definition are:

$$\begin{aligned} N_c &= \frac{V_{\mathrm{ca}}}{V^{\mathrm{I}}} \times 100, \\ \bar{K} &= \left(1 - \frac{V^{\mathrm{T}}}{V^{\mathrm{I}}}\right) \times 100, \text{ and} \\ C &= \frac{V_{\mathrm{ca}}}{V^{\mathrm{T}} - V_{\mathrm{f}}}. \end{aligned} \tag{7-11}$$

Also by definition,

$$\phi_{\mathrm{ca}} = \frac{V_{\mathrm{ca}}}{V^{\mathrm{T}}}, \quad \phi_{\mathrm{cl}} = \frac{V_{\mathrm{cl}}}{V^{\mathrm{T}}}, \quad \phi = \frac{V_{\mathrm{f}}}{V^{\mathrm{T}}} \quad \text{and } V^{\mathrm{T}} = V_{\mathrm{f}} + V_{\mathrm{ca}} + V_{\mathrm{cl}}. \tag{7-12}$$

By inserting these expressions into Eq. 7-10 and rearranging, one regains Eq. 7-9.

To quantitatively describe the deformation of a rock composed of a solid skeleton of calcite grains plus pore filling clay and fluid, it is necessary to include both elastic and inelastic effects. Instantaneously, or on the time scale of laboratory observation in the absence of an imposed deformation velocity, elastic effects may be the dominant deformation mechanism (e.g., Zimmerman et al., 1986), whereas over intervals of geologic time, inelastic effects will likely dominate rock deformation (Palciauskas and Domenico, 1989). To account for both elastic and inelastic effects in the domain where inelastic effects are dominantly chemical, acting only at grain contacts as opposed to throughout the grains, one needs to include a description of fluid-pressured, elastic porous media. The two deformation mechanisms are then integrated into a self-consistent scheme via the reaction–transport–mechanical model. A means for describing an elastically isotropic and yet inhomogeneous porous medium (in which the macroscopic elastic properties are dependent on the elastic constants of the solid skeleton, fluid pressure, and porosity) is summarized in the next section.

Equations for macroscopic effective stress and force balance

The purpose of this section is to outline the derivation of the partial differential equations necessary to describe elastic interactions as a function of applied stresses, fluid pressure, and attendant changes in the textural properties of the load-supporting mineral. These take the form of three second-order Navier equations for the three components of elastic displacement, w_x, w_y, and w_z. To derive these, a constitutive relationship between the macroscopic stress and strain tensors, a condition for mechanical equilibrium (force balance), and an expression relating the displacement vector with components of the strain tensor (Jaeger and Cook, 1979) are required.

The macroscopic stress ($\boldsymbol{\sigma}^{\mathrm{m}}$) and strain ($\boldsymbol{\varepsilon}^{\mathrm{m}}$) tensors are related by a fourth-rank tensor of elastic compliances $\mathbf{C}^{\mathrm{m}}$, fluid pressure p, and the effective stress coefficient α^{m}:

$$\boldsymbol{\sigma}^{\mathrm{m}} + \alpha^{\mathrm{m}} p \mathbf{I} = \mathbf{C}^{\mathrm{m}} \boldsymbol{\varepsilon}^{\mathrm{m}} \quad \text{(I being the identity tensor).} \tag{7-13}$$

This representation is similar to that of Biot and Willis (1957), except that here thermoelastic effects are ignored. In the case of an isotropic medium, the compliance tensor is assumed to be related to a macroscopic shear modulus μ^{m} and Lamé's constant λ^{m} by:

$$C^{\mathrm{m}}_{ijkl} = \mu^{\mathrm{m}}(\delta_{ik}\delta_{jl} + \delta_{il}\delta_{jk}) + \lambda^{\mathrm{m}}\delta_{ij}\delta_{kl} \tag{7-14}$$

and α^{m} is related to the bulk modulus of both the porous solid skeleton, κ^{m} (drained of pore fluid) and the solid composing the skeleton, κ, by (Zimmerman et al., 1986):

$$\alpha^{\mathrm{m}} = 1 - \kappa^{\mathrm{m}}/\kappa. \tag{7-15}$$

κ^{m} is related to μ^{m} and λ^{m} (and similarly κ is related to μ and λ). A number of authors have derived upper and lower bounds for the isotropic moduli of porous media as a function of porosity. Expressions from Eshelby (1957) are used here:

$$\begin{aligned}\mu^{\mathrm{m}} &= \mu\left\{1+\frac{5(3\kappa+4\mu)\phi}{f\kappa+8\mu)(1-\phi)}\right\}^{-1}\\ \kappa^{\mathrm{m}} &= \kappa\left\{1+\frac{3(3\kappa+4\mu)\phi}{12\mu(1-\phi)}\right\}^{-1}\end{aligned} \tag{7-16}$$

Although such dependencies are ignored in the present chapter, the macroscopic moduli may depend on fluid pressure, temperature, or microscopic textural factors. For example, Zimmerman et al. (1986) showed a non-linear dependence of the macrocompressibility on the difference between confining and fluid pressures; this effect becomes prominent as fluid pressure approaches the confining pressure. Single crystal elastic constants for calcite are given as a function of temperature by Dandekar (1969). To estimate representative isotropic moduli, the VHR averages are employed here.

Balance of forces implies

$$\sum_{j=1}^{3}\frac{\partial\sigma_{ij}^{\mathrm{m}}}{\partial x_j}-[\phi\Gamma_{\mathrm{f}}+(1-\phi)\Gamma_{\mathrm{s}}]\delta_{i3} \tag{7-17}$$

The bracketed factor in Eq. 7-17 accounts for the gravitational body force; Γ_{f} and Γ_{s} are the gravitational acceleration multiplied by the mass density of pore fluid and solid skeleton, respectively; and $i,\ j=3$ denotes the vertical coordinate.

For linear elasticity, the strain tensor ε^{m} and the vector of elastic displacements w are related via:

$$\varepsilon_{ij}=\tfrac{1}{2}\left\{\frac{\partial w_{ij}^{\mathrm{m}}}{\partial x_j}+\frac{\partial w_j}{\partial x_i}\right\} \tag{7-18}$$

By substituting Eqs. 7-13 and 7-18 in Eq. 7-17, one obtains:

$$\begin{aligned}&\frac{\partial}{\partial x}\left\{(\lambda^{\mathrm{m}}+2\mu^{\mathrm{m}})\frac{\partial w_x}{\partial x}+\lambda^{\mathrm{m}}\frac{\partial w_y}{\partial y}+\lambda^{\mathrm{m}}\frac{\partial w_z}{\partial z}+\alpha^{\mathrm{m}}p\right\}=0\\ &\frac{\partial}{\partial y}\left\{(\lambda^{\mathrm{m}}+2\mu^{\mathrm{m}})\frac{\partial w_y}{\partial y}+\lambda^{\mathrm{m}}\frac{\partial w_x}{\partial x}+\lambda^{\mathrm{m}}\frac{\partial w_z}{\partial z}+\alpha^{\mathrm{m}}p\right\}=0\\ &\frac{\partial}{\partial z}\left\{(\lambda^{\mathrm{m}}+2\mu^{\mathrm{m}})\frac{\partial w_z}{\partial z}+\lambda^{\mathrm{m}}\frac{\partial w_x}{\partial x}+\lambda^{\mathrm{m}}\frac{\partial w_y}{\partial y}+\alpha^{\mathrm{m}}p\right\}-(1-\phi)\Gamma_{\mathrm{s}}-\phi\Gamma_{\mathrm{f}}=0\end{aligned} \tag{7-19}$$

Calcite reaction rates: mechanisms and driving forces

Quantification of the rates of growth and dissolution at the various grain facets requires an account of both driving forces and rate limiting steps involved in the transfer of mass between solid and fluid phases at each facet type. As grain reaction reflects stresses at the grain scale, the connection must be made between grain texture, microscopic stresses, and the macroscopic stress field as developed in the previous subsection.

The average vertical normal stress across grain contacts is found by equating the average force within a horizontal plane to the area-weighted average of forces in that plane acting within both solid and fluid. If P_z is the normal pressure across the z contact (which is equal to minus the normal stress as per the sign convention of negative compressive stresses) and $L_x L_y$ is the horizontal area of the "unit cell", then (Jaeger and Cook, 1979)

$$-L_x L_y \sigma_{zz}^{\mathrm{m}} = A_z P_z + (L_x L_y - A_z)\, p. \tag{7-20}$$

Relations similar to Eq. 7-20 may be obtained for P_x and P_y.

The average stress within grains is determined from the macroscopic mean stress $(= -\operatorname{tr}\sigma^{\mathrm{m}}/3)$ by averaging the contributions by fluid and solid weighted by the appropriate volume fractions of solid $(1-\phi)$ and fluid (ϕ):

$$-\operatorname{tr}\sigma^{\mathrm{m}} = -(1-\phi)\operatorname{tr}\sigma + 3\phi p. \tag{7-21}$$

In Eq. 7-21, σ is the average stress tensor within a grain, and "tr" denotes the trace of a tensor.

The dependence of grain-free energy on local stress follows from the stress dependence of Gibb's free energy. The molar Gibb's free energy U of a grain face is given by:

$$U(P_{\mathrm{n}}, \sigma) = \frac{P_{\mathrm{n}}}{\rho} + \frac{F}{\rho_{\mathrm{o}}}. \tag{7-22}$$

Here ρ and ρ_{o} are the molar densities of the solid in the stressed and reference states, respectively; F is the Helmholtz or strain energy; and P_{n} is the pressure normal to the grain face under consideration. It is assumed in the present treatment that the strain energy and molar density of the solid depend only on the average stress σ in an isotropic, elastic solid:

$$F = F(\sigma), \quad \rho = \rho(\sigma). \tag{7-23}$$

The average elastic strain energy in the solid is then taken in the form:

$$F = \tfrac{1}{2}\operatorname{tr}(\varepsilon\sigma); \tag{7-24}$$

F can be expressed solely in terms of two elastic constants and the mean and deviatoric parts of the average stress tensor:

$$\begin{aligned} \operatorname{tr}(\varepsilon) &= \frac{1}{3\kappa}\operatorname{tr}(\sigma), \text{ and} \\ \hat{\varepsilon} &= \frac{1}{2\mu}\hat{\sigma}. \end{aligned} \tag{7-25}$$

The diagonal components of the average stress tensor are found from the macroscopic stress tensor by expressions similar to Eq. 7-21, i.e.,

$$\phi p \delta_{ij} - (1-\phi)\sigma_{ij} = -\sigma_{ij}^{\mathrm{m}}, \quad i, j = 1, 2, 3 \tag{7-26}$$

such that by putting $j = i$, summing over i and dividing by three one regains Eq. 7-21. The components of the deviatoric part of the tensor are then found from:

$$\hat{\sigma}_{ij} = \sigma_{ij} - \tfrac{1}{3}\mathrm{tr}\,\sigma\,\delta_{ij}, \tag{7-27}$$

and the strain energy is expressed as:

$$F = \tfrac{1}{2}\left\{\frac{1}{9\kappa}\mathrm{tr}\,(\sigma)^2 + \frac{1}{2\mu}\mathrm{tr}\,(\hat{\sigma}^2)\right\}. \tag{7-28}$$

Stress-induced dissolution at grain contacts is thought to proceed by one of two mechanisms (Tada et al., 1987). In the water-film diffusion mechanism, reaction occurs by means of thin aqueous fluid films which support the stress across the contact. The rate of reaction is limited by diffusion through the film and is driven by the normal stress dependence of Gibb's free energy. In the free-face pressure dissolution mechanism (Tada et al., 1987), reaction is driven by elastic or permanent (dislocation) strain energies or possibly microfracturing at grain contacts, and may be limited by detachment or attachment kinetics or by diffusion.

The question arises as to which pressure solution mechanism will be the active one in argillaceous carbonates. Experimental documentation of thin aqueous films (differing in properties from bulk water) at quartz–quartz and mica–mica interfaces shows that they are approximately 1–5 nm thick and can support differential stresses (i.e., $P_z - p$) up to at least 1 kbar (Pashley and Kitchener, 1979; Pashley and Israelachvili, 1984; Tada et al., 1987). Experiments of Hay and Evans (1988) on limestones, however, show no evidence for such films existing at clean natural or artificial calcite grain boundaries, at least at temperatures exceeding 300°C. Tada and Siever (1986) convincingly demonstrated the operation of free-face dissolution in halite, which appeared to involve both elastic and dislocation strain energies.

Uniaxial shortening rates of grains in simple cubic packing for the water film mechanism show a textural dependence that goes inversely with the product of grain size and horizontal contact area, whereas those for the free-face mechanism go inversely with grain size (Dewers and Ortoleva, 1990b). In this work, simulations of intergranular pressure solution-induced compaction were carried out by the present authors using reaction rates determined from both of the above mechanisms. The results were then compared with data on sandstones from Houseknecht (1988) on the effect of grain size on the estimated volume loss at grain contacts. In short, it was found that clean sandstones of Houseknecht (1988) exhibited a grain-size dependence consistent with the free-face mechanism, whereas sandstones containing coatings of clay exhibited grain size trends consistent with the water-film diffusion mechanism. These studies and the common suggestion in the literature on the relative enhancement of diffusion along clay mineral surfaces have led the authors to use the water-film diffusion mechanism to describe pressure solution at grain–grain contacts in argillaceous carbonates. Clay minerals and zeolites in fact have anomalously high lattice diffusivities compared to other minerals (Freer, 1981); therefore, the treatment of grain boundary diffusion in this chapter is approximated by the lattice diffusivity of phyllosilicates.

Virtually all authors concerned with the kinetics of pressure solution processes characterize rates in the form of constitutive laws between stress and strain rate, in which the pore fluid concentration is buffered by grain facets in equilibrium with pore fluid at pressure p. This is only the case for slow reaction rates at grain contacts relative to that at free faces. For cases where the rate of contact dissolution is not negligible compared to free-face rates, the pore fluid composition will reflect a compromise between the different driving forces and kinetics at contacts and free faces. If free-face reaction is sufficiently inhibited, then pore fluid composition may approach equilibrium with grain facets in contact.

Dewers and Ortoleva (1989) showed that a diffusion-controlled reaction rate law describing pressure solution at circular grain contacts takes the following form:

$$G_z = \frac{2\pi\,\Delta r_o}{A_z \rho}\, J_\alpha^z, \tag{7-29}$$

where Δ is the fluid film thickness, r_o is the contact radius, and J_α^z is the diffusive flux of α out of the contact. Equation 7-29 was derived by combining a number of results: a condition for equilibrium between solid and the aqueous film lining vertical contacts, a phenomenological relation between chemical potential gradients and the flux of the least mobile solute, a relation giving the dependence of stress on the radial coordinate along circular contacts, and a condition for force balance across the contacts.

Weyl (1959) showed that for a constant approach of two grains due to dissolution along their mutual interface, solute flux along the contact is independent of the radial coordinate from the center to the edge of a circular contact. This implies a condition for the dependence of normal stress on distance along the contact. The resulting form of the flux, which follows from considerations of diffusion down chemical potential gradients, was shown by Dewers and Ortoleva (1990a) to be given by (in mol/cm^2 s):

$$J_\alpha^z = \frac{D_\alpha^c}{1000\gamma_\alpha r^o} \left\{ a_\alpha - \left[K \Big/ \prod_{\beta\neq\alpha}^{N} {a_\beta}^{\nu_\beta} \right]^{\nu_\alpha^{-1}} \times \exp\left[\frac{(P_{\max} - p)}{\nu_\alpha RT} \left(\frac{1}{\rho} - \sum_{\beta\neq\alpha=1} \nu_\beta \overline{V}_\beta \right) \right] \right\}. \tag{7-30}$$

The normal stress along the contact varies from $P_{\max}$ at the center to p (i.e., fluid pressure) at the contact edge. This follows from the dependence of the normal stress along the radial-coordinate measuring distance from the center of the contact and a force balance condition (Dewers and Ortoleva, 1990a). $P_{\max}$ is related to the average normal stress applied across the contact and the fluid pressure by (Dewers and Ortoleva, 1990a):

$$P_{\max} - p = 3\,(P_z - p). \tag{7-31}$$

Similar relations connecting solute flux to the horizontal stresses P_x and P_y can be derived for the x and y contacts. The α diffusion coefficient in Eq. 7-30 is taken to be

TABLE 7-2

Temperature-dependence of rate and diffusion coefficients

$$D^{c} = 9.4 \times 10^{-4} \exp\left[\frac{+5076.47}{T\,(\mathrm{K})}\right], \quad 293 < T\,(\mathrm{K}) < 395^{a}$$

$$k^{+} = (k_1 a_{\mathrm{H}^+} + k_2 a_{\mathrm{H_2CO_3^0}} + k_3 a_{\mathrm{H_2O}})\,(1000\rho) - 1^{b}$$

$$\log k_1 = 0.198 - 444/T\,(\mathrm{K})$$
$$\log k_2 = 2.840 - 2177/T\,(\mathrm{K})$$
$$\log k_3 = 1.10 - 1737/T\,(\mathrm{K})$$

$$D_{\mathrm{w}} = 6.70 \times 10^{-3} \exp\left[\frac{-1996.9}{T\,(\mathrm{K})}\right]^{c}$$

	0°C	25°C	70°C
D^{c} ($\mathrm{cm^2/s}$)	2.6×10^{-12}	1.3×10^{-11}	1.5×10^{-10}
k^{+} (cm/s; pH = 6)	1.4×10^{-9}	1.9×10^{-9}	3.0×10^{-9}
D_{w} ($\mathrm{cm^2/s}$)	4.5×10^{-6}	8.3×10^{-6}	2.0×10^{-5}

[a] Data for $\mathrm{Ca^{2+}}$ diffusion in biotites from Freer (1981).

[b] Plummer et al. (1979).

[c] Fit of data for $\mathrm{Ca^{2+}}$ tracer diffusion coefficients at 25, 50, and 100°C given in table 4 from Oelkers and Helgeson (1988).

equal to the $\mathrm{Ca^{2+}}$ lattice diffusion coefficient in phyllosilicates as tabulated in Freer (1981). The temperature dependence in an Arrhenius form is given in Table 7-2.

Reaction at calcite grain facets exposed to hydrostatically stressed pore fluid may be limited by interface detachment kinetics, or by diffusion through a leached layer (Berner and Morse, 1974). In either case, the rate of reaction at free faces, G_{f}, may be expressed as follows:

$$G_{\mathrm{f}} = -k a_i \left[1 - \exp\left(\frac{-A_i^{\mathrm{f}}}{nRT}\right)\right] \tag{7-32}$$

where k is the dissolution rate coefficient (in cm/s), a_i is the activity of the solid, A_i^{f} is the affinity for reaction at free faces, R is the gas constant, T is temperature, and n is a constant, close to unity. The coefficient k depends on temperature, pore fluid chemistry, and other factors.

The form of k for calcite employed in this paper is given in Table 7-2, after Plummer et al. (1979) and Busenberg and Plummer (1986). The affinity follows from the equilibrium condition at free faces, which are normally stressed by the fluid pressure, and retain (in this treatment) a strain energy equal to its grain-average value. Letting K be the equilibrium constant for the calcite reaction given in Table 7-4 at p and T, the rate of calcite reaction at free faces is written as follows:

$$G_{\mathrm{f}} = \frac{k}{K}\left\{a_{\mathrm{Ca^{2+}}} a_{\mathrm{CO_3^{2-}}} - K \exp\left(\frac{\Omega}{RT}\right)\right\} \tag{7-33}$$

where:

$$\Omega = \rho_o \left\{ \frac{p \operatorname{tr} \sigma}{3\kappa} + \frac{p^2}{\kappa} + F(\sigma, p) - F(p) \right\}. \tag{7-34}$$

The activities in Eq. 7-33 are related to molal concentrations by:

$$m_\alpha = \gamma_\alpha^{-1} a_\alpha, \tag{7-35}$$

and molal concentrations may be approximated in terms of molar concentrations by:

$$m_\alpha = c_\alpha 1000/\Delta_w,$$

where Δ_w is the mass density of water.

Boundary conditions and other constraints

The present model is cast in terms of coupled partial differential equations describing grain growth, dissolution, mass transport, and texture-dependent effective stress. To simulate the evolution of texture in argillaceous carbonates one must simultaneously solve the model equations by numerical methods. To complete the analysis, further considerations must be made as follows.

This study is concerned with modeling systems over which lithology varies on a length scale no larger than a few meters. Mass conservation considerations in marl/limestone alternations (Ricken, 1986) show that diagenesis in a meter-scale subvolume of these systems may proceed as a closed system, with diffusion dominating as a mechanism for solute transport. Thus, this chapter explores meter-scale subvolumes of rock, which are closed to mass transport at the boundaries. The banded symmetry involved in stylolites and diagenetic bedding planes allows solution of the model equations along the dimension perpendicular to the putative bands/beds. In other words, compaction and mass transport are in these examples predominantly in the direction normal to the plane defined by the banding. For simplicity, no gradients in temperature, fluid pressure, fluid composition, or stress arising from body forces are imposed across the simulation domain. In order to simulate the effects of burial, the column of pore fluid is taken to be in hydrostatic equilibrium, so that fluid pressure increases linearly with depth. Similarly, temperature increases with depth via a specified geothermal gradient. The stress on the upper boundary of the simulation domain is found from the weight of overburden, represented by a constant wetted bulk density of rock of 2.2 g/cm^3. Boundary conditions for a subvolume of rock during burial used in the one-dimensional simulations discussed in the remainder of this chapter are summarized in Table 7-3.

Increases in free energy due to stress arising from overburden loading at diagenetic conditions are relatively small. In order to numerically simulate stress-driven diagenetic reactions, the authors have found it necessary to introduce a new dimensionless deviatoric concentration variable ψ_α defined by

$$c_\alpha = \bar{c}_\alpha(p, T)(1 + \psi_\alpha) \tag{7-36}$$

TABLE 7-3

Boundary and initial conditions for sinking-subvolume

Boundary conditions:

$$J_\alpha = 0 \text{ at } z = z_{\text{top}}, z_{\text{bottom}}$$

$$\frac{\partial w_y}{\partial y} = f(\sigma_z) \text{ at } z = z_{\text{top}}$$

$$w_y = \text{constant at } z = z_{\text{bottom}}$$

$$\frac{\partial L_i}{\partial z} = 0 \text{ at } z = z_{\text{top}}, z_{\text{bottom}}$$

$$\frac{\partial \phi_{\text{clay}}}{\partial z} = 0 \text{ at } z = z_{\text{top}}, z_{\text{bottom}}$$

Initial conditions:

c_α found from $\sum_i \tilde{A}_i G_i = 0$ and rock texture, L_i and ϕ_{cl} are given initially as a function of space.

where $\overline{c}_\alpha(p, T)$ is the concentration of α in equilibrium with the solid at fluid pressure and temperature. This enables the pressure solution effects to be brought out in the equations above the level of background numerical noise.

The horizontal components of the macroscopic stress tensor, and from them the horizontal derivatives of w_x and w_y, are found from a lateral constraint on the pressure solution-induced deformation. A medium in which the compaction mechanism is predominantly chemical will cease compaction along a given direction when reaction at grain facets normal to this direction ceases. The normal components of the grain stresses, P_x and P_y, are thus determined by setting the horizontal growth rates G_x and G_y equal to zero (that is, setting G_x and G_y equal to 0 using analogous expressions to that given for G_z in Eq. 7-29). The macro-stress components σ^{m}_{yy} and σ^{m}_{xx} are found from the local texture, P_x, and P_y from relations analogous to Eq. 7-20. The mechanical model can then be summarized as follows:

$$\begin{aligned}
\sigma^{\text{m}}_{zz} &= \lambda^{\text{m}}\frac{\partial w_x}{\partial x} + \lambda^{\text{m}}\frac{\partial w_y}{\partial y} + (\lambda^{\text{m}} + 2\mu^{\text{m}})\frac{\partial w_z}{\partial z} + \alpha^{\text{m}} p, \\
\sigma^{\text{m}}_{xx} &= \sigma^{\text{m}}_{yy} = -\left((P_y - p)\frac{A_y}{L_x L_y} + p\right), \\
\frac{\partial w_x}{\partial x} &= \frac{\partial w_y}{\partial y} = \left(\frac{\sigma yy - \lambda^{\text{m}}\frac{\partial w_z}{\partial z} - \alpha^{\text{m}} p}{2(\lambda^{\text{m}} + \mu^{\text{m}})}\right), \\
P_x &= P_y = p + \psi_\alpha \rho R T,
\end{aligned} \tag{7-37}$$

and:

$$\frac{\partial}{\partial z}\left((\lambda^{\text{m}} + \mu^{\text{m}})\frac{\partial w_z}{\partial z} + \lambda^{\text{m}}\frac{\partial w_x}{\partial x} + \lambda^{\text{m}}\frac{\partial w_y}{\partial y} + \alpha^{\text{m}} p\right) - (1 - \phi)\Gamma_{\text{s}} - \phi\Gamma_{\text{f}} = 0.$$

Methods for mapping the equations describing a compacting domain onto a constant rectilinear grid, and for numerical solution of the system of equations, are given in Dewers and Ortoleva (1990b).

THERMODYNAMICS AND KINETICS OF CALCITE–WATER REACTION

Speciation and linear dependency of concentrations

Equations describing reaction and transport for the calcite/water system are derived from conditions of mass conservation. The treatment adopted for carbonate speciation is similar to that used by Plummer and Busenberg (1982) for carbonate equilibria. The species involved and the appropriate equilibrium constants are defined in Table 7-4. Conservation of mass for these species is expressed as (Ortoleva et al., 1987; Chen and Ortoleva, 1990):

$$\begin{aligned}
\nabla \cdot J_{\mathrm{Ca}^{2+}} &= \phi[-W_{\mathrm{CaCO}_3^0} - W_{\mathrm{Ca(OH)}^+} - W_{\mathrm{CaHCO}_3^-}] + n\rho \sum_i \tilde{A}_i G_i \\
\nabla \cdot J_{\mathrm{CO}_3^{2-}} &= \phi[-W_{\mathrm{CaCO}_3^0} - W_{\mathrm{HCO}_3^-}] + n\rho \sum_i \tilde{A}_i G_i \\
\nabla \cdot J_{\mathrm{CaHCO}_3^+} &= \phi W_{\mathrm{CaHCO}_3^+} \\
\nabla \cdot J_{\mathrm{CaCO}_3^0} &= \phi W_{\mathrm{CaCO}_3^0} \\
\nabla \cdot J_{\mathrm{Ca(OH)}^+} &= \phi W_{\mathrm{Ca(OH)}^+} \\
\nabla \cdot J_{\mathrm{HCO}_3} &= \phi[W_{\mathrm{HCO}_3^-} - W_{\mathrm{H_2CO}_3^0} - W_{\mathrm{CaHCO}_3^+}] \\
\nabla \cdot J_{\mathrm{H_2CO}_3^0} &= \phi W_{\mathrm{H_2CO}_3^0} \\
\nabla \cdot J_{\mathrm{OH}^-} &= -\phi W_{\mathrm{H_2O}} - \phi W_{\mathrm{Ca(OH)}^+} \\
\nabla \cdot J_{\mathrm{H}}^{+} &= -\phi[-W_{\mathrm{H_2O}} - W_{\mathrm{HCO}_3^-} - W_{\mathrm{H_2CO}_3^0}].
\end{aligned} \tag{7-38}$$

It is likely that the aqueous reaction rates are fast compared to calcite–water reactions and hence are maintained at equilibrium. The aqueous species are then not necessarily independent but related through the various equilibrium conditions.

TABLE 7-4

Chemical model for calcite reaction

Reaction	Equilibrium constant at p and T
$\mathrm{CaCO_3}$ (calcite) $\rightleftharpoons$ $\mathrm{Ca^{2+} + CO_3^{2-}}$	K_c
$\mathrm{H^+ + OH^-}$ $\rightleftharpoons$ $\mathrm{H_2O}$	K_w
$\mathrm{H^+ + CO_3^{2-}}$ $\rightleftharpoons$ $\mathrm{HCO_3}$	K_2
$\mathrm{H^+ + HCO_3^-}$ $\rightleftharpoons$ $\mathrm{H_2CO_3}$ (or $\mathrm{CO_2^*}$)	K_1
$\mathrm{Ca^{2+} + CO_3^{2-}}$ $\rightleftharpoons$ $\mathrm{CaCO_3^0}$	$K_{\mathrm{CaCO_3^0}}$
$\mathrm{Ca^{2+} + OH^-}$ $\rightleftharpoons$ $\mathrm{Ca(OH)^+}$	$K_{\mathrm{CaOH^+}}$
$\mathrm{Ca^{2+} + HCO_3}$ $\rightleftharpoons$ $\mathrm{CaHCO^+}$	$K_{\mathrm{CaHCO_3^+}}$
$\mathrm{CO_2}$ (gas) $\rightarrow$ $\mathrm{CO_2^*}$	K_H

By taking linear combinations of the reaction–transport relations in Eq. 7-38 and invoking aqueous equilibria conditions, one may express these relations in terms of a smaller set of equations that do not contain the aqueous reaction terms (Ortoleva et al., 1987). This methodology is both convenient and practical for usage in numerical solution algorithms. To carry out this program for the present problem, it is convenient to introduce the following variables:

$$\begin{aligned} \beta &\equiv m^{\mathrm{T}}_{\mathrm{Ca}} - m^{\mathrm{T}}_{\mathrm{CO_3}} \\ \chi &\equiv m_{\mathrm{H^+}} - m_{\mathrm{OH}} + m_{\mathrm{HCO_3}} + 2m_{\mathrm{H_2CO_3^0}} + m_{\mathrm{CaHCO_3^+}} - m_{\mathrm{Ca(OH)^+}} \end{aligned} \tag{7-39}$$

where total calcium is denoted $m^{\mathrm{T}}_{\mathrm{Ca}}$,

$$m^{\mathrm{T}}_{\mathrm{Ca}} = m_{\mathrm{Ca^{2+}}} + m_{\mathrm{CaCO_3^0}} + m_{\mathrm{CaHCO_3^+}} + m_{\mathrm{Ca(OH)^+}} \tag{7-40}$$

and total carbonate is denoted $m^{\mathrm{T}}_{\mathrm{CO_3}}$

$$m^{\mathrm{T}}_{\mathrm{CO_3}} = m_{\mathrm{CO_3^{2-}}} + m_{\mathrm{HCO_3^-}} + m_{\mathrm{H_2CO_3^0}} + m_{\mathrm{CaCO_3^0}} + m_{\mathrm{CaHCO_3^+}}.$$

If diffusion coefficients of all species are equal, it is found:

$$-\nabla \cdot J_{\chi} = 0. \tag{7-41}$$

A relation similar to Eq. 7-41 applies to β. Because the system boundaries are closed to the flux of all aqueous species, Eq. 7-41 and its analog for β imply that β and χ are constants of motion at a given temperature, fluid pressure, and ionic strength. Recognition of this fact allows reduction of the number of equations needed to describe the evolution of the pore fluid chemistry.

When $\beta = 0$ (i.e., total calcium equals total carbonate), charge neutrality is satisfied if (Plummer and Busenberg, 1982):

$$2\beta + \chi = 0. \tag{7-42}$$

These two conditions, plus the reaction–transport relation:

$$\nabla \cdot J^{\mathrm{T}}_{\mathrm{Ca}} = n\rho \sum_i \tilde{A}_i G_i, \tag{7-43}$$

are sufficient to determine the evolution of the pore fluid chemistry, when subject to boundary and initial conditions.

Corrections to carbonate equilibria due to fluid pressure, ionic strength, and p_{CO_2}

Calcite solubility varies over many orders of magnitude, depending on ionic strength, pressure, temperature, and the partial pressure of carbon dioxide. Rates of calcite reaction at the various calcite–fluid interface sites, which display different dependencies on the thermodynamics of the calcite–water system, are sensitive to these variables. The present model was developed to include options for both dilute or sea water (the latter having ionic strength of 0.725 molal) and to also allow for either the imposition of a partial pressure of CO_2 (open system) or the internal

TABLE 7-5

Sources for temperature-dependence of equilibrium constants (S = saline, I = 0.725 m, F = fresh)

Value	Model	log $K(T, 1\text{ atm})$	Activity coefficients
K_c	S	Rabinowicz et al., 1985	Rabinowicz et al., 1985
	F	Plummer and Busenberg, 1982	Plummer and Busenberg, 1982
$K_{HCO_3^-}$	S	Patterson et al., 1982	Patterson et al., 1982
	F	Plummer and Busenberg, 1982	Plummer and Busenberg, 1982
$K_{H_2CO_3^0}$	S	Patterson et al., 1984	Patterson et al., 1984
	F	Plummer and Busenberg, 1982	Plummer and Busenberg, 1982
$K_{Ca(OH)^+}$	S	Anórsson et al., 1982	Plummer and Busenberg, 1982
	F	Anórsson et al., 1982	Plummer and Busenberg, 1982
$K_{CaHCO_3^+}$	S	Jacobson and Langmuir, 1974	Plummer and Busenberg, 1982
	F	Jacobson and Langmuir, 1974	Plummer and Busenberg, 1982
$K_{CaCO_3^0}$	S	Reardon and Langmuir, 1974	Plummer and Busenberg, 1982
	F	Reardon and Langmuir, 1974	Plummer and Busenberg, 1982
K_{H_2O}	S	Plummer and Busenberg, 1982	Becker and Bilal, 1985
	F	Plummer and Busenberg, 1982	Plummer and Busenberg, 1982
K_H	S	Plummer and Busenberg, 1982	Plummer and Busenberg, 1982
	F	Plummer and Busenberg, 1982	Plummer and Busenberg, 1982

determination of it (closed system). Sources for the temperature dependence of equilibrium constants for both dilute and saline (ionic strength $I = 0.725\ m$) cases are given in Table 7-5.

When data was available, corrections for fluid pressure were applied in the following form:

$$K(p, T) = K(1\text{ bar}, T)\exp\left\{\sum_{\alpha=1}^{N} \nu_\alpha \left(V_\alpha(p-1) + \frac{\beta_\alpha}{2}(p-1)^2\right)\right\}, \tag{7-44}$$

where V_α and β_α are the partial molar volume and compressibility for solute α. Molar volume data for $CaOH^+$, $CaCO_3$ and $CaHCO_3^+$ were not found, and so equilibrium constants for reactions involving these species were not corrected for fluid pressure. Where equilibrium constants were given at a temperature and fluid pressure equal to the vapor pressure of water, the reference pressure of 1 bar appearing in Eq. 7-44 was replaced by the appropriate vapor pressure.

In the case of the first and second dissociation constants of carbonic acid at ionic strengths equal to that of sea water, pressure corrections are given in Patterson et al. (1982; 1984). Sources for data and temperature dependencies for V_α and β_α are given in Table 7-6 for both fresh and saline examples.

Ionic strength corrections for fresh-water chemistry are determined using the extended Debye–Huckel theory as carried out by Plummer and Busenberg (1982), with an iterative procedure.

TABLE 7-6

Sources for partial molar volumes and compressibilities of solutes (S = saline, I = 0.725 M, F = fresh)

Solute	Model	Sources
Ca^{2+}	S	Millero, 1982
	F	Millero, 1982
CO_3^{2-}	S	Millero, 1982
	F	Millero, 1982
HCO_3^-	S	Millero, 1982
	F	Millero, 1982
$H_2CO_3^0$	S	Ellis, 1972
	F	Ellis, 1972
OH^-	S	Millero, 1982
	F	Millero, 1982

For saline waters, enough data exists at ionic strengths near sea water to allow one to model calcite–water equilibria at $I = 0.725\ m$ as a special case. The temperature dependence of the equilibrium constant for calcite, K_c, at this ionic strength is taken from an expression used by Rabinowicz et al. (1985); at 25°C, K_c ($I = 0.725\ m$) determined from this expression corresponds to that of Harvie et al. (1984, p. 743). At 100°C this expression yields a K_c equal to that determined by Ellis (1963). First and second dissociation constants for carbonic acid (K_1 and K_2) at $I = 0.725$, temperature, and fluid pressure are found from expressions in Patterson et al. (1982, 1984). Osmotic coefficients for use in these expressions were taken from Liu and Lindsay (1972).

Despite the apparent complexity of this chemical model, the present reaction transport model actually requires only a few parameters determined from solution chemistry. This is due to the assumption of equal diffusion coefficients. Only the relationship between total calcium concentration and the deviatoric calcium ion concentration, $\psi_{Ca^{2+}}$, the relationships between $\psi_{Ca^{2+}}$, ψ_{H^+}, and $\psi_{CO_3^{2-}}$, and the value of calcium ion concentration in equilibrium with calcite at temperature, fluid pressure, and ionic strength are needed. The relations $\beta = 0$ and $\chi = 0$ are sufficient to determine the interdependence of the deviatoric concentrations $\psi_{Ca^{2+}}$, $\psi_{CO_3^{2-}}$, and ψ_{H^+}.

In cases where the partial pressure of CO_2 is internally determined (i.e., closed systems), the writers simultaneously solved the equations χ, $\beta = 0$ by a Newton–Raphson iterative method. In the case of an imposed p_{CO_2}, the activity of dissolved CO_2, $a_{H_2CO_3^0}$, is equal to the partial pressure of carbon dioxide multiplied by K_H (Henry's Law constant) and a fugacity coefficient. This fixes the pH of the solution for a given calcium ion concentration; one can show that:

$$a_{H^+} = (K_H\, p_{CO_2}\, K_{HCO_3} - K_{H_2CO_3^0}\, a_{Ca^{2+}}/K_c). \tag{7-45}$$

For the case of imposed carbon dioxide fugacity, Eq. 7-45 plus the condition in Eq. 7-41 were solved simultaneously by a bisection-iterative algorithm to give the dependence of $\psi_{\mathrm{Ca}^{2+}}$ on $\psi_{\mathrm{CO}_3^{2-}}$.

INHIBITION OF FREE-FACE RATES DUE TO SOLUTE INHIBITORS AND GRAIN COATINGS

An important premise of this chapter is that the rate of reaction at grain free-faces relative to that at grain contacts determines which of the various stable and unstable compactional behaviors are obtained. This is discussed in detail in the context of numerical simulations in the next section. There are at least two factors, one chemical and one physical, which can greatly influence the reaction rate at free faces. These are ionic inhibitors dissolved in the pore fluid solution (chemical) and clay coatings (physical).

Much in the calcite reaction kinetics literature has been devoted to surface poisoning of calcite dissolution or precipitation by Mg^{2+}, SO_4^{2-}, PO_4^{3-}, or organic acids (Morse, 1974; Reddy and Wang, 1980; Busenberg and Plummer, 1986; Amjad, 1987). A few examples are discussed in this chapter for illustrative purposes. Inhibition of calcite by these solute species is commonly described in terms of a Langmuir adsorption isotherm:

$$\frac{k}{k^{\circ}} = 1 - \left\{1 + \frac{k_{\mathrm{d}}}{k^{\mathrm{a}}} \Big/ m_{\alpha}\right\}^{-1}, \tag{7-46}$$

where k is the uninhibited dissolution rate coefficient; $k_{\mathrm{d}}/k_{\mathrm{a}}$ is the ratio of the desorption to adsorption coefficient rates for inhibitor α; and m_{α} is the molal concentration of α. For Mg^{2+}, Reddy and Wang (1980) found:

$$\frac{k}{k_{\mathrm{o}}} = 1 - (1.12 + 0.4 \times 10^{-4}/m_{\mathrm{Mg}}^{\mathrm{T}})^{-1}$$

where $m_{\mathrm{Mg}}^{\mathrm{T}}$ is the total amount of magnesium in solution.

Gieskes (1983) gave examples of concentrations of pore fluid obtained within pelagic sediments from cores of the Deep Sea Drilling Project. Table 7-7 lists some

TABLE 7-7

Example concentrations, Langmuir isotherm coefficients, and kinetic inhibition of calcite free-face rate coefficient

Inhibitor	Concentration [a]	$k_{\mathrm{d}}/k_{\mathrm{a}}$	k^{+}/k_{0}^{+}
Mg^{2+}	20.0×10^{-3}	$\approx 0.46 \times 10^{4}$ (Reddy and Wang, 1980)	0.168
	53.0×10^{-3}		0.107
PO_4^{3}	4.0×10^{-6}	2.0×10^{-6} (Amjad, 1987)	0.333
	32.0×10^{-6}		0.058
SO_4^{2-}	3.7×10^{-4}	0.2×10^{-4} (Berner and Morse, 1974)	0.095

[a] Concentrations from DSDP pore fluids from Gieskes (1983), in mol/kg.

concentrations taken from that study, the adsorption /desorption parameter for use in Eq. 7-46 and the resulting k/k_o. These are used in the next section to demonstrate the possibility that ionic inhibition in sea water–calcite interaction can play a role in the transition from (stable) pervasive intergranular pressure solution to (unstable) (stylolitized or otherwise diagenetically layered) compaction in limestones.

To account for kinetic inhibition in calcite due to clay coatings, the thickness of the coating is expressed in terms of the volume fraction of clay, ϕ_{cl}, surface area available for coating, and density of the coating on a single grain. The thickness is a key variable, as the rate of reaction at free faces may be limited by diffusion through the clay film. The coating thickness, δ, can be approximated by the ratio of the volume of clay per unit cell serving as coating, V_{cl}, and the free-face area of a grain, A_{f}:

$$\delta = \frac{V_{\mathrm{cl}}}{A_{\mathrm{f}}}. \tag{7-47}$$

The clay volume is equal to the volume fraction of clay divided by the number of "coating entities" per unit volume. The latter is equal to the number of calcite grains per unit volume (i.e., one coating per grain), denoted n as in Table 7-1. δ then takes the following form:

$$\delta = \frac{\phi_{\mathrm{cl}}\, L_x L_y L_z}{A_{\mathrm{f}}}$$

Implicit in this treatment is the assumption that all of the clay serves as a coating, and, as compaction proceeds, the decrease in calcite free-face area is covered by a progressively thickening coating.

The form of the rate law for free-face reaction rates in the diffusion controlled limit are similar to expressions for "leached layer" kinetics (e.g., Berner and Morse, 1974):

$$G^{\mathrm{f}} = \frac{D^{\mathrm{c}}\tau}{\delta\rho}(c_\alpha - c_\alpha^{\mathrm{eq}}) \tag{7-48}$$

where α is the species which diffuses the slowest, τ is the tortuosity of the clay film, and c_α^{eq} is the equilibrium concentration of α. For calcite, Ca^{2+} is likely the slowest diffusing species, and $c_{\mathrm{Ca}^{2+}}^{\mathrm{eq}}$ is equal to $K/c_{\mathrm{CO}_3^{2-}}$.

Using the above formulas, the rate of calcite reaction at free faces is inversely proportional to the clay volume fraction. This is consistent with the inverse relationship of calcite grain size with clay amount seen by Bausch (1968), and shown in Fig. 7-4. This relationship between clay content and free face growth rate is very important in the development of marl/limestone alternations, as shown in the next section.

NUMERICAL SIMULATIONS

Numerical solution of the system of coupled partial differential equations constituting the present model simulates the spatio-temporal evolution of the system variables. It thereby is essential to compare model predictions with natural systems.

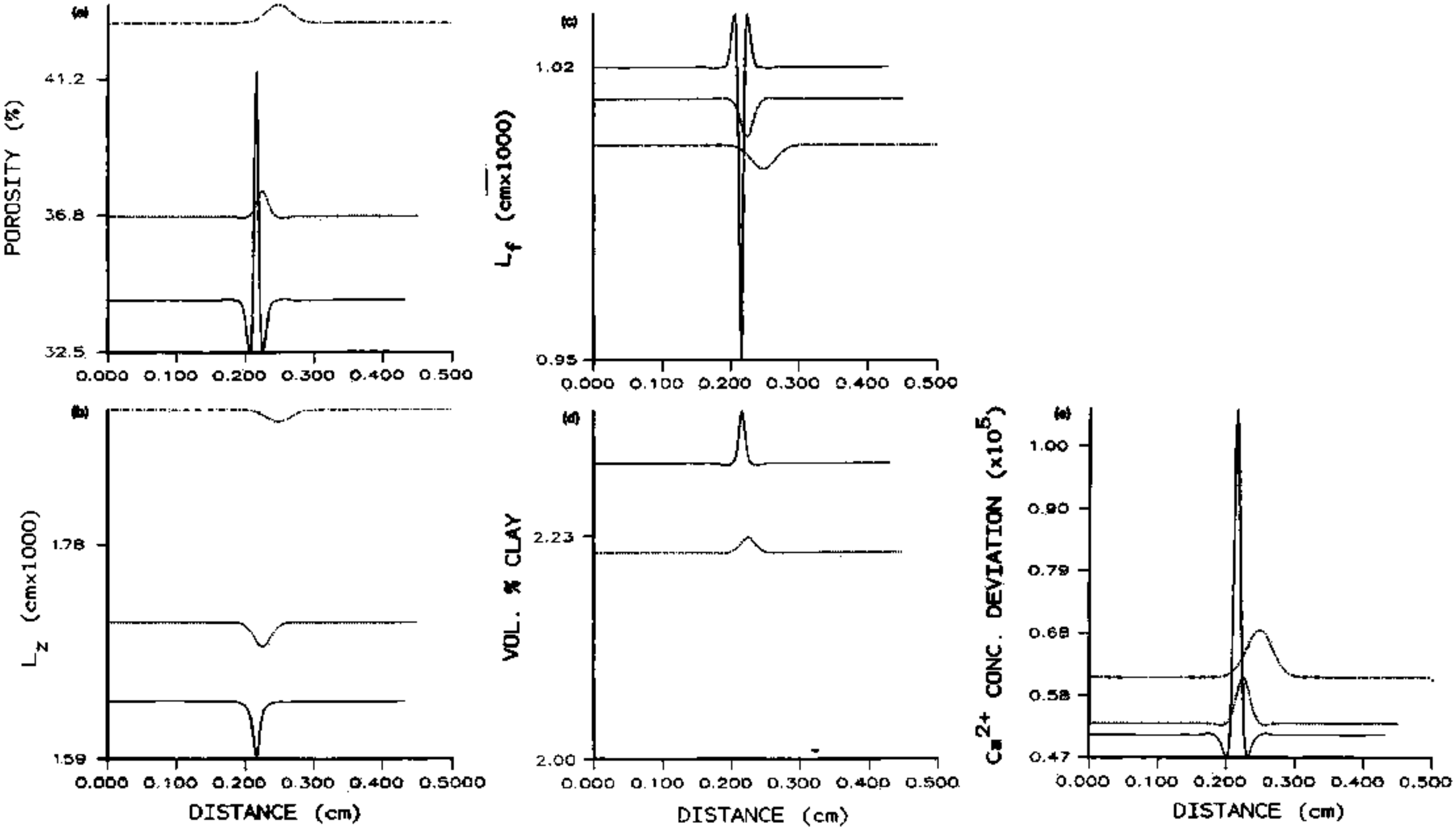

Fig. 7-7. Evolution of a one-dimensional porous calcite–clay system for a burial rate of 10 m/million years. Shown are the profiles of textural variables and deviatoric concentration of Ca^{2+} at 0 (broken line), 500 (dashed line), and 1000 years (solid line). The temperature gradient is 25°C/km. The size of the simulation domain decreases with time because of compactional shortening. For this model, clay serves only as "insoluble residue". $p_{CO_2} = 10^{-3}$ atm, ionic strength is fixed at 0.725 *m*, and $k/k_0 = 0.06$, reflecting an inhibition by Mg^{2+}. (a) Porosity versus distance, showing the amplification of a small initial heterogeneity in porosity. (b) L_z versus distance, showing the localization of compaction at the minima. Zones of greater compaction occur when L_z is the smallest, and thus height of grains the least. (c) L_f versus distance, showing localized dissolution at the initial heterogeneity and heightened concentration in adjacent localities. (d) Volume % clay versus distance, showing greater collection of clay in the zone of heightened compaction. (e) Deviatoric concentration of Ca^{2+} showing concentration gradients that arise because of, and which in turn modify, the evolution of texture.

To begin the numerical analyses, first the limit is examined wherein clay does not influence the free-face reaction rates. Depending on reaction kinetics, the simulated water–rock system may respond to burial by compacting relatively pervasively (intergranular pressure solution), or compaction may become localized (as during stylolitization). Next, the implications of a clay-coating-dependent free-face reaction kinetics are examined. If clay content lies within a certain range, alternations in cementation and compaction are predicted to occur which bear a striking resemblance to natural examples of marl–limestone alternations. Finally, a model is discussed for the post-compactional segregation between calcite and clay, where the same kinetic mechanism operates at all interfaces in a low-porosity rock.

Stylolitization in relatively clean limestones

Dewers and Ortoleva (1990b) showed that for sandstones a transition between pervasive intergranular pressure solution and stylolitization accompanied an increase in the ratio between free-face and contact rate coefficients. In limestones, such a change may reflect variations in fluid chemistry, specifically due to the concentrations of solute inhibitors. In Figs. 7-7 through 7-9 this transition is shown to occur in an open system saline fluid chemistry with $p_{CO_2} = 10^{-3}$ bar, following a change in k/k_o of 0.06 (Fig. 7-7), 0.01 (Fig. 7-8), and 0.001 (Fig. 7-9). An initial small negative perturbation in grain size, taking the form of a small negative bump in L_z and L_f in the center of the simulation domain, may strongly auto-enhance, as shown in Fig. 7-7, weakly enhance, as in Fig. 7-8, or experience very little change, as in Fig. 7-9. In interpreting Figs. 7-7, 7-8, 7-9 and the results of simulations to follow, one should note the overall shortening of this system and consequent displacement of maxima and minima associated with the ongoing compaction. In all simulations, the left-hand side of the system was taken to be the origin and distance was measured relative to this.

In Fig. 7-7, small minima in L_z and L_f are seen to amplify with time. In the case of L_f, free-face dissolution driven by elastic strain energy increases the local porosity and decreases the horizontal contact area. As a result, local stress (and thus strain energy) increases, which increases the rate of dissolution, thus completing a positive feedback loop. In the case of L_z, contact dissolution becomes localized because horizontal contact areas in the dissolution zone decrease, which serves to increase the stress (force per unit area) across the contacts. The localized compaction that occurs can be seen in the evolution of the spatial profile of the clay volume fraction in Fig. 7-7d. More clay collects in the zones of greater compaction.

As the rate of free-face reaction relative to contact dissolution reaction decreases, this instability becomes more and more repressed. As a result, compaction and dissolution become less localized and more pervasive throughout the domain. This can be seen in the sequence of Figs. 7-7 through 7-9.

Figure 7-7 best demonstrates the tendency of an initial textural heterogeneity to induce secondary or "satellite" stylolites, as first suggested by one of the authors (Merino et al., 1983), as well as the greater amounts of cementation that occur adjacent to the dissolution "seam". The latter has been observed in limestones (Wong and Oldershaw, 1981; Ricken, 1986). The mass lost at stylolitic or other

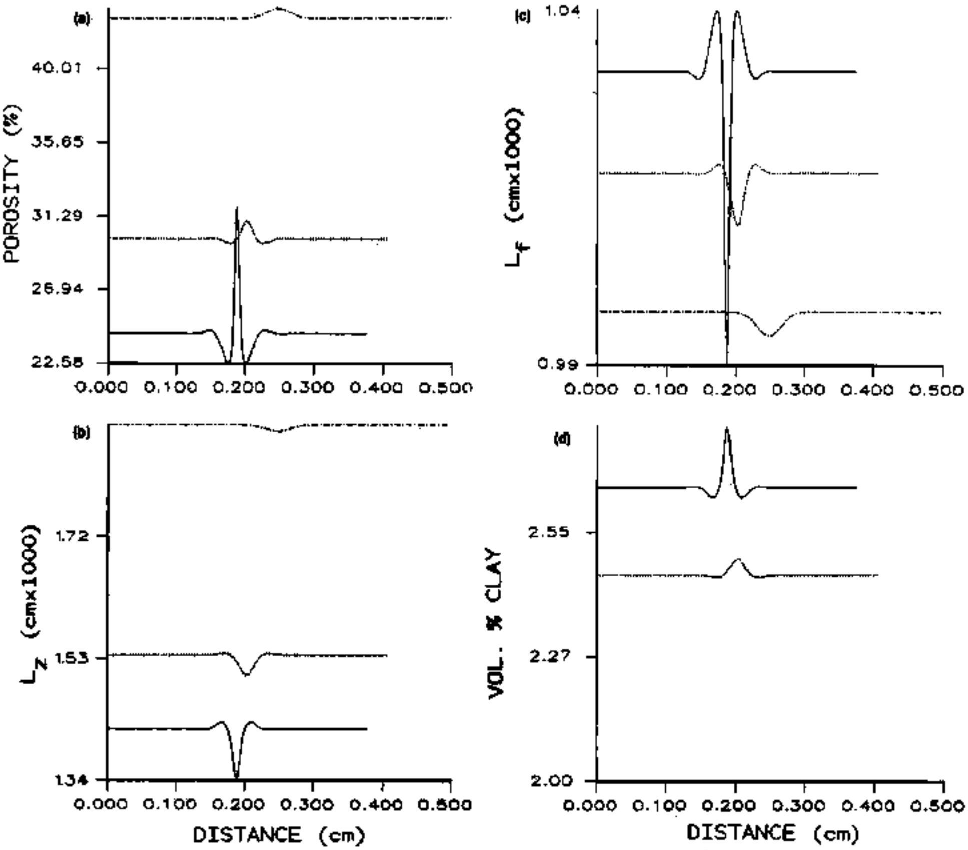

Fig. 7-8. Same as in Fig. 7-7, except k/k_0 equals 0.01. Shown are the spatial profiles of (a) porosity, (b) L_z, (c) L_f, and (d) volume % clay at 0.0 years (broken line), 2235 years (dashed line), and 4470 years (solid line). The instability leading to localized dissolution and compaction is damped somewhat from that in Fig. 7-7 because of the lower k/k_0.

dissolution seams will diffuse down chemical potential gradients and precipitate in the adjacent regions. The distance it may diffuse prior to precipitation is roughly equal to the square root of the product of the pore-fluid diffusion coefficient multiplied by a characteristic reaction time, i.e., a time over which reaction may act to produce an appreciable textural change, which varies inversely with the magnitude of the net calcite–water reaction rate. The contrast between the rock texture (porosity, contact areas, etc.) in the cemented zones and the outlying regions induces the secondary dissolution zones, both through macroscopic stress, as mediated by porosity-dependent macro-elastic constants and concentration gradients.

In Fig. 7-10, the "satellite induction length" (Feeney et al., 1983), or distance between the initial textural heterogeneity and the satellite stylolite it induces, is plotted as a function of k/k_0. The decreasing spacing with increasing k/k_0 occurs because the characteristic stylolitization time in the present model is inversely

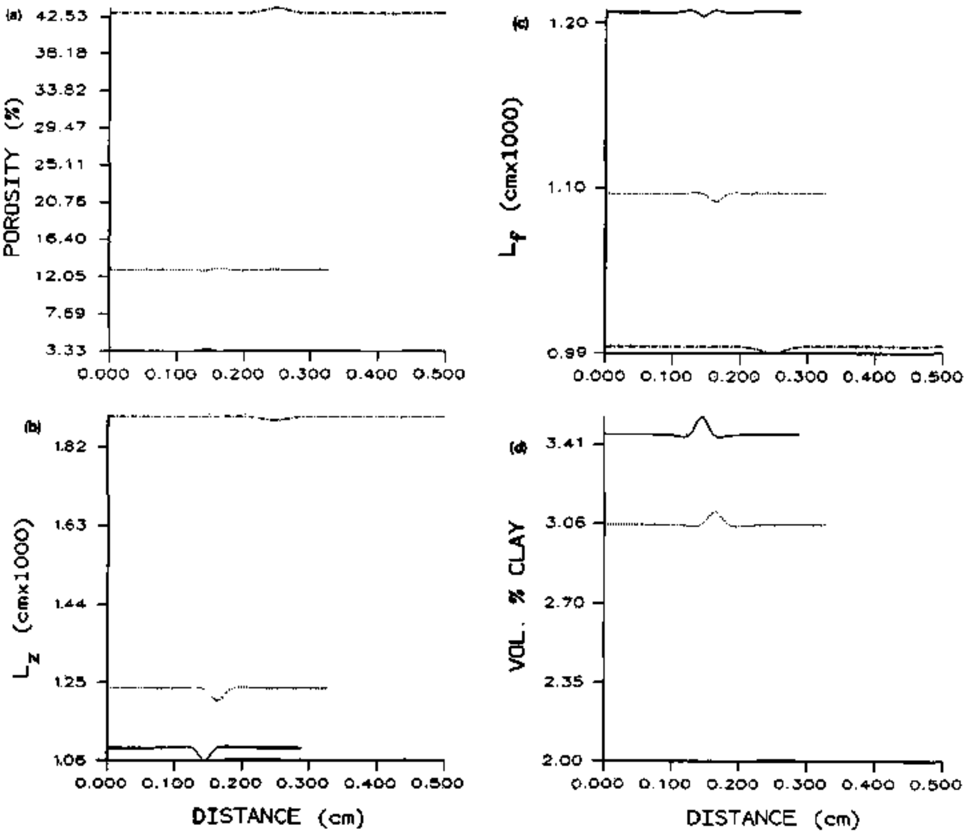

Fig. 7-9. Same as in Fig. 7-7, except k/k_0 equals 10^{-3}. Shown are the spatial profiles of (a) porosity, (b) L_z, (c) L_f, and (d) volume % clay at 0.0 years (broken line), 9150 years (dashed line), and 18,300 years (solid line). Because of the slower rate of free face dissolution, there is no local enhancement of textural variations, and compaction is essentially pervasive.

proportional to the rate coefficient, k, and the diffusion length increases with the square root of the reaction time.

A number of simulations were also carried out using small-amplitude initial random deviations from the initial average texture. Figure 7-11 shows the change with time of the root-mean-square (RMS) average of porosity for several simulations of this type in which k/k_0 also varied. Textural fluctuations from the average increase parabolically with time. The development of dissolution seams as mediated by the free-face/strain energy mechanism thus appears to be very unstable, or almost explosively rapid on a geologic time scale, especially for k/k_0 near unity.

Other parameters can be expected to exert an influence on the timing (and thus length scale) of stylolitization. In Figs. 7-12 and 7-13, the RMS deviations are plotted versus time for several simulations (initialized as in Fig. 7-11 with initial random texture) in which the temperature gradient (Fig. 7-12) and the partial

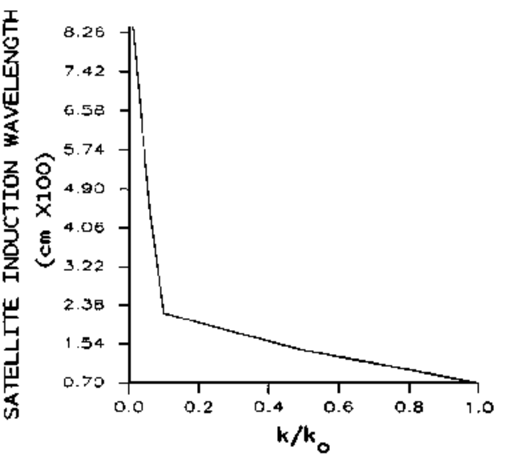

Fig. 7-10. Distance between initial dissolution seam and the adjacent "satellite" seam which it induces as a function of k/k_0.

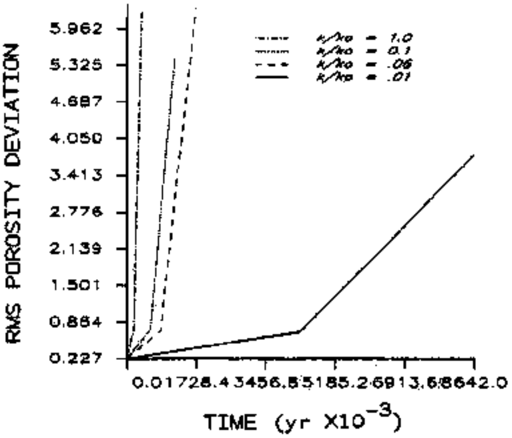

Fig. 7-11. The root-mean-square average of the fluctuations in porosity for four simulations in which the ratio of the inhibited to uninhibited rate coefficient is changed. Large variations in porosity, due to dissolution and cementation attending "stylolitization" in these simulations, develop faster for k/k_0 near unity.

pressure of p_{CO_2} (Fig. 7-13) are varied. The rate of stylolitization increases with both temperature and p_{CO_2} through their effect on the rate coefficient k.

The evolution of small textural variations of random amplitude and wavelength in the initial spatial profiles of L_z and L_f are seen in Fig. 7-14. The small variations amplify with time, with zones of greatest compaction and greatest porosity alternating with zones of greatest cementation. The distance between maxima in, for example, the L_f profiles suggests a characteristic length scale of approximately 0.05 cm. This is a similar separation distance to the fine-scale laminations of (apparent) dissolution

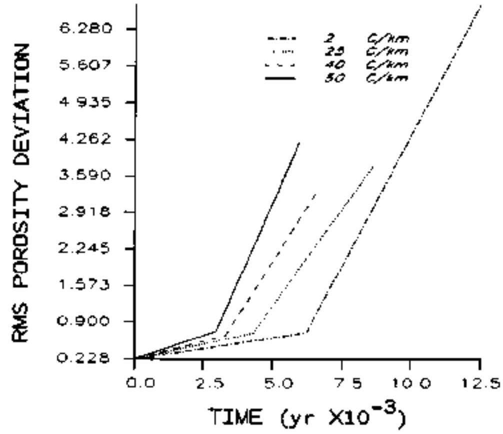

Fig. 7-12. Same as in Fig. 7-11 except that $k = k_0$ and the temperature gradient is varied. Porosity variations develop faster for higher geothermal gradients, due to the effect of temperature on the rate coefficient k.

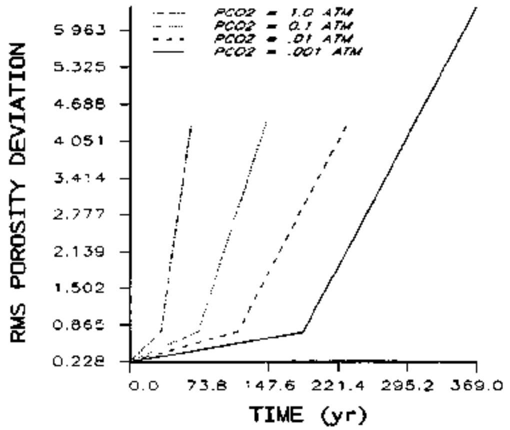

Fig. 7-13. Same as in Fig. 7-11 except that $k = k_0$ and that the partial pressure of carbon dioxide in the pore fluid is varied. Porosity variations develop faster for larger p_{CO_2}, due to its influence on the free-face rate coefficient.

seams in chalk discussed by Ekdale and Bromley (1988). The connection between diffusion and this characteristic length is demonstrated in the maxima and minima of the (deviatoric) concentration profile in Fig. 7-14e. The dissolution features, which have taken off somewhat explosively, correspond to maxima in the spatial profile of the deviatoric concentration of Ca^{2+}.

Figures 7-15, 7-16, and 7-17 show the localization of compaction at the interface between two adjacent regions characterized by a slight contrast in grain size and porosity. The initial textural gradients (i.e., change in porosity, L_z and L_f with distance) decrease in going from Fig. 7-15 through Fig. 7-17; other data used in the

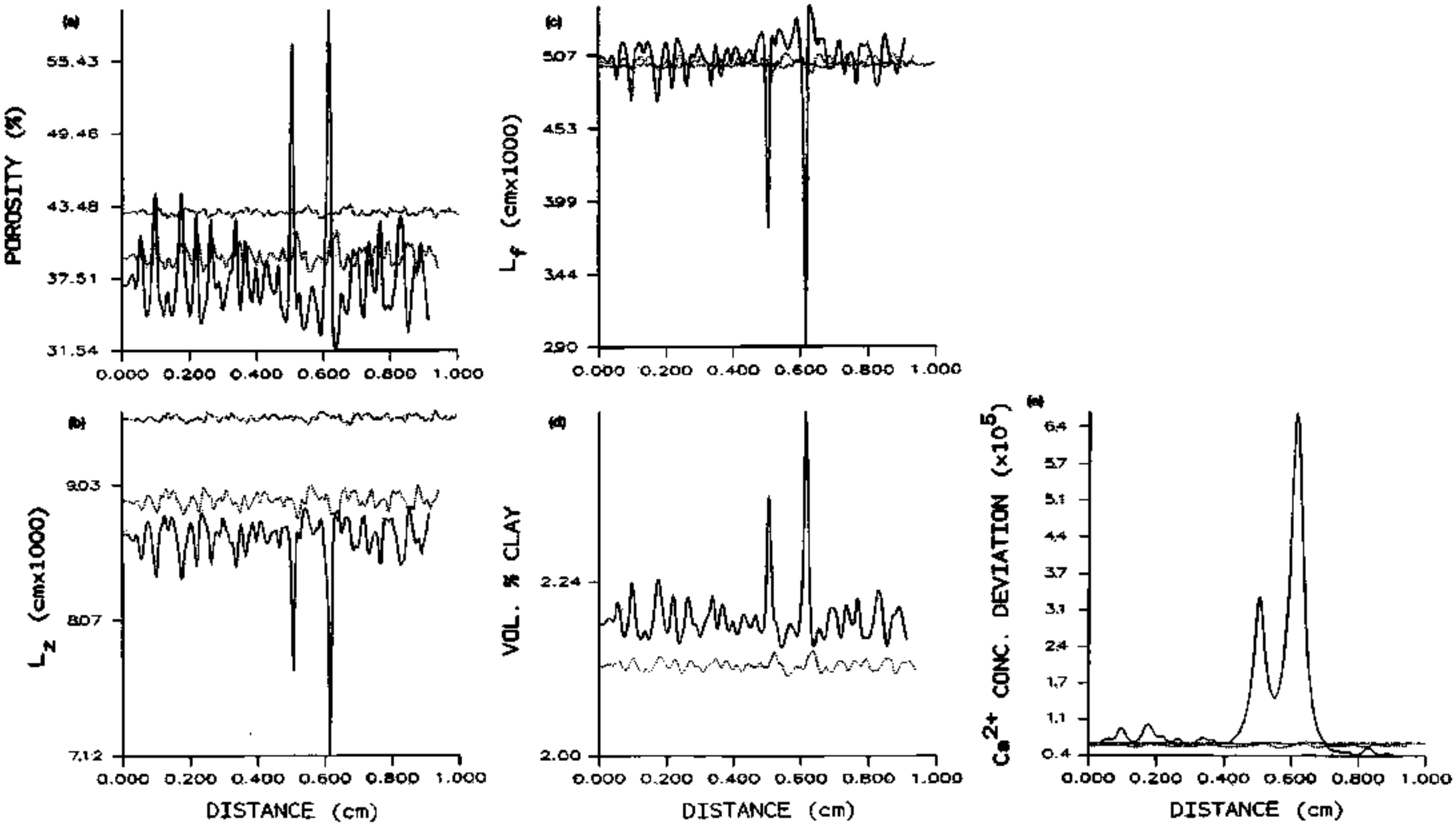

Fig. 7-14. Evolution of small nonuniformities of initial random amplitude and wavelength. Shown are the textural and concentration profiles at 0 years (broken line), 4321 years (dashed line), and 8142 years (solid line). The size of the simulation domain decreases because of compaction during burial from 200 m beneath the sediment–water interface at a rate of 10 m/million years. Zones of greater compaction alternate with zones of greater cementation. The length scale of the two textural variations is similar to that observed in clean chalks by Ekdale and Bromley (1988). (a) Porosity vs. distance; (b) L_z vs. distance; (c) L_f vs. distance; (d) volume % clay vs. distance; (e) deviatoric concentration of Ca^{2+}. The maxima and minima of the concentration profile reflect a characteristic diffusion length determined by the interplay of reaction rates and diffusion. p_{CO_2} equals 10^{-3} atm, and $k/k_o = 0.01$.

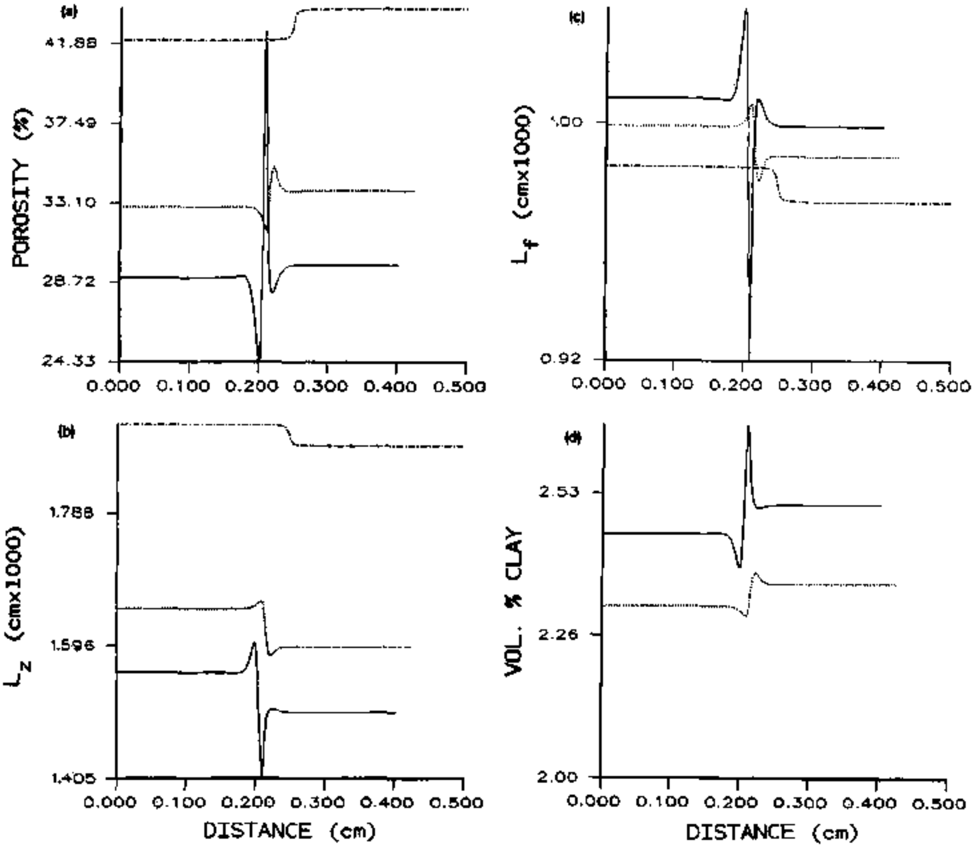

Fig. 7-15. Simulation of a 0.5 cm length domain showing localization of chemical compaction and free-face dissolution at spatial locality where the lithology, here taking the form of grain size and porosity, changes. Shown are the textural profiles at 0 years (broken line), 1385 years (dashed line), and 2770 years (solid line). (a) Porosity vs. distance, showing the generations of secondary porosity at the initial lithologic change and loss of porosity in adjacent regions. (b) L_z vs. depth, showing local shortening occurring at initial lithologic change. Shortening accompanying compaction is greatest in the finer-grained lithologic unit (the right hand side of the simulation domain). (c) L_f vs. distance, showing locally enhanced free-face dissolution and domains of heightened cementation. (d) Volume % clay vs. distance, showing greater collection of clay in zones of greatest compaction. The profile representing the initial clay content coincides with the horizontal axis (at 2 vol.% clay).

simulations are the same. This suggests that the existence and timing of stylolitization is dependent on the size of any initial textural heterogeneity. The development of stylolites at such changes in lithology is commonly observed (Buxton and Sibley, 1981; Simpson, 1985). In this way, depositional bedding surfaces may be considerably enhanced through mechanochemical diagenesis.

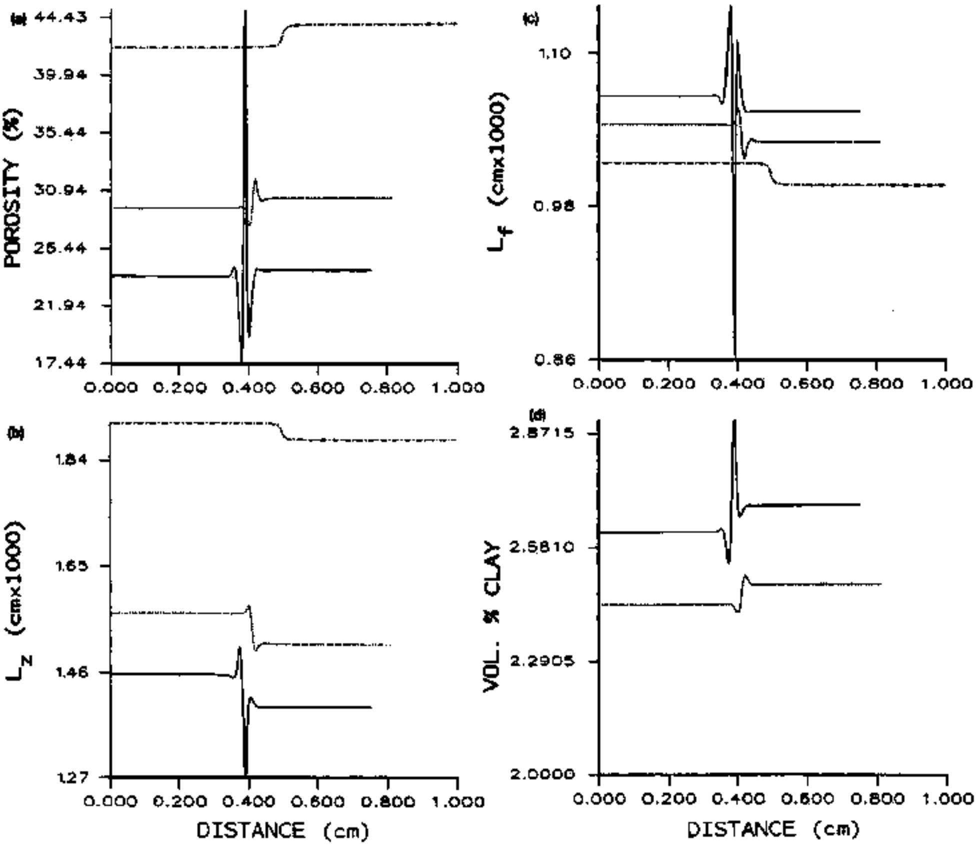

Fig. 7-16. Same as in Fig. 7-15 except that the simulation domain is 1 cm in length. The final time shown (solid line) represents 3890 years. Because of the longer length of the system, the initial spatial gradients in texture are half as large as in Fig. 7-15. As a result, textural variations here take approximately 1.5 times longer to achieve the same state of enhancement as in Fig. 7-15. (a) Porosity vs. distance; the secondary satellite porosity maxima are much more evident here than in Fig. 7-15. (b) L_z vs. distance; (c) L_f vs. distance; (d) volume % clay vs. distance.

Marl/limestone alternations in argillaceous carbonates

Another type of diagenetic bedding is associated with marl/limestone alternations. Figure 7-18a shows a one-dimensional spatial profile of the three textural variables of porosity, compaction, and carbonate content (expressed as a percent of the total solid fraction) in an example of diagenetically enhanced marl/limestone alternations after Ricken (1986). The spatial alternation of zones of compaction and higher porosity with zones of greater cementation are, as mentioned earlier, characteristic of diagenetic alteration. An example of alternating marl and limestone layers reflecting a depositional cyclicity is shown in Fig. 7-18b. There is a relative lack of any spatial correlation between the textural variables, in contrast to that apparent in Fig. 7-

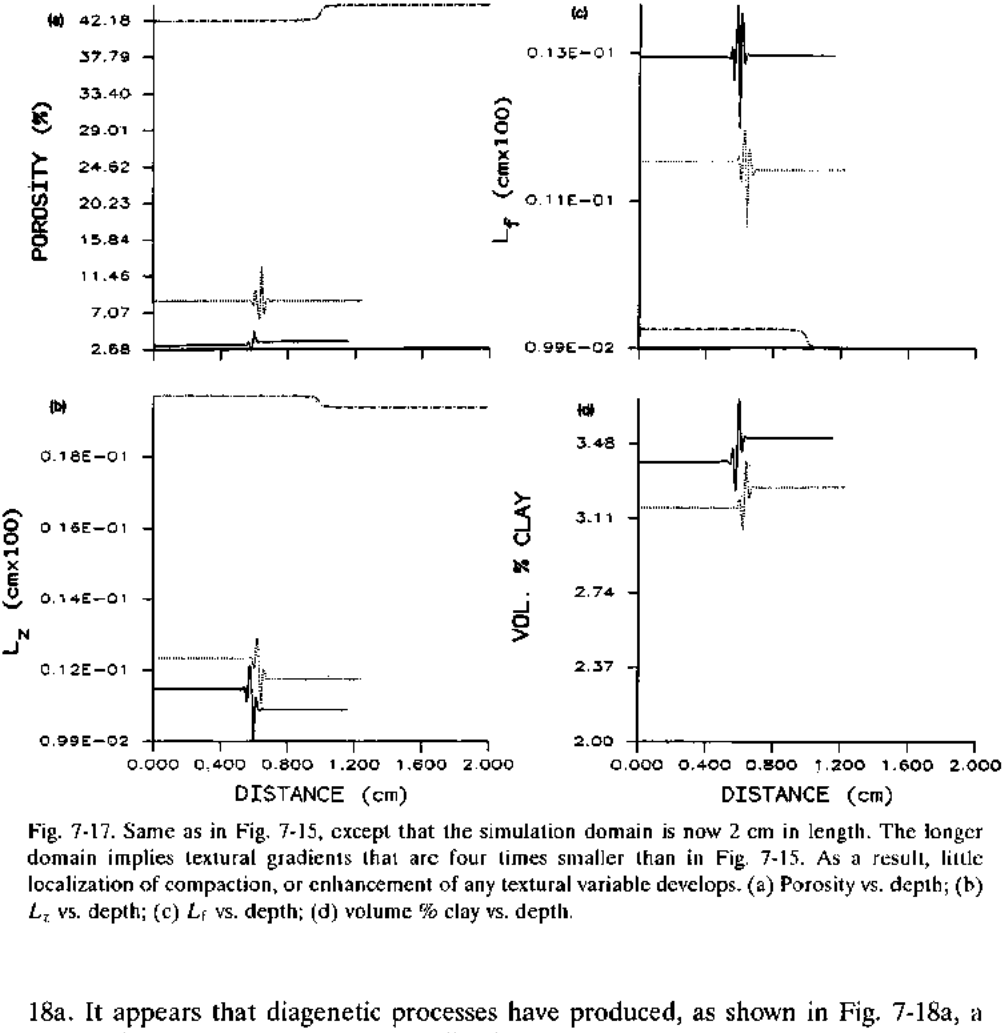

Fig. 7-17. Same as in Fig. 7-15, except that the simulation domain is now 2 cm in length. The longer domain implies textural gradients that are four times smaller than in Fig. 7-15. As a result, little localization of compaction, or enhancement of any textural variable develops. (a) Porosity vs. depth; (b) L_z vs. depth; (c) L_f vs. depth; (d) volume % clay vs. depth.

18a. It appears that diagenetic processes have produced, as shown in Fig. 7-18a, a (roughly) regular, correlated spatial distribution in texture.

The initial uncompacted state of the depositional precursor to, e.g., the lithologic characteristics plotted in Fig. 7-18a, is not perfectly uniform but inherits some non-uniformity due to depositional processes. This is evident in Fig. 7-18b. To understand the development of diagenetic bedding, one must understand how this sedimentary textural "noise" becomes enhanced or otherwise evolved into the observed textural distributions. It is to be expected that this noise, particularly that which has undergone mechanical compaction, is typically "colored", i.e., bears the overprint of some characteristic length corresponding to climatic or other cycles imposed during deposition. The coloring or wavelength embedded in the sedimentary noise can be filtered and amplified by the textural instability that likely underlies the development of diagenetic marl/limestone alternations. This viewpoint is now investigated via some numerical experiments.

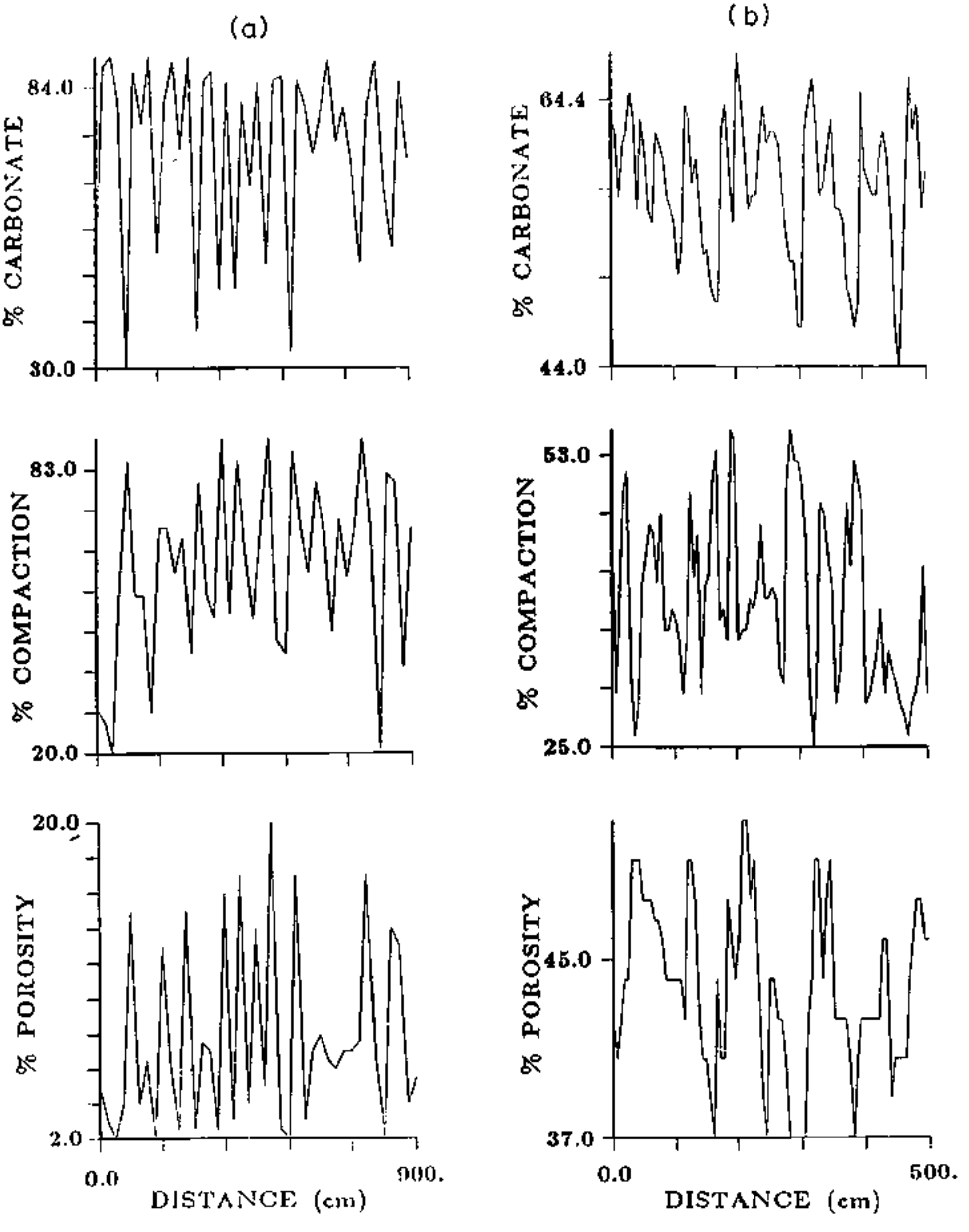

Fig. 7-18. (a) One-dimensional spatial profiles of textural variables from an example of diagenetically enhanced marl/limestone alternations from Ricken (1986). Regions of greater carbonate content (reflecting locally greater cementation) alternate with regions of greater compaction. (b) Same as in (a) except for an example of uncemented marl from Ricken (1986). The textural distributions reflect mechanical compaction; regions of lower porosity sometimes coincide with regions of greater (mechanical) compaction, the opposite case to that shown in (a). Chemical compaction during diagenesis thus results in a correlated pattern of textural alternations.

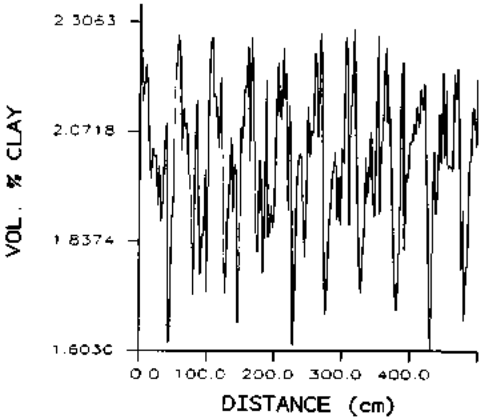

Fig. 7-19. Initial textural "noise" in the spatial distribution of volume % clay, taken to reflect a cyclic depositional precursor with a superimposed degree of randomness.

The initial colored textural noise used in the present simulations was developed in the following form. Letting ψ be a textural variable and $\overline{\psi}$ be its average value in the unlithified sediment, the initial distribution of ψ with space, r, is taken in the following form:

$$\psi(r,0) = \overline{\psi}\left(1 + \sum_{n=1}^{n_{\max}} a_n \sin[k_n r + \phi_n]\right). \tag{7-49}$$

The amplitude factor a_n is a function that is peaked about some value of the "mode number" n. If a_n is narrowly peaked about n_o, the textural perturbation is nearly monochromatic with wavelength near $2\pi/k_{n_o}$. The wave vectors k_n were chosen from the following formula:

$$k_n = \frac{2\pi n}{L}(1 + \varepsilon\eta) \tag{7-50}$$

where η is a random number uniformly distributed in the interval -1 to 1 and $0 < \varepsilon < 1$ is a parameter that gives a measure of the deviation of the noise from a pattern with well defined fundamental wavelength. Finally the ϕ_n are random phases chosen in the interval $0 < \phi_n < 2\pi$. In Fig. 7-19, an example of such an initial noise is shown for the case:

$a_n = 2^{-2}(1+n)^{-1}$,
$L = L_C$ (fundamental wavelength of the initial noise), and
$\varepsilon = 0.3$.

The resulting pattern varies on a length scale roughly equal to L, but retains a strongly random character — what might be expected for a typical situation for deposited and bioturbated sediment.

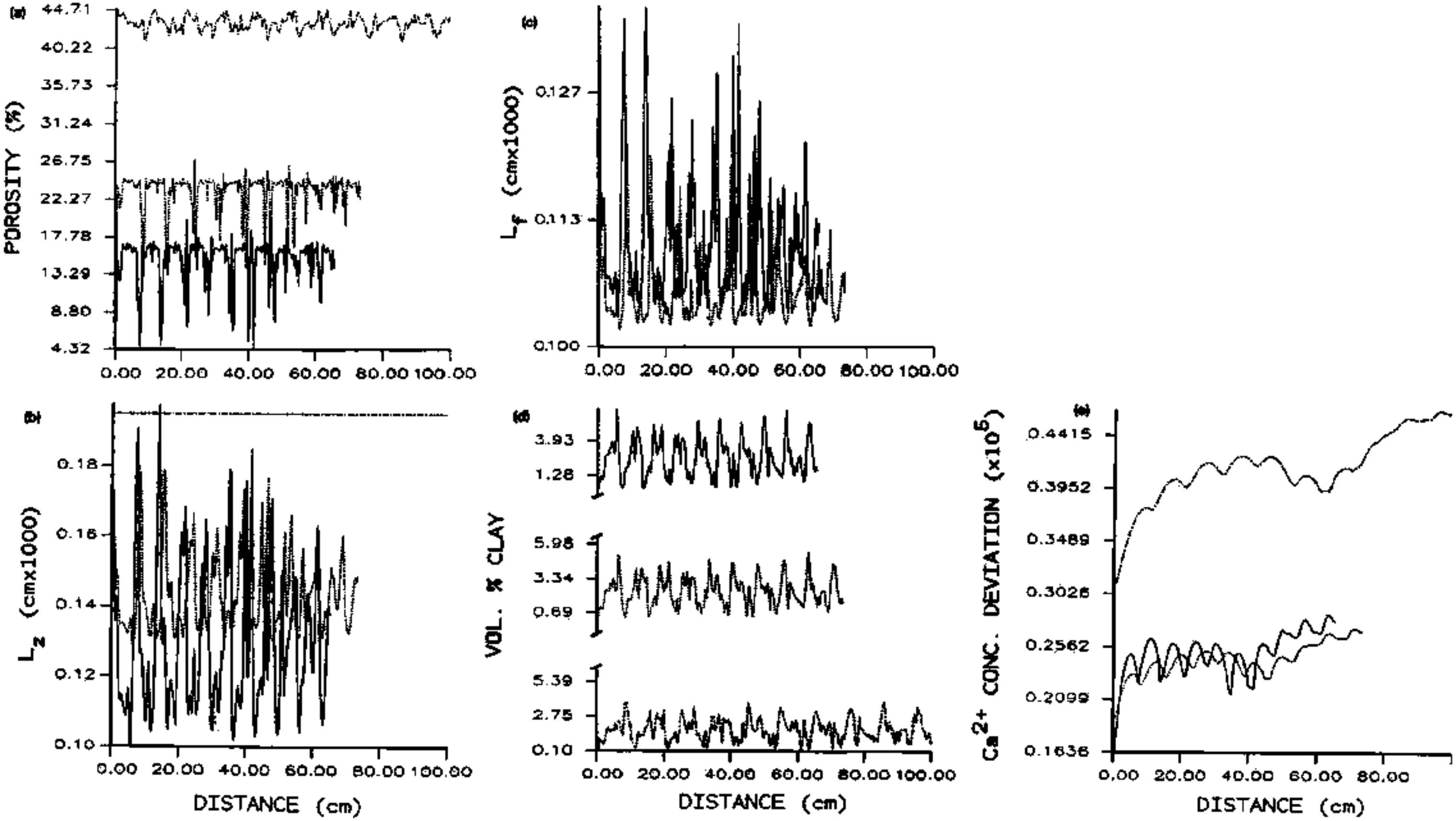

Fig. 7-20. Simulation showing the development of marl/limestone-type textural alternations. At the initial time, porosity minima correspond spatially to clay maxima, and calcite texture, represented by L_z and L_f, is constant in space. By the final time shown (1 million years), porosity maxima correspond to clay maxima demonstrating the diagenetically differentiated textural correlation referred to in Fig. 7-18. As in the example portrayed in Fig. 7-18, zones of greater compaction (lesser L_z), greater clay content, and greater porosity alternate with zones of greater cementation and lower porosity. The simulations are for a saline pore fluid (ionic strength = 0.725 *m*), and $p_{CO_2} \approx 10^{-3}$ atm. Burial rate equals 10 m/million years. The maxima in concentration correspond to regions of dissolution, i.e., zones of greater compaction and clay content.

Numerical experiments were carried out, using the above scheme to generate an initial "noisy" distribution in clay mode. This initial textural distribution is then evolved in space and time via numerical solution of the model equations. To emphasize the important influence of spatial inhomogeneity in clay content, the other variables, which characterize calcite grain size and shape, are kept uniform in the initial state. Any subsequent variation in these variables that arises during a simulation does so as a direct consequence of the mechanochemical dynamics.

Four examples of such simulations are shown in Figs. 7-20, 7-21, 7-22, and 7-23. In going from Fig. 7-20 through 7-22, only the initial average volume fraction of clay is changed: 2% in Fig. 7-20, 3% in Fig. 7- 21, and 8% in Fig. 7-22. Figure 7-23 is the same as Fig. 7-20, except for the reduction in amplitude of the initial clay fluctuations. Figure 7-20a shows the development of large-amplitude porosity fluctuations from the initial clay-induced variations. As evident from comparison of the initial and final porosity profiles, the porosity has become positively correlated with compaction, i.e., the maxima in the initial profile now correspond to minima in the subsequent profiles so that porosity is now a maximum where compaction is greatest. This is characteristic of the development of diagenetic bedding of the type studied by Ricken (1986), and is discussed further below. As was shown in Fig. 7-18a, porosity minima correlate with maxima in the L_f profiles (reflecting cementation), and porosity maxima correlate with L_z minima (reflecting greater compaction). Somewhat counterintuitively, but as is well documented in studies of marl/limestone alternations, clay maxima in Fig. 7-20 correlate with porosity maxima. The development of the positive correlation between porosity and compaction occurs as follows: mechanical compaction, acting in the earlier stages of burial, is concentrated in clay-rich zones and results in a higher-than-average porosity loss there (Bathurst, 1987; Ricken, 1986). Chemical compaction is also concentrated in the clay-rich zones, becoming influential after an initial phase of mechanical compaction, because the clay preserves relatively small contact areas by inhibition of overgrowth precipitation. The smaller contact areas yield a greater magnitude of normal stress across contacts (for a constant far-field stress), and, thus, a faster rate of dissolution. The solutes resulting from calcite dissolution diffuse to adjacent regions, increase contact areas of grains there by cementation, and reduce porosity to a greater extent than in the compacting zones. Early in chemical compaction, greater porosity loss is due to dissolution at grain contacts, but at later stages, as free-face area decreases, greater porosity loss accompanies cementation at the free faces (Rittenhouse, 1971). This could explain the spatial variations in the textural variables of porosity, cementation, clay content, and compaction.

The spatial profile of the L_z variable in Fig. 7-20c demonstrates an interesting feature. Some of the peaks in the final L_z profile rise above the initial one. These peaks correlate with cementation zones and indicate growth of the L_z variable against a normal stress. Thus, the supersaturation within the cementing zones has in this case resulted in a "force-of-crystallization", producing a net "negative" compaction. A similar "thickening" of limestone beds adjacent to, and apparently at the expense of, clay rich zones has been documented by Hallam (1986); this may be due to the effect described here. Closely related force-of-crystallization effects have also been used to explain some types of siliceous concretion growth in a lithified carbonate host (Dewers and Ortoleva, 1990c).

In Fig. 7-20e, distances between adjacent maxima or minima in the profile of the deviatoric Ca^{2+} concentration profile suggest the characteristic diffusion length. It is much larger than the "satellite induction length" for stylolite development discussed earlier. This is because stylolitization dynamics, which the authors argue is controlled by calcite–water reaction kinetics, occurs on a shorter time scale than the development of diagenetic marl–limestone alternations. In the present model, clay inhibition of the interface detachment kinetics imparts a much slower rate to the dynamics of diagenetic marl/limestone differentiation. Hence the diffusion length, proportional to the square root of the characteristic reaction time, is longer.

With an increase in average clay content, the tendency toward instability, or enhancement of textural contrast, decreases. Figure 7-21 shows results of a simulation with an initial 3% clay by volume. The positive porosity–compaction correlation still

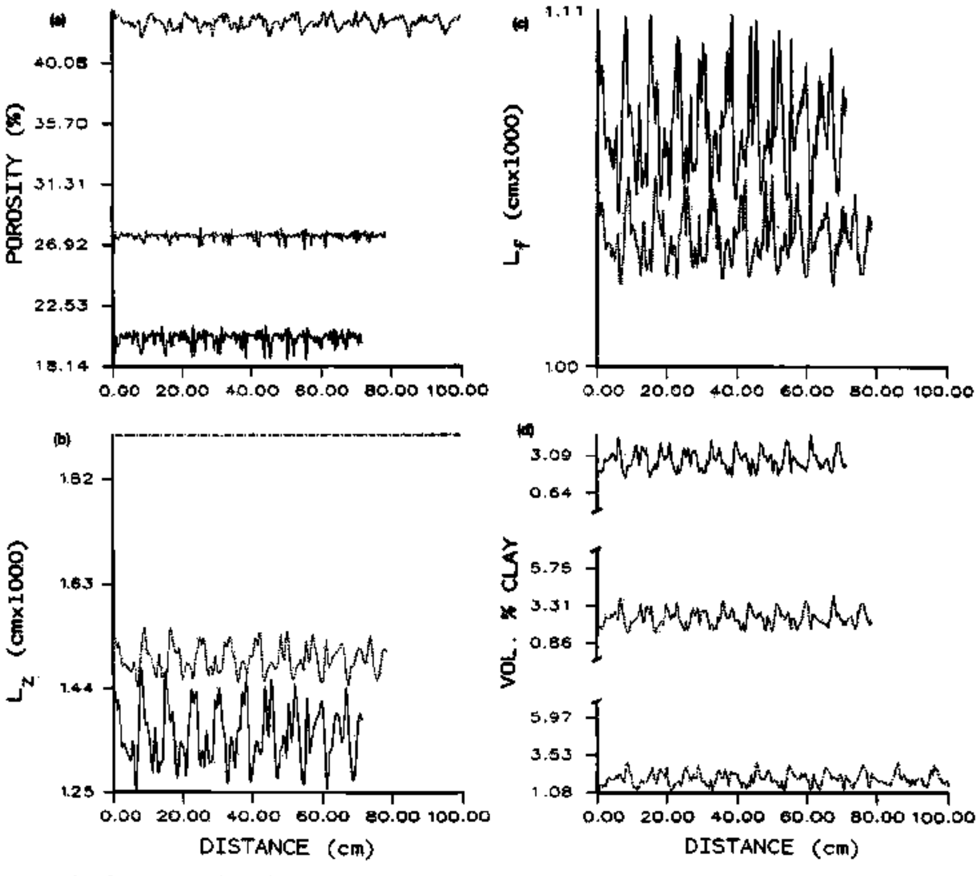

Fig. 7-21. Similar to Fig. 7-20 except that the average clay content here is 3 vol.%. As a result, by the final time shown (1 million years) the amplitude of the textural fluctuations are not as great as in Fig. 7-20.

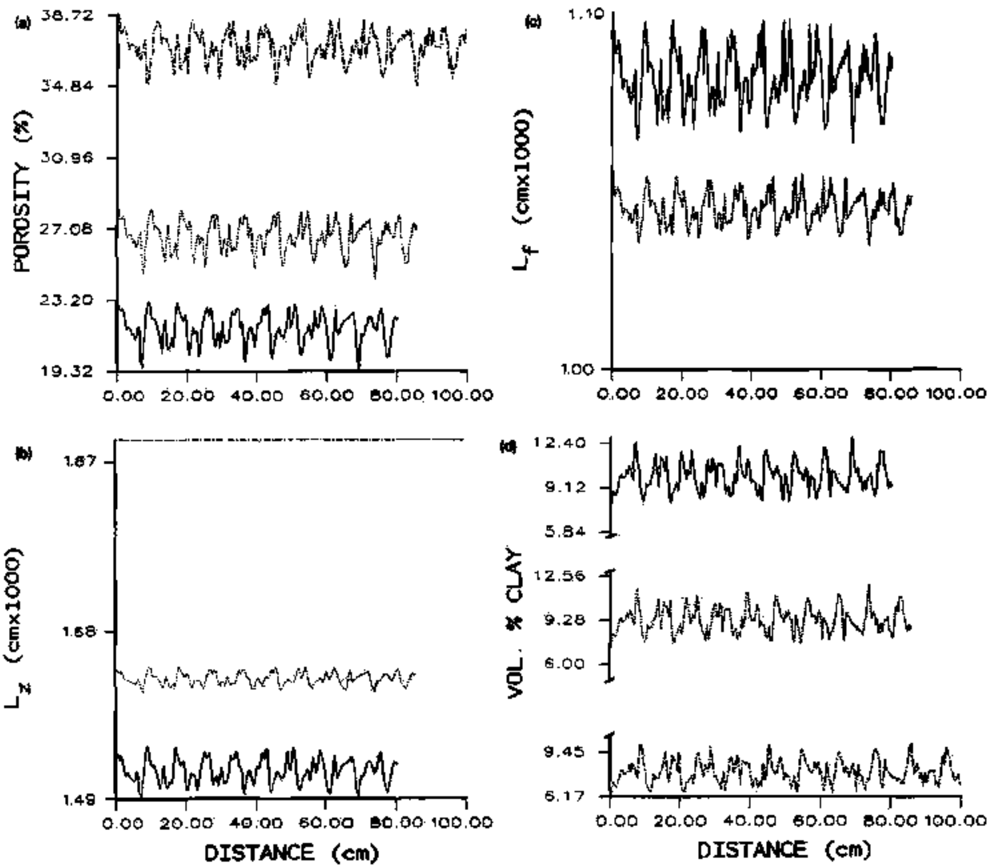

Fig. 7-22. Similar to Fig. 7-20 except that the average clay content here is 8 vol.%. As in Figs. 7-20 and 7-21, maxima of compaction shortening and clay content alternate with maxima in cementation through space, by the final time shown, but the amplitudes of the fluctuations are not as large as in the previous two figures. Also, zones of lesser porosity correspond to zones of greater clay; no development of textural correlation is evident by comparing the initial and final porosity profiles. As shown by the data of Barrett (1964), plotted in Fig. 7-4, argillaceous carbonates containing too much clay do not develop localized compaction and the accompanying clay segregation.

develops, but the amplitude of the final textural variations is much lower. Figure 7-22, with 8% initial clay content, shows a profile of porosity variations that exhibits very little change with time. The L_z and L_f variables still show a break-up into zones of greater compaction alternating with zones of greater cementation, but the variations in texture are slight when compared to those presented in Figs. 7-20 and 7-21.

A similar dampening of unstable behavior accompanies a decrease in the amplitude of the initial clay noise. In Fig. 7-23, the amplitude of clay noise is one-half of that used in Fig. 7-20. The amplitudes of the textural variations in the final profiles shown in Fig. 7-23 are, as a result of the different initial conditions, smaller than those plotted in Fig. 7-20.

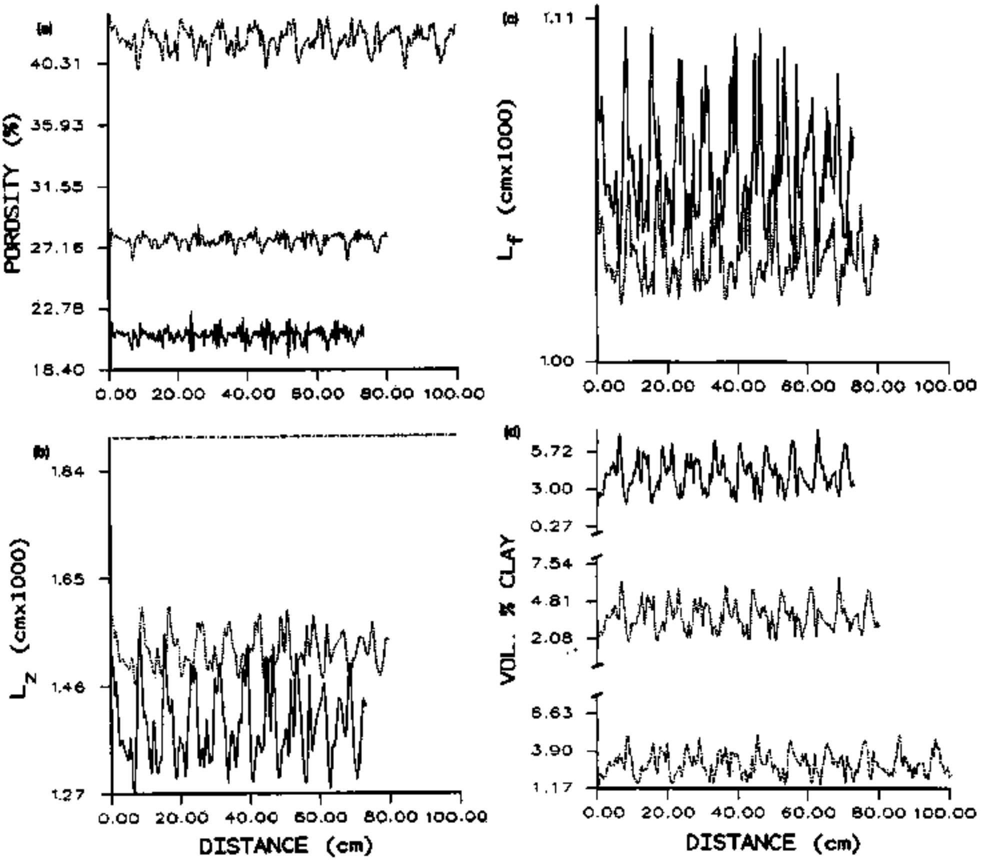

Fig. 7-23. Same as in Fig. 7-20, except that the amplitude of the initial clay fluctuations is half of that used to initialize the simulation in Fig. 7-20. The amplitudes of the textural variations at the final time shown (the solid lines corresponding to 1 million years) are smaller than those in Fig. 7-20.

The results given in Fig. 7-24 were obtained from a simulation initialized with clay variations of random amplitude and wavelength. By the second time shown (0.5 million years), the small initial textural variations have amplified into a large amplitude pattern. Upon weathering, one might expect the spatial distribution of textural variables to yield a "tendency toward periodicity" of the type mentioned by Ricken (1986). In any case, the number of limestone layers evident by the simulation time of 0.5 million years, shown in Fig 7-24, is fewer than the number expected from the variations in the initial profile.

Interestingly, by the final time shown in Fig. 7-24 (1 million years), the fluctuations in porosity have begun to die out with further compaction and cementation; however, the L_z, L_f, and clay profiles retain large fluctuations, thus exhibiting a "memory" of the diagenetic history the simulated rock experienced.

The influence of the average clay content and the amplitude of the initial spatial variation in clay content on the development of diagenetic marl/limestone

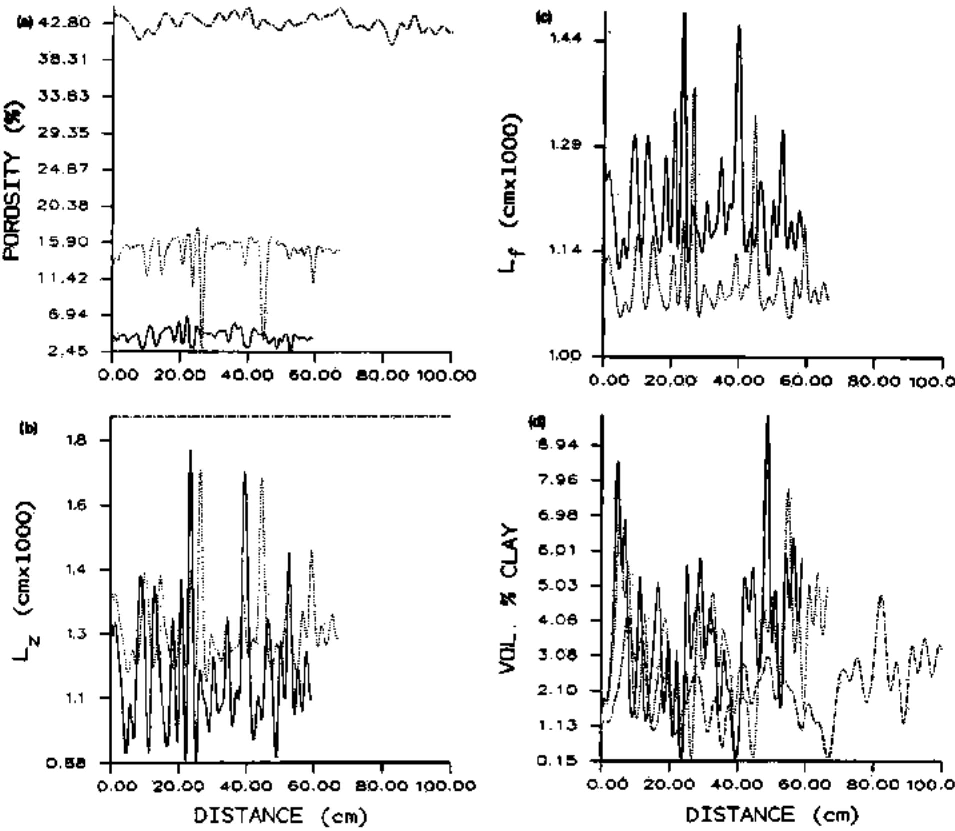

Fig. 7-24. Simulation showing the development of differential chemical compaction and cementation from initial noise of random amplitude and wavelength. The number of regions in which compaction is enhanced is fewer than the number of initial clay maxima. By the final time shown (2 million years), the fluctuations in porosity begin to die out.

alternations may be understood in terms of the influence of clay on the reaction rates at calcite free faces. In Fig. 7-25, the ratio of the contact and free-face rate coefficient is plotted as a function of the volume fraction of clay, contoured by the product of grain size, tortuosity of the pore-lining clay film, and the reciprocal of the fluid film width. Next the writers consider the case of two regions which are spatially separate, yet close enough to communicate via diffusion, and which contain slightly different amounts of clay. One sees from Fig. 7-25 that the difference in the ratio k^f/k^c between these two regions becomes larger as one moves from greater to lesser average clay amounts, indicating a higher sensitivity to clay content variations at lower average clay contents. Differentiation into zones of differing compaction and cementation becomes more intense with larger spatial variations in the growth and dissolution rates. The differences in the reaction rate ratio between two regions of slightly different amounts of clay become less as the overall clay

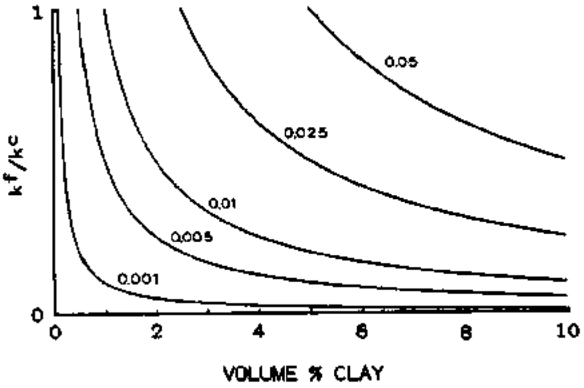

Fig. 7-25. Ratio of the free-face and contact reaction rate coefficients ($k^{\mathrm{f}} \equiv D^{\mathrm{c}}\tau/S\rho$; $k^{\mathrm{c}} \equiv 2\pi D^{\mathrm{c}}\Delta/A_z p$; and $S = L_y^2 L_z \phi_{\mathrm{cl}}/A_{\mathrm{f}}$) as a function of the reciprocal of volume % clay, ϕ_{cl}. Larger variations in the reaction rates between spatially separate regions with varying clay content accompany a smaller overall amount of clay.

content increases. Thus, the tendency toward localization of compaction decreases with increasing clay. The relationship between growth rates and texture portrayed in Fig. 7-25 may also explain why this type of diagenetic bedding is confined to very fine-grained carbonates. Holding everything else constant, as grain size increases, the contours in Fig. 7-25 become displaced upward and to the right. As a result, the free-face rate ceases to be the rate-limiting factor. It is the inhibition of the calcite free-face reaction rate which is responsible for the development of the diagenetic bedding.

The correlation between the textural variables of carbonate content in %, porosity, and compaction for marl/limestone sequences has been demonstrated by Ricken (1986) by plotting textural variables at different spatial localities as a function of one another. Figure 7-26 shows a plot of regression lines from Ricken (1986) showing porosity as a function of carbonate content (expressed as a percentage of the solid fraction). The labels on the various lines correspond to Ricken's samples (see Ricken, 1986; table 11, p. 84). The one-dimensional profiles plotted in Fig. 7-18b correspond to the line labeled *PE* in Fig. 7-26. The samples corresponding to the textural profiles in Fig. 7-18a (the Angles 2 section studied by Ricken, 1986) are not plotted in Fig. 7-26; however, it has a form similar to those labeled *A1* and *A3*. When plotted in this manner, the development of textural correlation mentioned earlier becomes quite apparent as a change in slope in the space of porosity vs. carbonate content in percent. Mechanical compaction results in the porosity being greater in regions greater in carbonate content, whereas chemical compaction results in porosity being greater in regions containing less carbonate.

When compaction is plotted as a function of carbonate content in %, a characteristic parabolic form is obtained, that is displaced upward and to the right as clay content decreases. Examples from Ricken (1986) plotted in this manner are shown in Fig. 7-27.

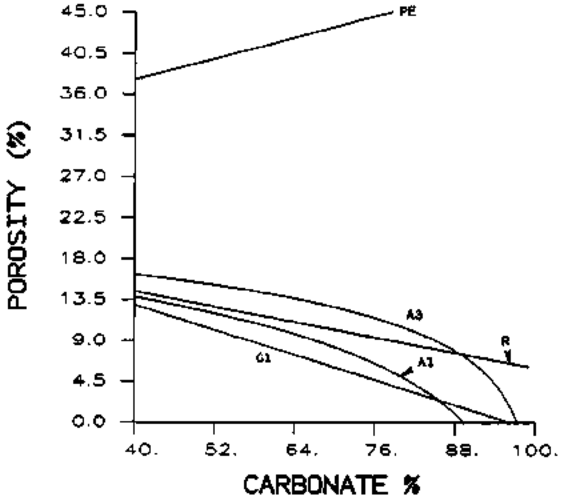

Fig. 7-26. Porosity in examples of marl-limestone alternations from Ricken (1986) plotted as a function of carbonate content in %. Labels refer to individual localities; the notation is that of Ricken (1986). *PE* is the Pleistocene marl shown in Fig. 7-18b, and has undergone mechanical compaction but little cementation. The remaining examples are Jurassic or Cretaceous in age, and have experienced both chemical compaction and cementation. Clay content of these rocks increases in going from *A3*, *A1*, *G1*, to *R*.

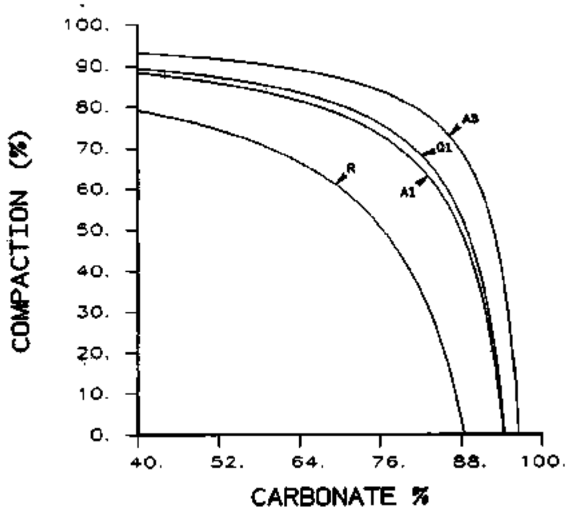

Fig. 7-27. Compaction % plotted as a function of carbonate content (%) for marl-limestone alternations from Ricken shown in Fig. 7-26. As clay content increases in these examples, the curves are displaced upward and to the right, demonstrating that spatial variations in the amount of compaction increase with decreasing clay content.

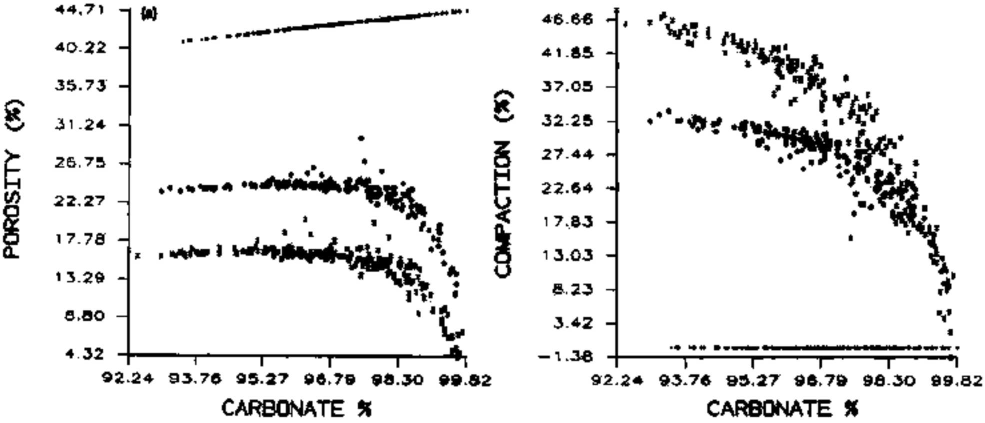
(a)
POROSITY (%)
44.71
40.22
35.73
31.24
26.75
22.27
17.78
13.29
8.80
4.32
92.24
93.76
95.27
96.79
98.30
99.82
CARBONATE %
COMPACTION (%)
46.66
41.85
37.05
32.25
27.44
22.64
17.83
13.03
8.23
3.42
−1.38
92.24
93.76
95.27
96.79
98.30
99.82
CARBONATE %

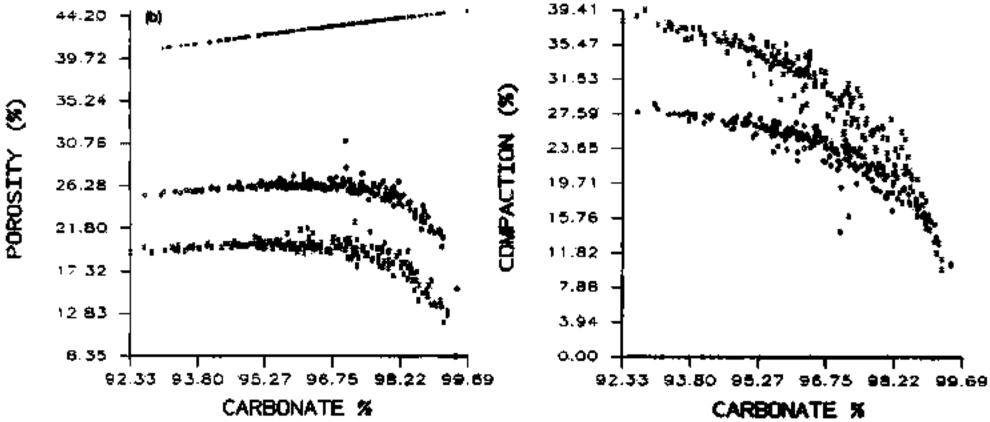
(b)
POROSITY (%)
44.20
39.72
35.24
30.76
26.28
21.80
17.32
12.83
8.35
92.33
93.80
95.27
96.75
98.22
99.69
CARBONATE %
COMPACTION (%)
39.41
35.47
31.53
27.59
23.65
19.71
15.76
11.82
7.88
3.94
0.00
92.33
93.80
95.27
96.75
98.22
99.69
CARBONATE %

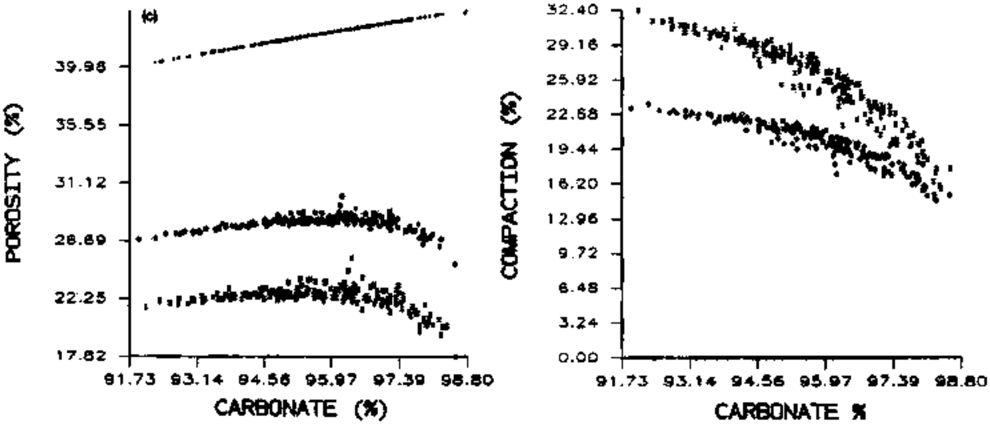
(c)
POROSITY (%)
39.98
35.55
31.12
26.69
22.25
17.82
91.73
93.14
94.56
95.97
97.39
98.80
CARBONATE (%)
COMPACTION (%)
32.40
29.16
25.92
22.68
19.44
16.20
12.96
9.72
6.48
3.24
0.00
91.73
93.14
94.56
95.97
97.39
98.80
CARBONATE %

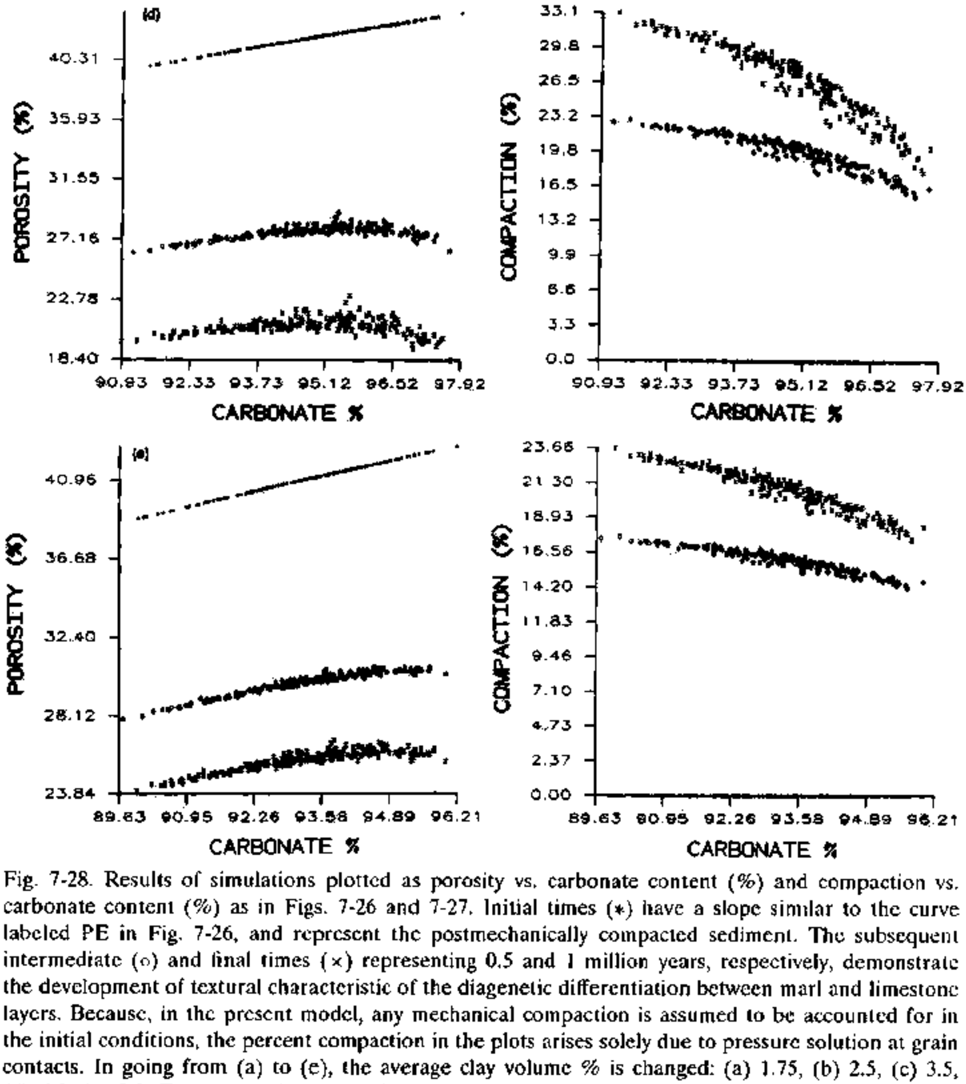

Fig. 7-28. Results of simulations plotted as porosity vs. carbonate content (%) and compaction vs. carbonate content (%) as in Figs. 7-26 and 7-27. Initial times (*) have a slope similar to the curve labeled PE in Fig. 7-26, and represent the postmechanically compacted sediment. The subsequent intermediate (○) and final times (×) representing 0.5 and 1 million years, respectively, demonstrate the development of textural characteristic of the diagenetic differentiation between marl and limestone layers. Because, in the present model, any mechanical compaction is assumed to be accounted for in the initial conditions, the percent compaction in the plots arises solely due to pressure solution at grain contacts. In going from (a) to (e), the average clay volume % is changed: (a) 1.75, (b) 2.5, (c) 3.5, (d) 4.0, (e) 8.0. The change in shape of the slope of the curves in (a) to (d) at the final times with a change in clay content agree qualitatively with the trends seen in Figs. 7-26 and 7-27. Example (e), however, retains the positive slope in the porosity vs. carbonate plot, reflecting little differential cementation or compaction. In this case, a diagenetic marl–limestone alternation has not formed.

Figure 7-28 shows the results of several simulations obtained by changing only the average volume fraction of clay, in the manner suggested by Ricken (1986), as porosity versus carbonate content % correlation plots (similar to Fig. 7-26). As clay content increases, the slopes of the curves representing the final simulation times decrease, and the shape changes from a parabolic to a more linear trend. This agrees, at least qualitatively, with the relationships seen in Fig. 7-26. Also, it is suggested that

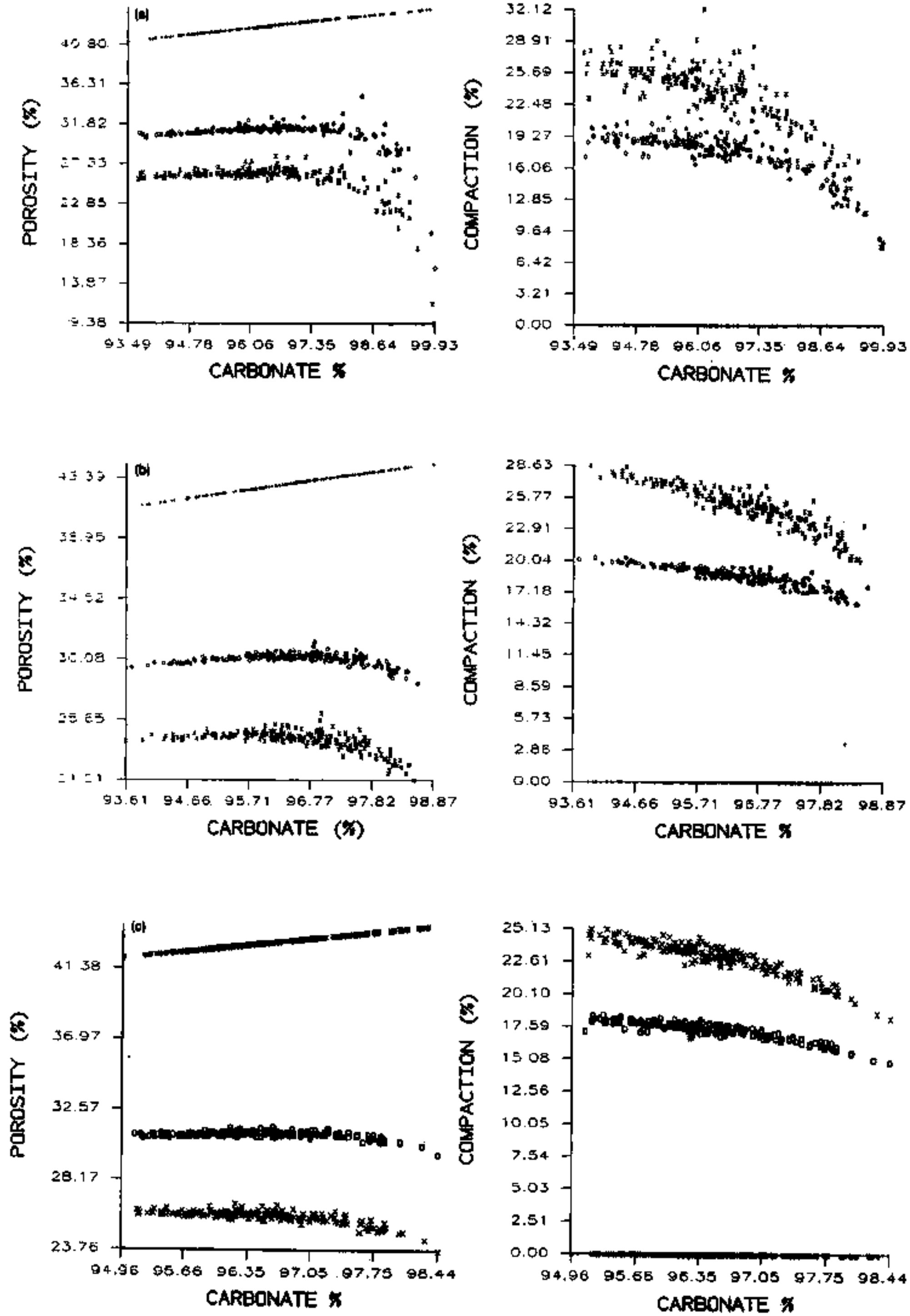
(a)
POROSITY (%)
40.80
36.31
31.82
27.33
22.85
18.36
13.87
9.38
93.49
94.78
96.06
97.35
98.64
99.93
CARBONATE %
COMPACTION (%)
32.12
28.91
25.69
22.48
19.27
16.06
12.85
9.64
6.42
3.21
0.00
93.49
94.78
96.06
97.35
98.64
99.93
CARBONATE %
(b)
POROSITY (%)
43.39
38.95
34.52
30.08
25.65
21.21
93.61
94.66
95.71
96.77
97.82
98.87
CARBONATE (%)
COMPACTION (%)
28.63
25.77
22.91
20.04
17.18
14.32
11.45
8.59
5.73
2.86
0.00
93.61
94.66
95.71
96.77
97.82
98.87
CARBONATE %
(c)
POROSITY (%)
41.38
36.97
32.57
28.17
23.76
94.96
95.66
96.35
97.05
97.75
98.44
CARBONATE %
COMPACTION (%)
25.13
22.61
20.10
17.59
15.08
12.56
10.05
7.54
5.03
2.51
0.00
94.96
95.66
96.35
97.05
97.75
98.44
CARBONATE %

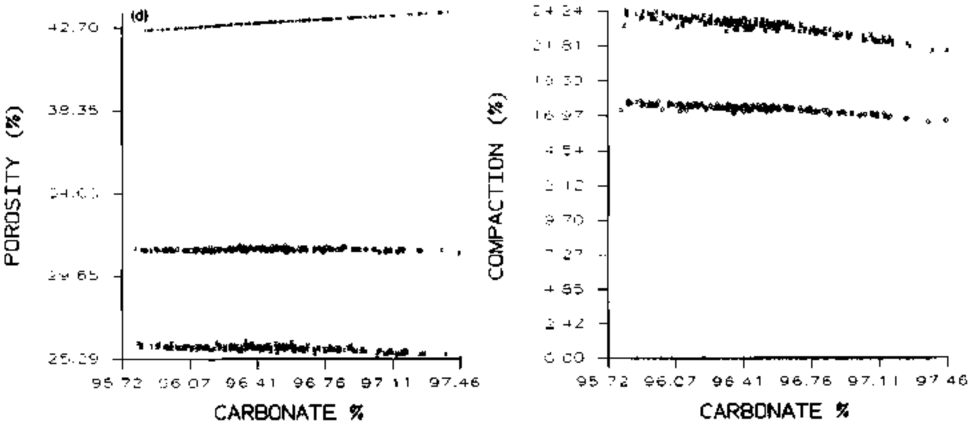

Fig. 7-29. Same as in Fig. 7-28, except that the amplitude of initial clay fluctuations is varied, keeping the average initial clay content constant at 3%. Clay amplitude is: (a) 4×10^{-2}, (b) 2×10^{-2}, (c) 1×10^{-2}, (d) 5×10^{-3}. Similar changes that were seen to accompany increases in average clay amount (Fig. 7-28) also arise with decreases in amplitudes of the initial clay fluctuations.

the type of textural correlations characteristic of marl–limestone alternations will not be found in carbonates containing greater than a critical clay content.

Figure 7-29 shows the effects of decreasing clay amplitude on the form of the porosity–carbonate % and compaction–carbonate % relationships as obtained from the simulations. Analogous to the situation of increasing clay vol. % shown in Fig. 7-28, decreasing the clay amplitude results in a transition from a parabolic to a linear form of the correlation between the carbonate and clay contents.

The influence by clay on the development of these textural patterns is also evident in Figs. 7-30 and 7-31. Figures 7-30a through 7-30c show a plot of the root-mean-square of the spatial deviations in porosity, L_z and L_f as a function of the initial average volume % of clay obtained from several simulations, each run to 0.5 million years. The minimum displayed in the porosity plot in Fig. 7-30a divides examples that display textural correlations characteristic of marl/limestone alternations (to the left of the minimum, for example, those shown in Figs. 7-20 and 7-21), from those that display a more-or-less spatially homogeneous texture (to the right of the minimum, similar to that shown in Fig. 7-22). It appears that marl/limestone type textures will result from a clay content smaller than a critical amount suggested by the minimum in Fig. 7-30a. No such minimum is evident in the L_z and L_f profiles of Fig. 7-30b and 7-30c. The RMS average fluctuation of these variables dies off rapidly with increasing clay content.

Plots of the RMS deviations in ϕ, L_z and L_f as a function of the initial amplitude of the clay noise are shown in Figs. 7-31a through 7-31c. Deviations in all three variables appear to increase parabolically with increasing amplitude.

The wavelength (or correlation length) of the initial noise influences as well the rate of textural enhancement. The RMS porosity deviation in several simulations that arose after 0.5 million years is plotted in Fig. 7-32 as a function of the reciprocal of

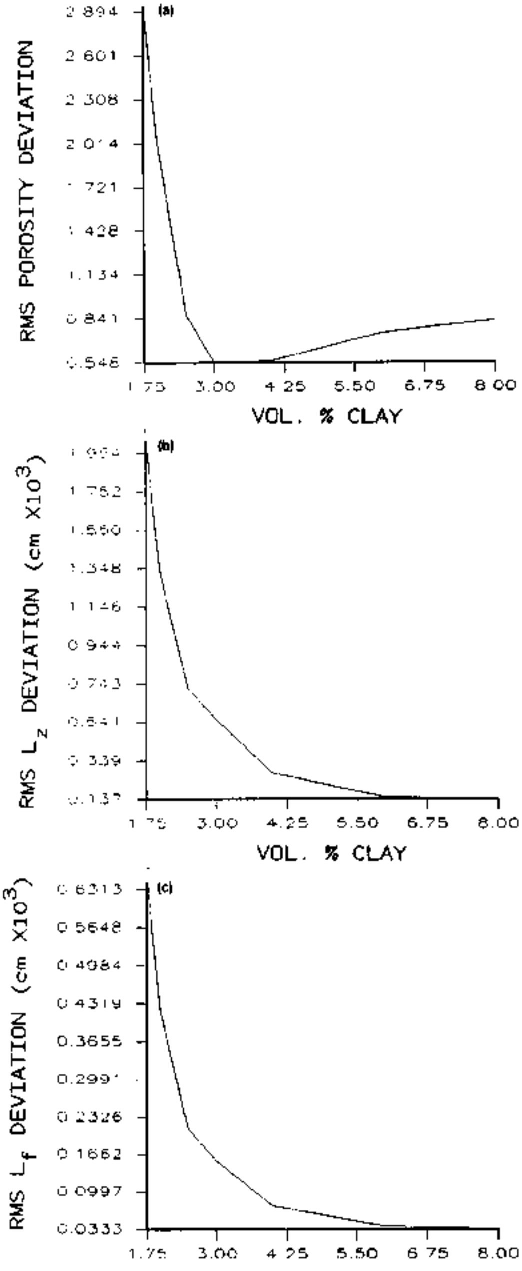

Fig. 7-30. Root-mean-square average of spatial fluctuations in porosity, L_z, and L_f, obtained from several simulations run to 1 million years, as a function of average initial volume % clay. (a) RMS porosity vs. vol.% clay; the minimum in the curve separates behavior characteristic of the localization of chemical compaction in marl–limestone alternations from a more spatially pervasive compaction. The RMS porosity fluctuations increase with clay from H 4% to 8% because the initial variations are essentially preserved. (b) and (c) show L_z and L_f vs. vol.% clay, respectively, demonstrating that the largest differentiated spatial variations in compaction and cementation arise in rocks containing relatively little clay; fluctuations in these variables die out with increasing clay, reflecting more or less pervasive compaction and cementation.

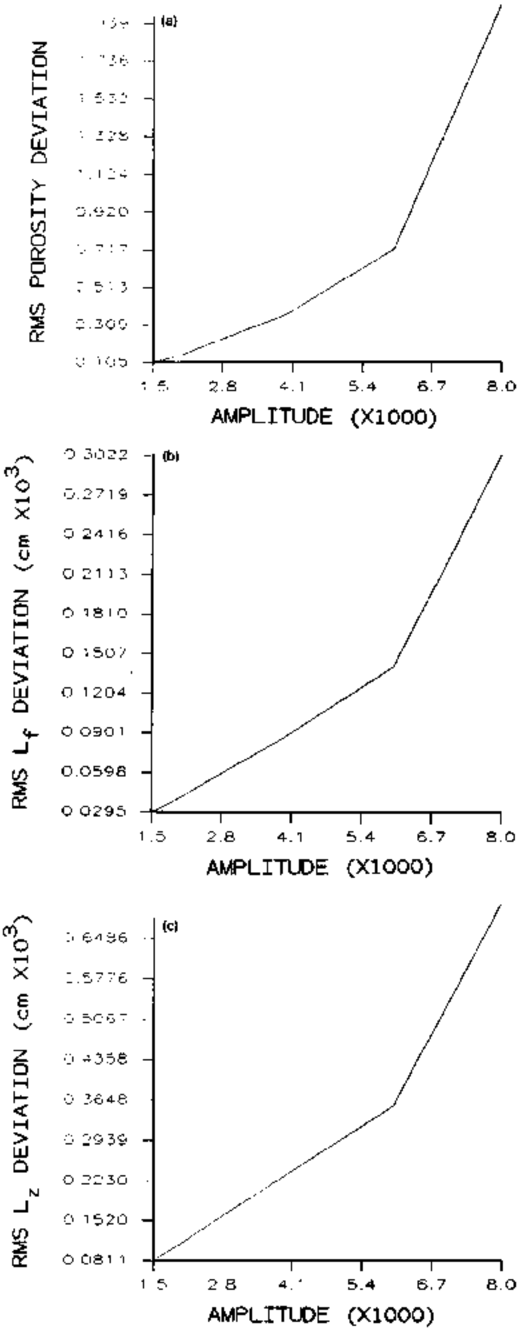

Fig. 7-31. The root-mean-square average of the fluctuations in (a) porosity, (b) L_f, and (c) L_z are shown as a function of the amplitude of the initial clay noise in several simulations. The average fluctuation of all variables increases parabolically with increasing amplitude.

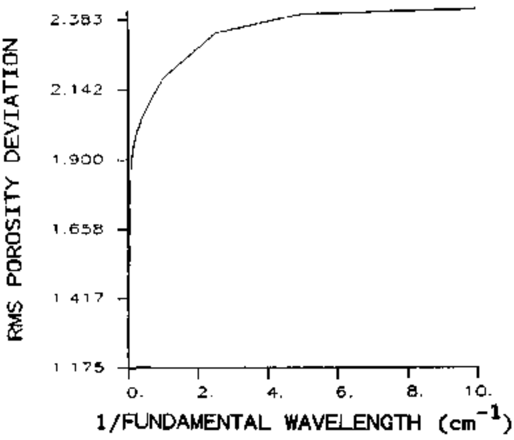

Fig. 7-32. The RMS average of porosity fluctuations from several simulations, each run to 1 million years, is shown as a function of the reciprocal of the fundamental wavelength of the distribution of clay used to initialize the simulations. This relationship suggests that the growth rate of the porosity deviations, and that for the development of diagenetically enhanced marl–limestone layers, increases as the wavelength (or repeat distance) of any initial depositional periodicity decreases. Because smaller wavelength patterns grow at a faster rate, large length-scale examples of marl–limestone alternations probably reflect a strongly periodic predecessor (e.g., depositional fluctuations or some early diagenetic alteration).

the fundamental wavelength used in construction of the noise. The fact that the curve in Fig. 7-32 rises monotonically with decreasing fundamental wavelength implies that smaller-wavelength perturbations display a faster growth rate than larger ones. At least for the parameters used in this study, the difference in growth rate for the initial noise displaying fundamental wavelengths of 2 cm versus, say, 20 cm is far greater than the difference in growth rate for noise having wavelengths between 2 and 5 cm. It is, therefore, likely that larger length-scale marl/limestone alternations, e.g., those on the order of meters, probably reflect enhancement of a depositional precursor to a greater degree than those with a spacing of 5–10 cm. This is because the smaller-length scale perturbations would grow with a faster rate. Longer-length scale perturbations, with slower growth rates, would not become manifest during diagenesis unless "forced" by a large amplitude depositional coloring of the same length scale.

Dissolution (clay) seams in low-porosity, clay-rich carbonates

Dewers and Ortoleva (1989) presented a reaction–transport model for the development of segregation between mineral phases in low-porosity rocks. The purpose of the present section is to illustrate that differentiation may occur in low-porosity carbonate rocks via a feedback mechanism which does not involve porosity.

The mechanical aspects of this model were described by a "mean-field" approach in which the grain-scale stresses were calculated by assuming that each mineral grain (taken to be spherical) resides in a homogeneous, elastically isotropic medium. The trace and deviatoric parts of the microscopic (grain-scale) stress tensor are related to their macroscopic counterparts by way of the elastic constants of the grain and the elastic constants of the matrix, the latter representing an average of the textural properties of the matrix. The macroscopic stress tensor, representing the average over a macrovolume element containing many grains, is obtained from a viscous continuum model. The bulk viscosity can, for example, depend on the volume fractions of the minerals making up each volume element, although, for the example discussed here, it is assumed constant.

Dewers and Ortoleva (1990a) explored differentiation between muscovite and quartz using this model, and found that behavior in a system with constant bulk viscosity was markedly different from behavior in a system in which viscosity varied with mineral content. In addition, they showed that enhanced diffusion along grain boundaries shared by both muscovite and quartz relative to that at quartz–quartz boundaries could increase the rate of differentiation between quartz and muscovite. This had the net effect of decreasing the spacing between differentiated muscovite domains as the volume fraction of muscovite in the bulk rock increased.

Using the above formalism, Dewers and Ortoleva (1989) showed that for a given stress on a macrovolume element, the free energy of a calcite grain in a low-porosity calcite–illite rock decreases with increasing calcite volume fraction. In the present studies, simulations were performed under the assumption that, as is typically the case at relatively low temperatures, the clay kinetics is much slower than that of calcite. Figure 7-33 demonstrates segregation between calcite and clay (elastically modeled as muscovite). In Fig. 7-33a, a small local increase in calcite volume fraction induces the growth of a spatially segregated calcite domain, shown in Fig. 7-33a as a maximum in calcite volume fraction, an adjacent minimum (or clay-rich region), and a secondary maximum approximately 2 mm away. The differentiation occurs because the local stress on a typical calcite grain is lower when the grain is immersed in a calcite-rich matrix than when the grain is immersed in a clay-rich matrix. This is essentially because the bulk modulus of a calcite–clay composite increases with increasing calcite content. The calcite maxima amplify with time because calcite grains are growing there. The two calcite minima at the final time in Fig. 7-33a have increased in depth because calcite grains dissolved there. As a result, it is seen in Fig. 7-33b that clay decreases in calcite-precipitation regions and increases in the calcite-dissolution regions, owing to rock flow induced by the differential calcite reaction. The rock deformation velocities in Fig. 7-33c show this; sites of clay concentration in Fig. 7-33b coincide with the localities where the velocity crosses the zero-axis, i.e., changes from positive to negative. This reaction-induced rock flow shows that the maximum strain rates occur both in the center of the clay segregation and in the center of the precipitation domains.

The influence by the clay-enhanced grain boundary diffusion mechanism referred to earlier on timing and length scales of clay-seam formation in clay–calcite rocks is shown in Figs. 7-34 and 7-35. The figures are contoured for the ratio of calcite/clay particle size. The spacing of segregational domains decreases with increasing clay content (and likewise, decreasing calcite content). The effect becomes stronger as

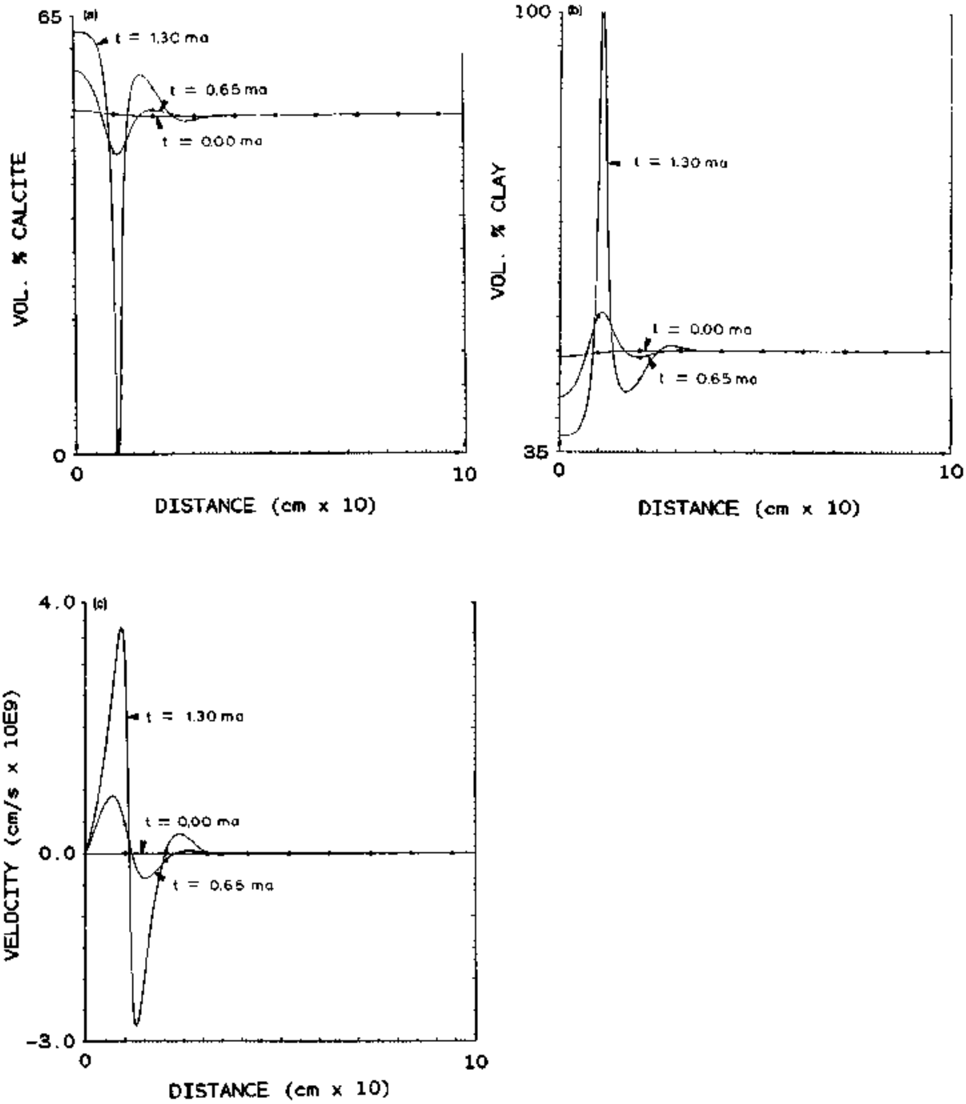

Fig. 7-33. Simulation showing the development of clay segregations due to differential dissolution and precipitation of calcite in a low-porosity argillaceous limestone, initiated by a small local change in mineralogy. The driving force for segregation involves stress concentrations arising in regions rich in clay due to the variation in elastic moduli of calcite–clay rocks as a function of clay content. In addition, dissolution rates at calcite grain contacts shared by clay (taken to be phyllosilicate minerals) are slightly faster than at calcite–calcite grain boundaries due to phyllosilicate-enhanced diffusion. (a) Calcite volume % as a function of distance; (b) clay volume % as a function of distance; and (c) velocity of rock deformation as a function of distance. The final time shown represents 5 million years. The change in sign and slope of the final velocity profile reflects a convergence of the rock at clay concentration sites, and a divergence of the rock at calcite growth sites.

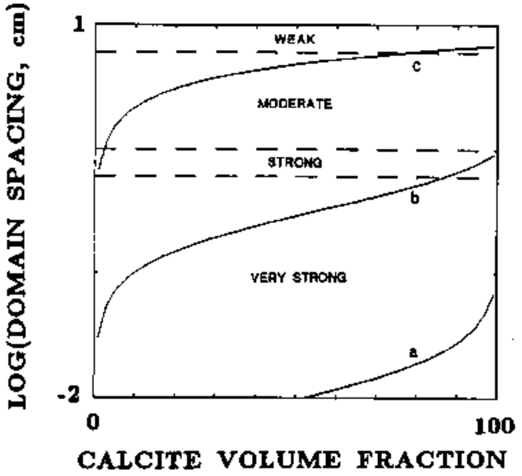

Fig. 7-34. Change in spacing (or repeat distance) of clay seams as a function of calcite volume fraction (equal to one minus the clay volume fraction) contoured for the ratio of clay to calcite grain sizes: (a) 0.1, (b) 0.01, and (c) 0.001. The decrease in spacing accompanying an increase in clay is due to enhanced diffusion at clay–calcite grain boundaries.

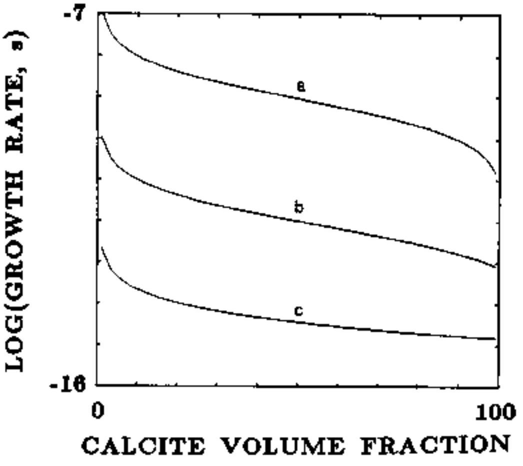

Fig. 7-35. Characteristic clay seam formation time as a function of calcite volume fraction contoured for the ratio of clay to calcite grain sizes (labeling is the same as in Fig. 7-34). Rates of clay seam formation increase with increasing clay because of enhanced diffusion at calcite–clay grain boundaries.

the clay-to-calcite grain size ratio decreases. The dashed lines in Fig. 7-34 represent the cleavage classification scheme of Alvarez et al. (1978). An increase in "cleavage intensity", here analogous to clay seam or segregation spacing, with increasing clay content has been observed by Wanless (1979). The decrease in length scale accompanying the increase in clay content is commensurate with an increase in the growth rate of textural perturbations, or simply stated, the rate of differentiation. The faster the reaction rates that are characteristic of a process, the smaller the length scale of the segregation the process produces.

CHANGES IN TIMING AND LENGTH SCALE ACCOMPANYING BURIAL

Because of the temperature dependence in the Arrhenius form of the rate coefficients, and increasing stress attending deeper burial, the rates of pressure solution-driven segregational processes increase with deeper burial. Accordingly, one expects the length-scales for segregations to decrease with deeper burial. This in fact has been observed for spaced cleavage in argillaceous carbonates by Mitra and Yonkee (1985). Furthermore, as different pressure-solution processes have different Arrhenius dependencies, and depend on porosity (and other textural variables) in different ways, it is expected that crossovers in behavior can occur with depth.

Reaction rates for free-face and grain contacts versus depth are plotted schematically for the cases with (see Fig. 7-36a) and without (Fig. 36b) clay. Based on results of numerical experiments presented in this chapter, one possible burial scenario for each case is shown. The situation for clay-rich carbonates implied by Fig. 7-36a shows that contact rates become faster than free-face rates at a relatively shallow depth,

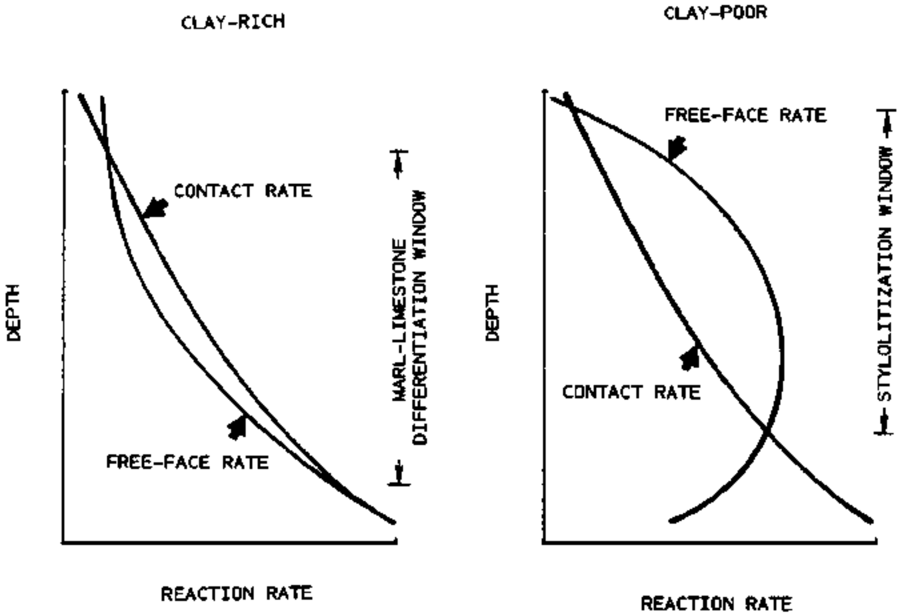

Fig. 7-36. Schematic change in the rates of free-face and contact reaction for the cases of clay-rich and clay-poor carbonates. (a) In porous clay-rich sediments, macroscopic marl–limestone segregation can arise from small initial fluctuations if free-face reaction rates are lower than contact rates. When placed within a burial scenario, a window in depth within which a diagenetic marl–limestone can form may be defined. (b) In porous clay-poor sediments, stylolitization can result if free-face reaction rates are faster than contact rates. A window similar to that in (a) can be defined within which stylolites may form.

possibly due to increasing stress. This may persist to relatively great depths until most porosity has been lost due to compaction. This scenario implies a "window" in depth at which the mechanism for marl/limestone development can operate. At greater depths, the contact and free-face reaction rates become equal as porosity is lost and the clay becomes "load-supporting". Thus, a crossover between the marl/limestone mechanism (in which free-face reaction is the rate-limiting step) and the low-porosity clay seam mechanism (in which reaction rates can be the same at all grain interfaces) takes place at this depth. Similarly, as shown in Fig. 7-36b, the free-face rate in clay-rich carbonates is expected to be much faster than contact reaction rates (when contact rates are diffusion-limited), because of the larger free-face rate coefficient of calcite. This situation may persist to greater depths, where, because of porosity loss and/or a decrease in free-face surface area, contact rates may become faster. As in Fig. 7-36a, this implies a window in depth for which unstable behavior can occur; here the operation of a faster free-face reaction could induce stylolitization as shown earlier. These scenarios are just two of many that are possible. Many variables influence the relative magnitude of the reaction rates, and factors not discussed here could enhance or detract from the tendency toward instability and enhancement of textural contrast (e.g., fluid overpressuring). The presence and amplitude of textural inhomogeneity, as might be inherited from depositional processes, are other important factors.

CONCLUSIONS AND DIRECTIONS FOR FUTURE STUDY

The following assertions can be made about the processes governing chemical compaction in argillaceous carbonates:

(1) Compaction may or may not become localized in space depending on the rate of reaction at grain contacts relative to that at grain free faces at the periphery of the contacts.

(2) Localization occurs if the increase in contact areas accompanying dissolution there does not proceed homogeneously in space, but is somehow impeded more in some localities than in others.

(3) One way in which compaction can be localized is when dissolution at grain-contact peripheries, which effectively serves to decrease contact areas, proceeds at a comparable or faster rate than contact dissolution. This dissolution may be driven by strain energy, and although this driving force is far less than that inducing pressure solution at grain contacts, the kinetics of free-face dissolution can be much faster. It is the combination of driving force and reaction kinetics that determines the efficiency of a reaction mechanism (Tada et al., 1987). If free-face dissolution proceeds faster in one locality, it locally decreases contact areas and increases porosity. This focuses stress, increases strain energy, and thus increases the rate of free-face dissolution. Also, with the decrease in contact areas, the rates of contact dissolution are also increased. In this way, the initial small local increase in dissolution rates, due to a local perturbation in texture, can auto-enhance through positive feedback, and localize compaction via dissolution.

(4) If grain-contact dissolution rates are faster than free-face rates, contact areas will increase both due to dissolution at contacts and overgrowth precipitation at free faces. This will tend to diminish any textural heterogeneity, because a locally greater rate of chemical compaction due to, say, a locally smaller contact area, will act to bring the contact area to a level more in line with the average in the rock.

(5) If overgrowth formation is locally impeded because of, for example, a physical coating of clay, pressure solution-induced compaction can proceed faster (the stress per contact being maintained due to relatively smaller contact areas) in a clay-rich region than in a clay-poor region. Compaction could then localize, in clay-rich regions. If the clay is insoluble relative to calcite, clay would collect in areas undergoing shortening, and the added clay would inhibit cementation and preserve the relatively faster compaction rate. This is another example of a positive feedback process.

(6) The prediction by the model of the correlated alternation of higher porosity preservation, clay content, and compactional rock shortening with zones of greater cementation appears to be a universal feature of diagenetically altered marl–limestone sequences.

The authors equate the compactional localization described in point (3) above to the development of stylolites, and that of point (5) to the development of clay seams and marl/limestone alternations in porous rocks. In porous rocks, both processes may be occurring simultaneously, and hence, at low clay contents, these two effects could be mutually enhancing.

Construction of a quantitative reaction–transport model that includes the processes of reaction at grain contacts and free faces, texture-dependent effective stress in a linear elastic porous medium, diffusional solute transport, and kinetic inhibition due to ionic inhibitors and clay coatings, offers the possibility of quantitatively describing the spatial and temporal evolution of these compactional features. This is a powerful tool, as the results can be directly compared to naturally occurring examples.

In addition to the porous model, the authors examine a model for low-porosity rocks which was developed in earlier studies, in which the stress on a grain possesses a functional dependence on the texture of the rock in which it is immersed. This model shows the development of segregations of calcite that alternate with clay segregations. These segregations may be similar to clay seams observed in deeply buried argillaceous carbonates.

There are a number of natural directions for the extension of this work. The mechanics of the problem could be improved by employing other periodic or random packing geometries. The extension to multiple load-supporting minerals for porous rocks is a challenging problem that is key to developing insights into the transition between the high- and low-porosity segregation phenomena of calcite (or quartz) from clays. Other important directions are the effects of fluid flow across the systems, macroscopic shear, effects in two- and three-dimensional systems, grain plastic deformation, and the interplay of heterogeneity arising from mechanochemical segregations and fracturing.

ACKNOWLEDGEMENTS

This work was supported in part by a grant from the National Science Foundation and a contract with the Gas Research Institute. P. Ortoleva gratefully acknowledges the John Simon Guggenheim Foundation for a fellowship award.

REFERENCES

Alvarez, W., Engelder, T. and Lowrie, W., 1976. Formation of spaced cleavage and folds in brittle limestone by dissolution. *Geology*, 4: 698–701.

Alvarez, W., Engelder, T. and Geiser, P.A., 1978. Classification of solution cleavage in pelagic limestones. *Geology*, 6: 263–266.

Amjad, Z., 1987. Kinetic study of the seeded growth of calcium carbonate in the presence of benzenepolycarboxylic acids. *Langmuir*, 3: 224–228.

Angevine, C.L. and Turcotte, D.L., 1983. Porosity reduction by pressure solution: a theoretical model for quartz arenites. *Geol. Soc. Am. Bull.*, 94: 1129–1134.

Arnórsson, S., Sigurdsson, S. and Svavarsson, H. 1982. The chemistry of geothermal waters in Iceland. I. Calculation of aqueous speciation from 0° to 370°C. *Geochim. Cosmochim. Acta*, 46: 1513–1532.

Baker, P.A., Kastner, M., Byerlee, J.D. and Lockner, D.A., 1980. Pressure solution and hydrothermal recrystallization of carbonate sediments — an experimental study. *Mar. Geol.*, 38: 185–203.

Barrett, P.J., 1964. Residual seams and cementation in Oligocene shell calcarenites, Te Kuiti Group. *J. Sediment. Petrol.*, 34: 524–531.

Bathurst, R.G.C., 1987. Diagenetically enhanced bedding in argillaceous platform limestones: stratified cementation and selective compaction. *Sedimentology*, 34: 749–778.

Bausch, W.M., 1968. Clay content and calcite crystal size of limestones. *Sedimentology*, 10: 71–75.

Beaudoin, B., El Khanchoufi, A., Monleau, C. and Pinault, M., 1989. Carbonate transfer in alternating limy/marly U. Bajocian–L. Bathonian of Sainte-Victoire (S.E. France). *C. R. Acad. Sci. Paris*, 308: 641–645.

Becker, P. and Bilal, B.A., 1985. Ion products of water in 1 *m* NaCl under hydrothermal conditions. *J. Solution Chem.*, 14: 367–373.

Berner, R.A. and Morse, J.W., 1974. Dissolution kinetics of calcium carbonate in sea water, IV. Theory of calcite dissolution. *Am. J. Sci.* 274: 108–134.

Biot, M.A. and Willis, D.G. 1957. Elastic coefficients of the theory of consolidation. *ASME J. Appl. Mech.*, 24: 594–603.

Busenberg, E. and Plummer, L.N., 1986. A comparative study of the dissolution and crystal growth kinetics of calcite and aragonite. In: F.A. Mumpton (Editor), *Studies in Diagenesis. U.S. Geol. Surv. Bull.*, 1578: 139–168.

Buxton, T.M. and Sibley, D.F., 1981. Pressure solution features in a shallow buried limestone. *J. Sediment. Petrol.*, 51:1, 19–26.

Chen, W. and Ortoleva, P., 1990. Reaction front fingering in carbonate cemented sandstones. In: P. Ortoleva, B. Hallet, A. McBirney, I. Meshri, R. Reeder and P. Williams (Editors), *Self-Organization in Geological Systems. Proceedings of a Workshop held 26–30 June 1988, University of California, Santa Barbara. Earth-Sci. Rev.*, 29: 183–198.

Dandekar, D.P., 1969. Variation in the elastic constants of calcite with temperature. *J. Appl. Phys.*, 39: 3694–3699.

Dewers, T. and Ortoleva, P., 1989. Mechano-chemical coupling in stressed rocks. *Geochim. Cosmochim. Acta*, 53: 1243–1258.

Dewers, T. and Ortoleva, P., 1990a. Geochemical self-organization, III. A mechano-chemical model of metamorphic differentiation. *Am. J. Sci.*, 290: 473–521.

Dewers, T. and Ortoleva, P., 1990b. A coupled reaction/transport/mechanical model for intergranular pressure solution, stylolites, and differential compaction and cementation in clean sandstones. *Geochim. Cosmochim. Acta*, 54: 1609–1625.

Dewers, T. and Ortoleva, P., 1990c. Force of crystallization during the growth of siliceous concretions. *Geology*, 18: 204–207.

Ekdale, A.A. and Bromley, R.G., 1988. Diagenetic microlamination in chalk. *J. Sediment. Petrol.*, 58: 857–861.

Ellis, A.J., 1963. The solubility of calcite in sodium chloride solutions at high temperatures. *Am. J. Sci.*, 261: 259–267.

Ellis, A.J., 1972. Partial molal volumes of ions in hydrothermal solutions. *Geochim. Cosmochim. Acta*, 36: 413–426.

Eshelby, J.D., 1957. The determination of the elastic field of an ellipsoidal inclusion and related problems. *Proc. R. Soc. London, Ser. A*, 241: 376–396.

Feeney, R., Schmidt, S.L., Strickholm, P., Chadam, J. and Ortoleva, P., 1983. Periodic precipitation and coarsening waves: Applications of the competitive particle growth model. *J. Chem Phys.*, 78: 1293.

Freer, R., 1981. Diffusion in silicate minerals and glasses: a data digest and guide to the literature. *Contrib. Mineral. Petrol.*, 76: 440–454.

Garrison, R.E. and Kennedy, W.J., 1977. Origin of solution seams and flaser structures in the Upper Cretaceous chalks of southern England. *Sediment. Geol.*, 19: 107–137.

Gieskes, J.M., 1983. The chemistry of interstitial waters of deep sea sediments: interpretation of deep sea drilling data. *Chem. Oceanogr.*, 8: 222–265.

Hallam, A., 1986. Origin of minor limestone–shale cycles: Climatically induced or diagenetic? *Geology*, 14: 609–612.

Harvie, C.E., Møller, N. and Weare, J., 1984. The prediction of mineral solubilities in natural waters: the Na–K–Mg–Ca–H–Cl–SO_4–OH–HCO_3–CO_3–CO_2–H_2O system to high ionic strengths at 25°C. *Geochim. Cosmochim. Acta.*, 48: 723–751.

Hay, R.S. and Evans, B., 1988. Intergranular distribution of pore fluid and the nature of high-angle grain boundaries in limestone and marble. *J. Geophys. Res.*, 93: 8959–8974.

Heald, M.T., 1956. Cementation of Simpson and St. Peter sandstones in parts of Oklahoma, Arkansas, and Missouri. *J. Geol.*, 64: 16–30.

Heald, M.T. and Anderegg, R.C., 1960. Differential cementation in the Tuscarora Sandstone. *J. Sediment. Petrol.*, 30: 568–577.

Houseknecht, D., 1988. Intergranular pressure solution in four quartzose sandstones. *J. Sediment. Petrol.*, 58: 228–246.

Jacobson, R.L. and Langmuir, D., 1974. Dissociation constants of calcite and $CaHCO_3^+$ from 0 to 50°C. *Geochim. Cosmochim. Acta*, 38: 301–318.

Jaeger, J.C. and Cook, N.G.W., 1979. *Fundamentals of Rock Mechanics*. Chapman and Hall, London, 3rd ed., 593 pp.

Liu, C. and Lindsay, W.T., Jr., 1972. Thermodynamics of sodium chloride solutions at high temperatures. *J. Solution Chem.*, 1: 45–69.

Marschner, H., 1968. Relationship between carbonate grain size and non-carbonate content in carbonate sedimentary rocks. In: G. Muller and G.M. Friedman (Editors), *Recent Developments in Carbonate Sedimentology in Central Europe*. Springer-Verlag, New York, pp. 55–57.

Marshak, S. and Engelder, T., 1985. Development of cleavage in limestones of a fold-thrust belt in eastern New York. *J. Struct. Geol.*, 7: 345–359.

Matter, A., 1974. Burial diagenesis of pelitic and carbonate deep-sea sediments from the Arabian Sea. *Init. Rep. DSDP*, 23: 421–470.

McKenzie, W.F. and Helgeson, H.C., 1984. Estimation of the dielectric constant of H_2O from experimental solubilities of quartz, and calculation of the thermodynamic properties of aqueous species to 900°C at 2 kb. *Geochim. Cosmochim. Acta*, 48: 2167–2177.

Merino, E., Ortoleva, P. and Strickholm, P., 1983. Generation of evenly spaced pressure solution seams during late diagenesis: a kinetic theory. *Contrib. Mineral. Petrol.*, 82: 360–370.

Meyers, W.J., 1980. Compaction in Mississippian skeletal limestones, Southwestern New Mexico. *J. Sediment. Petrol.*, 50: 457–474.

Meyers, W.J. and Hill, B.E., 1983. Quantitative studies of compaction in Mississippian skeletal limestones, New Mexico. *J. Sediment. Petrol.*, 53: 231–242.

Millero, F.J., 1982. The effect of pressure on the solubility of minerals in water and seawater. *Geochim. Cosmochim. Acta*, 46: 11–22.

Mitra, G. and Yonkee, W.A., 1985. Relationship of spaced cleavage to folds and thrusts in the Idaho–Utah–Wyoming thrust belt. *J. Struct. Geol.*, 7: 361–373.

Morse, J.W., 1974. Dissolution kinetics of calcium carbonate in sea water, V. Effects of natural inhibitors and the position of the chemical lysocline. *Am. J. Sci.*, 274: 638–647.

Morse, J.W. and Casey, W.H., 1988. Ostwald processes and mineral paragenesis in sediments. *Am. J. Sci.*, 288: 537–560.

Neugebauer, J. 1974. Some aspects of cementation in chalks. In: K.J. Hsu and C. Jenkyns (Editors), *Pelagic Sediments: On Land and Under the Sea. Int. Assoc. Sedimentol., Spec. Publ.*, 1: 149–176.

Oelkers, E.H. and Helgeson, H.C., 1988. Calculation of the thermodynamic and transport properties of aqueous species at high pressures and temperatures: Aqueous tracer diffusion coefficients of ions to 1000°C and 5 kb. *Geochim. Cosmochim. Acta*, 52: 63–85.

Ortoleva, P., 1994. Development of diagenetic differentiated structure through reaction–transport feedback. In: K.H. Wolf and G.V. Chilingarian (Editors), *Diagenesis, IV. Developments in Sedimentology 51.* Elsevier, Amsterdam, pp. 79–94 (this volume).

Ortoleva, P., Merino, E. and Strickholm, P., 1982. Kinetics of metamorphic layering in anisotropically stressed rocks. *Am. J. Sci.*, 282: 617–643.

Ortoleva, P., Merino, E., Chadam, J. and Moore, C.H., 1987. Geochemical self-organization, I. Feedback mechanisms and modeling approach. *Am. J. Sci.*, 287: 979–1007.

Palciauskas, V.V. and Domenico, P.A., 1989. Fluid pressures in deforming porous rocks. *Water Resour. Res.*, 25: 203–213.

Pashley, R.M. and Israelachvili, J.N., 1984. Molecular layering of water in thin films between mica surfaces and its relation to hydration forces. *J. Colloid Interface Sci.*, 101: 511–523.

Pashley, R.M. and Kitchener, J.A., 1979. Surface forces in adsorbed multilayers of water on quartz. *J. Colloid Interface Sci.*, 71: 491–500.

Patterson, C.S., Slocum, G.H., Busey, R.H. and Mesmer, R.E., 1982. Carbonate equilibria in hydrothermal systems: first ionization of carbonic acid in NaCl media to 300°C. *Geochim. Cosmochim. Acta*, 46: 1653–1663.

Patterson, C.S., Busey, R.H. and Mesmer, R.E., 1984. Second ionization of carbonic acid in NaCl media to 250°C. *J. Solution Chem.*, 13: 647–659.

Plummer, L.N. and Busenberg, E., 1982. The solubilities of calcite, aragonite and vaterite in CO_2–H_2O solutions between 0 and 90°C, and an evaluation of the aqueous model for the system $CaCO_3$–CO_2–H_2O. *Geochim. Cosmochim. Acta*, 46: 1011–1040.

Plummer, L.N., Parkhurst, D.L. and Wigley, T.M.L., 1979. Critical review of the kinetics of calcite dissolution and precipitation. In: E.A. Jenne (Editor), *Chemical Modeling in Aqueous Systems. ACS Symp. Ser. 93.* American Chemical Society, Washington, D.C., pp. 537–573.

Rabinowicz, M., Dandurand, J.C., Jakubowski, M., Schott, J. and Cassan, J.P., 1985. Convection in a North Sea oil reservoir: inferences on diagenesis and hydrocarbon migration. *Earth Planet. Sci. Lett.*, 74: 387–404.

Reardon, E.J. and Langmuir, D., 1974. Thermodynamic properties of the ion pairs $MgCO_3^0$ and $CaCO_3^0$ from 10 to 50°C. *Am. J. Sci.*, 274: 599–612.

Reddy, M.M. and Wang, K.K., 1980. Crystallization of calcium carbonate in the presence of metal ions, I. Inhibition by magnesium ion at pH 8.8 and 25°C. *J. Crystal Growth*, 50: 470–480.

Ricken, W., 1986. *Diagenetic Bedding. Lecture Notes in Earth Sciences, 6.* Springer-Verlag, Berlin, 210 pp.

Ricken, W., 1987. The carbonate compaction law: a new tool. *Sedimentology*, 34: 571–584.

Rittenhouse, G., 1971. Pore-space reduction by solution and cementation. *Am. Assoc. Pet. Geol. Bull.*, 55: 80–91.

Schlanger, S.O. and Douglas, R.G., 1974. Pelagic ooze–chalk–limestone transition and its implications for marine stratigraphy. In: K.J. Hsü and C. Jenkyns (Editors), *Pelagic Sediments: On Land and Under the Sea. Int. Assoc. Sedimentol., Spec. Publ.*, 1: 117–148.

Scholle, P.A., 1977. Chalk diagenesis and its relation to petroleum exploration: Oil from chalks, a modern miracle? *Am. Assoc. Pet. Geol. Bull.*, 61: 982–1009.

Simpson, J., 1985. Stylolite-controlled layering in an homogeneous limestone: pseudo-bedding produced by burial diagenesis. *Sedimentology*, 32: 495–505.

Spang, J.H., Oldershaw, A.E. and Stout, M.Z., 1979, Development of cleavage in the Banff Formation at Pigeon Mountain, Front Ranges, Canadian Rocky Mountains. *Can. J. Earth Sci.*, 16: 1108–1115.

Stockdale, P.B., 1922. Stylolites: their nature and origin. *Ind. Univ. Stud.*, 9: 1–55.

Sujkowski, Zb. L., 1958. Diagenesis. *Am. Assoc. Pet. Geol. Bull.*, 42: 2692–2717.

Tada, R. and Siever, R., 1986. Experimental knife-edge pressure solution of halite. *Geochim. Cosmochim. Acta*, 51: 2295–2301.

Tada, R. and Siever, R., 1988. Pressure solution during diagenesis: *Annu. Rev. Earth Planet. Sci.*, 17: 89–118.

Tada, R., Maliva, R. and Siever, R., 1987. A new mechanism for pressure solution in porous quartzose sandstone. *Geochim. Cosmochim. Acta*, 51: 2295–2301.

Thomson, A., 1959. Pressure solution and porosity. In: H.A. Ireland (Editor), *Silica in Sediments, Soc. Econ. Paleontol. Mineral., Spec. Publ.*, 7: 92–110.

Tillman, R.W. and Almon, W.R., 1979. Diagenesis of Frontier Formation offshore bar sandstones, Spearhead Ranch Field, Wyoming. In: P.A. Scholle and P.R. Schluger (Editors), *Aspects of Diagenesis. Soc. Econ. Paleontol. Mineral., Spec. Publ.*, 26: 175–207

Wanless, H.R., 1979. Limestone response to stress: pressure solution and dolomitization. *J. Sediment. Petrol.*, 49: 437–462.

Weyl, P.K., 1959. Pressure solution and the force of crystallization — a phenomenological theory. *J. Geophys. Res.*, 64: 2001–2025.

Wong, P.K. and Oldershaw, A., 1981. Burial cementation in the Devonian, Kaybob Reef Complex, Alberta, Canada. *J. Sediment. Petrol.*, 1: 507–520.

Zimmerman, R.W., Somerton, W.H. and King, M.S., 1986. Compressibility of porous rocks. *J. Geophys. Res.*, 91: 12,765–12,777.

Diagenesis, IV. Developments in Sedimentology 51
edited by K.H. Wolf and G.V. Chilingarian
© 1994 Elsevier Science B.V., Amsterdam. All rights reserved.

Chapter 8

MORPHOCHEMICAL AND REPLACEMENT DIAGENESIS OF BIOGENIC CARBONATES

UWE BRAND

INTRODUCTION

Morphological diagenesis of biogenic carbonates addresses the problem of physical changes at both the macro- and microstructural levels. In addition, chemical diagenesis refers to the concomitant mineralogical and elemental/isotopic changes that take place during the postdepositional alteration of primary and pristine carbonate allochems. This alteration generally takes place in the presence of a fluid which may have its origin either in the oceanic or continental realm or a combination of these within the hydrologic cycle. The fluid(s), of whatever origin, acts as a catalyst in diagenetic alteration processes which allows the reaction to proceed at a geologically rapid rate. Without such a catalytic fluid(s), solid-state alteration of sedimentary grains may be an invariably slow geological process under normal Earth surface (pressure–temperature) conditions.

Alteration encompasses a number of different processes such as lithification, compaction, micritization, calcitization, cementation, dolomitization, neomorphism, and inversion. All of these terms and processes have been described in detail by Bathurst (1975) and other researchers. Replacement defines a special process in the realm of diagenesis, and refers to the partial- to full-scale replacement of the primary or diagenetic mineral phase by an authigenic mineral; for instance, silica, pyrite, phosphate and dolomite replacing calcite. During replacement, macrostructures of a particular biogenic allochem are usually maintained and well-preserved. Most of these processes, however, have an overall destructive consequence for the more delicate and intricate microstructures of a carbonate allochem. Microstructures, though, may be preserved as ghosts under special postdepositional conditions conducive to maintenance of these delicate structures.

Preservation, in the strictest sense, infers in all instances not only preservation of macro- and microstructures of carbonate allochems, but also of the original mineralogy and geochemistry of the endo/exoskeleton shell. Described and identified fossils represent a best estimate of only 9% of the actual populations, and preserved material exemplifies an even smaller percentage. Despite such low preservation potential, fossil material may be preserved when it is entombed in a matrix which effectively seals out air, water and other fluids, and actively prevents or minimizes biological interaction. Amber, chert, ice and tar as well as fine-grained sediments and possibly organic matter in sediments may provide suitable protection from the catalytic effect of water in slowing down the transformation of meta- and unstable carbonate mineral phases such as aragonite (ARAG) and high-Mg calcite (HMC), and even the alteration of relatively stable phases such as intermediate-Mg calcite (IMC) and low-Mg calcite (LMC). If this protection is coupled with generally inhospitable depositional conditions and/or rapid sedimentation rates, biological activity may be suppressed as a contributing factor in enhancing and accelerating diagenetic processes. Concholin of shells/skeletons which encloses individual crystallites and layers, may suppress early diagenetic reactions during disarticulation and degradation of an organism after its demise. In addition, the overall size and morphology of the biogenic carbonate grain (e.g., Anderson et al., 1973; Walter and Morse, 1984), in some instances, may further influence the rate of diagenetic alteration under certain physicochemical conditions.

Geologic time, in addition to physical and chemical constituents of diagenetic environment(s), plays an essential role in either enhancing or suppressing diagenetic reactions in a multitude of settings otherwise conducive to postdepositional transformation. In some unusual instances, microstructural features are preserved in fossil material, whereas the original mineralogical and to some degree the geochemical properties have been moderately to severely changed. Even under the best preservation conditions possible, time (geologic) may be the critical ingredient for small-scale but continual aggressive action and reaction of the fluid(s) with the carbonate allochem.

Mineralogy to some degree may also influence the preservation potential of a specific carbonate allochem. This control in addition to the other parameters already discussed above, may provide for the right conditions and the ultimate preservation of the fossil in its original mineralogy, microstructures and geochemistry. This "pristine" material may be an essential cornerstone, a rosetta stone, in unravelling some of the Earth's complicated and mysterious exogenic processes in the geologic past and their ultimate controls and causes and interactions with endogenic processes. Thus, the diagenetic evaluation process in itself is a cornerstone of identifying the material which must meet very stringent conditions. A clear understanding of the relevant basic principles and concepts of depositional and diagenetic processes increases one's confidence of identifying the "best" preserved material whether it be a biogenic carbonate or another mineral phase.

BASIC PRINCIPLES

An understanding of the basic concepts is essential pertaining to mineralogical and microstructural controls, major, minor and trace elements as well as stable and radiogenic isotope re-distribution which may be influenced during the initial deposition or subsequent diagenetic alteration of the studied biogenic mineral. These may include factors such as growth/precipitation rate and osmotic equilibrium between body fluids and ambient water. Other factors such as redox potential of the water may apply equally to those in depositional and diagenetic environments. In diagenetic environments, the water/rock ratio in addition to the type of water(s) involved in the catalytic alteration of the shell/skeleton play significant roles in "shaping" the morphogeochemistry of the ultimate diagenetic product(s).

Mineralogy

One school of thought postulates that organisms appear to exercise a major physiological control over the type of mineral, and consequently mineralogy that is used in the construction of their shell/skeleton. The other suggests that seawater composition (Mg/Ca ratio or dissolved Ca^{2+}) imparted a controlling influence on the mineralogy of biogenic carbonates (cf., Chilingar, 1962; Wilkinson, 1979; Kázmierczak et al., 1985). Interaction of mid-ocean ridge basalt with seawater is an effective mechanism for removing fluvial Mg as well as supplying Ca to the oceans (Holland, 1984). At present it is unclear whether the distribution and evolution of calcium carbonate shells/skeletons, or for that matter silica/phosphates, is an evolutionary process controlled by the organism or the chemistry of past oceans influenced by mid-ocean ridge basalt cycling (cf., Lowenstam, 1963; Rosenberg, 1990). Nor is it certain that phosphatic organisms were necessarily ancestral to the carbonate secreting biota of the Phanerozoic. Palmer (1981, 1983) suggested that secreting organic-rich shells/skeletons requires more energy than those consisting of mostly inorganic calcium carbonate. Thus, a metabolic consideration of conserving energy by organisms may have been possibly the physiological driving force for the evolution and secretion of calcium carbonate endo- and exoskeletons.

Calcium carbonate

Detailed analysis of the major Phanerozoic fossil groups shows no definite trend towards a gradual shift from calcite to aragonite with time (Fig. 8-1). The only exception are the coelenterata, with specimens documenting a definite shift from precipitating low-Mg and intermediate-Mg calcite exoskeletons to predominantly aragonitic ones, which was initiated during the early to mid Mesozoic. The only other fossil groups which show an evolutionary shift in mineralogy are the bivalvia and gastropoda. Unlike the corals, the trend is reversed in these two groups (cf., Rosenberg, 1990). Paleozoic gastropods and especially bivalves were mostly monomineralic aragonite; few genera possessed thin calcitic outer layers. Truly monomineralic and bimineralic low to intermediate-Mg calcite secreting bivalves did not become abundant until the mid Mesozoic (e.g., Carter, 1980; Rosenberg, 1990); similar observations apply to gastropods but mineralogical changes are less prevalent. Late Paleozoic through Mesozoic belemnites are the only known cephalopods to have secreted mostly low-Mg calcite exoskeletons (rostrum), which is in stark contrast to a preference for aragonite by all other extinct as well as extant groups. Unlike the other fossil groups, coralline sponges have a most assorted evolutionary mineralogical history (Fig. 8-1). A more detailed account of the diversity in biomineralization products shows that besides calcium carbonates, phosphates, halides oxalates, sulphates, silica, Fe-oxides, Mn-oxides and Fe-sulphides may be used as a building material by extant organisms (Lowenstam, 1981). Specific mineralogical changes in fossil groups are discussed in more detail in the subsequent sections.

Silica/phosphate

Much less attention has been paid to siliceous and phosphatic marine and nonmarine organisms than their calcareous counterparts. Two groups, the radiolaria and

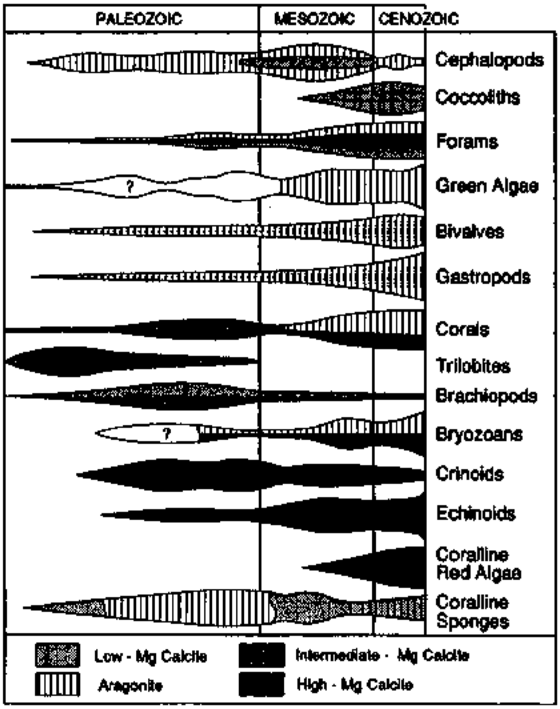

Fig. 8-1. Relative abundance and mineralogy of major carbonate-secreting Paleozoic, Mesozoic and Cenozoic fossil groups (? = mineralogical uncertainty). Information based mainly on work by Lowenstam (1963), Brand and Morrison (1987a), and Carter (1990).

porifera, dominate the geologic record only to be dominated by the later-evolving siliceous algae such as diatoms (Fig. 8-2). Of the phosphatic groups, the conodonts listed under the problematica have dominated the geochemical field in recent years

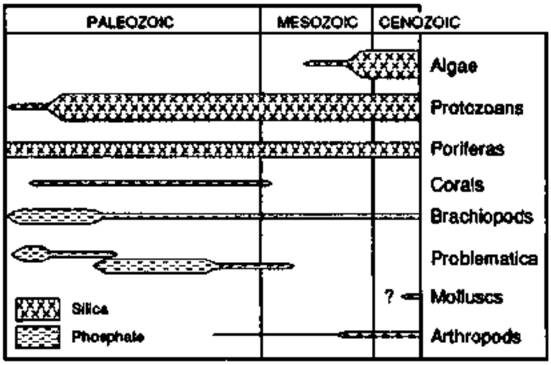

Fig. 8-2. Relative abundance of silica and phosphate-secreting Paleozoic, Mesozoic and Cenozoic fossil groups. (Modified from Lowenstam, 1963.)

supplementing the work carried out on fish teeth and scales. Their potential was recently challenged, because of doubts expressed concerning their diagenetic stability (Shemesh, 1990).

Biomineralogical evolution and diversity does not seem to play a major role in controlling or influencing the preservation potential of specific carbonate/silica/phosphate secreting invertebrates during the Phanerozoic. But it may have a profound effect on influencing shell/skeleton resistance to diagenetic attack and alteration.

Microstructures

Calcium carbonate

To some degree the layers of microstructural arrangements in the major fossil groups are quite complex and intricate (Table 8-1). These reflect some basic biomechanical properties best suited to some of the groups/organisms to exploit the multitude of environmental niches of this planet (e.g., Currey, 1990). Some structures are well suited in providing strength, whereas others are ideal in providing flexibility which may be supplemented by the organic matrix surrounding individual crystallites as well as layers and whole shells/skeletons in response to environmental stresses. This component may vary from a low of 0.1% in corals to a high of 96% in coralline sponges (Table 8-1). Current thought suggests that the organic matter concholin,

TABLE 8-1

Major microstructures, mineralogy and organic matter in shells/skeletons of carbonate-secreting marine organisms (e.g., Lowenstam, 1963; Nicol, 1968; Brand and Morrison, 1987a; Carter, 1990)

Group	Microstructures	Organic matter (%)
Cephalopods	$\mathrm{N_A}$, $\mathrm{P_{AC}}$, $\mathrm{H_A}$	2.0–6.9
Bivalves	$\mathrm{N_A}$, $\mathrm{P_{AC}}$, $\mathrm{H_A}$, $\mathrm{F_C}$, $\mathrm{CL_A}$, $\mathrm{CCL_A}$	2.0–3.2
Gastropods	$\mathrm{N_A}$, $\mathrm{P_{AC}}$, $\mathrm{F_C}$, $\mathrm{CL_A}$, $\mathrm{CCL_A}$	2.0–3.2
Coccoliths	OLC, ER	
Foraminiferas	$\mathrm{G\text{-}E_C}$, $\mathrm{RF_{AC}}$, $\mathrm{S_C}$, NL	1.3–3.2
Corals	$\mathrm{TF_{AC}}$, LF, $\mathrm{G_C}$, $\mathrm{SP_C}$	0.1–40.9
Trilobites	$\mathrm{H_C}$, $\mathrm{G_{CP}}$, $\mathrm{E_C}$	
Brachiopods	$\mathrm{KF_C}$, $\mathrm{P_C}$, $\mathrm{B_C}$	1.0–3.5
Bryozoans	$\mathrm{G_C}$, $\mathrm{LC_C}$, $\mathrm{SR_C}$, $\mathrm{F_A}$	6.9–35.1
Crinoids/echinoids	$\mathrm{PFE_C}$	8.6–46.7
Green algae	$\mathrm{MCF_A}$	
Coralline red algae	$\mathrm{MCF_C}$	
Coralline sponges	$\mathrm{G_A}$, $\mathrm{F_{AC}}$, $\mathrm{SP_{AC}}$, $\mathrm{C_{AC}}$, $\mathrm{O_{AC}}$	0.4–96.0

B = bladed, C = clinogonal, CL = crossed-lamellar, CCL = complex-crossed-lamellar, E = equant, ER = elongate rhombohedra, F = fibrous, H = homogeneous, KF = keeled-fibrous, LC = laminated calcite, LF = lamellar fibrous, MCF = micro-calcite fibers, G = granular, N = nacreous, NL = needle-laths, O = orthogonal, OLC = overlapping crystals, P = prismatic, PFE = polycrystalline fenestrate, RF = radial fibers, S = spiculate, SP = spherulitic, SR = skeletal rods, TF = trabeculae fibers.

Subscripts: A = aragonite, C = calcite.

composed of proteins and several polysaccharides (e.g., Grégoire et al., 1955) provides the organizational framework for the shell, and that acidic macromolecules are involved in the actual mineral nucleation and deposition processes (e.g., Crenshaw, 1990; Lowenstam and Weiner, 1989). The reader is referred to the last two citations for more comprehensive discussions on the topic of biomineralization and related processes and functions (Rhoads and Lutz, 1980; Carter, 1990).

Most organisms deposit shells with layers of mono-, bi-, or variable mineralogy and different microstructures. Table 8-1 summarizes major microstructures recognized in shells/skeletons of carbonate-secreting marine invertebrates. No order of importance or evolutionary succession is implied by the listings. A comprehensive analysis of the types of microstructures, number of layers and degree of calcification are areas of research that deserve more attention. This research may be important in unravelling some evolutionary processes and their possible role in influencing the complex procedure(s) involved in the transformations and replacement of original shell/skeletal material during postdepositional reactions. Until then, their primary role consists of identifying the best preserved fossil allochem; to document the morphological changes in both shell/skeleton macro- and microstructures during diagenetic alteration.

Silica/phosphates

Most information about microstructures in siliceous and phosphatic organisms is based on diatoms, fish teeth, brachiopods and conodonts. In sponges, the spicules consist of amorphous, opaline and hydrated silica which dissolve rapidly after death of the organisms (e.g., Jones, 1971). Thus microstructures of modern and especially fossil spicules are relatively unknown. In protozoans, similar to spicules the skeletal material consists of amorphous phosphate. Crystalline calcium phosphate has only been reported in teeth of polyplacophorans, the periostracum of some bivalves, and the shells of atremate brachiopods (e.g., Iwata, 1981a, b; Waller, 1983; Watabe, 1990). In polyplacophoran teeth, initially deposited as amorphous phosphate but transformed to dahllite, crystals are aligned nearly perpendicular to the tooth surface. Molluscan phosphate may occur as an irregular mass or hexagonal cylinders. In atremate brachiopods three microstructural arrangements have been recognized, (1) acicular crystallites, (2) coarse-coalescent acicular crystallites, and (3) minute granules of calcium phosphate.

Interesting details are known about the microstructure of apatite, a phosphate mineral, found in conodonts. Apatite in the crown probably accreted concentrically, and consists of elongated parallel rods (e.g., Lindström and Ziegler, 1981; Wright, 1990). "White matter" present in denticles and in the growth axis consists of microspheres. Fish teeth may be covered by dentine depending on phylogenetic level (Carlson, 1990). Major structures recognized in fish teeth are orthodentine, trabecular dentine, and plicidentine which are covered by an outermost layer of virtodentine or enameloid (Peyer, 1968). In sharks this outer layer may resemble that found in some reptilian and mammalian teeth. Excellent discussions on phosphate, silica and carbonate-based microstructures of organisms are found in the chapters of the book edited by Carter (1990).

Trace elements

Geochemistry has been become an integral part of geological work; in particular fossil studies. Trace elements and their redistribution patterns are part of this advance in not only defining the degrees and pathways of diagenetic processes, but they also play a major role in unravelling some of the cycles and reactions between and within the various exogenic processes.

Trace elements are essential to the targeted and multi-method approach of deciphering diagenetic processes in biogenic carbonates. After mineralogical (where applicable) and microstructural analysis, concentrated trace chemistry evaluation is instrumental in defining and delineating the best preserved material. A clear understanding of the principles of partitioning and its limitations are fundamental to deriving realistic trends and reaching plausible interpretations. Cations, minor and trace elements, may substitute for Ca^{2+}in the $CaCO_3$ lattice in the following manner: (1) by direct or diadochic substitution of the foreign element for the major element, (2) by interstitial lattice-position substitution, (3) by adsorption on crystal surface, and 4) by substitutions involving crystal defects. These substitutions are governed or elucidated by a number of structural controls (i.e., ionic radius, charge, bond characteristics, and crystal coordination), non-thermodynamic controls (i.e., partition coefficient), and kinetic controls (i.e., diffusion, growth/precipitation rate).

Precipitation and subsequent dissolution–reprecipitation of calcium carbonate in the presence of water and carbon dioxide can be expressed by the simplified reaction (McIntyre, 1963):

$$CaCO_3 + H_2O + CO_2 \rightarrow Ca^{2+} + 2\,HCO_3^- \tag{8-1}$$

and the distribution (D) of a specific trace element between liquid and solid phase is usually expressed by the homogeneous non-thermodynamic relationship:

$$({}^{m}t/{}^{m}C)_{S} = D({}^{m}t/{}^{m}C)_{L}, \tag{8-2}$$

where t is the trace/minor element, C is the major or carrier element expressed in moles (m) in the solid (S) and liquid (L) phases (Henderson and Kraeck, 1927). Systems governed by non-equilibrium conditions, which most likely pertains to partly closed/closed diagenetic systems (intermediate to low water/rock ratios), the heterogeneous distribution applies:

$$\log({}^{m}t_{i}/{}^{m}t_{f}) = D\log {}^{m}Ca_{i}/{}^{m}Ca_{f}), \tag{8-3}$$

where "i" and "f" are the initial and final concentrations of the tracer and Ca in solution (Gordon et al., 1959). The activity of elements is important in defining the "thermodynamic" distribution of species and is related to the equilibrium constant K by:

$$D = K(\lambda_{t}/\lambda_{Ca})/(\gamma_{t}/\gamma_{Ca}), \tag{8-4}$$

where λ and γ are, respectively, solid and solution phase activity coefficients (Morse and Mackenzie, 1990). Thus the prevalent coefficients in the literature are good approximations of reactions that are most likely temperature, pressure and rate dependent (e.g., Lorens, 1981; Morse and Mackenzie, 1990). Although, it is undeniable that partition coefficients may be also strongly influenced by crystal morphology, they are useful in delineating first-order trends of trace elements during postdepositional alteration processes. Some of the "accepted" partition coefficients are listed in Table 8-2. Preference for specific elements for incorporation into six-fold coordinated calcite or nine-fold coordinated aragonite is also governed, in part, by the ionic radius of the element substituting for Ca in the crystal lattice. A partition coefficient of unity infers that there is no significant difference in the molar ratio of tracer/carrier between liquid and solid phase. In the case where $D > 1$, the tracer will be enriched in the solid phase relative to the tracer/carrier of the liquid phase. A state of depletion is evident in the solid when $D < 1$. This in conjunction with concentrations (activities) of elements in seawater and diagenetic fluids such as meteoric water, will bring about the depletion in some elements and the enrichment of others during the diagenetic alteration process (cf. Veizer, 1983b; Brand and Morrison, 1987a).

A most interesting case is the partitioning of Sr into biogenic aragonite (Table 8-2). Marine aragonite of algae contains twelve times more Sr than is predicted by the postulated distribution coefficient of 0.095 at 25°C (Plummer and Busenberg, 1987; Table 8-2). This suggests that Sr in algal aragonites is not controlled by equilibrium or stoichiometric saturation with ambient seawater. Indeed, molluscan aragonite with a distribution coefficient of 0.24 is closer to equilibrium conditions than either algal or coral aragonite. This Sr variance observed in biogenic/non-biogenic carbonates is probably related to some control by precipitation/growth rate kinetics.

TABLE 8-2

Valences, ionic radii and partition coefficients of important elements substituting for Ca^{2+} in the calcium carbonate lattice of biogenic calcite (VI) and aragonite (IX) (e.g., Lorens, 1981; Veizer, 1983a; Boyle, 1988; Brand, 1989a; Faure, 1991; Smith et al., 1991)

	Valence	VI	D_C	IX	D_A
Ca	2	1.08	1.26		
Mg	2	0.80	0.06	>0.97	0.00025
Na	1	1.10	0.000025	1.40	0.00063
Mn	2	0.75–0.92	15.0	1.01	57.0
Fe	2	0.69–0.86	10.0		9.7
Zn	2	0.83	20.0	>0.98	5.0
Sr	2	1.21	0.05	1.36	0.24/1.12
Cd	2	1.03	2.5	>1.15	≈4
Ba	2	1.44	0.25	1.55	2.0
Nd	3	1.06		1.17	
Pb	2	1.26	250	1.41	7.2
Ir	3	0.81			
Al	3	0.61			
U	4	0.89–097		1.13	≈0.01

Note: $D^{Sr}_{CaCO_3} = 0.24$ for molluscan aragonite, and 1.12 for coelenterate–algae aragonite.

Equilibrium incorporation of elements and isotopes into biogenic carbonates are subject, in some instances, to both kinetic and metabolic fractionation processes. These may increase or decrease the composition relative to the carrier and ratio expected in seawater and iso-osmotic hemolymph in marine invertebrates. These processes will be discussed further in subsequent sections.

Cathode luminescence

A relatively new tool in studies of carbonate diagenesis is cathode luminescence. Initially it held much promise for rapidly differentiating between preserved and altered material. It was extensively used in diagenetically assessing Paleozoic brachiopods (e.g., Popp et al., 1986b). But most recently detailed work by Mason (1987) and Barbin et al. (1991) demonstrated some of the pitfalls of relying exclusively on luminescence patterns in identifying altered regions/material in carbonate specimens (cf., Pedone et al., 1990; Rush and Chafetz, 1990). Cathode studies (Fig. 8-3A and B) demonstrate that modern unaltered biogenic aragonite has differential luminescence (Fig. 8-3A to C) which are interpreted to reflect chemical variations in environmental conditions, both macro- and microenvironmental, during shell growth and not simply selective alteration. Otherwise it is possible that the pattern displayed in the fossil cephalopod, which based on mineralogical, microstructural and geochemical interpretations is pristine aragonite (Brand, 1989a), may be construed wrongly as indicating selective alteration of growth layers (Fig. 8-3D). Similar patterns of luminescence related to growth variations were also observed in modern brachiopods (Barbin et al., 1991). Furthermore, luminescence patterns in diagenetically altered ooids may either follow the predicted trends or are diametrically opposed to generally accepted concepts (Brophy et al., in prep.). Thus, cathode luminescence although it is a useful tool in differentiating between calcite and dolomite, and identifying zonations in cements, caution must be exercised in ascribing luminescence in biogenic carbonates solely to diagenetic processes.

Stable isotopes

Stable isotopes, in particular carbon and oxygen, are imparted increasingly important roles in assessing not only the diagenetic state of carbonate allochems but also to wrestle information from them about their depositional environment and Earth's exogenic systems. Carbon and oxygen isotope incorporation into carbonate minerals is governed by the fractionation factor α:

$$R_{\mathrm{S}} = \alpha_{\mathrm{S\text{-}W}} R_{\mathrm{W}}, \tag{8-5}$$

where R is the ratio of relative abundances of the studied isotope (e.g., $^{18}\mathrm{O}/^{16}\mathrm{O}$, $^{13}\mathrm{C}/^{12}\mathrm{C}$), subscript S represents the solid phase, and W the liquid (in most instances it is water). The α values are close to unity and vary mostly in the third decimal place; to facilitate expression of differences, ratios are usually expressed as whole numbers in permil (‰):

$$\Delta_{\mathrm{S\text{-}W}} = [(R_{\mathrm{S}}/R_{\mathrm{W}}) - 1] \times 10^3 = (\alpha_{\mathrm{S\text{-}W}} - 1) \times 10^3, \tag{8-6}$$

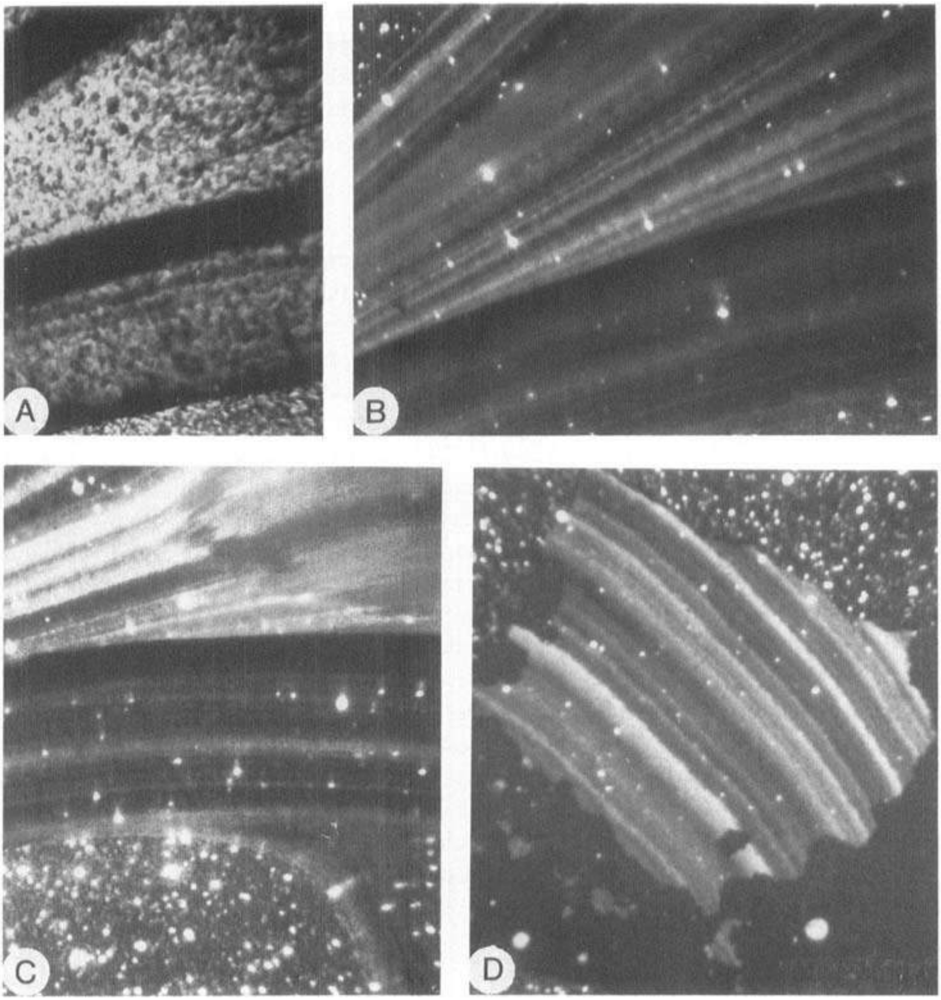

Fig. 8-3. Cathode luminescence patterns of Recent (*Nautilus pompilius*) and Pennsylvanian (*Orthoceras* sp.) cephalopods (courtesy of V. Barbin, University of Bern). A is a plane polarized-light view of external shell material from *Nautilus*. B and C are cathode luminescence views of external shell. D is a cathode image of a septum from *Orthoceras* sp. (B81-36a) showing prominent growth layers.

but this relationship is more commonly expressed by the delta (δ) value of the sample and standard:

$$\delta_S = [(R_S/R_W) - 1] \times 10^3. \tag{8-7}$$

The fractionation between two phases, such as calcite (S) and water (W), may be related to the enrichment factor (ϵ) in the following manner:

$$\epsilon_{S\text{-}W} \simeq \delta_S - \delta_W \simeq \Delta_{S\text{-}W} \simeq 10^3 \ln \alpha_{S\text{-}W} \tag{8-8}$$

Isotopic compositions of carbonates are usually given in permil relative to the PDB standard based on *Belemnitella americana* from the Cretaceous Peedee Formation of South Carolina. It is further customary to express isotopic compositions of waters relative to the SMOW standard (Standard Mean Ocean Water). These two standards are related by the following equation (Coplen et al., 1983):

$$\delta^{18}O_{(SMOW)} = 1.03086 \times \delta^{18}O_{(PDB)} + 30.86 \tag{8-9}$$

Aragonites and magnesian calcites tend to concentrate preferentially the heavier isotopes ^{18}O and ^{13}C of oxygen and carbon relative to low-Mg calcite (Rubinson and Clayton, 1969; Tarutani et al., 1969). At 25°C, the ^{13}C enrichment in aragonite relative to syngenetic calcite is about 1.8–2.0‰, whereas the ^{18}O enrichment is about 0.6‰ (Rubinson and Clayton, 1969; Grossman and Ku, 1986). Fractionation of both isotopes is temperature sensitive; however, oxygen is the more responsive of the two. This principle has become a major tool of geochemistry in solving complex geological problems such as the hydrogeochemistry and water temperature of ancient oceans. Similar to trace elements, fractionation processes of stable isotope are influenced by a number of kinetic factors such as precipitation/growth rate and metabolic processes, which are discussed further in the next section.

The temperature relationship between calcite and water of $\delta^{18}O$ was recognized very early in the establishment of stable isotopes as a tool in geochemistry (e.g., Urey, 1947). Based on experiments performed in the lab and in natural settings, the temperature–^{18}O relationships for calcite and aragonite were formulated as follows:

$$16.9 - 4.3(\delta^{18}O_C - \delta^{18}O_W) + 0.14(\delta^{18}O_C - \delta^{18}O_W)^2 \tag{8-10}$$

$$19.9 - 4.0(\delta^{18}O_A - \delta^{18}O_W) + 0.08(\delta^{18}O_A - \delta^{18}O_W)^2, \tag{8-11}$$

where the $\delta^{18}O_C$ and $\delta^{18}O_A$ are the oxygen isotopic compositions of the calcite and aragonite, respectively (Urey et al., 1951; Grossman and Ku, 1981), and the $\delta^{18}O_W$ is the composition of the ambient water. The underlying assumption here is that the calcium carbonate is precipitated in isotopic equilibrium with the water, and thus the calculated T°C represents ambient depositional conditions.

Radiogenic isotopes

Application of radiogenic isotope systematics to geological problems is expanding. Foremost, applications revolve about carbon, strontium, uranium and, lead isotopes. Radiocarbon dating is a well established procedure and is covered in more detail in specialist books and articles. Strontium isotope systematics has been applied to geological problems, but the field did not expand rapidly until recently. A relative newcomer to the field is the research specialty of lead isotope systematics. Only these two will be discussed in more detail.

Strontium isotope systematics

Strontium has four isotopes, and these are incorporated into carbonate minerals without any fractionation effects. Radiogenic ^{87}Sr is generated by the emission of negative β-particles from ^{87}Rb:

$$^{87}_{37}\mathrm{Rb} \longrightarrow {}^{87}_{38}\mathrm{Sr} + \beta^- + \overline{\nu} + Q \tag{8-12}$$

where β^- is the beta particle, $\overline{\nu}$ is an antineutrino, and Q represents the decay energy in million electron volts (MeV). The magnitude of ^{87}Sr present in modern environments (M) is directly related to the sum of primordial Sr (P) and radiogenic Sr generated by the decay of ^{87}Rb, and normalized to the stable Sr isotope. This is expressed as follows:

$$(^{87}\mathrm{Sr}/^{86}\mathrm{Sr})_{\mathrm{M}} = (^{87}\mathrm{Sr}/^{86}\mathrm{Sr})_{\mathrm{P}} + (^{86}\mathrm{Rb}/^{86}\mathrm{Sr})\,(e^{\Delta t} - 1) \tag{8-13}$$

Results of this expression are usually stated as the ratio of the two isotopes (^{87}Sr/^{86}Sr), relative to standard N.B.S. SRM-987, Atlantic seawater, or Eimer & Amend $SrCO_3$, which for modern seawater and carbonates are 0.709241 ± 32 and 0.709211 ± 37 for the two standards, respectively (Elderfield, 1986; Brand, 1991). Generally, the Sr isotopic composition of carbonates reflects the composition of the ambient seawater, if they escaped any postdepositional alteration processes. Otherwise, the ratio may be influenced by one or more of the major reservoirs of the strontium exogenic cycle (e.g., Palmer and Elderfield, 1985; Hess et al., 1986; Veizer, 1989).

Lead isotope systematics

This is a new and exciting field in carbonate geochemistry, with its application to unravelling diagenetic time frames. Uranium has three radioactive isotopes, whereas thorium has only one long-lived isotope (Faure, 1977). The decay of ^{238}U produces stable ^{206}Pb as follows:

$$^{238}_{92}\mathrm{U} \longrightarrow {}^{206}_{82}\mathrm{Pb} + 8\,^{4}_{2}\mathrm{He} + 6\,\beta + Q \tag{8-14}$$

where Q is the sum of the decay energy in MeV. The radioactive decay of ^{235}U gives rise to stable ^{207}Pb in the following manner:

$$^{235}_{92}\mathrm{U} \longrightarrow {}^{207}_{82}\mathrm{Pb} + 7\,^{4}_{2}\mathrm{He} + 4\,\beta^- + Q \tag{8-15}$$

and thorium decay into stable lead follows the summary pathway of:

$$^{232}_{90}\mathrm{Th} \longrightarrow {}^{208}_{82}\mathrm{Pb} + 6\,^{4}_{2}\mathrm{He} + 4\,\beta^- + Q. \tag{8-16}$$

A total of 43 isotopes of 12 elements are intermediate products of these decay series. In a closed system under secular equilibrium, free from contamination and resetting, the production rate of the stable endproducts is equal to those of their respective parents (Faure, 1977). Under these circumstances the use of these isotopes in conjunction with "stable" ^{204}Pb, enables one to date the isotope-bearing carbonate mineral using the familiar and simplified equation, provided reasonable values for the initial lead isotope ratios have been determined:

$$t_{206} = \frac{1}{\lambda_l} \ln\left[\frac{^{206}\mathrm{Pb}/^{204}\mathrm{Pb} - (^{206}\mathrm{Pb}/^{204}\mathrm{Pb})_0}{^{238}\mathrm{U}/^{204}\mathrm{Pb}} + 1\right], \tag{8-17}$$

where subscript "0" designates the initial isotope ratios of lead incorporated into the mineral at time of formation, and t is the time elapsed since closure of the primary/diagenetic carbonate mineral to uranium, thorium and lead.

DEPOSITIONAL CONTROLS

Depositional controls may be of an intrinsic or extrinsic nature, and some of these factors are not well defined or as yet unknown. In some instance, the organism may "accept" the geochemical signal of its surrounding environment without modification. Under certain circumstances for some specific element(s)/isotope(s), the organism during the calcification process may metabolically modify the composition/ratio of the particular ingredient. Three of these factors are discussed in detail in the following section.

Growth/precipitation rate

Growth/precipitation rate of organisms may be controlled by both extrinsic as well as intrinsic factors, which may be recorded in the form of change in shell shape and form, micro/macrogrowth increments, mineralogy or chemistry. Of the extrinsic factors (dissolved oxygen, substratum conditions, water turbidity, salinity), water temperature and chemistry, and nutrient level (and contaminants in the modern environment) may be the most important ones in influencing the growth rate of marine and non-marine invertebrates. Of the intrinsic factors, phylogenetic level of the organism may be the overriding factor in the ultimate rate of growth/accretion of shell/skeletal material. Changes in, or different growth rates from the norm, may result in mineralogical variability in species/genera from different environments and "growth" habitats (Rhoads and Lutz, 1980). The mineralogical variability of the bivalve *Mytilus* is a classic example of changes in shell mineralogy attributed to water temperature (Lowenstam, 1954). This mineralogical/chemical variability has also been observed in other marine invertebrates (e.g., Dodd, 1965; Moberly, 1968; Kolesar, 1978). The most pronounced effect of variable growth/precipitation rate, whether or not it is induced by ecological stress, is on non-thermodynamic distribution coefficients/fractionation factors and consequently the trace element/stable isotope composition of biogenic carbonate (e.g., Lowenstam, 1961; Rosenberg, 1980; Lorens, 1981; Turner, 1982). Although not well established, it may be possible that differences in growth rate, such as faster for algae/corals and slower for molluscs, is responsible for the observed differences in Sr contents of some biogenic aragonites. This may in part explain the wide variation of Sr observed in extant and fossil molluscan aragonite, and exhibited by their divergent distribution coefficients (Table 8-2).

Figure 8-4 is a good example of the effect of precipitation/growth rate on the partition coefficient (D) for Sr between liquid and calcite. Similar observation of growth rate control were also made by a number of researchers, but with inverse results for Cd, Mn, Co and Mg in calcite (Lorens, 1981; Kolesar, 1978). Thus,

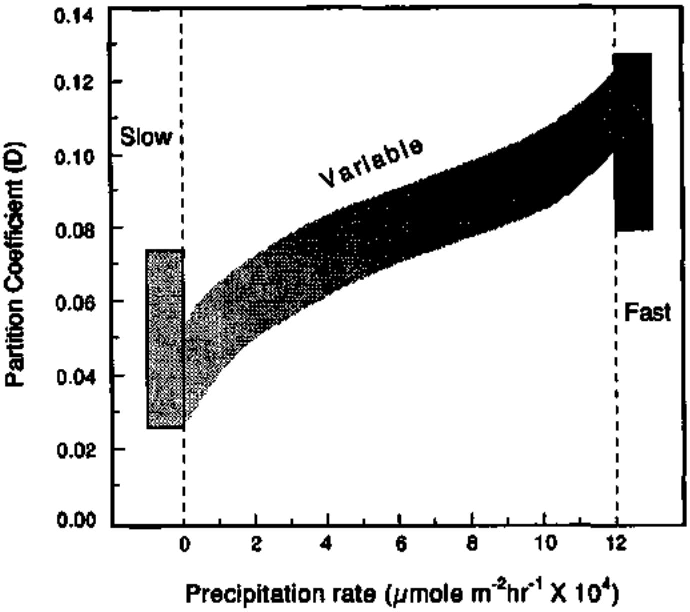

Fig. 8-4. Variation of Sr partition coefficient (*D*) with precipitation rate of calcite (Katz, 1973; Lorens, 1981; Pingitore and Eastman, 1986). Similar trends but with inverse direction have been observed for Cd, Mn, Co (Lorens, 1981) and Mg (Kolesar, 1978).

environmentally induced stress, whether extrinsic or intrinsic, must be recognized in fossil material before "realistic" and "logical" interpretations can be made and conclusions reached about the geochemistry of biogenic carbonates. The recognition of this phenomenon is still in its infancy and more studies evaluating the geochemical changes with growth rate, which are "sealed" in growth increments, are necessary for deriving truly realistic assessments of local/regional habitat/paleoenvironments and ultimately the Earth's exogenic processes and system.

Osmotic equilibrium

Osmotic equilibrium is one of the most important factors governing trace element and stable isotope incorporation into shell/skeletal carbonate (Burton, 1983; Simkiss, 1983; McConnaughey, 1989a, b). During "equilibrium" incorporation, the trace element composition or stable isotope ratio is not significantly modified by the organisms relative to that in the ambient, depositional fluid, as it moves through the various cells and body fluids (Fig. 8-5) to its permanent/temporary "storage" in the calcium carbonate shell/skeleton. Essentially, the ionic composition or proportion and osmotic pressure of the hemolymph are similar to that of the ambient seawater for many marine organisms (Burton, 1983). In this essentially isosmotic phase, ions should be passively distributed between the hemolymph and seawater. Usually this state of "Donnan equilibrium" is approached in groups such as coelenterates, echinoderms, polychaetes, bivalves, gastropods, ascidians and, possibly, brachiopods

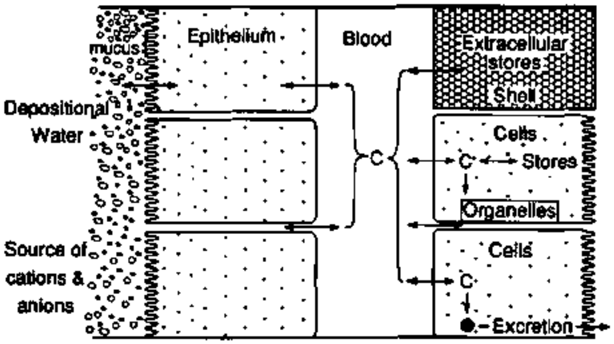

Fig. 8-5. Transportation and incorporation mechanisms of anions and cations (*C*) into the various biologic compartments of organisms (cf. Burton, 1983; Simkiss, 1983; McConnaughey, 1989a, b). Material stored in extracellular stores (exo- and endoskeletons) may be resorbed during ecdysis (e.g., trilobites).

(Nicol, 1967), whereas cephalopods and crustaceans actively regulate their ion concentration in the hemolymph. Donnan equilibrium requires that the product of diffusible cations and anions in the hemolymph (i) is equal to that in the ambient depositional water (o):

$$\mathrm{Na_i \times Cl_i = Na_o \times Cl_o}, \tag{8-18}$$

but because some of the cation is held by protein,

$$\mathrm{Na_i > Na_o} \quad \text{and} \quad \mathrm{Cl_i < Cl_o}. \tag{8-19}$$

Primitive marine animals have hemolymph ion compositions in equilibrium with seawater. The blood of higher forms, such as vertebrates, differs in its ionic proportions from expected concentrations. This ionic regulation of hemolymph composition is believed to be an expression of evolutionary processes between major groups.

In organisms from brackish marine environments, the hemolymph may not be in a steady state with seawater for Na and Mg. To this end, sodium pumps exist in freshwater organisms for active osmoregulation of Na. Although absolute concentrations may be significantly lower in the hemolymph, the ionic proportions will be similar to those of normal seawater. Under fluctuating salinity, many marine organisms especially molluscs, effectively terminate communication with the ambient seawater through shell closure. This action may lead to acidosis through anaerobic respiration, which possibly increases both the $p_{\mathrm{CO_2}}$ and leads to production of organic acids (Crenshaw and Neff, 1969). In this instance, the shell of an invertebrate is an important reservoir of alkali ions to counter the effects of acidosis (Fig. 8-5) in the following manner:

$$\mathrm{H^+ + CaCO_3 \longrightarrow Ca^{2+} + HCO_3^-} \tag{8-20}$$

In this process, Ca levels are maintained at osmotic levels in the hemolymph. Organisms inhabiting tidal environments may be subject to involuntary acidosis on a regular basis. In the case of the extinct trilobites, acidosis may have been a means to control and preserve alkali material during molting of the exoskeleton.

Deviations from expected values of Na in shells of marine and non-marine organisms may simply be an expression of the efficacy of the specific ion pump. Nutrient supply has been postulated to regulate to some degree the hemolymph composition of some gastropods (DeWith and Sminia, 1980). But terrestrial organisms, for example land snails, are not effective hemolymph osmoregulators (e.g., Riddle, 1981; Burton, 1983). Variations in body fluids may reflect decreases due to evaporation and increases due to absorption of water from food. Thus climatic conditions may greatly influence the water content of terrestrial molluscs and ultimately the chemical composition of the carbonate shell/skeleton, which may be a powerful tool in deciphering differences in environmental conditions (cf., Brand et al., 1986). To minimize the effects of body fluid loss due to evaporation, the organisms may aestivate until more hospitable conditions recur. This process is very effective in reducing water loss, and some snails have been able to survive without water for up to six years (Machin, 1975).

Osmotic equilibrium may be suppressed or enhanced by some organisms for specific cations and anions. These ions may be sequestered in the shell carbonate in proportions dictated by the ratios in the seawater and the respective partition (D) and fractionation factors (α). When this relationship breaks down, it is usually assumed that the elemental and/or isotopic composition is biologically controlled or shows the so-called vital effect. This disequilibrium may be caused by kinetic effects such as variable growth rate or metabolic processes. The metabolic effect is caused mainly by incorporation of products derived from photosynthesis and respiration into the hemolymph (e.g., Urey et al., 1951; McConnaughey, 1989a, b).

Strontium content of aragonite-secreting molluscs (marine and non-marine) is a classic example of biological fractionation. The measured Sr content is normally about 2.5 times of that expected under strictly osmotic equilibrium and seawater saturation conditions (e.g., Plummer and Busenberg, 1987). This control can be traced back to aragonitic Carboniferous molluscs, and it probably evolved in molluscs of early Paleozoic time (Brand and Morrison, 1987a). Another example of biological fractionation is the Na content of brachiopods which is greater by up to almost one order of magnitude compared to levels encountered in calcite precipitated in equilibrium with ambient seawater (e.g., Brand and Veizer, 1980). They postulated that excess Na incorporation into brachiopod shell calcite served to regulate the $MgCO_3$ composition of the calcium carbonate (cf., Bates and Brand, 1991). The elemental incorporation of Na into the calcium carbonate lattice, however, may not follow strictly diadochic substitution, but may be also located in interstitial positions (e.g., Ishikawa and Ichikuni, 1984). Similarly, carbonate-bound relationships were demonstrated for Cd and Mn in bulk carbonates and foraminifera (Span and Gaillard, 1986; Boyle, 1988).

Oxygen and carbon isotopes are subject to disequilibrium conditions in biogenic carbonates. Kinetic disequilibrium usually involves simultaneous enrichment of ^{16}O and ^{12}C in rapidly growing shells/skeletons (McConnaughey, 1989a, b). This enrichment may be by as much as one order of magnitude. Metabolic disequilibrium processes (photosynthesis and respiration) influence the $\delta^{13}C$ of shells/skeletons by raising or lowering the $\delta^{13}C$ of the organism's dissolved inorganic carbon (DIC) reservoir. Recognition of elemental and isotopic biologic disequilibrium fractionation effects in marine organisms will surely improve data recovery and interpretation of fossil material.

Redox potential

Redox effects on shell/skeletal geochemistry are mostly unresolved or in their infancy. Distributions of redox sensitive elements such as Fe and Mn common in a variety of waters may be reflected by the shell chemistry of marine and non-marine organisms. Natural environments have a wide range of redox potential (Fig. 8-6), and many of these are inhabited by organisms. Of the metals required by organisms, Mn and Fe play major roles as metaloenzymes and ion-activated enzymes in molluscs (e.g., Simkiss and Mason, 1983). Iron is intricately involved in oxygen transport in addition to anaerobic metabolism where it is supplemented by Mn, Cu, Mo, Co, and Zn. The reduction of oxygen to water produces a number of toxic intermediates, where the intervention of metal enzymes such as superoxide dismutases (Cu, Zn, Mn) and cataclases (Fe) protects cells from potential toxic effects (Fridovich, 1978). These aerobic and protective processes evolved probably in response to an increasingly oxygen-rich atmosphere.

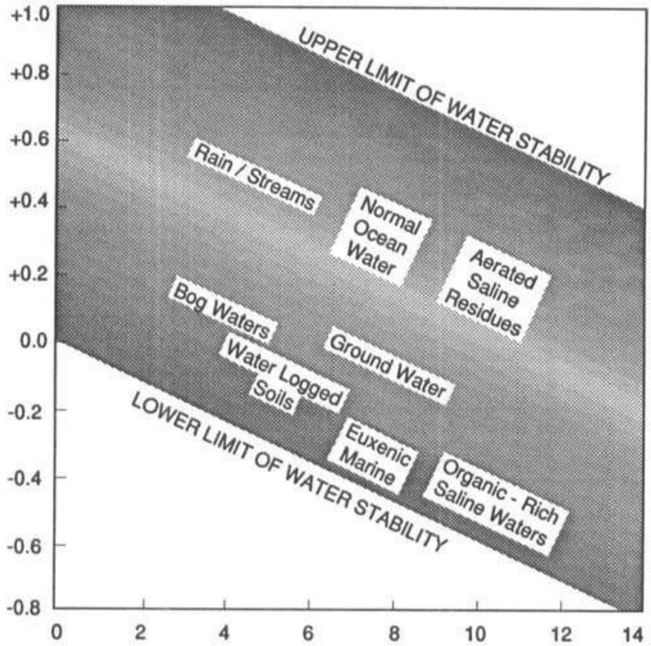

Fig. 8-6. General redox parameters of natural waters under various surface conditions. (Modified from Garrels and Christ, 1965.)

The low solubility of Mn and Fe represent considerable difficulties to uptake and transport within an organism's body. Thus many organisms have evolved storage systems to counter and balance both cellular deficiencies as well as excesses. By this definition, Fe and Mn among other metals are considered essential in the well-being of organisms, if they are (a) present in all tissues, (b) maintained at a fairly constant concentration, and (c) capable of inducing physiological abnormalities if in excess or deficient quantities. Thus, animals living in slightly dysaerobic seawater with its potential for greater solubility of Mn and Fe, may store excess quantities of these metals in their shells/skeletons out of harms way. Variations in Fe and Mn contents of marine invertebrates, therefore, may reflect biogenic feedback mechanisms to an influx of potentially toxic concentrations of metals in redox-influenced environments (Veizer, 1977; Morrison and Brand, 1986; Brand, 1987).

Overall, the solubility of calcite in aqueous solutions is further controlled/influenced by the H^+ concentration (e.g., Berner and Morse, 1974; Sjöberg and Rickard, 1984). In H^+-dependent systems, the dissolution of calcite is controlled essentially by transport mechanisms. Under aqueous conditions, which are independent of H^+ concentration, the dissolution is generally controlled by mixed kinetics (Sjöberg and Rickard, 1984). Thus, redox conditions are important both at the precipitation and postdepositional alteration stage of biogenic calcite and possibly aragonite.

DIAGENETIC CONTROLS

Diagenetic processes are so multifarious and complex that the products of these reactions are at times too difficult to interpret and relate to their original and pristine material. The difficulty becomes most apparent in recognizing early-diagenetic alteration processes in especially submodern biogenic carbonates, because depositional and diagenetic controls may be highly varied with no definitive trends and rarely be equilibrium reactions (e.g., Zolotarev, 1976; Ragland et al., 1979; Cross and Cross, 1983; Swart, 1984; Bischoff et al., 1987). However, the relative solubility of the organic mineral and anticipated water/rock ratio and hydrologic character may provide subtle but distinct signals of the alteration and its degree.

Solubility

A general principle of solubility is that an equilibrium state may exist between a liquid and a solid (carbonate mineral) so that no change takes place in the solid due to the catalytic effect of natural waters. Solubility may be enhanced by mineralogical heterogeneity and excess free energy of a specific grain, and which may be further influenced by the surface area of the particle (e.g., Flessa and Brown, 1983; Morse and Mackenzie, 1990). The reactivity of the water, and with it the solubility of carbonate grains, is also dependent on the physicochemical parameters of the fluid (e.g., Sjöberg and Rickard, 1984; Mucci et al., 1989). The solubility of calcites with varying $MgCO_3$ content under ideal conditions is presented in Fig. 8-7,

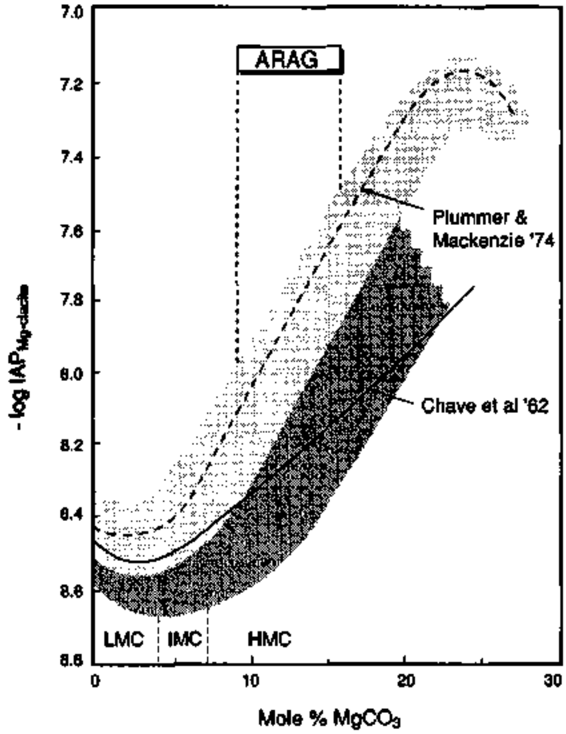

Fig. 8-7. Summary diagram of relative solubilities for low-Mg calcite (*LMC*), intermediate-Mg calcite (*IMC*), high-Mg calcite (*HMC*) and aragonite (*ARAG*). Trends and curves based, in part, on work by Plummer and Mackenzie (1974) and Chave et al. (1962).

with the determined solubility of aragonite relative to magnesian calcites. Differences in solubilities between biogenic and synthetic samples (Fig. 8-7) lies in the physical and chemical properties of these distinct carbonate species (Bischoff et al., 1987). Stability of a magnesian calcite or aragonite is usually expressed by the stoichiometric ion activity product (IAP):

$$\mathrm{IAP}_{\mathrm{CaCO_3}} = (a_{\mathrm{Ca}^{2+}})^{1-X}(a_{\mathrm{Me}^{2+}})^{X}(a_{\mathrm{CO}_3^{2-}}) \qquad (8\text{-}21)$$

where a is the activity of the ion in solution and X is the mole fraction of $MgCO_3$ or $SrCO_3$ (Me^{2+}) in the solid phase (e.g., Bischoff et al., 1987).

Textural and morphological properties may play a greater role in the dissolution kinetics of biogenic carbonate than mineralogic stability. Extensive studies have demonstrated the importance of primary porosity in dissolution kinetics and alteration processes of calcium carbonate (e.g., Martin et al., 1986). The complexities of calcite and aragonite solubilities are discussed in further detail by Morse and Mackenzie (1990).

Low-Mg calcite

Solubility of low-Mg calcite (LMC) is greatly influenced by its low Mg content, which by definition varies from 0 to 4 mol% $MgCO_3$ (Chave, 1954; Milliman, 1974). Calcite with these low Mg contents is the most resistant to dissolution, and calcium carbonate with a $MgCO_3$ content of about 1–2 mol% represents the most stable configuration at standard Earth surface conditions (Fig. 8-7). This relative mineralogical stability, however, may be greatly influenced by the particle size (e.g., Morse and Mackenzie, 1990), surface ornamentation, morphology, and porosity (primary/secondary) of the biogenic carbonate grain (Flessa and Brown, 1983; Walter and Morse, 1985). Microstructural features and layers may also influence dissolution rates of calcareous hard parts. LMC is not unique to any particular marine organisms, because its employment as a building material is widespread and was used throughout the Phanerozoic (Fig. 8-1). Relative "thermodynamic" stability of LMC is evidenced by the fact that in the same rock unit brachiopod valves may be well preserved in their pristine state, whereas molluscs may be only preserved as molds or filled by calcite spar.

Intermediate-Mg calcite

Solubility of calcite increases exponentially with increasing Mg content (Fig. 8-7). The $MgCO_3$ content of intermediate-Mg calcite varies between 4 and 7 mol%. The distinction between LMC and IMC shells/skeletons precipitated by organisms is rarely characterized by a sharp division. Few organisms except for brachiopods and trilobites, and possibly rugose corals, are recognized to precipitate all or part of their shells/skeletons of IMC (Fig. 8-1). This of course does not infer that other groups, which are less well studied, do not have representatives that deposited shells/skeletons of IMC. In rock units containing coeval specimens with LMC and IMC shells, the former are usually slightly better preserved at the microstructural and geochemical levels (Brand, 1983).

High-Mg calcite

Of all the calcite species, high-Mg calcite is the "thermodynamically" least stable of the group at Earth's surface conditions (Fig. 8-7). The $MgCO_3$ content is generally greater than 7 mol%, and the common marine groups with shells/skeletons of this mineralogy are the Echinodermata (Fig. 8-1). Fossils which precipitated originally HMC shells/skeletons show usually well preserved macrostructures, but the more delicate microstructures and mineralogy are usually altered to diagenetic low-Mg calcite, at the same time when LMC and IMC biogenic materials are still well preserved in the same rock unit (McAllister and Brand, 1989b). It is reasonable that some organisms may have highly variable $MgCO_3$ contents influenced, in part, by ambient conditions such as water temperature and/or nutrient levels. This variability has been clearly demonstrated for echinoderms and foraminifers and this may complicate their diagenetic evaluation.

Aragonite

The orthorhombic polymorph of calcite, aragonite, has a solubility that under ideal conditions overlaps with calcium carbonate of 9–15 mol% $MgCO_3$ (Fig. 8-7). Aragonite is not usually preserved in rocks older than 100,000 years, but if it is preserved then some special physical and/or chemical circumstances were active to counter the aggressive and catalytic nature of the omnipresent diagenetic fluid, water. The ravenous character of even seawater is demonstrated by the extensive erosion/dissolution that has been observed on reef carbonates. Despite the omnipotent diagenetic potential of water, primary biogenic aragonite has been documented from sedimentary units as old as Carboniferous and relics and ghost microstructures in Devonian/Silurian horizons (Stehli, 1956; Grandjean et al., 1964; Rollins et al., 1971; Brand, 1981).

Hydrologic regime(s)

Alteration of carbonate and other sedimentary minerals may proceed in the presence of the various fluids of the hydrologic cycle (Fig. 8-8). The aggressiveness of the reaction may in part be related to the calcium carbonate saturation index. All of the regimes in the hydrologic cycle depending on the water/rock ratio will impart characteristic chemical signatures on the diagenetic product. In addition to the water rock ratio, the chemistry of the diagenetic fluid and the partition coefficient will influence the degree of the alteration process. The catalytic nature of water is well established, and it has demonstrated to be further influenced by dissolved ions, compounds and complexes (e.g., Morse et al., 1980; Sjöberg and Rickard, 1985; Mucci et al., 1989).

Some distinctly different diagenetic reactions proceed in the various hydrologic settings. Commonly, cementation (hardgrounds) and alteration take place in the marine phreatic environment (Fig. 8-8). In the marine vadose (beach) environment, particles may be dissolved and/or cemented and distinct zones of consolidated beachrock/rubble/sand at or within the splash and wash zone may form. Material formed in this regime needs to be protected from the aggressive nature of even seawater. Otherwise it may fall pray to physical and chemical degradation. In the mixing zone of meteoric and marine waters, the diagenetic products are characteristically dolomite as well as other carbonate species (e.g., Hanshaw et al., 1971).

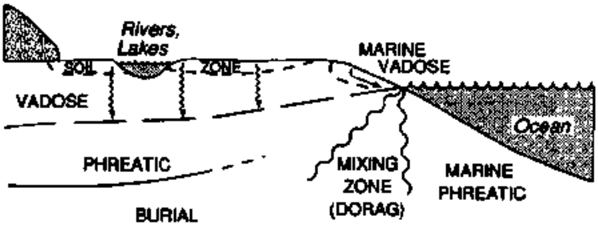

Fig. 8-8. Generalized model of hydrologic regimes and cycles. Various alteration/precipitation processes and rates are operative in the different zones.

Vadose meteoric environments, with their reactive soil horizons, may be zones of active dissolution and some alteration with characteristic geopetal cementation and sedimentation. It is believed that wholesale alteration of marine carbonates takes place in continental phreatic and burial environments; in the latter realm, dolomitization may also be a prominent process (Fig. 8-8; e.g., Taylor and Sibley, 1986). Fluids in these realms exhibit a wide range of dissolved solids, and may range from freshwater to brines, which also include formation and connate waters. Thus the precise aggressiveness of these different fluids is difficult to predict, but is certainly reflected in the wide spectrum of fabrics and chemistries observed in diagenetic carbonates and other authigenic minerals. It is highly unlikely that any particular model will ever be able to satisfactorily explain the diagenetic "pathway" of all natural carbonates. Simplification of these most complex processes, reactions and conditions, however, provides some insights considered invaluable in deciphering the diagenetic and ultimately the depositional histories of both inorganic and biogenic carbonates.

Water/rock ratio

The water/rock ratio in addition to the water chemistry and thermodynamic stability of the carbonate mineral may be the ultimate control on the degree and type of alteration of biogenic carbonates. In the absence of water, diagenetic process may be invariably slow to improbable. But in the presence of diagenetic water(s), alteration may proceed at an accelerated pace. The alteration of carbonates is defined by water and mineral(rock)-controlled end-members of the diagenetic transition series (Fig. 8-9). These end-members are also known as open, fluid-controlled and fluid-chemistry-dominated systems for the high water/rock system (Fig. 8-9). In contrast, the other end-member defined by a low water/rock ratio, is also known in the literature by closed, diffusion-controlled and rock/mineral chemistry-dominated diagenetic microenvironments with transformation taking place across a thin (messenger) water film (e.g., Pingitore, 1978; Brand and Veizer, 1980; Brand, 1990).

Alteration of carbonate minerals involves complex reaction kinetics which are difficult to factualize under Earth surface conditions (Morse, 1983). A number of mechanisms have been recognized and a typical sequence of dissolution–reprecipitation in a carbonate would involve: (1) diffusion of the reactant calcium carbonate material through a diffusion boundary layer (DBL, Fig. 8-9), (2) adsorption of the reactant material on the surface, (3) diffusion on the surface to a reactive or high-energy site such as a lattice defect, (4) reaction of the reactant material with the solid, (5) diffusion of carbonate products away from the reaction site, (6) desorption of products, and (7) diffusion of products to bulk solution regime (Fig. 8-9; Morse, 1983). The overall dissolution rate is also dependent on the surface area and morphology of the dissolving carbonate grain, and it may be further influenced by the thickness of the diffusion boundary layer which is strongly dependent on hydrodynamic conditions of the aquifer system (Fig. 8-9). At any given time one of these mechanisms will be slower than the others, and this particular process is then the rate-controlling mech-

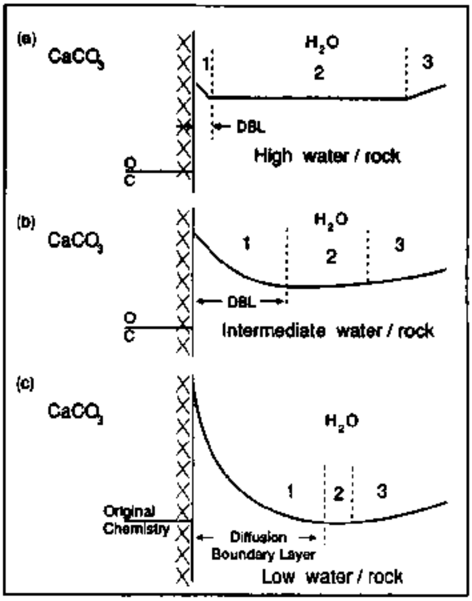

Fig. 8-9. Conceptualized models of calcium carbonate diagenesis (dissolution–reprecipitation) under various water/rock ratio systems. Initial congruent dissolution proceeds through a diffusion boundary layer (*DBL*) adjacent to the surface layer of the original carbonate. Second phase of the dissolution process involves incongruent dissolution dominated by aquifer water. Supersaturation in stage 3 leads to the eventual precipitation of diagenetic calcium carbonate from bulk solution (cf. Plummer and Mackenzie, 1974; Brand and Veizer, 1980; Pingitore and Eastman, 1989). High water/rock ratio systems are also known as fluid-controlled, open, fluid-chemistry-dominated systems. Systems of intermediate water/rock ratio are known in the literature as partly closed diagenetic microenvironments. The low water/rock system is also known as closed, diffusion-controlled and rock-mineral chemistry-dominated diagenetic environments.

anism of the diagenetic alteration process. Lastly, it is possible that surface-adsorbed inhibitors such as magnesium and phosphate, may also influence the rate of diagenetic reaction (e.g., Sjöberg, 1978; Lahann, 1978; Reddy and Wang, 1980). There are two ways in which these ions can influence the diagenetic dissolution process: (1) they can form complexes with the reaction ions and thus alter the activity coefficient, and (2) occupy high-energy lattice positions, preferred for dissolution, on the surface of the mineral grain (Morse, 1983). Holes and kinks are examples of higher potential energy sites, with more potential than plain surfaces or simple corners (Burton et al., 1951). Much less is known about the potential of other trace elements and/or organic matter on the diagenetic reaction rates (e.g., Nestaas and Terjesen, 1969; Morse, 1974). Delineating precise reaction kinetics for biogenic carbonates is fraught with problems, because natural waters are complex and naturally formed carbonates are messy. But, the process of defining first-order reactions may contribute significantly to the understanding of diagenetic processes and their products in carbonates.

High water/rock system

In the high water/rock ratio idealized diagenetic microenvironment, three distinct steps are recognized in the dissolution–repreciptation process (Fig. 8-9a). Adjacent to the dissolving carbonate, a small chemical gradient is realized which is essentially in disequilibrium with the chemistry of the solid. The hydrogeochemistry of this diffusion boundary layer in a high water/rock system is insignificant in magnitude and influence compared to that of the bulk aquifer on the $CaCO_3$ transformation. Furthermore, Plummer and Mackenzie (1974) postulated that the dissolution process at this stage is essentially congruent with active dissolution of the depositional carbonate. Only a short distance from the solid, the chemical contribution derived from the solid phase is completely amalgamated and homogenized with that of the fluid phase (bulk aquifer; e.g., Brand and Veizer, 1980), and dissolution becomes an essentially incongruent process (Fig. 8-9a). This flooding of the thin-film water system by cations and anions from the dissolving solid changes the saturation state of the fluid to the point where homogeneous as well as heterogeneous precipitation of a diagenetic phase may commence. Overall, dissolution and subsequent precipitation are greatly influenced by relative rates of calcite growth and hydraulic flow (e.g., Carlson, 1983). The third phase represents the whole-sale precipitation of $CaCO_3$ from the bulk solution of the thin-film (Fig. 8-9a), with general geochemical contents and trends characteristic of those of the bulk aquifer system (cf. Pingitore, 1978; Brand and Veizer, 1980). Precipitation at this stage is controlled by the partition coefficient, ion activity, inhibitory ions and complexes in the water, and saturation state of the diagenetic fluid. The chronospatial aspect will depend largely on flow rates within the overall diagenetic system. At low rates, precipitation may occur across an open and wide thin-film, whereas at high flow rates precipitation of the diagenetic carbonate phase may take place removed from the site of initial dissolution; thus outside the local system.

At the macroscopic level, this high water/rock alteration process is characterized by the development of first moldic and intraskeletal porosity, which may be followed by filling with fine- to coarse-grained calcite (sparite). Original microstructures are usually lost in this transformation process, and the geochemistry of the diagenetic carbonate product is almost exclusively controlled by that of the bulk aquifer water(s). In the literature, high water/rock systems are also referred to as "open" and fluid (water) controlled systems.

Intermediate water/rock system

Development of a chalky zone is a prominent characteristic of the process of alteration in intermediate water/rock systems (Pingitore, 1976). Development of a chalky appearance in fossils may be related to the early degradation of the organic tissue which coats individual cystallites, shell layers and whole carbonate shells and skeletons. In systems with intermediate water/rock characteristics, the thin-film is much reduced in width compared to that of a system with high water/rock ratio. But similarly, a chemical gradient is build up adjacent to the reaction surface of the dissolving grain, and dissolution is generally a congruent process (Fig. 8-9b). Furthermore, this stagnant diffusion boundary layer is marked by a chalky transition zone adjacent to the zone of active dissolution and thin-film mixing. Because this layer is so much more prominent in this system, more of the primary chemical and possibly macrostructural information is transmitted to and through the thin-film (2: Fig. 8-9b) to the precipitating carbonate phase; stage three of the bulk precipitation process (Fig. 8-9b). Dissolution in stage 2 may be incongruent and the supply of components from the dissolving solid may greatly influence the final composition of the diagenetic product as well as may initiate the precipitation process. Differential solubilities and relative saturation states within the thin-film fluid ensures the maintenance of the reaction as well as the continual enlargement of the space between the dissolving and precipitating phases. Microscopic intraskeletal porosity develops during this transformation process, and this space between original aragonite and diagenetic low-Mg calcite has been captured in a few partly altered specimens (e.g., Pingitore, 1976; Brand, 1989a). Recognition of a chalky appearance in fossil specimens is not always a sign of carbonate diagenesis, because colors are produced by the scattering, diffraction and interference of incoming light by the structural arrangements of the shell/skeletal crystallites (Nicol, 1967). For example, the nacreous luster of pearls is produced by light diffraction of slightly inclined regularly spaced nacreous plates. A white appearance may simply reflect the irregular nature of the chalky surface layer which diffuses the incoming light, and not the onset of diagenesis in biogenic carbonates. Color in organisms may also be produced by pigments and in this case its disappearance may be treated as the onset and sign of early diagenetic reactions involving the organic matter so prevalent in biogenic materials.

Most diagenetic processes and carbonate products exhibit characteristics typical of high to intermediate water/rock ratio alteration. Although a myriad of textures and geochemical signatures may form and be preserved within any particular rock unit, later diagenetic reactions may further complicate the end product and the geochemical signature it carries over from that of the primary carbonate grain. But normally, carbonates formed in these systems retain sufficient microstructural and geochemical information providing linkage with their precursor carbonate mineral and mineralogy. These carbonates are also referred to as products of partly closed diagenetic microenvironments.

Low water/rock system

Most important characteristic of this alteration process is the retention of essentially depositional geochemical and microstructural features and signatures of both biogenic and inorganic precursor carbonates in their diagenetic products. The classic ghost structures are excellent examples of carbonate alteration in a diagenetic system with relatively low water/rock ratio. In diffusion boundary layer-dominated thin-film microenvironments, through congruent dissolution of the solid and non- or minor mixing with the external bulk aquifer, the chemical gradient in the thin-film fluid may approach levels similar to those of the reacting $CaCO_3$ (Fig. 8-9c). A steady state is readily attained between the thin-film fluid and dissolving carbonate. This state and further dissolution of the original carbonate mineral is then controlled by the removal rate of ions from solution by the precipitating diagenetic carbonate (e.g., Carlson, 1983). Degradation of organic matter or increased packing may account for some of the 8% volume differential between biogenic aragonite and diagenetic calcite. The slight changes observed in trace element and stable isotope in diagenetic specimens, however, suggest some minor, albeit important exchange of thin-film fluid with water of the bulk aquifer. This "diffusion" influx of highly reactive bulk aquifer fluid may be sufficient to provide the necessary driving force for the reaction process.

The width of the thin-film is so minuscule that it is even difficult to identify with the scanning electron microscope (cf. Morse, 1983). In only a few instances has this thin-film been documented in fossil material (e.g., Pingitore, 1976; Brand, 1989a). In settings of unusual circumstances, thermodynamically un- and metastable, pristine carbonate minerals may be preserved. Examples are the La Brea tar pits of California or the Buckhorn asphalt deposits of southern Oklahoma. In these instances, structural and pigmentation coloration may also be preserved in the fossil material. This unique and special diagenetic system with low water/rock ratio, is also referred to as closed, diffusion-controlled and rock/mineral-controlled systems.

It has been demonstrated that the type and degree of water/rock ratio is influenced by the diffusion coefficient of each and every element/isotope (e.g., Pingitore, 1982). Thus, under similar water/rock conditions, the degree of change may vary considerably between the various elements and isotopes. In this instance, the penultimate geochemistry of the diagenetic calcium carbonate is controlled to some degree by (1) the respective diffusion coefficients, (2) the absolute geochemical contents of the solid and liquid reservoirs, and (3) the relative differences in contents between the solid and fluid reservoirs. Overall, kinetic and hydrologic factors may greatly control and influence the calcium carbonate diagenetic process and consequently the morphochemical state of the diagenetic product.

MORPHOCHEMICAL DIAGENESIS

The following sections discuss the morphological, mineralogical and geochemical changes that take place during the transformation of pristine biogenic carbonates into diagenetic low-Mg calcite in various settings and water/rock systems. Discussion is divided into the four major carbonate species encountered in carbonate-secreting marine organisms.

Aragonite–calcite transformation

In this chapter only the alteration of biogenic aragonite (ARAG) in the presence of diagenetic fluid(s) is considered, because solid-state transformation is inferred to be a geologically unimportant process (Carlson, 1983). The complexities of the reactions, fluids, products and environments are further complicated by the interaction of the allochems/diagenetic fluid(s) with the morphology, mineralogy, geochemistry of matrix components and cements present in sediments. The goal is to simplify the complexities/chaos of natural geological processes into comprehensible qualitative/quantitative reactions. A multi-method and coordinated approach is the best and maybe the only way to decipher the degree of preservation of fossil biogenic carbonates (cf. Brand and Veizer, 1980). This is particularly important, when the geochemical content is to be further used for modelling paleoecological and paleoenvironmental settings and habitats at local, regional or global levels.

Mineralogy

Changes in mineralogy of original aragonite are easily detectable in biogenic carbonates. These changes are usually accompanied by a loss of lustre and pigmentation, and a white appearance of a normally pearly shell is a good, but albeit qualitative, indication of early(?) postdepositional alteration. Transformation of original aragonite to diagenetic low-Mg calcite is easily discernable through X-ray diffraction analysis. Mineralogical change may be rapid, in which instance the original shell/skeletal aragonite will be replaced by calcite spar or be preserved as a mold. In special circumstances, a rock unit may contain material that covers the complete transition in variable amounts from all aragonite to complete replacement by diagenetic low-Mg calcite (Fig. 8-10). The degree of transformation can be traced by the shift of the 2θ angle from 26.2 to 29.4 on the diffractogram. In addition, Mg is an excellent tracer of the mineralogical aragonite–calcite transformation. Ultimately, the time and/or degree of transformation may depend in large extent on the chemical nature of the diagenetic fluid(s) and the water/rock ratio of the diagenetic microenvironment.

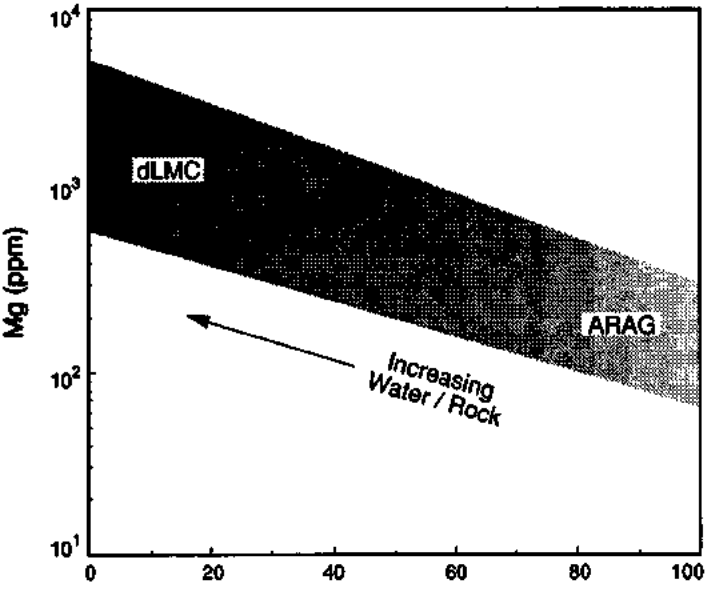

Fig. 8-10. Mineralogical transition of aragonite (*ARAG*) to diagenetic low-Mg calcite (*dLMC*). Alteration is strongly rate-dependent on the water/rock ratio (e.g., Brand, 1989a).

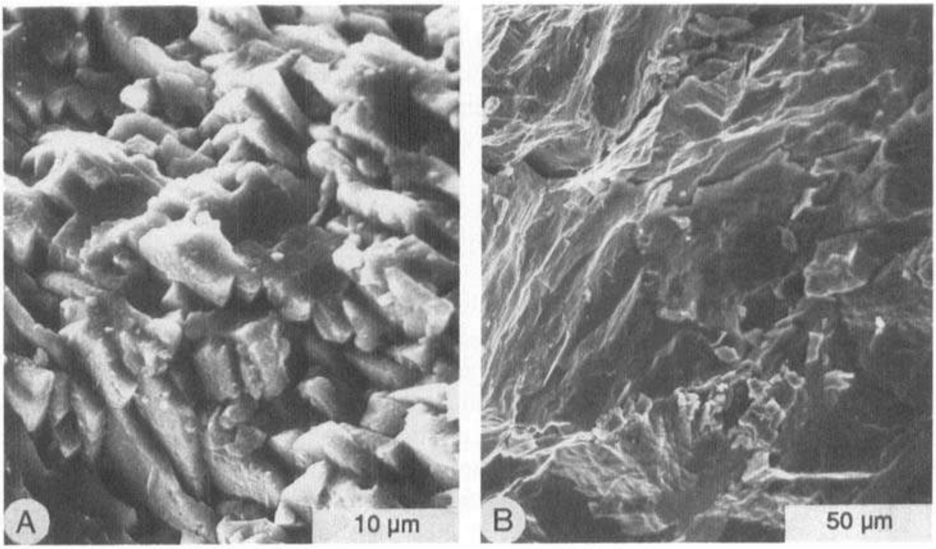

Fig. 8-11. Microstructures in biogenic aragonite. A shows nacreous tablets in a bivalve specimen from the Pennsylvanian Brush Creek Member (BC 104; Morrison et al., 1985). B is an example of calcite mosaic replacing nacre in a bivalve from the Pennsylvanian Kendrick Member (K81-15; Brand, 1981).

Microstructures

In the multi-faceted approach, microstructures and their morphological characterization are another invaluable tool in enhancing the evaluation process to delineate the degree of the aragonite–calcite transformation. Aragonite is a very common building material in many marine invertebrates (Fig. 8-1), but the structural arrangement of the individual building blocks is a myriad of different configurations (Table 8-1). These microstructural features recognized in modern specimens are used to infer an original mineralogy in extinct and extant fossil samples. Nacreous tablets (nacre) form a common microstructure in molluscs, which in all instances is either aragonite or indicative of an aragonite mineralogy precursor (Fig. 8-11A). This stacked arrangement of tablets and the other microstructures are seldom preserved in fossils older than Pleistocene. In special circumstances, fossils are preserved in their original and pristine state in sediments as old as Carboniferous (e.g., Stehli, 1956; Brand, 1989a). Filled molds are common preservation states for originally aragonitic fossils, which may preserve external morphological features but the internal microstructures are usually replaced by calcite crystals (Fig. 8-11B). This mosaic of crystallites may range from large, coarse- to fine-grained anhedral diagenetic low-Mg calcite. Preservation of "ghost structures" of the original microstructures and layers depends to a large degree on the water/rock ratio of the diagenetic system. Specimens altered in systems with large ratio seldom retain any microstructural information of the precursor carbonate mineral. Specimens which were subjected to diagenetic systems with low water/rock ratio, however, may contain relics or ghost structures of the primary building blocks and their structural arrangement (Rollins et al., 1971, fig. 3).

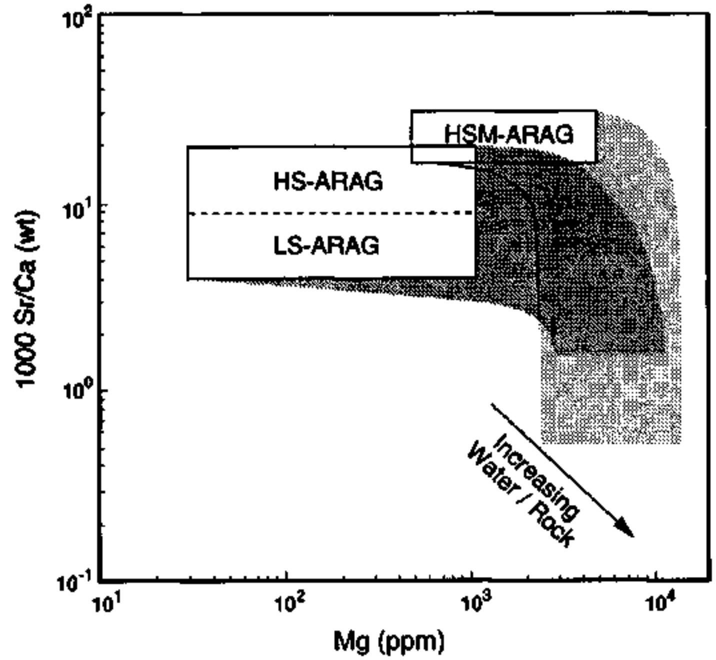

Fig. 8-12. Postdepositional alteration trends of Sr and Mg in biogenic and inorganic aragonite. Three geochemically distinct aragonites are recognized with disparate diagenetic trends. Biogenic aragonites fall into low-Sr and high-Sr with mutually low-Mg content categories. Inorganic aragonites tend to be high in both Sr and Mg relative to biogenic ones.

Elemental geochemistry

Changes in elemental geochemistry usually complement those documented by the mineralogy and microstructures (Figs. 8-10, 8-11, 8-12). Shell/skeletal chemistry of biogenic aragonite falls into distinct fields apart from that for non-biogenic (algal?) aragonite (Fig. 8-12). Subtle changes in biogenic aragonite Sr are accompanied by more extensive ones in the Mg contents with postdepositional alteration. The penultimate contents of the diagenetic low-Mg calcite are controlled by that of the original aragonite, the chemistry of the intervening diagenetic fluid(s), and the water/rock ratio of the diagenetic system. The rate-limiting process in low water/rock systems is generally the original mineralogy, whereas in high water/rock systems the water is usually the controlling factor of the degree of alteration and contents of the diagenetic product (Pingitore, 1976; Brand and Veizer, 1980; Carlson, 1983; Brand, 1989a). Remnants of original nacre may be "trapped" in a mass of calcite, and the space between the aragonite–calcite interphase has been related to the size of the diagenetic front (zones 1 and 2; Fig. 8-9) and ultimately to the magnitude of the water/rock ratio of the system (Pingitore, 1976, 1978; Brand, 1989a). Aragonite altered in systems with low water/rock ratio, may preserve ghost structures without mineralogical preservation, but may have elemental contents closely resembling those of the precursor carbonate. In contrast, aragonite subject to high water/rock

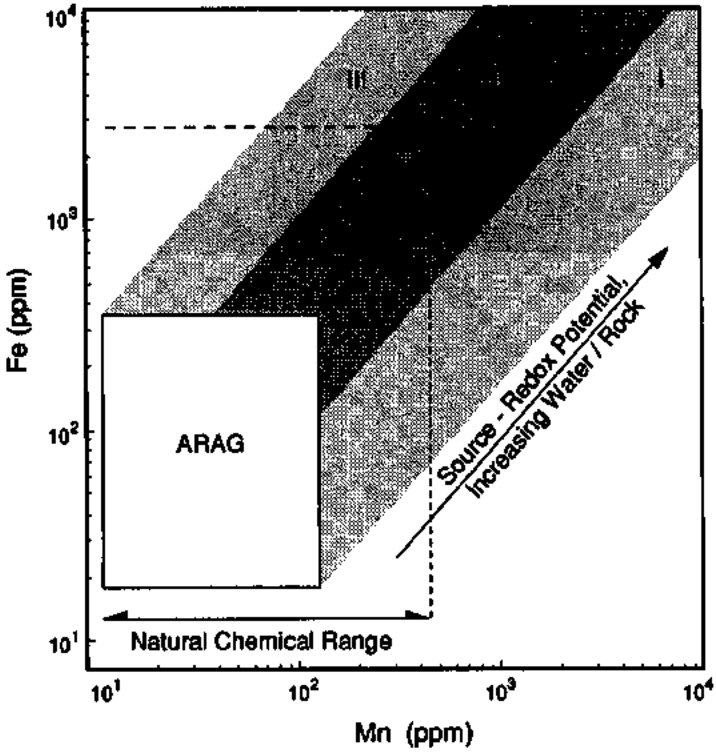

Fig. 8-13. Postdepositional alteration trends of Fe and Mn in biogenic and inorganic aragonite (*ARAG*). Variations in source and redox potentials of fluid(s) control the Fe and Mn contents as depicted in the trends (*I–III*) of the postdepositional alteration. In conjunction with water/rock ratio, the redox potential ultimately controls the content of the diagenetic product. The white field outlines Fe and Mn contents usually encountered in aerobic conditions, but under dysaerobia the field expands to the "Natural Chemical Range" in depositional carbonates (cf. Veizer, 1977; Morrison et al., 1985; Brand, 1987).

ratios during alteration usually shows a lack of mineralogical, microstructural and elemental geochemistry association with the original material. In this instance, the catalytic reactivity and composition of the diagenetic water controls to a large extent the morphochemical nature of the diagenetic low-Mg calcite. High-Sr/Mg aragonite (HSM-ARAG) follows similar trends and behavior during interaction with diagenetic fluids as do LS and HS-ARAG (Fig. 8-12). Although in the case of HSM-ARAG, the change in Sr is more drastic and extensive than expected for Mg during postdepositional alteration in comparison to trends of Sr and Mg encountered in LS and HS-ARAG. The invariant geochemical trends may be related to differences in original chemistry and grain size of the various aragonite species.

Additional information about depositional and diagenetic conditions and processes can be gleaned from other trace element analyses of carbonate minerals. In particular, Mn and Fe are very sensitive and most useful indicators of redox and source potential of the ambient waters from the depositional through the diagenetic phase (Fig. 8-13). Depositional aragonites fall into two regimes. One defines the oceanic realm with waters of normal oxygen conditions, whereas the second reflects oxygen-minimum zones and dysaerobic conditions in both oceanic, shelf and epeiric seas. The source potential strongly controls the diagenetic trend(s) for Mn and Fe, with the water/rock ratio being the rate-limiting step of the diagenetic product. From the geochemical data, it is possible to identify three distinct trends (Fig. 8-13). Thus, a coordinated multi-method of studying the geochemical content of carbonate minerals is a very powerful tool for evaluating both depositional and diagenetic processes.

Isotope geochemistry

Isotope analyses are rapidly becoming an accepted tool in diagenetic process evaluation and identification. But to do so at the expense or deletion of the other evaluation methods may lead to conclusions that are subject to misinterpretation. The distribution and composition of $\delta^{13}C$ and $\delta^{18}O$ in carbonates are a complex myriad of a number of interactive depositional and diagenetic processes (Fig. 8-14). The field of "Normal Seawater" represents modern carbonates precipitated in isotopic equilibrium and thus reflecting ambient water conditions (cf. Lowenstam, 1961; Milliman, 1974; Brand and Veizer, 1981). In the case of geological samples a strong potential for secular variation exists for material older than Carboniferous

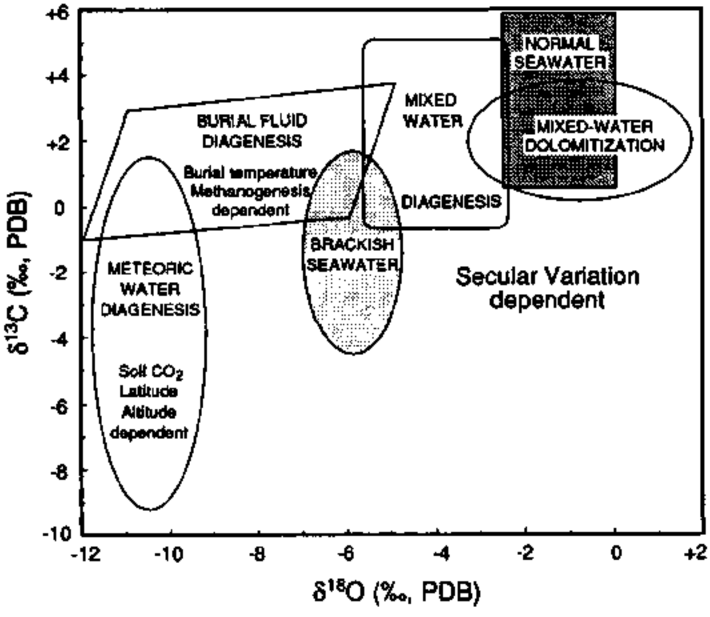

Fig. 8-14. Isotopic distribution in depositional and diagenetic carbonates. The field for normal seawater is based on data of modern carbonates. Isotopic compositions of carbonates precipitated/altered in seawater (normal to brackish) and mixed water (seawater–meteoric water) are dependent on secular/regional/local variations in oceanic/continental waters.

(e.g., Brand and Veizer, 1981; Popp et al., 1986b; Veizer et al., 1986; Hudson and Anderson, 1989). But there is increasing evidence that secular variation of seawater carbon and oxygen isotopes may not be a dominant influence for late Paleozoic carbonates (e.g.; Karhu and Epstein, 1986; Brand, 1990), and there is insufficient data to comment on the seawater composition of early Paleozoic marine carbonates. Despite this apparent paradox, it is possible to define both normal and brackish marine regimes based on the isotopic and elemental composition of carbonates (Fig. 8-14). Furthermore, it is possible to isolate isotopic compositions that are characteristic of mixed-water, burial fluid and meteoric water diagenesis in diagenetic products of the aragonite–calcite transformation process. A number of possible modifiers to the isotopic compositions of carbonates are listed within the respective fields. Results may not always be so equivocal and distinct, instead the norm is usually reflected by complete transition series and diffusive trends because the role of the water/rock ratio and the original mineralogy must be considered as rate-limiting step(s).

Another tool in the evaluation of diagenetic alteration are Sr isotopes. Their importance to depositional processes is without doubt one of the great advances of carbonate geochemistry (Peterman et al., 1970; Burke et al., 1982). But even Sr isotope compositions are subject to redistribution during diagenesis of marine carbonates (e.g., Brand, 1991). Magnitude of the redistribution is dependent on the type of water and the water/rock ratio involved in the transformation process(es) (Fig. 8-15). Furthermore these trends must be time dependent, although this concept remains untested because of lack of data, and should be influenced by the secular variation of seawater $^{87}Sr/^{86}Sr$ with geologic time. The trends of Fig. 8-15 are currently applicable to Pennsylvanian–Mississippian carbonates. Whether or not these trends are appropriate to carbonates of other time periods is uncertain now. In any case, the study of Sr isotopes has important implications for defining further the paleohydrology of diagenetic systems as well as significant connotations in evaluating the fluxes and reservoirs of the sedimentary exogenic cycle. Use of other isotopes, such as U and Pb, are in their infancy as tracers of diagenetic processes in marine and non-marine carbonates (e.g., Smith et al., 1991). These may lead eventually to data and results that can not only identify the paleohydrology of the system but also the chronology of the reaction(s).

High-Mg calcite–calcite transformation

Magnesium calcites are subdivided according to their Mg contents into high-Mg calcite (HMC), intermediate-Mg calcite (IMC) and low-Mg calcite (LMC). These carbonates will be discussed in sequence following their relative metastability (Fig. 8-7). Similar to the aragonite–calcite transformation, the alteration of magnesium calcites also proceeds in the presence of catalytic diagenetic fluid(s). Despite the similar solubilities between ARAG and HMC, the diagenetic products usually have many dissimilar morphochemical characteristics. Only in units with the highest water/rock ratio will the chemistry of the various carbonate grains approach diagenetic unity (Brand and Veizer, 1980, 1981).

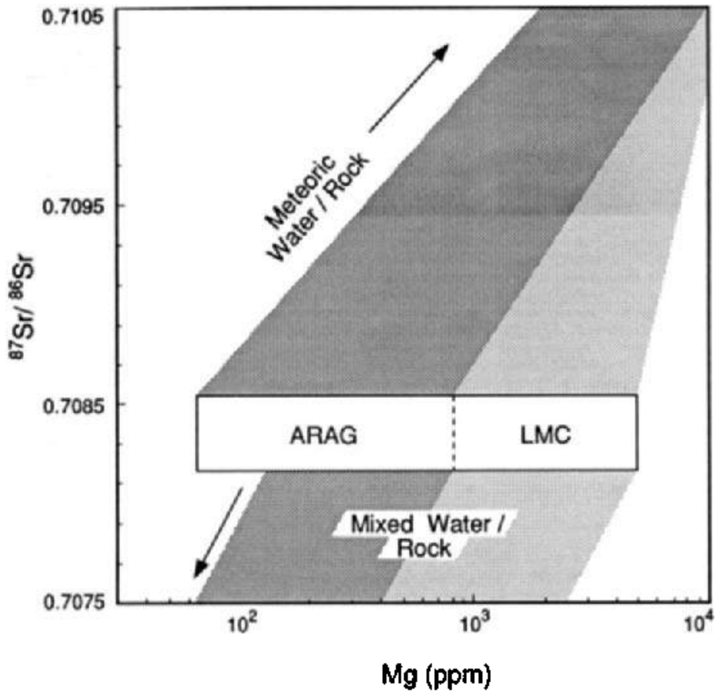

Fig. 8-15. Postdepositional alteration trends of $^{87}Sr/^{86}Sr$ in biogenic aragonite (*ARAG*) and low-Mg calcite (*LMC*) in the presence of specific diagenetic fluids. (After Brand, 1991.)

Mineralogy

Only in a few instances is biogenic HMC preserved in specimens older than the Mesozoic (Richter, 1974) and is defined to originally have $MgCO_3$ content greater than 7 mol%. Often, aragonite allochems are found in the same unit in conjunction with Mg calcite fossils. The oldest well-preserved material is represented by the echinoderm spines from the Buckhorn asphalt pits of southern Oklahoma (Blake et al., 1982), the Kendrick beds of Kentucky (Brand, 1981), and the Brush Creek of Pennsylvania (Brand and Morrison, 1987b). Despite these occurrences, preservation of echinodermal and crinoidal material is rare because of the open-mesh (stroma) nature of the skeletal material. The stroma is generally rapidly filled by diagenetic syntaxial cements after death and disarticulation of the organism, which distorts mineralogical examinations and tests. Mineralogical alteration of the stereom and filling of the stroma, whether it occurs in a system with low or high water/rock ratio, is a rapid process with little evidence of the original phase retained by the diagenetic product.

Microstructures

Mineralogical preservation is usually accompanied by microstructural preservation. Specimens from the above-mentioned localities show the typical open stereom–

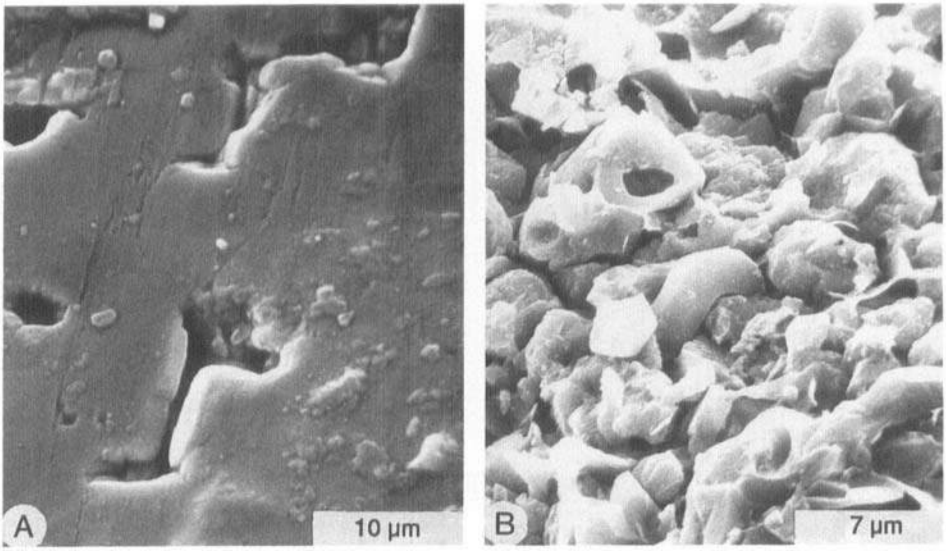

Fig. 8-16. Microstructures in biogenic high-Mg calcite. A shows partial preservation of stereom space in a crinoid columnal (Bangor Limestone; Brand, 1990). B shows the extensive recrystallization and filling of the stereom and stroma by diagenetic calcite (Naco Formation; Brand, 1990).

stroma arrangement found in their modern counterparts (e.g., Neugebauer, 1978; Brand, 1981; Blake et al., 1982; Brand and Morrison, 1987b, fig. 2). The organic matter occupying the stromal space is rapidly oxidized and consumed by bacteria on the seafloor, with equally geologically rapid occlusion of the generated pore space by diagenetic cement (Fig. 8-16). The occlusion may range from partial to complete and in all instances consists of syntaxial calcite cement. Neugebauer (1979) observed two modes of calcite cement growth in echinoderms from the Pleistocene of Greece. Growth of tooth cement (model b, Fig. 8-17) commences in numerous individual places mitigated by possible construction flaws in the stereom calcite surface. Individual cement crystals grow slowly and continue with the typical *c*-axis alignment of stereom polycrystalline calcite (Towe, 1967). The cement growth model proposed in (b) (Fig. 8-17) proceeds in the absence of construction flaws, but generates multiple steps and corners in the early growth stages. With continued precipitation of cement, the number of these steps and corners are reduced until all the pore space is filled by syntaxial calcite. Neugebauer (1979) further concluded that extensive external cementation of ossicles proceeds only after microstructural occlusion of internal pore space (stroma) is almost complete. During the cementation of the stroma and concomitant Mg reduction of stereom calcite, some of the liberated Mg may be utilized in the construction of the microdolomite crystals found in crinoidal/echinodermal skeletal fragments (Richter, 1974; Lohmann and Meyers, 1977). Generally, internal pore space of crinoidal/echinodermal material is represented by homogeneous (Fig. 8-16A) or mottled (Fig. 8-16B) syntaxial cement, which may have its origin in the facet and tooth growth models of Neugebauer (1979).

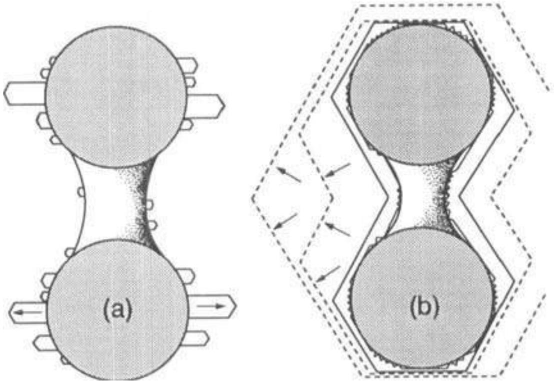

Fig. 8-17. Conceptualized models of syntaxial cement development on biogenic high-Mg calcite. Model (a) refers to the growth of "tooth" (zahn) cement, whereas model (b) applies to the growth of facet cement on stereom echinodermal calcite. (Modified from Neugebauer, 1979.)

Elemental geochemistry

The rapid destruction, occlusion by tooth-facet cement, of stromal pore space can also be documented geochemically. During the alteration of the stereom and concomitant cementation of the stroma, the overall Sr and Mg contents of relatively well-preserved specimens may strongly reflect that of the original high-Mg calcite skeletal material (Fig. 8-18). But despite this generally small degree of Sr and Mg degradation, the loss of Na from the structure is larger by several orders of magnitude (e.g., Brand, 1990). Brand ascribed this Na decrease to biogenic decomposition of organic tissue and fluids from the skeletal material during early diagenesis shortly after death of the organism. Subsequent changes in Na with postdepositional alteration are then more in line with the trends depicted for the other trace elements (Fig. 8-18). The ultimate geochemical composition of the diagenetic product is dictated mostly by the water/rock ratio of the diagenetic system (cf. Brand and Veizer, 1980; Brand, 1990). But, data from individual populations tend to form single clusters distinct from specimens within the unit but from other localities, as well as from other units. This "stepwise" alteration of crinoidal/echinodermal HMC leads to the concomitant decrease of Sr, Mg and Na in progressively more altered specimens.

The geochemical trend for Mn and Fe in crinoidal/echinodermal HMC is more complicated than that for the other diagenetic tracers. Depending on the source and redox potential of both the depositional and diagenetic fluids, the Mn and Fe elemental content of the diagenetic product may either show decreases or increases with progressive alteration (Fig. 8-19). Of course, as is the case with all other carbonate transformations, the water/rock ratio ultimately controls the magnitude of the elemental changes, but the redox and source potentials control the direction of the elemental redistribution. Their metastable configuration encourages rapid alteration and cementation. Thus, biogenic HMC material should be most useful in depicting and identifying diagenetic processes under various hydrologic conditions.

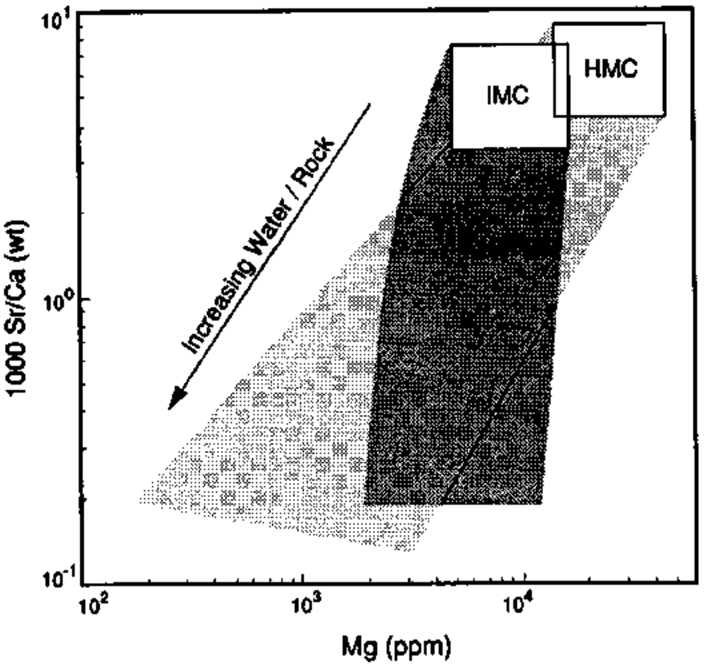

Fig. 8-18. Postdepositional alteration trends of Sr and Mg in biogenic high-Mg (*HMC*) and intermediate-Mg calcites (*IMC*). The degree of alteration is strongly dependent on the water/rock ratio and the catalytic aggressiveness of the diagenetic fluid (cf. Brand, 1990).

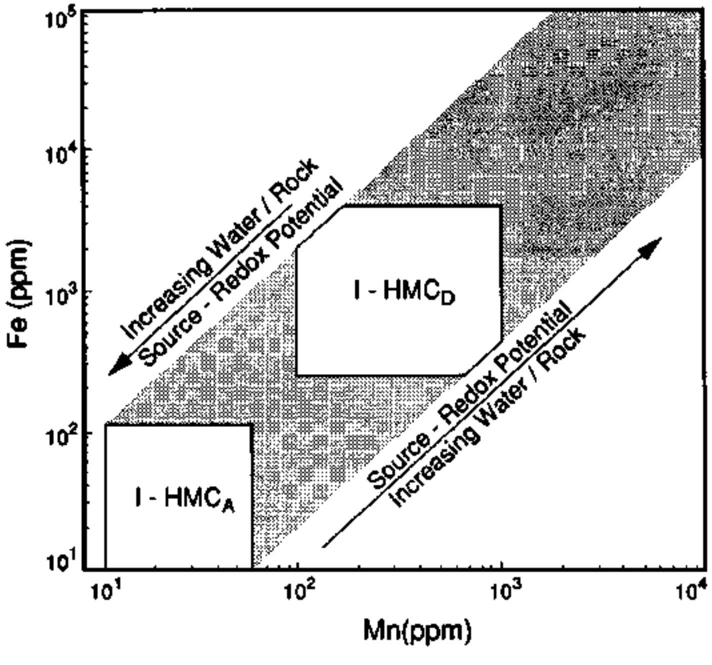

Isotope geochemistry

Isotopic compositions and redistribution of originally HMC biogenic material with postdepositional alteration are more difficult to interpret because crinoids/echinoderms as a group metabolically modify their skeletal isotopic ratios (Weber, 1968). This intrinsic modification of the isotopic compositions makes it a most difficult task to set a reference value or range for their $\delta^{13}C$ and $\delta^{18}O$ values in unaltered specimens (Fig. 8-14). Although difficult, it is not impossible to use the complement of trace element and isotope data to postulate on the hydrologic conditions and parameters that were responsible for the alteration process of biogenic HMC material (cf. Brand, 1990).

A comprehensive study of experimental morphochemical alteration of biogenic high-Mg calcite was carried out by Turner et al. (1986). Dissolution of the HMC was mostly homogeneous and congruent. Isotopic and elemental shifts in the echinoderm material were small, and possibly controlled by the texture of the exoskeleton. In natural systems, the water/rock ratio and isotopic composition of the ambient water influenced by a number of extrinsic factors control the ultimate isotopic composition of the diagenetic end products.

Intermediate-Mg calcite–calcite transformation

Intermediate-Mg calcite is not readily recognized or identified in the scientific literature. But a number of important fossil groups apparently secreted shells/skeletons with Mg contents in between those recognized in low-Mg calcite brachiopods and high-Mg calcite echinoderms (Fig. 8-1). Thus their increasing importance in geochemical work requires a discussion of observations and results separate from the other calcite species.

Mineralogy

Intermediate-Mg calcite shells/skeletons contain about 4–7 mol% $MgCO_3$ (Milliman, 1974; Morrison and Brand, 1986). Previously, biogenic specimens with such levels of Mg were deemed to have undergone some alteration from a postulated originally HMC mineralogy. Extensive studies, however, have demonstrated that a number of fossil groups originally secreted skeletons of intermediate-Mg calcite, such as the rugose corals and trilobites (e.g., Brand and Veizer, 1980; Brand, 1981; McAllister and Brand, 1989a, b). Wilmot and Fallick (1989) inferred an original low-Mg calcite mineralogy for trilobite cuticles, and among others, Oekentorp (1980) postulated that Permian rugose corals originally possessed aragonitic skeletons (cf. Wendt, 1990). Perhaps an evolutionary transition, between the calcitic corals of the early Phanerozoic and the aragonitic ones of the late Phanerozoic, is represented by the Permian rugose corals. Oekentorp (1980) presented an excellent discussion

Fig. 8-19. Postdepositional alteration trends of Fe and Mn in biogenic high-Mg (*HMC*) and intermediate-Mg calcites (*IMC*). The redox potential and chemistry of depositional/diagenetic fluid(s) strongly influences the original (A = aerobic, D = dysaerobic) contents and ultimate trends and compositions of the diagenetic reaction/calcite (cf. Brand, 1983, 1990).

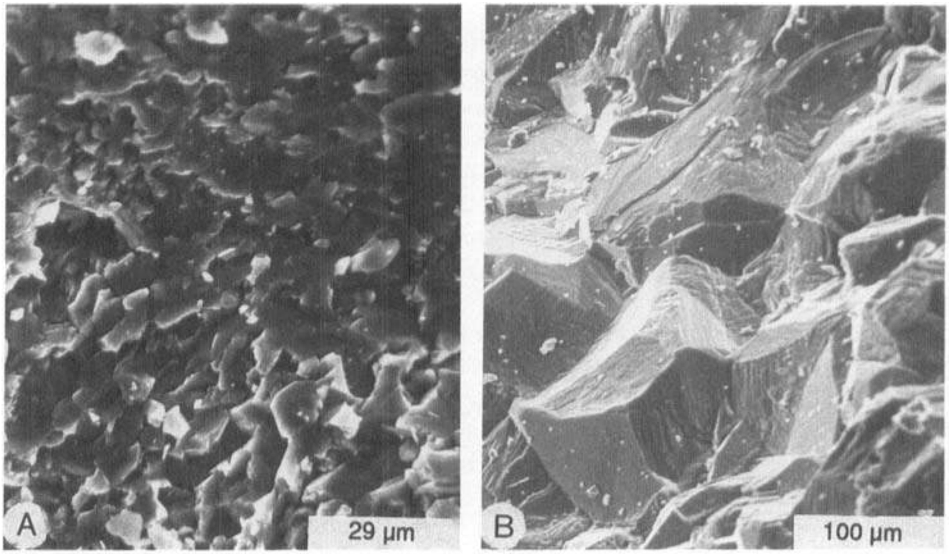

Fig. 8-20. Microstructures in biogenic intermediate-Mg calcite. A shows the trabecular fibers in a rugose coral (Shawnee Group). B shows diagenetic calcite mosaic replacement of original septal fibers and intermediate-Mg calcite (Sausbee Formation; Brand, 1990).

of the original mineralogy controversy for rugose corals. More incisive studies are needed to resolve the interesting dichotomy in the postulated original mineralogy for trilobites and rugose corals.

Microstructures

Rugose corals older than Permian have trabecular microstructures typical of a pristine calcian mineralogy (Fig. 8-20A). For a detailed discussion of microstructures in rugose corals and their original mineralogy one may consult Kato (1963), Sorauf (1971) and Oekentorp (1980). Intermediate-Mg calcite, being metastable (Fig. 8-7) eventually alters to diagenetic low-Mg calcite in the presence of catalytic fluids, and the trabecular crystals are transformed into larger calcite grains (Fig. 8-20B). Another group of marine invertebrates with postulated IMC exoskeletons are the trilobites. Primary and diagenetic microstructures in trilobites are quite complex and beyond the scope of this review, but are fully discussed by McAllister and Brand (1989a) and Wilmot (1990). However, the generally better preservation of microstructures in coeval brachiopod shells, but worse microstructural conditions for coeval crinoid columnals, argues for an originally intermediate-Mg calcite mineralogy for trilobite cuticles (McAllister and Brand, 1989b).

Elemental geochemistry

The elemental geochemistry is governed largely by the mineralogy and, consequently, Sr and Mg contents of intermediate-Mg calcites are between those encountered in HMC and LMC. Thus, the fields defining the original chemistry are distinct for IMC and HMC (Fig. 8-18). Furthermore, the diagenetic trends of the reaction pathways for Mg are significantly different for the two mineral species. Biogenic HMC loses its Mg content much faster than IMC during postdepositional alteration; proportional to their original compositions (Fig. 8-18). Thus, diagenetic products of high water/rock ratio for IMC will have retained more of their original geochemistry than coeval biogenic HMC. Differentiation between the two calcite phases is especially difficult during alteration in diagenetic systems with low to intermediate water/rock ratios. But with careful evaluation of all available parameters it should be possible to differentiate between the various calcite species and the degree/magnitude of postdepositional alteration.

Manganese and Fe trends with diagenesis of IMC and HMC are essentially indistinguishable (Fig. 8-19). This may hamper identification of the original calcite mineralogy, but is invaluable in assessing the redox and source potentials of both the depositional and diagenetic fluids. Depending on the original parameters, Mn and Fe contents may either increase or decrease during the alteration process. Ultimate composition of the diagenetic carbonate phase is then dependent on the "potential" and water/rock ratio of the catalytic reaction system. At the same time it is possible in conjunction with other morphochemical evidence to assess the ratio of the diagenetic water/rock system and degree of alteration.

Isotope geochemistry

The stable isotope data derived from intermediate-Mg calcites are usually very distinct from that of biogenic low- and high-Mg calcites (cf. McAllister and Brand, 1989b). The enhanced metastability of IMC subjects this material to greater alteration than LMC. Thus more material has to be evaluated to find suitably and sufficiently well-preserved samples for evaluation of paleoenvironmental conditions. Although, the database is rapidly expanding, more results are required to bring it to the level of confidence currently applicable to brachiopod low-Mg calcite. This is particularly important before depositional interpretations are attempted based only on isotope data of populations of biogenic IMC, such as trilobites, without corroborating support from that of biogenic LMC.

Low-Mg calcite–calcite transformation

It is generally believed that low-Mg calcite is relatively resistant to diagenetic processes active under Earth surface pressure and temperature conditions, and even in the presence of diagenetically reactive fluids. Low-Mg calcite as building material is widespread in the animal kingdom and the most important invertebrates using LMC in construction of their shell/skeleton are the brachiopods (Fig. 8-1). They, as a group except for few genera precipitating phosphatic shells (Fig. 8-2), have built LMC shells throughout their known geologic history. Despite their acclaim to producing a shell most resistant to diagenetic alteration than any other organism, postdepositional effects have been documented in ancient (e.g., Al-Aasm and Veizer, 1982) and modern brachiopod shells (e.g., Brand and Logan, 1991) by a variety of fluids in various settings.

Mineralogy

The mineralogical transition from low-Mg calcite to diagenetic low-Mg calcite is difficult to ascertain using standard X-ray diffraction techniques. Generally, LMC contains less than 4 mol% $MgCO_3$, with modern brachiopod LMC averaging about 4010 ppm Mg (600–18,000 ppm; Brand and Logan, 1991). Proton nuclear magnetic resonance spectrometry may solve the dilemma of original mineral resolution for LMC, but the availability of the other methods does not justify the use of this complex method for mineralogy identification. Another tool, cathode luminescence may not be as reliable as previously thought in identifying pristine biogenic LMC (Barbin et al., 1991). Luminescence patterns may be hampered by growth banding and zoning in biogenic material, and depending on the redox/source potential of the diagenetic fluids luminescence of diagenetic phases may be the inverse of expected trends (Brophy et al., in prep.). This reinforces the assertion that using singular methods for identifying transformed calcium carbonate is fraught with difficulty. Instead, whenever possible a coordinated multi-method approach is the only reliable tool for identifying pristine carbonate material.

Microstructures

Inasmuch as mineralogical determinations are of little help in defining unaltered material, microstructural evaluations take on a greater prominence in selecting pristine brachiopod material. Post-mortem degradation and alteration of brachiopod shells is rapid under normal environmental conditions (Emig, 1990). Degradation of organic matrix, shell softening (maceration), and structural disaggregation occurs in articulated brachiopods with two calcite layers within seven months. Species with three or more calcite layers are only slightly more resistant to disaggregation (Emig, 1990) and, thus, are poor sediment contributors. Preservation of brachiopods in rock units, therefore, infers burial process that must have been faster than a few months and as such are geologically instantaneous for the many brachiopods found throughout the geologic column.

Good success of obtaining pristine specimens is attained by detailed evaluation of microstructures within the shell/skeleton of the two major and important groups of LMC-secreting fossils. Excellent preserved calcite fibers have been recognized in brachiopods as old as Cambrian (Wadleigh and Veizer, 1990). The primary prismatic layer is seldom preserved in Paleozoic specimens or removed by the researcher to limit incorporation of diagenetic geochemical signals into the database. In contrast, the bladed and keeled fibers of the secondary layer(s) are commonly well preserved in Phanerozoic brachiopods (Fig. 8-21A). Despite the general resistance of biogenic LMC to the catalytic action of diagenetic fluids, brachiopod and belemnite shells/skeletons may undergo subtle changes in specimens as young as modern. Depending on the water/rock ratio of the diagenetic system and the overall aggressiveness of the fluid, biogenic LMC may be dissolved out and even be replaced by calcite spar (Fig. 8-21B). Dissolution features are common in belemnites and brachiopods, however, if the vug/void space is not occluded by diagenetic calcite, the remainder of the specimen is still suitable for geochemical study and subsequent evaluation. The relatively fragile nature of brachiopod shells and their susceptibility to rapid

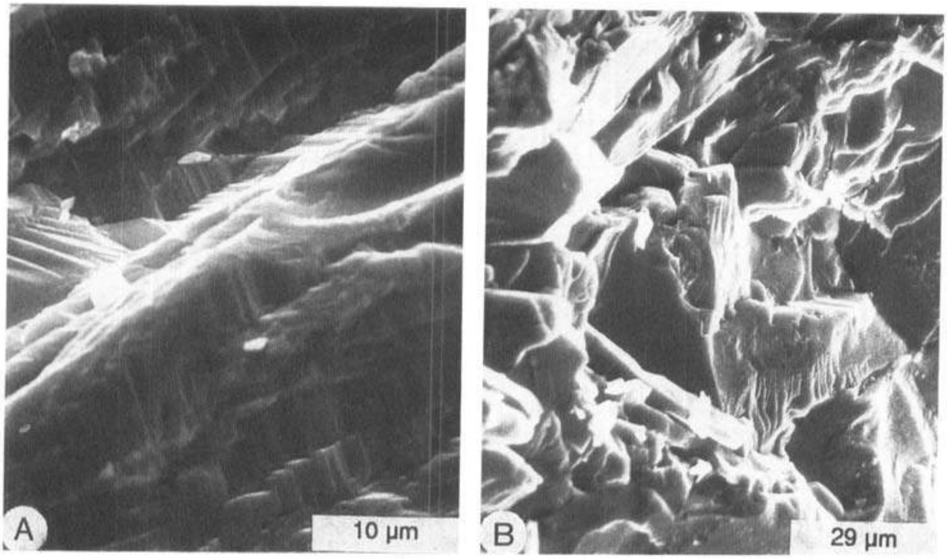

Fig. 8-21. Microstructures in biogenic low-Mg calcite. A shows pristine prismatic, keeled fibers in the secondary layer of brachiopods (Bangor Limestone; Brand, 1989b). B shows extensive dissolution and alteration of primary microstructural fibers (Merriton Formation; Bates, 1990).

disaggregation, thus makes any fossils found in submodern units and those as old as Cambrian probably the most important tool for paleoceanographic studies.

Elemental geochemistry

Once it was believed that no biogenic carbonate species preserved their original mineralogy and geochemistry. This concept of omnipotent diagenesis was gradually challenged, and over the past decade was replaced by the concept of potential preservation in the absence of diagenetic fluid(s). It was recognized that low-Mg calcite of brachiopods was relatively stable under most surface conditions. This universal concept of diagenetic inviolability for LMC has been challenged, and both physical and geochemical evidence has proven the potential for postdepositional alteration in even this most stable of carbonate species under specific conditions (Al-Aasm and Veizer, 1982; Brand and Logan, 1991). This, however, has not changed the importance of brachiopod and belemnite LMC geochemistry as an indicator of paleoceanographic evolution.

Geochemically, pristine brachiopod calcite can be subdivided into two subspecies of low-Sr with variable Mg LMC and high-Sr and Mg LMC (Fig. 8-22; Brand and Logan, 1991). The transition between the two is diffuse in modern brachiopods and not well defined in fossil material. Thus, this geochemical–mineralogical distinction in modern and fossil brachiopods needs to be studied further for its possibly important paleoecological potential.

Despite the alteration of even LMC in the presence of catalytic and aggressive diagenetic fluids, biogenic LMC remains one of the most important and significant

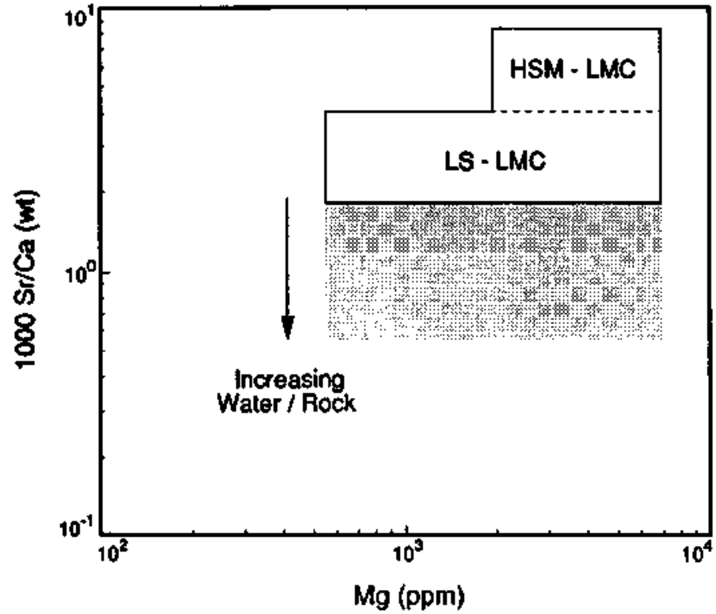

Fig. 8-22. Postdepositional alteration trends of Sr and Mg in biogenic low-Mg calcite (*LMC*). The Sr content is significantly altered during diagenesis with only minimal changes in Mg content. Original shell chemistry of brachiopods falls into two geochemical fields of low-Mg calcite; *1* = low Sr and low–high Mg (*LS-LMC*); *2* = high Sr and Mg (*HSM-LMC*; Brand and Logan, 1991).

ingredients for unravelling the paleoenvironmental/ecological systems and fluxes of the Earth's exogenic cycle. Within this context, it is of utmost importance to be able to identify the specimen/material that has been subject to minor degrees of postdepositional alteration. In conjunction with detailed microstructural examination, careful elemental analysis is able to achieve just this, and effectively identify and consequently remove this sample and specimen from further evaluations (Fig. 8-22). A loss of Sr from brachiopod shell calcite, relative to its stratigraphic and local population, is usually easily detectable in specific samples (Brand, 1981). Unlike Sr, Mg is not a diagnostic tracer of LMC diagenesis (Fig. 8-22). Only subtle differences in Mg content within populations and between unaltered and altered specimens are discernable in belemnite as well as brachiopod LMC. Manganese and Fe double as diagenetic and environmental indicators in LMC (Fig. 8-23), where the source and redox potentials have significant effect on the ultimate elemental content. Despite this complexity in elemental redistribution, it is possible to identify diagenetically altered material in conjunction with other available information to discern the water/rock ratio of the diagenetic dissolution–repreciptation process (e.g., Brand, 1983; 1989b; Popp et al., 1986a).

Isotope geochemistry

It is generally believed that brachiopods incorporate both carbon and oxygen isotopes into shell calcite in equilibrium with ambient water (e.g., Epstein et al.,

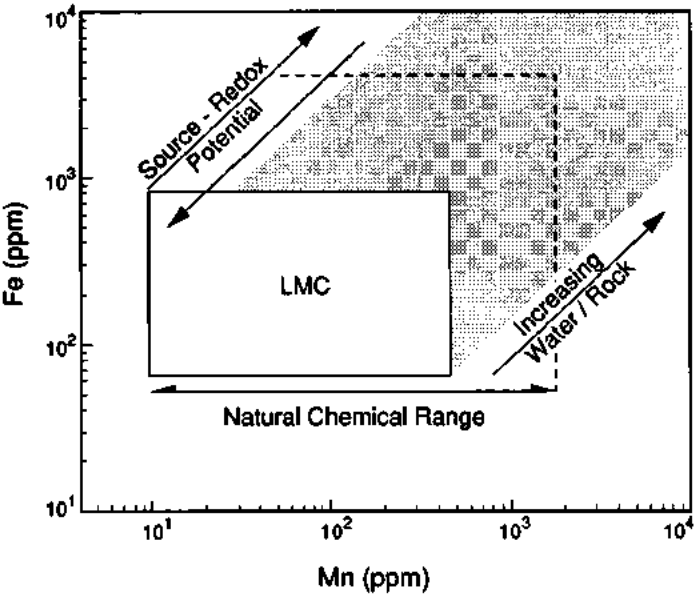

Fig. 8-23. Postdepositional alteration trends of Fe and Mn in biogenic low-Mg calcite (*LMC*). The redox potential and chemistry of depositional/diagenetic fluid(s) strongly influences the initial contents (Natural Chemical Range) and ultimate trends of the diagenetic reaction and biogenic calcite (cf. Brand, 1983, 1990).

1953; Lowenstam, 1961; Brand, 1989b). Similar observations also have been made for the isotopic composition of belemnites (e.g., Saelen and Karstang, 1989; Morrison, 1991). Thus the isotopic compositions should reflect the oxygen and temperature variations of the ambient seawater, and brachiopods and belemnites in addition to other unaltered fossil material with their pristine elemental chemistries should be extremely useful indicators/recorders of paleoenvironmental/climatic conditions and perturbations (cf. Brand, 1981; Popp et al., 1986b).

If this is the case, diagenetic changes should be discernable in brachiopod/belemnite material after careful assessment of the depositional parameters and any possible effect due to the secular variation and/or thermal evolution of seawater (Fig. 8-14; Weber, 1967; Perry,; Brand and Veizer, 1981; Karhu and Epstein, 1986; Veizer et al., 1986). Inclusion of Sr isotope systematics into the diagenetic evaluation process may prove to be highly profitable in defining the most pristine specimen (Fig. 8-15). This additional, albeit expensive tool, may be especially useful for specimens which were both deposited and subsequently altered in tropical regimes that are characterized by low elemental/isotopic gradients between the various hydrologic regimes.

Summary

Using a coordinated approach in alteration studies, allows for the sophisticated determination of the water/rock ratio and the nature of the fluid(s) involved in carbonate transformations. With the tools available to carbonate geochemists it is possible to identify pristine and altered material and derive conclusions regarding both depositional and diagenetic parameters. Not all methods, however, are equally effective and important in identifying the pristine specimen because of the varied mineralogy–morphology of the different carbonate species. A coordinated approach will yield most promising results in elucidating a most intriguing process in low-temperature sedimentary geochemistry (e.g., Reeder, 1983). Physicochemical complexity of both depositional and diagenetic realms demands that limits on possible geochemical contents and variations in morphological features be most responsive and subject to verification by independent paleontological/sedimentological data, and it requires a high degree of flexibility on part of the carbonate geochemist studying carbonate allochems.

There are four major biogenic carbonate minerals (ARAG, HMC, IMC and LMC) precipitated by organisms in construction of shells and skeletons. Many different architectural methods are used by these organisms to obtain ecologically sound "gehäuse" suitable to its specific environment. This best of plans does not provide omnipotent protection during life and especially in death from the ravenous actions of diagenetic fluids within the shallow-deep burial realms of the sedimentary column. Morphological features such as shell layering, ornamentation, porosity and individual crystal size may greatly influence the degree of ultimate postdepositional alteration. This alone is not sufficient force to drive the alteration process, but in conjunction with mineralogy, physicochemical nature of the diagenetic fluid(s) and the degree of the water/rock ratio of the diagenetic microenvironment an effective set of parameters for the transformation of any biogenic carbonate species may be built under a number of settings at Earth's surface and subsurface conditions.

Three major members of the mineralogical transformation have been identified and recognized in carbonate fossil allochems. In most instances the original and pristine material of biogenic carbonates has been transformed into a more stable variety under Earth's surface conditions. The end-product of these transformations is usually diagenetic low-Mg calcite (dLMC). Biogeochemical information about the pristine specimen within the diagenetic product is greatly dependent on the degree of alteration. Rate-limiting parameters of the postdepositional process are the original mineralogy of the pristine biogenic allochem, the physicochemical nature of the diagenetic fluid, the water/rock ratio of the diagenetic microenvironment, and thermodynamic properties of both the dissolving and precipitating carbonate phases. The slowest reaction of the catalytic alteration will be the rate-limiting step for the overall transformation process. The three members of the reaction process generally recognized are systems with low water/rock ratio (cf. closed, diffusion controlled), intermediate water/rock ratio (cf. partly closed, fluid/diffusion dominated), and high water/rock ratio (cf. open, fluid controlled).

Transformation systems with low water/rock ratios are characterized by reactions dominated by the thermodynamic properties of the dissolving calcium carbonate mineral. Thus, the mineral phase is the rate-limiting step, whereas the diagenetic fluid plays a secondary role. In this process much of the original geochemistry and microstructural features may be transmitted through the "messenger-film" to the diagenetic product. The biogenic carbonate product irrespective of original mineralogy is always diagenetic low-Mg calcite (dLMC).

Systems representing intermediate water/rock ratios are more influenced by the diagenetic fluid. For originally aragonite and high-Mg calcite allochems, the diagenetic fluid may be the rate-limiting step. In contrast, for intermediate- and low-Mg calcite the thermodynamic properties of the mineral phase probably still control the rate and extent of the transformation reaction. In this instance, some of the original geochemical content and microstructures in the form of ghost structures may be retained by the diagenetic LMC product providing strong affiliation to its precursor.

Biogenic allochems subjected to high water/rock ratios seldom contain geochemical or microstructural information indicative of the precursor carbonate specimen. This definitely applies to originally aragonite and the high- and intermediate-Mg calcites, whereas some diagnostic information may be retained by diagenetic LMC of an originally LMC mineralogy. In this transformation process the diagenetic fluid is the rate-limiting factor and imposes a strong control over the geochemistry of the diagenetic end-product. Specimens altered in these reactions usually reflect the physicochemical conditions and fluctuations of the diagenetic fluid.

REPLACEMENT DIAGENESIS

Replacement diagenesis involves the wholesale substitution of the original and diagenetic calcium carbonate by another mineral. In some instances, although the original shell/skeletal geochemistry is lost, valuable macro- and microstructural information may be retained in the replacement mineral mimicking the original features. This morphological replacement of biogenic carbonates by authigenic minerals requires that the transformation is controlled by a process intricately linked to the growth of the crystallites. Furthermore, because of the highly stable nature of some of these authigenic minerals, biogenic information may be preserved that otherwise would have been obliterated by the ravenous actions of diagenetic fluids. Four major processes dominate in replacing original carbonate phases: pyritization, silicification, phosphatization and dolomitization. These will be discussed in turn.

Pyritization

Of all the processes, pyritization of carbonate allochems is fairly well understood and the geological implications are based on a solid sedimentological–geochemical foundation. In contrast to some other replacement processes, pyrite/marcasite replaces the original calcium carbonate, fills vugs and voids or lines the original shell material. Every known fossil shell/skeleton can be potentially replaced by pyrite (cf. Brand and Morrison, 1987b).

Mineralogy

The common mineral of the pyritization process is pyrite (FeS_2) with less frequent occurrence of dimorphous marcasite. This replacement process is assumed to be a generally rapid process in which iron combines with elemental sulphur to form pyrite within 24 hours (e.g., Berner, 1964; Howarth, 1979).

Microstructures

In rare instances are the original microstructures of the carbonate allochem preserved as "ghost structures" by the pyritization process (e.g., Hudson, 1982; Brand and Morrison, 1987b). Macrostructures are usually well preserved in pyritized carbonate material. Microstructures and layers of carbonate shells/skeletons may be partially to totally disrupted by the formation of intrinsic pyrite. Four types of pyrite are encountered in carbonate allochems, one is framboidal pyrite which consists of regular spheroids that are about 1 mm in size. Another variety found in carbonates is nanopyrite, which occurs as singular euhedral crystals less than 0.5 mm in size (Fig. 8-24B). An additional type of pyrite replacing $CaCO_3$ is aggregate pyrite which consists of coalescent, irregular masses, and the last type is micropyrite which occurs as euhedral crystals about 15 to 40 μm in size (Fig. 8-24A).

Presence/absence of pyrite as an extrinsic or intrinsic component of fossil material is a diagnostic indicator of some special environmental/postdepositional conditions. These may have been operative while the organism was still alive (e.g., Howarth, 1979), although in most instances pyritization occurs soon after death within the shallow burial realm of the sediment column (Raiswell and Berner, 1985). This process is of course strongly dependent on the right redox potential (dysaerobia to anaerobia) and availability of the required elemental ingredients (Fe and S) in the burial realm. More importantly, the relative preservation of shell/skeletal integrity by

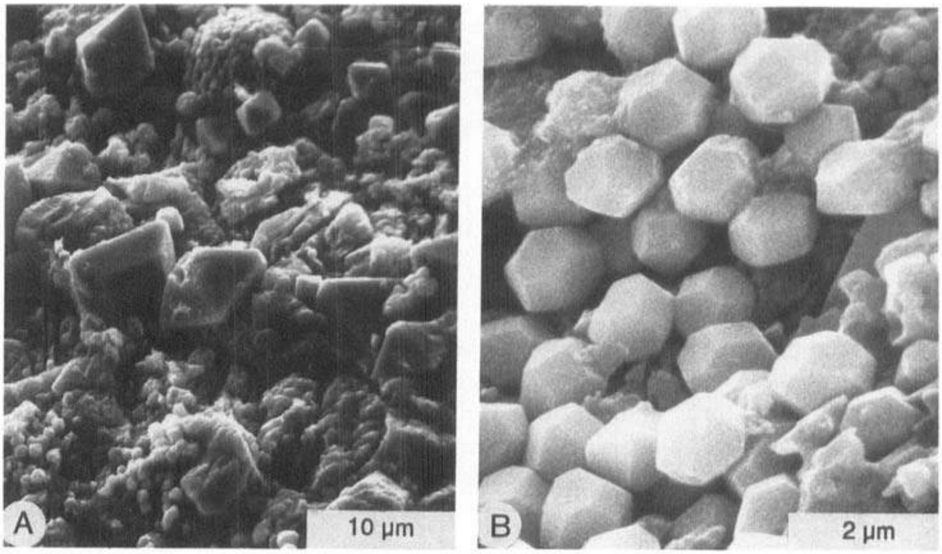

Fig. 8-24. Pyritization microstructures of primary biogenic and secondary calcium carbonate. A shows the replacement of crinoidal calcite by euhedral macro- and micropyrite. B shows the filling of crinoidal pore space by framboidal micropyrite. (After Brand and Morrison, 1987b.)

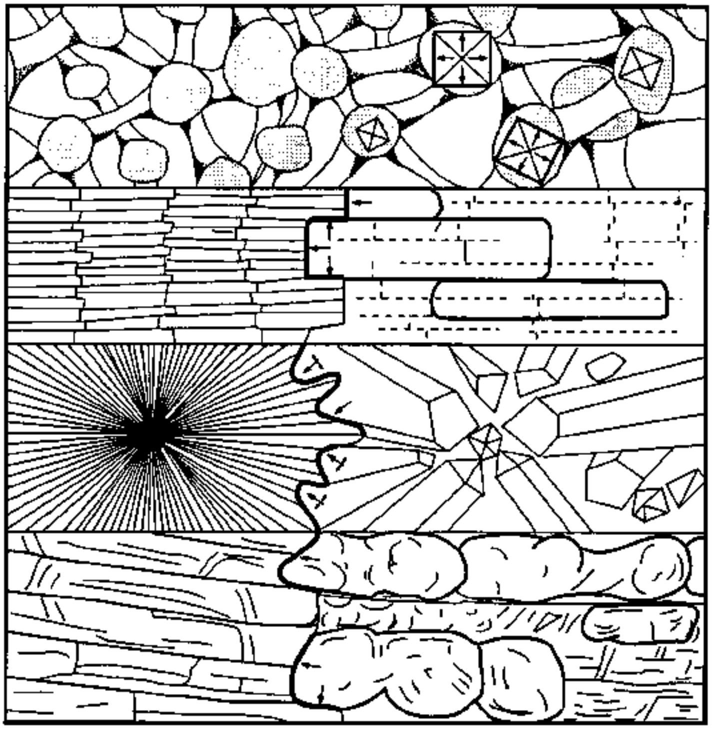

Fig. 8-25. Replacement process model (RPM) for biogenic and diagenetic calcium carbonates by authigenic minerals. The process is mediated by the force of crystallization (FC) through the thin-film front (TIFF). Important replacement minerals are pyrite, silica, phosphate and dolomite.

the pyritization process (Fig. 8-24A) precludes wholesale dissolution of the biogenic carbonate prior to pyrite formation. It is reasonable to assume that replacement proceeds through a thin-film, similar to that for the $CaCO_3$–calcite transformations, where the force of crystal (FC) formation in conjunction with solution diffusion of required elements out off and to the crystallization front (TIFF) maintains the redox and source requirements of the system (Fig. 8-25).

Replacement process

Two reaction pathways describe the formation of pyrite in biogenic carbonates (e.g., Berner, 1964; Brand and Morrison, 1987b):

$$FeO \cdot OH + HS^- \longrightarrow (FeS_{0.9}) \longrightarrow Fe_3S_4 \longrightarrow FeS_2 \qquad (8\text{-}22)$$

and

$$FeO \cdot OH + HS^- \longrightarrow (FeS_{0.9}) \longrightarrow FeS_2 \qquad (8\text{-}23)$$

The reaction in 8-22 represents the formation of framboidal pyrite via the metastable intermediates, mackinawite and possibly greigite (Sweeney and Kaplan, 1973; Hallberg, 1972). The reaction in 8-23 represents the formation of euhedral pyrite directly from Fe and S with a possibility of the intermediate mackinawite (Goldhaber and Kaplan, 1974). Besides the proper redox conditions either within the local environment or within the confines of the carbonate allochem, the local environment must contribute the necessary Fe and S to the formation of authigenic pyrite replacing biogenic carbonates. As long as the redox/source conditions are maintained, pyritization may continue in replacing the biogenic carbonate. The replacement process can be described by the following reaction pathway:

$$CaCO_3 + FeO \cdot OH + HS^- \xrightarrow{\text{TIFF}} FeS_2 + Ca^{2+} + HCO_3^- \tag{8-24}$$

where dissolution of the carbonate host and formation of the authigenic pyrite proceeds simultaneously in the thin-film front (TIFF) under the right redox/source potential. Thus the major rate-limiting step in the pyritization of carbonates may be any combinations of redox potential, source availability, and force of crystallization (FC). This process gave rise to some outstanding paleontological specimens with a wealth of paleobiological and geochemical information trapped by the formation of pyrite in the shells/skeletons.

Silicification

Silicification or chertification is another diagenetic replacement process common in carbonate allochems of all ages (Maliva and Siever, 1988; Hesse, 1990) and sometimes in conjunction with pyritization (e.g., Loope and Watkins, 1989). Replacement by silica is highly allochem selective while generally leaving the host rock material unaffected. This process probably proceeds before or after carbonate-controlled diagenetic processes and is highly dependent on chemical-crystal growth conditions of the replacement microenvironment.

Mineralogy

Silica in the form of quartz (SiO_2) with its many equigranular and fibrous varieties may replace original biogenic carbonate. Replacement silica may be equigranular micro- and megaquartz, whereas the common fibrous forms are length-fast chalcedony, length-slow chalcedony (quartzine) and lutectite. Microquartz consists of crystals between 5 and 20 μm in size with pinpoint extinction pattern. Macroquartz is generally larger than 20 μm and in fossil replacement replete with carbonate inclusions. In length-fast chalcedony, fibers are arranged perpendicular to the crystallographic *c*-axis. In contrast, in quartzine fibers are aligned parallel to the crystallographic *c*-axis, and lutectite is a fibrous quartz variety morphologically situated in between chalcedony and quartzine in which the fibers are inclined about 30° to the crystallographic *c*-axis (e.g., Milliken, 1979; Hesse, 1990).

Microstructures

Generally, silicification is an excellent means of preserving macromorphological and trapping microstructural features in biogenic carbonate allochems. In contrast, intricate carbonate layering and crystal arrangements are usually degraded in the replacement process, but they may be interned as solid inclusion. Replacement may proceed preferentially along lines or surfaces of weakness within biogenic carbonates. Primary biogenic fractures (areas of original organic tissue) in belemnites are excellent avenues and provide the right conditions for silica replacement by crystallization force (Fig. 8-26A), but are not necessarily the sole catalyst for the process to proceed. Direct replacement by silica also proceeds readily within biogenic carbonates on a layer-by-layer process (Fig. 8-26B). In some instances, void formation through active carbonate dissolution without "instantaneous" quartz precipitation may precede silicification. But, the more common process is for megaquartz, preceded possibly by its metastable opal precursors, to fill the shell/skeleton through a thin-film front (TIFF) with retention of some large-scale morphological features such as the radial nature of the trabecular structure in rugose corals (Fig. 8-26C). Maintenance of the carbonate shell/skeleton integrity strongly argues for a model envisaging a one-for-one dissolution of the host carbonate and precipitation of the authigenic silica (Fig. 8-26; cf. Maliva and Siever, 1988). The formation of authigenic micro- and megaquartz may be preceded by an opal-CT precursor, although, incontrovertible evidence is lacking for this in fossils. This precursor scenario is not plausible for the formation of fibrous chalcedony, which would require preservation of carbonate microstructures in the opal-CT which would have to survive subsequent recrystallization to quartz. The most reasonable explanation is the direct replacement of the host carbonate by authigenic silica, which would accommodate the retention of micro- and macro-ghost structures (Maliva and Siever, 1988; Hesse, 1990).

Replacement process

Silicification of biogenic carbonate allochems may occur at any time in their geologic and diagenetic history. Evidence is mounting that silicification of carbonate allochems occurs prior to extensive cementation of the host sediment, and either before, during or after the aragonite–calcite and high-Mg calcite–calcite transformations (e.g., Choquette, 1955; Richter, 1974; Jacka, 1974; Hesse, 1987). It has been proposed that siliceous organisms, such as sponge spicules which dissolve during diagenesis of the host rock, may be a sufficient silica source for the silicification process (Siever, 1962).

Carbonate allochems are readily replaced by silica, but the process does not readily apply to matrix material. If the matrix was derived from degraded biogenic material, then it should have a similar potential for silicification. Early diagenetic processes such as compaction, cementation, oxidation of organic matter and carbonate transformation, however, may have decreased the potential of matrix carbonates for silicification. In addition to bioturbation of sediments, their larger specific grain size makes matrix more susceptible to these processes than the generally larger biogenic allochems (Maliva and Siever, 1988).

Two models may explain the silicification of biogenic carbonate allochems: (1) the dissolution of the shell/skeletal calcite with efflux of calcium and carbonate ions, followed by the influx of silica and subsequent precipitation of quartz into the resulting void space, and (2) the simultaneous dissolution of biogenic calcium carbonate and the precipitation of silica (cf. Maliva and Siever, 1988). Physical

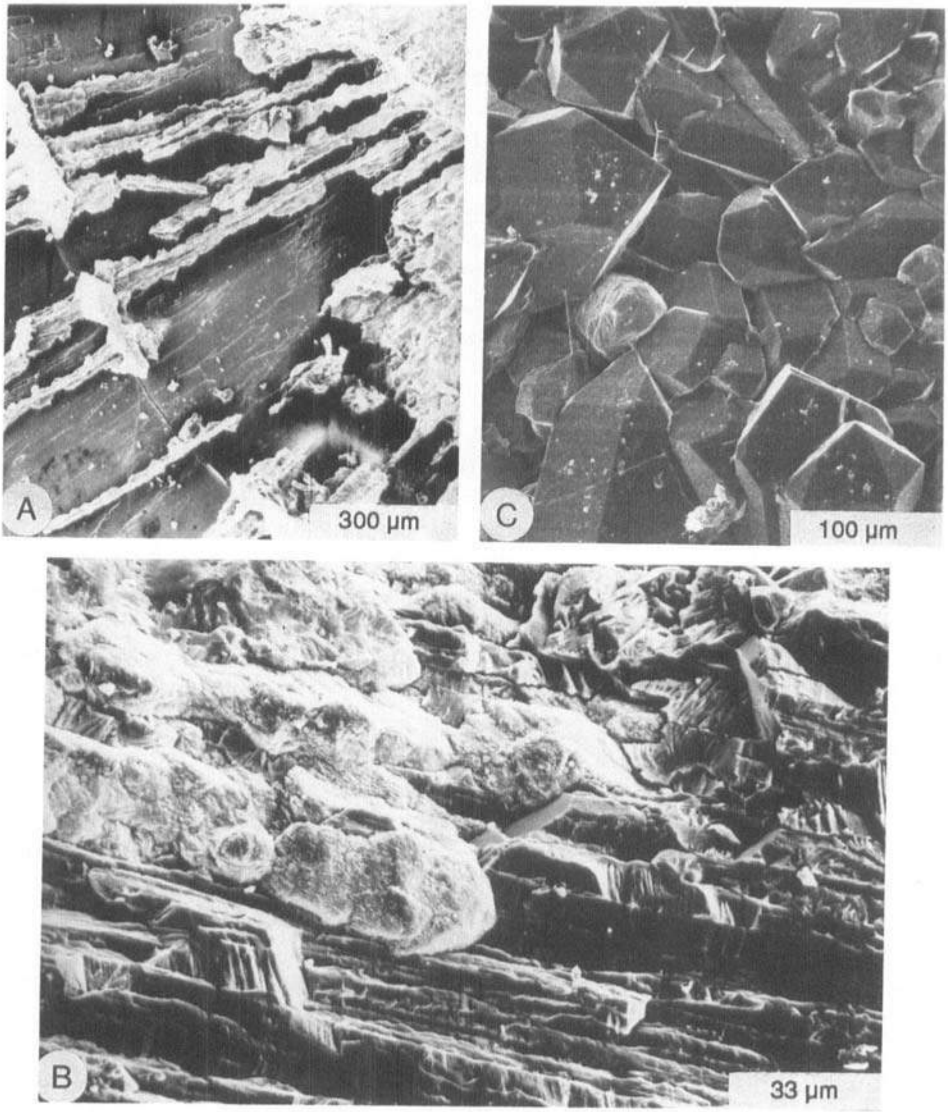

Fig. 8-26. Silicification microstructures of primary biogenic and secondary calcium carbonate. A shows contact silica replacement along biogenic fractures in a belemnite rostrum. B shows silica replacing *en mass* prismatic calcite fibers in a belemnite (after Morrison, 1991). C shows the complete replacement of trabecular calcite in a rugose coral by euhedral megaquartz (Onondaga Formation).

evidence is lacking for the first model, whereas solid inclusions within quartz (Fig. 8-26B), ghost structures in quartz (Maliva and Siever, 1988), pseudomorphing of skeletal structures (Fig. 8-26C), and overall preservation of structural integrity (Fig. 8-26A) support the second model for silica replacement of biogenic carbonate.

Ramberg (1947) described the force of crystallization as the pressure a crystal can endure or grow against at a given state of supersaturation. Crystals only grow in the region of stress if a solution thin-film separates the crystal from its solid host constraint (Weyl, 1959). The thickness of the thin-film is in the order of microns, similar to that postulated for the calcium carbonate transformation processes (e.g., Pingitore, 1976; Brand and Veizer, 1980).

The silicification of biogenic carbonates may be explained by the following reaction pathway:

$$CaCO_3 + Si^{4+} \xrightarrow{\text{TIFF}} SiO_2 + Ca^{2+} + HCO_3^- \tag{8-25}$$

where the resulting crystallization force through increased surface stress coupled with a solution slightly supersaturated for silica would effectively increase the Gibbs free energy and consequently the solubility of the biogenic calcite at the quartz–calcite interface. Silica replacement may take place through the thin-film zone (TIFF) in bulk pore waters effectively at calcite saturation (Maliva and Siever, 1988). The solubility of calcite may increase by several factors depending on effective stress produced at the TIFF and type of diagenetic water in the bulk pore/aquifer system and thin-film microenvironment. Although the replacement process is reversible, the silicification of carbonate is favoured over the inverse process because of the greater force of crystallization and lower solubility with increasing pressure of both opal-CT and quartz.

Maliva and Siever (1988) found no correlation between shell mineralogy and replacement silica type, but noticed an apparent correlation between shell microstructure and quartz type. It is uncertain as to whether the influence is related to crystal size, organic matter content, or intra-shell permeability. Several different silica types may be present within a single carbonate horizon and possibly involved a sequential replacement process in pore waters of different compositions. Silica was probably derived by the intraformational dissolution of siliceous sponge spicules, and its concentration varied with the amount of spicules present in the sediments, kinetics of silica dissolution and rate of quartz/chalcedony precipitation. According to Maliva and Siever (1988, p. 396) "... we would expect opal-CT at highest concentrations, chalcedony at lower values, microcrystalline quartz at even lower values, and granular megaquartz and quartz euhedra at the lowest concentrations". Replacement would continue until all available silica were exhausted and thus represents an early diagenetic process controlled by localized silica supersaturation and force of crystallization.

Phosphatization

Phosphate may occur in invertebrates as a biogenic (primary) or replacement mineral of shells/skeletons. Biogenic phosphate is found as spherulitic, matted, homogeneous, fine complex-crossed lamellar, irregular complex-crossed lamellar and as spicules and spikes (cf. Carter et al., 1990). Among the marine invertebrates, some brachiopods, corals, annelids, conodonts, scolecodonts and molluscs use phosphate (apatite) in the construction of their shells/skeletons. Replacement phosphate is known in diagenetically altered molluscs from Cambrian units, but is of uncertain existence in younger specimens due to lack of data.

Mineralogy

There are a large number of anhydrous, hydrated and uranyl phosphate minerals with members of the apatite group being most important constituents of biogenic shells/skeletons. Biogenic phosphate is mostly hydroxylapatite ($Ca_5[PO_4]_3[OH]$), whereas there is no definitive mineral species identification of replacement phosphate in fossil specimens.

Microstructures

Overall phosphatization degrades the microstructures in calcitic shells/skeletons with little or no recognition of original features. In some instances, however, the phosphate has preserved surficial as well as internal microstructures of replaced mollusc shells. Massive dissolution of biogenic calcite/aragonite under its special chemical requirements and subsequent replacement by phosphate with its special prerequisites would not result in the excellent preservation noted in Cambrian molluscs (Runnegar, 1985). Nor is it possible for a precursor to have preceded the replacement phosphate, for it would have transmitted the delicate structural information to the final mineral phase which is highly unlikely. Instead, it is postulated, similar to the silicification process, that phosphatization of biogenic calcium carbonate is a direct replacement process.

A number of surficial and internal features preserved in phosphatized molluscs argue that original calcite and aragonite molluscan microstructures were already well-developed in Cambrian monoplacophorans (Fig. 8-27). Polygonal prism ends are well preserved in phosphatized specimens of *Latouchella*? n.sp. (Fig. 8-27A). Other evidence of original calcite microstructures is documented by the well-preserved fibers of foliated calcite in *Pseudomyona queenslandica* (Fig. 8-27B). Precursor aragonite microstructures maintained in phosphatized specimens are nacre (Fig. 8-27C), tangential fibers (Fig. 8-27D), spherulitic prisms, and crossed-lamellar crystals (Runnegar, 1985). This excellent preservation of molluscan microstructures in early middle Cambrian specimens argues for the direct replacement of the biogenic carbonate phase. Other diagenetic processes would be unable to preserve the delicate microstructures documented in the Cambrian molluscs.

Replacement process

The massive and disruptive replacement of carbonate shells/skeletons would argue for the wholesale dissolution of the biogenic calcium carbonate prior to precipitation of the phosphate mineral. But microstructural evidence supports the concept of a direct replacement process. Two processes are involved in phosphatization: (1) the dissolution of shell calcium carbonate with outflow of carbonate, and (2) subsequent inflow of phosphorous and mixing with Ca to precipitate phosphate. The replacement mechanism involving bulk dissolution of shell/skeletal carbonate and subsequent precipitation of phosphate into pre-existing void space is discounted based on the excellent preservation of original microstructures (Fig. 8-27). Instead, it is more

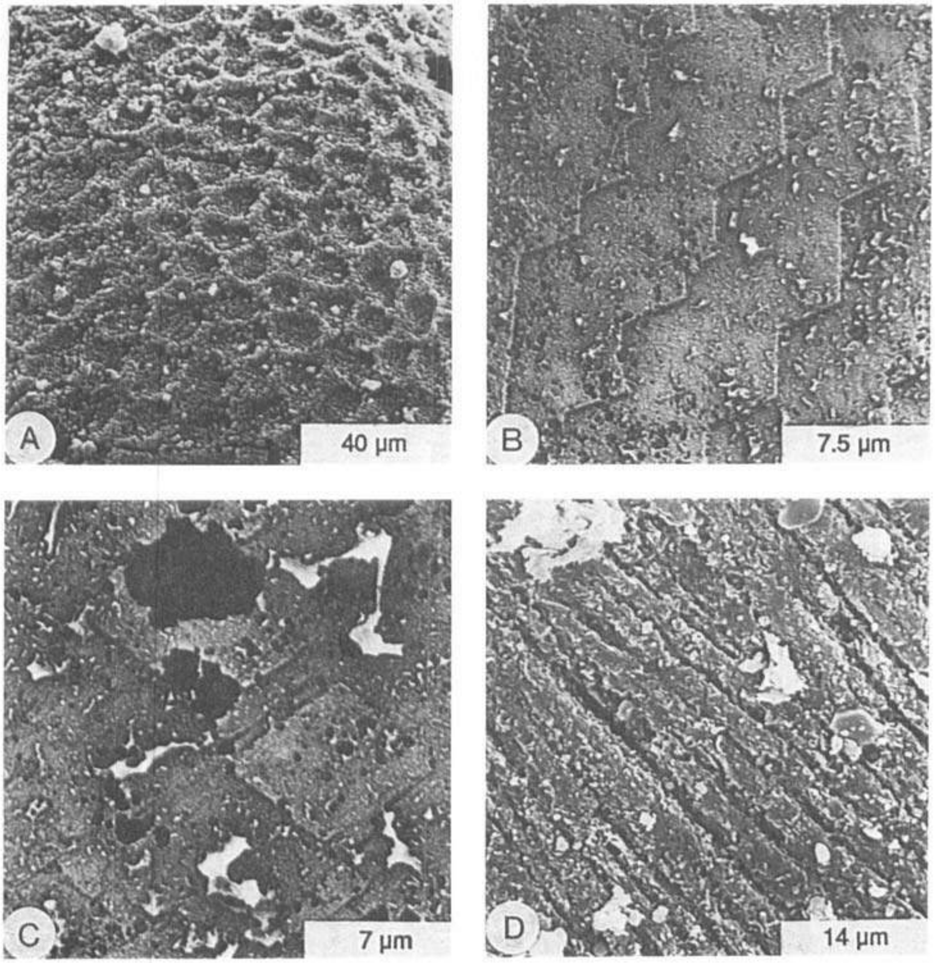

Fig. 8-27. Phosphatization microstructures of primary biogenic calcium carbonate (Runnegar, 1984). A shows replicas of prism ends in the ridges of an internal mould of *Latouchella*? n.sp. B is an electronically inverted image of foliated calcite of *Pseudomyona queenslandica*. C is an inverted image of nacreous tablets of *Mellopegma georginensis*. D represents "preserved" fibrous phosphate crystals of precursor aragonite in *Pelagiella subangulata* (reproduced with permission of B. Runnegar).

likely that replacement of biogenic shell/skeletal carbonate by phosphate proceeds simultaneously via water in a thin-film in disequilibrium with the bulk aquifer water system (e.g., Fig. 8-25). The micron-sized thin-film front (TIFF) would advocate the transmission of the micrometer shell microstructure information and foster their consequent preservation in the replacement phosphate. Conodonts and other biogenic phosphatic allochems as well as abiogenic phosphorites may be possible sources for the replacement phosphate. Despite precise lack of knowledge about the source and formation process, it must be clear that the fluids in the thin-film front must be supersaturated with phosphate relative to the saturation state for calcite/aragonite. Furthermore, force of phosphate crystallization, analogous to that of silica, may provide the necessary driving force for the replacement process. It is possible that this may increase the solubility of the calcium carbonate and at the same time allow for the precipitation of phosphate across the thin-film front (TIFF). Ultimately, the supply of phosphorous to the site of precipitation and its concentration may be one of the rate-limiting parameters in the extent and degree of the replacement process.

Precise physicochemical parameters for the phosphatization process and products are lacking, but probably follow a methodology similar to that for silica replacement of biogenic carbonates. Cryptocrystalline and euhedral forms and framboids of rhombs are known for authigenic phosphate in detrital sediments but unproven in replacement of primary biogenic calcium carbonates. This important aspect of fossilization requires more attention and research.

Dolomitization

Unlike the previously discussed replacement processes, dolomitization does not usually retain much of the original microstructures in the replacement product. Although, preservation is usually poor, many carbonate sequences and allochems have been preserved by the dolomitization process. All biogenic allochems of all ages are known to be susceptible to dolomite replacement.

Mineralogy

Biogenic calcium carbonates seem to be readily replaced by dolomite. The difference in the chemical composition between calcite/aragonite and dolomite is the incorporation of Mg to form $CaMg(CO_3)_2$. Unlike the various dolomite types recognized in sedimentary sequences, the mineral formed in biogenic allochems is always the replacement type. Four isotypes such as ankerite ($Ca[Mg,Fe][CO_3]_2$), kutnahorite ($CaMn[CO_3]_2$), minrecordite ($CaZn[CO_3]_2$) and the synthetic phase of cadmium dolomite ($CdMg[CO_3]_2$) crystallize with the dolomite structure (Reeder, 1983). Sedimentary dolomite contains Ca and Mg in the proportions of about 55 and 45 mol% which may vary at surface temperature–pressure conditions (Goldsmith, 1983). The best known species besides dolomite is ankerite and the less Fe-rich variety is ferroan dolomite. One precise X-ray structural assessment by Beran and Zeman (1977) is known for ankerite with a formula of: $Ca_{1.05}Mg_{0.27}Fe_{0.63}Mn_{0.05}(CO_3)_2$.

In dolomites, increasing amounts of Fe are incorporated into the dolomite lattice which may vary from a few hundred ppm to several percent. Within this general classification, two major groups of ferroan dolomite have been recognized in originally calcitic/aragonitic biogenic allochems. The general replacement of biogenic carbonate allochems can be represented by the following reaction:

$$2\,CaCO_3 + Mg^{2+}(Fe^{2+}) \longrightarrow CaMg(CO_3)_2 + Ca^{2+} \qquad (8\text{-}26)$$

where variable amounts of Fe may substitute into the dolomite lattice depending on the source availability and redox of the diagenetic system.

Microstructures

Biogenic carbonates subjected to dolomite replacement usually do not retain fine and detailed microstructural information, although there are exceptions to this observation. In contrast to microstructural features, exoskeletal/shell morphology is usually well maintained during the replacement process. Figure 8-28A shows a calcitic crinoid columnal which was readily etched by dilute acid, whereas a dolomitized counterpart from the same unit (Read Bay Group, Cape Rescue, Cornwallis Island) was resistant to any etching attempt (Fig. 8-28B). The observed porosity is not primary but secondary due to the replacement of calcite by dolomite. In some instances, micro- (Meyers and Lohmann, 1975; Burke et al., 1982) and macrodolomite crystals may be trapped within an otherwise still calcitic allochem. If dolomitization occurred after calcitization/transformation of the original biogenic specimen, microstructural information because of multiple alteration effects is usually not retained by the studied allochem. In the case that ghost structures are visible, replacement probably proceeded before the onset of transformation in a system controlled by intermediate to low water/rock ratios. Thus, type of preservation may provide important clues about the dolomitization process in biogenic carbonates.

The retention of microdolomite integrity suggests that the force of crystallization model is possibly also operative in the replacement of biogenic calcite by dolomite.

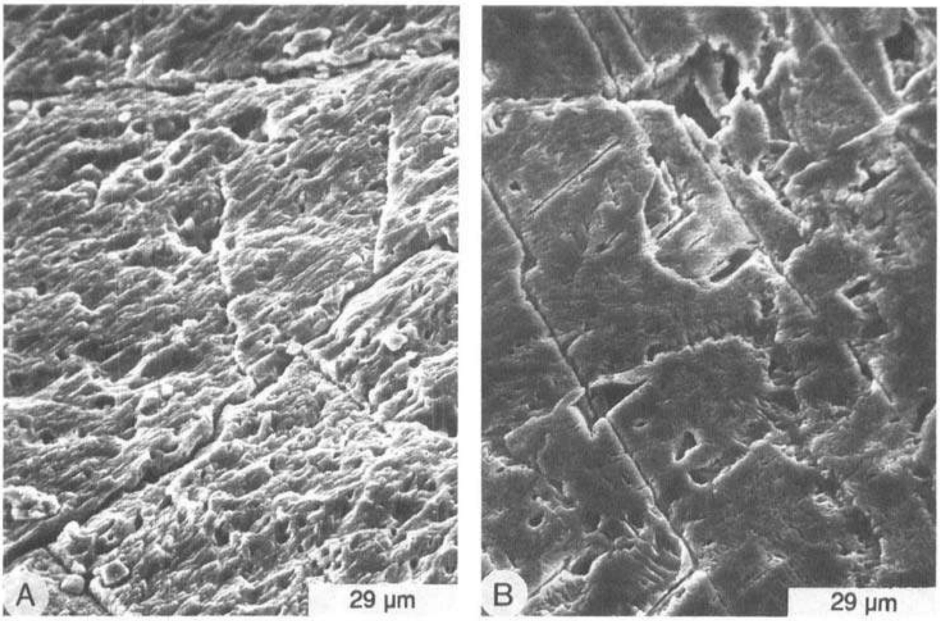

Fig. 8-28. Dolomitization microstructures of primary biogenic and secondary calcium carbonate. A shows the acid-etched surface of crinoidal calcite. B shows the acid-etched but resistant surface of crinoidal calcite replaced by dolomite.

Furthermore, void space formation and subsequent precipitation are usually not a factor, and may be ruled out for most observed dolomite replacement. Instead it is postulated that replacement proceeds across a thin-film front (TIFF) to preserve the structural integrity commonly observed in affected specimens.

Elemental geochemistry

The trace element composition of replacement dolomites is strongly influenced by source and redox potentials (in particular Mn and Fe) of the diagenetic fluid(s) and of course the water/rock ratio of the diagenetic microenvironment. By definition (see Chilingar, 1957), dolomitic calcite specimens contain between 10 and 50% dolomite, calcareous dolomite specimens contain between 50 and 90% dolomite, and dolomite specimens contain >90% dolomite. Magnesium, in conjunction with X-ray diffraction, is a good tracer of the extent of dolomitization (Fig. 8-29). The most likely source for the Mg required by the dolomitization process is probably seawater-Mg, although other fluid(s) under certain thermodynamic conditions within

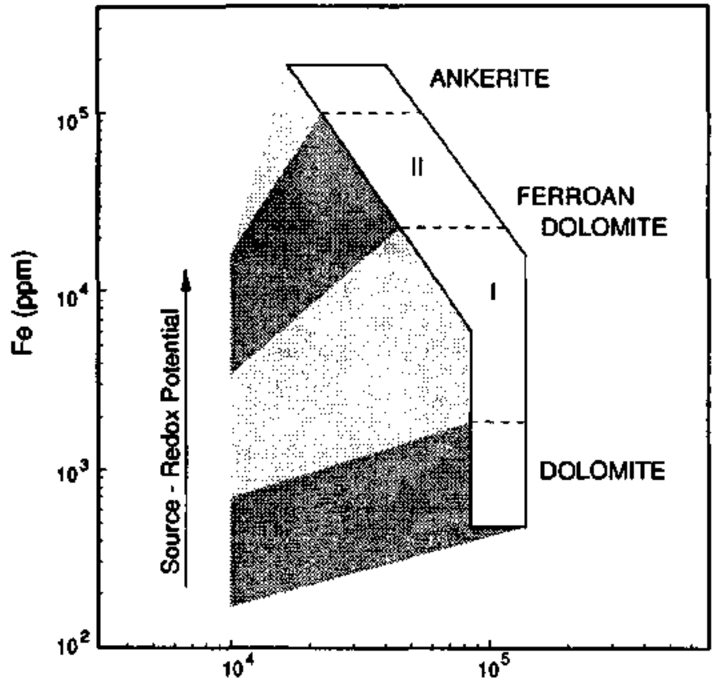

Fig. 8-29. Dolomitization trends of Fe and Mg in biogenic carbonates. The amount of Fe incorporation is strongly influenced by redox potential and source of the diagenetic fluid(s). A total of four fields are recognized in sedimentary dolomites and ankerites (Brand, 1990). Dolomite usually has less than 2000 ppm Fe; ferroan dolomite is subdivided into low-Fe (2000–20,000 ppm) and high-Fe (20,000–100,000 ppm) regimes (cf. Goldsmith et al., 1962). The Fe composition of ankerite is variable within 10–20% (Beran and Zeman, 1977).

the TIFF of the diagenetic regime also may be possible sources (e.g., Hanshaw et al., 1971; Badiozamani, 1973). Relative saturation states of the carbonate species within the fluids of the TIFF and possibly bulk aquifer system may allow the process to proceed under a number of diagenetic settings (summary in Zenger et al., 1980).

Studies of crinoids from the Douro and Irondequoit formations, replaced by dolomite, shows that the samples fall into two distinct fields. The specimens from the Douro Formation (Arctic Canada) are low in Fe with generally less than 1.5%, whereas specimens from the Irondequoit Formation (southern Ontario) are enriched and contain from 2 to 25% Fe (Fig. 8-29). Thus these two data sets fall into the "DOLOMITE" and "FERROAN DOLOMITE I" fields, respectively (Fig. 8-29). The replacement for these specimens proceeded probably in TIFF's with fluid composition controlled by mixed waters of meteoric and seawater parentage. Specimens from burial environments or from areas with higher source and redox potential fall into "FERROAN DOLOMITE II" field. Only in special circumstances does the chemical composition of the replacement mineral approach that of ankerite (Fig. 8-29). Not only are the fields distinct, but this applies to the trends as well, with no crossover detected at this time by these studies for the different populations (cf. Brand, 1990).

Isotope geochemistry

The stable isotope compositions of replacement dolomite is specific of the diagenetic realm. For example, previously calcitized samples during the subsequent dolomitization process showed no significant change in $\delta^{13}C$ values but a definite trend towards more positive values for $\delta^{18}O$ (PDB; Brand, 1990). This trend towards heavier values is consistent with dolomitization by mixed waters, where the enrichment is about 2–4‰ in the dolomite relative to the calcite precursor (Fig. 8-14; Land, 1983; Budai et al., 1987; Brand, 1990).

In contrast, specimens replaced in the presence of burial fluids in the TIFF, show a marked difference in their isotopic re-distribution. These specimens show a definite trend towards more negative $\delta^{18}O$ and slight one for $\delta^{13}C$ values relative to their unaltered counterparts (Fig. 8-14). Thus based on their isotopic compositions, it is possible to identify shallow subsurface dolomite from deep-burial replacement dolomite. Furthermore, it is possible to speculate on the type of water(s)/fluid(s) involved in the replacement process (cf. Brand, 1990).

Replacement process

Despite the poor retention of primary microstructures by replacement dolomite in biogenic carbonate shells/skeletons, it is believed that the process is probably controlled by the force of dolomite crystallization. The preservation of euhedral microdolomite crystals within originally HMC biogenic carbonates without any appreciable spaces between host and replacement product supports the concept of a thin-film front. Within this front, dissolution of the host and precipitation of the replacement product occurs almost simultaneously across the thin-film (Fig. 8-25). Whether or not this model applies to macrodolomite within biogenic carbonate allochems is uncertain, but indications from crinoids of the Douro Formation suggest a process that approaches those advanced by the replacement model for the general formation of authigenic minerals within biogenic carbonates.

Summary

Replacement diagenesis of biogenic carbonates, whether still in their original state or as transformation products, is dependent largely on the amount and availability of the source, the saturation state of the fluid with respect to the host and replacement mineral, and the force of crystallization induced by localized stress of the system. The major replacement minerals are silica, phosphate, pyrite and dolomite. These minerals precipitate simultaneously from the liquid in the thin-film front as the host carbonate mineral dissolves and its constituents are dispersed eventually into the bulk aquifer system. The driving mechanism of the replacement process is the force of crystallization of the specific mineral, the degree of which will depend largely on the continued availability of source material. Geochemically there are significant differences between the host and replacement minerals, and microstructures of the biogenic allochem are at best preserved as ghost structures. Replacement is considered an early to intermediate diagenetic process which may have started already in the living allochem, but commonly occurs in the early stages of the postdepositional transformation process. Although late stage replacement of biogenic carbonate allochems can not be discounted as a viable timeframe, structural evidence suggests that the replacement of calcium carbonate by the aforementioned minerals occurs across a migrating thin-film front driven by the stress of the system fuelled by the force of crystallization.

This postulated hypothesis is supported by microstructural evidence, where euhedral replacement minerals formed in the carbonate host without the prior formation of void space for their growth. This replacement proceeds across a thin-film, analogous to that in calcium carbonate transformation. This preserves the macromorphology of the biogenic allochem but only rarely microstructural features.

GENERAL SUMMARY

It is becoming more apparent that fossil material, in general, and the wealth of geochemical information, in specific, stored in the shell/skeleton must be treated as a dynamic system that is in constant flux and interphase with the ambient environment. Thus, extrapolation of geochemical databases based on a “local” population must be avoided in the context of global environmental and secular reconstructions. Despite these cautionary words, we have gleaned an enormous amount of information from biogenic material about the changes and fluxes of the exogenic system of our planet. The future holds much promise for even greater accomplishments with a better understanding of organism dynamics and technological advances to unravel and solve both past and future ecological problems facing the Earth and mankind.

ACKNOWLEDGEMENTS

I thank Dr. K.H. Wolf (Bureau of Mineral Resources, Canberra) for his invitation to contribute to the volume on Diagenesis and improving the manuscript together with Professor George V. Chilingarian. M. Lozon and H. Melville (Brock University) are acknowledged for their drafting and scanning electron microscopy expertise, respectively. I also thank the numerous colleagues who provided me with reprints of their work and permission to republish some of their figures and plates. This work was financially supported by grants (#7961) from the Natural Sciences and Engineering Research Council of Canada.

REFERENCES

Al-Aasm, I.S. and Veizer, J., 1982. Chemical stabilization of low-Mg calcite: an example of brachiopods. *J. Sediment. Petrol.*, 52: 1101–1109.

Anderson, T.F., Bender, M.L. and Broecker, W.S., 1973. Surface areas of biogenic carbonates and their relation to fossil ultrastructure and diagenesis. *J. Sediment. Petrol.*, 43: 471–477.

Badiozamani, K., 1973. The Dorag dolomitization model — application to the middle Ordovician of Wisconsin. *J. Sediment. Petrol.*, 43: 965–984.

Barbin, V., Ramseyer, K., Debenay, J.P., Schein, E., Roux, M. and Decrouez, D., 1991. Cathodoluminescence of Recent biogenic carbonates: an environmental and ontogenetic fingerprint. *Geol. Mag.*, 128: 19–26.

Bates, N.R. and Brand, U., 1991. Environmental and physiological influences on isotopic and elemental compositions of brachiopod shell calcite: implications for the isotopic evolution of Paleozoic oceans. *Chem. Geol.*, 94: 67–78.

Bathurst, R.G.C., 1975. *Carbonate Sediments and Their Diagenesis. Developments in Sedimentology 12.* Elsevier, Amsterdam, 2nd ed., 658 pp.

Beran, A. and Zeman, J., 1977. Refinement and comparison of the crystal structures of a dolomite and an Fe-rich ankerite. *Tschermaks Mineral. Petrogr. Mitt.*, 24: 279–286.

Berner, R.A., 1964. Distribution and diagenesis of sulfur in some sediments from the Gulf of California. *Mar. Geol.*, 1: 117–140.

Berner, R.A. and Morse, J.W., 1974. Dissolution kinetics of calcium carbonate in sea water, IV. Theory of calcite dissolution. *Am. J. Sci.*, 274: 108–134.

Bischoff, W.D., Mackenzie, F.T. and Finley, C., 1987. Stabilities of synthetic magnesian calcites in aqueous solution: comparison with biogenic materials. *Geochim. Cosmochim. Acta*, 51: 1413–1423.

Blake, D.F., Peacor, D.R. and Wilkinson, B.H., 1982. The sequence and mechanism of low-temperature dolomite formation: calcian dolomites in a Pennsylvanian echinoderm. *J. Sediment. Petrol.*, 52: 59–70.

Boyle, E.A., 1988. Cadmium: chemical tracer of deepwater paleoceanography. *Paleoceanography*, 3: 471–489.

Brand, U., 1981. Mineralogy and chemistry of the Lower Pennsylvanian Kendrick Fauna, eastern Kentucky, U.S.A., 1. Trace elements. *Chem. Geol.*, 32: 1–16.

Brand, U., 1983. Mineralogy and chemistry of the Lower Pennsylvanian Kendrick Fauna, eastern Kentucky, U.S.A., 3. Diagenetic and paleoenvironmental analysis. *Chem. Geol.*, 40: 167–181.

Brand, U., 1987. Depositional analysis of the Breathitt Formation's marine horizons, Kentucky: trace elements and stable isotopes. *Chem. Geol.*, 65: 117–136.

Brand, U., 1989a. Aragonite–calcite transformation based on Pennsylvanian molluscs. *Geol. Soc. Am. Bull.*, 101: 377–390.

Brand, U., 1989b. Biogeochemistry of Late Paleozoic North American brachiopods and secular variation of seawater composition. *Biogeochemistry*, 7: 159–193.

Brand, U., 1990. Chemical diagenesis and dolomitization of Paleozoic high-Mg calcite crinoids. *Carbonates and Evaporites*, 5: 179–195.

Brand, U., 1991. Strontium isotope diagenesis of biogenic aragonite and low-Mg calcite. *Geochim. Cosmochim. Acta*, 55: 505–513.

Brand, U. and Logan, A., 1991. Brachiopod geochemistry: a tracer tool of present and past ocean circulation, chemistry and cycles. *Geol. Assoc. Can., Prog. Abstr.*, 16: A14.

Brand, U. and Morrison, J.O., 1987a. Paleoscene #6. Biogeochemistry of fossil marine invertebrates. *Geosci. Can.*, 14: 85–107.

Brand, U. and Morrison, J.O., 1987b. Diagenesis and pyritization of crinoid ossicles. *Can. J. Earth Sci.*, 24: 2486–2498.

Brand, U. and Veizer, J., 1980. Chemical diagenesis of a multicomponent carbonate system, 1. Trace elements. *J. Sediment. Petrol.*, 50: 1219–1236.

Brand, U. and Veizer, J., 1981. Chemical diagenesis of a multicomponent carbonate system, 2. Stable isotopes. *J. Sediment. Petrol.*, 51: 987–997.

Brand, U., Wassenaar, L. and Kanip, J., 1986. Variation in shell chemistry of terrestrial gastropods, *Cerion incanum, Cerion uva,* and *Tudora maculata)* from the Florida Keys and Bonaire. *Can. J. Zool.*, 64: 2399–2404.

Brophy, C.M., Brand, U. and Bell, S., in prep. Geochemistry of Cambrian ooids: a re-evaluation of mineralogical trends.

Budai, J.M., Lohmann, K.C. and Wilson, J.L., 1987. Dolomitization of the Madison Group, Wyoming and Utah overthrust belt. *Bull. Am. Assoc. Pet. Geol.*, 71: 909–924.

Burke, W.H., Denison, R.E., Heatherington, E.A., Koepnick, R.B., Nelson, H.F. and Otto, J.B., 1982. Variation of seawater ^{87}Sr/^{86}Sr throughout Phanerozoic time. *Geology*, 10: 516–519.

Burton, R.F., 1983. Ionic regulation and water balance. *The Mollusca*, 5: 291–352.

Burton, W.K., Carbrera, N. and Frank, F.C., 1951. The growth of crystals and the equilibrium structure of their surfaces. *Philos. Trans. R. Soc. London, Ser. A*, 243: 299–358.

Carlson, S., 1990. Vertebrate dental structures. In: J.G. Carter (Editor), *Skeletal Biomineralization: Patterns, Processes and Evolutionary Trends*. Van Nostrand Reinhold, New York, N.Y., pp. 531–556.

Carlson, W.D., 1983. The polymorphs of $CaCO_3$ and the aragonite–calcite transformation. In; R.J. Reeder (Editor), *Carbonates: Mineralogy and Chemistry*. Mineral. Soc. Am., Bookcrafters Inc., Chelsea, Mich., pp. 191–225.

Carter, J.G., 1980. Guide to bivalve shell microstructures. In: D.C. Rhoads and R.A. Lutz (Editors), *Skeletal Growth of Aquatic Organisms*. Plenum, New York, N.Y., pp. 645–673.

Carter, J.G., 1990. *Skeletal Biomineralization: Patterns, Processes and Evolutionary Trends*. Van Nostrand Reinhold, New York, N.Y., 832 pp.

Carter, J.G., Lutz, R.A. and Tevesz, M.J.S., 1990. Shell microstructural data for the bivalvia. Part VI: Orders Modiomorphoida and Mytiloidea. In: J.G. Carter (Editor), *Skeletal Biomineralization: Patterns, Processes and Evolutionary Trends*. Van Nostrand Reinhold, New York, N.Y., pp. 391–412.

Chave, K.E., 1954. Aspects of the biogeochemistry of magnesium, 1. Calcareous marine organisms. *J. Geol.*, 62: 266–283.

Chave, K.E., Deffeyes, K.S., Weyl, P.K., Garrels, R.M. and Thompson, M.E., 1962. Observations on the solubility of skeletal carbonates in aqueous solutions. *Science*, 137: 33–34.

Chilingar, G.V., 1957. Classification of limestones and dolomites on the basis of Ca/Mg ratio. *J. Sediment. Petrol.*, 27: 187–189.

Chilingar, G.V., 1962. Dependence on temperature of Ca/Mg ratio of skeletal structures of organisms and direct chemical precipitates out of sea water. *Bull. S. Calif. Acad. Sci.*, 61 (1): 45–60.

Choquette, P.W., 1955. A petrographic study of the "State College" siliceous oolite. *J. Geol.*, 63: 337–347.

Coplen, T.B., Kendall, C. and Hopple, J., 1983. Comparison of stable isotope reference samples. *Nature*, 302: 236–238.

Crenshaw, M.A., 1990. Biomineralization mechanisms. In: J.G. Carter (Editor), *Skeletal Biomineralization: Patterns, Processes and Evolutionary Trends*. Van Nostrand Reinhold, New York, N.Y., pp. 1–10.

Crenshaw, M.A. and Neff, J.M., 1969. Decalcification at the mantle–shell interface in molluscs. *Am. Zool.*, 9: 881–885.

Cross, T.S. and Cross, B.W., 1983. U, Sr, and Mg in Holocene and Pleistocene corals. *J. Sediment. Petrol.*, 53: 587–594.

Currey, J.D., 1990. Biomechanics of mineralized skeletons. In: J.G. Carter (Editor), *Skeletal Biomineralization: Patterns, Processes and Evolutionary Trends.* Van Nostrand Reinhold, New York, N.Y., pp. 11–26.

DeWith, N.D. and Sminia, T., 1980. The effects of the nutritional state and the external calcium concentration on the ionic composition of the haemolymph and on the calcium cells in the pulmonate freshwater snail *Lymnaea stagnalis*. *Proc. K. Ned. Akad. Wet., Ser. C*, 83: 217–227.

Dodd, J.R., 1965. Environmental control of strontium and magnesium in *Mytilus*. *Geochim. Cosmochim Acta*, 29: 385–398.

Elderfield, H., 1986. Strontium isotope stratigraphy. *Palaeogeogr., Palaeoclimatol., Palaeoecol.*, 57: 71–90.

Emig, C.C., 1990. Examples of post-mortality alteration in Recent brachiopod shells and (paleo)ecological consequences. *Mar. Biol.*, 104: 233–238.

Epstein, S., Buchsbaum, R., Lowenstam, H.A. and Urey, H.C., 1953. Revised carbonate–water isotopic temperature scale. *Bull. Geol. Soc. Am.*, 62: 417–425.

Faure, G., 1977. *Principles of Isotope Geology.* Wiley and Sons, New York, N.Y., 464 pp.

Faure, G., 1991. *Principles and Applications of Inorganic Geochemistry.* MacMillan, New York, N.Y., 626 pp.

Flessa, K.W. and Brown, T.J., 1983. Selective solution of macroinvertebrate calcareous hard parts: a laboratory study. *Lethaia*, 16: 193–205.

Fridovich, I., 1978. The biology of oxygen radicals. *Science*, 201: 875–879.

Garrels, R.M., and Christ, C.L., 1965. *Solutions, Minerals, and Equilibria*. Harper, New York, N.Y., 450 pp.

Goldhaber, M.B. and Kaplan, I.R., 1974. The sulphur cycle. In: E.D. Goldberg (Editor), *The Sea, Vol. 5, Marine Chemistry.* Wiley Interscience, London, pp. 569–655.

Goldsmith, J.R., 1983. Phase relations of rhombohedral carbonates. In: R.J. Reeder (Editor), *Carbonates: Mineralogy and Chemistry.* Mineral. Soc. Am., Bookcrafters Inc., Chelsea, Mich., pp 49–76.

Goldsmith, J.R., Graf, D.L., Witters, J. and Northrop, D.A., 1962. Studies in the system $CaCO_3$–$MgCO_3$–$FeCO_3$: 1. Phase relations; 2. Method for major element spectrochemical analysis; 3. Compositions of some ferroan dolomites. *J. Geol.*, 70: 659–688.

Gordon, L., Salutsky, M.L. and Willard, H.H., 1959. *Precipitation from Homogeneous Solution.* Wiley and Sons, New York, N.Y.

Grandjean, J., Grégoire, C. and Lutts, A., 1964. On the mineral components and the remnants of organic structures in shells of fossil molluscs. *Acad. R. Belg. Bull. Sci.*, 50: 562–595.

Grégoire, C., Duchateau, G. and Florkin, M., 1955. La trame protidique des nacres et des perles. *Ann. Inst. Oceanogr., Paris*, 31: 1–36.

Grossman, E.L. and Ku, T.L., 1986. Oxygen and carbon isotope fractionation in biogenic aragonite: temperature effects. *Chem. Geol.*, 59: 59–74.

Hallberg, R.O., 1972. Iron and zinc sulphides formed in a continuous culture of sulphate-reducing bacteria. *Neues Jahrb. Mineral., Abh.*, 11: 481–500.

Hanshaw, B.B., Back, W. and Deike, R.G., 1971. A geochemical hypothesis for the dolomitization by groundwater. *Econ. Geol.*, 66: 710–724.

Henderson, Lm. and Kracek, F.C., 1927. The fractional precipitation of barium and radium chromates. *J. Am. Chem. Soc.*, 49: 739.

Hess, J., Bender, M.L. and Schilling, J.G., 1986. Evolution of the ratio of strontium-87 to strontium-86 in seawater from the Cretaceous to present. *Science*, 231: 979–984.

Hesse, R., 1987. Selective and reversible carbonate–silica replacements in lower Cretaceous carbonate-bearing turbidites of the eastern Alps. *Sedimentology*, 34: 1055–1077.

Hesse, R., 1990. Silica Diagenesis: origin of inorganic and replacement cherts. In: I.A. McIlreath and D.W. Morrow (Editors), *Diagenesis. Geosci. Can. Ser.*, 4: 253–275.

Holland, H.D., 1984. *The Chemical Evolution of the Atmosphere and Oceans*. Princeton Press, Princeton, N.J., 582 pp.

Howarth, R.W., 1979. Pyrite — its rapid formation in a salt marsh and its importance in ecosystem metabolism. *Science*, 203: 49–51.

Hudson, J.D., 1982. Pyrite in ammonite-bearing shales from the Jurassic of England and Germany. *Sedimentology*, 29: 639–667.

Hudson, J.D. and Anderson, T.F., 1989. Ocean temperatures and isotopic compositions through time. *Trans. R. Soc. Edinburgh: Earth Sci.*, 80: 183–192.

Ishikawa, M. and Ichikuni, M., 1984. Uptake of sodium and potassium by calcite. *Chem. Geol.*, 42: 137–146.

Iwata, K., 1981a. Ultrastructure and calcification of the shells in inarticulate brachiopods. Part 1: Ultrastructure of the shell of *Lingula unguis*. *J. Geol. Soc. Jpn.*, 87: 405–415.

Iwata, K., 1981b. Ultrastructure and mineralization of the shell of *Lingula unguis* Linné (inarticulate brachiopod). *J. Fac Sci. Hokkaido Univ.*, 20: 35–65.

Jacka, A.D., 1974. Replacement of fossils by length-slow chalcedony and associated dolomitization. *J. Sediment. Petrol.*, 44: 421–427.

Jones, W.C., 1971. Spicule formation and corrosion in recently metamorphosed *Sycon ciliatum*. In: D.J. Crisp (Editor), *European Marine Biology Symposium*. Cambridge Univ. Press, Cambridge, pp. 301–320.

Karhu, J. and Epstein, S., 1986. The implications of the oxygen isotope records in coexisting cherts and phosphates. *Geochim. Cosmochim. Acta*, 50: 1745–1756.

Kato, M., 1963. Fine skeletal structure in *Rugosa*. *J. Fac Sci. Hokkaido Univ.*, 11: 571–630.

Katz, A., 1973. The interaction of magnesium with calcite during crystal growth at 25–90°C and one atmosphere. *Geochim. Cosmochim. Acta*, 37: 1563–1586.

Kázmierczak, J., Ittekot, V. and Degens, E.T., 1985. Biocalcification trough time: environmental challenge and cellular response. *Paläontol. Z.*, 59: 15–33.

Kolesar, P.T., 1978. Magnesium in calcite from a coralline alga. *J. Sediment. Petrol.*, 48: 815–819.

Lahann, R.W., 1978. A chemical model for calcite crystal growth and morphology control. *J. Sediment. Petrol.*, 48: 337–344.

Land, L.S., 1983. The application of stable isotopes to study of the origin of dolomite and to problems of diagenesis of clastic sediments. In: M.A. Arthur, T.F. Anderson, I.R. Kaplan, J. Veizer and L.S. Land (Editors), *Stable Isotopes in Sedimentary Geology. Soc. Econ. Paleontol. Mineral., Short Course*, 10 (4): 1–22.

Lindström, M. and Ziegler, W., 1981. Surface microornamentation and observations on internal composition. In: R.A. Robinson (Editor), *Treatise on Invertebrate Paleontology, Part W*. Geol. Soc. Am./Univ. Kansas Press, pp. W41–W52.

Lohmann, K.C. and Meyers, W.J., 1977. Microdolomite inclusions in cloudy prismatic calcites: a proposed criterion for former high-Mg calcites. *J. Sediment. Petrol.*, 47: 1078–1088.

Loope, D.B. and Watkins, D.K., 1989. Pennsylvanian fossils replaced by red chert: early oxidation of pyritic precursors. *J. Sediment. Petrol.*, 59: 375–386.

Lorens, R.B., 1981. Sr, Cd, Mn and Co distribution coefficients in calcite as a function of calcite precipitation rate. *Geochim. Cosmochim. Acta*, 45: 553–561.

Lowenstam, H.A., 1954. Factors affecting the aragonite:calcite ratios in carbonate-secreting marine organisms. *J. Geol.*, 62: 284–322.

Lowenstam, H.A., 1961. Mineralogy, O^{18}/O^{16} ratios, and strontium and magnesium contents of Recent and fossil brachiopods and their bearing on the history of the oceans. *J. Geol.*, 69: 241–260.

Lowenstam, H.A., 1963. Biological problems relating to the composition and diagenesis of sediments. In: T.W. Donnelly (Editor), *The Earth Sciences*. Univ. Chicago Press, Chicago, Ill., pp. 137–195.

Lowenstam, H.A., 1981. Minerals formed by organisms. *Science*, 211: 1126–1131.

Lowenstam, H.A. and Weiner, S., 1989. *On Biomineralization*. Oxford Univ. Press, New York, N.Y., 324 pp.

Machin, J., 1975. Water relationships. In: V. Fetter and J. Peake (Editors), *Pulmonates*. Academic Press, London, pp. 105–163.

Maliva, R.G. and Siever, R., 1988. Mechanism and controls of silicification of fossils in limestones. *J. Geol.*, 96: 387–398.

Martin, G.D., Wilkinson, B.H. and Lohmann, K.C., 1986. The role of skeletal porosity in aragonite neomorphism — *Strombus* and *Montastrea* from the Pleistocene Key Largo Limestone, Florida. *J. Sediment. Petrol.*, 56: 194–203.

Mason, R.A., 1987. Ion microprobe analysis of trace elements in calcite with an application to the cathode luminescence zonation of limestone cements from the lower Carboniferous of South Wales, U.K. *Chem. Geol.*, 64: 209–224.

McAllister, J.E. and Brand, U., 1989a. Primary and diagenetic microstructures in trilobites. *Lethaia*, 22: 101–111.

McAllister, J.E. and Brand, U., 1989b. Geochemistry of some Ordovician and Devonian trilobite cuticles from North America. *Chem. Geol.*, 78: 51–63.

McConnaughey, T., 1989a. ^{13}C and ^{18}O isotopic disequilibrium in biological carbonates: I. Patterns. *Geochim. Cosmochim. Acta*, 53: 151–162.

McConnaughey, T., 1989b. ^{13}C and ^{18}O isotopic disequilibrium in biological carbonates: II. *In vitro* simulation of kinetic isotope effects. *Geochim. Cosmochim. Acta*, 53: 163–171.

McIntyre, W.L., 1963. Trace element partition coefficients — a review of theory and applications to Geology. *Geochim. Cosmochim. Acta*, 27: 1209–1264.

Meyers, W.J. and Lohmann, K.C., 1975. Stable isotope geochemistry of regionally extensive calcite cement zones and marine components in Mississippian limestones, New Mexico. In: N. Schneiderman and P.M. Harris (Editors), *Carbonate Cements. Soc. Econ. Paleontol. Mineral., Spec. Publ.*, 36: 223–240.

Milliken, K.L., 1979. The silicified evaporite syndrome — two aspects of silicification history of former evaporite nodules from southern Kentucky and northern Tennessee. *J. Sediment. Petrol.*, 49: 245–256.

Milliman, J.D., 1974. *Marine Carbonates.* Springer-Verlag, Berlin, 375 pp.

Moberly, R., 1968. Composition of magnesian calcites of algae and pelecypods by electron microprobe analysis. *Sedimentology*, 11: 61–82.

Morrison, J.O. and Brand, U., 1986. Paleoscene #5. Geochemistry of Recent marine invertebrates. *Geosci. Can.*, 13: 237–254.

Morrison, J.O., Brand, U. and Rollins, H.B., 1985. Paleoenvironmental and chemical analysis of the Pennsylvanian Brush Creek fossil allochems, Pennsylvania, U.S.A. *10th Int. Carboniferous Congr., Madrid, Sept. 12–17, 1983. C. R. (Madrid)*, 2: 271–280.

Morse, J.W., 1974. Dissolution kinetics of calcium carbonate in seawater, V: Effects of natural inhibitors and the position of the chemical lysocline. *Am. J. Sci.*, 274: 638–647.

Morse, J.W., 1983. The kinetics of calcium carbonate dissolution and precipitation. In: R.J. Reeder (Editor), *Carbonates: Mineralogy and Chemistry.* Mineral. Soc. Am., Bookcrafters Inc., Chelsea, Mich., pp. 227–264.

Morse, J.W. and Mackenzie, F.T., 1990. *Geochemistry of Sedimentary Carbonates.* Elsevier, Amsterdam, 707 pp.

Morse, J.W., Mucci, A. and Millero, F.J., 1980. The solubility of calcite and aragonite in seawater of 35‰ salinity and atmospheric pressure. *Geochim. Cosmochim. Acta*, 44: 85–94.

Mucci, A., Canuel, R. and Zhong, S., 1989. The solubility of calcite and aragonite in sulfate-free seawater and the seeded growth kinetics and composition of the precipitates at 25°C. *Chem. Geol.*, 74: 309–320.

Nestaas, I. and Terjesen, S.G., 1969. The inhibiting effect of scandium ions upon the dissolution of calcium carbonate. *Acta Chem. Scandinavica*, 23: 2519–2531.

Neugebauer, J., 1978. Micritization of crinoids by diagenetic dissolution. *Sedimentology*, 25: 267–283.

Neugebauer, J., 1979. Drei Probleme der Echinodermendiagenese: Innere Zementation, Mikroporenbildung und der Übergang von Magnesiumcalcit zu Calcit. *Geol. Rundsch.*, 68: 856–875.

Nicol, J.A.C., 1967. *The Biology of Marine Animals.* Sir Isaac Pitman and Sons, London, 2nd ed., 699 pp.

Oekentorp, K., 1980. Aragonit und diagenese bei jungpaläozoischen Korallen. *Münster. Forsch. Geol. Paläontol,*. 52: 119–239.

Palmer, A.R., 1981. Do carbonate skeletons limit the rate of body growth? *Nature*, 292: 150–152.

Palmer, A.R., 1983. Relative cost of producing skeletal organic matrix versus calcification: evidence from marine gastropods. *Mar. Biol.*, 75: 287–292.

Palmer, M.R. and Elderfield, H., 1985. The Sr isotopic composition of seawater over the past 75 million years. *Nature*, 314: 526–528.

Pedone, V.A., Cercone, K.R. and Burruss, R.C., 1990. Activators of photoluminescence in calcite: evidence from high-resolution, laser-excited luminescence spectroscopy. *Chem. Geol.*, 88: 183–190.

Peterman, Z.E., Hedge, C.E. and Tourtelot, H.A., 1970. Isotopic composition of strontium in sea water throughout Phanerozoic time. *J. Geochem. Meteorol. Soc.*, 34: 105–120.

Peyer B., 1968. *Comparative Odontology.* Chicago Univ. Press, Chicago, Ill., 347 pp.

Pingitore, N.E., Jr., 1976. Vadose and phreatic diagenesis processes, products, and their recognition in corals. *J. Sediment Petrol.*, 46: 985–1006.

Pingitore, N.E., Jr., 1978. The behavior of Zn^{2+} and Mn^{2+} during diagenesis: theory and application. *J. Sediment. Petrol.*, 48: 799–814.

Pingitore, N.E., Jr., 1982. The role of diffusion during carbonate diagenesis. *J. Sediment. Petrol.*, 52: 27–39.

Pingitore, N.E., Jr. and Eastman, M.P., 1985. Barium partitioning during the transformation of corals from aragonite to calcite. *Chem. Geol.*, 48: 183–187.

Pingitore, N.E., Jr. and Eastman, M.P., 1986. The coprecipitation of Sr^{2+} with calcite at 25°C and 1 atm. *Geochim. Cosmochim. Acta*, 50: 799–814.

Pingitore, N.E., Jr. and Eastman, M.P., 1989. Barium variation in *Acropora palmata* and *Montastrea annularis*. *Coral Reefs*, 8: 31–36.

Plummer, L.N. and Busenberg, E., 1987. Thermodynamics of aragonite–strontianite solid solutions: results from stoichiometric solubility at 25 to 76°C. *Geochim. Cosmochim. Acta*, 51: 1393–1411.

Plummer, L.N. and Mackenzie, F.T., 1974. Predicting mineral solubility from rate data: application to the dissolution of magnesian calcites. *Am. J. Sci.*, 274: 61–83.

Popp, B.N., Anderson, T.F. and Sandberg, P.A., 1986a. Textural, elemental, and isotopic variations among constituents in Middle Devonian limestones, North America. *J. Sediment. Petrol.*, 56: 715–727.

Popp, B.N., Anderson, T.F. and Sandberg, P.A., 1986b. Brachiopods as indicators of original isotopic compositions in some Paleozoic limestones. *Geol. Soc. Am. Bull.*, 97: 1262–1269.

Ragland, P.C., Pilkey, O.H. and Blackwelder, B.W., 1979. Diagenetic changes in the elemental composition of unrecrystallized mollusk shells. *Chem. Geol.*, 25: 123–134.

Raiswell, R. and Berner, R.A., 1985. Pyrite formation in euxinic and semieuxinic sediments. *Am. J. Sci.*, 285: 710–724.

Ramberg, H., 1947. The force of crystallization as a well definable property of crystals. *Geol. Foren. Stockholm Forh.*, 69: 189–194.

Reeder, R.J. (Editor), 1983. *Carbonates: Mineralogy and Chemistry.* Mineral. Soc. Am., Bookcrafters Inc., Chelsea, Mich., 394 pp.

Reddy, M.M. and Wang, K.K., 1980. Crystallization of calcium carbonate in the presence of metal ions, I. Inhibition of magnesium ion at pH 8.8 and 25°C. *J. Crystal Growth*, 50: 470–480.

Rhoads, D.C. and Lutz, R.A., 1980. *Skeletal Growth of Aquatic Organisms.* Plenum Press, New York, N.Y., 750 pp.

Richter, D.K., 1974. Zur subaerischen Diagenese von Echinidenskeletten und das relative Alter pleistozäner Karbonatterrassen bei Korinth (Griechenland). *Neues Jahrb. Geol. Paläontol., Abh.*, 146: 51–77.

Riddle, W.A., 1981. Hemolymph osmoregulation and urea retention in the woodland snail. *Comp. Biochem. Physiol.*, 69: 493–498.

Rollins, H.B., Eldredge, N. and Spiller, J., 1971. Gastropoda and monoplacophora of the Solsville members (Middle Devonian, Marcellus Formation) in the Chenango Valley, New York State. *Am. Mus. Nat. Hist.*, 144: 131–170.

Rosenberg, G.D., 1980. An ontogenetic approach to the environmental significance of bivalve shell chemistry. In: D.C. Rhoads and R.A. Lutz (Editors), *Skeletal Growth of Aquatic Organisms.* Plenum Press, New York, N.Y., pp. 133–168.

Rosenberg, G.D., 1990. The "vital effect" on skeletal trace element content as exemplified by magnesium. In: J.G. Carter (Editor), *Skeletal Biomineralization: Patterns, Processes and Evolutionary Trends*. Van Nostrand Reinhold, New York, N.Y., pp. 567–578.

Rubinson, M. and Clayton, R.N., 1969. Carbon-13 fractionation between aragonite and calcite. *Geochim. Cosmochim. Acta*, 33: 997–1002.

Runnegar, B., 1985. Shell microstructures of Cambrian molluscs replicated by phosphate. *Alcheringa*, 9: 245–257.

Rush, P.F. and Chafetz, H.S., 1990. Fabric-retentive, non-luminescent brachiopods as indicators of original $\delta^{13}C$ and $\delta^{18}O$ composition: a test. *J. Sediment. Petrol.*, 60: 968–981.

Saelen, G., 1989. Diagenesis and construction of the belemnite rostrum. *Palaeontology*, 32: 765–798.

Saelen, G. and Karstang, T.V., 1989. Chemical signatures of belemnites. *Neues Jahrb. Geol. Paläontol., Abh.*, 177: 334–346.

Shemesh, A., 1990. Crystallinity and diagenesis of sedimentary apatites. *Geochim. Cosmochim. Acta*, 54: 2433–2438.

Siever, R., 1962. Silica solubility, 0–200°C, and the diagenesis of siliceous sediments. *J. Geol.*, 70: 127–150.

Simkiss, K., 1983. Trace elements as probes of biomineralization. In: P. Westbroek and E.W. deJong (Editors), *Biomineralization and Biological Metal Accumulation*. Reidel, Dordrecht, pp. 363–371.

Simkiss, K. and Mason, A.Z., 1983. Metal ions: metabolic and toxic effects. In: P.W. Hochadika (Editor), *The Mollusca*. 2: 101–164.

Sjöberg, E.L., 1978. Kinetics and mechanism of calcite dissolution in aqueous solutions at low temperatures. *Acta Univ. Stockholm, Contrib. Geol.*, 332: 1–92.

Sjöberg, E.L. and Rickard, D.T., 1984. Calcite dissolution kinetics: surface speciation and the origin of the variable pH dependence. *Chem. Geol.*, 42: 119–136.

Sjöberg, E.L. and Rickard, D.T., 1985. The effect of added dissolved calcium on calcite dissolution kinetics in aqueous solutions at 25°C. *Chem. Geol.*, 49: 405–413.

Smith, P.E., Brand, U. and Farquhar, R.M., 1991. U-Pb systematics with trace element and stable isotope geochemistry: a new tool for carbonate diagenesis. *Geol. Assoc. Can., Prog. Abstr.*, 16: A116.

Sorauf, J.E., 1971. Microstructure in the exoskeleton of some *Rugosa* (Coelenterata). *J. Paleontol.*, 45:, 23–32.

Span, D. and Gaillard, J.F., 1986. An investigation of a procedure for determining carbonate-bound trace metals. *Chem. Geol.*, 56: 135–141.

Stehli, F.J., 1956. Shell mineralogy in Paleozoic invertebrates. *Science*, 123: 1031–1032.

Swart, P.K., 1984. U, Sr, and Mg in Holocene and Pleistocene corals: discussion. *J. Sediment. Petrol.*, 54: 326–328.

Sweeney, R.E. and Kaplan, I.R., 1973. Pyrite framboid formation — laboratory synthesis and marine sediments. *Econ. Geol.*, 68: 618–634.

Tarutani, T., Clayton, R.N. and Mayeda, T.K., 1969. The effect of polymorphism and magnesium substitution on oxygen isotope fractionation between calcium carbonate and water. *Geochim. Cosmochim. Acta*, 33: 987–996.

Taylor, T.R. and Sibley, D.F., 1986. Petrographic and geochemical characteristics of dolomite types and the origin of ferroan dolomite in the Trenton Group, Ordovician, Michigan Basin, U.S.A. *Sedimentology*, 33: 61–86.

Towe, K.M., 1967. Echinoderm calcite: single crystal or polycrystalline aggregate. *Science*, 157: 1048–1050.

Turner, J.V., 1982. Kinetic fractionation of carbon-13 during calcium carbonate precipitation. *Geochim. Cosmochim. Acta*, 46: 1183–1191.

Turner, J.V., Anderson, T.F., Sandberg, P.A. and Goldstein, S.J., 1986. Isotopic, chemical and textural relations during the experimental alteration of biogenic high-Mg calcite. *Geochim. Cosmochim. Acta*, 50: 495–506.

Urey, H.C., 1947. The thermodynamic properties of isotopic substances. *J. Am. Chem. Soc.*, 57: 321.

Urey, H.C., Lowenstam, H.A., Epstein, S. and McKinney, C.R., 1951. Measurement of paleotemperatures and temperatures of the upper Cretaceous of England, Denmark, and the southeastern United States. *Bull., Geol. Soc. Am.*, 62: 399–416.

Veizer, J., 1977. Geochemistry of lithographic limestones and dark marls from the Jurassic of southern Germany. *Neues Jahrb. Geol. Paläontol., Abh.*, 153: 129–146.

Veizer, J., 1983a. Chemical diagenesis of carbonates: theory and applications of trace element technique. In: M.A. Arthur, T.F. Anderson, I.R. Kaplan, J. Veizer and L.S. Land (Editors), *Stable Isotopes in Sedimentary Geology. Soc. Econ. Paleontol. Mineral., Short Course*, 10 (3): 1–100.

Veizer, J., 1983b. Trace elements and isotopes in sedimentary carbonates. In: R.R. Reeder (Editor), *Carbonates: Mineralogy and Chemistry.* Mineral. Soc. Am., Bookcrafters Inc., Chelsea, Mich., pp. 265–300.

Veizer, J., 1989. Strontium isotopes in seawater through time. *Annu. Rev. Earth Planet. Sci.*, 17: 141–167.

Veizer, J., Fritz, P. and Jones, B., 1986. Geochemistry of brachiopods: oxygen and carbon isotopic records of Paleozoic oceans. *Geochim. Cosmochim. Acta*, 50: 1679–1696.

Wadleigh, M.A. and Veizer, J., 1990. Oxygen and carbon record of Paleozoic brachiopods. *Geol. Soc. Am. Abst. Prog.*, A114.

Waller, T.R., 1983. Dahllite in the periostracum of *Lithophaga nigra* (Mollusca: Bivalvia) and its taxonomic and functional implications. *Am. Malacol. Bull.*, 1: 1–101.

Walter, L.M. and Morse, J.W., 1984. Reactive surface area of skeletal carbonates during dissolution: effect of grain size. *J. Sediment. Petrol.*, 54: 1081–1090.

Walter, L.M. and Morse, J.W., 1985. The dissolution kinetics of shallow marine carbonates in seawater: a laboratory study. *Geochim. Cosmochim. Acta*, 49: 1503–1513.

Watabe, N., 1990. Calcium phosphate structures in invertebrates and protozoans. In: J.G. Carter (Editor), *Skeletal Biomineralization: Patterns, Processes and Evolutionary Trends.* Van Nostrand Reinhold, New York, N.Y., pp. 35–44.

Weber, J.N., 1967. Possible changes in the isotopic composition of the oceanic and atmospheric carbon reservoir over geologic time. *Geochim. Cosmochim. Acta*, 31: 2343–2351.

Weber, J.N., 1968. Fractionation of the stable isotopes of carbon and oxygen in calcareous marine invertebrates — the Asteroidea, Ophuiroidea, and Crinoidea. *Geochim. Cosmochim. Acta*, 32: 33–70.

Wendt, J., 1990. The first aragonitic rugose coral. *J. Paleontol.*, 64: 335–349.

Weyl, P.W., 1959. Pressure solution and the force of crystallization — phenomenological theory. *J. Geophys. Res.*, 64: 2001–2025.

Wilkinson, B.H., 1979. Biomineralization, paleoceanography, and the evolution of calcareous marine organisms. *Geology*, 7: 524–527.

Wilmot, N.V., 1990. Primary and diagenetic microstructures in trilobite exoskeletons. *Hist. Biol.*, 4: 51–65.

Wilmot, N.V. and Fallick, A.E., 1989. Original mineralogy of trilobite exoskeleton. *Paleontology*, 32: 297–304.

Wright, J., 1990. Conodont apatite: structure and geochemistry. In: J.G. Carter (Editor), *Skeletal Biomineralization: Patterns, Processes and Evolutionary Trends.* Van Nostrand Reinhold, New York, N.Y., pp. 445–460.

Zenger, D.H., Dunham, J.B. and Ethington, R.L., 1980. Concepts and Models of Dolomitization. *Soc. Econ. Palaeontol. Mineral., Spec. Publ.*, 28: 320 pp.

Zolotarev, V.N., 1976. Early diagenetic alterations in the chemical composition of marine mollusk shells. *Litol. Polezn. Iskop.*, 3: 20–29.

Diagenesis, IV. Developments in Sedimentology 51
edited by K.H. Wolf and G.V. Chilingarian
© 1994 Elsevier Science B.V., Amsterdam. All rights reserved.

Chapter 9

MULTIPLE DOLOMITIZATION OF THE WARSAW AND SALEM FORMATIONS (MIDDLE MISSISSIPPIAN), WESTERN FLANK OF THE ILLINOIS BASIN: TEXTURAL, TRACE ELEMENTAL, AND ISOTOPIC SIGNATURES OF FOUR TYPES OF DOLOMITE — A CASE STUDY

DEBA P. BHATTACHARYYA and MARK R. SEELY

INTRODUCTION

Sediments go through a sequence of diagenetic changes influenced by their depositional and diagenetic environments, both of which exert major control on the composition of the pore fluid responsible for the changes. In a marginal marine depositional system the coastal water, along with the underlying sediment pore water, develops coast-parallel compositional belts by processes inherent in the depositional environment, i.e., evaporation, freshwater influx, nature of circulation, etc., which influence the diagenesis of associated sediments. During diagenesis, too, the pore fluid constantly evolves through processes inherent in the diagenetic system such as, among others, dissolution–reprecipitation, oxidation–reduction, rate of fluid migration and thermal state of the basin. Inasmuch as carbonate sediments respond easily to any change in the composition of the interstitial fluid, both these controls should have perceptible influence on their diagenesis. Moreover, in an open system the diagenetic processes are gradational from one to the other. As a result, the product of an earlier process continuously reequilibrates to the new environment imposed on it, and the "process-fingerprints" on the final product are often of those related to the final phase of diagenesis (Land, 1980, 1985). The "openness" of a diagenetic system, however, is dependent on the permeability of the rocks involved. It may vary widely not only from facies to facies but also within the same facies, and may be enhanced or reduced during any stage of diagenesis. This is particularly true for carbonate rocks which are susceptible to drastic changes in permeability at every stage of their diagenesis. Consequently, a system which is open during a stage of diagenesis may or may not remain open during the subsequent stage(s), and the products of each of the diagenetic stages may be partially preserved within specific parts of the rock that remained closed to subsequent diagenetic episodes.

The carbonate sequences of the Warsaw and Salem formations (Middle Mississippian) of eastern Missouri along the western margin of the Illinois basin represent a case in point. These rocks were affected by a number of diagenetic processes. Some of these processes operated concurrently, but independently, in different parts of the sequence, whereas others acted in temporal succession variably modifying the product(s) of earlier episode(s). The purpose of this study was to: (1) elucidate the various controls and episodes of dolomitization in this sequence, (2) characterize the petrographic, chemical and isotopic properties of the products of each of these diagenetic episodes, and (3) to evaluate the extent of modification caused by the subsequent episodes in order to reconstruct the diagenetic history of these rocks. This information is useful in better understanding the dolomitization process, and in the exploration of energy resources in parts of the Illinois Basin where equivalent sequences with similar depositional and diagenetic histories are hydrocarbon reservoirs (Cluff and Lineback, 1981; Cluff, 1984; Carpenter and Keller, 1986; Nellist, 1987). In addition, the latest generation of dolomite in the Warsaw–Salem sequence is probably equivalent to the ferroan "ore stage" dolomite associated with the Mississippi Valley-type (MVT) Pb–Zn mineralization in the area (Choquette and Steinen, 1980; Cobb, 1981; Cander et al., 1988; Gregg, 1988; Gregg and Shelton, 1990). The data on this type of dolomite, therefore, may provide further constraints on the genesis of the MVT ore deposits.

METHODS OF STUDY

Thirteen representative stratigraphic sections were measured and sampled in the study area (Fig. 9-1). Prior to the petrographic studies the thin-sections were stained with combined alizarin red and potassium ferricyanide (Evamy, 1963) in order to distinguish various carbonate mineral types in the samples. Major and trace elements were analyzed on a fresh set of doubly polished thin-sections by a Jeol 733 superprobe for Ca, Mg, Fe, Na and Sr. The analytical precision are: better than 0.5 relative percent for Ca and Mg, 5 relative percent for Fe, 50 relative percent for Mn and Sr, and 25 relative percent for Na.

For isotopic analyses, the dolomites were disaggregated from the rock by treatment with 1% hydrochloric acid solution. Subsequent treatment with 2.5% HCl removed all calcite from the disaggregated grains. Thoroughly washed, clay-free disaggregates were then dried at room temperature and sieved to −325 mesh (−44 μm) to remove the coarser dolomites and other impurities. Because of the inherent size difference between the major dolomite types in the studied samples, a significant separation of these types from the −325 mesh fractions of the samples was achieved by repeated settling from distilled water suspensions. Further separation into principal subsamples by type was done by a magnetic separator. Only the dominant dolomite type from each sample was selected for analysis. The purity of each analyzed subsample was checked by staining and X-ray diffractometry.

The CO_2 gas liberated from each sample by reaction with anhydrous phosphoric acid at 75°C for 24 hours was analyzed for carbon and oxygen isotopes by a Finnigan Delta-E mass spectrometer having a 9 cm deflection radius. The average yield of CO_2 by this method was better than 99% with an analytical precision of 0.05‰ or better. A fractionation factor of 1.00932 for the reaction temperature of 75°C was used to correct the oxygen isotopic analyses with respect to SMOW. The data were then converted to the PDB standard using the equation $\delta^{18}O_{(PDB)} = [\delta^{18}O_{(SMOW)} - 30.86]/1.03086$ (Land, 1980).

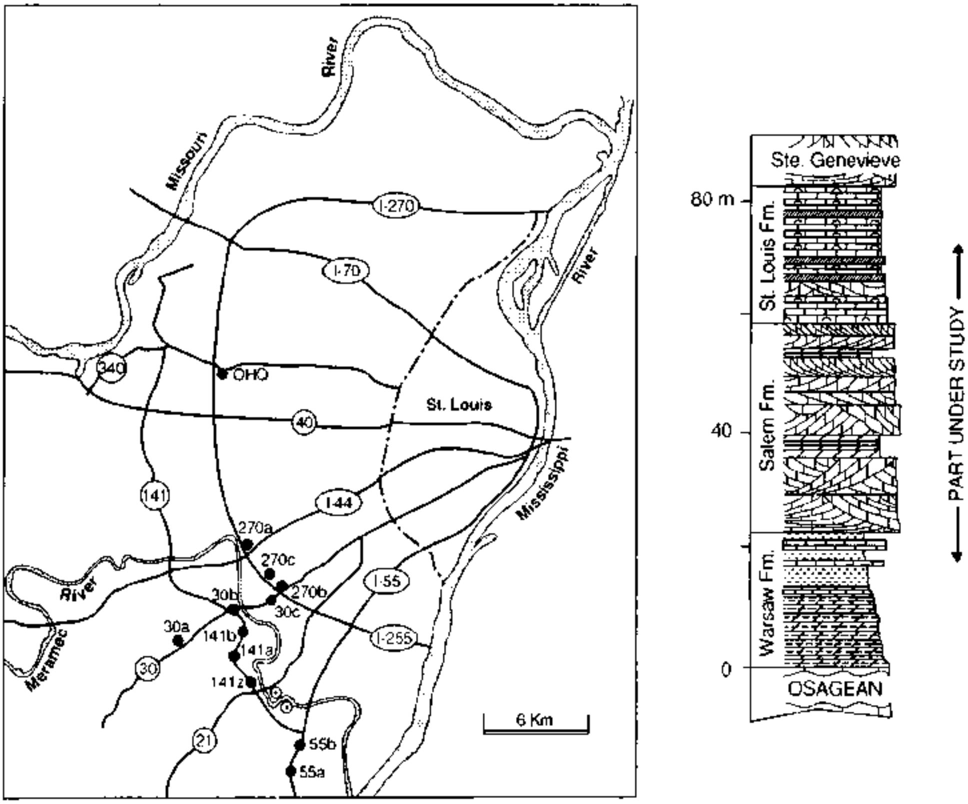

Fig. 9-1. Study area and generalized stratigraphic succession of the Middle Mississippian rocks in eastern Missouri.

GEOLOGICAL SETTING

The Meramecian (Middle Mississippian) sequence of eastern Missouri consists of four formations (Howe and Koenig, 1961). From bottom to top these are: the Warsaw, Salem, St. Louis, and Ste. Genevieve formations (Fig. 9-1). In the study area (Fig. 9-1), however, only the lower three formations are present. The following brief descriptions, therefore, are restricted to these three formations.

The Warsaw Formation consists of a gray, shaly, dolomitic mudstone with thin intercalations of very coarse- to coarse-grained grainstones. The lower half of the unit is a shaly dolostone, whereas the upper half is composed of a dark fissile dolomitic shale.

The Salem Formation is composed of very coarse- to medium-grained grainstone and packstone with interbedded mudstone and wackestone units. The grainstone and packstone are light gray to brownish gray and pale yellow in color, locally oolitic, and are conspicuously cross-bedded, cross-laminated or ripple-laminated. The mudstone and the wackestone, on the other hand, are tan and brown in color, and are generally massive and structureless.

Bluish-gray, finely laminated lime mudstone with intercalations of pale-yellow, medium- to fine-grained, cross-bedded to cross-laminated grainstone and tan-brown, massive dolomitic mudstone comprise the St. Louis Formation.

Extended discussions about the spatial distribution, paleontology, and regional correlations of the Meramecian formations of Missouri are given by Howe and Koenig (1961) and Stichcomb and Fellows (1968).

LITHOFACIES AND DEPOSITIONAL HISTORY

The Warsaw and Salem formations, with a cumulative thickness of about 80 m, consist of six major lithofacies (Fig. 9-2): (F1) graded grainstone and packstone; (F2) gray dolomitic mudstone; (F3) biohermal mudstone; (F4) cross-bedded, very coarse-grained grainstone and packstone; (F5) massive brown dolomitic mudstone and wackestone; and (F6) medium-grained, well-sorted and cross-laminated grainstone. The diagnostic characters of these facies are summarized in Table 9-1.

The Warsaw Formation is composed of facies F1 to F3, and the Salem Formation comprises facies F4 to F6 described above (Fig. 9-2).

The lithologic characters and associated sedimentary structures of the Warsaw–Salem lithofacies suggest that the facies sequence represents the deposits of a single

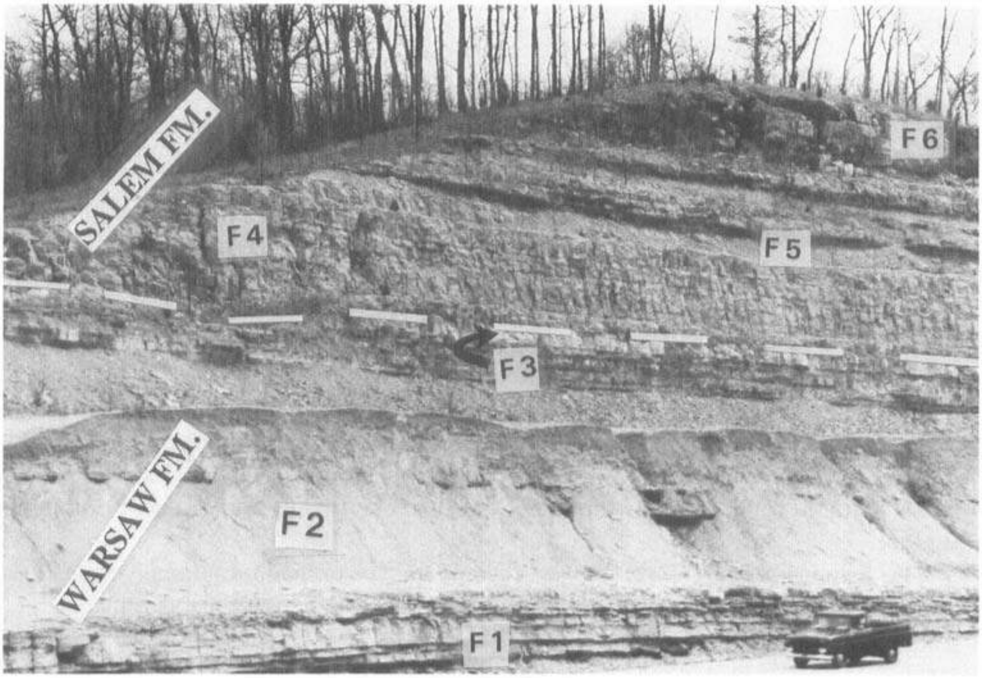

Fig. 9-2. Lithofacies sequence of the Warsaw–Salem formations at location 141Z in Fig. 9-1. *F1–F6* = Facies 1 to 6.

TABLE 9-1

Diagnostic characters and inferred depositional environments of the Warsaw and Salem lithofacies

Facies	Lithology	Diagnostic characters	Inferred depositional environment
F1	Graded grain- and packstone, coarse- to fine-grained.	Thin, graded-bedded, sheet-like individual beds with erosional base, and hummocky cross-stratification, rippled and planar laminanation in the upper part. Commonly in stacks of top-truncated Bouma sequences.	Storm-surge deposits on shallow open marine shelf below fair weather but above storm-wave base.
F2	Dark gray mudstone.	Laminated to bioturbated, massive, rich in organic and argillaceous matter.	Shallow open marine shelf below fair-weather wave base.
F3	Biohermal mudstone.	Light gray to tan with biohermal mounds delicately preserving a diverse biota, but dominated by bryozoa.	Open marine shallow subtidal shelf. Biohermal barrier.
F4	Cross-bedded, very coarse-grained grain- and packstone.	Lenticular sandbodies with channeled base and large-scale bipolar trough cross-beds.	Tidal channels, shoals, washover deposits.
F5	Massive, brown mud- and wackestone.	Massive, bioturbate to poorly laminated.	Subtidal lagoon to intertidal mudflat.
F6	Cross-laminated grainstone.	Medium-grained, well-sorted grainstone with highly abraded grains and small-scale cross-beds, rippled beds and ripple-laminations.	Shoreface to strandplain.

regressive outbuilding or shoaling of a carbonate ramp similar to those of the modern Campeche Bank of Mexico, or the Jurassic Smackover–Cotton Valley formations in the subsurface of the Gulf Coast of U.S.A. (Ahr, 1973; Mullins et al., 1988). Table 9-1 summarizes the diagnostic characters and inferred depositional environments of the Warsaw–Salem lithofacies, and Fig. 9-3 represents a depositional model of this ramp.

The critical stage in this ramp outbuilding, however, was the development of a chain of biohermal mud-mounds (i.e., F3) that divided the shelf into two distinct depositional regimes (Fig. 9-3): (1) an eastern open, shallow marine shelf of normal marine sedimentation; and (2) a western restricted part of the ramp where shoals, lagoons, tidal flats, and strandplains developed under fluctuating marginal marine conditions. Incidentally, these two depositional regimes nearly conform to the two stratigraphic formations, the Warsaw and the Salem, respectively, designated in the area. The uppermost member of the Warsaw Formation, i.e., the biohermal mound of F3, thus, formed a transition zone between the normal marine and restricted

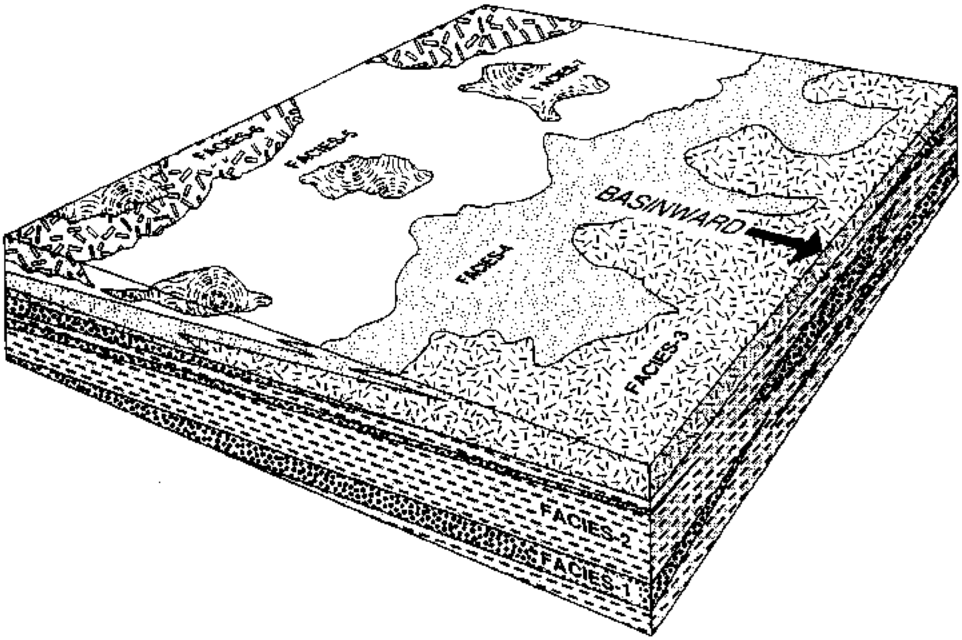

Fig. 9-3. Depositional model for the Warsaw–Salem lithofacies in eastern Missouri.

marine depositional environments, and was influenced, in part, by the depositional and diagenetic processes of both regimes. But, by virtue of being a physical barrier of dense mudstone lithology, it also served as a barrier to the fluids of early diagenetic origin within the two regimes.

Along the outer margin of this ramp, the argillaceous lime mudstones (F2) were deposited under shallow, open marine condition below the influence of wave or current energies prevalent during fair weather. During periodic high-energy (storm) events, storm-generated surges brought in the coarser inner-shelf bioclastic material across the biohermal mound barrier on to the open shelf as density currents from which the graded grainstones (F1) were deposited as thin sheets on the muddy, open marine shelf. The transition from F3 to F4 illustrates the transition from open marine shelf to a restricted shelf under the influence of tidal currents and waves. The trough cross-bedded grainstones of the F4 represent the deposits of tidal channels, shoals and washover fans. The mudstones of F5 were deposited in restricted lagoons and tidal flats behind the complex of biohermal barrier and tidal channels so that, unlike the F3, the stenohaline biota could not colonize it. The final phase of the first shoaling event is represented by the strandplain grainstones of F6 with its characteristic texture and very shallow wave and current-dominated structures.

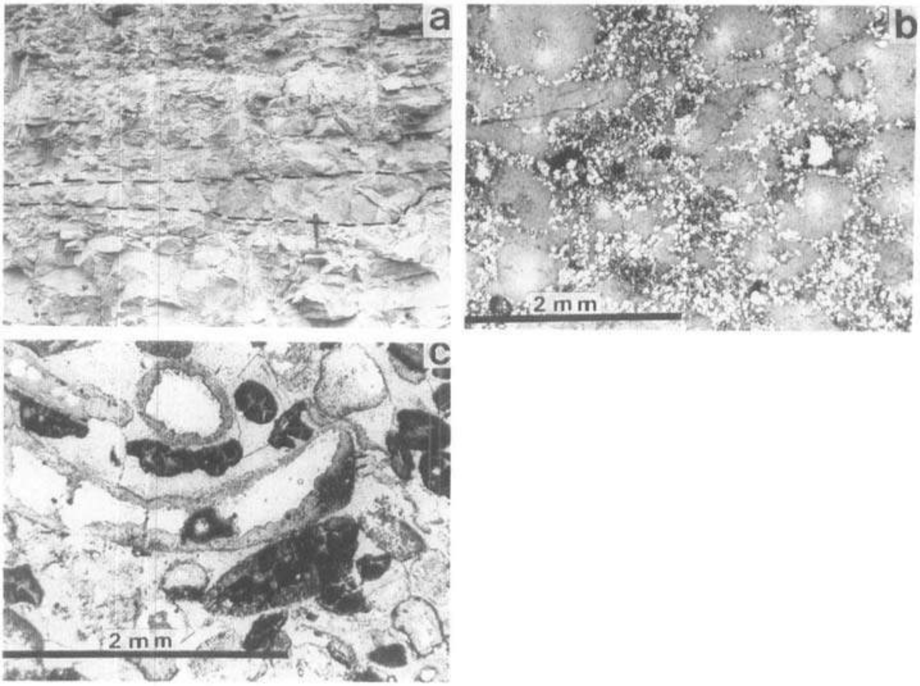

Fig. 9-4. Facies- and fabric component-selective dolomitization in the Middle Mississippian rocks of eastern Missouri. (a) Totally dolomitized lagoonal/tidal flat mudstone (F5) interbed in undolomitized tidal channel grainstone (F6) sequence. (b) Thin-section of a tidal channel packstone (F4) with dolomitized matrix and stabilized bioclasts. (c) Extensive spar-cementation and selective silicification of the bioclasts by microcrystalline quartz in matrix-free tidal channel grainstone (F4).

DOLOMITES

The dolomites in the Warsaw and Salem formations are facies- and fabric component-selective (Fig. 9-4) such that all mudstones and the matrix mud of the grainstones, packstones and wackestones are totally dolomitized (Fig. 9-4a, b). The matrix-free grainstones, on the other hand, are not dolomitized at all, but are cemented by blocky spar (Fig. 9-4c). Four types of dolomites occur in these rocks (Table 9-2). Two of these types are matrix-replacive, whereas the other two types occur as cement. Table 9-2 summarizes the distinguishing characteristics of the dolomite types in the Warsaw–Salem sequence.

In addition to being facies- and fabric component-selective, each one of the dolomite types T1 through T3 occurs in the lithofacies of a specific depositional regime (Table 9-3). For example, the matrix-replacive T1 and the associated T2 cement dolomites occur only in the restricted marine shoreline facies association (F3 to F5). The limpid cement dolomite (T2) is also restricted to the shoreline facies association. In samples where both T1 and T2 occur together, the T2 dolomites aggrade from T1 matrix into the adjoining pores (Fig. 9-5c). The amount of T2

TABLE 9-2

Dolomite types in the Warsaw and Salem formations

Type	Mode of occurrence and texture	Diagnostic characters	Figure illustrations
T1	Matrix-replacive, xenotopic.	Fine-grained (<10 μm), non-ferroan, non-zoned; cloudy and dusty in appearance due to numerous fluid inclusions.	Fig. 9-5a, b.
T2	Cement; limpid, idiotopic.	Coarser (30–50 μm), clear, locally slightly to moderately ferroan, non-zoned.	Fig. 9-5c, d.
T3	Matrix-replacive, idiotopic to subidiotopic.	Fine-grained (10–15 μm) clear, iron zoned with diffused zone boundaries.	Fig. 9-5e, f.
T4	Cement; idiotopic saddle dolomite.	Strongly ferroan, clear and non-zoned; commonly occurs as >100 μm isolated rhombs in pore spaces, or as a sharply defined outer-most rim around all other types. Commonly, the larger rhombs contain a core of other types.	Fig. 9-5g, h.

dolomite, however, is highly variable not only between samples but also within any specific sample even in the scale of a thin section (Fig. 9-5a), and is clearly related to the permeability of any specific sample, or part of the sample, prior to the formation of this type of cement. For example, the massive, tan-brown dolostones (F5) without any pores, or even those with isolated moldic pores, contain very little, if any, T2 dolomite (Fig. 9-5a). On the other hand, a zone of limpid T2 dolomite cement forms along zones of spar-filled moldic pores in a sample that originally contained thin laminae of scattered skeletal debris which, during T1 dolomitization, gave rise to linked moldic pores due to dissolution of the skeletal grains. Inasmuch as the T1 and T2 dolomites have very distinctive appearance in thin section, it is, therefore, not uncommon to find patchy, pore-centered or lamina-parallel zones of concentration of T2 dolomite in the thin sections of samples (Figs. 9-5a and 9-5c) which, in hand sample, appear massive and homogeneous. Thus, the absence or presence and the frequency of occurrence of these bright patches and zones of T2 dolomite in thin sections of the dolomitic mudstones of Facies 5 can be used to estimate the relative

---

Fig. 9-5. Dolomite types in the Warsaw–Salem formations. (a) Matrix-replacive, fine-grained, xenotopic T1 dolomite. No modification of the T1 dolomite in the right two-thirds of the picture although there are large but scattered moldic pores (i.e., high porosity–low permeability), whereas the left one-third part shows aggradational texture and extensive development of T2 dolomite because of higher permeability in that part. (b) Backscattered Electron Image (BEI) of T1 dolomite. There are large number of inclusion cavities, probably due to fluid inclusions. (c) Larger, clear, limpid, idiotopic T2 dolomite cement. There is aggradation from T1 in the secondary pore. (d) BEI of T2 showing idiotopic habit and smooth, inclusion-free character. (e) Matrix-replacive, fine-grained, iron-zoned T3 dolomite. (f) BEI of T3 dolomite showing characters common to both T1 and T2 dolomites. (g) Large rhombs of T4 ferroan saddle dolomite cement in the secondary pore. Nucleus of T2 dolomite within the saddle dolomite grains. (h) BEI of T4 dolomite.

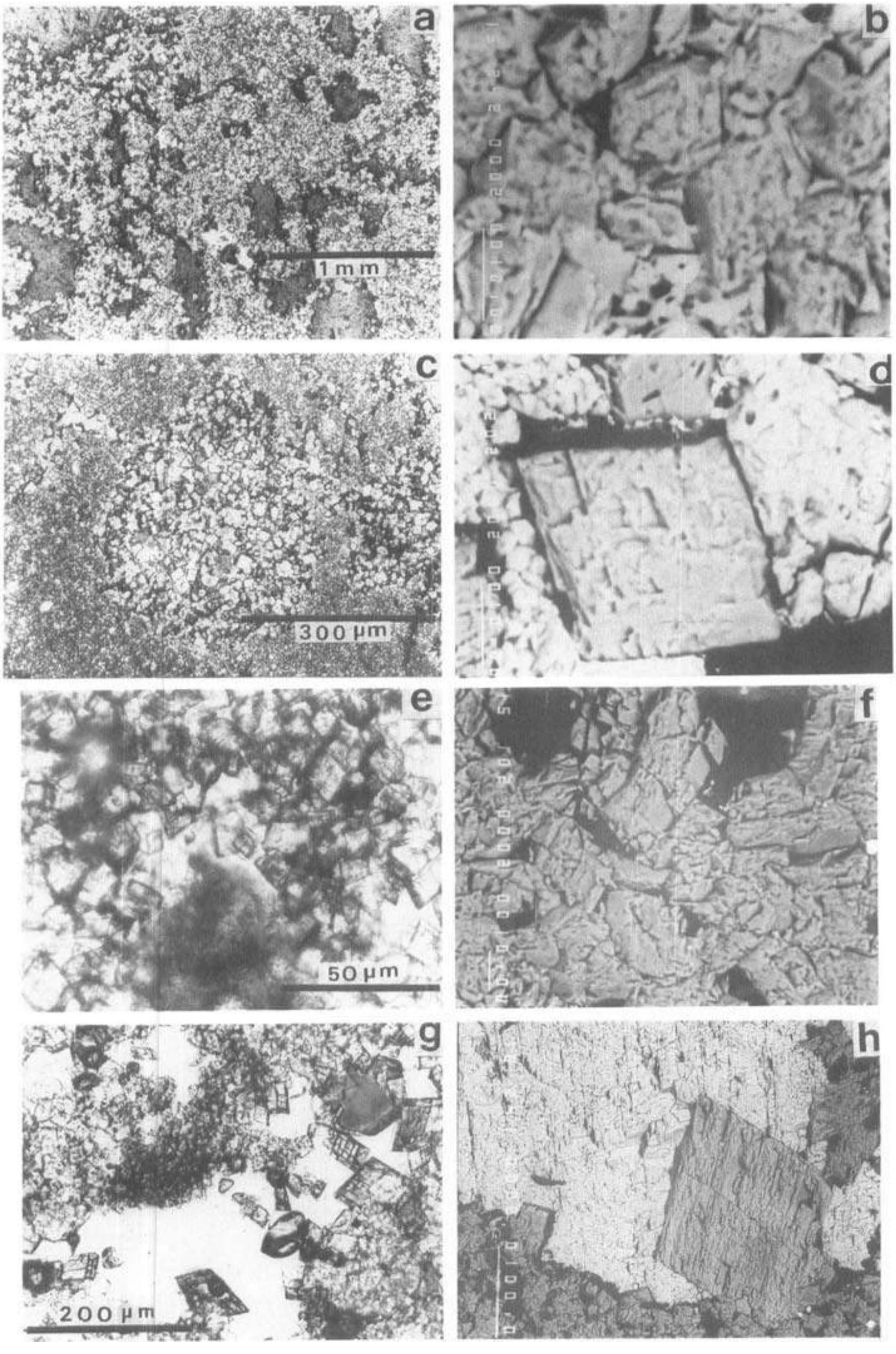
a
1 mm
b
c
300 µm
d
e
50 µm
f
g
200 µm
h

TABLE 9-3

Association and other significant characters of the dolomite types

Facies association	Dolomite types	Significant characters and association
Near-shore, restricted marine, F3 (in part)–F4–F5.	T1–T2–T4	1. T1 matrix-replacive, fine-grained, xenotopic, fluid inclusion-rich, and associated with gypsum/anhydrite casts. 2. Occurrence of mudclasts with T1 dolomite in undolomitized Facies 6. 3. T2 cement, coarser, idiotopic, limpid, and aggrade from T1 into nearby pore spaces. 4. Notable iron content in T2 dolomite; T1 dolomites extremely iron-poor. 5. T4 dolomite strongly ferroan, non-zoned, ankeritic in composition, commonly forms large idiotopic rhombs in the pores. 6. T4 dolomite also forms sharp outermost rim around T1 and T2 dolomites. 7. Generally, the T4 rhombs contain a core of T1 and T2 dolomites in the genetic sequence: T1–T2–T4, or T2–T4.
Off-shore, open marine, F1–F2–F3 (in part)	T3–T4	1. T3 matrix-replacive, fine-grained, idiotipic to subidiotopic, strongly iron-zoned, and associated with glauconite and pyrite. 2. Diffused zone boundaries of the T3 dolomite. 3. T4 dolomite strongly ferroan, non-zoned, ankeritic in composition, commonly forms large idiotopic rhombs in the pores. 4. T4 dolomite also forms sharp outermost rim around T3 dolomites. 5. Generally, the large T4 rhombs contain a core of T3 dolomites.

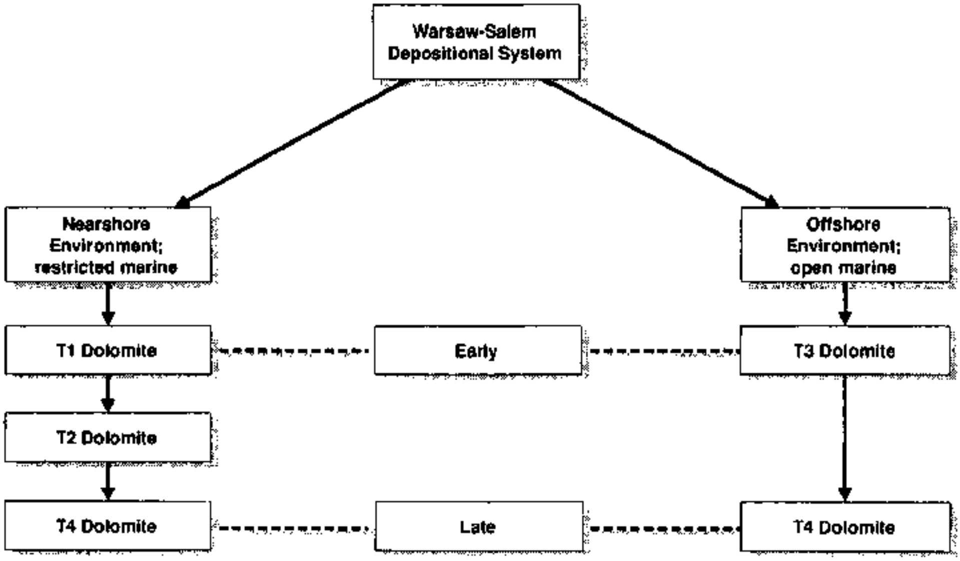

Fig. 9-6. Dolomitization sequence in the Warsaw–Salem formations.

permeability of the samples prior to the formation of the T2 dolomite cement in these samples, and were very successfully utilized in determining the degree to which a specific sample was affected by the T2 dolomitization process.

The matrix-replacive, iron-zoned dolomites (T3), on the other hand, are restricted only to the lithofacies of the open marine depositional regime (F1–F3). Finally, the ferroan saddle dolomite cement (T4) occurs in all the dolomite-bearing facies of the sequence. A summary of the relations between the dolomite types, in terms of their texture and association with specific depositional and diagenetic environments which have a bearing on their mode and sequence of formation, is given in Table 9-3.

The temporal evolution of the dolomite types in the sequence, as suggested by the relationships described above, is illustrated in Fig. 9-6.

CHEMISTRY OF THE DOLOMITE TYPES

Major and trace elements

Four hundred and eight (408) dolomite grains from seven samples representing all 4 dolomite types from two stratigraphic profiles 141Z and 30B (locations shown in Fig. 9-1) were microanalyzed for major and trace elements. The summary of these analyses are given in Table 9-4.

None of the dolomite types exhibits stoichiometric composition (Table 9-4). The xenotopic T1 dolomite, however, is closest to stoichiometric composition: (average) $Ca_{50.7}Mg_{49.15}Fe_{0.15}$. All others are calcian with average compositions: T2: $Ca_{52.3}Mg_{47.2}Fe_{0.5}$; T3: $Ca_{52.5}Mg_{47.2}Fe_{0.3}$; and T4: $Ca_{52.6}Mg_{45.6}Fe_{1.8}$, respectively.

Both types of matrix-replacive dolomites (T1 and T3) show a significant concentration of Na, in excess of 500 ppm, compared to the cement dolomites (T2 and T4). The latter contain, on an average, 260 ppm Na. But the T1 dolomites have slightly higher average Na content (630 ppm) than the T3 dolomites (570 ppm).

Considering the low analytical precision for Sr and Mn, these elements do not show any significant difference in concentration among the different dolomite types (Table 9-4). Nevertheless, the T3 dolomite has the highest average Sr content (average 320 ppm), and the T4 dolomite contains highest average Mn (330 ppm). The Fe/Mn ratio of the four dolomite types, however, is consistently high (6, 15, 6, 33, respectively), which probably accounts for the uniform dull orange-red to non-luminescent character of these dolomites under cathodoluminescent microscope. Figure 9-7 illustrates the differences in major and trace element compositions between the four dolomite types. It clearly demonstrates that the T1 and T3 dolomites have very similar chemical properties, except for their iron contents, probably suggesting that similar pore fluids were involved during diagenesis in the formation of these dolomites under varying redox conditions inherent in each diagenetic regime. The cement dolomites, on the other hand, are not only different from the matrix-replacive dolomites but also are distinctly different themselves, especially in their iron and sodium contents (Fig. 9-7). Most of the T2 dolomites have quite low Na content (majority with ≈200 ppm), and about 0.4%

TABLE 9-4

Average compositions (by type per sample) of the dolomite types (ranges in parentheses)

Sample No.	Na (ppm)	Sr (ppm)	Mn (ppm)	$CaCO_3$ (mol%)	$MgCO_3$ (mol%)	$FeCO_3$ (mol%)	N[a]
Type 1							
141Z-13	360	230	180	49.5	50.3	0.2	39
	(n.d.–1050)	(n.d.–390)	(n.d.–270)	(45–52.6)	(47.4–54.5)	(0.02–0.5)	
30B-19	860	260	200	52.0	47.9	0.1	40
	(500–1480)	(n.d.–490)	(n.d.–330)	(47.8–58.1)	(41.7–52.1)	(0.03–0.6)	
Type 2							
141Z-12	200	240	210	53.0	46.6	0.4	43
	(n.d.–320)	(n.d.–1520)	(n.d.–320)	(46.6–57.7)	(42.1–53.2)	(0.2–0.6)	
141Z-14	220	290	240	53.3	46.1	0.6	45
	(n.d.–680)	(n.d.–410)	(n.d.–500)	(47.5–57.3)	(42.0–52.4)	(0.07–0.8)	
30B-19	330	270	230	50.5	49.2	0.3	20
	(n.d.–570)	(n.d.–520)	(n.d.–470)	(46.7–54.9)	(45.0–52.9)	(0.05–0.5)	
30B-20	200	230	250	51.2	48.1	0.7	33
	(n.d.–330)	(n.d.–430)	(n.d.–430)	(46.2–55.8)	(43.5–53.2)	(0.4–1.1)	
Type 3							
141Z-6	550	330	210	52.5	47.3	0.2	53
	(n.d.–1220)	(n.d.–1350)	(n.d.–380)	(47.9–59.5)	(40.4–51.6)	(0.02–0.6)	
30B-9	600	300	280	52.6	47	0.4	33
	(n.d.–1330)	(n.d.–590)	(n.d.–570)	(49.4–55.8)	(44.1–50.5)	(0.1–1.1)	
Type 4							
141Z-6	280	290	340	51.3	46.4	2.3	13
	(n.d.–610)	(n.d.–420)	(n.d.–710)	(47.7–54.6)	(41.6–50.6)	(0.8–7.9)	
141Z-12	210	140	510	51.3	47.5	1.2	9
	(n.d.–250)	(n.d.–190)	(n.d.–980)	(48.8–52.8)	(45–50.1)	(0.9–2.2)	
141Z-13	120	260	160	51.9	46.5	1.6	1
141Z-14	200	230	250	54.5	44.4	1.1	46
	(n.d.–360)	(n.d.–400)	(n.d.–520)	(49.3–68.4)	(30.5–49.9)	(0.8–3.4)	
30B-9	260	220	280	50.9	47.3	1.8	8
	(n.d.–390)	(n.d.–250)	(n.d.–500)	(49.2–52.6)	(45.7–49.1)	(1.3–2.8)	
30B-19	580	290	450	50	46.5	3.5	16
	(n.d.–1280)	(n.d.–540)	(n.d.–1150)	(47.9–52.5)	(40–51.2)	(0.7–8.4)	
30B-20	270	220	360	51.9	45.9	2.2	9
	(n.d.–310)	(n.d.–350)	(150–570)	(48.4–57.5)	(40.4–49.9)	(1.4–3.2)	

[a] N = number of grains analyzed.

n.d.= not detected. Detection limits: Na = 120 ppm; Sr = 135 ppm; Mn = 120 ppm; Fe = 0.02%

(Fe + Mn)O, suggesting their formation from a very mildly reducing pore fluids of low salinity. Strongly ferroan T4 dolomites (Table 9-4), in contrast, formed from strongly reducing pore fluids, the salinity of which fluctuated between a much wider limits.

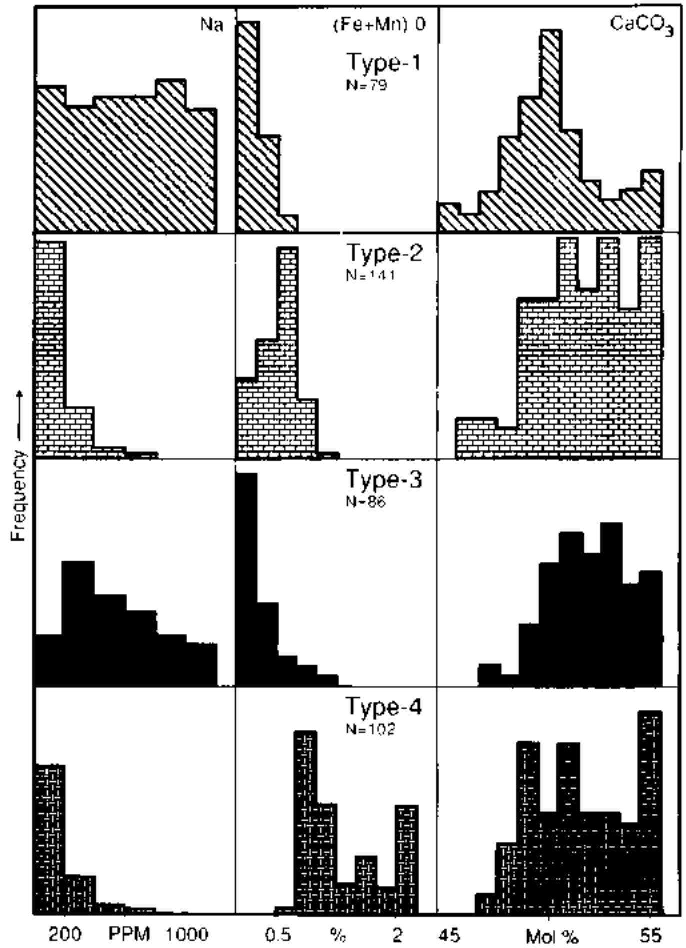

Fig. 9-7. Frequency distribution of $CaCO_3$, (Fe + Mn)O and Na in the dominant dolomite types.

Isotopes

Twenty-seven samples from the two profiles mentioned above have been analyzed for the carbon and oxygen isotopic compositions of the dominant dolomite type in each sample. Enough sample of the T4 dolomites could not be separated for isotopic analyses. The results are presented in Table 9-5 and Figs. 9-8 and 9-9. The dolomite types are distinctive in their isotopic compositions (Table 9-5, Fig. 9-9). On an average, the T1 dolomites have −1.43‰ $\delta^{18}O$ (range: +0.33 to −3.94) and +3.77‰ $\delta^{13}C$ (range: +3.57 to +3.9); the T2 has −7.38‰ $\delta^{18}O$ (range: −5.68 to −8.7) and +3.56‰ $\delta^{13}C$ (range: +3.3 to +3.8), and the T3 dolomites contain −0.87‰ $\delta^{18}O$ (range +0.43 to −2.63) and +3.02‰ $\delta^{13}C$ (range: +2.35 to +3.69).

TABLE 9-5

Isotopic composition of dolomite

Sample No.	$\delta^{18}O$ (‰, PDB)	$\delta^{13}C$ (‰, PDB)	Dolomite type	Rock type	
30B-3	−2.63	2.35	T-3	GS	F1
30B-9	−2.61	3.29	T-3	WS	F2
30B-11	−6.7	3.39	T-2	WS	F5
30B-14	−6.86	3.77	T-2	GS	F4
30B-15	−8.7	3.73	T-2	WS	F3
30B-16	−2.77	3.7	T-1	WS	F5
30B-19	0.136	3.8	T-1	MS	F5
30B-20	−7.53	3.5	T-2	PS	F4
30B-21	−0.25	3.7	T-1	MS	F5
30B-23	0.136	3.9	T-1	MS	F5
30B-23A	−5.68	3.5	T-2	WS	F5
30B-24	−1.51	3.7	T-1	MS	F5
30B-26	−7.82	3.6	T-2	PS	F4
141Z-3	0.43	2.5	T-3	PS	F1
141Z-6	0.33	3.57	T-3	MS	F2
141Z-6A	−1.31	3.69	T-1	PS	F4
141Z-7	0.15	3.26	T-3	MS	F2
141Z-10	−3.94	3.8	T-1	MS	F5
141Z-11	−8.21	3.7	T-2	GS	F4
141Z-12	−8.11	3.7	T-2	WS	F5
141Z-13	−3.55	3.9	T-1	MS	F5
141Z-14	−7.04	3.8	T-2	PS	F4
141Z-17	−7.53	3.5	T-2	GS	F4
141Z-18	−7.72	3.5	T-2	GS	F4
141Z-19	−7.53	3.4	T-2	WS	F5
141Z-20	−6.76	3.4	T-2	WS	F5
141Z-21	−7.12	3.3	T-2	GS	F6

PS = packstone; WS = wackestone; MS = mudstone; GS = grainstone. F1–F6 = Facies 1 to 6.

DOLOMITIZATION

Taken together, the occurrence of multiple varieties of dolomites, their specific association as two groups, textural relations between the coexisting dolomite types in each group, and restricted distribution of each of these two groups to two specific facies associations suggest that the rocks of the Warsaw–Salem formations have gone through two sequences of dolomitization processes (Fig. 9-10): (1) T1–T2–T4 and (2) T3–T4, along two parallel diagenetic regimes coincident with two coast-parallel belts of depositional environments, one nearshore, restricted (i.e., the Salem Formation), and the other offshore, open marine (i.e., the Warsaw Formation), respectively. The earliest of these dolomitization processes in both facies associations were concurrent but independent of each other, and were controlled by the pore fluids inherent in each depositional environment.

In the nearshore lagoons and tidal flats, the mudstones (F5) and, in part, the

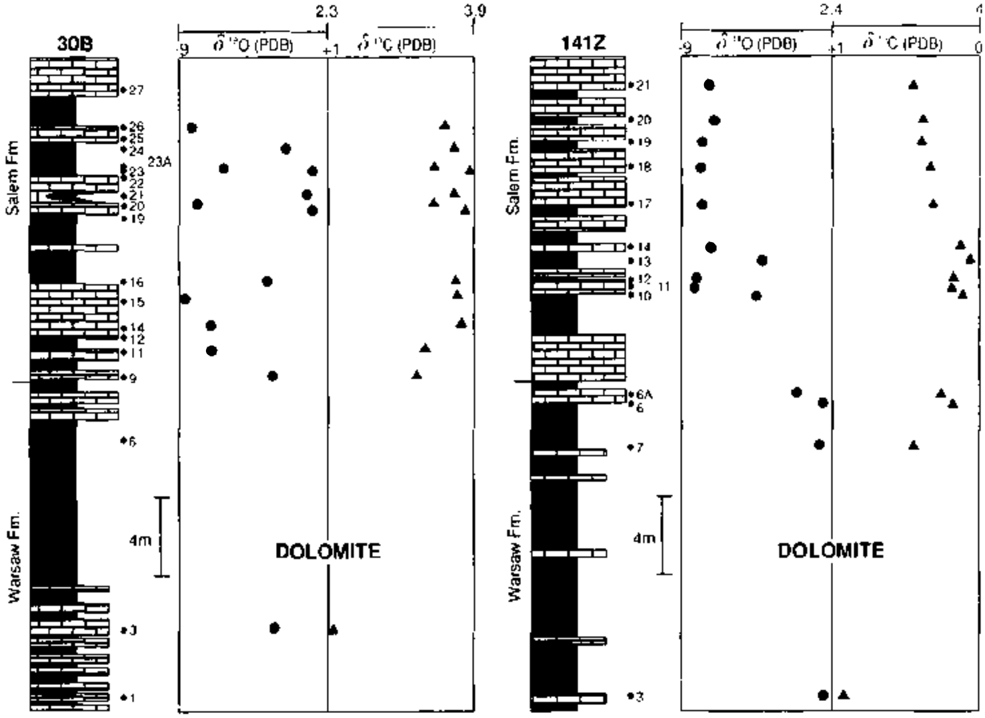

Fig. 9-8. Profiles of isotopic composition of dolomite in samples along two stratigraphic sections, 30B and 141Z (location in Fig. 9-1).

adjoining biohermal mounds (F3) were dolomitized early into the matrix-replacive T1 dolomites either by tidally recharged seawater (Carballo and Land, 1984) or by refluxion of the evaporative brine from the lagoons and tidal flats (Adams and Rhodes, 1960). The latter mechanism is more probable as indicated by the occurrence of pseudomorphs and molds of gypsum/anhydrite in these rocks. The mud matrix of the associated grainstones, packstones and wackestones (F4) was also similarly dolomitized into T1 during this early phase. In addition, the bioclastic components of the mud-rich facies were either stabilized or partially to completely dissolved during this stage, producing moldic porosity. The chemical and isotopic compositions of the xenotopic T1 dolomites (Figs. 9-6 and 9-8; Tables 9-4 and 9-5), and the chemistry of the stabilized brachiopods (Table 9-6) both point to the influence of hypersaline brine during the T1 dolomitization and grain stabilization.

The dominant early diagenetic process in the open marine shelf part of the sequence (i.e., in the lithofacies of the Warsaw Formation), concurrent with the T1 dolomitization in the Salem Formation, was the replacement of matrix mud of these facies by T3 dolomite. Both elemental and isotopic compositions of this dolomite (Figs. 9-6 and 9-8; Tables 9-4 and 9-5) suggest diagenesis under the influence of seawater. Gradual zoning of these dolomites with respect to iron, and association with pyrite and glauconite, however, indicate that a moderate reducing environment grad-

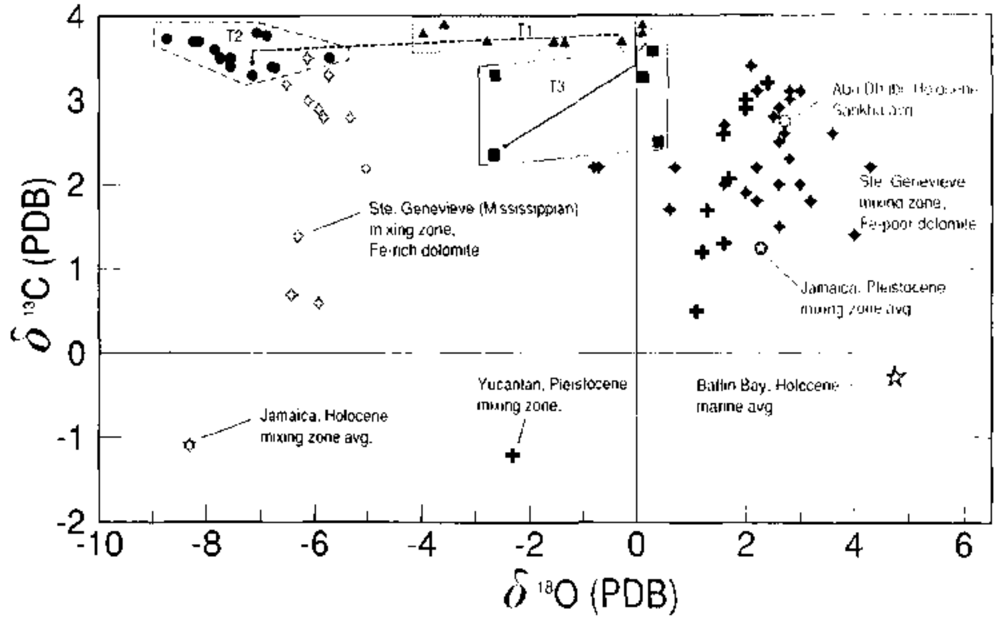

Fig. 9-9. Carbon and oxygen isotopic compositions of the dolomite types of the Warsaw–Salem formations compared with other dolomites of various modes of origin. Data for other dolomites are from: Behrens and Land (1972), Land (1973a, b), Choquette and Steinen (1980), McKenzie(1981), and Ward and Halley (1985). All oxygen isotopic analyses, except for those in the present study, were not corrected for phosphoric acid fractionation.

TABLE 9-6

Average composition of blocky calcite cement and associated stabilized bioclasts (ranges in parentheses)

Sample No.	Na (ppm)	Sr (ppm)	Mn (ppm)	$CaCO_3$ (mol%)	$MgCO_3$ (mol%)	$FeCO_3$ (mol%)	*N*
Secondary pore-fill cement							
30B-19	<120	790	350	97.4	2.1	0.5	12
	(n.d.)	(n.d.–980)	(n.d.–620)	(95.0–99.2)	(0.3–4.7)	(0.3–0.6)	
141Z-12	320	220	200	98.0	1	1	15
	(n.d.–380)	(n.d.–240)	(n.d.–250)	(95.9–99.4)	(0.6–1.6)	(n.d.–2.5)	
Stabilized brachiopod							
30B-19	3420	500	130	99.5	0.4	0.1	10
	(480–5200)	(n.d.–720)	(n.d.–200)	(99.2–99.8)	(0.2–0.8)	(n.d.–0.2)	

Abbreviations and detection limits are as shown in Table 9-4.

ually developed in the host facies during the T3 dolomitization. Bacterial degradation of organic matter during early sulfate reduction, methanogenesis or fermentation (Spotts and Silverman, 1966; Claypool and Kaplan, 1974; Compton, 1988) probably generated the necessary reducing environment. Relatively light carbon isotopic com-

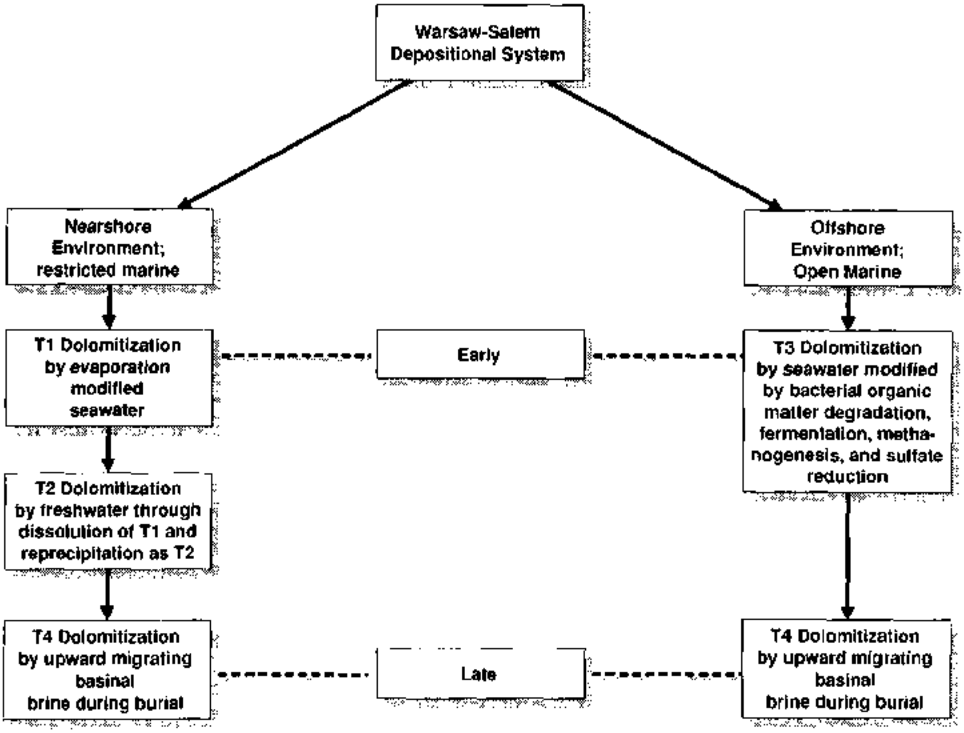

Fig. 9-10. Dolomitization processes in the Warsaw–Salem lithofacies.

position of the T3 dolomites (Fig. 9-9; Table 9-5) is in conformity with such a mode of formation.

Following the formation of the evaporative T1 dolomites in the Salem Formation, the entire shoreline facies sequence was gradually inundated by freshwater as a result of progradational regression. Under these conditions, part of the bioclasts in the grainstones were silicified, and the limpid T2 dolomite cement was produced in these facies at the expense of the preexisting T1 dolomites. The textural attributes (Fig. 9-5b), and both elemental and oxygen isotopic compositions (Figs. 9-7 and 9-9; Tables 9-4 and 9-5) of the T2 dolomites suggest such a mode of formation. The closeness of carbon isotopic compositions of the T1 and T2 dolomites, however, indicates that the system was still rock-dominating. It is noteworthy in this context that the T2 dolomites are found only in the matrix-bearing parts of the shoreline facies in association with T1 dolomites, whereas the matrix-free parts are free from any dolomite.

Finally, the T4 dolomite represents the last stage of dolomitization in all the lithofacies of the Warsaw and Salem formations. Their facies-pervasive occurrence, textural attributes (for example, saddle-type individual crystals, and relatively large but sparse distribution, especially in the secondary pores), distinctive iron-enrichment, and variable Na content suggest formation from fluids which were quite distinct from

TABLE 9-7

Models and constraints on diagenetic dolomitization

Model (dolomitization by)	Constraints			Comments
	Mg-source	Recharge mechanism	Chemistry and kinetics	
Normal seawater.	Seawater.	Diffusion.	Supersaturation with respect to dolomite.	Operative below sediment–water interface. Diffusive processes are slow.
do	do	Tidal pumping.	do	do
Evaporation-modified seawater.	do	Gravity reflux, and hydrodynamic pumping.	do	Operative in peritidal zones.
do	do	Pumping due to loss of hydrodynamic head by evaporation.	do	do
Seawater modified by mixing with freshwater.	do	Topography-driven.	Appropriate mix may become supersaturated with respect to dolomite, and undersaturated with respect to calcite.	Operative in coastal zones of mixing. Low sulfate concentration is conducive to dolomitization.
Dissolution–reprecipitation from freshwater influx.	Early-formed dolomite or high-Mg calcite.	do	Undersaturated pore-water capable of dissolving earlier Mg-phase and become supersaturated.	do
Deep-seated connate brine.	Pressure solution; clay diagenesis.	Thermal convection; lithostatic pressure.	Higher temperature of fluid is conducive to dolomitization.	Operative during burial.

the fluids responsible for the formation of other dolomite types in the sequence. These probably precipitated from an upward migrating pore fluid from the deeper parts of the basin during burial.

DISCUSSION

There is a general consensus that the majority of the dolomites in the geologic record is secondary, a product of diagenesis, and the primary dolomite described from a few Holocene occurrences (Alderman and Skinner, 1957; Jones, 1961; Miller, 1961; Skinner, 1963; Barnes and O'Neil, 1969; Behrens and Land, 1972) "... represents an insignificant contribution towards the total mass of ancient dolomites" (Chilingar et al., 1979, p. 439). (See Chilingar, 1956, *however*.)

The major dolomitization processes, so far proposed under various constraints (Table 9-7), such as Mg-source, recharge mechanism (i.e., pump), and the kinetics of the dolomitizing fluid, can be grouped under four principal categories: (a) by diffusion from (Sass and Katz, 1982) or tidal pumping of normal seawater (Carballo and Land, 1984); (b) by seepage refluxion of evaporation-modified seawater (Adams and Rhodes, 1960; Chilingar and Bissell, 1961; Deffeys et al., 1965), or by evaporative pumping of seawater (Hsü and Siegenthaler, 1969); (c) under the influence of freshwater by a process of dissolution of earlier phase(s) and reprecipitation as a new phase, or at the mixing zone with marine water (Hanshaw et al., 1971; Badiozamani, 1973); and (d) by basinal brine evolved during burial (Illing, 1959). Despite the thermodynamic and kinetic difficulties (Machel and Mountjoy, 1986; Hardie, 1987) these processes are considered viable, and numerous examples have been cited in the literature (see Friedman and Sanders, 1967, and Chilingar et al., 1979, for reviews and references) describing the field, petrographic and chemical characters of the products of each of the processes. The effects of more than one process acting on a single sequence, however, have not been adequately documented because of the problem of textural and chemical modifications (Land, 1967, 1983, 1985), although the theoretical basis for such changes are presumably well-understood (Veizer, 1978, 1983a, b). In addition, the process of dolomite neomorphism from a preexisting dolomite phase by dissolution–reprecipitation has only been mentioned (Land, 1983, 1985), but has not been documented.

The Middle Mississippian carbonate sequence of eastern Missouri, as illustrated earlier, provides an example where all of these processes operated, some contemporaneously and others in succession. Two combinations of the four processes mentioned above — (a) and (d) in the offshore part, and (b), (c) and (d) in the nearshore part of the sequence — resulted in two temporal sequences or trends of dolomitization: (1) T3–T4, and (2) T1–T2–T4, respectively, with characteristic chemical properties of each and textural relationships between the dolomite types. Each of these dolomitization trends is the result of multiple, sequential dolomitization in two different, but contemporaneous, diagenetic regimes. During the operation of the sequential processes in each regime, the product of an earlier process was modified by subsequent processes. But the degree of modification was variable, and was controlled both by the diagenetic environments as well as the lithofacies characters, especially by the porosity and permeability of the host facies.

The point is well-illustrated by the ternary plots [CaO–MgO–Na_2O and CaO–MgO–(Fe + Mn)O] of three samples (Fig. 9-11) from the measured stratigraphic section 30B, and also by their isotopic compositions (Table 9-5; Fig. 9-9). In this section (Fig. 9-8), the sample 30B-19 was collected from a massive lagoonal mudstone (F5) that was extensively dolomitized early into T1 dolomite by the evaporative hypersaline seawater during which the porosity might have been enhanced by bioclast dissolution, but the permeability of the rock was drastically reduced. Subsequent dolomitization processes, first under freshwater influx and later under burial condition, produced only limited amounts of the T2 and T4 dolomite cements, respectively, because of limited permeability of the rock during each of these subsequent stages of dolomitization. The final compositional trend (Fig. 9-11a) is the result of these three sequential dolomitization processes. A major part of the rock acted as relatively closed system during the freshwater influx and burial dolomitization stages, however, and a substantial amount of the earliest evaporative dolomite was left in the rock that had not been significantly modified by the subsequent processes as indicated by the elemental and isotopic composition of the dolomite type in this sample (Tables 9-4 and 9-5).

The sample 30B-20 (Fig. 9-8), in contrast, is a tidal channel packstone (F4) interbedded within the lagoonal F5 mudstones. The matrix mud in this sample was dolomitized first into T1 dolomite by the evaporative brines from the adjoining lagoons, and the bioclasts were partially to completely dissolved during the process generating a significant amount of interconnected secondary porosity that resulted in high permeability within the lithofacies following the formation of the T1 dolomite. The rock, therefore, was fairly open during the subsequent dolomitization episode, and a major part of the early T1 dolomite was cannibalized to produce the T2 dolomite cement during the freshwater influx that followed. But, in the process, a substantial amount of secondary porosity of the rock was also lost, and extensive cementation by T2 dolomite reduced the permeability of the rock to a substantial degree. Yet, the permeability of the sample 30B-20 at this stage was higher than that in the sample 30B-19 described above and, as a result, a notable amount of late ferroan dolomite cement (T4) had been added to it during its dolomitization under late burial condition. Figure 9-11b shows the resultant modifications in the major and trace elemental compositions. But the degree of chemical modification is very clearly illustrated by the isotopic composition of the dominant dolomite type in the sample (Table 9-5), which reflects the results of relative openness of the system during the T2 and T4 dolomitization episodes.

In the open marine argillaceous mudstone (F2) represented by the sample 30B-9 (Fig. 9-8), the interaction of the processes (a) and (d) described above produced a trend shown in Fig. 9-11c that is almost identical to Fig. 9-11a, but was caused by an initial continuous evolution of the phreatic marine pore fluid during early diagenesis (i.e., during T3 dolomitization) in an organic-rich, gradually reducing environment that was superposed by a late T4 dolomitization under burial condition similar to that in samples 30B-19. It is noteworthy, however, that despite the parallelism between the trace elemental trends in these two samples (Fig. 9-11) the isotopic compositions

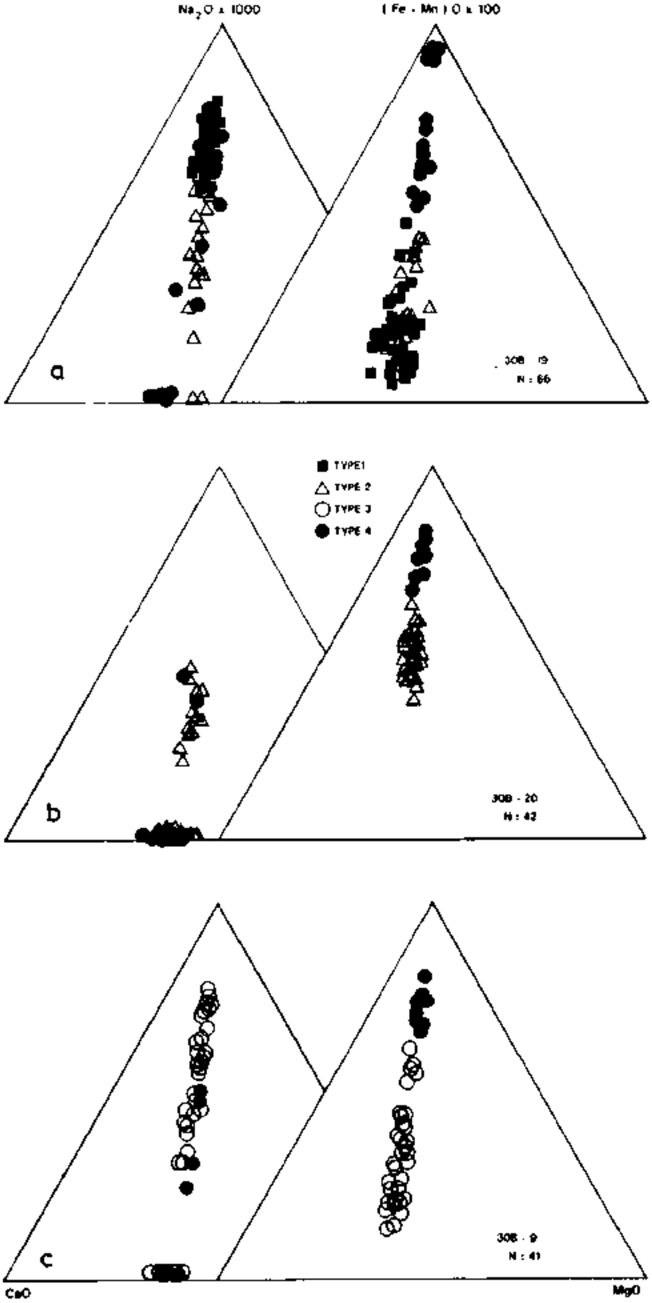

Fig. 9-11. Trace element compositional trends of dolomites in three samples in the stratigraphic profile 30B (see text for explanation).

of the dominant dolomite types in these two samples (Table 9-5) are quite distinct and characteristic of the processes of formation in each regime. Similar relationships were also observed in the equivalent samples from the measured stratigraphic section 141Z (Figs. 9-1 and 9-8), suggesting that the effects were regional rather than local.

A large number of published isotopic compositions of marine- and freshwater-influenced dolomites show wide scatter (Fig. 9-9) not only because of compositional evolution of the diagenetic pore fluids but also due to variable rock/water ratios during dolomitization (Lohmann, 1982; Coniglio et al., 1988). The meteoric diagenetic processes in a system presumably defines an "Inverted-J" curve on the $\delta^{18}O$–$\delta^{13}C$ bivariate plot (Lohmann, 1982) in response to the differences in the isotopic compositions and volumes of the initial sediment and meteoric fluid. The horizontal part of the "Inverted-J" represents proximal to distal transitions of the meteoric fluid at essentially invariant carbon values of the rock, and the vertical part represents the proximality to the soil gas sources at invariant oxygen isotopic composition of the meteoric fluid (Coniglio et al., 1988). In rocks affected by multiple diagenesis, such as the rocks of the present study area, the situation is further complicated. In this area, the products of two different but contemporaneous diagenetic regimes define two isotopic trends T1–T2 and T3 in Fig. 7-9. The T1–T2 trend is characterized by a relatively narrow range of carbon but a wide range of oxygen isotopic ratios. The narrow range of carbon isotopic composition suggests a rock-dominating system. Yet, the wide range in oxygen isotopic composition of these dolomites might suggest that the rock/water ratio in the system varied considerably. The textural evidence suggest, however, that the trend resulted from a variable degree of reequilibration of the preexisting phase in response to variable permeabilities of the affected lithofacies at the time of the freshwater influx. The T3 trend, on the other hand, resulted from a continuous evolution of pore water by diagenetic processes (i.e., diffusion, organic matter degradation, bacterial sulfate reduction, methanogenesis, and fermentation) inherent in the system.

The T4 dolomite in the sequence requires special attention in view of its probable relationship with the Mississippi Valley-type (MVT) Pb–Zn mineralization in the area. The MVT deposits of the Missouri lead belt are associated with a strongly ferroan late dolomite (Gregg, 1988; Gregg and Shelton, 1990) which is similar to the T4 dolomite of the Warsaw–Salem formations described above. Similar late generation, facies-pervasive, coarse ferroan dolomite also occurs in minor amounts in other parts of the Mississippian sequence in Illinois and Missouri (Choquette, 1971, Choquette and Steinen, 1980; Banner et al., 1988a, b, c; Cander et al., 1988), and the entire sequence of Cambrian to Pennsylvanian age in the area is characterized by sporadic to massive MVT mineralization (Leach, 1973, 1979; Cobb, 1981). The MVT ore-associated ferroan dolomites are considered to be the ore stage dolomite in the paragenetic sequence of the MVT sulfides (Leach and Rowan, 1986; Gregg, 1988), both of which reportedly owe their origin to deep-seated basinal brines (White, 1958; Noble, 1963; Jackson and Beales, 1967; Leach et al., 1975, 1983, 1984; Ohle, 1980; Ludvigson et al., 1983; Sverjensky, 1984; Leach and Rowan, 1986). A similar origin for the T4 and equivalent late ferroan dolomites of the Warsaw–Salem formations (present work) and other sequences in the area (Banner et al., 1988a, c; Cander et al., 1988, respectively), and sporadic sulfide mineralization in these sequences suggest a genetic relationship of these late ferroan dolomites with the MVT ore deposits. The T4 and similar dolomites in the Mississippian sequence of the area probably represent the precipitates from the last stage of the upward migrating basinal brine that was responsible for the formation of massive sulfide deposits in the older (Cambrian) carbonate sequence in the vicinity.

CONCLUSIONS

The conclusions can be summarized as follows:

(1) The Warsaw and Salem formations have experienced multiple dolomitization processes, which produced four types of texturally, chemically and isotopically distinct dolomites — T1 through T4.

(2) Three of the dolomitization processes (T1, T2 and T3) were facies-specific; the pore fluids responsible for these processes were inherent in the depositional systems of specific facies associations. The fourth process (T4) was facies-pervasive, and was related to deep-seated diagenetic evolution and upward migration of the pore fluids during burial.

(3) Interactions of the facies-specific and facies-pervasive processes produced two temporal sequences of dolomites: (1) T1–T2–T4, and (2) T3–T4, in the Warsaw–Salem formations along two coast-parallel depositional and diagenetic environments — one restricted, nearshore, and the other offshore, open marine, respectively, separated by a barrier that behaved as an aquitard during the preburial diagenesis.

(4) In each dolomite sequence, the degree of reequilibration of an earlier phase of dolomite by a subsequent process was controlled principally by the permeability of the rocks at the advent of the process.

(5) Consequently, relicts of an earlier phase with textural, chemical and isotopic fingerprints of the process responsible for its formation were preserved in the rocks, the amount of which was dictated by the permeability of these rocks at the end of the earlier process.

(6) The facies-pervasive T4 dolomite is considered equivalent to the "ore-stage" dolomite in the adjoining MVT province, and may represent the last precipitate from the deep basinal brine that formed massive sulfide deposits in the Cambrain carbonate sequence of the area.

ACKNOWLEDGEMENTS

The authors are grateful to Dr. Edward Ripley for making available the stable isotope analytical facilities at Indiana University, Bloomington. Randy Olson helped with sample preparation, and Lisa Dunn helped with parts of X-ray diffraction and cathodoluminescence analyses. Comments and suggestions on an early version of the manuscript by Drs. J. Robert Dodd, Loretta A. Williams, Timothy Hayes and Lisa M. Pratt, and reviews and editorial comments by Drs. K.H. Wolf and G.V. Chilingar helped in improving the final manuscript.

REFERENCES

Adams, J.E. and Rhodes, M.L., 1960. Dolomitization by seepage refluxion. *Bull. Am. Assoc. Pet. Geol.*, 44: 1912–1921.

Ahr, W.M., 1973. The carbonate ramp: An alternate to the shelf model. *Gulf Coast Geol. Soc. Trans.*, 23: 221–225.

Alderman, A.R. and Skinner, H.C.W., 1957. Dolomite sedimentation in the southeast of South Australia. *Am. J. Sci.*, 255: 561–567.

Badiozamani, K., 1973. The dorag dolomitization model — application to the middle Ordovician of Wisconsin. *J. Sediment. Petrol.*, 43: 965–984.

Banner, J.L., Hanson, G. and Meyers, W.J., 1988a. Rare earth elements and Nd isotopic variations in regionally extensive dolomites from the Burlington–Keokuk Formation (Mississippian): implications for REE mobility during carbonate diagenesis. *J. Sediment. Petrol.*, 58: 415–432.

Banner, J.L., Hanson, G. and Meyers, W.J., 1988b. Determination of initial Sr isotopic compositons of dolostones from the Burlington–Keokuk Formation (Mississippian): constraints from cathodoluminescence, glauconite paragenesis, and analytical methods. *J. Sediment. Petrol.*, 58: 673–687.

Banner, J.L., Hanson, G. and Meyers, W.J., 1988c. Water–rock interaction history of regionally extensive dolomites of the Burlington–Keokuk Formations (Mississippian): isotopic evidence. In: V. Shukla and P.A. Baker (Editors), *Sedimentology and Geochemistry of Dolostones. Soc. Econ. Paleontol. Mineral., Spec. Publ.*, 43: 97–114.

Barnes, I. and O'Neil, 1969. The nature of secondary dolomite formation. *Trans. Am. Geophys. Union*, 50: 347 (abstract).

Behrens, E.W. and Land, L.S., 1972. Subtidal Holocene dolomite, Baffin Bay, Texas. *J. Sediment. Petrol.*, 42: 155–161.

Cander, H.S., Kaufman, J., Daniels, L.D. and Meyers, W.J., 1988. Regional dolomitization of shelf carbonates in the Burlington–Keokuk Formation (Mississippian), Illinois and Missouri: Constraints from cathodoluminescent zonal stratigraphy. In: V. Shukla and P.A. Baker (Editors), *Sedimentology and Geochemistry of Dolostones. Soc. Econ. Paleontol. Mineral., Spec. Publ.*, 43: 129–144.

Carballo, J.D. and Land, L.S., 1984. Holocene dolomitization of Sugarloaf sediments by active tidal pumping, Sugarloaf Key, Florida. *Bull. Am. Assoc. Pet. Geol.*, 68: 459.

Carpenter G.L. and Keller, S.J., 1986. Oil Development and Production in Indiana During 1985. *Indiana Geol. Surv., Min. Econ. Ser.*, 32: 49pp.

Chilingar, G.V., 1956. Use of Ca/Mg ratio in porosity studies. *Bull. Am. Assoc. Pet. Geol.*, 40: 2489–2493.

Chilingar, G.V. and Bissell, H.J., 1961. Dolomitization by seepage refluxion — discussion. *Bull. Am. Assoc. Pet. Geol.*, 45: 679–683.

Chilingar, G.V., Zenger, D.H., Bissell, H.J. and Wolf, K.H., 1979. Dolomites and dolomitization. In: G. Larsen and G.V. Chilingar (Editors), *Diagenesis in Sediments and Sedimentary Rocks. Developments in Sedimentology, Vol. 25A*. Elsevier, Amsterdam, pp. 423–536.

Choquette, P.W., 1971. Late ferroan dolomite cement, Mississippian carbonates, Illinois Basin, U.S.A. In: O.P. Bricker (Editor), *Carbonate Cements. Johns Hopkins Univ. Stud. Geol.*, No. 19: 339–348.

Choquette, P.W. and Steinen R.P., 1980. Mississippian non-supratidal dolomites, Ste. Genevieve Limestone, Illinois Basin: evidence for mixed water dolomitization. In: D.H. Zenger and R.L. Ethington (Editors), *Concepts and Models of Dolomitization. Soc. Econ. Paleontol. Mineral., Spec. Publ.*, 28: 163–196.

Claypool, G.E. and Kaplan, I.R., 1974. The origin and distribution of methane in marine sediments. In: I.R. Kaplan (Editor), *Natural Gases in Marine Sediments.* Plenum Press, New York, N.Y., pp. 99–140.

Cluff, R.M., 1984, Carbonate sand shoals in the Middle Mississippian (Valmeyran) Salem–St. Louis–Ste. Genevieve Limestones, Illinois Basin. In: P.M. Harris (Editor), *Carbonate Sands, a Core Workshop. Soc. Econ. Paleontol. Mineral., Core Workshop*, 5: 94–135.

Cluff, R.M. and Lineback, J.A., 1981. Middle Mississippian carbonates of the Illinois Basin. *Ill. Geol. Soc./Ill. Geol. Surv., Seminar and Core Workshop*, 88 pp.

Cobb, I., 1981, *Geology and Geochemistry of Sphalerite in Coal.* Ph.D. Dissertation, Univ. of Illinois, Urbana–Champaign, Ill., 204 pp.

Compton, J.S., 1988. Degree of supersaturation and precipitation of organogenic dolomite. *Geology*, 16: 318–321.

Coniglio, M., James, N.P. and Aissaoui, D.M., 1988. Dolomitization of Miocene carbonates, Gulf of Suez, Egypt. *J. Sediment. Petrol.*, 58: 100–119.

Deffeys, K.S., Lucia, F.J. and Weyl, P.K., 1965. Dolomitization of Recent and Pleistocene sediments by evaporite waters on Bonaire, Netherlands Antilles. In: L.C. Pray and R.C. Murray (Editors), *Dolomitization and Limestone Diagenesis. Soc. Econ. Paleontol. Mineral., Spec. Publ.*, 13: 71–87.

Evamy, B.D., 1963. The application of chemical staining techniques to the study of dedolomitization. *Sedimentology*, 2: 164–170.

Friedman, G.M. and Sanders, J.E., 1967. Origin and occurrence of dolostones. In: G.V. Chilingar, H.J. Bissell and R.W. Fairbridge (Editors), *Carbonate Rocks, Origin, Occurrence, and Classification.* Elsevier, Amsterdam, pp. 267–348.

Gregg, J.M., 1988. Origin of dolomite in the offshore facies of the Bonnterre Formation (Cambrian), southeast Missouri. In: V. Shukla and P.A. Baker (Editors), *Sedimentology and Geochemistry of Dolostones. Soc. Econ. Paleontol. Mineral., Spec. Publ.*, 43: 67–84.

Gregg, J.M. and Shelton, K.L., 1990. Dolomitization and dolomite neomorphism in the backreef facies of the Bonterre and Davis formations (Cambrian), southeastern Missouri. *J. Sediment. Petrol.*, 60: 549–562.

Hanshaw, B.B., Beck, W. and Deike, R.G., 1971. A geochemical hypothesis for dolomitization by groundwater. *Econ. Geol.*, 66: 710–724.

Hardie, L.A., 1987. Dolomitization: A critical view of some current views. *J. Sediment. Petrol.*, 57: 166–183.

Howe, W.B. and Koenig, J.W., 1961. The stratigraphic succession in Missouri. *Mo. Geol. Surv. Water Resour., 2nd Ser.*, 40: 13 pp.

Hsü, K.J. and Siegenthaler, C., 1969. Preliminary experiments on hydrodynamic movements induced by evaporation and their bearing on the dolomite problem. *Sedimentology*, 12: 11–25.

Illing, L.V., 1959. Deposition and diagenesis of some upper Paleozoic carbonate sediments in Western Canada. *5th World Pet. Congr. Proc., New York, N.Y., Sect. 1*, pp. 23–52.

Jackson, S.S., and Beales, F.W., 1967. An aspect of sedimentary basin evolution, the concentration of Mississippi Valley-type ores during the late stage diagenesis. *Can. Pet. Geol. Bull.*, 15: 393–433.

Jones, B.F., 1961. Zoning of saline minerals in Deep Spring Lake. In: *Geological Survey Research, 1961: Short Papers in Geologic and Hydrologic Sciences. U.S. Geol. Surv. Prof. Pap.*, 424-B: 199–202.

Land, L.S., 1967. Diagenesis of skeletal carbonates. *J. Sediment. Petrol.*, 37: 914–930.

Land, L.S., 1973a. Contemporaneous dolomitization of middle Pleistocene reefs by meteoric water, North Jamaica. *Bull. Mar. Sci.*, 23: 64–92.

Land, L.S., 1973b. Holocene meteoric dolomitization of Pleistocene limestones, North Jamaica. *Sedimentology*, 20: 411–424.

Land, L.S., 1980. The isotopic and trace element geochemistry of dolomites: state of the art. In: D.H. Zenger and R.L. Ethington (Editors), *Concepts and Models of Dolomitization. Soc. Econ. Paleontol. Mineral., Spec. Publ.*, 28: 87–110.

Land, L.S., 1983. The application of stable isotopes to studies of origin of dolomite and to problem of diagenesis of clastic sediments. In: M.A. Arthur and T.F. Anderson (Editors), *Stable Isotopes in Sedimentary Geology. Soc. Econ. Paleontol. Mineral., Short Course Notes*, 10 (4): 1–22.

Land, L.S., 1985. Origin of massive dolomite. *J. Geol. Education*, 3: 112–125.

Lane, H.R. and De Keyser, T.L., 1980. Paleogeography of late early Mississippian (Tournaisian) in the central and southwestern United States. In: T.D. Fouchs and E.G. Magathan (Editors), *Paleozoic Paleogeography of the West-Central United States. Rocky Mtn. Sect. SEPM Symp. 1 on West-Central U.S. Paleogeography*, pp. 149–162.

Leach, D.L., 1973. Possible relationship of Pb–Zn mineralization in the Ozarks to the Ouachita orogeny. *Geol. Soc. Am. Abst. Prog.*, 5: 269.

Leach, D.L., 1979. Temperature and salinity of the fluid responsible for minor occurrence of sphalerite in the Ozark region of Missouri. *Econ. Geol.*, 74: 931–937.

Leach, D.L. and Rowan, E.L., 1986. Genetic link between Ouachita foldbelt tectonism and the Mississippi Valley-type lead–zinc deposits of the Ozarks. *Geology*, 14: 931–935.

Leach, D.L., Nelson, R.C. and Williams, D., 1975. Fluid inclusion studies in the northern Arkansas Zinc district. *Econ. Geol.*, 70: 1084–1091.

Leach, D.L., Rowan, E.L. and Hedal, J.A., 1983. Evidence for ore-fluid migration in the Bonterre Formation, Southeast Missouri. *Geol. Soc. Am. Abst. Prog.*, 15: 625.

Leach, D.L., Viets, J.G. and Rowan, E.L., 1984. Appalachian–Ouachita orogeny and Mississippi Valley-type lead–zinc deposits. *Geol. Soc. Am. Abst. Prog.*, 16: 572.

Lees, A., 1961. The Waulsortian "reef" of Eire: A carbonate mudbank complex of Lower Carboniferous age. *J. Geol.*, 69: 101–109.

Lohmann, K.C., 1982. "Inverted-J" carbon and oxygen isotopic trends: a criterion for shallow phreatic meteoric diagenesis. *Geol. Soc. Am. Abst. Prog.*, 14: 548.

Ludvigson, G.A., Bunker, B.J. and Garvin, P.L., 1983. Burial diagenetic model for the emplacement of Zn–Pb sulfide ores in the Upper Mississippi Valley, U.S.A. In: G. Kisvarsanyi, S.K. Grant, W.P. Pratt and J.W. Koenig (Editors), *Proc. Int. Conf. on MVT Pb–Zn Deposits.* Univ. Missouri Press, Rolla, Mo., pp. 497–515.

Machel, H.G. and Mountjoy, E.W., 1986. Chemistry and environment of dolomitization — a reappraisal. *Earth-Sci. Rev.*, 23: 175–222.

McKenzie, J., 1981. Holocene dolomitization of calcium carbonate sediments from the coastal sabkhas of Abu Dhabi, U.A.E.: a stable isotope study. *J. Geol.*, 89: 185–198.

Miller, D.N., Jr., 1961. Early diagenetic dolomite associated with salt extrusion process, Inagua, Bahamas. *J. Sediment. Petrol.*, 31: 473–476.

Mullins, H.T., Gardulski, A.F., Hinchey, E.J. and Hine, A.C., 1988. The modern carbonate ramp slope of central west Florida. *J. Sediment. Petrol.*, 58: 273–290.

Nellist, W.E., 1987. Economic geology of the Valmeyran carbonate rocks of southern Indiana. In: J.R. Dodd (Editor), *Valmeyran (Middle Mississippian) Carbonate Rocks of Southern Indiana. Guideb. for Great Lake Sect. SEPM Annu. Field Trip*, pp. 49–60.

Noble, E.A., 1963. Formation of ore deposits from water of compaction. *Econ. Geol.*, 58: 1145–1156.

Ohle, E.L., 1980. Some consideration in determining the origin of ore deposits of the Mississippi Valley-type, Part II. *Econ. Geol.*, 75: 161–172.

Sass, E. and Katz, A., 1982. The origin of platform carbonates: new evidence. *Am. J. Sci.*, 282: 1184–1213.

Skinner, H.C.W., 1963. Precipitation of calcian dolomites and magnesian calcites in the southeast of South Australia. *Am. J. Sci.*, 261: 449–472.

Spotts, J.H. and Silverman, S.R., 1966. Organic dolomite from Point Fermin, California. *Am. Mineral.*, 51: 1144–1155.

Stichcomb, B.L. and Fellows, L.D., 1968. Geology of the Maxville Quadrangle, Jefferson and St. Louis Counties, Missouri. *Mo. Geol. Surv. Water Resour. Circ.*, 386: 20pp.

Sverjensky, D.H., 1984. Oil-field brines as ore-forming solutions. *Econ. Geol.*, 79: 23–37.

Veizer, J., 1978. Simulation of limestone diagenesis: a model based on strontium depletion — discussion. *Can. J. Earth Sci.*, 15: 1683–1685.

Veizer, J., 1983a. Trace elements and isotopes in sedimentary carbonates. In: R.J. Reeder (Editor), *Carbonate: Mineralogy and Chemistry. Reviews in Mineralogy, Vol. 11. Mineral. Soc. Am.*, pp. 265–299.

Veizer, J., 1983b. Chemical diagenesis of carbonates: theory and application of trace element technique. In: M.A. Arthur and T.F. Anderson (Editors), *Stable Isotopes in Sedimentary Geology. Soc. Econ. Paleontol. Mineral., Short Course Notes*, 10 (3): 1–100

Ward, W.C. and Halley, R.B., 1985. Dolomitization in a mixing zone of near seawater composition, Late Pleistocene, Northeastern Yucatan Peninsula. *J. Sediment. Petrol.*, 55: 407–420.

White, D.E., 1958. Liquid of inclusions in sulfides from Tristate (Mossouri–Arkansas–Oklahoma) is probably connate in origin. *Geol. Soc. Am. Bull.*, 69: 1660.

Wilson, J.L., 1975. *Carbonate Facies in Geologic History.* Springer-Verlag, Berlin, 471 pp.

Diagenesis, IV. Developments in Sedimentology 51
edited by K.H. Wolf and G.V. Chilingarian
© 1994 Elsevier Science B.V., Amsterdam. All rights reserved.

Chapter 10

DIAGENESIS OF ORGANIC MATTER

ALFRED HOLLERBACH and JANET DEHMER

INTRODUCTION

Organic matter in sediments represents a complex mixture of organic compounds of different types and molecular size, which are mostly derived from plant material. The organic compounds present are composed mainly of carbon and hydrogen atoms and are sometimes accompanied by other elements, such as oxygen, nitrogen and sulphur. The term diagenesis is defined here as a geotransformation of organic matter under low temperatures, generally less than 50°C, which is controlled by physical, chemical and biological processes.

Most of the organic matter produced in the biosphere is formed by biosynthesis with the help of solar energy and has a high energy content and a low thermodynamic stability. During the course of diagenesis, thermodynamic stabilization takes place producing more stable compounds with simplified chemical structures. This period of stabilization is characterised by a transition phase, which is represented by the occurrence of substances with a wide range of chemical structures. Further transformations (hydrocarbon generation and aromatization), where high temperatures and pressures are involved (coalification), lead to increasing crystallographic order of the carbon; the end-product being graphite.

In the last few decades, progress in analytical chemistry has made it possible to analyze complex mixtures of organic compounds, which has stimulated the knowledge of the fate of organic matter in the geosphere and has lead to the established science of organic geochemistry. This chapter gives a brief description of the chemistry, occurrence and diagenesis of different types of organic substances present in recent sediments. For further information the reader should refer to the reference list at the end of this chapter.

BIOCHEMICAL DECOMPOSITION OF ORGANIC MATTER

The decomposition and transformation of organic matter occurs mainly in soils, water columns and aquatic sediments. The main decomposers are a wide variety of microorganisms (bacteria, fungi and yeasts), which have the ability to adapt to different environments. Bacteria play an especially important role in oxygen-lean (anaerobic) sites, where they are exclusively responsible for the biochemical decomposition of organic material. The most widespread species of bacteria are: *Pseudomonas*, *Arthrobacter*, *Clostridium*, *Achromobacter*, *Bacillus*, *Micrococcus* and *Flavobacteria*. In addition, unicellular and mycelium-forming *Actinomycetes*, *Streptomycetes* and *Norcardia* are responsible for the decomposition of resistant organic

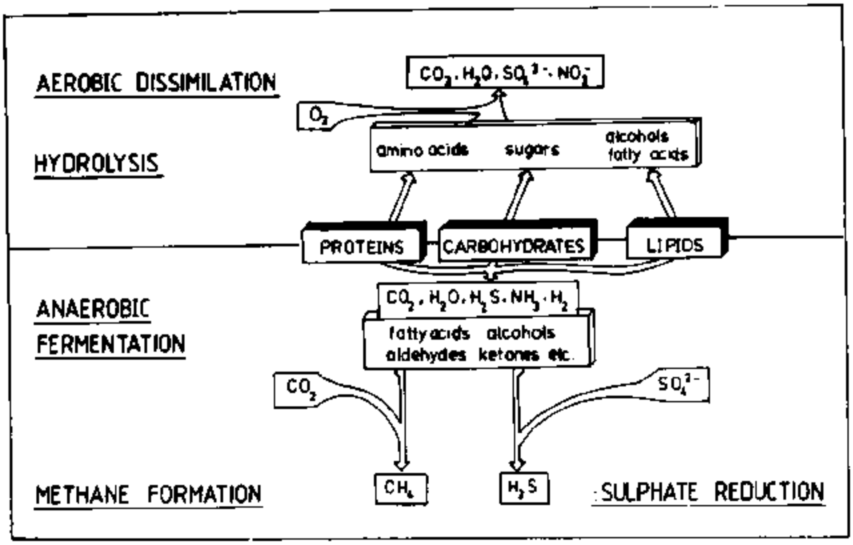

Fig. 10-1. Biological decomposition of organic matter.

matter, e.g., lignin and chitin. A third group of microorganisms is related to the fungi: *Basidiomycetes* are very effective in destroying one of the main components of wood, namely, lignin. Despite the importance of these microorganisms and their role in the decomposition of organic matter, macro-fauna, e.g., various annelids and arthropods, living in the soil or sediment, play an important part in the preparatory work of the mechanical disintegration of organic matter.

The activity of microorganisms is normally restricted to the first meter of sediment and decreases with increasing depth. As light can not penetrate the sediments, photosynthesis does not take place; therefore, reduced carbon (organic matter) is used for respiration to obtain energy. Under the access of oxygen, aerobic respiration (dissimilation) is responsible for the destruction of organic matter, which leads to the end-products carbon dioxide and water (Fig. 10-1). Microbial decomposition of hydrocarbons can only take place when molecular oxygen is present, which with the help of enzymes can be introduced in the form of functional groups into the carbon skeleton.

In water columns and fine-grained sediments with restricted water circulation, anaerobic conditions occur rapidly due to the uptake of oxygen and its limited access. The absence of oxygen initiates a microbial ecosystem in which organic material is decomposed by anaerobic dissimulation and respiration. At first, primary anaerobic organisms transform proteins, lipids and polysaccharides by fermenting hydrolysis processes into low-molecular-weight carboxylic acids, alcohols, aldehydes and ketones together with CO_2, H_2 and H_2O. These metabolites are then further used as a substrate by sulphur-reducing and methane-producing bacteria (secondary anaerobic organisms). During anaerobic respiration, sulphate (and nitrate) and carbon dioxide undertake the function of hydrogen acceptors and are thereby transformed into hydrogen sulphide (nitrogen) and methane as follows:

$$\begin{array}{lll} 2\mathrm{R(CH_2OH)} + \mathrm{SO_4^{2-}} & \longrightarrow \mathrm{H_2S} + 2\mathrm{CO_2} + \mathrm{H_2O} + 2\mathrm{R} & \text{sulphate reduction} \end{array}$$

$$\left.\begin{array}{ll} 4\mathrm{H_2} + \mathrm{CO_2} & \longrightarrow \mathrm{CH_4} + 2\mathrm{H_2O} \\ \mathrm{CH_3COOH} & \longrightarrow \mathrm{CH_4} + \mathrm{CO_2} \end{array}\right. \quad \text{methanogenesis}$$

Reduction of carbon dioxide to methane is common in sedimentary environments and is achieved by methanogenic bacteria. These methane-forming bacteria are archaebacteria, which distinguish themselves from normal eubacteria by their differing cell wall structure. About half of the organic material that undergoes anaerobic decomposition is transformed to methane. The fact that low amounts of methane are found in the atmosphere stems from the oxidation of methane into CO_2 by methanotrophic bacteria resident in the upper layers of the sediment.

In a natural anaerobic ecosystem, low-molecular-weight compounds are simultaneously formed and destroyed, whereby these substrates may accumulate under favorable conditions as intermediate products within the sediment. In addition, organic substances from plant-derived matter, which are resistant to decomposition, and the remnants of the last remaining active bacterial population become enriched and preserved within the sediment. Bacterial activity in sediments does not end abruptly but rather depends on the presence of decomposition products as nutrients and adequate pH and temperature conditions. Sulphate reduction and methane formation is possible, however, in sediments many hundreds of meters deep.

Among the substances which are more resistant to decomposition are the carbohydrates, lignin, chitin and hydrocarbons. These substances are important due to their quantitative distribution in the biosphere. Carbohydrates (cellulose, xylane and starch) are the basic components of plant substances and are produced in great quantities more than any other natural substance. Carbohydrates and chitin are utilized under aerobic conditions by fungi, myxobacteria and eubacteria, and under anaerobic conditions by *Clostridium*. Under both conditions, hydrolysis takes place using exoenzymes to break down the polymers into dimer- and monomer-components (glucose and glucosamine, respectively).

Lignin, a major component of wood, possesses a non-uniform chemical structure, which is biologically difficult to decompose. Microbial breakdown of lignin is undertaken by fungi (*Basidiomycetes*) and bacteria and provides the main source for the formation of humic substances in soils and peats.

The degradation of hydrocarbons, especially the large quantities of methane produced by methanogenesis, occurs only under aerobic conditions whereby yeasts preferentially oxidize longer-chained aliphatic hydrocarbons.

ORGANIC SUBSTANCES IN RECENT SEDIMENTS

Organic material in the geosphere can be divided into two basic groups, those which are soluble in water or organic solvents (e.g., benzene) and those which are insoluble in both (e.g., cell remains). The insoluble organic material is also termed as kerogen. It is, however, the group of substances that are soluble in organic solvents which are of special interest to organic geochemists.

In comparison to organic matter in water, soluble organic substances in sediments are bound to mainly inorganic and organic detritus. Only the organic substances which are highly water soluble, such as sugars and nucleic and amino acids, are able to exist freely within the pore spaces. Thus, in the upper sedimentary layers, the following groups of soluble organic material are present:

- water-soluble organic substances, which are easily transported by the pore waters to the surface, where they are utilized by microorganisms;
- lipophilic (hydrophobic) compounds, which remain adsorbed to the mineral matrix and, therefore, have a greater chance of being preserved if they are able to escape from the biologically-active zone;
- hydrocarbons, which can only be broken down in considerable amounts under strong aerobic conditions and, therefore, are preferentially preserved;
- highly reactive organic substances, which are able to react with functional groups present on particulate (organic) matter; and
- other organic molecules, which have been transformed by diagenetic processes into stable forms (e.g., hydrocarbons) by the removal of functional groups.

During diagenesis and catagenesis the original organic matter changes significantly from its initial form in the organism to its form in the sediment and, finally, in the rock. In sediments, the lipophilic compounds, i.e., water-insoluble compounds, are preferentially enriched and preserved. Biologically-derived molecules are found in Recent sediments and new compounds form during diagenesis and catagenesis.

LIPOPHILIC SUBSTANCES

Lipophilic (fat-like) substances are geochemically very significant organic compounds. They are grouped as compounds which are soluble in certain organic solvents, but insoluble in water. The organic solvents used for their extraction are also immiscible with water and include benzene, ether and chlorinated hydrocarbons. The group of lipophilic substances include fats, oils, waxes and also long-chained alcohols and carboxylic acids. Moreover, hydrocarbons and other compounds which possess a hydrogen-rich hydrophobic carbon skeleton also belong to this group.

Hydrocarbons

Hydrocarbons are chemically very simple compounds as they are only composed of the elements carbon and hydrogen. Each tetravalent carbon atom is saturated with monovalent hydrogen atoms. The carbon atom is capable of bonding with other carbon atoms to form chains, which can be unbranched (normal); e.g., *n*-butane:

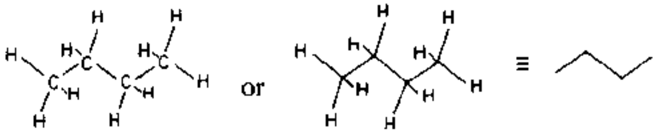

Normal-butane (n-butane) — C_4H_{10}

When more than four carbon atoms are involved a branched chain can also occur; e.g., iso-butane:

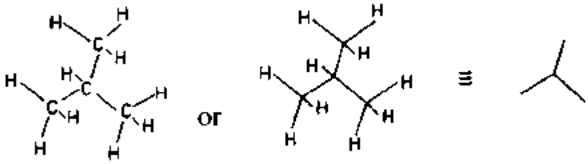

Iso-butane (i-butane) — C_4H_{10}

Carbon to carbon bonds possess a spatial orientation which allows carbon skeletons with five or more carbon atoms to form rings. Cyclohexane is an example for a non-planar ring structure:

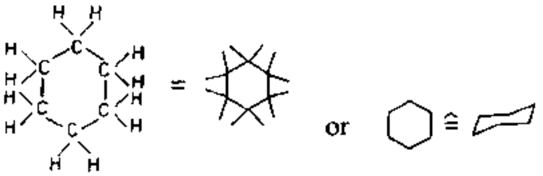

Cyclohexane (C_6H_{12})

In simple carbon to carbon bonding, where the carbon atoms carry the maximum number of hydrogen atoms possible one speaks of saturated hydrocarbons (alkanes or paraffins). A double bond can also form between two carbon atoms. In this case, the trigonal C=C bond requires two hydrogen atoms less than its saturated counterpart and is, therefore, designated as an unsaturated hydrocarbon, e.g., n-butene:

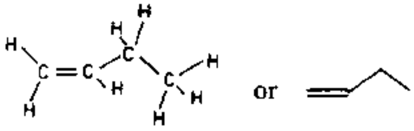

n-Butene (C_4H_8)

With cyclic hydrocarbons, as in the case of cyclohexane, it is possible to introduce three C=C double bonds into the structure. This leads to a new substance group known as the aromatic hydrocarbons (aromatics); e.g., benzene:

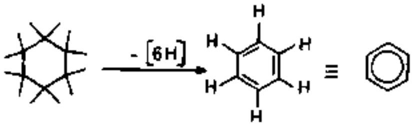

Cyclohexane (C_6H_{12}) Benzene (C_6H_6)

These hydrocarbons represent, in the chemical sense, end products of hydrogenation or dehydrogenation (aromatization) processes and are chemically and thermally very stable compounds.

If the organic compound contains other elements other than carbon and hydrogen, one speaks of so-called heterocompounds. Atoms, which are involved in the chemical structures of heterocompounds are mostly oxygen, nitrogen and sulphur. Their introduction into a carbon molecule leads to changes in its chemical behavior. The structure of the carbon molecule, however, does not change significantly.

Thus, one can classify hydrocarbons as (1) branched or unbranched chain-like aliphatic compounds, (2) alicyclic and aromatic with ring systems, and (3) heterocyclic compounds if they contain a hetero-atom within a ring system.

Aliphatic hydrocarbons (alkanes)

Alkanes are relatively volatile compounds which have lower boiling and melting points than other organic compounds having a similar molecular weight (see Table 10-1). Under normal conditions of temperature and pressure, C_1 to C_4 alkanes are gaseous, C_5 to C_{17} compounds are liquid and from C_{18} upwards the alkanes are solid in form.

Long-chained unbranched aliphatic hydrocarbons occur in plant organisms, where the odd-numbered *n*-alkanes dominate the even-numbered *n*-alkanes. This is due to the fact that odd-numbered *n*-alkanes are biologically derived from even-numbered carboxylic acids, which have undergone defunctionalization (in this case, the loss of the COOH group).

Differences in the occurrence and distribution of *n*-alkanes exist between those *n*-alkanes derived from aquatic organisms and those derived from higher plants. Higher plants possess hydrophobic cuticles which protect them from desiccation. These cuticles contain *n*-alkanes in the range between *n*-C_{23} and *n*-C_{33} (see Fig. 10-2). Consequently, one finds this *n*-alkane distribution in recent terrestrial sedi-

TABLE 10-1

Boiling and melting points of *n*-alkanes under normal conditions of temperature and pressure

Hydrocarbon	Melting point (°C)	Boiling point (°C)
Methane (CH_4)	−184	−164
Ethane (C_2H_6)	−172	−89
Propane (C_3H_8)	−190	−42
Butane (C_4H_{10})	−135	−0.5
Pentane (C_5H_{12})	−129	36
Heptadecane ($C_{17}H_{36}$)	22	303
Octadecane ($C_{18}H_{38}$)	28	317
Tetracontane ($C_{40}H_{82}$)	81	n.a.

n.a. = not available

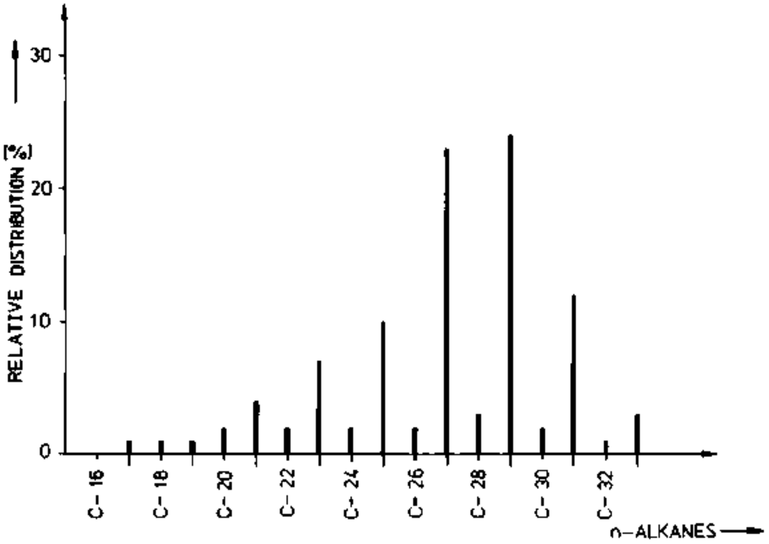

Fig. 10-2. *n*-Alkane distribution from stream sediment.

ments (e.g., peats). Similarly, this *n*-alkane distribution is also found in suspended and sedimentary particles from hydrological systems, which have a large input of terrestrial material (Fig. 10-2).

In large lakes and in the marine environment, the alkane distribution is influenced by the presence of aquatic organisms. Phytoplankton preferentially gives rise to *n*-alkanes with 15, 17, 19, and 21 carbon atoms; *n*-C_{17} is commonly found in photosynthetic algae and bacteria. One can, therefore, assume that *n*-C_{17} is an indicator or so-called biomarker for the presence of autochthonous organic matter from algae or bacteria. Some bacteria can, however, synthesize about the same amounts of odd and even *n*-alkanes between *n*-C_{25} and *n*-C_{32}. In hydrophyta (water plants) and *Phaeophyceae* (brown algae), the odd-numbered *n*-alkanes between *n*-C_{21} and *n*-C_{31} dominate.

Due to the interaction of a wide variety of aquatic organisms and allochthonous terrestrial material in aquatic sediments, one often obtains a bimodal *n*-alkane distribution, as shown in Fig. 10-3. Furthermore, olefinic hydrocarbons (mainly alkenes) of the type $C_{23}H_{46}$, $C_{25}H_{50}$ and $C_{27}H_{54}$, which are derived from fresh water algae (*Botryococcus braunii*), can be also present. Due to their highly reactive nature, these alkenes and other unsaturated hydrocarbons are not normally found within deeper lying sediments.

The proportion of *n*-alkanes in recent sediments can vary considerably (on a moisture-free basis). In forest soils and also in fresh-water sediments they amount to about 200 ppm. In unpolluted lakes, depending on their size and oxygen status, *n*-alkane content ranges normally between 5 and 300 ppm. In polluted areas, however, the amounts can rise to over 1000 ppm. Unpolluted coastal regions have between 0.01 and 5 ppm of *n*-alkanes.

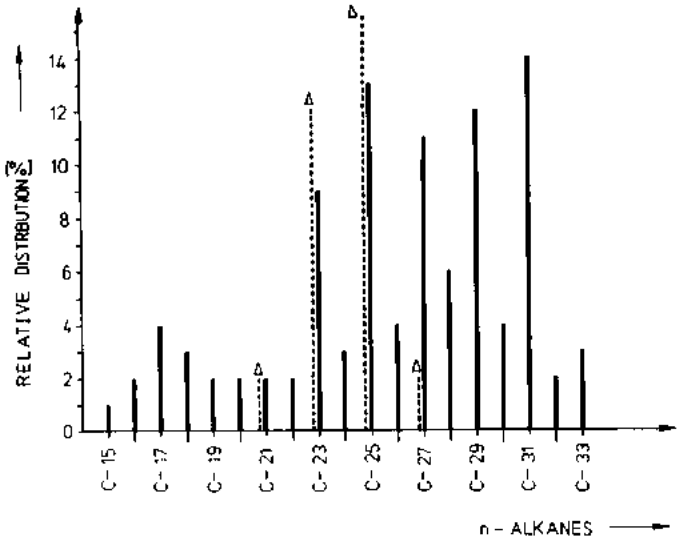

Fig. 10-3. *n*-Alkane distribution from an aquatic sediment. Those designated with Δ are corresponding *n*-alkenes.

Branched (iso and anteiso alkanes) and cyclic hydrocarbons are only found in low amounts in recent sediments. The isoprenoid hydrocarbon, pristane, is very common, however, in marine sediments, whereas phytane occurs only in trace amounts.

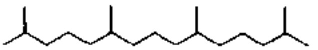

Pristane ($C_{19}H_{40}$)

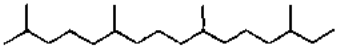

Phytane ($C_{20}H_{42}$)

Pristane and phytane shown above, are derived from the compound phytol, which is present as the alcohol side chain of the chlorophyll molecule found in photosynthetic plants. During diagenesis, the chlorophyll molecule undergoes a cleavage reaction, whereby phytol is released and is biochemically transformed via various stages to pristane (or phytane). Pristane occurs also in marine animals, especially in the copepod, *Calanus*.

In aquatic sediments, where terrestrial plant detritus is common, various phytadienes (containing two double bonds) may be found. Phytadienes are products formed from the dehydration of phytol. Terrestrial soils do not contain phytadienes, as the double bonds quickly undergo hydrogenation to form the corresponding *n*-alkanes or they disappear by condensation reactions with other compounds. Conservation of reactive double bonds can be sometimes explained when plant antioxidizing agents (e.g., tocopherols) are present.

Red-to-yellow-colored extracts obtained from Recent sediments are normally attributed to carotinoids, which are common hydrophobic plant pigments. Members of this group include the orange-colored polyene-hydrocarbon of the carotene type (e.g., β-carotene)and the relatively functional group-rich, yellow-colored xanthophylls (e.g., *Zeaxanthene*). In deeper layers of sedimentary material, diagenetic products from carotinoids are rare, which is probably due to degradation processes.

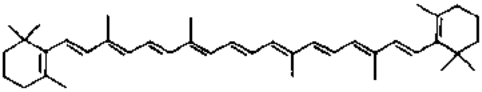

β-Carotene

Alicyclic hydrocarbons, except for certain pentacyclic triterpenoids, are seldom found in autochthonous Recent sediments.

Polycyclic aromatic hydrocarbons

Polycyclic aromatic hydrocarbons (PAH) consist of three or more condensed aromatic ring systems linked together. Although they are not formed in living organisms, as far as it is known today, they are present in the environment and the geosphere, where their source of emission is not always certain. PAHs can be formed from organic material by natural pyrolytic (forest fires) and anthropogenic processes (incomplete combustion). They are easily adsorbed by soot and dust particles and are consequently locally and globally transported and deposited. Airborne particles contain mainly benzo(ghi)perylene, coronene, indeno(1,2,3-cd)-pyrene, benz(a)anthracene, chrysene, benzofluoranthene and benzopyrene. Street dust mainly includes compounds such as fluoranthene, pyrene and various benzofluorenes. Investigations have shown that the exhaust from internal combustion engines and diesel motors contain large quantities of fluoranthene and pyrene.

Bituminous coals and coal tar can contain large amounts of phenanthrene, benzopyrene, coronene and perylene, as well as their methylated homologs. Petroleum and its products consist of less significant quantities of chrysene, benzopyrene and other PAHs with methyl groups and those with long aliphatic side chains.

Transportation processes succeed in depositing PAHs uniformly into the sedimentary system. They are found worldwide. Even the relative abundances of these compounds vary little in uncontaminated surface sediments of terrestrial and aquatic origin. An example is shown in Fig. 10-4. The total contents of PAHs in forest soils range between 1 and 4 ppm (on a moisture-free basis). Uncontaminated lakes contain, depending on allochthonous influences, between 2 and 10 ppm of PAHs.

It is also important to note that certain PAHs can be formed by natural biogeochemical processes. These PAHs are derived from mostly diterpenoid and triterpenoid compounds (see section below).

Oxygenated compounds

Lipids, such as fats, oils and waxes can be classified as esters. Esters are synthesized from alcohols and carboxylic acids. Contrary to hydrocarbons, these lipid-like substances contain oxygen.

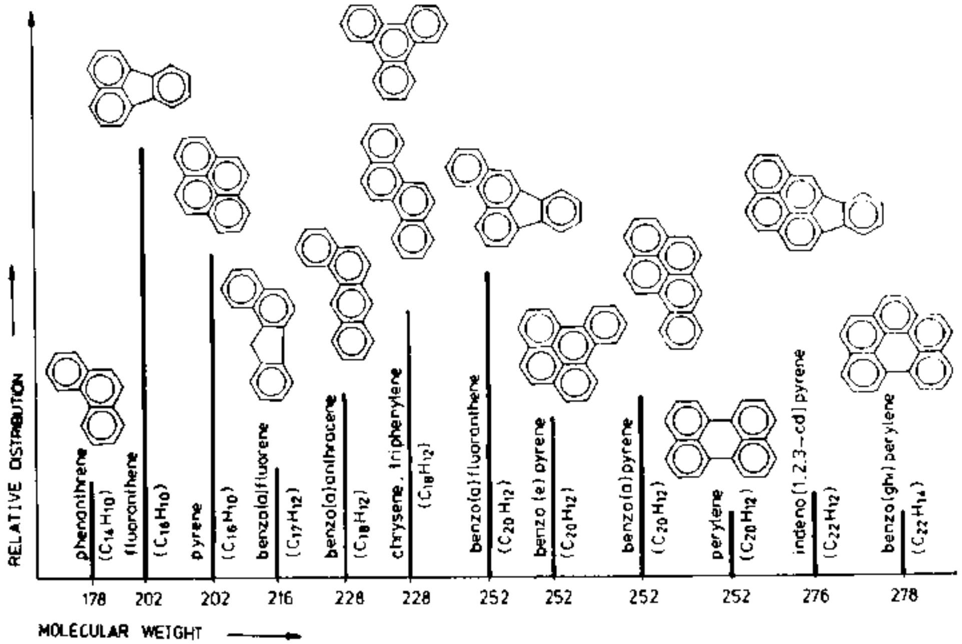

Fig. 10-4. Occurrence and distribution of polycyclic aromatics in recent surface sediments of aquatic origin.

Alcohols

Alcohols can be represented as a water molecule which has one of its hydrogen atoms replaced by an organic rest (R):

R—O—H

R can consist of an aliphatic CH_3 (methyl), C_2H_5 (ethyl) or a C_nH_{2n+1} group or even an alicyclic group. When the molecule contains one, two or more hydroxyl (OH) groups, one speaks of mono-, di- or polyvalent alcohols. Furthermore, one can differentiate between primary, secondary and tertiary alcohols depending on whether the OH-group is bound to the primary, secondary or tertiary carbon atom:

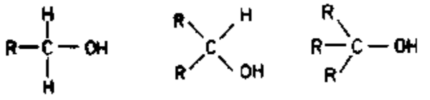

Primary, Secondary, Tertiary alcohol

The boiling points of the lower members of the alcohols are as follows:

methanol (CH_3-OH):	64.6°C
ethanol (C_2H_5-OH):	78.4°C
propanol (C_3H_7-OH):	97.2°C

They are water soluble due to their hydrophilic nature. In comparison to hydrocarbons, they are characterized by higher boiling points. As in the analogous case of water, this is due to the formation of hydrogen bridges. Alcohols with 4 to 11 C-atoms are only miscible in water to a certain extent. Consequently, as the R-group becomes larger its influence increasingly exceeds that of the hydroxyl group, so that higher alcohols possess physical and chemical properties similar to those of hydrocarbons.

Alcohols are found widely distributed in organisms. They occur esterified with acids in waxes or as unbound forms. In the aquatic organisms, alcohols in the range of C_{12} to C_{20} predominate, the most common of which are:

n-dodecanol (lauryl alcohol):	$C_{12}H_{25}OH$
n-tetradecanol (myristyl alcohol):	$C_{14}H_{29}OH$
n-hexadecanol (cetyl alcohol):	$C_{16}H_{33}OH$

The waxy coating of higher terrestrial plants contain long-chain primary alcohols, for example:

n-hexacosanol (ceryl alcohol):	$C_{26}H_{53}OH$
n-octacosanol:	$C_{28}H_{57}OH$
n-triacontanol (myricyl alcohol):	$C_{30}H_{61}OH$

n-Alcohols in aquatic sediments often show a bimodal distribution, as shown in Fig. 10-5. The first major area lies between C_{14} and C_{16}, whereas the second lies at C_{26}. The reason for this is due to the mixed nature of the input materials: the higher *n*-alcohols from C_{22} to C_{32} are derived from terrestrial plant material, whereas

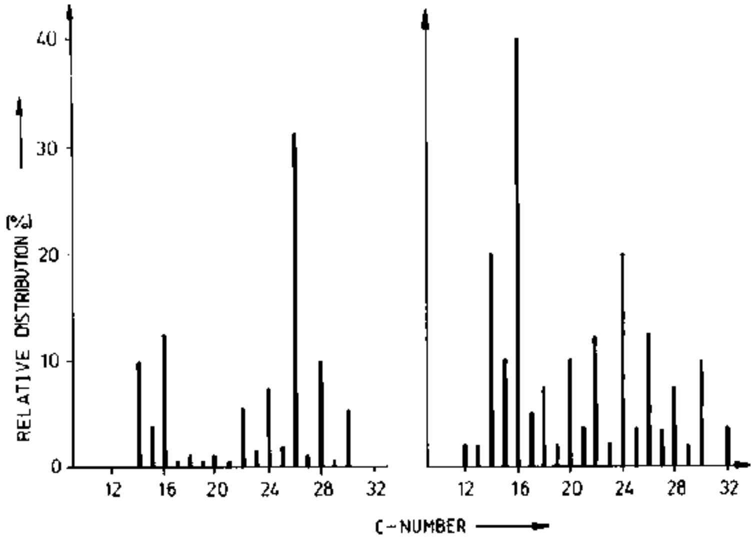

Fig. 10-5. Occurrence of *n*-alcohols in aquatic sediments. Left: free alcohols; right: bound alcohols.

the alcohols less than C_{20} are derived from autochthonous phytoplankton. A shift in the bimodal distribution in one or the other direction points to differences in the composition of the organic matter input. In aquatic sediments, alcohol contents normally range from 400 to 1500 ppm (moisture-free basis).

As well as long-chained alcohols, iso- and anteiso-alcohols in the range of C_{15} to C_{21} are found in aquatic sediments. A number of algae are known to synthesize these types of compounds. Occasionally, a C_{15}-iso-alcohol may be present, which points to a microbial input.

Carboxylic acids

The dehydration and oxidation of primary alcohols produces carboxylic acids via aldehyde formation.

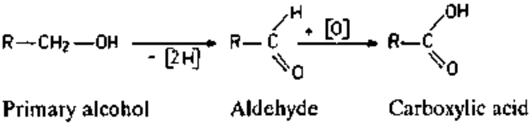

Carboxylic acids are characterized by their carboxyl group (COOH). Contrary to alcohols, carboxylic acids are acidic in nature, which is due to the ability of the hydrogen atom sitting on the carboxyl group to cleave as a proton, thus leaving a carboxylate anion. The carboxylate anion possesses the ability to build salts such as mineral acids do. The acidity of carboxylic acids is low, however — they are only weak acids. The marked solubility in water of lower carboxylic acids decreases rapidly with increasing length of the R-group:

formic acid:	$HCOOH$
acetic acid:	CH_3-COOH
propionic acid:	CH_3-CH_2-COOH

Carboxylic acids with more than ten carbon atoms are solid and possess a paraffinic nature. The biosynthesis of long, unbranched carbon chains is accomplished with the help of acetyl-coenzyme A, a C_2-compound-unit. Thus, long-chained carboxylic acids and also alcohols possess carbon atoms with an even-numbered preference.

The carboxylic acids are structural units of fats, oils, and waxes. The C_6- to C_{18}-carboxylic acids are present in fats and oils, whereas long-chained C_{20} to C_{32} compounds occur in waxes. These compounds consist of mono-carboxylic acids, i.e., those with only one carboxyl group.

Typical fatty acids and oils are:

n-tetradecanic acid (myristic acid):	$C_{13}H_{27}COOH$
n-hexadecanic acid (palmitic acid):	$C_{15}H_{31}COOH$
n-octadecanic acid (stearic acid):	$C_{17}H_{35}COOH$
n-octadec-(11)-enic acid (oleic acid):	$C_{17}H_{33}COOH$
n-octadec-(9,12)-dienic acid (linoleic acid):	$C_{17}H_{31}COOH$
n-octadec-(9,12,15)-trienic acid (linolenic acid):	$C_{17}H_{29}COOH$

Planktonic organisms consist of a high proportion of C_{12} to C_{18} unsaturated fatty acids. Furthermore, certain bacteria living in sediments contain C_{14} to C_{16} iso- and anteiso-fatty acids, e.g.:

2-Methyl-carboxylic acid (iso-carboxylic acid)

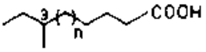

3-Methyl-carboxylic acid (anteiso-carboxylic acid)

In the waxes of higher terrestrial plants, long-chained carboxylic acids from C_{20} to C_{32} are found; typical examples are:

n-tetracosanic acid (carnaubic acid):	$C_{23}H_{47}COOH$
n-hexacosanic acid (carotic acid):	$C_{25}H_{51}COOH$
n-octacosanic acid (montanic acid):	$C_{27}H_{55}COOH$

Hydroxylated carboxylic and dicarboxylic acids (α and ω types) occur in the sea grasses (e.g., *Zostera*) in the C_{20} to C_{28} range:

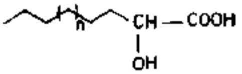

α-Hydroxy-carboxylic acid

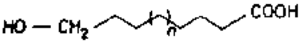

ω-Hydroxy-carboxylic acid

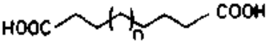

α,ω-Dicarboxylic acid

Short chained α-hydroxy-carboxylic acids (less than C_{20}) are found in microorganisms living in soil. Marine sediments contain predominately C_{14} to C_{18} fatty acids (Fig. 10-6). In lacustrine sediments, however, long-chained carboxylic acids from plant waxes and, therefore, from terrestrial detritus provide for a bimodal distribution as shown in Fig. 10-7. Thus, sedimentary carboxylic acids have a similar distribution to that of the alcohols.

Periodic fluctuations in the sedimentation rate and phytoplankton population give rise to variable amounts of iso- and anteiso-fatty acids. The unsaturated fatty acids have C_{16} to C_{22} carbon chains, whereas the iso- and anteiso-fatty acids lie between C_{14} and C_{16}. In aquatic sediments both types of acids can be found, as illustrated in Fig. 10-8, which indicates an input from aquatic organisms. Unsaturated C_{16}- and C_{18}-fatty acids represent phytoplankton, whereas the long-chained fatty acids could point to the input of higher plant detritus or zooplankton. The iso- and anteiso-carboxylic acids are produced by bacteria living in sediment and, thus, implies the input of microbial biomass into the sediment. When these branched acids increase

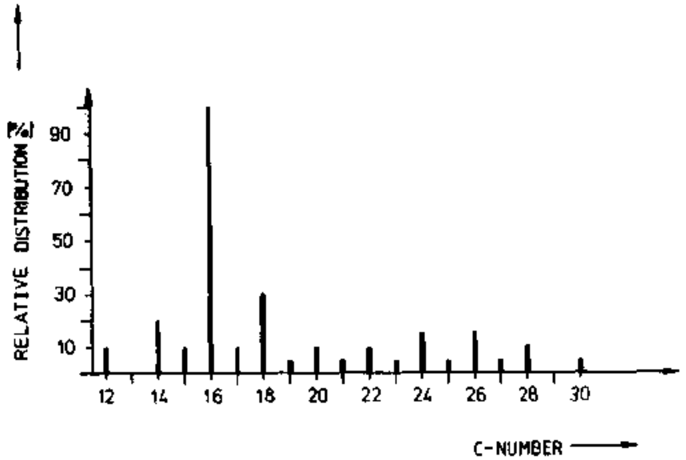

Fig. 10-6. Carboxylic acids in marine sediments.

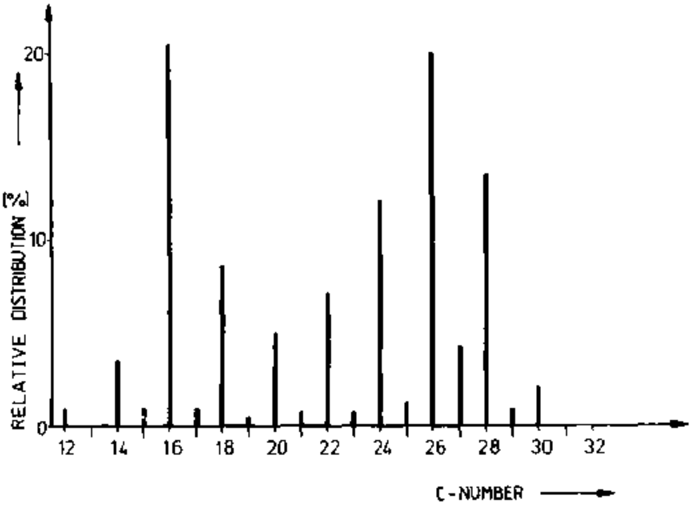

Fig. 10-7. Carboxylic acids in lacustrine sediments.

with increasing depth of the sediment, then one has a clear indication of in situ activity.

In the acid fraction, hydroxy-carboxylic acids and dicarboxylic acids occur in low quantities. These acid types can provide information on the origin of the organic matter in the sediment. Long-chained α-hydroxy- and α,ω-dicarboxylic acids (C_{22} to C_{28}) are present in higher aquatic plants. The C_{10}- to C_{20}-, α-, β- and ω-hydroxy-carboxylic acids are found in almost all Recent sediments, which indicates microbial reworking. On the contrary, di- and polyhydroxy-carboxylic acids do not owe their origins to the microorganisms and only occur in sediments which have a large input

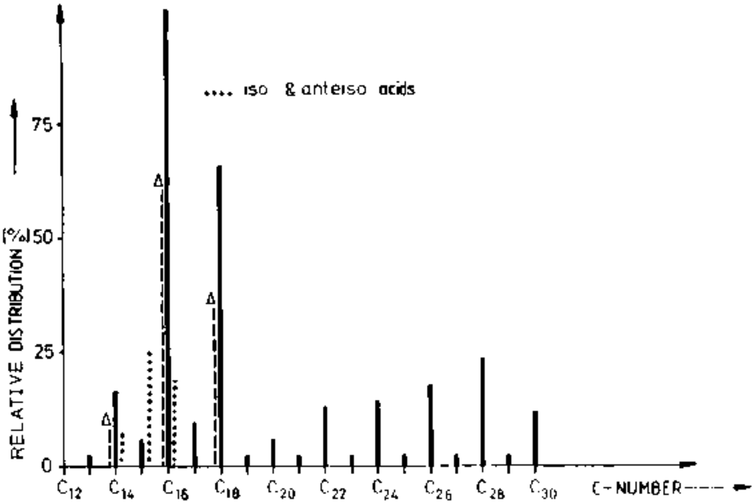

Fig. 10-8. Occurrence and distribution of carboxylic acids from a lacustrine sediment (Δ designates unsaturated carboxylic acids).

of terrestrial material. Higher plants contain large quantities of these acids, as they are structural components for the biopolymers cutin and suberin. The acid fraction, therefore, is especially suitable for the biogeochemical investigations regarding the input of organic matter in sediments.

Fatty acids are the favored nutrients for heterotrophic organisms and, therefore, are quickly assimilated, so that their amounts in deeper parts of the sedimentary column decreases significantly. Their preservation can be influenced by a suitable redox potential; thus, anaerobic sediments in productive lakes contain higher amounts and better preserved unsaturated fatty acids than aerobic sediments. Amounts vary from 100 ppm in fjord areas to 17,000 ppm in mesotrophic lakes. Furthermore, sediments of oligotrophic lakes contain more branched fatty acids than those of the eutrophic lakes.

Fats, oils, and waxes

Fats, oils, and waxes belong chemically to the group of carboxylic acid esters. Carboxylic acid esters are formed from carboxylic acids and alcohols under an equilibrium reaction in which water is formed as a byproduct (esterification):

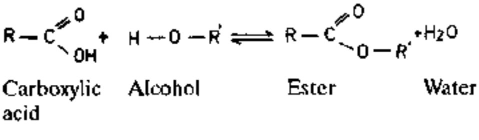

$$R-C(=O)OH + H-O-R' \rightleftharpoons R-C(=O)-O-R' + H_2O$$

By hydrolytic cleavage (reaction proceeds right to left) the original starting materials carboxylic acid and alcohol are produced again. Esters are neutral compounds and are immiscible in water. Long-chained fatty acids are esterified with the trivalent glycerol to form fats and oils. In each fat or oil molecule, three fatty acids with chain lengths of generally C_{12} to C_{18} are bound to the glycerol molecule (triglyceride). When different esterified fatty acids are involved in fat or oil formation, one speaks of the so-called mixed triglycerides:

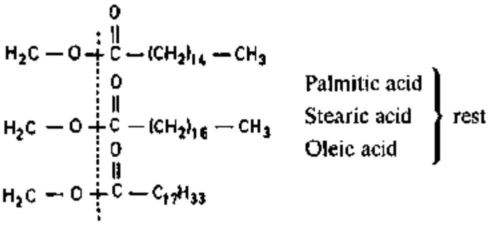

Glyceryl rest

Plant oils are not very stable as they contain a large proportion of unsaturated fatty acids with one or more double bonds, that are easily polymerised by molecular oxygen into solid high-molecular resins. Due to their insolubility in water and poor osmotic property, fats and oils are especially suitable as storage substances for plants and animals. Their high hydrogen content, for instance, is an excellent energy reserve and so they are mostly found in the seeds of flowering plants or are simply deposited in large quantities in the cells of algae.

Carboxylic acids not only esterify with glycerol but also with a variety of monovalent long-chained alcohols, that react together to form wax esters. The chain lengths of these two components lie generally between C_{20} and C_{30}. Carnauba wax is predominately a n-C_{26}-carboxylic acid esterified with a n-C_{30}-alcohol:

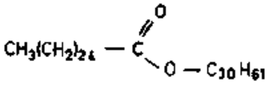

Cerotic acid-myricyl ester

Long-chained wax esters with more than 40 carbon atoms are solid, hydrophobic, and chemically-resistant compounds that are considerably more difficult to hydrolyze than fat esters. In higher plants, they are used to construct water repellent protective layers as well as waterproof partition zones between cell walls. In many types of zooplankton, wax esters with slightly shorter chain lengths between C_{30} and C_{34} are used as energy reserves.

Both triglycerides (fats and oils) and wax esters represent energy reserves. They are very sought after sources of nutrition, which are quickly utilized by living organisms, with the triglycerides being preferentially metabolized. Furthermore, due to the ease with which the hydrolytic cleavage occurs, their chemical stability is limited in aquatic environments.

Wax esters with chain lengths between C_{26} and C_{44} occur in suspended marine material, with C_{30}, C_{32}, C_{34} and C_{36} being most commonly present. Some triglycerides can contain 40 to 60 carbon atoms per molecule. Their maximum distribution peaks occur at C_{46} and C_{48}. These wax esters normally occur in small amounts and are usually derived from zooplankton and not higher plants.

The proportion of intact triglycerides and waxes can vary considerably and can make up to 50% of the total lipid fraction. Generally, their amounts decrease rapidly with increasing sediment depth. Hydrolysis and biochemical processes degrade these substances quickly, so that their rate of conservation is low.

Ketones

When secondary alcohols undergo oxidation at the oxygen carrying carbon atom, ketones are formed:

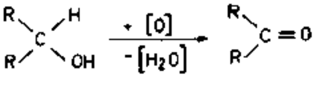

Secondary alcohol Ketone

Ketones are characterized by their carbonyl group (>C=O) and their two organic carbon rests. The simplest ketone is acetone:

$CH_3-CO-CH_3$

Acetone

Ketones with more than three carbon atoms already possess a lipid character.

In lacustrine and marine sediments, low amounts of methyl-ketones (*n*-alkan-2-ones) with a carbon chain length between C_{20} to C_{35} are found, where the odd-numbered varieties dominate:

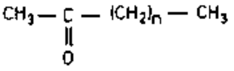

$$CH_3-\underset{\underset{O}{\|}}{C}-(CH_2)_n-CH_3 \qquad n = 16 \cdots\cdots\cdots 31$$

Their origin in aquatic sediments is uncertain, although it can not be excluded that methyl ketones are a microbial in situ product formed by an appropriate *n*-alkane or *n*-carboxylic acid (via β-oxidation and decarboxylation, respectively). In terrestrial soils, *n*-C_{26} to *n*-C_{39} methyl-ketones are also detectable and thus it can not be excluded that there is a possibility of an allochthonous input into the aquatic sediments. Unsaturated C_{37}- to C_{39}-ketones may be derived from phytoplankton, as they have been found in the coccolith, *Emiliana huxleyi*. Methyl-ketones have a high geochemical stability and are well preserved in sediments, especially under anaerobic conditions.

Terpenoid compounds

In nature, there are a group of special compounds which carry out various biochemical functions of regulation. Terpenoid compounds belong to this category. Terpenoids are based on the C_5-isoprene unit (2-methylbutadiene). Due to the methyl groups situated at characteristic sites on the carbon skeleton, terpenoids are able to form chains and ring systems.

Terpenoids are classified in terms of how many terpene units they possess, these being hemiterpenes (C_5), monoterpenes (C_{10}), sesquiterpenes (C_{15}), diterpenes (C_{20}), triterpenes (C_{30}) and tetraterpenes (C_{40}). The hemi- and monoterpenes are very volatile compounds. The sesquiterpene, farnesol is found in certain photosynthetic bacteria (e.g., *Clorobium*), where it substitutes phytol on the chlorophyll molecule.

Diterpenes

In contrast to monoterpenes and sesquiterpenes, diterpenes are not volatile compounds. They are components of higher plant resins, which represent complex excretion products. The most important diterpene and probably the most synthesized compound, however, is phytol, an unsaturated branched alcohol, that is linked to the chlorophyll molecule by an ester bond:

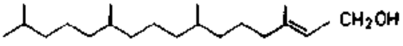

Phytol ($C_{20}H_{39}OH$)

As mentioned before, phytol is transformed via various chemical steps into the hydrocarbon end-products, pristane and phytane. The first stage of diagenesis consists of the release of phytol from the chlorophyll molecule by a hydrolysis reaction at the ester linkage. Thereafter, a step-wise transformation process occurs, which depends on whether the environment of deposition is oxidizing or reducing. Under oxidizing conditions, the following products are formed:

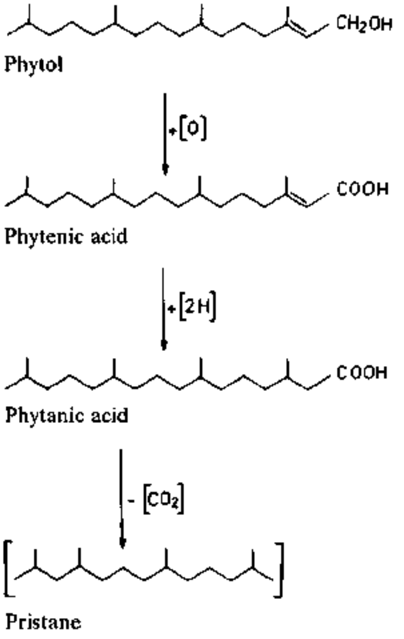

Under reducing conditions the double bond of the phytol molecule undergoes saturation and at the same time hydrogenolysis:

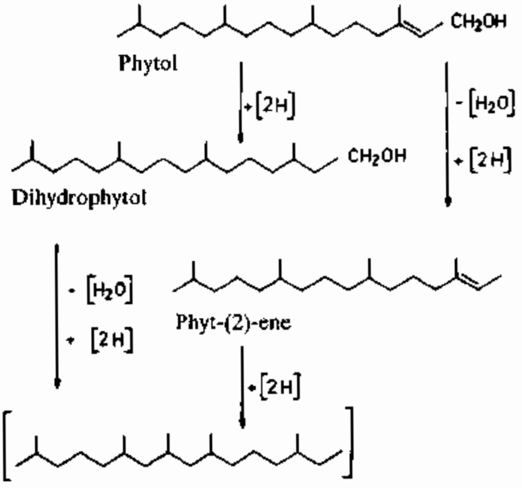

Phytane

As diagenesis continues decarboxylation of phytanic acid or dihydrophytol leads to the formation of pristane (C_{19}) or phytane (C_{20}), respectively. As it is seldom that either strongly oxidizing or reducing conditions exist in Recent sediments, both isoprenoid hydrocarbons, pristane and phytane, are found together. Furthermore, a C_{18}-ketone may also be present, which is formed from phytol by oxidative microbial decomposition:

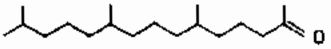

6,10,14-Trimethylpentadecan-2-one

Unlike phytol, most of the other diterpenes are not chain-like structures, but are normally three-ringed systems. The three-ringed diterpenes are divided into two main groups, namely abietane and pimarane. Abietane-type diterpenes have an isopropyl side chain on ring C, whereas the pimarane-types have an ethyl and methyl group.

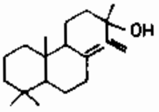

Manool

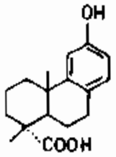

Podocarpic acid

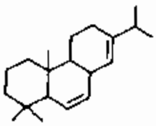

Cupressene

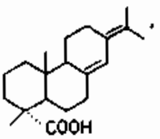

Neoabietic acid

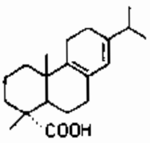

Palustrinic acid

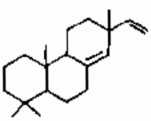

Pimaradiene

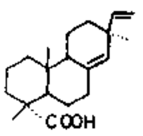

Pimaric acid

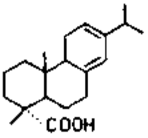

Levopimaric acid

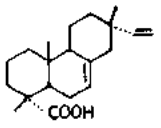

Isopimaric acid

Moreover, a four-ringed diterpene of the following type also occurs:

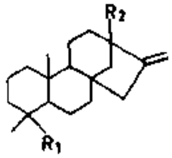

$R_1 = R_2 = H$: phyllocladene or kaurene
$R_1 = COOH, R_2 = OH$: steviol

Phyllocladene and kaurene are differentiated by their steric ring structure. Phyllocladene is found in certain shrub-like conifers belonging to the groups, *Podocarpaceae*, *Araucariaceae* and some *Cupressaceae*. In contrast, conifer resins (e.g., from *Piceae*) are composed of an isomeric mixture of diterpenoid-carboxylic acids having the pimarane and abietane structure.

As cyclic diterpenes are not formed in aquatic organisms, these compounds can be used as indicators (or biomarkers) for the input of terrestrial organic matter derived from gymnosperms. In aquatic sediments of marine or lacustrine origin, one of the main diterpene compounds found is dehydroabietic acid. Via dehydrogenation and decarboxylization, it is diagenetically transformed to the aromatic hydrocarbon, retene. These products are derived from the starting material, abietic acid, which is easily formed by acid-catalyzed rearrangement of the unstable double bond present in the other isomeric diterpenoidal acids, levopimaric acid, neoabietic acid and palustric acid:

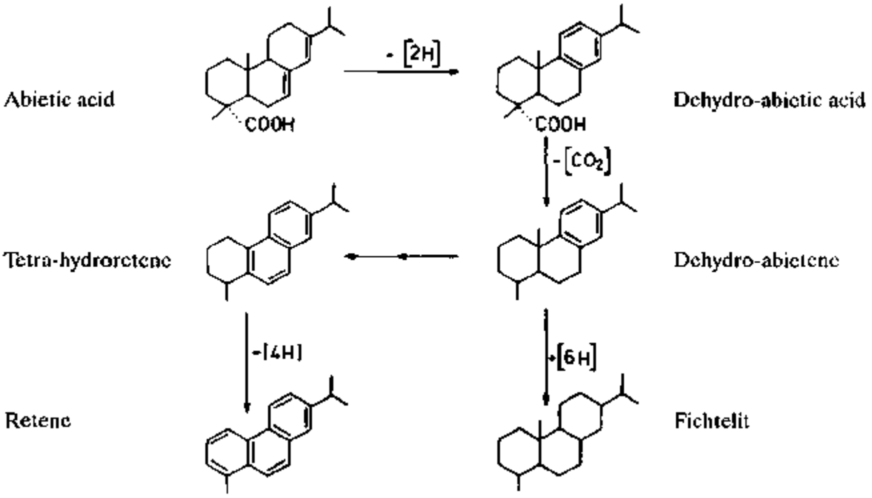

Other diagenetic products of diterpenes include the classes of aromatic compounds:

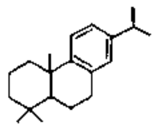

Dehydro-abietane

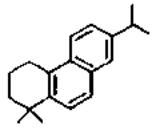

Simonellite

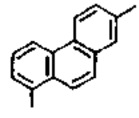

Pimanthrene

Anoxic sediments contain larger amounts of partly or completely aromatized diterpenes than corresponding sediments deposited under oxic conditions. The mode of formation of aromatized diterpenes, however, is unclear.

Triterpenes

Pentacyclic triterpenes are common compounds of plants and microorganisms. In the plant kingdom, the cyclization of squalane (C_{30} isoprenoid) in the presence of oxygen leads to the formation of three different basic triterpene types:

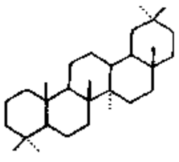

Oleanane-type

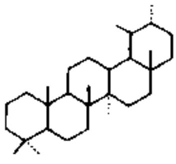

Ursane-type

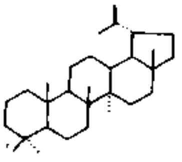

Lupane-type

At different positions on the triterpene skeleton, often hydroxyl- and carboxyl-groups are present. Thus, most of the pentacyclic triterpenes belong to the chemical groups of alcohols, carboxylic acids, and hydroxy-carboxylic acids. The commonly-found β-amyrin and taraxerene, which have been isolated from lichens, belong to the oleanane-type triterpene including oleanolic acid:

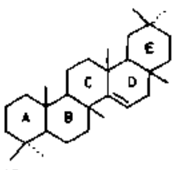

Taraxerene

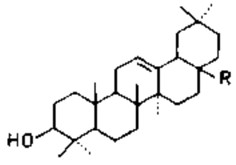

R = CH_3: β-amyrin
R = COOH: oleanolic acid

Another arrangement of the methyl groups on ring E gives rise to representatives of the ursane group:

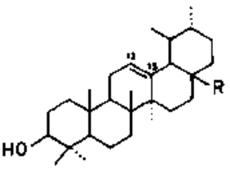

R = CH_3: α-amyrin
R = COOH: ursolic acid

Pentacyclic triterpenes of the lupane type are also commonly found in higher plants. In this group, ring E is formed of five carbon atoms and possesses an isopropenyl side chain:

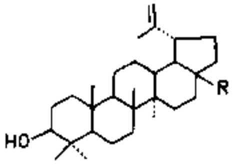

R = CH_3: lupeol
R = CH_2OH: betulin

A similar structural arrangement is found in arborene (arborinol) present in tropical plants and fernene, which is derived from ferns and microbial organisms:

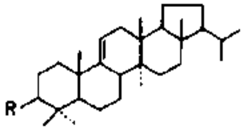

R = H: arborene
R = OH: isoarborinol

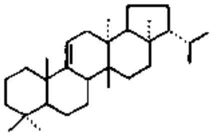
Fernene

In (lower) algae and some bacteria, pentacyclic triterpenes of the hopane type occur. In the absence of oxygen, some of these organisms are able to synthesize these compounds by the acidic catalyzation of squalene, which induces cyclization. Although hopanoids have the same A to D ring structure, differences occur in ring E and the length of the side chains present, which can reach up to five carbon atoms. Hop-17(21)-ene and diploptene are such examples and are found in blue-green algae:

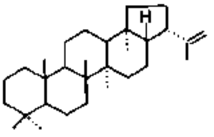
Hop-22(29)-ene (diploptene)

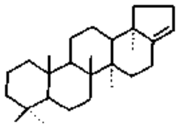
Hop-17(21)-ene

Hopanoids with longer side chains are present in many types of bacteria. So far, they have been found in the following eubacteria: *Rhodospirillaceae*, the obligate methanotrophic bacteria and many cyanobacteria. One of the most commonly found hopanoids is the tetra-hydroxy-C_{35}-hopane:

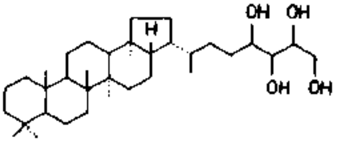

Tetrahydroxybacteriohopane

Pentacyclic triterpenes are often found in recent sediments. Terrestrial sediments contain the triterpenes of higher plants, for example, α- and β-amyrin, betulin and triterpenoidal carboxylic acids. During diagenesis some triterpenes undergo oxidization at the hydroxy-groups to form ketones. Marine and lacustrine sediments show a complex spectrum of different pentacyclic triterpenes depending on their source input. Commonly found pentacyclic triterpenes include saturated C_{27}-, C_{29}-, C_{30}- to C_{32}-hopanes, unsaturated C_{27}- and C_{30}-triterpenoids (trisnorhopene and diploptene) as well as C_{31}- to C_{33}-hopanoic acids, of which C_{32}-hopanoic acid is the most common:

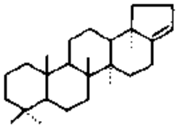

Trisnorhop-17(21)-ene

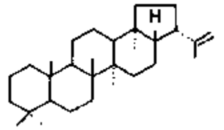

Diploptene

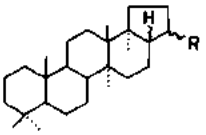

R=H: C_{27}-hopane (trisnorhopane)
R=C_2H_5: C_{29}-hopane (adiantane)
R=C_3H_7: C_{30}-hopane
R=C_4H_9: C_{31}-hopane (homohopane)
R=C_5H_{11}: C_{32}-hopane (bishomohopane)

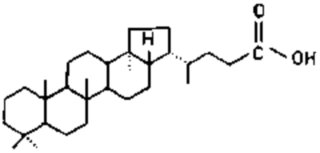

C_{32}-Hopanic acid

As well as the originally-present biogenic pentacyclic triterpenes, others occur which are formed by biogeochemical processes. Thus, the range of different pentacyclic triterpenes becomes more complex, as not only recent triterpenes from various sources are present, but also geohopanes which are derived from fossil organic matter input. These fossil geohopanes, which are formed from biohopanes by thermo-catalytic processes, are completely saturated and possess the thermodynamically stable 17α(H)-configuration on ring E. The unstable 17β(H)-isomer is only present in hopanes with a biological mode of formation. In those recent sediments that have been hardly influenced by fossil material, therefore, only the 17β(H)-hopane series from C_{27} to C_{32} occur. It is also important to note, that the 17β(H)-configuration can be transformed to the 17α(H)-form by acid catalyzation.

Pentacyclic triterpenes from higher plants often contain a special endocyclic double bond that is very slow to react. This applies to the case of the double bond present between positions 12 and 13 in α- and β-amyrin and its reluctance to undergo hydrogenation. Despite this, the presence of the double bond can act as a starting point for the introduction of more double bonds into the cyclic structure to give aromatic triterpenoids. During the aromatization process many different intermediates are formed.

Further aromatization of these intermediate naphtheno-aromatics leads to the formation of the polycyclic aromatic hydrocarbons (PAH), chrysene and picene (see Fig. 10-9). These compounds may occur with or without methyl groups attached. These compounds can be found in the deeper (older) parts of recent sedimentary sequences in lakes and large rivers, in which a large proportion of terrestrial plant material has been deposited under anaerobic conditions. They have also been found in the deeper layers of some peat sections. The reason for their formation can be probably attributed to anaerobic microbial processes, which create suitable environmental conditions for the biogeochemical aromatization process.

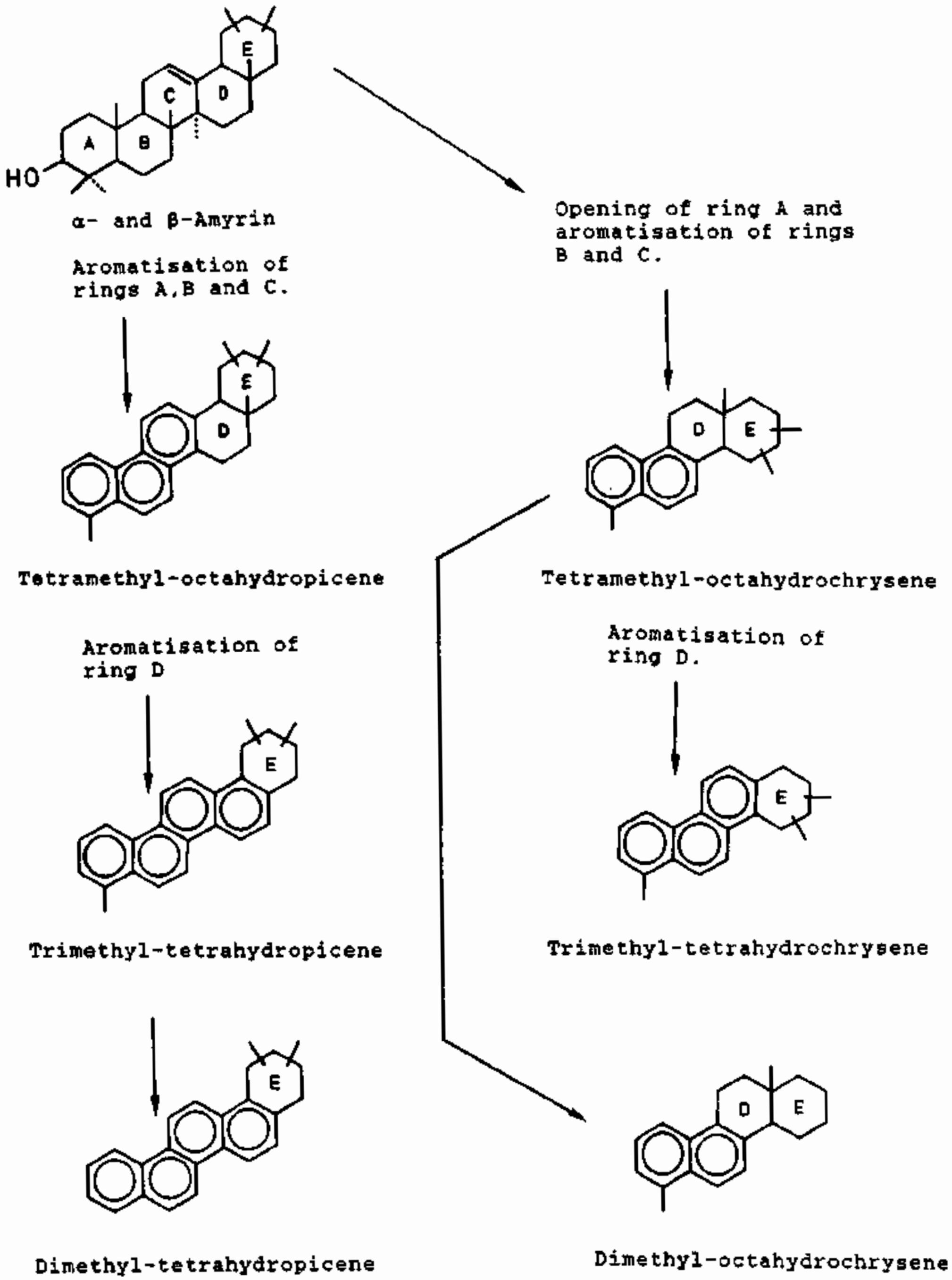

Fig. 10-9. Aromatization of α- and β-amyrin.

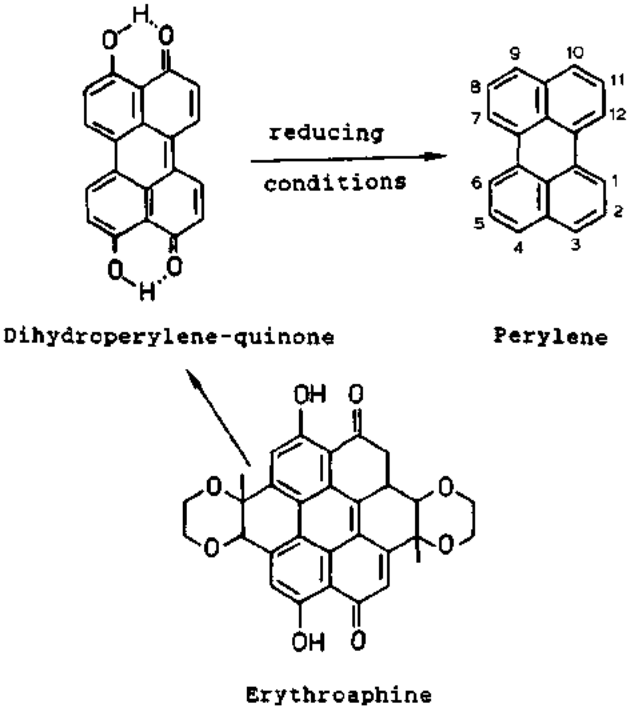

Fig. 10-10. Formation of perylene.

In addition to the natural formation of PAHs of the phenanthrene, chrysene and picene type, diagenetic processes can give rise to the formation of perylene which is derived from hydroxy-quinone pigments (see Fig. 10-10). Compounds of this structure are commonly found in plants and especially fungi. The original source material is the compound dihydroperylene-quinone. Perylene, however, can be formed by the reduction of erythroaphine. During this process small amounts of 1,12-benzperylene and coronene are formed.

A general increase in the concentration of perylene with increasing depth of sediment infers in situ formation. Perylene is a suitable geochemical indicator for anaerobic conditions and also for terrestrial input. High sedimentation rates with a high input of terrestrial detritus results in a high proportion of perylene present in the PAH fraction. Under aerobic conditions with a low rate of accumulation and terrestrial input, the deposited sediment normally contains very little of this compound.

Steroids

Steroids can be described as derivatives of the C_{30}-triterpene, squalene. From squalene, lanosterol is formed via various intermediate stages, which, in turn, is transformed into cholesterol. The principal structure of cholesterol is an alicyclic cyclopentano-perhydrophenanthrene ring system with a branched C_8-side chain:

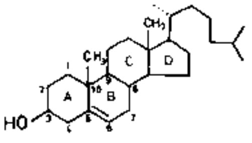

Cholesterol ($C_{27}H_{45}OH$)

Normally, alicyclic six-ringed structures are not planar, as each ring is able to connect to the next in a different position, thus forming a three-dimensional molecule. In steroids, however, the trans-linkage of all four rings is responsible for producing a flat molecule. Two methyl groups at positions 10 and 13 on the ring system project above the molecule plane. The dotted line (···) situated on the side chain indicates that the methyl group points back into the page. In many sterols there is also a double bond present between the C-atoms 5 and 6 (Δ^5) in ring B. Furthermore, sterols possess a hydroxy-group, which sits on the third carbon atom in ring A. Chemically, cholesterol can be looked upon as an unsaturated alcohol.

All steroids have the same basic tetracyclic structure, but differ in their substituent R groups. They are found in both animals and plants. Although cholesterol is the main steroid present in vertebrates, it is also widely found in plants and in low amounts in some algae. Typical higher plant (tracheophyta) steroids are shown in Fig. 10-11.

Some steroids have a more complicated ring and side chain structure. Of these, higher plant steroids appear to have the general property of being able to utilize the two stereospecific possibilities of the R and S configuration at C_{24}, on which sits a methyl and an ethyl group (e.g., 24R and 24S in campesterol).

The main steroid found in fungi (*Ascomycetes* and *Basidomycetes*) is ergosterol, which has an additional double bond (Δ^5 and Δ^7) in its ring system.

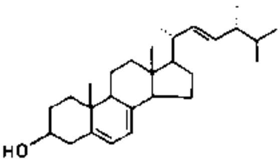

Ergosterol

Marine organisms are capable of synthesizing a variety of steroid compounds. These are shown in Table 10-2. Red algae are found to contain mainly C_{27}-sterols, whereas brown and green algae additionally contain C_{29}-sterols. The C_{29}-sterols also occur in higher terrestrial plants and mainly comprise stigmasterol and sitosterol. As these sterols are absent in marine algae, their presence in recent sediments indicate the input from higher plant material. The C_{28}-sterols are found in a mixture of organisms, including plants (campesterol) and some algae (dihydroergosterol). In comparison to plants and algae, invertebrates possess a complex mixture of C_{26}-, C_{27}-, C_{28}- and C_{29}-sterols. Procaryotes (bacteria) do not appear to have any steroids at all. It is suggested that the hopanoids present in procaryotes take on the regulatory function of steroids.

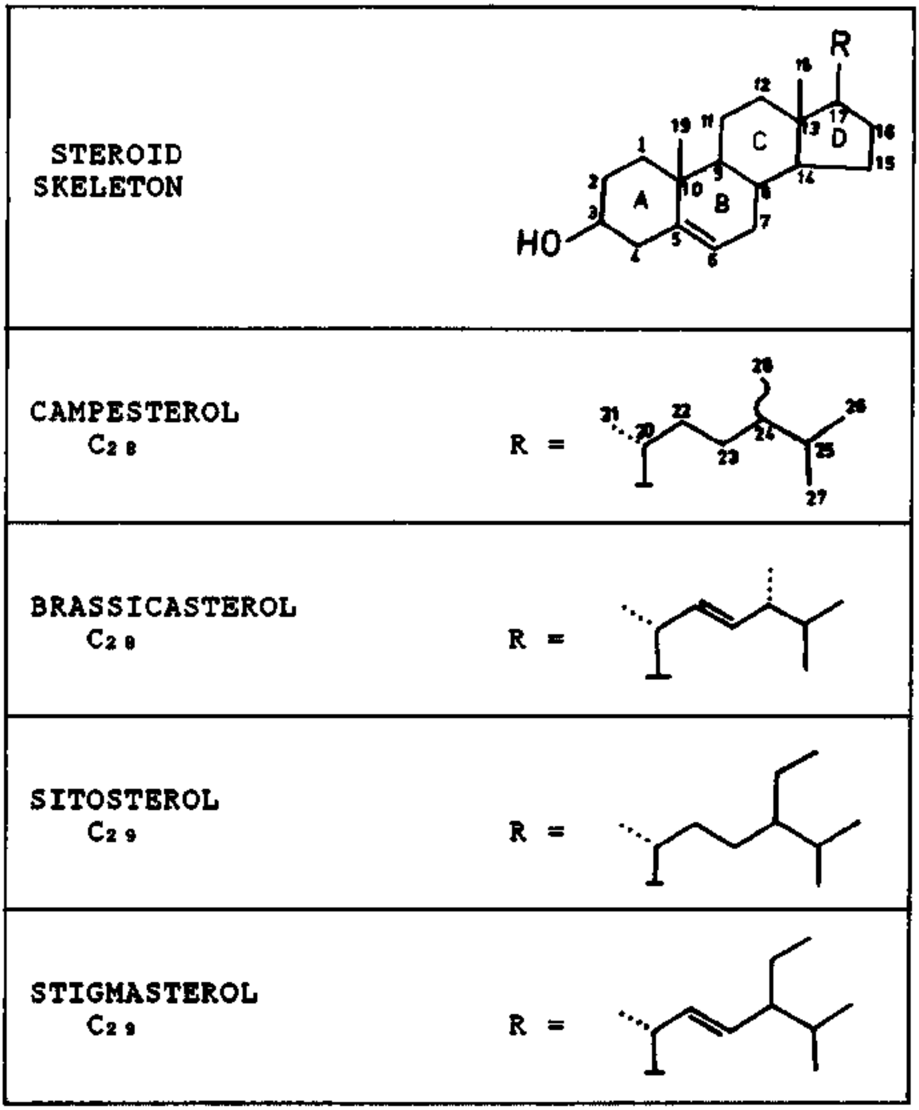

Fig. 10-11. Typical sterols in higher plants.

In recent soils, the main sterols found comprise those derived from higher plants. These are shown in Table 10-3. This table shows that the main representative of the steroid fraction isolated from soils is sitosterol. The cholesterol present is derived from the fauna living in soil. In addition to the higher-plant sterols, small amounts of 5α-stanols are found. The stanol does not contain a double bond in ring B and is an early diagenetic product. Further diagenetic products include Δ^2-sitostene and a series of sitostadienes, of which the latter consists mainly of Δ^3,Δ^5-sitostadiene. Hydrocarbons of this type are formed from appropriate precursors by dehydration

TABLE 10-2

Occurrence of sterols in different organisms

ORGANISM	STEROID	SIDE CHAIN
Rhodophyceae (red algae)	Cholesterol	
	Desmosterol	
Phaeophyceae (brown algae)	Fucosterol Cholesterol	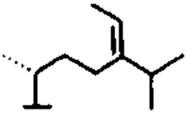
Chlorophycaea (green algae)	Isofucosterol	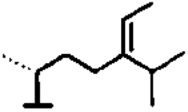
	24-Methylencholesterol Cholesterol	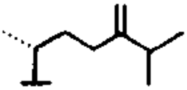
Bacillarophyceae (Diatoms : silica algae)	Brassicasterol	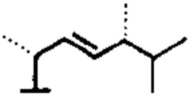
Porifera (sponges)	Cholesterol Clionasterol Poriferasterol	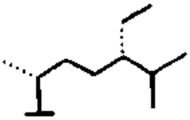 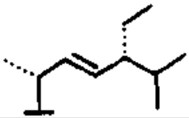
Coelenterata	Cholesterol 22-Dehydrocholesterol Gogosterol	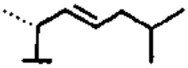 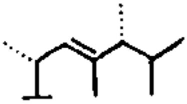
Arthropoda (crustaceans)	Cholesterol Desmosterol	

TABLE 10-3

Composition of the steroid fraction found in soils

Steroid	Relative amount (%)
Cholesterol	0– 8
Brassicasterol	0– 5
Campesterol	5–15
Sitosterol	55–75
Δ^2-Sitostene	2– 6
Δ^3,Δ^5-Sitostadiene	3–25
Δ^3-Sitosten-3-one	10–30

(loss of water molecule) mediated by biological or chemical processes:

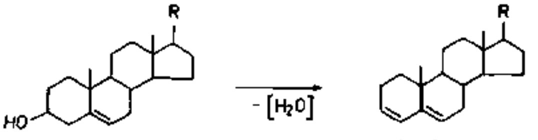

Sterol Δ^3,Δ^5-Steradiene

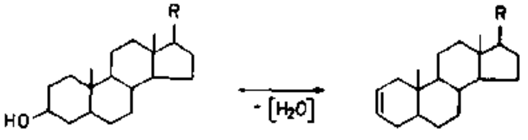

Stanol Δ^2-Sterene

Diasterenes represent other diagenetic products that do not occur in living organisms. They can be formed under acidic conditions, when Δ^4- and Δ^5-sterenes undergo backbone rearrangement by ring cleavage.

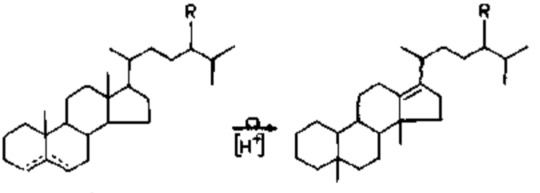

Δ^4- or Δ^5-Sterene $\Delta^{13(17)}$-Diasterene

In addition to undergoing dehydration, secondary alcohols on steroids can undergo oxidation to form ketones. This induces a double bond rearrangement at the favorable position 4:

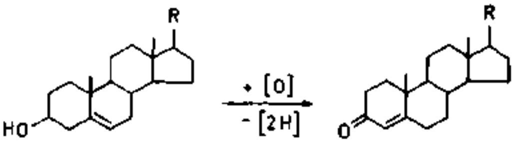

Δ^5-Sterol Δ^4-Sten-3-one

TABLE 10-4

Composition of the steroid fraction found in lacustrine sediments

Steroid	Relative amount (%)
Cholesterol	5–45 (65)
22-Dehydrocholesterol	2– 5
Campesterol	5–35
Brassicasterol	2– 4
Stigmasterol	5–10
Sitosterol	20–35
5α(H)-Cholestanol	5–55
5β(H)-Cholestanol	0–75
5α(H)-Sitostanol	5–30
5β(H)-Sitostanol	0–45

Table 10-4 shows the composition of the steroid fraction in lacustrine sediments, which varies depending on the input of terrestrial allochthonous and littoral plant detritus. The interpretation of steroid composition in recent lacustrine sediments depends also on the trophic status. One can assume that in sediments from oligotrophic lakes the influence of autochthonous organic matter can be reflected by the ratio of cholesterol to sitosterol. This, however, is not valid for mesotrophic or eutrophic lake sediments, as for example, waste water from sewage plants contain high amounts of cholesterol and even greater amounts of 5β-(H)-cholestanol (coprostanol). The formation of 5α(H)- and 5β(H)-sterols depends on how the saturation of the double bond of Δ^5-sterols occurs. If the hydrogen at position 5 is taken up below the molecular plane [5α(H)], then the elongated molecule is retained as the rings A and B are joined in the trans position. The addition of the hydrogen above the molecular plane in the 5β-position leads to the bending of ring A and thus a change in the molecular architecture (configuration), so that a cis-linkage of rings A and B occurs:

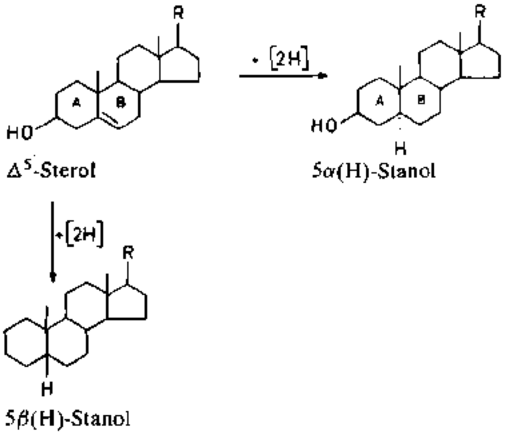

Δ^5-Sterol

5α(H)-Stanol

5β(H)-Stanol

TABLE 10-5

Occurrence of sterols in marine sediments

Skeleton type	Name of steroid
C_{27}-Sterols	Cholesterine, 22-dehydrocholesterol, desmosterol, 22-dehydrocholesterol
C_{28}-Sterols	Campesterol, brassicasterol, ergosterol, 24-methylenecholesterol, 4-methylcholesterol, 22-dihydrobrassicasterol, campostanol, spongesterol
C_{29}-Sterols	Sitosterol, stigmasterol, clionasterol, gorgosterol

The 5α(H)-stanols are formed only in small amounts in organisms. There are various microorganisms, however, especially those which live in the intestinal tract, that can hydrogenate Δ^5-sterols to 5β(H)-stanols (e.g., cholesterol to coprostanol). Thus, a high content of 5β(H)-stanols can point to fecal contamination. Under a reducing environment, which is often found in lacustrine sediments, the formation of 5α(H)-stanols takes place under normal diagenetic conditions. Reduction processes of this type give rise to an increasing 5α(II)-stanol/sterol ratio with increasing sediment depth. Moreover, there appears to be a certain relationship between the amount of sterols present and the degree of pollution. Oligotrophic lakes contain 100 to 500 ppm sterols, whereas in mesotrophic lakes the amounts rise to over 1000 ppm (moisture free basis).

The steroid fraction in marine sediments is much more complex in composition. The main input of sedimentary sterols, however, is derived from "primitive" marine organisms. A summary of marine sterols based on their carbon number is shown in Table 10-5.

Typical for marine sediments are the sterols which are methylated and dimethylated at position 4. They include the commonly-found dinosterol (4,23,24-trimethycholest-22-enol), which is present in different species of dinoflagellates:

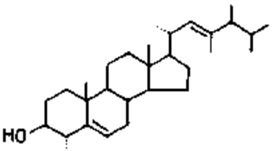

Dinosterol

The main sterols present in the sapropelic layers of the Black Sea are dinosterol, its hydrogenated analogue and 4,24-dimethyl-cholestanol. In addition to the hydrogenated 5a(H)-stanols, diagenetic products include sterenes and keto-steroids. With increasing sediment depth, the amount of original sterol material and its diagenetic products decrease rapidly.

CHLOROPHYLL

As well as the above-mentioned plant pigments with a carotin and xanthophyll structure, chlorophyll is the most important pigment in the plant world.

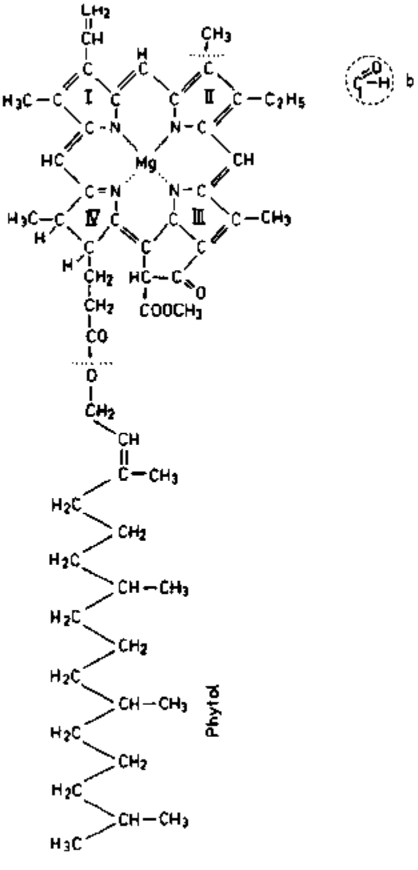

CHLOROPHYLL – a

Chlorophylls are the main substances that facilitate photosynthetic activity in plants. There are several kinds of chlorophyll, of which chlorophyll *a*, *b* and *c* are the most important. Chlorophyll *a* and *b* occur in higher plants and green algae, whereas chlorophyll *a* and *c* are found in marine plankton. Of the three chlorophyll types, chlorophyll *a* is the most common photosynthetic pigment. It is built from four pyrrole rings connected by four methine bridges, which form a porphyrin ring. The hydrophilic porphyrin ring is linked to the lipophilic side-chain alcohol, phytol, by an ester bond. Chlorophyll contains a magnesium ion, which is bound to the center of the porphyrin ring system as a chelate. The magnesium in chlorophyll gives it its green color. Different chlorophylls present in living systems do not differ much from one another. In chlorophyll *b*, the most important associate of chlorophyll a, a methyl group is replaced by a formic group (—CHO). On the other hand, chlorophyll *c* does not possess a phytol side chain at all, but that of farnesol, a C_{15}-isoprenoid alcohol. Bacteriochlorophyll a has a CH_3-CO-group instead of a $CH_2=CH-$ side chain and a reduced ring II.

The decomposition of chlorophyll begins already in the plant cell, as is evident by the bright-colored leaves produced during the autumn. The first diagenesis product to be formed, even before sedimentation occurs, is pheophytin which is formed by the loss of the magnesium ion. Under oxic conditions, hydrolysis occurs by the cleavage of the ester group. Afterwards, oxidative opening of the isocyclic ring takes place to form chlorin-P6 and a series of altered chlorins and purpurins. Thereafter, further rapid opening of the tetrapyrrole ring leads to the destruction of the molecule, so that the chance of preservation is very low in oxic sediments. Not only does the redox potential affect preservation but also the pH. A high pH leads to the rapid decomposition of the chlorophyll molecule, whereas a low pH accelerates the transformation of chlorophyll to pheophytin.

In anoxic environments phylloerythin is formed. The consequent loss of functional groups leads to the formation of deoxophyllo-erytroetio-porphyrins (DPEP) or when the isocyclic ring opens, etioporphyrin III (ETIO). During the diagenetic transformation from the pheophorbids to the stable DPEP or ETIO compounds, complete defunctionalization and aromatization of the tetrapyrrole ring takes place. This diagenetic transformation is illustrated in Fig. 10-12. The qualitative difference between the occurrence of chlorophyll derivatives in terrestrial, lacustrine and marine sediments is not significant. Nevertheless, one can say that terrestrial soils contain more chlorophyll and its diagenetic products, although strongly reducing environments are necessary for their preservation in the sedimentary record.

A further diagenetic transformation occurs in fossil sediments, where the metal-free DPEP- and ETIO-porphyrin may normally chelate with Ni^{2+} or VO^{2+} ions to form nickel- and vanadyl-porphyrins, as shown below. Cu-porphyrins are also known. The occurrence of petroporphyrins in crude oils provide circumstantial evidence for the biogenetic origin of petroleum.

Metallo-DPEP-porphyrin

X = VO, Ni
R = H, CH_3, C_2H_5

Metallo-ETIO-porphyrin

CARBOHYDRATES

Cellulose, starch and sugar belong to the important natural substance group of the carbohydrates, which have the general formula of $C_nH_{2n}O_n$. In terms of the amount, carbohydrates represent the most produced organic substance on earth.

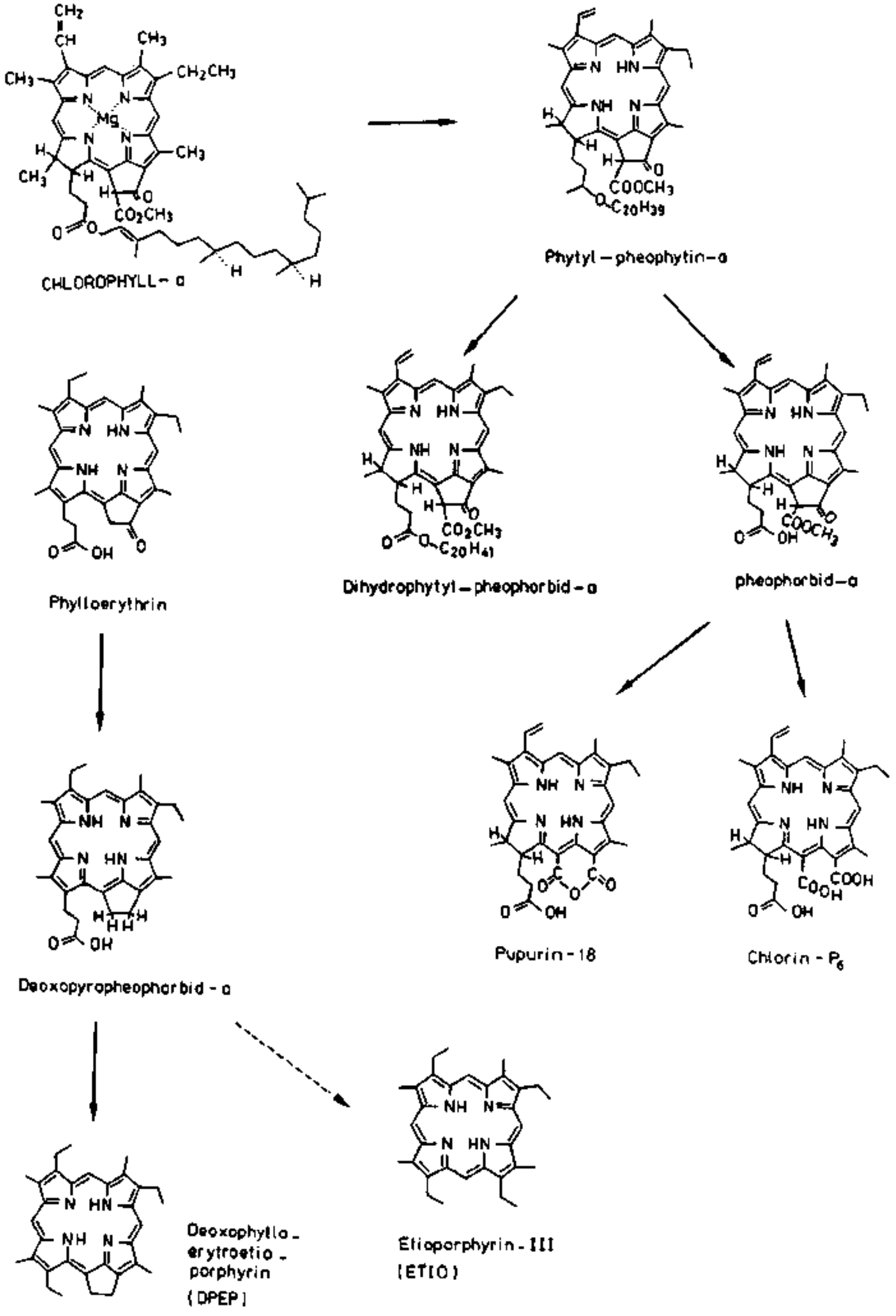

Fig. 10-12. Diagenetic products of chlorophyll.

In the extensive subject of carbohydrate chemistry, carbohydrates are divided into three main groups: the water soluble, monosaccharides (a simple sugar unit), the oligosaccharides (comprising of several sugar units), and the high-molecular-weight water-insoluble polysaccharides.

The monosaccharides consist of the sub-groups pentoses (C_5-sugars) and hexoses (C_6-sugars). These simple sugars can be looked upon as oxidation products of polyalcohols (polyhydroxy-alcohols), which carry an aldehyde (aldoses) or a keto-group (ketoses) depending on whether the primary or secondary alcohol group has been oxidized. Furthermore, aldohexoses and ketohexoses possess four and three asymmetrical C-atoms, respectively. This provides the possibility of producing 16 (2^4) or 8 (2^3) stereoisomers, respectively; however, these isomers are not all present in nature.

Cyclic sugars, which are formed mostly by an intra-molecular bond between the carbonyl- and hydroxy-groups on the same molecule to give either 6-membered rings (pyranoses) or 5-membered rings (furanoses), occur as well as the open chained aldoses and ketoses. These ring systems exist as α- and β-forms. The most important hexose and pentose representatives are glucose and ribose, respectively.

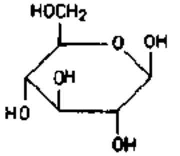

β-D-Glucopyranose

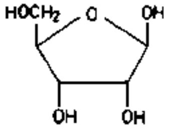

β-D-Ribofuranose

In the plant kingdom, the pentoses occur mainly as polysaccharides in wood (pentosanes) and in all other organisms as a component of nucleic acids. Among the group of hexoses, glucose is certainly the most important sugar, as it represents the main product of photosynthesis.

Naturally-occurring pentoses and hexoses are:

Pentose:	Hexose:
Ribose	Glucose
Xylose	Galactose
Arabinose	Fructose
	Rhamnose
	Fucose

Disaccharides belong to the group of oligosaccharides. They are formed from two monosaccharides bonded together via dehydration, i.e., a hydroxy-group from each molecule reacts upon the expulsion of water. Important examples of disaccharides are (1) sucrose (table sugar), which is formed from glucose and fructose, and (2) lactose (milk sugar), which is formed from glucose and galactose. Maltose and cellobiose, which are also disaccharides, both consist of two glucose molecules. They differ from one another by their stereometric linkage. Cellobiose is a break-down product of cellulose.

The most important polysaccharides are cellulose, starch and glycogen, which are formed by poly-dehydration reactions of numerous D-glucose molecules. This gives rise to the above-mentioned macromolecules, which differ from each other only in the way they link together. Cellulose is formed when supportive structures are needed in plants, whereas starch is synthesized as a storage product. In animals, glycogen serves as an energy reserve. It is also present in some bacteria and fungi.

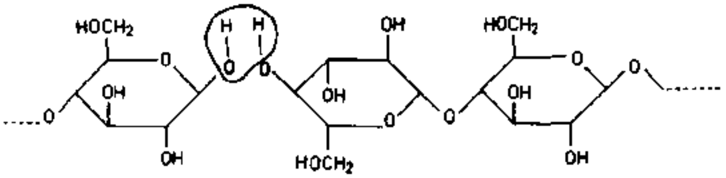

Cellulose

Another important polysaccharide is the compound chitin, which is used as a supportive tissue in fungi and for making the exo-skeletons of crustaceans and insects. Like cellulose, it is a linear macromolecule. Its monomer building-unit, however, is an altered form of glucose, namely, *N*-acetyl-glucosamine, which possesses an acetylated amino-group instead of a hydroxy-group.

The hydrolysis of oligo- and polysaccharides results in the cleavage of the molecule and the release of the monosaccharides. Thus, by using different techniques it is possible to differentiate between "free" sugars and "bonded" sugars from macromolecules.

Whereas terrestrial organic material does not differ significantly in its monosaccharide composition, i.e., mainly glucose, the carbohydrate composition of marine plankton varies considerably. The relative order of abundance of "free" and "bonded" sugars in plankton and marine sediments is given in Table 10-6. As shown in this table, hexoses occur more frequently than the pentoses; also galactose is the main monosaccharide present. In marine sediments, one finds very similar relative compositions to those presented in Table 10-6. The total amount of monosaccharides per gram of dry marine sediment is about 2 milligrams.

In lacustrine sediments from oligotrophic lakes, the concentrations of "free" sugars are very low. Eutrophic lakes, on the other hand, contain higher amounts of

TABLE 10-6

Free and bound monosaccharides in planktonic organisms and marine sediments

	Marine plankton	Marine sediment
Decreasing concentration ↓	Galactose	Galactose
	Glucose	Mannose
	Mannose	Glucose
	Ribose	Rhamnose
	Xylose	Ribose
	Fucose	Xylose
	Rhamnose	Arabinose
	Arabinose	

glucose and maltose. In the hydrolysate ("bonded" sugars) fraction, galactose, glucose, arabinose, xylose and mannose occur. The occurrence of these monosaccharides show little differentiation in both oxic and anoxic sediments. The ratio of glucose to ribose, however, appears to be a facies indicator for the type of organic matter present. A high ratio of more than 20 implies that the organic detritus is derived from the land plants, whereas a low ratio (less than 4) points to the input of material with a predominately planktonic origin.

As carbohydrates, especially sugars, are favored nutrient sources and are also very water soluble (the polymers are fairly easy to hydrolyze), they have only a small chance of survival in the aquatic environment. Even under anaerobic conditions, they undergo decomposition so quickly that at shallow sediment depths only trace quantities are detected. They occur only in fossilized sediments where they have been protected by certain depositional mechanisms, e.g., in biologically formed carbonates, silicates and phosphate deposits.

AMINO ACIDS AND PROTEINS

On the basis of their high structural order, proteins are of the utmost importance to living organisms. Proteins are high-molecular-weight colloidal natural substances, which are composed of combinations of different α-amino acids (there is a maximum of 22 different types). Amino acids are similar to monosaccharides in that they are water soluble. Almost all of the natural α-amino acids (with the exception of glycine) possess an asymmetric α-carbon atom. In proteins amino acids belong exclusively to the L-series:

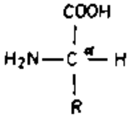

$$\begin{array}{c} COOH \\ | \\ H_2N-\overset{\alpha}{C}-H \\ | \\ R \end{array}$$

R = aliphatic, aromatic or heterocyclic group

L-amino acid

Important amino acids include for example, glycine, alanine and glutamic acid:

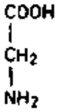

$$\begin{array}{c} COOH \\ | \\ CH_2 \\ | \\ NH_2 \end{array}$$

Glycine

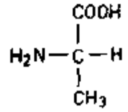

$$\begin{array}{c} COOH \\ | \\ H_2N-C-H \\ | \\ CH_3 \end{array}$$

L-alanine

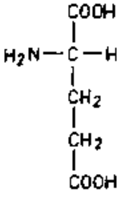

$$\begin{array}{c} COOH \\ | \\ H_2N-C-H \\ | \\ CH_2 \\ | \\ CH_2 \\ | \\ COOH \end{array}$$

L-glutamic acid

Amino acids can be classified as being neutral, acidic or basic. Neutral amino acid molecules have the same number of amino and carboxyl groups. When this is not the case, their chemical behavior shows either acidic or basic characteristics, which is dependent on whether the acidic (COOH) or amino (NH_2) groups dominate. There are also amino acids which contain sulphur; these include cysteine and methionine.

The bonding of single amino acids to form a long peptide chain, that may consist of a sequence of over 100 amino acids, occurs via the formation of peptide bonds. These peptide bonds form from the linkage of a carboxyl group of one amino acid with an amino group of another amino acid. This linkage occurs with the expulsion of a water molecule. The reaction is also reversible, which implies that peptide chains can be cleaved into single monomer units by hydrolysis:

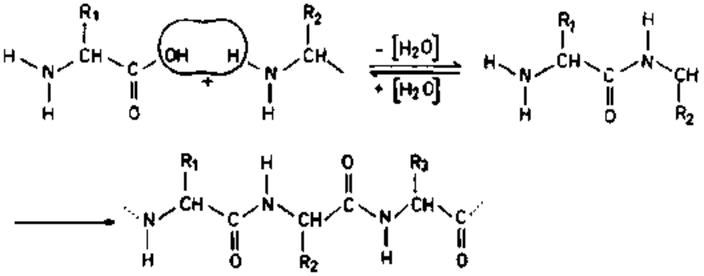

Peptide chain

Proteins are polypeptides, which are differentiated into two general groups depending on whether they have a structural or control function. Structural proteins are responsible for cell construction, whereas the other protein group are regulators and biocatalysts.

The cell wall of bacteria consists mostly of the gluco-peptide, mureine. This macromolecule is a heteropolymer and consists of chains of *n*-acetyl-muramic acid units (*n*-acetyl-glucosamine derivative). These are cross-linked together by peptide-like bonds of amino acid units, which are composed mainly of L-alanine and D-glutamic acid.

In contrast to the terrestrial environments, in aquatic environments the proteins constitute the major component of the biomass. They make up between 50% and 75%, and 35% and 55% of the organic material in bacteria and phytoplankton, respectively. In the hydrolysate fraction (free and bound amino acids), one finds the following relevant L-amino acids (see Table 10-7).

The main source of amino acids in sediments is derived from the breakdown of proteins from dead plant material and the decomposed remains of microorganisms.

TABLE 10-7

Free and bound amino acids in marine plankton and sediments

	Marine plankton	Marine sediment
Decreasing concentration ↓	Glycine	Arginine
	Alanine	Glutamic acid
	Glutamic acid	Alanine, valine, glycine, isoleucine, leucine, proline, threonine, gerine, rhemylalanine, aspartic acid, lysine
	Aspartic acid	
	Leucine	
	Serine	
	Threonine	

Soils contain very small amounts of free amino acids. They are mostly present in the bound form. The dominant amino acids are arginine, glutamic acid or alanine, glycine and proline. The other amino acids show a relatively uniform distribution. Thus, aquatic sediments show a very similar amino acid distribution to that of humus.

Under reducing conditions, recent sediments contain between 200 ppm and 800 ppm (dry weight) of amino acids. They do not show any general trend in the upper layers of the sedimentary column. In oxic sediments, however, there is a rapid loss of amino acids with increasing depth. In both facies, the most frequent amino acids are glycine, alanine and aspartic acid. This is also valid for recent fresh-water sediments. Aspartic and glutamic acids occur in plankton as extra-cellular products, which control the calcium balance. When one differentiates amino acids by their structure and chemical behavior, one finds that amino acids with cyclic structures are predominantly found in terrestrial detritus, whereas marine organic matter have amino acids with an acidic character.

There are very large differences recorded in the amino acid spectrum, which are not derived from the decomposition of proteins. It is thought that a series of special amino acids form during microbial degradation. This perhaps explains the occurrence of D-alanine and D-glutamic acid in freshly-deposited sediments. Obviously, in this case one could not subscribe to a thermal transformation process in which the L-form amino acids are isomerized into the thermodynamically more stable D-form.

In general, the amount of amino acids in fossil sediments is low. The chance of amino acids being preserved may be attributed to the fact that they are preferentially adsorbed by the residual organic matter, for example, humic substances. Also the nitrogen contents found in fossil sediments can be assigned to amino acid precursors.

COMPLEX BIOPOLYMERS

In addition to the above-mentioned biopolymers (cellulose, starch and protein, which are formed from well-defined chemical units), there are other biopolymers which occur in nature, that have a more or less non-uniform and complex structure. These substances include cutin, suberin and lignin.

Cutin and suberin

Cutin and suberin are hydrophobic plant materials. Cutin is a structural component of plant cuticles and is a polyester synthesized from hydroxy- and epoxy-fatty acids having 14 to 26 carbon atoms. Suberin (cork tissue) is found inside plant tissues and is formed from hydroxy- and dicarboxylic acids (C_8 to C_{22}). The degree of polymerization in suberin is probably lower than that in cutin.

Chemically related, but having a much higher degree of polymerization, is the biopolymer, sporopollenin. This substance forms the basis of exines of fungal spores and pollen.

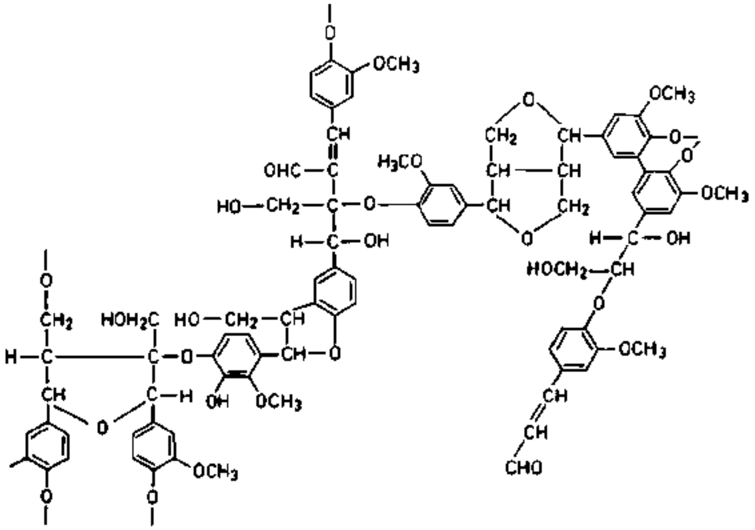

Fig. 10-13. Part of a lignin molecule containing phenylpropane units.

Cutin, suberin and, especially, sporopollenin are biochemically and chemically very inert substances. Some microorganisms, however, are capable of decomposing these substances with the help of extracellular enzymes (cutinases) to hydroxy-carboxylic acids.

Lignin

Wood is composed of the fibrous and tensile material, cellulose, which is enclosed by the pressure-resistant biopolymer, lignin. Lignin is, after cellulose, the most important organic substance as far as quantity is concerned and is a typical product of higher plants. It is formed by the dehydrogenated polymerization of the phenylpropylalcohols: cumaryl alcohol, coniferyl alcohol and sinapyl alcohol:

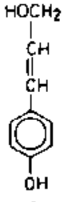

p-Cumaryl alcohol

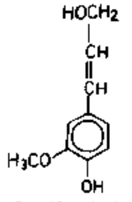

Coniferyl alcohol

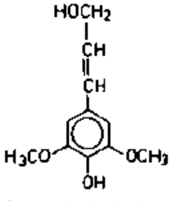

Sinapyl alcohol

By enzyme-controlled dehydrogenation reactions radicals are formed, which polymerize together in various ways to produce a three-dimensional macromolecule. Lignin is, therefore, not a chemically uniform compound but a very complex substance (see Fig. 10-13).

Gymnosperms (coniferous plants) contain lignin which is composed predominately of coniferyl alcohol units. Angiosperms (flowering plants) have different lignin types depending on their botanical affiliation. Thus, lignin from dicotyledons (flowering plants with two seed leaves) contain roughly equal proportions of coniferyl and sinapyl alcohol, whereas lignin from monocotyledons (flowering plants with one seed leaf) contains not only the above-mentioned components, but also a large amount of p-cumaryl alcohol units. Due to the differences in the methoxyl group content of the structural units and their relative abundance in different plant groups, the methoxyl group content can be used as a parameter for determining the source of lignin present in woody material found in sediments and recent peats.

Lignin is a phytogenic bulk product and is decomposed very slowly by biological activity. This is due to the presence of C—C and C—O bonds, which are not easy to hydrolyze. Thus, this gives rise to the fact that lignin is the main source of organic material, especially for the formation of humic substances, in soils and peats. Lignin is decomposed in significant quantities in aerobic environments by fungi. Some species of bacteria, however, are also able to undertake this task. The intermediate products of lignin decomposition include a series of phenol-aldehydes and aromatic acids. These decomposition products are, in part, very unstable (e.g., the aldehydes) and reactive and so they tend to form condensation products with other substances. These include such substances as:

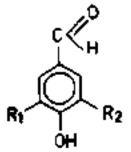

$R_{1,2}$ = H: p-hydroxy-benzaldehyde
R_1 = H; R_2 = OCH_3: vanillin
$R_{1,2}$ = OCH_3: syringal-aldehyde

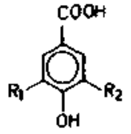

$R_{1,2}$ = H: p-hydroxy-benzoic acid
R_1 = H; R_2 = OCH_3: vanillinic acid
$R_{1,2}$ = OCH_3: syringic acid

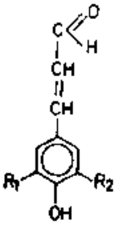

$R_{1,2}$ = H: p-cumar-aldehyde
R_1 = H; R_2 = OCH_3: coniferyl-aldehyde
$R_{1,2}$ = OCH_3: sinapin-aldehyde

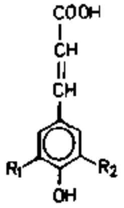

$R_{1,2}$ = H: p-cumric acid
R_1 = OCH_3; R_2 = H: ferulic acid
$R_{1,2}$ = OCH_3: sinapic acid

FORMATION OF HUMIC SUBSTANCES

The main sedimentary organic matter in soils and peats are humic substances, as most of the decomposition of dead organic matter takes place in the terrestrial environment. Easily degradable substances, such as sugars and amino acids are quickly endoxidized. The remaining organic matter left for the microorganisms is composed of resistant plant substances, such as lignin, wax, fats, carbohydrates and protein constituents. These substances and their decomposition products are converted together with the metabolites from microorganisms into very complex polymers. The metabolites of microorganisms consist of hydroquinones, polyphenols and polyphenolic carboxylic acids, examples of which are shown below:

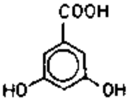

Dihydroxy-benzoic acid

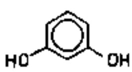

Resorcinol

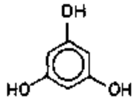

Phloro-glucinol

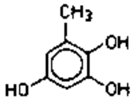

Methyl-hydroxy-hydroquinone

The polyphenols combine together by oxidative condensation reactions to form large molecular bodies. For example, quinones can form condensation products with amino acids. These condensation products react further to form brown undefined nitrogen-containing polymers:

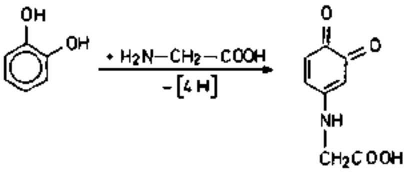

Brown, nitrogen-containing polymers

Amino acids and sugars can react together to form brown compounds called melanoidins ("Maillard reaction"). In the first phase, carbohydrates and amino acids form extremely reactive polyfunctional di- and tricarbonyl compounds, which stabilize in the second phase via aldimine and ketimine to hetero-polymeric brown melanoidins. The melanoidins are also in a position to take up phenols and lipid substances with functional groups. This combined interaction with humic substances produced by various pathways proceed to build a heteropolymerisate with an extremely high molecular weight.

Reactive substances can also penetrate particulate organic matter and react during the humification process to form humus. The preservation of humic substances depends on the speed of the endoxidation reactions, which are controlled by the access of oxygen. Humic substances thus form from a combination of different plant substances, which, depending on their composition, give nitrogen-poor or nitrogen-rich humus (see Fig. 10-14). They also represent a mixture of more or less reactive molecules of different origins with a large range of different molecular weights. They can also form very large molecular aggregates of up to 100 Å in diameter and more than 10^5 Daltons in weight.

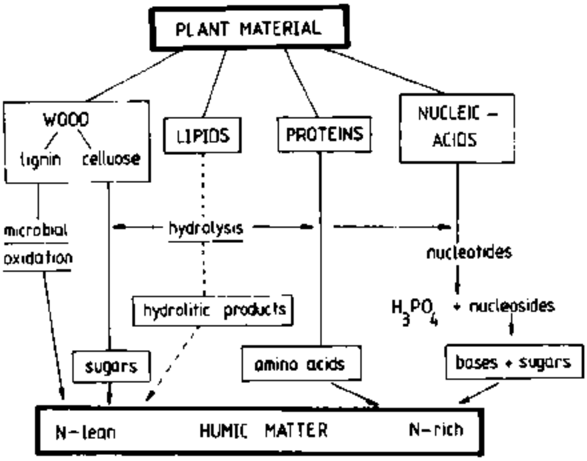

Fig. 10-14. Formation of humic substances from plant material.

Another characteristic of humic substances is the presence of different functional groups, which include:

carboxyl: –COOH
phenolic hydroxyl: ar–OH
alcoholic hydroxyl: aliph–OH
carbonyl: R–CO–R
methoxyl: –O–CH3
heteroatoms: N and S

Much has been speculated about the structural elements of humic substances. Estimates of the molecular weights of these substances deviate greatly. Thus, one can only assume that humic substances represent complex polyanions with an indefinable chemical structure. Investigations on the structural analysis of humic substances have shown that a large proportion of aromatic complexes and aliphatic chains are present. The aromatic complexes are thought to be derived from the decomposition products of lignin, whereas the aliphatic chains are explained as unsaturated or functional group containing lipids (especially from microbial activity), which have been incorporated into the macromolecule. The humic substances can be divided into three main groups on the basis of their solubility and insolubility in acids and alkalis: (1) alkali insoluble humin, (2) alkali-soluble humic acids, and (3) alkali-soluble fulvic acids. In contrast to the humic acids, fulvic acids are also soluble in acids. This physicochemical differentiation between the two acid types is based on their molecular weight and proportion of carboxyl groups (see Table 10-8).

The figures quoted for the molecular weights of the humic and fulvic acids differ significantly. The molecular weights of humic acids range from 1000 to 10,000 Daltons, whereas those of fulvic acids range from 500 to 1000 Daltons. In general, humic and fulvic acids from aquatic environments appear to have a lower molecular

TABLE 10-8

Elemental composition of humic and fulvic acids

	Humic acids	Fulvic acids
Carbon	58 –62% (wt.)	43 –52% (wt.)
Hydrogen	2.9– 5.4% (wt.)	3.4– 5.1% (wt.)
Nitrogen	3.4– 4.8% (wt.)	1.2– 4.1% (wt.)
Oxygen	29 –32% (wt.)	43 –51% (wt.)
H/C atomic ratio	0.56–1.12	1.27–1.42
O/C atomic ratio	0.35–0.41	0.62–0.63
Average molecular weight	1000–10,000	500–1000
—COOH-groups (meq/100 g)	150– 300	610– 910
Phenolic OH-groups (meq/100 g)	290– 570	270– 570

weight than terrestrial derivatives. Also, there are differences between terrestrial and marine humic and fulvic acids in terms of their aromaticity; terrestrially-derived acids being more aromatic than marine-derived humic compounds. Thus, phenolic compounds are predominately found in terrestrial humic acids, whereas aliphatics in the form of polyethers are predominant in marine (aquatic) humic acids. Marine and lacustrine humic and fulvic acids, however, may often have a detrital character as they are derived from a mixed source, i.e., mostly terrestrial and aquatic. In the hydrolysate fraction of humin, the humic and the fulvic acids, the amino acids β-alanine and γ-amino butyric acid have been identified. These amino acids are not derived from proteins but are metabolic products of microbial activity.

Humic and fulvic acids from sapropelic sediments contain not only a high proportion of sulphur (cf. 4%: terrestrial — 0.5%), but also a large proportion of partly decomposed polysaccharides in the form of, for example, polyuronic acid.

In contrast to the amino acids and sugars, humic substances are better equipped to complex with inorganic ions, especially metals. This inorganic–organic interaction depends on the effectiveness of the polyanionic groups of the humic and fulvic acids. In an aquatic environment, therefore, metal–humic complexes are much more stable than inorganic–metal complexes. The formation of metal complexes depends on the concentration of the humic compounds present and their complexing ability to compete with the main inorganic cations for the trace elements, Fe, Cu, Pb, Zn, Cd, and Al and also U, Ni, Mn, Co, etc. Investigations on model humic compounds showed that the bonding ability of humic substances and metals depends on the affinity of the metal ion for organic matter. Thus Fe, Hg, Cu, and Pb are preferentially taken up to form very stable complexes, whereas Ni, Cr, Zn, Mn and Co have a low sorption ability for humic matter. For all metals, there is a general relationship between the pH and the sorption ability. With increasing pH, the sorption ability increases, i.e., metals form stable complexes at high pH values and go into solution at low pHs. At a pH of 5.8, the affinity for metals to complex with humic substances is as follows:

$$\mathrm{Hg} = \mathrm{Fe} = \mathrm{Pb} = \mathrm{Al} = \mathrm{Cr} = \mathrm{Cu} > \mathrm{Cd} > \mathrm{Zn} > \mathrm{Ni} > \mathrm{Co} > \mathrm{Mn}$$

The proportions of the different fractions of humic substances changes with increasing sediment depth. The proportion of alkali-insoluble humin increases, whereas the content of humic and fulvic acids decreases. The fulvic acids present decrease more rapidly than the humic acids so that ratio of their contents can be used as a measure of advancing diagenesis.

CONCLUSIONS

Organic matter in the biosphere is normally assimilated by macrophages, fungi, and microorganisms. When specific conditions prevail in the geosphere and the organic matter can be preserved, cleavage reactions, aromatization and other transformations take place, which produce thermodynamically more stable products. Unlike catagenesis, where the various transformation processes of organic (and inorganic) matter are governed by high temperatures and pressures and where great depths of burial are involved, diagenesis is controlled predominately by biochemical and chemical reactions, which take place at shallow depths and at temperatures of less than 50°C.

ACKNOWLEDGEMENTS

The help extended by Drs. G.V. Chilingarian and K.H. Wolf is greatly appreciated by the writers.

BIBLIOGRAPHY AND REFERENCES

Biochemical decomposition of organic matter

Anderson, J.M. and MacFadyan, A., 1976. Role of terrestrial and aquatic organisms in decomposition processes. In: *17th Symposium of the British Ecological Society, 15–18 April, 1975.* Blackwell, Oxford, 474 pp.

Blumer, M., 1975. Organische Verbindungen in der Natur; Die Grenze unseres Wissens. *Angew. Chem.*, 87: 527–554.

Froelich, P.N., Klinkhammer, G.P., Bender, M.L., Luedtke, N.A., Heath, G.R., Cullen, D., Dauphin, P., Hammond, D., Hartman, B. and Maynard, V., 1979. Early oxidation of organic matter in pelagic sediments of the eastern equatorial Atlantic: suboxic conditions. *Geochim. Cosmochim. Acta*, 43: 1075–1090.

Given, P.H., Spackman, W., Painter, P.C., Rhoads, C.A., Ryan, N.J., Alemany, L. and Pugmire, R.J., 1984. The fate of cellulose and lignin in peats: an exploratory study of the input to coalification. *Org. Geochem.*, 6: 399–407.

Grundmanis, V. and Murray, J.W., 1982. Aerobic respiration in pelagic marine sediments. *Geochim. Cosmochim. Acta*, 46: 1101–1120.

Kuester, E., 1978. Microbiology of peat. In: W.E. Krumbein (Editor), *Environmental Biogeochemistry and Geomicrobiology, Vol. 2: The Terrestrial Environment.* Ann Arbor Science Publishers, Ann Arbor, pp. 439–449.

Martens, C.S. and Goldhaber, M.B., 1978. Early diagenesis in transitional environments of the White Oak River Estuary, North Carolina. *Limnol. Oceangr.*, 23(3): 428–441.

Metzner, H., 1973. *Biochemie der Pflanzen.* Enke-Verlag, Stuttgart, 376 pp.

Oremland, R.S. and Taylor, B.F., 1978. Sulphate reduction and methanogenesis in marine sediments. *Geochim. Cosmochim. Acta*, 42: 209–214.

Premuzic, E.T., Benkovitz, C.M., Gaffney, J.S. and Walsh, J., 1982. The nature and distribution of organic matter in the surface sediments of world oceans and seas. *Org. Geochem.*, 4: 63–77.

Reed, W.E., 1977. Biogeochemistry of Mono Lake, California. *Geochim. Cosmochim. Acta*, 41: 1231–1245.

Tan, F.C. and Strain, P.M., 1983. Sources, sinks and distribution of organic carbon in the St. Lawrence Estuary, Canada. *Geochim. Cosmochim. Acta*, 47: 125–132.

Organic substances in Recent sediments

Barnes, M.A. and Barnes, W.C., 1978. Organic compounds in lake sediments. In: A. Lehrman (Editor), *Lakes, Chemistry, Geology, Physics.* Springer Verlag, New York, N.Y., pp. 127–152.

Brassell, S.C. and Eglington, G., 1986. Molecular geochemical indicators in sediments. In: M.L.Sohn (Editor), *Organic Marine Chemistry. Am. Chem. Soc. Symp. Ser.*, 305: 2–32.

Brown, F.S., Baedecker, M.J., Nissenbaum, A. and Kaplan, I.R., 1972. Early diagenesis in a reducing fjord, Saanich Inlet, British Columbia, III. Changes in organic constituents of sediment. *Geochim. Cosmochim. Acta*, 36: 1185–1203.

Hatcher, P.G., Simoneit, B.R.T., Mackenzie, F.T., Neumann, A.C., Thorstenson, D.C. and Gerchakov, S.M., 1982. Organic geochemistry and pore water chemistry of sediments from Mangrove Lake, Bermuda. *Org. Geochem.*, 4: 93–112.

Ishiwatatari, R., Ogura, K. and Horie, S., 1980. Organic geochemistry of a lacustrine sediment (Lake Haruna, Japan). *Chem. Geol.*, 29: 261–280.

Philp, R.P., Maxwell, J.R. and Eglington, G., 1976. Environmental organic geochemistry of aquatic sediments. *Sci. Progr. Oxford*, 63: 521–545.

Simoneit, B.R.T., 1978. The organic chemistry of marine sediments. In: J.P. Riley and R. Chester (Editors), *Chemical Oceanography, Vol. 7.* Academic Press, London, pp. 233–311.

Lipophilic substances

Blumer, M., Guillard, R.L. and Chase, T., 1971. Hydrocarbons of marine phytoplankton. *Mar. Biol.*, 8: 183–189.

Braids, O.C. and Miller, R.H., 1975. Fats, waxes and resins in soil. In: J.E. Gieseking (Editor), *Soil Components: Organic Components.* Springer-Verlag, Berlin, pp. 343–368.

Cardoso, J.N., Watts, C.D., Maxwell, J.R., Goodfellow, R., Eglington, G. and Golubic, S., 1978. A biogeochemical study of the Abu Dhabi algal mats: a simplified ecosystem. *Chem. Geol.*, 23: 273–291.

De Leeuw, J.W., 1986. Sedimentary lipids and polysaccharides as indicators for sources of input, microbial activity and short-term diagenesis. In: M.L. Sohn (Editor), *Organic Marine Geochemistry. Am. Chem. Soc. Symp. Ser.*, 305: 34–61.

Erwin, J.A., 1973. *Lipids and Biomembranes of Eukaryotic Microorganisms.* Academic Press, London, 339 pp.

Peake, E., Casagrande, D.J. and Hodgson, G.W., 1974. Fatty acids, chlorins, hydrocarbons, sterols and carotenoids from a Black Sea core. In: E.T. Degens and D.A. Ross (Editors), *The Black Sea — Geology, Chemistry and Biology. Am. Assoc. Pet. Geol., Mem.*, 20: 505–523.

Tevini, M. and Lichtenhaler, H.K. (Editors), 1977. *Lipids and Lipid Polymers in Higher Plants.* Springer-Verlag, Berlin, 306 pp.

Volkman, J.K., Johns, R.B., Gillan, F.T., Perry, G.J. and Bavor, H.J., Jr., 1980. Microbial lipids of an intertidal sediment, I. Fatty acids and hydrocarbons. *Geochim. Cosmochim. Acta*, 44: 1133–1143.

Hydrocarbons

Aizenshtat, Z., 1973. Perylene and its geochemical significance. *Geochim. Cosmochim. Acta*, 37: 559–567.

Blumer, M., Mullin, M.H. and Thomas, D.W., 1964. Pristane in the marine environment. *Helg. Wiss.*

Meeresunters., 10: 187–201.

Blumer, M., Blumer, W. and Reich, T., 1977. Polycyclic aromatic hydrocarbons in soils of a mountain valley: correlation with highway traffic and cancer incidence. *Environ. Sci. Technol.*, **11**: 1082–1091.

Borges del Castillo, J., Brooks, C.J.W., Cambie, R.C., Eglington, G., Hamilton, R.J. and Pellitt, P., 1967. The taxonomic distribution of some hydrocarbons in gymnosperms. *Phytochemistry*, 6: 391–398.

Giger, W., Schaffner, C. and Wakeham, S.G., 1980. Aliphatic and olefinic hydrocarbons in recent sediments of the Greifensee, Switzerland. *Geochim. Cosmochim. Acta*, 44: 119–129.

Gschwend, P.M. and Hites, R.A., 1981. Fluxes of polyaromatic hydrocarbons to marine and lacustrine sediments in the northeastern United States. *Geochim. Cosmochim. Acta*, 45: 2359–2367.

Laflamme, R.E. and Hites, R.A., 1978. The global distribution of polycyclic aromatic hydrocarbons in recent sediments. *Geochim. Cosmochim. Acta*, 42: 289–303.

Laflamme, R.E. and Hites, R.A., 1979. Tetra- and pentacyclic, naturally-occurring aromatic hydrocarbons in recent sediments. *Geochim. Cosmochim. Acta*, 43: 1687–1691.

Louda, J.W. and Baker, E.W., 1984. Perylene occurrence, alkylation and possible sources in deep-ocean sediments. *Geochim. Cosmochim. Acta*, 48: 1043–1058.

Romanowski, T., Funcke, W., Koenig, J. and Balfanz, E., 1981. Detection of PAH of molecular weight between 300 and 402 in airborne particulate matter by fused silica capillary GC and GC/MS. *J. High Resolut. Chromatogr. Column Chromatogr.*, 4: 209–214.

Spyckerelle, C., Greiner, A.Ch., Albrecht, P. and Ourisson, G., 1977. Aromatic hydrocarbons from geological sources. Part III: A tetrahydrochrysene derived from triterpenes in recent and old sediments: 3,3,7-trimethyl-1,2,3,4-tetrahydrochrysene. *J. Chem. Res. (S)*, pp. 330–331.

Stánsky, K., Streibl, M. and Sorm, F., 1968. On natural waxes, VII. Lipid hydrocarbons of the alga. *Collect. Czech. Chem. Commun.*, 33: 416–424.

Tan, Y.L. and Heit, M., 1981. Biogenic and abiogenic polynuclear aromatic hydrocarbons in sediments from two remote Adirondack lakes. *Geochim. Cosmochim. Acta*, 45: 2267–2279.

Venkatesan, M.I. and Kaplan, I.R., 1982. Distribution and transport of hydrocarbons in surface sediments of the Alaskan Outer Continental Shelf. *Geochim. Cosmochim. Acta*, 46: 2135–2149.

Wakeham, S.G., Schaffner, C. and Giger, W., 1980a. Polycyclic aromatic hydrocarbons in Recent lake sediments, I. Compounds having anthropogenic origins. *Geochim. Cosmochim. Acta*, 44: 403–413.

Wakeham, S.G., Schaffner, C. and Giger, W., 1980b. Polycyclic aromatic hydrocarbons in Recent lake sediments, II. Compounds derived from biogenic precursors during early diagenesis. *Geochim. Cosmochim. Acta*, 44: 415–429.

Oxygenated compounds

Boon, J.J., de Leeuw, J.W. and Schenk, P.A., 1975. Organic geochemistry of Walvis Bay diatomaceous ooze, I. Occurrence and significance of the fatty acids. *Geochim. Cosmochim. Acta*, 39: 1559–1565.

Brooks, P.W., Eglington, G., Gaskell, S.J., McHugh, D.J., Maxwell, J.R. and Philp, R.P., 1976. Lipids of Recent sediments. Part I: Straight chain hydrocarbons and carboxylic acids of some temperate lacustrine and sub-tropical lagoonal-tidal flat sediments. *Chem. Geol.*, 18: 21–38.

Brooks, P.W., Maxwell, J.R. and Patience, R.L., 1978. Stereochemical relationships between phytol and phytanic acid, dihydrophytol and C_{18} ketone in Recent sediments. *Geochim. Cosmochim. Acta*, 42: 1175–1180.

Cardoso, J.N. and Eglington, G., 1983. The use of hydroxyacids as geochemical indicators. *Geochim. Cosmochim. Acta*, 47: 723–730.

Casagrande, D.J. and Ferguson, A., 1983. The distribution of fatty acids in coal precursors in the Okefenokee Swamp, Georgia. In: M. Bjoroy (Editor), *Advances in Organic Geochemistry, 1981*. John Wiley and Sons, New York, N.Y., pp. 628–634.

Cranwell, P.A., 1974. Monocarboxylic acids in lake sediments: indicators derived from terrestrial and aquatic biota of paleoenvironmental trophic levels. *Chem. Geol.*, 14: 1–14.

Cranwell, P.A., 1977. Organic geochemistry of Cam Loch (Sutherland) sediments. *Chem. Geol.*, 20: 205–221.

Cranwell, P.A., 1980. Branched/cyclic alkanols in lacustrine sediments (Great Britain): recognition of iso- and anteiso-branching and stereochemical analysis of homologous alkan-2-ols. *Chem. Geol.*, 30: 15–26.

Cranwell, P.A., 1981. The stereochemistry of 2- and 3-hydroxy fatty acids in Recent lacustrine sediment. *Geochim. Cosmochim. Acta*, 45: 547–552.

Cranwell, P.A., 1985. Long chain unsaturated ketones in Recent lacustrine sediments. *Geochim. Cosmochim. Acta*, 49: 1545–1551.

Eglinton, G. and Hamilton, R.J., 1967. Leaf epicuticular waxes. *Science*, 156: 1322–1334.

Kawamura, K. and Ishiwatari, R., 1981. Polyunsaturated fatty acids in a lacustrine sediment as a possible indicator of paleoclimate. *Geochim. Cosmochim. Acta*, 45: 149–155.

Kolattukudy, P.E., 1969. Plant waxes. *Lipids*, 5, 259–275.

Lee, R.F., Nevenzel, J.C. and Paffenhoefer, G.A., 1972. The presence of wax esters in marine planktonic copepods. *Naturwissenschaften*, 59: 406–411.

Marlowe, I.T., Brassell, S.C., Eglington, G. and Green, J.C., 1984. Long chain unsaturated ketones and esters in living algae and marine sediments. *Org. Geochem.*, 6: 135–141.

Meyers, P.A. and Takeuchi, N., 1979. Fatty acids and hydrocarbons in surficial sediments of Lake Huron. *Org. Geochem.*, 1: 127–138.

Perry, G.J., Volkman, J.K., Johns, R.B. and Bavor, H.J., Jr., 1979. Fatty acids of bacterial origin in contemporary marine sediments. *Geochim. Cosmochim. Acta*, 43: 1715–1725.

Philp, R.P., Brown, S., Calvin, M., Brassel, S. and Eglington, G., 1978. Hydrocarbons and fatty acid distribution in recently deposited algal mats at Laguna Guerrero, Baja California. In: W. Krumbein (Editor), *Environmental Biogeochemistry and Geomicrobiology, Vol 1. The Aquatic Environment*. Ann Arbor Science Publishers, Ann Arbor, pp. 255–264.

Snyder, F. (Editor), 1972. *Ether Lipids — Chemistry and Biology.* Academic Press, London, 433 pp.

Van Vleet, E.S. and Quinn, J.G., 1979. Early diagenesis of fatty acids and isoprenoid alcohols in esturine and coastal sediments. *Geochim. Cosmochim. Acta*, 43: 289–303.

Volkman, J.K., Eglington, G., Corner, E.D.S. and Sargent, J.R., 1980. Novel unsaturated straight chain C_{37}-C_{39} methyl and ethyl ketones in marine sediments and a coccolithophore, *Emiliania huxleyi*. In: A.G. Douglas and J.R. Maxwell (Editors), *Advances in Organic Geochemistry, 1979.* Pergamon Press, Oxford, pp. 219–229.

Wakeham, S.G., 1982. Organic matter from a sediment trap experiment in the equatorial North Atlantic: wax esters, steryl esters, triacylglycerols and alkyldiacylglycerols. *Geochim. Cosmochim. Acta*, 46: 2239–2257.

Terpenoid compounds

Barnes, M.A. and Barnes, W.C., 1983. Oxic and anoxic diagenesis of diterpenes in lacustrine sediments. In: M. Bjoroy (Editor), *Advances in Organic Geochemistry, 1981.* John Wiley and Sons, New York, N.Y., pp. 289–298.

Barrick, R.C. and Hedges, J.J., 1981. Hydrocarbon geochemistry of the Puget Sound region, II. Sedimentary diterpenoid, steroid and triterpenoid hydrocarbons. *Geochim. Cosmochim. Acta*, 45: 381–392.

Dehmer, J., 1988. *Petrographische und organisch-geochemische Untersuchungen an rezenten Torfen und teriaren Braunkohlen — Ein Beitrag zur Fazies und Genese gebänderter Braunkohlen.* Doctoral Thesis, Rheinisch-Westfälischen Techischen Hochschule Aachen, 340 pp.

De Rosa, M., Gambacorta, A., Minale, L. and Bu'Lock, J.D., 1971. Bacterial triterpenes. *Chem. Comm.*, pp. 619–620.

Goodwin, T.W., 1973. Recent developments in the biosynthesis of plant triterpenes. In: V.C. Runeckles and T.J. Mabry (Editors), *Terpenoids: Structure, Biogenesis and Distribution. Recent Advances in Phytochemisty, Vol.6.* Academic Press, London, pp. 97–115.

Ourisson, G., Albrecht, P. and Rohmer, M., 1979. The Hopanoids — paleochemistry and biochemistry of a group of natural products. *Pure Appl. Chem.*, 51: 709–729.

Peakman, T.M. and Maxwell, J.R., 1988. Early diagenetic pathways of steroid alkenes. *Org. Geochem.*, 13(4–6): 583–592.

Quirk, M.M., Patience, R.L., Maxwell, J.R. and Wheatley, R.E., 1980. Recognition of the sources of isoprenoid alkanes in recent environments. In: J. Albaiges (Editor), *Analytical Techniques in Environmental Chemistry*. Pergamon Press, Oxford, pp. 23–31.

Quirk, M.M., Wardroper, A.M.K., Wheatley, R.E. and Maxwell, J.R., 1984. Extended hopanoids in peat environments. *Chem. Geol.*, 42: 25–43.

Rohmer, M. and Ourisson, G., 1976a. Dérivés du bactériohopane: Variations structurales et répartition. *Tetrahedron Lett.*, 40: 3637–3640.

Rohmer, M. and Ourisson, G., 1976b. Structur des Bactériohopane-tétrols d'*Acetobacter xylinum*. *Tetrahedron Lett.*, 40: 3633–3636.

Rohmer, M., Dastillung, M. and Ourisson, G., 1980. Hopanoids from C_{30} to C_{35} in recent muds — chemical markers for bacterial activity. *Naturwissenschaften*, 67: 456–458.

Rowland, S.J. and Maxwell, J.R., 1984. Reworked triterpenoid and steroid hydrocarbons in a recent sediment. *Geochim. Cosmochim. Acta*, 48: 617–624.

Ruecker, G., 1973. Sesquiterpene. *Angew. Chem.*, 85: 895–907.

Simoneit, B.R.T., 1977. Diterpenoid compounds and other lipids in deep-sea sediments and their geochemical significance. *Geochim. Cosmochim. Acta*, 41: 463–476.

Thomas, B.R., 1970. Modern and fossil plant resins. In: J.B. Harbourne (Editor), *Phytochemical Phylogeny*. Academic Press, London, pp. 59–79.

Steroids

Björkheim, I. and Gustafsson, J.-Å., 1971. Mechanism of microbial transformation of cholesterol into coprostanol. *Eur. J. Biochem.*, 21: 428–432.

Gagosian, R.B. and Heinzer, F., 1979. Stenols and stanols in the oxic and anoxic waters of the Black Sea. *Geochim. Cosmochim. Acta*, 43: 471–486.

Gagosian, R.B. and Smith, S.O., 1979. Steroids ketones in surface sediments from the south-west African shelf. *Nature*, 277: 287–289.

Gagosian, R.B., Smith, S.O., Lee, C., Farrington, J.W. and Frew, N.M., 1980. Steroid transformations in Recent marine sediments. In: A.G. Douglas and J.R. Maxwell (Editors), *Advances in Organic Geochemistry, 1979*. Pergamon Press, Oxford, pp. 407–419.

Gaskell, S.J. and Eglington, G., 1976. Sterols of a contemporary lacustrine sediment. *Geochim. Cosmochim. Acta*, 40: 1221–1228.

Goad, L.J., 1976. The steroids of marine algae and invertebrate animals. In: D.C. Malins and J.R. Sargent (Editors), *Biochemical and Biophysical Perspectives in Marine Biology, Vol. 3*. Academic Press, London, pp. 213–319.

Grunwald, C., 1975. Plant sterols. *Ann. Rew. Plant Physiol.*, 26: 209–236.

Lee, C., Gagosian, R.B. and Farrington, J.W., 1977. Sterol diagenesis in Recent sediments from Buzzards Bay, Massachusetts. *Geochim. Cosmochim. Acta*, 41: 985–992.

Nishimura, M. and Koyama, T., 1976. Stenols and stanols in lake sediments and diatoms. *Chem. Geol.*, 17: 229–239

Nishimura, M. and Koyama, T., 1977. The occurrence of stanols in various living organisms and the behavior of sterols in contemporary sediments. *Geochim. Cosmochim. Acta*, 41: 379–385.

Schmitz, F.J., 1978. Uncommon marine steroids. In: P.J. Scheuer (Editor), *Marine Natural Products, Vol. 1*. Ed. Academic Press, London, pp. 241–297.

Chlorophyll

Baker, E.W. and Louda, J.W., 1983. Thermal aspects in chlorophyll geochemistry. In: M. Bjoroy (Editor), *Advances in Organic Geochemistry, 1981*. John Wiley and Sons, Chichester, pp. 401–421.

Louda, J.W. and Baker, E.W., 1986. The biochemistry of chlorophyll. In: M.L. Sohn (Editor), *Organic Marine Geochemistry. Am. Chem. Soc. Symp. Ser.*, 305: 107–126.

Staub, E., 1976. Stratigraphy of diatoms and chlorophyll derivatives in the uppermost sediment of a Swiss lake. In: F. Goldman, *Interactions between Sediments and Fresh-Water*. W. Junk, The Hague, pp. 161–164.

Carbohydrates

Degens, E.T. and Mopper, K., 1979. Early diagenesis of sugars and amino acids. In: G. Larsen and G.V. Chilingar (Editors), *Diagenesis in Sediments and Sedimentary Rocks. Developments in Sedimentology, Vol. 25A*. Elsevier, Amsterdam, pp. 143–205.

De Leeuw, J.W., 1986. Sedimentary lipids and polysaccharides as indicators for sources of input, microbial activity and short-term diagenesis. In: M.L. Sohn (Editor), *Organic Marine Geochemistry. Am. Chem. Soc. Symp. Ser.*, 305: 34–61.

Amino acids and proteins

Casagrande, D.J. and Given, P.H., 1980. Geochemistry of amino acids in some Florida peat accumulations, II. Amino acid distributions. *Geochim. Cosmochim. Acta*, 44: 1493–1507.

Degens, E.T. and Mopper, K., 1979. Early diagenesis of sugars and amino acids in sediments. In: G. Larsen and G.V. Chilingar (Editors), *Diagenesis in Sediments and Sedimentary Rocks. Developments in Sedimentology, Vol. 25A*. Elsevier, Amsterdam, pp. 143–205.

Dungworth, G., 1979. Optical configuration and the racemisation of amino acids in sediments and in fossils — a review. *Chem. Geol.*, 17: 135–153.

Dungworth, G., Thijssen, M., Zuurveld, Van der Velden, W. and Schwartz, A.W., 1977. Distibution of amino acids, amino sugars, purines and pyrimidines in a Lake Ontario sediment core. *Chem. Geol.*, 19: 295–308.

Complex biopolymers

Krueger, G., 1976. Lignin — seine Bedeutung und Biogenese. *Chemie in Unserer Zeit*, 10: 21–29.

Martin, F., Saiz-Jimenez, C. and Gonzalez-Vila, F.J., 1979. Pyrolysis — gas chromatography–mass spectrometry of lignins. *Holzforschung*, 33: 210–222.

Sarkanen, K.V. and Ludwig, C.H. (Editors), 1971. *Lignins, Occurrence, Formation, Structure and Reactions*. Wiley-Interscience, London. 916 pp.

Schraudolf, H. and Haag, R., 1985. The sporopollenin of the schizaeaceous fern *Anemia phyllitidis*. *Naturwissenschaften*, 72: 433–434.

Formation of humic substances

Angrick, M. and Rewiciki, D., 1980. Die Maillard-Reaktion. *Chemie in Unserer Zeit*, 5: 149–157.

Dereppe, J-M., Moreaux, C. and Debyser, Y., 1980. Investigation of marine and terrestrial humic substances by ^{1}H and ^{13}C nuclear magnetic resonance and infrared spectroscopy. *Org. Geochem.*, 2: 117–124.

Flaig, W., Beutelspacher, H. and Rietz, E., 1975. Chemical composition and properties of humic substances. In: J.E. Gieseking (Editor), *Soil Components — Organic Components*. Springer-Verlag, New York, N.Y. pp. 1–211.

Hatcher, P.G., Vanderhart, D.L. and Earl, W.L., 1980a. Use of solid-state ^{13}C NMR in structural studies of humic acids and humin from Holocene sediments. *Org. Geochem.*, 2: 87–92.

Hatcher, P.G., Rowan, R. and Mattingly, M.M., 1980b. ^{1}H and ^{13}C NMR of marine humic acids. *Org. Geochem.*, 2: 77–85.

Hatcher, P.G., Maciel, G.E. and Dennis, L.W., 1981. Aliphatic structure of humic acids; a clue to their origin. *Org. Geochem.*, 3: 43–48.

Hedges, J.I. and Mann, D.C., 1979. The lignin geochemistry of marine sediments from the southern Washington coast. *Geochim. Cosmochim. Acta*, 43: 1809–1818.

Hedges, J.I., Ertel, J.R. and Leopold, E.B., 1982. Lignin geochemistry of a Late Quaternary sediment core from Lake Washington. *Geochim. Cosmochim. Acta*, 46: 1869–1877.

Jackson, T.A., 1975. Humic matter in natural waters and sediments. *Soil Sci.*, 119(1): 56–64.

Kononova, M.M., 1961. *Soil Organic Matter*. Pergamon Press, Oxford, 450 pp.

MacFarlane, R.B., 1978. Molecular weight distribution of a humic and fulvic acids of sediments from a north Florida estuary. *Geochim. Cosmochim. Acta*, 42: 1579–1582.

Matsumoto, G. and Hanya, T., 1980. Gas chromatographic–mass spectrometric identification of phenolic acids in Recent sediments. *J. Chromatogr.*, 193: 89–94.

Schnitzer, M. and Khan, S.U., 1978. Humic substances — chemistry and reactions. In: M. Schnitzer and S.U. Khan (Editors), *Soil Organic Matter. Developments in Soil Science, Vol. 8.* Elsevier, Amsterdam, pp. 1–64

Thurman, E.M., Wershaw, R.L., Malcolm, R.L. and Pinckney, D.J., 1982. Molecular size of aquatic humic substances. *Org. Geochem.*, 4: 27–35.

Wilson, M.A., Barron, P.F. and Gillam, A.H., 1981. The structure of freshwater humic substances as revealed by ^{13}C-NMR spectroscopy. *Geochim. Cosmochim. Acta*, 45: 1743–1750.

This Page Intentionally Left Blank

Diagenesis, IV. Developments in Sedimentology 51
edited by K.H. Wolf and G.V. Chilingarian
© 1994 Elsevier Science B.V., Amsterdam. All rights reserved.

Chapter 11

PART I. POSTDIAGENETIC FERRUGINIZATION OF SEDIMENTARY ROCKS (SANDSTONES, OOLITIC IRONSTONES, KAOLINS AND BAUXITES) — INCLUDING A COMPARATIVE STUDY OF THE REDDENING OF RED BEDS

ARNO MÜCKE

INTRODUCTION

Ferruginization is defined as the alterations owing to weathering close to the surface in the presence of iron-bearing aqueous solutions. The intensity of such alterations is proportional to:
- the time the rocks are exposed to these alteration processes;
- the quantity of water circulating through the rocks;
- the porosity of rocks;
- the grain size of minerals of the rocks;
- the Eh and pH conditions of aqueous solutions; and
- the climatic conditions (e.g., see Wopfner and Schwarzbach, 1976; Mücke and Agthe, 1988).

This ferruginization operates at temperatures of generally about 50°C. In a narrow zone close to the surface, however, an upper temperature of 80°C may be attained in arid environments, thus excluding volume diffusion in solid state as shown in the diagram of Rubie and Thompson (1985) (Fig. 11-1). The diagram implies that, for

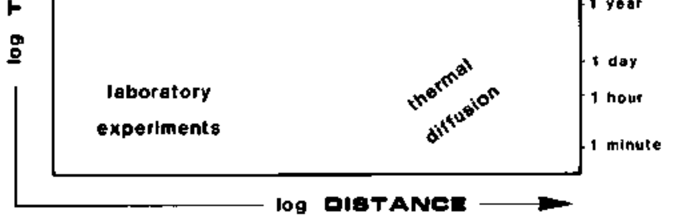

Fig. 11-1. Simplified time–distance diagram of diffusity. (After Rubie and Thompson, 1985, fig. 1.) Modified slightly by including the inferred field of diagenesis.

example, metamorphic reactions generally operate in a temperature range of about 300–600°C. The intensity of diffusion largely depends on temperature and, in the above-mentioned temperature range, diffusion increases with increasing temperature by a factor of 1000. In general, the relation between temperature and diffusion is characterized by an Arrhenius-type function, thus clearly indicating that the observed low-temperature alterations discussed here cannot be explained by solid-state volume diffusion processes.

The alterations during ferruginization are characterized by the presence of unstable precursor minerals. These minerals decompose either into pseudomorphic alteration products after the precursors, or they are completely dissolved. Consequently, specific elements or groups of elements are removed, whereas others — especially Fe — accumulate. Inasmuch as Eh and pH are the main controlling factors, elements that predominate in the alteration phenomena are those with various valencies and which thus exhibit variable migration behavior. This variability is shown, for instance, by the elements Fe, Mn, Cr, V, Ni, Co, Th, and U. Because of Fe's comparativly high Clark value, it is of major importance in the present context.

As the intensity of these alterations depends partly upon the porosity of rocks, ferruginization is particularly marked in porous and permeable sandstones; therefore, they are frequently referred to below. However, other sedimentary rocks with high porosity, such as oolitic ironstones, are also dealt with. A humid and warm climate particularly favors these alterations. Inasmuch as ferruginized sandstones appear to be identical to continental red beds, the various theories concerning red beds are reviewed next.

A COMPARATIVE STUDY OF THE REDDENING OF RED BEDS

Continental red beds

Turner (1980) made a comprehensive study of continental red beds. A summary is provided here which is required for the subsequent discussions. The summary also includes genetic ideas by Folk (1976), van Houten (1964, 1973), Mücke and Agthe (1988), and Walker (1967a, b, 1974, 1976).

Definition

Red beds are sedimentary rocks of reddish-brown (also yellowish-brown to orange and dark-brown) color produced by iron hydroxides and/or oxides. Red beds often form variegated sequences of alternating layers of red (at least 60% of the rock has to be red in order to be classified as a red bed; Bates and Jackson, 1987) and differently-colored (sometimes green, grey and colorless to white) intercalations. In contrast to the uniformly pigmented red beds, the variegated sequences can show a speckled distribution of iron hydroxides and/or oxides, and thus of coloration. Sandstone with as little as 0.1 wt.% of extractable Fe (not identical with Fe-total; Walker and Honea, 1969) may show coloration; 1.5% hematite, calculated from chemical analyses, is required for mudstones to have a red coloration (Franke and

Paul, 1980). Fine-grained iron hydroxide causes a yellowish coloration, whereas the fine-grained hematite, a red one. Sandstone with lower concentrations of extractable iron than 0.1% may be colorless to white. The coloration may be due to film-like coatings around grain boundaries and cavities or to finely-distributed mineral phases in cement or matrix, both often consisting of various types of clay minerals.

Red beds date from the Late Precambrian and Phanerozoic to the Recent, and have been commonly formed in non-marine to paralic facies (van Houten, 1973). They may also be formed in fluvial to fluvial–marine transitional environments (Walker, 1967a) and in environments on or close to land (Franke and Paul, 1980). The older red beds are called "*ancient red beds*", whereas younger and recent types are termed "*modern red beds*". According to van Houten (1973), ancient red beds are of different petrographic and facial types with two end-members (Fig. 11-2):

- one end-member comprises extensive uniformly pigmented quartz-rich sandstone and siltstone, both of which interfinger with marine calcites, evaporites and aeolian sandstones, indicating arid climatic conditions; whereas
- the other end-member consists of thick and usually variegated sequences of immature sandstones and mudstones, passing laterally into conglomerate. Many of these sandstones and mudstones constitute fining-upwards cycles. In the lower layers, coarse-grained drab sandstones or conglomerates are dominant (coarse member); in the top layers, however, there is mainly mudstone (fine member)

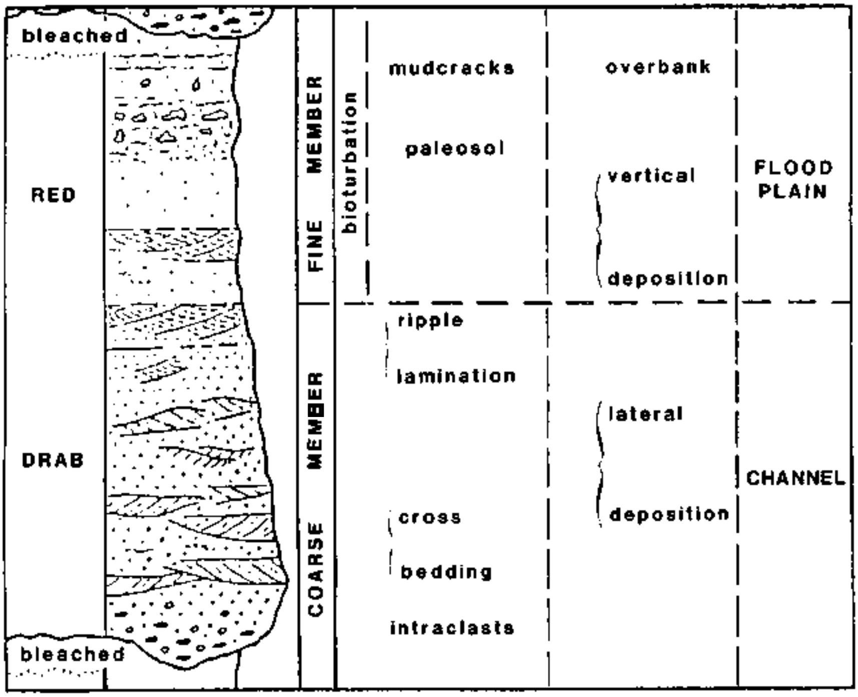

Fig. 11-2. Model of variegated asymmetric fining-upwards fluvial cycle. (From van Houten, 1973, fig. 2.)

having a speckled reddish-brown pigmentation. Red beds of this latter end-member have plants and vertebrate relics that existed in a warm-humid climate. The top of these sequences exhibits evidence of bioturbation.

Amount of iron in red beds

The total iron content of red beds varies considerably and calculated averages range from 1.7 to 3.5% Fe by weight (Turner, 1980, table 6.5 on p. 376). As reported by Pettijohn (1963) and Middleton (1960), the average total iron content of sandstones is 2.35 and 2.9% Fe by weight, respectively. From these values, Turner (1980) concluded that there is no evidence of iron enrichment in red beds in contrast to sandstones and, therefore, no evidence of any overall process of iron-enrichment.

The iron content of red beds is predominantly linked to the cement of sandstones rather than to the detrital material (quartz crystals), as demonstrated by a close correlation between the quartz crystal sizes and the iron content of sandstones (van Houten, 1961; Picard, 1965; Walker and Honea, 1969; Turner, 1974). Turner (1974) has illustrated this relationship: the iron content increases with increasing grain-size of the quartz crystals (Fig. 11-3). This is the consequence of increasing size of voids between neighboring grains in sandstones. Voids are filled with cementing material in lithified sandstone, and iron is mostly present within the cement as ferrous Fe-silicates.

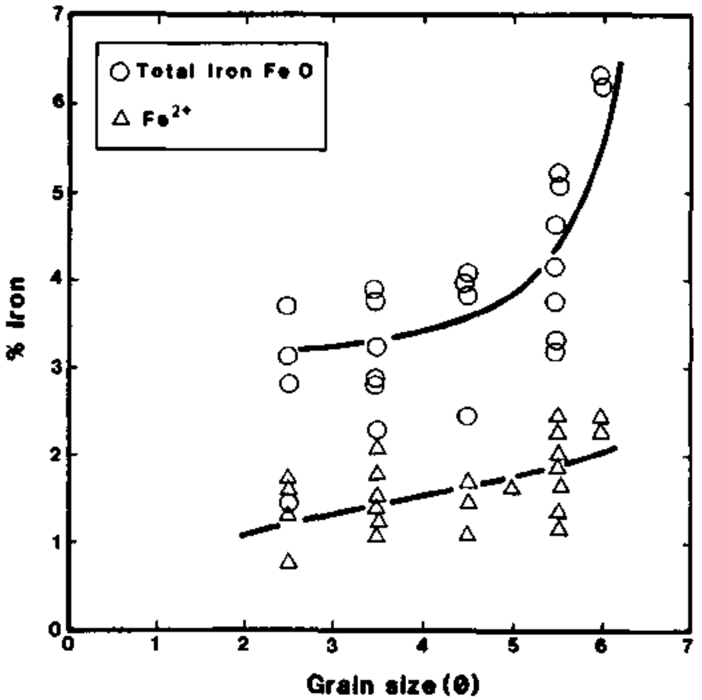

Fig. 11-3. Relationship between grain size and ferric iron and ferrous iron contents in ancient red beds (Ringerike Group, Silurian). (After Turner, 1974.)

TABLE 11-1

Total iron content of different types of red beds (values obtained from literature)

Literature	Origin of material	Type of sediment	Total iron content (wt%)		No. of analyses
			Aver.	Min.–Max.	
Walker (1967, table 1)	Baja California Sequence		3.3	2.6–3.8	16
	Sonoran Desert, Mexico	Red mudstone	3.2	2.7–3.7	10
Walker and Honea (1969, tables 6 and 3)	Sonoran Desert, Mexico	Recent alluvial sand	1.63	0.7–2.9	23
	Different locations	Ancient red beds	1.7	0.2–5.1	31
	Sonoran Desert		2.52	28	
Walker (1975, table 3)	Orinoco Basin	Modern alluvium	0.92	25	
	Puerto Rico		5.80		9
Schlugar and Roberson (1975, table 1)	Patapsco Formation, Maryland	Sandstone, siltstone	4.13	1.32–9.14	20
Picard (1965, table 1)	Chugwater Formation, Wyoming	Red sandstone	0.91	0.66–1.38	6
		Red siltstone	1.63	0.88–2.16	16
		Red claystone	4.86	4.08–5.29	4
McBride (1974, table 1)	Difunta Group, Mexico	Red claystone	3.81	3.71–4.25	7
Braunagel and Stanley (1977, table 1)	Wasatch Formation, Wyoming	Red mudstone	4.66	3.09–6.65	11

Table 11-1 summarizes the total iron content of red beds from the literature and shows a range from 1.31% to 4.72% Fe by weight. Additional data are presented in Table 11-2. In comparing these two tables to the data presented by Turner (1980), however, there appears to be some reason to doubt his statement mentioned above. Furthermore, the total iron content of sandstones does not necessarily have a direct relationship to the intensity of the coloration. There are two reasons for this as discussed below:

(1) The total iron content of sandstone is linked to various minerals (a, b, c), which contribute to the coloration:

(a) ferrous iron, which is a constituent of clay minerals; the latter are white to colorless, grey, or green and constitute the matrix (or cement) of the sandstones;

(b) ferric and/or ferrous iron, which are constituents of coarse-grained detritus; the latter either occurs as black oxide minerals (magnetite, ilmenite, and hematite–ilmenite solid solutions with and without exsolution bodies), or as iron-bearing silicates (e.g., hornblende and biotite);

(c) ferric iron, which is concentrated in yellow to brown fine-grained hydroxides and red fine-grained hematite, commonly disseminated in cement (and/or matrix).

In their study of ancient red beds from the Sonoran Desert, Walker and Honea (1969) removed the red pigmentation (= extractable iron) with reducing agents.

TABLE 11-2

Elemental concentrations of hilltop iron layers — analyses 1–14 (for localities compare with Fig. 11-10)

	El Heiz						Radwan				Sandstone Hill		El Ris	
	1 138/81	2 142/81	3 143/81	4 129/81	5 134/81	6 122/81	7 128/81	8 118/81	9 121/81	10 130/81	11 155/81	12 165/81	13 136/81	14 137/81
Ca (%)	1.1	1.2	1.4	0.7	1.8	1.7	1.4	1.4	0.8	1.5	1.4	1.9	1.3	0.9
Ti	3395	330	2185	910	7575	1975	1530	2065	9305	1210	2660	1930	540	1180
Cr	39	64	87	37	107	69	56	41	88	45	35	51	70	58
Mn	295	285	1070	260	1885	215	220	5385	600	5045	2080	605	1125	580
Fe (%)	17.5	17.5	35.1	19.0	27.0	22.8	18.1	15.2	21.4	20.1	15.1	14.1	22.4	19.8
Ni	–	–	–	–	–	–	–	15	16	–	–	–	13	–
Cu	–	–	–	11	17	–	–	–	11	–	–	–	–	–
Zn	–	–	–	54	29	26	–	40	13	–	–	–	–	15
Sr	34	46	75	29	102	100	66	56	15	62	60	62	28	12
Zr	380	–	290	70	275	160	140	210	590	140	320	200	245	130
Hf	–	–	–	–	–	–	–	–	119	–	–	–	–	–
Ba	205	825	330	–	770	460	600	2120	–	1700	1090	210	315	475
Pb	–	–	–	121	–	140	–	–	–	–	–	–	–	–
Nb	–	–	–	–	17	–	–	–	–	–	–	–	–	–

Note: If not otherwise indicated, data is in ppm. Elements with atomic numbers smaller than 19 were not analyzed.

They showed that the amount of pigmentary material varied from 0.1 to 2.1% Fe by weight and that some bright red samples have only 0.1% extractable iron, as in the newly-formed fine-grained hydroxides and oxides mentioned above (c). In general, red beds with excess ferric iron and Fe_2O_3/FeO ratios greater than two are common (Turner, 1980).

(2) The iron content of fine-grained and newly-formed hematite [mentioned under (c) above] will produce a markedly more intense red coloration of sandstones than shown by those associated with coarser-grained detrital hematite [mentioned under (b)]. Coarse-grained hematite will hardly influence the color, even though it may be present in a greater proportion. This can be easily demonstrated in reflected light and crossed polars: coarse-grained hematite shows only a few, fine-grained abundant red internal reflections. Thus, the total iron content of sandstone is not an indication as to whether the rock is a genuine "red bed".

Distinctive features in red-bed research

As Turner (1980, preface) stated, the origin of continental red beds and their color "has been hotly debated for over 100 years"; the hypotheses have changed further since then. Even today (1991) most of the problems remain. Earlier classifications of continental red beds are either almost exclusively based on color variations or special emphasis is placed on the provenance of the pigmentary hematite. Today, however, it is known that the red beds' origin largely depends on the basin type in which the sediments form (Turner, 1980), i.e., *senso lato* determined by tectonic conditions (Mücke and Agthe, 1988). Tectonism controls the rate of uplift and thus erosion of the source rocks, the amount of material fed into the basin, the rate of sedimentation, and finally the development of the basin after sedimentation. Red color alone, however, is not directly diagnostic of a specific tectonic framework (van Houten, 1973).

In the center of red-bed research one mineral is of particular importance: hematite, the pigment of red beds. The theories of red beds genesis, therefore, depend on the answers to the following questions:

(1) How was the pigmentary hematite introduced into the sediment? Directly or indirectly?

(2) What is the age relationship between sedimentation and the origin of pigmentary hematite? Did reddening occur (a) during or after the deposition or (b) during or after the diagenesis (= postdiagenetic)?

(3) What is the source of pigmentary hematite? Did it originate from lateritic soil, from detritus derived from igneous or metamorphic rocks, from redeposited red beds, or from iron-bearing solutions penetrating the sediments?

(4) Is there any relationship between the hematite formation and climate? What type of climate is required for the formation of hematite?

The major conflicting hypotheses seeking to answer (at least partially) these questions are briefly summarized as follows:

(1) Many geologists (at the beginning of the 20th century) thought, that red beds originated under desert conditions in analogy to the many tropical deserts with red sand dunes. Their arguments were based on the low water table and the lack of

vegetation in deserts causing an oxygenated environment. Here, the intense desert heat resulted in dehydration of ferric hydroxide to form hematite.

(2) According to the second theory, the hematite or its precursor ferric hydroxide has a lateritic-soil origin and a wet tropical or subtropical source area. After erosion of the soil, hematite or its precursor were transported to desert basins to be incorporated into sediments. Whereas Krynine (1949) believed that sediments were red when deposited, according to van Houten's (1968, 1973) model reddening may have occurred during the postdepositional period, due to in-situ dehydration of ferric hydroxide (of soil-origin) to hematite or in-situ alterations of igneous or metamorphic detritus.

(3) The third model, introduced by Walker (1967a), discussed intrastratal alteration of iron-bearing detrital grains during diagenesis that originates hematite.

(4) Mücke and Agthe (1988) demonstrated that hematite originates from ferric hydroxides, namely, that it is of postdiagenetic age replacing pre-existing cement of the sandstones.

The above discussion shows that it is impossible to develop a genetic red-bed model of general validity (Turner, 1980). There is still a wide range of problems regarding the origin of continental red beds. The following discussion deals exclusively with the theoretical genetic background of pigmentation, and the more significant red-bed models are discussed in some detail. For further information, the reader is referred to the contribution by Turner (1980).

The development of colors in sediments: transport, precipitation, and stability of pigmentary phases

The origin of pigments and their imparting color to sandstones, siltstones, mudstones, and other lithologies like associated limestones and evaporites often represents the central problem in red-bed research.

Within a red-pigmented sequence, i.e., sediments of red coloration, there can be variegated yellow, yellowish-red, red, reddish-brown and blackish-brown, as well as green and grey deposits; even white to colorless ones have been observed (Worral, 1969; van Houten, 1973; McBride, 1974; Folk, 1976; Braunagel and Stanley, 1977).

The pigmentation of sediments depends on characteristic features of the pigmenting mineral(s). Inasmuch as the pigment of red beds *sensu strictu* (e.g., exclusively variegated deposits), is strictly connected with iron hydroxides and oxides, their genetic–environmental characteristics must be discussed. These are: (a) the transport of iron, (b) the external conditions leading to the precipitation of iron, and (c) the stability of the iron minerals being formed.

(a) Iron is transported in the sedimentary environment in a variety of forms:

- in true solution especially under more acid and/or reducing conditions;
- as crystalline hydroxide associated with quartz-grain coatings (Folk, 1976) and/or adsorbed on the surface of clay minerals (van Houten, 1968, 1973);
- within silicate minerals [amphibole, biotite (Walker, 1976) and iron oxides (Mücke and Agthe, 1988)]; and
- in solution in the form of organic complexes (Bafor and Mücke, 1990).

(b) Precipitation and accumulation may take place at various stages during sediment deposition and diagenesis, and also postdiagenetically:

- by infiltration of lateritic material during deposition (Krynine, 1949; van Houten, 1968, 1973; Folk, 1976);
- by alteration of iron-bearing minerals postdepositionally both above and below the water table (van Houten, 1968, 1973);
- by the surface waters during diagenesis (Walker, 1967a);
- by the circulating groundwaters during diagenesis (Schluger and Roberson, 1975; Walker et al., 1978); and
- by the descending water during postdiagenetic alterations (Mücke and Agthe, 1988).

The precipitated iron minerals are hydroxides rather than oxides (hematite) the formation of which is discussed under (c). Precipitation of iron occurs from aqueous solutions as amorphous $Fe(OH)_3$, goethite and lepidocrocite (FeOOH), and is generally caused by changes in the Eh/pH-conditions. The genetic conditions and their identification have been discussed by Schwertmann and Fischer (1974), Schwertmann and Taylor (1977), and Stucki et al. (1985).

(c) The stability of iron hydroxides is largely a function of grain size, crystallinity, and contamination (usually by Al and Si). Depending on their quantity in the sediment and mode of distribution, these hydroxides impart a yellow to brown color to the sediments. Such colorations are frequently observed in younger sediments. In older red beds, however, hydroxides occur more rarely, as they have been replaced by red hematite. This hematite is formed by dehydration of iron hydroxides under arid conditions (van Houten, 1964, 1973; Schmalz, 1968; Turner, 1974; Walker, 1967a). The minimum reaction temperature for goethite transformation into hematite as a result of dehydration has been determined to be 40°C by Berner (1969) under laboratory conditions. The grain size of hydroxides is another factor significantly affecting the dehydration reaction (Langmuir, 1971; Langmuir and Whittemore, 1971; Goss, 1987). With decreasing grain size of the iron hydroxides, the intensity of dehydration increases. Under natural conditions, however, the dehydration is largely restricted to amorphous Fe-hydroxides (Turner, 1980).

To explain the green and colorless sediments, the rehydration hypothesis should be considered. Changing of red sediments into yellow, green or even colorless types is a reduction phenomenon (Hartmann, 1963; McBride, 1974; Folk, 1976; Braunagel and Stanley, 1977). During this process, the red turns yellow as a result of rehydration of hematite into iron hydroxides (van Houten, 1968; Folk, 1976), and finally green and colorless contemporaneously with the occurrence of newly-formed green ferrous silicates. Contrary to the yellow sediments of this type, the formation of colorless and green sediments is slightly different: subsequent to reduction, complete depletion in iron is brought about by the high mobility of Fe^{2+} ions in colorless sediments (McBride, 1974), whereas in green sediments, Fe^{2+} is incorporated into the lattice of associated silicates with simultaneous development of the green particles (Folk, 1976).

This rehydration hypothesis of hematite contradicts kinetic considerations advanced by Langmuir (1971), who demonstrated the impossibility of rehydration on

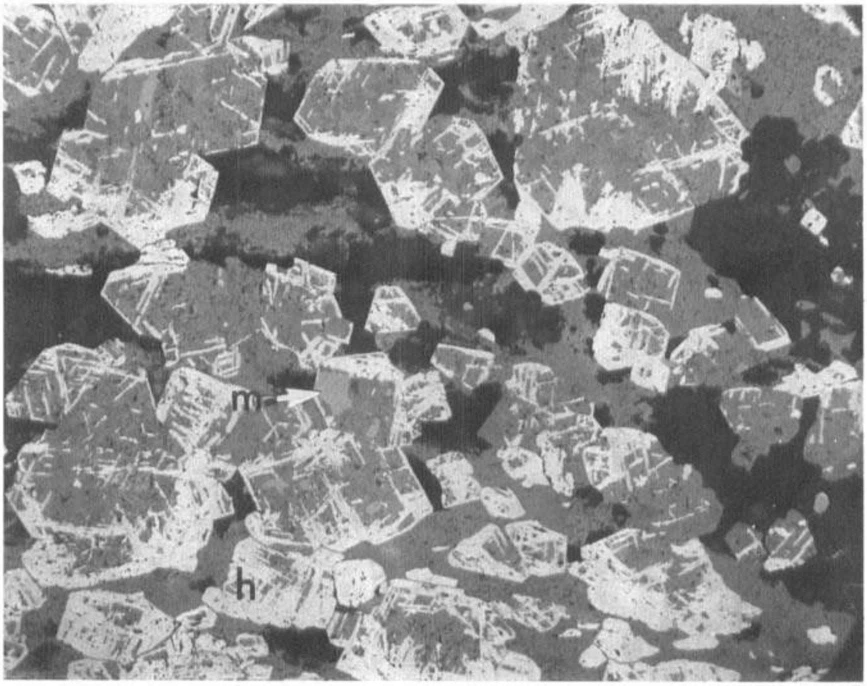

Fig. 11-4.* Partially martitized idiomorphic magnetite crystals replaced by goethite. The replacement affected only magnetite, which was preserved as relics (*m*). Martite [present in the form of oriented hematite needles (*h*)] is resistant against the process of goethite replacement. The gruneritic cement of the magnetite is also replaced by goethite. Banded Iron Formation of the Maru Belt, Nigeria.

theoretical grounds. Also, according to Palache et al. (1944), there is no known goethite pseudomorphism after hematite. The present author agrees with this observation (Fig. 11-4).

Models of red-bed formation

After the above discussion of general aspects and some details on red-bed research, genetic theories of red beds are discussed below. In addition to older concepts (a), two current models are considered in detail. These are:

(1) The detrital model (b): considerations are divided into two parts according to Folk (1976) who discussed microscopic observations (b_1) and the ideas of van Houten (1968, 1973) who considered not only the sedimentological–environmental aspects of the red-bed formation but also the stability relation of the minerals (b_2).

(2) The diagenetic model (c) of Walker (1967a, b, 1974, 1976).

---

* Unless otherwise stated: all the photos were prepared in reflected light using an oil-immersion objective. Length of the longer edge of the photo is 270 μm.

The classical theories (a)

The classical theories, related to the red-colored sediments, can be summarized as follows:

A low water-table and absence of organic matter are the prerequisites, together with a prevailing oxidizing environment (Dawson, 1848), so that ferric hydroxides can form. Dehydration of these hydroxides is assumed to occur in arid regions forming hematite, which imparts the red color to sands (Crosby, 1885, 1891; Barrell, 1908). In analogy to unconsolidated red-colored desert sands, ancient red bed equivalents are believed to be of similar origin, i.e., formed under desert conditions.

Three models have been discussed by Krynine (1949) to explain how the pigment hematite became associated with sandstones. No details on the models can be provided here and one can merely state that the red color of the sandstones, according to these three models, originates from:

(1) detrital material,
(2) precipitation from the Fe-bearing solutions migrating through the sandstone, and
(3) authigenic growth of Fe-minerals brought about by oxidation and/or alteration of detrital Fe-bearing minerals in situ.

Krynine favored the first theory based on the hematite being formed by lateritic weathering under a tropical or subtropical climate and deposited synsedimentarily in a desert basin with quartz grains. Owing to the detrital hematite, the sediment is red.

The detrital model (Simpson Desert, Australia) (b_1)

Folk (1976) examined active dunes of the Simpson Desert (Central Australia) overlying Pleistocene fluviatile sediments, by sampling their crests and flanks (consisting of well-sorted and fine-grained sands) as well as the intervening coarser-grained deflatory flats or reg (= desert surface covered with small pebbles). Folk (1976), after studying the fine-grained dune material and the more coarse-grained reg samples, established the following relationship between color and grain size:

(1) the fine to very fine fraction of the dune material showed intense dark-red effects, whereas the coarser-grained fraction of the same material exhibited orange color hues; and
(2) the reg samples revealed a similar distribution of colors. A decrease in grain size corresponded to an increase in intensity of the color. Thus, the coarser fraction of the reg material was of a lighter and rather yellow color, whereas the finer fraction was reddish-orange.

Before the relationship between grain size and color can be explained, the coloration phenomenon of single quartz grains, as observed by Folk (1976) using the binocular microscope must be considered. He reached an interesting conclusion: the color distribution of single quartz grains was of bimodal nature. Early in their history, the quartz grains were coated with a reddish-orange hematitic clay (the clay was identified microscopically and by the qualitative microprobe analysis). This original coating is at present preserved only as relics, i.e., occurring merely as incomplete remainders or traces on the grain surfaces (Fig. 11-5). Superimposed on this, there may be a silica coating enveloping the grains. This secondary silica has a bumpy

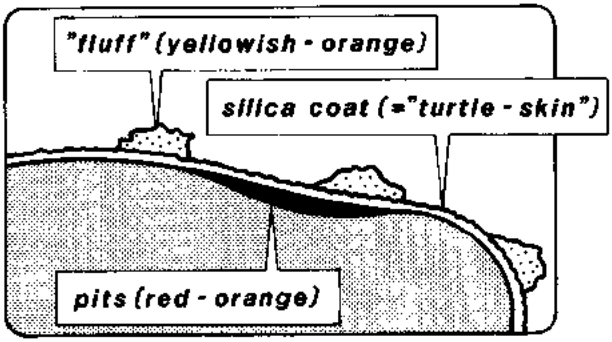

Fig. 11-5. Sketch showing the sequence of grain coatings: (1) hematite clay cutan preserved only in pits; (2) thin silica coat with bumpy surface; and (3) limonitic surface "fluff". (Redrawn from Folk, 1976, fig. 3.)

surface with a greasy luster, named by Folk (1976) "turtle skin". A yellowish-orange "fluff", consisting of limonitic clay, forms a final coating. Whereas the limonitic "fluff" originated during the Holocene to present time, the hematitic clay coating is believed to be of Pleistocene age.

In accordance with these observation made on single grains, Folk (1976) explained the color difference between quartz grains of different sizes as follows: the finer fraction is the saltation population that has a more intensive transportation history in contrast to the coarser one. Thus, the smaller grains were unable to accumulate limonitic "fluff" on their surface, and consequently the finer fraction merely shows the older Pleistocene clay–iron oxide coating (responsible for the red color) underneath the secondary quartz. On the contrary, the coarser grains had underwent lesser intensive transportation and were able to accumulate the yellow "fluff" on their surfaces. Folk (1976) concluded, therefore, that the color of red beds is dependent on both the geological age and the condition of deposition.

Subsequent investigations by Folk (1976) established a sequence of colors from a pale apricot hue in recent (Holocene) sandy sediments, through a deep brick-red for Pleistocene, to a lighter red for younger Paleozoic, and finally to maroon or liver-color (and even shades of green) for older Paleozoic and Precambrian rocks. These relationships are presented in Fig. 11-6 with quantitative color data (for details see Folk, 1976).

The quantitative color data by Folk (1976) in rocks of different ages resulted in his proposed diagenetic succession:

(1) Primary sediments are colorless, white or grey if they consist of uncoated quartz grains. Any iron that may be present, is linked to heavy minerals or to clay which imparts color to the sandstone.

(2) With the onset of alteration (i.e., hydration and oxidation), the iron-bearing detrital minerals become unstable and dissociate to form limonite. As a result, the sediment becomes yellow to yellowish-orange. As the alteration advances, the limonite content increases and so does the depth of color, which then changes to apricot-orange.

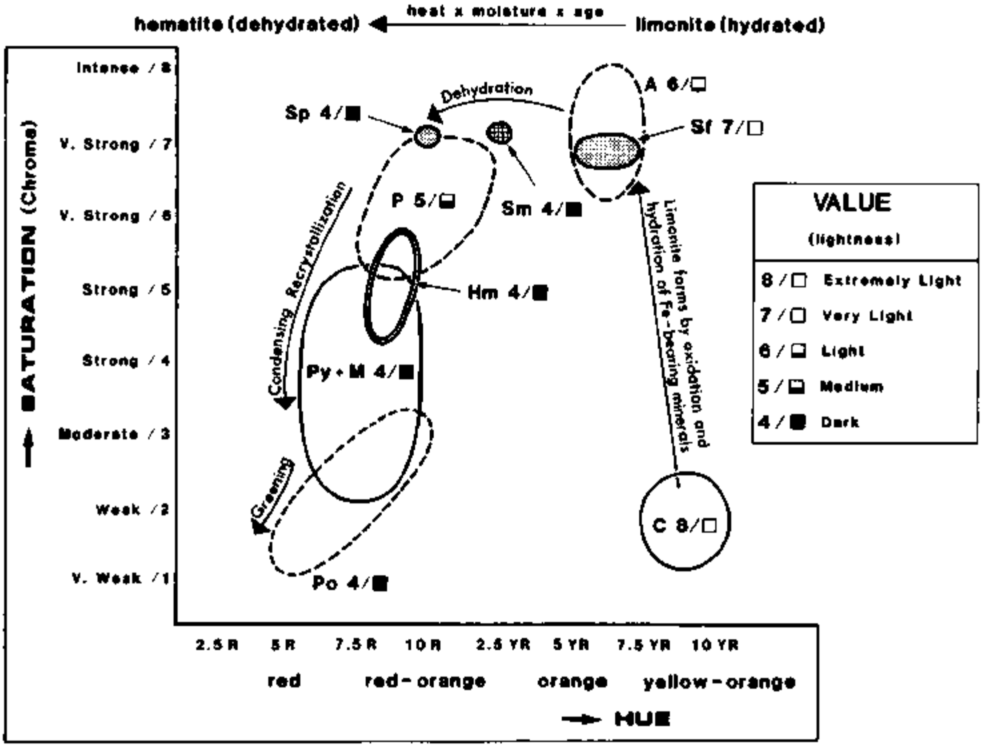

Fig. 11-6. Change of color with geologic age as shown on hue vs saturation plot. The third color dimension of lightness is shown by numbers (4/etc.), and the degree of darkening of the squares. C = initial unweathered quartzose sand; A = Saharan sands; S_f = surface fluff of Holocene age (Simpson Desert); S_m = modal color en masse of fine sands (Simpson Desert); S_p = color of hematite-clay cutans in pits formed during Pleistocene lateritization (Simpson Desert); P = other Pleistocene sediments; H_m = color of powdered hematite; $P_y + M$ = color of Mesozoic and younger Paleozoic rocks; P_o = Older Paleozoic and Precambrian rocks. Process causing these changes shown by the "evolutionary" arrows. (Redrawn from Folk, 1976, fig. 4.)

(3) Dehydration of limonite results in hematite and color changes towards red. In hot regions, both arid or humid, such alteration has taken place since the Pleistocene.

(4) Recrystallization of hematite grains, resulting in an increase in crystal size, occurs with age. Owing to the reduction in total grain surface areas of the hematite, the recrystallization process led to a color change from initially red, observable in rocks older than Mississipian, to maroon occurring in rocks of Late Paleozoic and younger formations (including the sands of the Simpson Desert).

(5) In some Mississipian to Precambrian rocks, the color is liver-like. Folk concluded that they have achieved their final "coloric resting-place" and further color changes are not possible under diagenetic conditions.

According to the above color sequence, potential further alterations are only possible through weathering, i.e., rehydration of hematite to limonite under oxidation. In reducing environments, however, Fe^{3+} (which imparts the red color to Paleozoic rocks in the form of hematite) is transformed into Fe^{2+} and incorporated into the lattices of "iron-hungry" clay minerals to produce the green pigmentation in some rocks.

Origin of detrital and soil-derived phases and their facies-related alterations (b_2)

The ideas of van Houten (1968, 1973) may be summarized under the above heading. He, like Folk (1976), favored the detrital origin, but incorporated in his model an in-situ alteration of the sediments. Van Houten's ideas, therefore, do not merely constitute a detrital model, but must be called detrital/postdepositional model.

Van Houten considered the occurrence and stability of minerals like magnetite, ilmenite and Fe-bearing silicates (as well as their secondary in-situ changes), to be essential for the development of pigmentation in sediments (Fig. 11-7). These minerals were derived from volcanic and metamorphic sources. Ilmenite, magnetite and iron-bearing silicates are present in nearly the same quantities in both the initial sediment of red beds and their associated drab deposits. Hematite is absent or rarely found in the above precursor rocks, but instead is predominantly formed either in soils or is developed in transit (during transportation of detritus). Van Houten's concepts of the environmental dependence of hematite genesis, therefore, has to be discussed:

(1) In *oxidizing alluvial fans and plains and high flats with a low water table*, where sediments are commonly subjected to small-scale organic and inorganic disturbance, most of the magnetite begins to alter to coarse-grained black hematite.

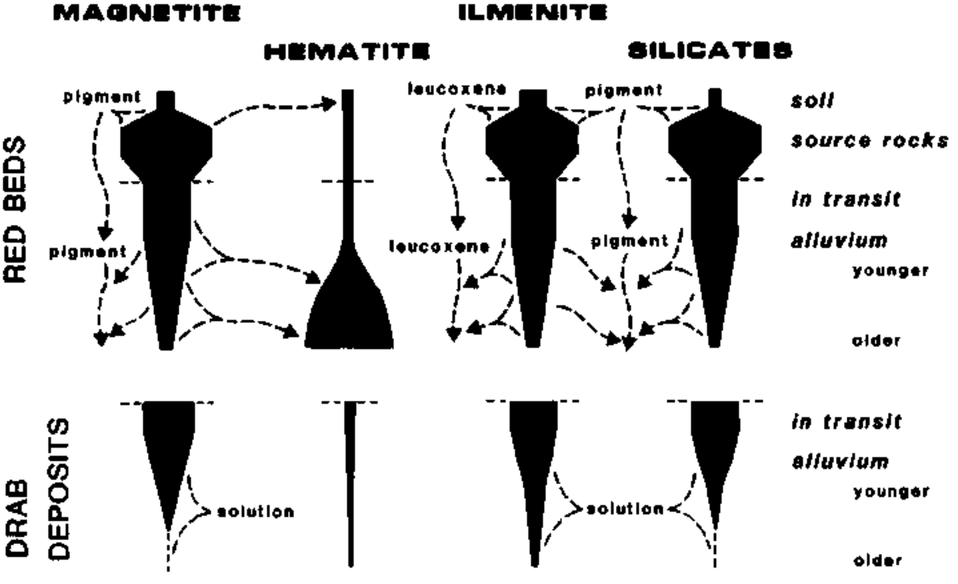

Fig. 11-7. Origin and fate of black minerals and pigment in red-bed sequences. Configuration suggest changes in abundance of each component relative to the amount in source rocks. (Redrawn from van Houten, 1968, fig. 3.)

As postdepositional oxidation proceeds, iron-bearing silicates become unstable as well, and alter in-situ into a mixture of clay and fine-grained hematitic pigment, which imparts the red color to sandstones. Ilmenite remains stable or decomposes in situ to leucoxene (Fig. 11-7).

(2) In *reducing environments*, magnetite, ilmenite and iron-bearing silicates begin to dissolve. Any hematite present at this stage has very likely been either newly-formed en route under oxidizing conditions or before the reducing environment replaced an oxidizing one.

(3) Under *warm humid conditions*, most of the magnetite, ilmenite and iron-bearing silicates inherited as detritus become unstable. In the upper horizons of soils, predominantly fine-grained hematite is formed, whereas in the lower ones, yellowish-brown, amorphous ferric hydroxide (= limonite) and goethite are formed.

(4) Under *cooler and drier climates*, the formation of ferric-hydroxide is favored over hematite.

(5) Both *tropical and temperate climatic source provenances* supply a tan-brown ferric hydroxide-bearing clay fraction that forms muddy sediments. After accumulating in an oxidizing environment, both the inherited and the newly-formed ferric hydroxides (together with clay resulting from the postdepositional decomposition of the iron-bearing silicates) are dehydrated in situ, forming the red hematitic color pigment.

(6) Most of the brown alluvium (consisting of ferric hydroxide-bearing clay) delivered to the *poorly-drained environments* becomes drab as the relatively easily-altered amorphous and poorly-crystallized hydrated ferric oxides are removed in solution. Lowering of the water table leads to the formation of a mottled soil. The process of mottling by solution and precipitation of iron that forms the drab deposits is essentially different from that leading to the red pigmentation as a consequence of dehydration of iron hydroxides. Notwithstanding these observed differences, mottled and uniformly pigmented deposits are formed under the same sedimentary environment and may thus occur in association with each other.

Van Houten (1968, 1973) concluded that:

(1) First-cycle red beds may be formed in two different ways: (a) muddy sediments which were derived largely from upland soils with brown ferric hydroxides; and (b) sandy deposits derived from soil-free uplands in hot, dry regions receiving the pigmenting hematite from detrital iron-bearing silicates which decompose into a mixture of clay and ferric hydroxides.

(2) Ferric hydroxides either inherited [see (a) above] or produced in situ [see (b) above] can transform slowly to hematite in an oxygenated burial environment. This may be achieved with a low water table and hot climate. Comparable conditions, necessary for the hematite formation, must also prevail below the water table, which is known to exist many hundreds of feet below the surface. The final red color, therefore, is not necessarily a climatic indicator of the source area.

(3) The following diagenetic processes are enhanced by long-continued increase in temperature during burial: (a) hematitization of detrital iron hydroxides; (b) alteration of unstable iron-bearing silicates to ferric hydroxides and clay; and (c) dehydration of ferric hydroxide to hematite.

(4) In associated drab deposits, ferric hydroxides (before they were converted to hematite) and less so detrital iron-oxides may be postdepositionally dissolved depending on the environmental conditions during deposition and burial.

The diagenetic model (Sonoran Desert) (c)

The diagenetic red-bed model first introduced by Walker (1967a) is discussed here together with additional details provided since then by Walker (1967b, 1974, 1976), Walker and Honea (1969), and by Walker et al. (1978). Walker's concepts are based on both modern (Sonoran Desert) and ancient deserts (Colorado).

Modern red beds of the Sonoran Desert. In the Sonoran Desert (in northwestern Mexico along the coastal plain of the north-eastern part of Baja California peninsula), the Baja California Sequence comprises Late Tertiary (Pliocene) and Quaternary desert alluvium associated with marginal marine deposits and aeolian sands (Fig. 11-8). With the exception of the Oyster Bioherm, only known in the Pliocene sequence, each facies shown in Fig. 11-8 occurs in sediments of Recent, Pleistocene, and Pliocene ages. In the Pleistocene deposits, the so-called "Red Desert Soils" (with four major types) are included. The facies associations reflect deposition in fluvial to fluvial–marine transition environments. The desert alluvium, which had been studied by Walker (1967a, 1976) and Walker et al. (1978), consists of first-cycle arkosic detritus derived from fresh crystalline basement that lacks any significant soil development. This indicates that there was no source of primary hematite. Since the early Pliocene time, the climate was arid and hot. During the Pleistocene, which included the pluvial periods, the climate was very similar to that of the present. Evaporite occurrences suggest that an arid climate existed throughout Quaternary times.

No pigmentation is found in the alluvium of the Sonoran Desert on deposition. The first traces of red color are observed in sediments of Late Paleozoic age. In the

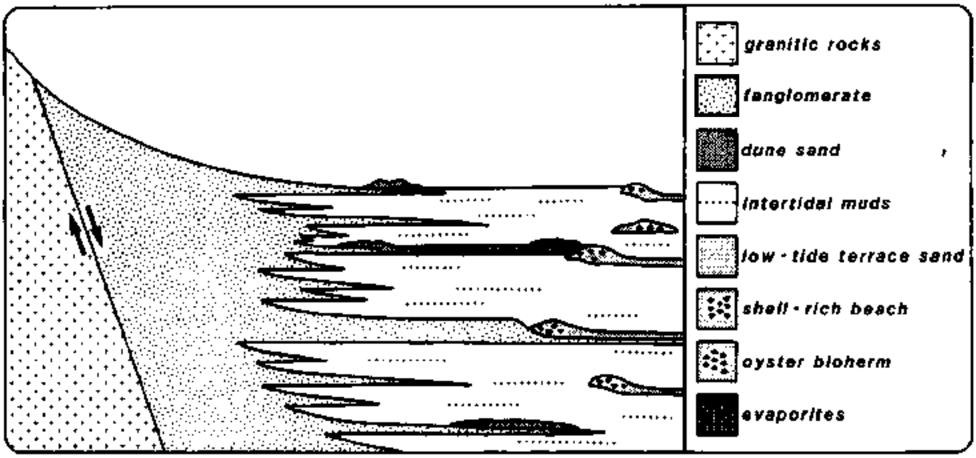

Fig. 11-8. Diagrammatic cross-section showing facies relationships of Recent, Pleistocene and Pliocene sediments, northeastern Baja California, Mexico. (Redrawn from Walker, 1967, fig. 2.)

early stage of this initial pigmentation, the agent consisted of ferric hydroxide/oxide that is amorphous using the X-ray analysis and which Walker (1976) obviously was unable to identify. Finely-crystalline hematite, which is responsible for the bright red coloration in the sediments, is restricted to the rocks of older Miocene age.

Walker's (1967a) petrographic observations in the sediments of the Sonoran Desert of different ages are as follows:

Recent alluvium. Recent alluvium deposits, only a few meters thick, comprise arkosic detritus (with accessories of hornblende and biotite) derived from dominantly granitic rocks. The alluvium, normally light grey in color is unconsolidated and shows no evidence of soil development. No pigmenting iron oxides and clayey matrix seem to be present.

Pleistocene alluvium. Owing to its greater age, Pleistocene alluvium has undergone mild chemical alterations, producing two significant characteristics, i.e., some incipient cementation and a reddish color. Both of these effects are related to weathering, which developed in the Pleistocene soils.

Pleistocene soils. Four major Pleistocene soils (so-called "Red Desert Soils") can be identified in the Pleistocene alluvium. The youngest soil shows a yellow-reddish color, whereas the oldest one is red. X-ray diffraction analyses of some soil samples reveal presence of montmorillonite, mixed-layer illite–montmorillonite, illite, and kaolinite. The pigmentary minerals in the Pleistocene soils are amorphous and thus can not be identified by X-ray analysis. These amorphous precipitates possibly are — according to Walker (1967a) — intermediary products of amorphous iron hydroxide and hematite.

Pliocene fanglomerates. Pliocene fanglomerates are calcite-cemented and contain, besides fragments of volcanic rocks, detrital iron-bearing minerals, such as hornblende, biotite, epidote, magnetite, and ilmenite. All the detritus is altered in situ as follows:

(1) hornblende is altered to montmorillonite, which is surrounded by a halo of hematite;
(2) biotite and epidote are commonly also surrounded by newly-formed hematite;
(3) magnetite is altered to hematite (martite); and
(4) ilmenite is altered to leucoxene.

Ancient red beds of Colorado. The Middle Pennsylvanian to Late Triassic red beds of Colorado (over 300 m thick) are comparable to the Sonoran Desert red beds, the former being their ancient analogs. Paleoclimatic indications suggest arid conditions. Judging from huge evaporites intercalated in the rock sequences, rainfall must have been negligibly low over a longer geological time; thus, Walker (1967a) excluded the formation of lateritic soil in the Colorado highlands. Granite and related rocks are the predominant rocks, which were the major sources of arkosic detritus in the adjacent basins, with a variable depositional setting. The fanglomerates flank the highlands and are interfingered basinward with sandstones, siltstones, mudstones, carbonates, and evaporites. This sequence implies a regional complex of continental and shallow-marine environments, including large tidal flats and/or playas and salt pans. Hematite is found in all these sediments, but generally is associated with finer-grained detritus.

Pigmenting hematite, as shown above, occurs in various rock types. Its distribution and origin in ancient and modern red beds are discussed below.

Origin and paragenetic position of pigmentary hematite

Walker (1967a) suggested that the hematitic pigment of both the modern (Sonoran Desert) and ancient (Colorado) red beds was formed after sedimentation by interstratal alteration. His arguments were:

(1) Iron-bearing detrital grains, predominantly biotite (occurring in the Pliocene fanglomerates of the Sonoran desert), are surrounded by a halo of hematite. Biotite is also abundant in red mudstones and red sandstones of the ancient red beds of Colorado, and is thus considered to be an important source of iron for the hematite pigment.

(2) Amphibole, representing the major accessory in the Recent alluvium of the Baja California Sequence (Colorado), is only preserved as relics in Pliocene red beds, which are about 10 million years old. Here, amphibole had been decomposed into a mixture of clay and hematite. Compared with the 250 million years-old late Paleozoic red beds of Colorado, Walker is not surprised that in the latter rocks amphibole is largely or nearly completely destroyed. Walker (1967a), therefore, concluded that amphibole had been a major accessory in Paleozoic red beds as well. The interstitial clay matrix in these red beds which contain hematite, probably also originated from decomposing hornblende.

(3) In the Minturn Formation, near the type area of the ancient red beds of Colorado, red beds are interstratified with green strata that owe their color to interstitial chlorite. Some beds grade from green to red, disclosing progressive stages of chlorite decomposition and the formation of authigenic hematite.

(4) The irregular nature of hematite/clay coatings on quartz and feldspar grains, and the absence of hematite at places of contact between quartz grains in ancient red beds of Colorado, are a clear indication of a postdepositional hematite origin.

Walker's model, depicting the interstratal alteration of mainly detrital hornblende into clay and hematite, is based predominantly on microscopic evidence as seen in transmitted light. In the following section, Walker's mechanism and stages of this alteration are discussed.

Mechanism and stages of decomposition of detrital iron-bearing silicates

Walker et al. (1978), studying first-cycle desert alluvium of Cenozoic age from southwestern USA and northwestern Mexico, differentiated two diagenetic alteration processes during which detrital silicates have been altered by (a) dissolution, and (b) replacement of clay.

Alteration by hydrolysis (a) covers all dissolution phenomena of detrital material. These are summarized in stage II in Fig. 11-9. The alterations, very difficult to observe in thin-sections (e.g., solution cavities cannot be distinguished from those resulting from polishing) may be easily observed using a scanning electron microscope (SEM). These SEM studies revealed alterations that were caused by solution, on the one

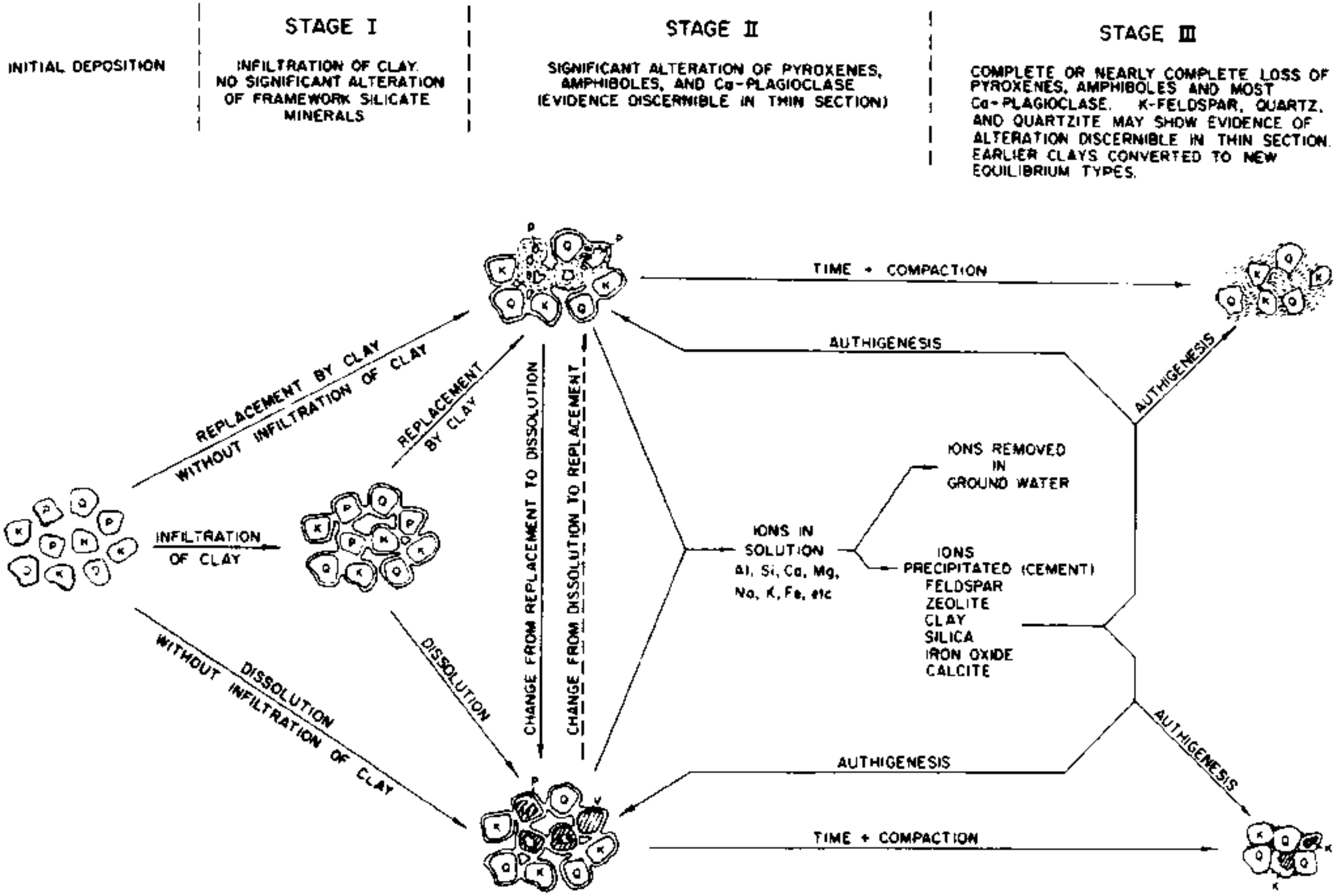

Fig. 11-9. Diagrammatic interpretation of observed and inferred stages of diagenetic alteration in first-cycle desert alluvium. (From Walker et al., 1978, fig. 12.)

hand, and by subordinate clay precipitation, on the other. Solution in hornblende forms either needle-like terminations along grain boundaries or develop "cockcomb" terminations. This indicates that disintegration starts either parallel to the *c*-axis or along lattice planes cutting across the *c*-axis. Plagioclase dissolution is more irregular. Usually, however, the dissolution process is unrecognizable. There are two reasons for this:

(1) open spaces produced by dissolution have coatings of either infiltrated or chemically-precipitated clay; and

(2) compaction of the sediment may force the clay coatings to collapse; thus, the clay coatings may become indeterminable from components of the interstitial matrix.

Replacements by clay (b) are identical with stage III of Fig. 11-9, where in-situ clay replacements of silicate detritus is shown. The clay replacements of detritic silicates may be irregular, either along grain boundaries or incipient fractures and either preferentially along crystallographic planes or cleavage planes. The replacing diagenetically-formed clay is randomly interstratified mixed-layer illite–montmorillonite containing between 80% and 95% expandable layers.

According to Walker et al. (1978), the sediments are modified texturally and mineralogically by these diagenetic processes (a) and (b) as follows:

(a) the modal composition shows in places up to 15 volume% clay of replacement origin; texturally such rock resembles graywacke; and

(b) with increasing intensity of alteration and particularly with depth of burial, intact pseudomorphs consisting of daughter clay after parent grains disappear. This is due to the fact that the soft clay is squeezed between more rigid grains and, thus, appears to be an original constituent of the interstitial matrix.

Iron liberated during clay replacement of hornblende, initiate authigenic formations (stage III of Fig. 11-9). Hematite and its precursor ferric-hydroxide are newly-formed and responsible for the pigmentation of sediments.

Walker (1976) summarized the two processes (alteration by hydrolysis and replacement by clay) as *late diagenetic reddening*. The mechanical infiltration of detrital clay into previously clay-free sediments, represents stage I in Fig. 11-9. This stage, however, is identical with his *early diagenetic reddening*. The ultimate reddening of desert sediments is the result of both early and late diagenetic reddening as: follows:

(1) Inflowing surface water carries suspended clay into permeable alluvium. This clay, coated with limonite and/or containing iron in its lattice (Walker and Honea, 1969), not as yet red when infiltrated, reacts with the oxygenated, alkaline surface water and turns red postdepositionally.

(2) Groundwater decomposes iron-bearing silicates intrastratally and releases iron, which precipitates in alkaline, oxygenated environments to form either hematite or a precursor ferric-hydroxide (the latter subsequently transforms to hematite by dehydration).

Walker (1974), investigating Holocene and Pleistocene alluvial deposits in Puerto Rico and the Orinoco Basin showed that diagenetic reddening is not necessarily related to arid climates. In the regions considered, reddening developed in a moist tropical climate. Thus, Walker (1974) suggested that red beds per se are not reliable indicators of climatic conditions. Finally, he concluded that environments in which the precursors of red beds (such as hornblende) can accumulate (and where favorable interstitial chemical conditions persist long enough for the yellow and brown ferric hydroxides to convert to red hematite) should be able to form red beds.

Final considerations and conclusion

Van Houten (1968) considered Walker's diagenetic model not to be applicable to all red beds, arguing that a mixture of clay and uniformly-distributed hematite, which Walker thought to be a product of alteration, can likewise be explained by his synsedimentary model. It may also be noted that (a) Walker's early diagenetic reddening is nearly identical with van Houten's in-situ alteration of detrital grains, and (b) the relative contributions of early and late diagenetic reddening to the final coloration of red beds is unknown. Braunagel and Stanley (1977) largely adopted the hypothesis of van Houten during their study of Eocene red beds of the Wasatch Formation, Wyoming, USA. These red beds do not show any indication of interstratal alteration, as the heavy minerals, including amphibole, were unaltered. Consequently, they considered clay-sized illite to be of detrital and not diagenetic origin.

The problems of red-bed genesis are summarized by Turner (1980, introduction): "The actual mechanisms of red bed formation are still only poorly understood and it is now clear that several different processes are involved in the genesis of a particular red-bed formation".

From the various models developed, it is concluded that the question of the origin of red beds is still open. For further information, the reader is referred to the works of Valeton (1953), Picard (1965), Friend (1966), Schlegelmilch (1968), McBride (1974), Schluger and Roberson (1975), Hubert and Reed (1978), Franke and Paul (1980), and Kowalczyk (1983).

The knowledge of red-bed genesis could certainly be more comprehensive if the geological–paragenetic position of iron oxides/hydroxides were better known. Van Houten (1968, p. 404) wrote: "There is no reliable way to determine whether the hematite pigment in red beds was: (1) inherited directly from red soil; (2) derived from limonite developed in the source area or *in transit*, by postdepositional conversion of brown oxides to red hematite; or (3) produced by interstratal alteration of iron-bearing silicates". Walker (1974, p. 636) also pointed out that: "Iron oxide of detrital origin cannot be distinguished... from those of authigenic origin".

Textural and structural studies of red-bed mineralizations have so far been undertaken almost exclusively by using transmitted-light microscopy. Mineral identifications have often been made by X-ray powder methods, probably on polymineralic material being partly amorphous. Occasionally, SEM is being used to determine structural characteristics. Another important method, reflected-light microscopy, which not only allows the determination of opaque minerals, but also their mutual age relationships with associated non-opaque minerals and replacements, has been widely neglected in red-bed investigations. This method has been used by the writer in his own investigations carried out on ancient red beds of the Bahariya Oasis, Western Desert, Egypt, and on the Phanerozoic ironstones and related deposits, the results of which are summarized below.

THE FERRUGINIZATION MODEL OF RED BEDS (BAHARIYA OASIS, WESTERN DESERT, EGYPT)

Observations first made by Mücke and Agthe (1988) in the red beds of Bahariya Oasis, Western Desert of Egypt, are presented here. Although the present data has been shortened, new information has been incorporated.

Occurrence of iron layers

The Bahariya Oasis in Egypt is a depression, the topography of which is controlled mainly by anticlines, and is characterized by isolated, cone-shaped residual hills. The latter are capped with iron-rich sandstone (with an average iron content of 20% by weight; Table 11-2) of brown to dark-brown color. These iron-rich hills were first described by Ball and Beadnell (1903). El Shazly (1962) estimated their iron reserves to be approximately 100×10^6 t ($1\ t = 10^3$ kg). Distribution of the iron mineralization in the sandstone is not arbitrary, but occurs mostly parallel to the anticlines and mainly in the southern and central parts of the oasis along the Radwan, El-Heiz, El-Ris, and Sandstone Hill anticlines (Figs. 11-10 and 11-11).

In the northern part of the oasis, the iron-capped residual hills are restricted to the Ghorabi anticline and are partly covered by the Ghorabi iron-ore deposit. In the earlier literature (e.g., El Shazly, 1962; El Akad and Issawi, 1963), these iron-rich sandstones were given special attention due to their geographically close association with three stratiform iron-ore deposits (inclusively the Ghorabi deposit) located at the northern border of the depression (Fig. 11-10). These deposits are genetically related to the basaltic volcanism of the region. The ores, which are of Eocene age, are of submarine hydrothermal synsedimentary origin (Agthe, 1986).

Iron layers within the Bahariya Oasis are not limited to hilltops (*hilltop iron layers*) (Fig. 11-12). They are frequently found at the flanks of the residual hills as well as at different levels where they form *foothill iron layers* (Fig. 11-12). Foothill iron layers may vary up to 1 m in thickness, whereas the average thickness of the hilltop iron layers is about 20 m. In addition, the eroded base of the depression is locally covered by a basal iron layer known as *groundfloor iron layer* (Fig. 11-12). Its thickness lies between 5 and 10 cm. The hilltop and foothill iron layers, the latter of which are covered by barren sandstone, are underlain by thinly-bedded fine-grained silt and clay sediments (maximum thickness of 2–5 cm). The latter themselves overlie barren grey to weakly yellowish sandstone. The groundfloor iron layer is underlain by barren sandstone.

Geological setting

The Bahariya Oasis is located in the northern part of the Western Desert of Egypt, about 350 km southwest of Cairo (Fig. 11-13). Like other depressions located farther south (Farafra, Dakhla, and Kharga), it is a basin without drainage, which was formed by wind erosion affecting only moderately-folded strata of the surrounding plateau.

The Bahariya depression lies on the Abu-Roash axis which belongs to a system of fold axes, known as Syrian fold-axes (Pfannenstiel, 1953). The southern end of this axis is located approximately 50 km southwest of Farafra in the depression of the Abu

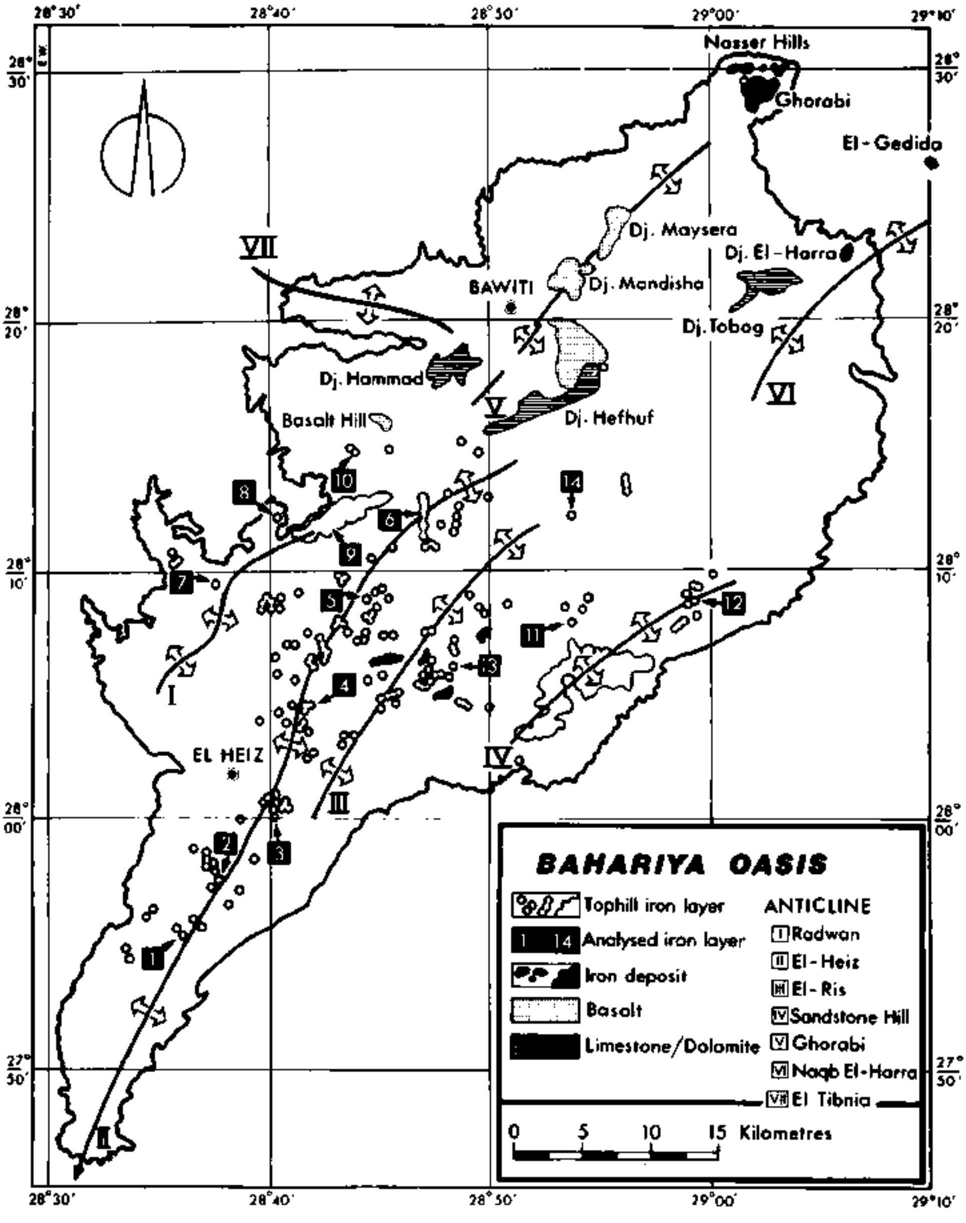

Fig. 11-10. Distribution of anticlines and ferruginized residual hills in the Bahariya Oasis, Western Desert, Egypt.

Munghar Oasis. From there, it strikes into the Farafra Oasis in a northeast direction up to Bahariya and beyond extending farther northwards (Fig. 11-13). In the area of the Bahariya Oasis, the Abu-Roash axis splits into several more or less parallel anticlines (Fig. 11-10).

Fig. 11-11. Residual hills along the El Heiz anticline in the southern part of the Bahariya Oasis, Western Desert, Egypt.

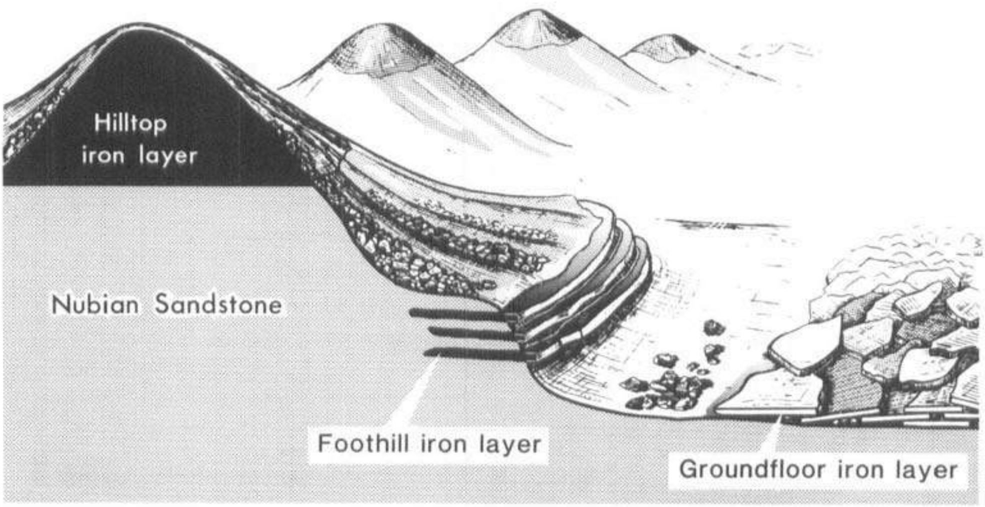

Fig. 11-12. Schematic position of different types of iron layers in the Bahariya Oasis, Western Desert, Egypt.

The uparching of the plateau began after the Cenomanian age and continued through the Maastrichtian to Oligocene time. The resulting ductile folds and extension joints in the crestal area of the anticlines offered favorable conditions for erosion, which had already begun in the Paleocene and continued up to the beginning

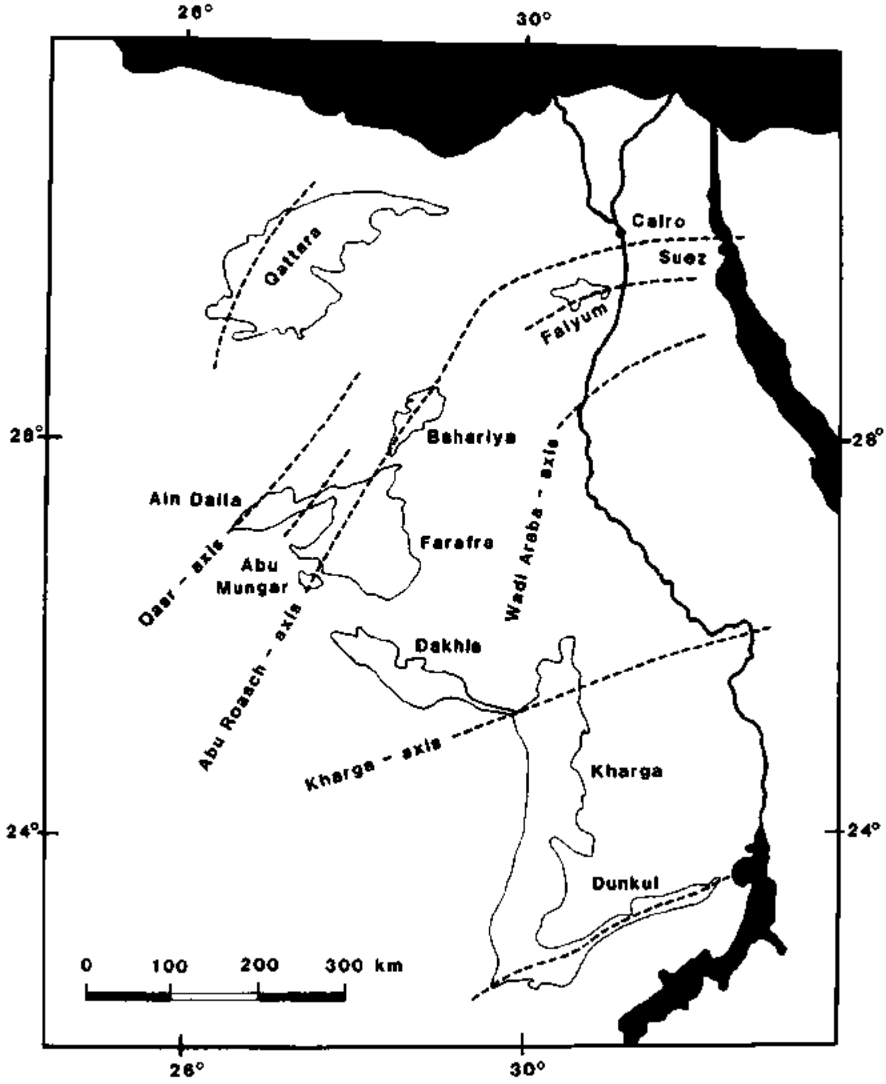

Fig. 11-13. Geologic setting of the Bahariya Oasis and the position of the Syrian fold axes. (According to Pfannenstiel, 1953.)

of the Miocene (Dominik, 1985). The sedimentary series, known as Bahariya Formation, incised by the depression, are of Cenomanian to Eocene age. The Bahariya Formation forms the base of the depression, the flanks of the residual hills, and parts of the surrounding escarpment locally up to 50 m high. All the three types of iron layers are part of the Bahariya Formation and are partly or completely enclosed by barren sandstones.

Petrographic characteristics of barren sandstones

The "barren" sandstones with an iron content of 3–4% by weight is so-named only in contrast to ferruginized sandstone that has approximately 20% by weight of iron (Table 11-2). The iron in the "barren" sandstone is fixed in detrital heavy minerals and within iron-bearing kaolinite in sandstone cement. In contrast to pure kaolinite which shows colorless to white internal reflections (in reflected light), mixtures of kaolinite and submicroscopic ferric hydroxides have light-yellow internal reflections. They are responsible for the macroscopic color of the sediment (Photo 1 of Fig. 11-14).

Apart from rounded grains of quartz and silicates, oxides of detrital origin may be found in the barren sandstones. In most cases, the heavy mineral resistates are black-colored. The oxide minerals are ilmenite ($FeTiO_3$) and its alteration products, pseudorutile ($Fe_2Ti_3O_9$) and leucoxene (TiO_2). Others are magnetite, magnesioferrite, pleonaste, chromite, rutile, anatase, and columbite. Less common minerals are silicates, comprising zircon, tourmaline, kyanite, staurolite, garnet, plagioclase, microcline, and titanite. Amphibole was not observed. Additional minerals include apatite and graphite (Photo 3 of Fig. 11-15).

Ilmenite has only rarely been preserved as relics, having been mostly altered to leucoxene and the whole range of its intermediate products (e.g., pseudorutile) as a result of the leaching of Fe. Strong leaching results in the development of shrinkage cracks in the leached residues. The final product of the whole process of leaching is a polycrystalline, fine-grained rutile (= leucoxene) (Mücke and Chauduri, 1991).

Magnetite, generally almost completely altered, is preserved only as relics. Occasionally, relics of titanomagnetite (trellis type) are also observed. The original magnetite is dissolved, whereas the ilmenite lamellae now consist of newly-formed pseudorutile (Photo 2 of Fig. 11-14). Magnesiospinel and pleonaste are stable under weathering and are thus preserved (Photo 3 of Fig. 11-14), whereas chromite shows peripheral leaching.

Petrographic characteristics of ferruginized sandstones

Minerals present in the "barren" sandstones are also found in the ferruginized ones. The original cementing material (quartz, kaolinite, illite, carbonate, anhydrite and bituminous substance), generally formed under diagenetic conditions (phyllomorphic stage, according to Dapples, 1967), has been partly or completely replaced (except for the quartzitic cement) by ferric-hydroxides (Photo 4 of Fig. 11-14). This results in a brown to dark-brown color of the sandstone. Quartz grains of the sandstone exhibit smooth surfaces (Photo 4 of Fig. 11-14), showing that they are not affected by the formation of ferric-hydroxides.

Sometimes, the iron-rich cement consists only of lepidocrocite, in which case quartz grains are corroded. Their original shape may either be still discernible (Photo 5 of Fig. 11-14) or disappear almost completely. The lepidocrocite-dominated layers show the highest iron content (up to 35% by weight; Table 11-2, analysis 3).

In the transition zones between ferruginized and barren sandstones and in flossary cavities (of stalactitic shape), the cement of the mineralized sandstones consists

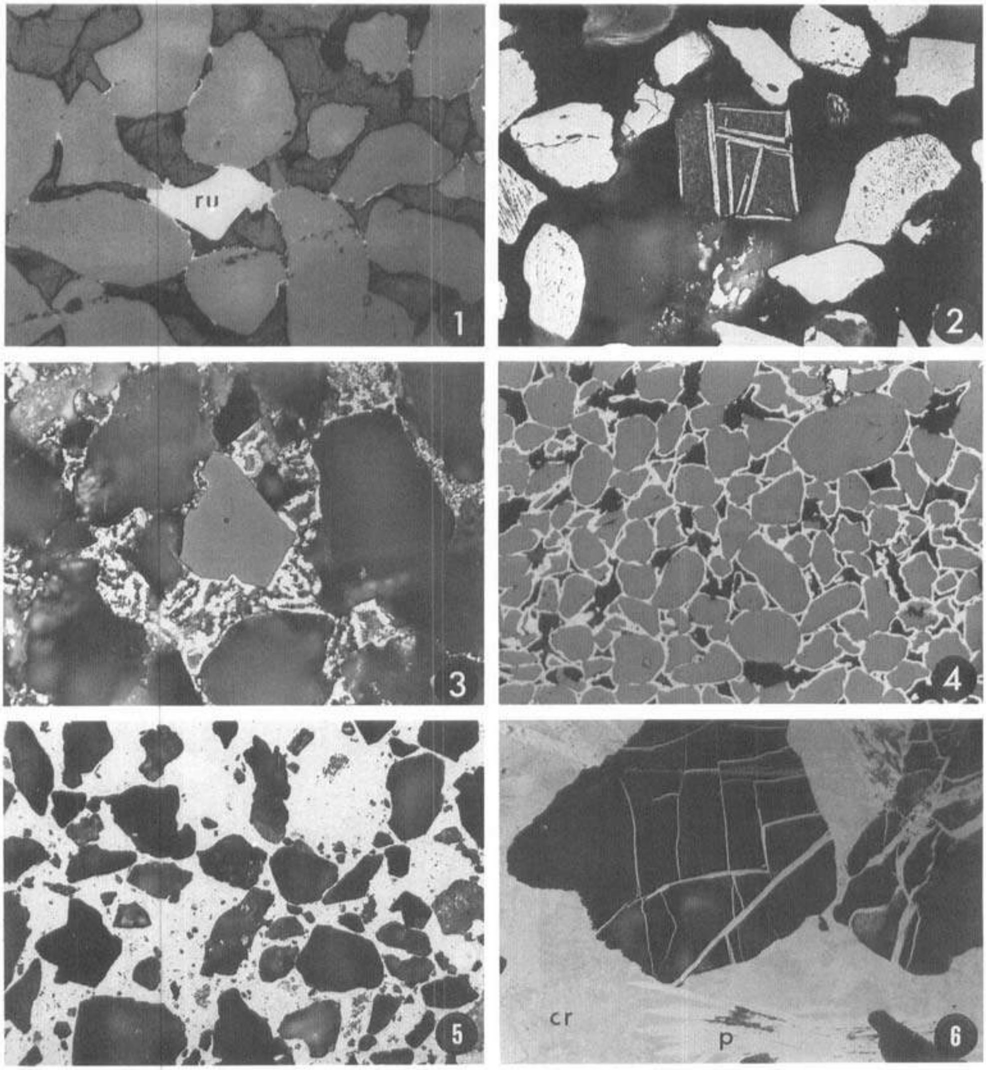

Fig. 11-14. Barren and ferruginized sandstones. 1. Rounded quartz grains and rutile (*ru*) in kaolinitic cement. Along grain boundaries, replacement of the quartz grains by ferric-hydroxide is visible. 2. The intergrown minerals titanomagnetite and ilmenite (trellis type) are strongly altered: titanomagnetite is completely transformed to a mixture of unknown phases; ilmenite is transformed to pseudorutile. Hilltop iron layer (concentrate of heavy minerals). 3. Spinel inclusion in ferruginized (ferric-hydroxide) sandstone. Foothill iron layer. 4. The original cement of the sandstone is replaced by goethite. Note the smooth grain boundaries of the quartz crystals. Length of the largest quartz crystal is 0.8 mm. Hilltop iron layer. 5. Lepidocrocite-mineralized sandstone with strongly corroded quartz grains. Hilltop iron layer. 6. The original cement is completely replaced by cryptomelane (*cr*), which is partially transformed into pyrolusite (*p*). The quartz crystals are strongly corroded and show solution fissures. Hilltop iron layer.

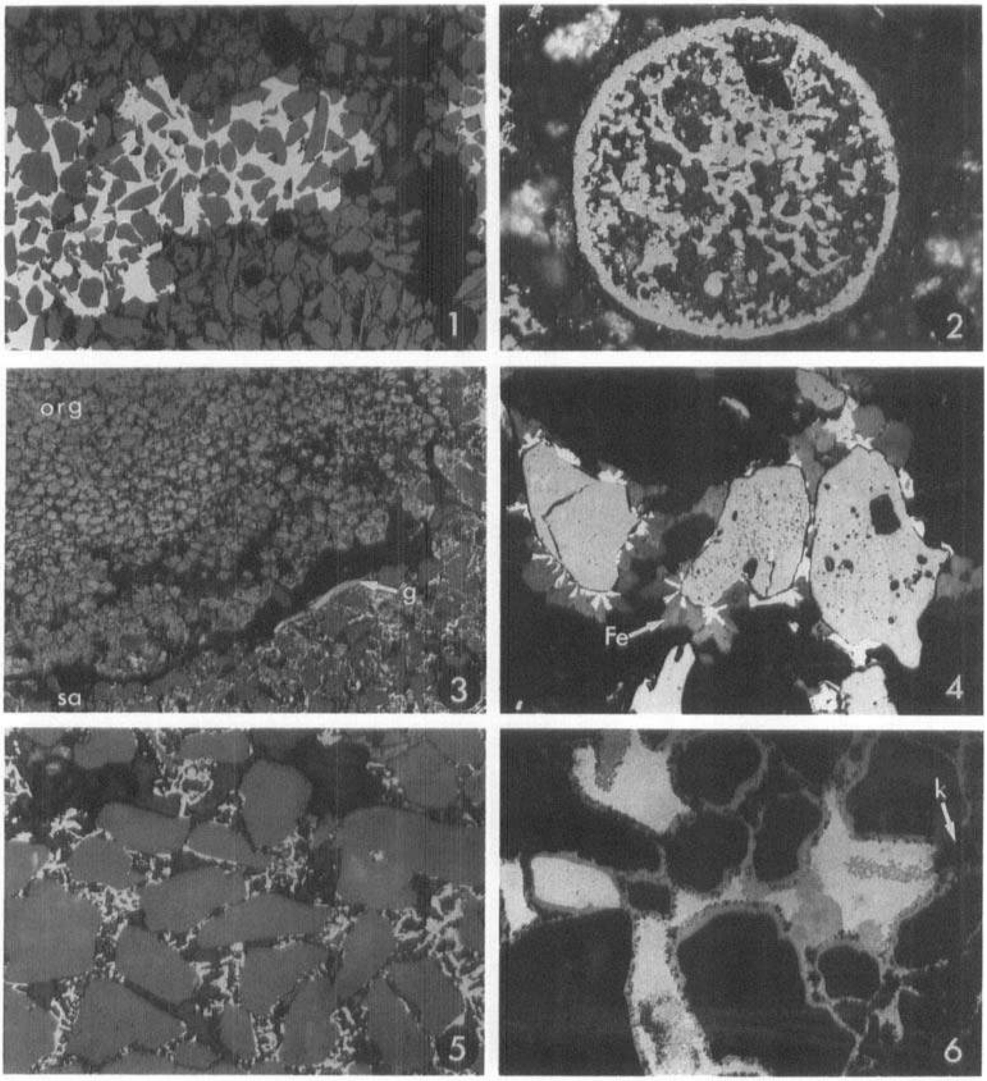

Fig. 11-15. Ferruginized sandstone. 1. Ferruginization front of ferric-hydroxide in sandstone. Quartz crystals are strongly corroded (also in parts of the barren sandstone). Normal objective; length of the mineralized zone is 220 μm. Hilltop iron layer. 2. Organic material incompletely replaced by goethite. Foothill iron layer. 3. Inclusion of organic material (*org*) is ferruginized by goethite and is embedded in ferruginized sandstone (*sa*); (*g* = graphite). Reflected light; normal objective; length of the graphite crystal is 0.6 mm. Groundfloor iron layer. 4. The cement of the sandstone containing leached ilmenite was partially replaced by ferric-hydroxide (*Fe*), which was subsequently partially transformed to hematite. The star-like arrangement reflects the original orientation of the goethite crystals. Groundfloor iron layer. 5. Quartz grains in kaolinitic cement, which was partially replaced by ferric-hydroxide. This hydroxide was transformed into hematite. Reflected light; normal objective; length of the longer edge of the photo is 3.2 mm. Groundfloor iron layer. 6. The cement of the sandstone consists dominantly of cryptomelane (white) with subordinate goethite (grey) or kaolinite (*k*), representing the primary cement. Hilltop iron layer.

exclusively of manganese minerals (e.g., cryptomelane and pyrolusite). In this association, quartz grains are also corroded and/or decomposed (Photo 6 of Fig. 11-14), indicating that manganese-bearing solutions are obviously much more aggressive to quartz than iron-rich ones. In rare cases, corroded quartz–grain boundaries occur in association with ferric-hydroxides. In the immediate neighborhood of these ferruginized sandstones, barren sandstone also contains corroded quartz grains, which are embedded in the original cement. Thus, this corrosion process, of unknown origin, is older, predating the ferruginization process (Photo 1 of Fig. 11-15).

Organic substances are frequently also found in the sandstone. They generally are pseudomorphously replaced by ferric-hydroxides (Photo 2 and 3 of Fig. 11-15).

Origin of iron layers

Foothill iron layers

The genetic development of the foothill iron layers was observed at an exposure in the El-Ris area. Several foothill iron layers (having a thickness varying from 20 to 50 cm) are interbedded with barren sandstones. At the base of such an iron-mineralized layer, intercalations of clay or silt with efflorescences of gypsum and anhydrite were found. Sandstone layers showing ferruginization on one side of an outcrop can be traced continuously along a horizontal distance of about 6 to 8 m towards the opposite side. Thereafter, no trace of ferruginization is observed in their lateral extensions. Compared with the neighboring sandstone, it appears to be heavily bleached. Thus, ferruginization is stratabound and projects tongue-like into the sandstone layer. Ferruginization is limited to those parts of the sandstone that are porous and are underlain by either a less porous sandstone or by an impervious horizon like silt (Fig. 11-16).

In nearly all sandstone samples, remains of plant material as well as various concentrations of bituminous substances were found. It is known that in the presence of rain water percolating through the sedimentary rock, the organic material decomposes, resulting in reducing conditions. Under these conditions, iron and manganese are dissolved predominantly from decomposing ilmenite, leaving behind an enrichment of immobile titanium in the form of leucoxene. Evidently, iron has also been derived from magnetite.

The above-mentioned iron- and manganese-bearing solutions of meteoric water-origin penetrate the sandstone, and move downwards by gravity. If an impervious layer is encountered by these solutions, their downward movement is changed into a lateral one. When sandstone, underlain by an impervious horizon, is exposed to atmospheric oxygen, the percolated solutions encounter an oxidation barrier (Perelman, 1972), along which iron and manganese become immobile and precipitate. The oxidation barrier penetrates into the sandstone in a tongue-like form (Fig. 11-16).

Hilltop iron layers

The residual hills are nearly always covered with ferruginized caps. At the center of the hilltop, where iron mineralization is less thick, barren parts are visible as a result of deep erosion. Intensive ferruginization is found at the outer zones of these

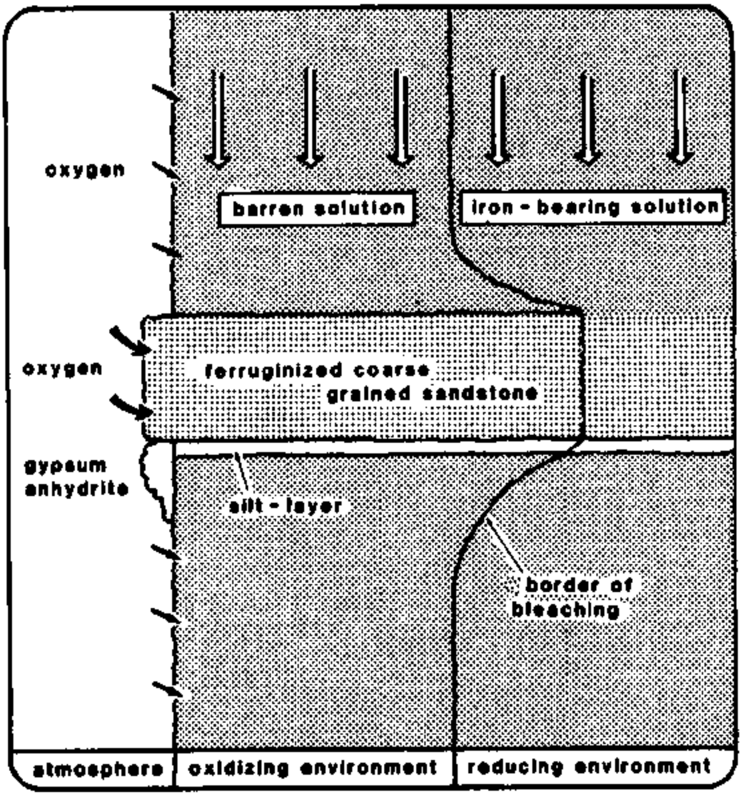

Fig. 11-16. Stratabound ferruginization of coarse-grained sandstone. Precipitation of iron, transported in reducing solution, is caused by the penetration of oxygen of the air into the sandstone.

hills. The hilltop layers thus do not represent continuous ferruginized horizons, but rather are arranged concentrically around the peaks. Hence, they should be classified along with the foothill layers, as stratabound oxidation products. It is, thus, concluded that there has never been a continuous ferruginized cover in the depression. Iron-rich layers could only have been formed in oxidizing environments.

A definite correlation exists between the formation of iron layers and tectonics. In the crestal area, fractures apparently developed during the formation of anticlines. Along these fractures, the atmospheric oxygen migrated to the deeper horizons of the sandstone (Fig. 11-17). The formation of fractures did not only facilitate the movement of supergene solutions, but also increased the amount of solution in the beds, resulting in effective leaching and greater concentration of precipitated iron. Both the solubility and the resultant strong leaching of iron and manganese would have been favored by the mildly acidic solutions of the reducing environments. Oxidation barriers alone, therefore, would probably not be sufficient to explain the formation of such large amounts of iron in the hilltop layers. In addition to oxidation, a process of evaporation (Perelman, 1972) appears to have been of equal importance in the precipitation of iron and manganese close to the outcrop (Fig. 11-17). This

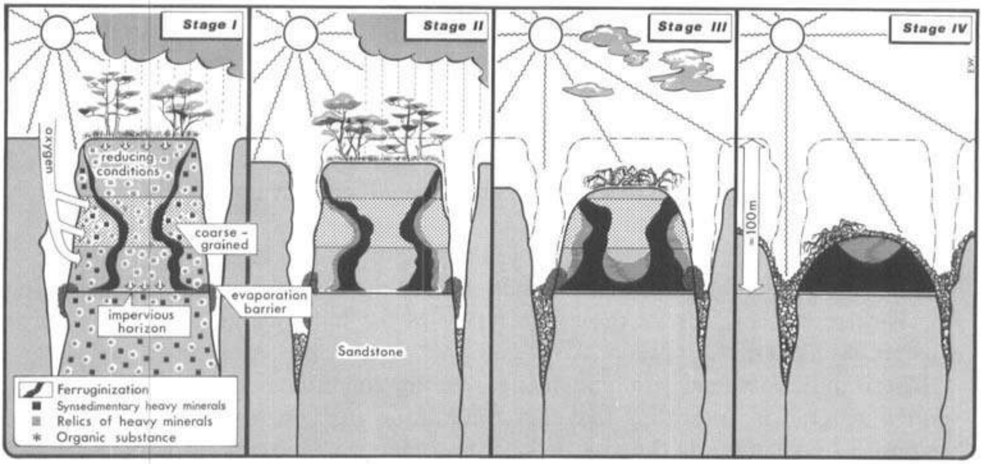

Fig. 11-17. Geologic-genetic development of residual hills (hilltop iron layers) presented in four stages, from stage I [beginning of iron (and/or manganese) impregnation of sandstone along oxidation barriers and subordinate along evaporation barriers] to stage IV (formation of residual hills after the process of ferruginization). Sandstones of stage II–IV are presented in a simplified manner, leaving out the heavy minerals, their relics, and the organic material.

is supported not only by the presence of gypsum-bearing outcrops in close spatial relationship with ferruginized bodies, but also by sandstone that has exclusively been mineralized by stalactite-like manganese precipitates.

Thus, in addition to a conducive lithology (porous rocks) and tectonics (deep fractures), the strong impregnation of sandstone required humid periods characterized by rapid rates of precipitation as well as warm-humid periods during which vegetation could develop and flourish. This resulted in a soil cover. Just like the organic substances already present in sandstones, the soil cover might also have contributed to the development of reducing conditions in the supergene solutions penetrating into the sandstones.

Comparison of different types of iron layers

Regarding the distribution of the detrital (e.g., syngenetic) and newly-formed (e.g., epigenetic–diagenetic) hydroxide–oxide minerals, there are no differences between the three types of iron layers (hilltop, foothill, and groundfloor iron layers; Fig. 11-12).

Both the groundfloor and the foothill layers, however, are different from the hilltop one in the following respects:

(1) quartz grains are usually larger and poorly sorted;
(2) the iron layer is much thinner (generally less than 1 m);
(3) the iron content is lower (about 12% by weight); and
(4) goethite has largely been replaced by hematite (Photos 4 and 5 of Fig. 11-15). The transformation of goethite into hematite is well-known in red beds, imparting the characteristic red color to sandstones.

Berner (1969) has shown a minimum temperature of 40°C to be sufficient for the formation of hematite by dehydration of ferric-hydroxides. As an indication of their higher iron concentration and of the fact that there is hardly any transformation of goethite into hematite, the hilltop iron layers exhibit a brown to dark-brown color. The transformation of ferric-hydroxides into hematite seems to be restricted to porous iron-rich sandstone layers that are less thick than the hilltop iron layer. Groundfloor and foothill iron layers are, thus, generally red-colored.

(5) There are more ilmenite grains remaining unaltered; and finally

(6) graphite is found both in the groundfloor and the foothill iron layers, thus being characteristic of both of these two types. In the hilltop iron layers, graphite is exceptionally rare.

These differences suggest modifications in the conditions of formation and subsequent alteration, indicating that the composition (e.g., in respect to the graphite content) of sandstones in the two, presumably older, iron layers is variable.

It was impossible to reconstruct the *genesis of the groundfloor iron layers* because of the absence of outcrops. They exist only as plate-like formations loosely lying adjacent to each other on the base of the oasis. The genesis of the groundfloor iron layer may be viewed differently, however, in that: the iron originated from the ground water which was moved to the surface by capillary action. Close to the surface, the water evaporated, with ferric hydroxides precipitating. The mutual arrangement of quartz grains and newly-formed hydroxides in the groundfloor iron layers is indistinguishable from that of the foothill and hilltop iron layers.

Geochemical analyses

Analyses were made of 14 ferruginized sandstone samples collected exclusively from the hilltop iron layers (Fig. 11-10). The Fe content varies (except for one sample (3) with 35.1% by weight; Table 11-2) between 14 and 27% by weight, with an average of 19.2. In all samples [with the exception of sample (3)], $Fe(OH)_3$ and goethite clearly dominate in contrast to lepidocrocite. In sample (3) only lepidocrocite is present. Owing to its strong replacement behavior towards quartz, resulting in increasing the size of voids between neighboring quartz grains, the iron content of this sample is very high.

In the samples with low manganese concentration, varying from 215 to 600 ppm, there is no manganese mineral. As a component of groutite (MnOOH), manganese has been incorporated into the lattice of goethite by isomorphic substitution. When the manganese content exceeds 1000 ppm, however, manganese occurs as cryptomelane and/or pyrolusite in addition to ferric hydroxides (Photo 6 of Fig. 11-15). The minor elements in the sandstone are reflected by the accessory minerals, and do not correlate with the secondary iron (and manganese) mineralization (Table 11-2). The presence of elements that are part of two overlapping parageneses may explain the reason why their element concentrations do not correlate. Whereas most minor elements are linked to the presence of heavy minerals, the concentration of iron and manganese depends on the pore volume previously existing in a sandstone, the type of cement (e.g., kaolin and quartz), the type of replacing mineral (e.g., goethite, lepidocrocite, and cryptomelane), the iron and manganese concentrations in circulating waters, and on the mechanism of their precipitation.

Sequence of events and age relationships

The events leading to the development of ferruginization of sandstone may be outlined in chronological order as follows:

(1) deposition of terrestrial–fluviatile sandstone with argillaceous–silty horizons and glauconite intercalations (e.g., Bahariya Formation);
(2) development of an extensive vegetation cover in a warm-humid climate;
(3) development of a reducing and mildly acidic environment in the substrata by decomposition of organic substances;
(4) mobilization of iron and manganese from heavy minerals (e.g., ilmenite and magnetite) present in barren sandstone;
(5) formation of anticlines resulting in the formation of extension joints in the crestal area, thus providing access for meteoric water and oxygen to deeper parts of the sandstone;
(6) precipitation of iron and manganese at oxidation barriers, mostly localized at impervious horizons, i.e., associated with iron-rich solutions of supergene character; and
(7) formation of residual hills by erosion of sandstone, with the ferruginized parts largely resisting weathering.

All of the sandstones belonging to the Bahariya Formation are of Cenomanian age. Thus, ferruginization could have taken place after that time. Since the depression came into existence during the Oligocene time (by erosion), the iron layers must have existed at that time. The facies formed during the Eocene were mainly marine, thus precluding them from the period of origin of these layers. During the Eocene time, the so-called Plateau-Limestone was formed in the Bahariya Oasis (Dominik, 1985). Consequently, it follows that the ferruginization originated between the Cenomanian and the Lower Middle Eocene times (i.e., the oldest unit of the Plateau-Limestone). Most probably, the transition period from the Cretaceous to the Tertiary time represents the period of ferruginization, with the anticlines developing at the same time. Furthermore, the large stratigraphic gap between the Turonian and the Paleocene, with the exception of the Campanian (Dominik, 1985), is characterized by a period of terrestrial conditions lasting long enough for a dense vegetation to develop. The depositional conditions favoring ferruginization of sandstones seem to be identical to those existing during this stratigraphic gap. That the period of the formation of ferruginized layers is pre-Eocene, as established above, is supported by the presence of isolated outcrops of ferruginized layers covered by the Eocene iron ores of submarine, hydrothermal, synsedimentary origin at Djebel El Ghorabi.

Discussion and comparison with other models

The following discussion only refers to ancient red beds and to those linked to consolidated sandstones and mudstones. In the ferruginization model, organic material is of great importance to permit mobilization of iron and manganese originally present within the barren sandstones in the form of heavy minerals. Infiltrating rainwaters caused the decomposition of organic material that resulted in a reducing environment in which iron and manganese became mobile. Precipitation occurred at an oxidation front, with iron being precipitated. In this process, the mineralization and the replacement fronts penetrate into the porous rock in a rollfront-like manner. Uparching caused by tectonic changes and the formation of fractures in an anticline enabled iron to become relatively highly enriched. The iron concentration is significantly greater in comparison to the other red beds (as indicated by comparing the Tables 11-1 and 11-2).

The processes of migration and precipitation may possibly be more complicated than described above. This can be illustrated using the detrital chromite present in these sandstones, which is usually an inert mineral. Chromite shows in its outer part a rim in which the chromium depletion is obvious as a result of leaching. The chromium was enriched in altered ilmenite and particularly in its strongly leached variety, ranging from 0.15 to 2.02% by weight Cr_2O_3. Such enrichment takes place along shrinkage cracks of leucoxene.

Both the mobilization of chromium from chromite and Cr-enrichment in leucoxene cannot simply be explained by repeated changes in Eh and pH. Possibly, chromium was dissolved as an organometallic complex; thus, an analogous mechanism of mobilization can then be assumed for other metals as well.

In conclusion, the diagenetic and detrital/postdepositional models have various aspects in common: both models involve the modification of synsedimentary material which is of bimodal origin (Table 11-3). In the ferruginization model, the iron was mobilized postdiagenetically from decomposing detrital oxides (e.g., ilmenite and magnetite) under reducing conditions. Iron was precipitated along the oxidation fronts. The most significant features of the three models are summarized in Table 11-3. The diagenetic model of Folk (1976) is not presented in this table, because there is no progressive development of the pigmenting material after sedimentation. In each of the three models (shown in Table 11-3), a clay cement with finely disseminated ferric-hydroxides and/or hematite are formed as an end-product. The origin and formation of this clay–hematite mixture can be summarized as follows:

(1) In the detrital/postdepositional model, lateritic material [a mixture of clay and iron hydroxide, which was subsequently (postdepositional) altered into hematite] was incorporated into the newly-formed cement during diagenesis. Lateritic material was also present as detrital heavy minerals, which decomposed to hematite prior to diagenesis via a ferric-hydroxide stage.

(2) In the diagenetic model, an early diagenetic alteration of infiltrated iron-bearing clay took place, followed by a late-diagenetic replacement of detrital hornblende and biotite by clay and hematite (ferric-hydroxide).

(3) In the ferruginization model, the postdiagenetic replacement of the clay cement in the sandstone by ferric-hydroxides occurred, which subsequently were altered to hematite by dehydration. In cases of incomplete ferruginization, clay relics are present together with ferric-hydroxides (and hematite).

Further investigations have to determine whether one or all of these three models

TABLE 11-3

Comparison of characteristic features of the three models leading to the formation of the pigmenting hematite

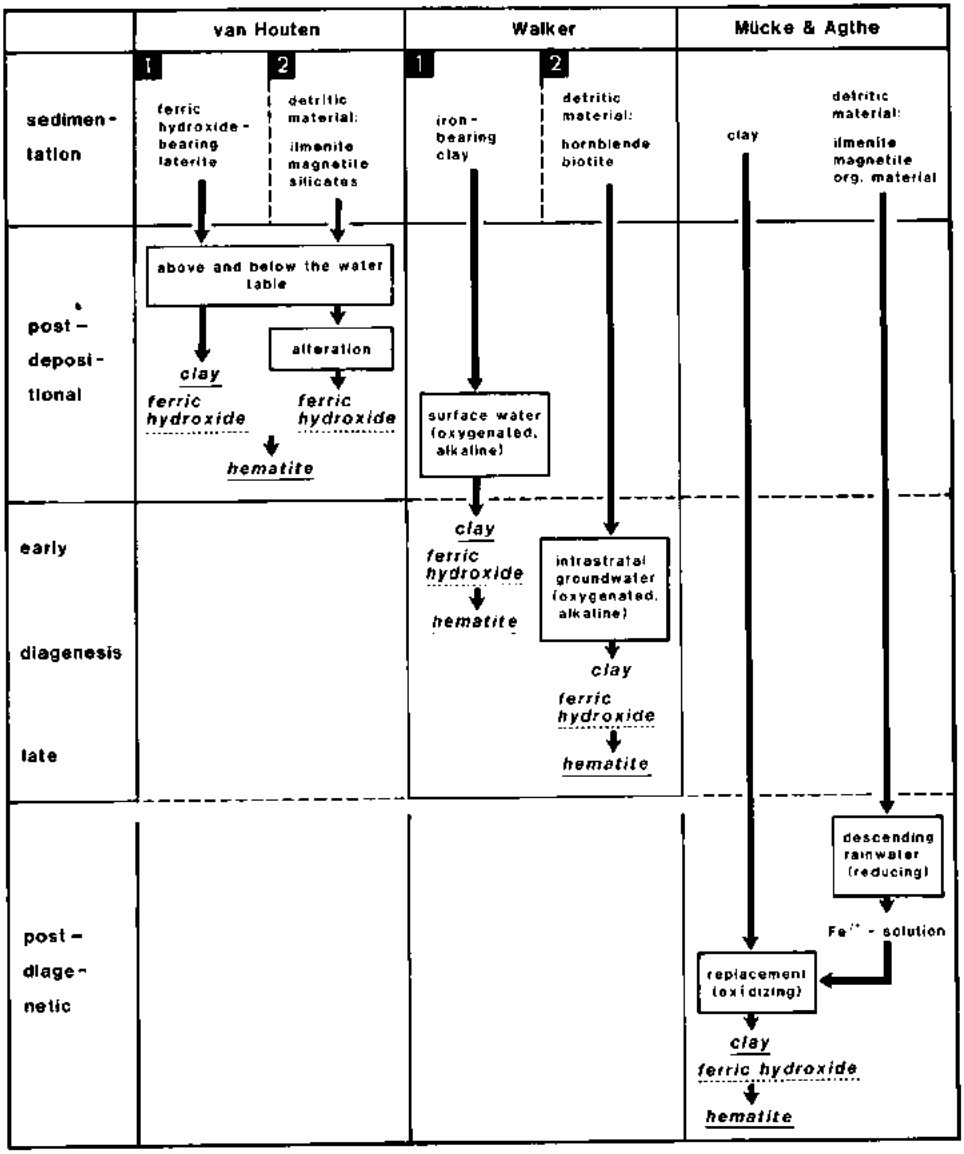

do, in fact, explain all observations, or whether the models merely represent different interpretations of the same data. Additional efforts will be required, which should, above all, include examinations in reflected light combined with microprobe analyses, and perhaps other techniques.

PART II. POSTDIAGENETIC FERRUGINIZATION OF PHANEROZOIC (OOLITIC) IRONSTONES: A CONTRIBUTION TO THEIR GENESES

INTRODUCTION

Phanerozoic ironstones have been the subject of scientific research for over 130 years. Initially, they were studied from the economic point of view, because of the worldwide mining operations. Because of their low iron content, exploitation of these ores has mostly been discontinued during the last 30 years. Although oolitic ironstones have always been investigated, scientific interest has been revived in recent years on a broader scale. Genetic and facies-analytical questions concerning these deposits have triggered this renewed interest, as exemplified by, for example, international congresses dealing exclusively with Phanerozoic ironstones (Young and Taylor, 1989; Odin, 1988), as well as reviews devoted to this subject (e.g., Wopfner and Schwarzmann, 1976).

In oolitic ironstones, even more than in red beds, the scientific interest is concentrated on the opaque minerals. Just as is the case with red beds, however, combined ore-microscopy and microprobe analyses are generally lacking. Thus, microscopic and micro-analytical investigations are discussed here. Particular attention is given to aspects related to secondary processes of mineralization.

A short introduction summarizes the development of Phanerozoic ironstone, which necessarily includes some references to the processes of diagenesis. The latter are a prerequisite for understanding postdiagenetic ferruginization.

Although a number of genetic models are available for this type of mineralization, none have as yet received general acceptance (see Berg, 1921; Hemingway, 1951; Borchert, 1952; Petranek, 1964; Petranek et al., 1988; Urban, 1966; Schellmann, 1969; Kolbe, 1970; Bubenicek, 1968, 1971; Adeleye, 1973; Siehl and Thein, 1978, 1989; Gygi, 1981; Battacharyya, 1980, 1989; van Houten and Battacharyya, 1982; Young, 1989; Harder, 1951, 1989; Doering, 1990). Almost all the models are based on a common assumption, i.e., that all material present is of synsedimentary origin and has been altered diagenetically after sedimentation (e.g., Schiavon, 1988; Williams and Owen, 1990; van Houten, 1990).

In general, mineralization of the Phanerozoic ironstones has the following features in common:

(1) comparable geologic setting;
(2) sedimentation in a marine environment;
(3) intercalations of sandstones, siltstones, claystones and limestones, in addition to repetitive horizons of iron mineralization, indicating frequent repetition of transgressions and regressions;

(4) similar mineralogy and structure of the iron-rich horizons; and
(5) the occurrence of ooids in iron-rich strata.

These features indicate a similar history of formation for all occurrences. To some extent, however, local differences and variations do exist. To provide a broad base of information, samples have been collected from various deposits and a total of more than 500 polished sections were studied. The localities sampled are: Minette ore from Luxembourg and France; oolitic iron ore from the Salzgitter area, Niedersachsen, Kressberg, Oberbayern and Schmiedefeld, Thüringen, Germany; Aswan, Bahariya Oasis, Kalabscha, Egypt; Wadi Halfa, Sudan; the Prague Basin, Czech Republic; Wales (localities such as Betws Garmon, Pen-y-Gear, Nant Ffrancon, and Tremadoc), United Kingdom; Agbaja, Mount Patti, Doko area, Niger Basin, Sokoto, Iullemmeden Basin, Potiskum, Chad Basin, Nigeria; Les Baux, France; Larymna, Greece; and Seydisehir, Turkey.

Development of oolitic ironstone: sedimentation and diagenesis

The initial material of oolitic ironstone is derived from the weathering of various rocks in the hinterland under lateritic conditions and subsequently transported into the marine basins via fluvial drainage systems. In these basins, unlithified sediments were formed consisting of three constituents:

(1) Ooids and peloids formed in agitated water. Ooids (usually with a nucleus and concentrically laminated) and peloids (without a nucleus and usually larger than ooids, showing a marked mammillary structure only at the periphery) dominate in these sediments.

(2) Detritus comprising quartz, biotite, muscovite, baryte, apatite, graphite, and heavy minerals, such as ilmenite, magnetite, rutile, zircon, monazite and chromite. In addition, fossils (mainly calcareous) and bituminous substances are present.

(3) Suspension-derived fine-grained material forming the matrix of the ooids, peloids, and detritus.

Matrix, ooids, and peloids originally consisted of clay minerals containing adsorbed $Fe(OH)_3$ and/or FeOOH on their surfaces (van Houten, 1973; Lemoalle and Dupont, 1973).

Subsequent diagenesis[1] affects the mineralogy and texture rather than the structure of the deposits: at the *phyllomorphic stage* (Dapples, 1967), taking place under reducing conditions (caused by decomposing organic substances), the iron-bearing clay minerals are transformed mainly into chamosite (berthierine)[2]. As a result of the loss of water during diagenesis, shrinkage cracks developed in ooids as well as in

---

[1] The reason that the term diagenesis is preferred to submarine weathering is that these postsedimentary alterations took place in the presence of abundant organic material (Berner, 1981). This follows accepted practice in the literature.

[2] Differentiation of whether the chemically investigated sheet silicate has a 14-Å structure (chamosite) or a 7-Å structure (berthierine) by X-ray methods was not undertaken. Compositionally, chamosite and berthierine are identical. The Mg content of chamosite must have been partly extracted from the seawater.

TABLE 11-4

Composition of carbonate solid solutions of dog-tooth shaped single crystals (I–V) and of coarse-grained cement (VI and VII) in weight and mole percent

	I	II	III	IV	V	VI	VII
FeO	47.61	48.48	48.17	54.55	50.89	53.50	54.17
MgO	5.13	5.55	5.04	–	3.65	4.13	3.55
CaO	6.69	5.55	5.17	5.35	4.99	2.51	2.81
MnO	0.33	0.40	1.24	1.42	1.32	0.20	–
TiO_2	0.23	0.11	–	–	–	–	–
$CO_{2(calc)}$	40.36	40.15	39.84	38.50	39.87	39.34	39.24
	100.35	100.24	99.46	99.82	100.72	100.08	99.77
Siderite	72.5	74.0	74.1	86.8	78.1	83.2	84.5
Magnesite	14.0	15.1	13.8	–	10.0	11.5	9.9
Calcite	13.0	10.8	10.2	10.9	9.8	5.0	5.6
Rhodochrosite	0.5	0.6	1.9	2.3	2.1	0.3	–

I–III = Konrad Schacht, Salzgitter, Germany; IV and V = Minette, France; VI = Nusice, Czech Republic, VII = Zdice, Czech Republic.

peloids leading to the formation of cavities. In the ooids, the cracks are tangentially oriented, whereas in peloids they exhibit a rather irregular arrangement. These cracks vary from about 1–2 μm (Photo 6 of Fig. 11-22) to about 15 μm in width (Photo 3 of Fig. 11-22). The cementing material, which has also been subjected to diagenetic alteration, also consists generally of berthierine (chamosite), but additional glauconite, kaolinite and illite may occur.

In the redoxomorphic stage (Dapples, 1967), following the phyllomorphic stage, porphyroblastic growth occurs, with pyrite (Photo 1 in Fig. 11-18) and marcasite being formed in the presence of organic substances. Pyrite may also be present as framboids. Additional new features of this stage are siderite-rich carbonate solid solutions (Table 11-4). In oolitic ironstones of Cretaceous to Tertiary age, siderite generally occurs as dog-tooth, i.e., euhedral-shaped single crystals which are finely distributed in the chamositic cement (Photo 2 in Fig. 11-18). In the Ordovician deposits, on the other hand, siderite may occur as cement replacing the chamositic ooids (Photo 3 of Fig. 11-18).

Apart from the iron of the siderite-rich Ordovician deposits, the iron of the other sediments is fixed in sheet silicates (e.g., berthierine and chamosite). Thus, the iron content cannot, as a rule, exceed the maximum Fe-content fixed in the lattice of chamosite (berthierine) (normally in the range of 30–40% by weight FeO). These are uneconomic and, therefore, identical to the so-called protore. The protore is characterized by a number of distinctive features:

(1) protore exhibits high porosity and a marked permeability to migrating waters;
(2) owing to the small grain size of sheet silicates, there is a fairly large intragranular space (and mineral-surface area) available to migrating waters; and
(3) due to the mineral association developed under reducing conditions (during diagenesis), the protore is unstable in an oxidizing environment.

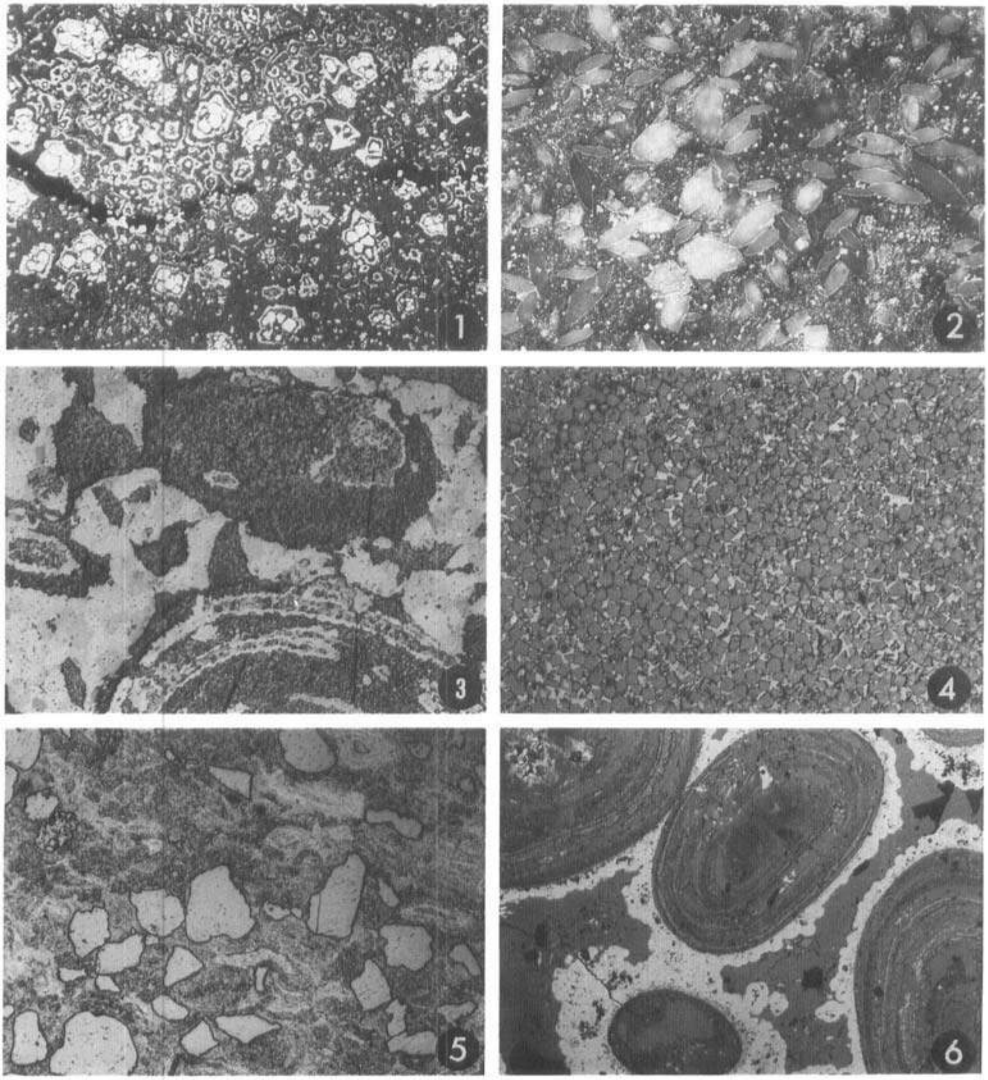

Fig. 11-18. Phanerozoic ironstones. 1. Framboidal to idiomorphic pyrite in chamositic cement. Salzgitter, Germany. 2. Dog-tooth-shaped porphyroblastic siderite in chamositic cement, showing the beginning of ferruginization along the siderite grain boundaries. Salzgitter, Germany. 3. Both chamositic ooids and chamositic cement replaced by siderite of diagenetic origin. Schmiedefeld, Thüringen, Germany; coarse-oolitic ore type; second deposit. 4. Idiomorphic pyrite porphyroblasts replaced by ferric-hydroxide are embedded in a cement consisting of hematite. Aswan, Egypt. 5. Corroded quartz grains in incompletely ferruginized (ferric-hydroxide) chamositic cement. Reflected light; normal objective; length of the longer edge of the photo is 3.2 mm. Aswan, Egypt. 6. Replacement by ferric-hydroxide affects the cement along grain boundaries of the ooids. Reflected light; normal objective; length of the longer edge of the photo is 3.2 mm. Bahariya Oasis, Western Desert, Egypt.

The protores, therefore, are most easily permeated by aqueous solutions (of unknown age) under continental conditions.

FERRUGINIZATION OF OOLITIC IRONSTONE

Postdiagenetic ferruginization results in a marked enrichment in iron, generally leading to concentrations of 60–70% by weight and rarely 80–90% Fe_2O_3 of the original sediment (= protore). This is common of the oolitic ironstone deposits investigated, except those of Ordovician age (e.g., the deposits of Thüringen, Germany, Wales, United Kingdom, and of the Prague Basin, Czech Republic).

This secondary alteration, which is unrelated to the lateritic processes, is the consequence of descending meteoric waters that cause oxidation. In the upper sequences, with abundant mudstones, both pyrite/marcasite and organic substances are widespread and common. The oxidizing descending fluids decompose the sulfide minerals, thus generating an acidic environment. Observations and interpretations of the writers are in full agreement with those of van Houten and Arthur (1989), who generally found black shales and mudstones in the stratigraphic sequences of Phanerozoic ironstones, with the mudstones being either rich in organic carbon or rich in pyrite with some subordinate organic matter. In each of the deposits studied, pyrite was particularly important with respect to secondary iron mobilization (Doering, 1990).

In secondarily-altered rocks, iron occurs as pseudomorphs of ferric-hydroxides after pyrite (Photo 4 of Fig. 11-18) and/or marcasite, but as pyrite (and/or marcasite) in rocks that were not subjected to secondary ferruginization. The latter rocks are usually green or grey in color, whereas the former are yellow or reddish-brown.

Iron-bearing descending acid solutions derived their iron from the upper sequences of chamosite-containing sediments. This leaching resulted in the bleaching of these rocks (Fig. 11-19). These solutions penetrated into the underlying sediments, decomposing fresh chamosite and leading to alkaline conditions which caused the precipitation of iron. The alkalinity is evidenced by the corroded quartz grains (Photo 5 of Fig. 11-18).

Ferruginization advanced through the permeable sediment in a roll-front-like manner (a feature so well-described by researchers of sandstone-hosted uranium deposits). As iron is deposited, other elements are dissolved. These are mainly Al, Si and Mg, which migrate ahead of the mineralization front (Fig. 11-20).

The above model is supported by replacement textures observed in reflected light. The intensity of the ferruginization of both cement and ooids varies considerably: some parts of the rocks are completely altered, whereas other parts show only little or no alteration (e.g., the Ordovician deposits). To quantify the degree of ferruginization, the replacements have subsequently been studied by microprobe analysis.

Ferruginization of cement

The ferruginization of cement may either occur along grain boundaries between ooids and cement (Photo 6 of Figure 11-18), or it may affect the chamositic cement at

Fig. 11-19. Ferric-hydroxide-pigmented bioturbated sediment (lower part), which is bleached by descending acid solutions with dissolution of iron (upper part). Aswan, Egypt.

first in a patchy manner but eventually involving all of the cement (Photo 1 of Figure 11-22). Figure 11-21 is a graph of the analyses of the patchy ferruginization which are summarized in Table 11-5. Stage 1 corresponds to the secondarily-oxidized chamosite, the bulk-chemical composition remaining largely constant. Oxidized chamosite is free of newly-formed hematite. The oxidation becomes visible under crossed polars in reflected light, where brown to yellow internal reflections occur. These are green in unaltered chamosite. Passing through an intermediate stage (stage 2; recognizable from its medium reflectivity), chamosite is altered to SiO_2- and Al_2O_3-rich and MgO-bearing ferric-hydroxide (stage 3; with the highest reflectivity).

With Fe-hydroxides being dehydrated, pseudomorphs of hematite are formed (Photo 2 of Fig. 11-22). Hematite can also develop directly, however, usually as thin-platy crystals, occurring preferentially in kaolinitic cement or in cavities (Photo 3 of Fig. 11-22).

Some authors have proposed that ferric-hydroxide and/or hematite are the products solely of oxidation of berthierine (chamosite) (e.g., see Foos, 1983). If that is accepted, Maynard (1986) assumed that Si and Mg must be mobile, concluding that newly-formed ferric-hydroxide should be rich in Al, on the one hand, but be largely depleted of Si and Mg, on the other. As the ferric-hydroxide analyzed by Maynard always had high quantities of both Al and Si, however, he ruled out oxidation as the cause of alteration. But Maynard's (1986) interpretation cannot be fully accepted: excluding any diffusion process, the low temperature involved suggests that iron mobilization must be related to leaching (Fig. 11-1). Ferric-hydroxide, therefore, is not a product of chamosite oxidation only.

Most of the Si and Al high contents in ferric-hydroxide (Fig. 11-21, stage 3, and Fig. 11-23, stage 5) is attributable to kaolinite (in addition to goethite, X-ray diffractograms always show major kaolinite reflections; Doering, 1990). The newly-formed submicroscopically-sized kaolinite (by decomposition of chamosite)

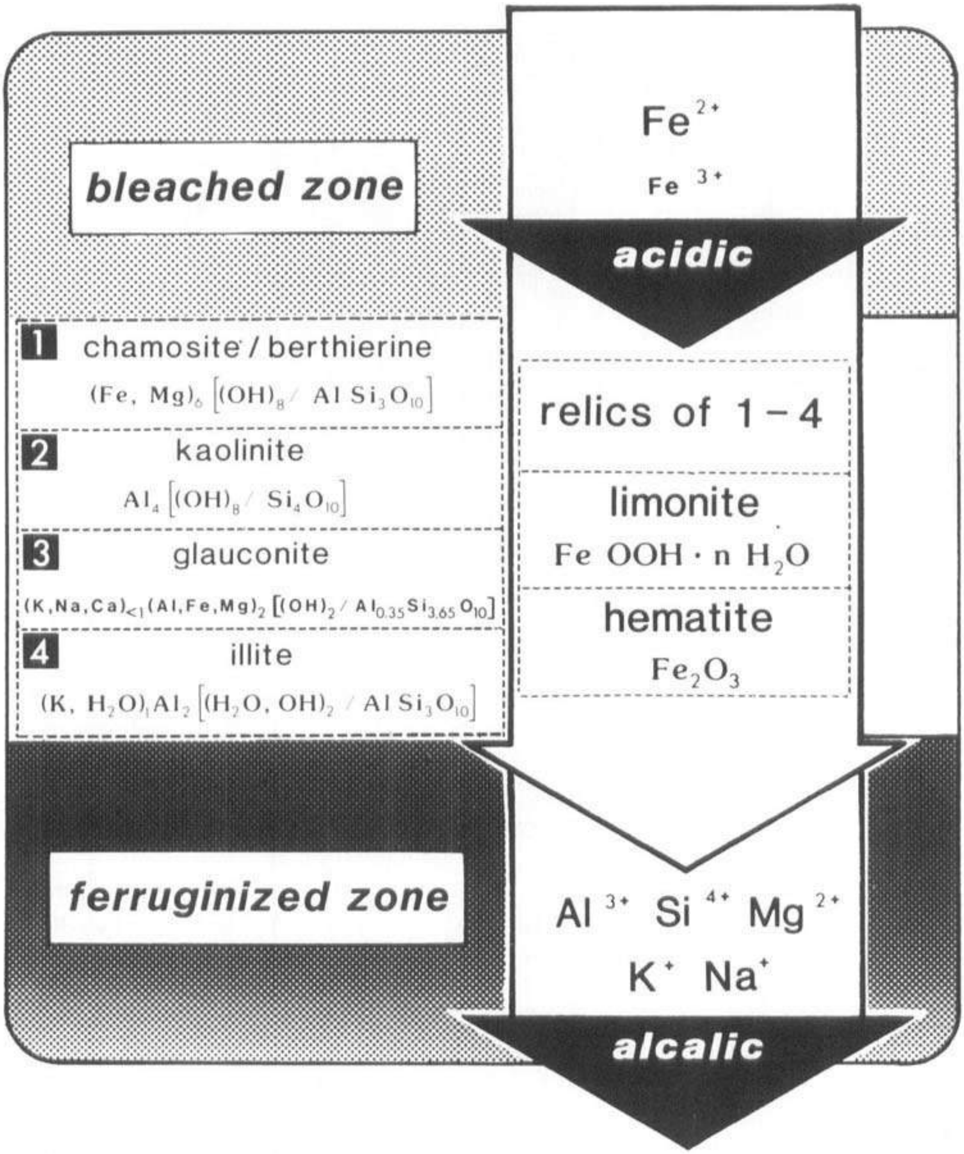

Fig. 11-20. Diagram of the replacement process of the pre-existing sheet silicates (1–4) by acidic Fe-bearing solutions resulting in newly-formed iron minerals and the newly-composed solution after the process of ferruginization.

was incorporated in situ into ferric-hydroxide (Doering, 1990). During dehydration of the Al-, Si- and Mg-bearing ferric-hydroxide, Al and Si were partially incorporated into the newly-formed hematite. Mg could not be detected in the latter, whereas Al_2O_3 and SiO_2 values reach a maximum of about 3% by weight.

TABLE 11-5

Different stages of cement ferruginization (II and III)

	I	II	III
FeO	23.72	50.32	67.83
Fe_2O_3	26.36	55.93	75.39
FeO	23.72	–	–
Fe_2O_3	–	–	34.85
FeOOH	–	62.23	45.10
MgO	7.27	2.69	1.18
MnO	0.15	0.20	–
Na_2O	0.41	1.89	0.31
K_2O	0.55	–	0.10
CaO	0.83	0.75	0.77
Al_2O_3	23.10	15.46	7.78
SiO_2	32.66	15.26	9.91
$H_2O_{(calc)}$	8.67		
	97.36	98.48	100.00
Fe^{2+}	2.131	6.000	
Mg	1.164		
Mn	0.014		
Na	0.085		
K	0.076		
Ca	0.096		
Al	2.434		
Si	3.509	4.000	
Al	0.491		
OH	6.218	8.000	
O	1.782		
O		10.000	

I = fresh chamosite (Aswan, Egypt).
Total Fe was determined as FeO (in Fig. 11-21 this was presented as Fe_2O_3; see above the line). Fe_2O_3 and FeOOH (under the line) are calculated as components of the analyses.

Ferruginization of ooids

Proof of ferruginization is of particular importance in the controversial discussion of ooid genesis. In the occurrences studied, a number of ooids of different compositions have been observed. Although these may, in part, be monomineralic, they are usually polymineralic. Common types of ooids (peloids) consist of:

- chamosite
- kaolinite
- chamosite + kaolinite
- chamosite + ferric-hydroxides

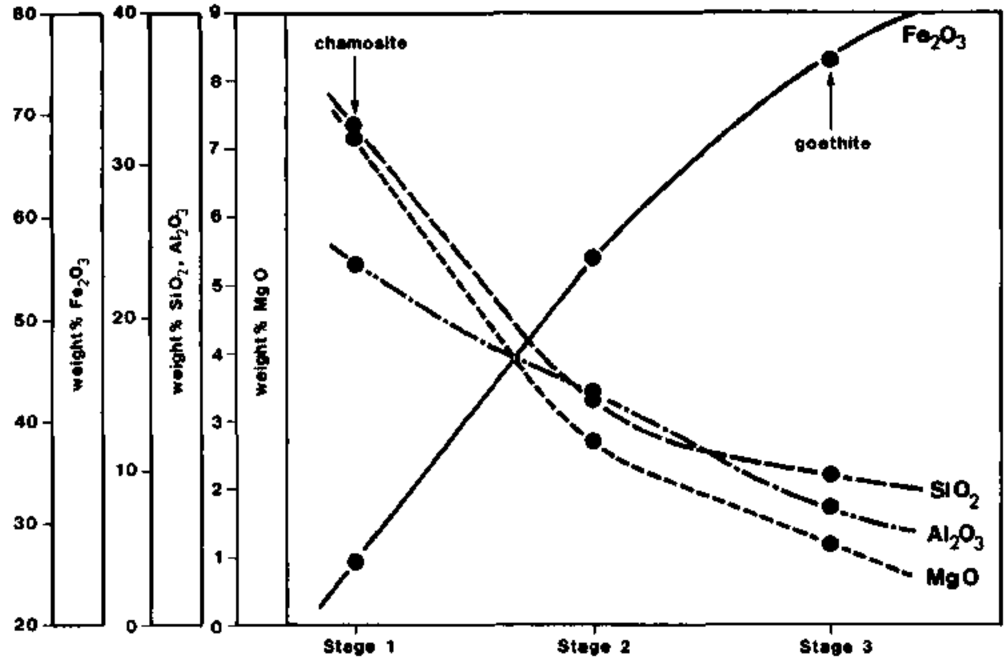

Fig. 11-21. Element distribution in chamositic cement during different stages of ferruginization (stage 1: fresh chamosite; stage 3: final stage of replacement). Aswan, Egypt.

- chamosite + ferric-hydroxides + hematite
- chamosite + hematite
- kaolinite + ferric-hydroxides
- kaolinite + ferric-hydroxides + hematite
- kaolinite + hematite
- ferric-hydroxides
- ferric-hydroxides + hematite
- hematite.

Carbonate and apatite are also occasional constituents of ooids. This multitude of ooid types resulted in a correspondingly large number of genetic hypotheses.

Almost all authors erroneously assume that genetic aspects of the mineralogy (e.g., the formation of FeOOH) and textures of ooids, as they are observed today, are the result of sedimentation and subsequent diagenesis. For this reason, complex mechanisms are frequently postulated to be responsible for their generation (see Berg, 1944; Schweigart, 1965; Bubenicek, 1968; Halbach, 1969; Schellmann, 1969; Siehl and Thein, 1978, 1989; Kimberley, 1979; Nahon et al., 1980; Gygi, 1981; Dahannayake and Krumbein, 1982; Battacharyya, 1980; Battacharyya and Kakimoto, 1982; Delaloye and Odin, 1988; Schiavon, 1988; Gehring, 1989; Kearsley, 1989; Odin et al., 1989; Chauvel and Guerrak, 1989; and Doering, 1990).

One of the problems regarding the origin of ooids, for instance, is the observed co-existence of ferric-hydroxides and ferrous iron-containing chamosite. This can be

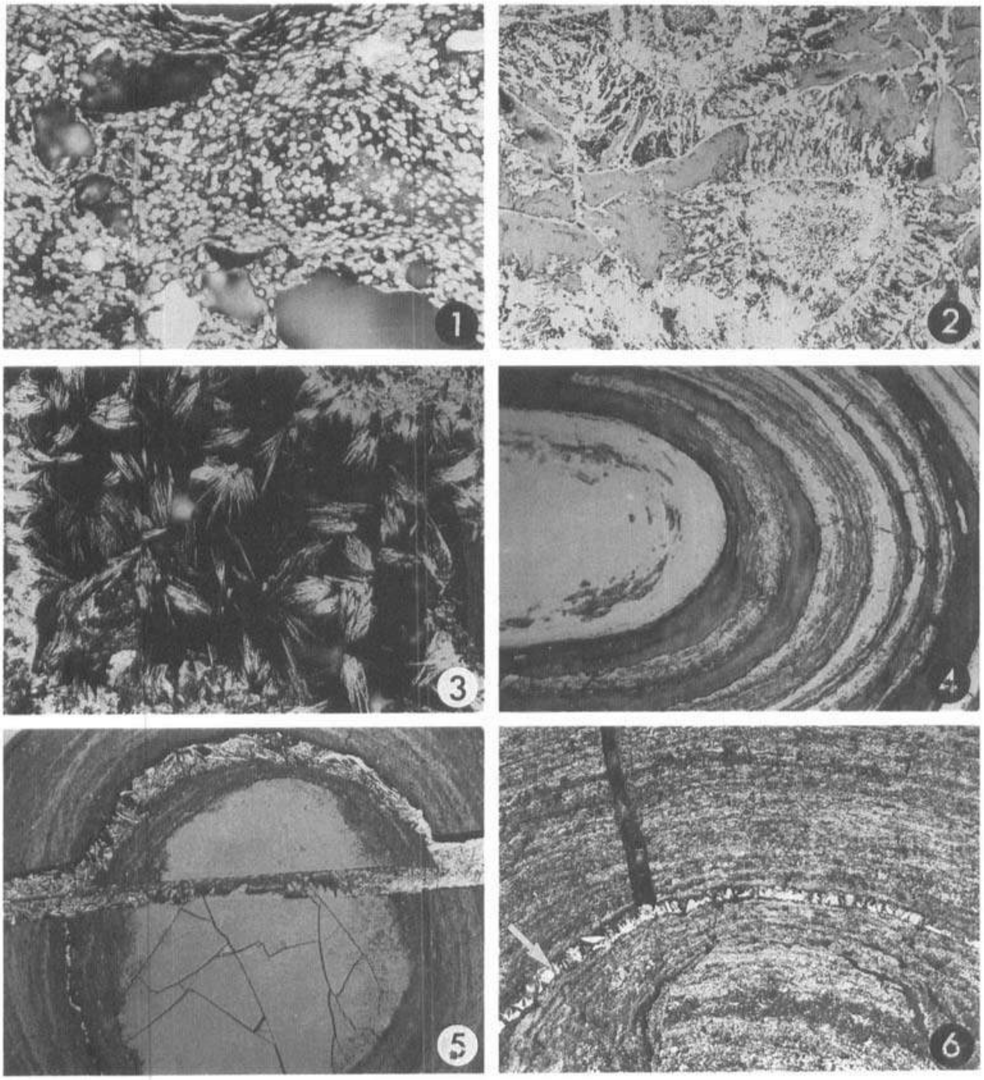

Fig. 11-22. Phanerozoic ironstones. 1. Spot-like distribution of ferric-hydroxide replacement of the chamositic cement in which quartz grains (transparent) and leucoxene (bright) are embedded. Aswan, Egypt. 2. Ferric-hydroxide (grey) of ferruginization origin, partially dehydrated to hematite (white). Aswan, Egypt. 3. Newly-formed platy hematite replacing kaolinite. Aswan, Egypt. 4. Discontinuous ferruginization along the mamillated ooid structure. Sokoto, Iullemmedden Basin, Nigeria. 5. Completely ferruginized (ferric-hydroxide) peloid with ooid-like outer zone and cement. Along a younger veinlet cryptomelane was introduced. In the ooid-structured outer part of the peloid, the manganese mineralization was followed by the tangentially developed structure. Wadi Halfa, Sudan. 6. Ferruginized ooid along fine and tangentially arranged cracks; open-space ferruginization along a wider and also tangentially arranged shrinkage crack (arrow). The small hematite crystals in the latter crack grew perpendicular to the vein border. Aswan, Egypt.

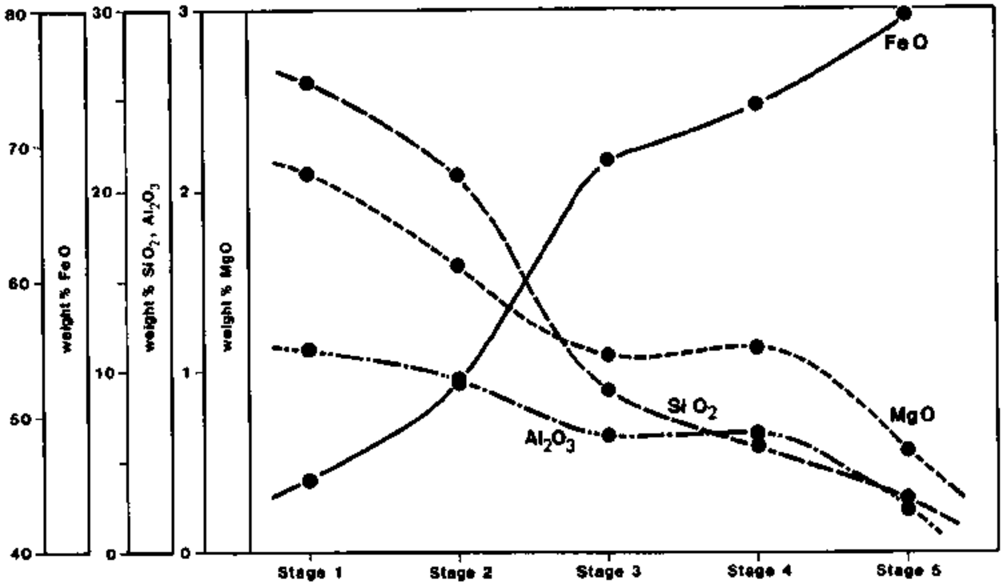

Fig. 11-23. Element distribution of a chamositic ooid in different stages of ferruginization (stage 1: nearly fresh chamosite; stage 5: final stage of ferruginization). Rumelange, Luxembourg.

explained, however, when under reflected light it becomes obvious that the chamosite ooids are partially replaced by ferric-hydroxide. The change in chemical composition resulting from advancing replacement of a chamosite ooid is illustrated in Fig. 11-23; stage 1 corresponds to a zone close to the nucleus, whereas stage 5 to the outer coating.

The continuous replacement of chamosite by Fe-rich solutions cannot normally be demonstrated on examining ooids as shown in Fig. 11-23 and Table 11-6. There are two reasons for this:

(1) due to the mammillated ooid structure, caused by the arrangement of the sheet-silicate chamosite, alteration proceeded at different intensities in individual tangentially arranged shells (Photo 4 of Fig. 11-22); and

(2) as a result of diagenetic dehydration, shrinkage occurs within the ooids, forming cracks often showing passive healing by ferric-hydroxides.

Thus, a distinction must be made between open-space ferruginization and replacement-type ferruginization, as defined by Happel (1930), particularly for ooids.

As a result of the tangential shrinkage and passive healing (= open-space ferruginization), sharply defined interbedding of layers (thicknesses varying from 1 to 15 μm) of different chemical composition is produced. The healing (the products being either carbonate- or apatite-rich) may already start during diagenesis. Open-space mineralization may also be younger than the ferruginization, in which case, veinlets of ferric-hydroxide, hematite or cryptomelane (Photo 5 of Fig. 11-22) occur (cryptomelane usually dominates). These minerals, precipitating along shrinkage cracks during passive emplacement, are characterized by radial arrangement of crystals. These grow vertically from the vein wall into free space (Photo 6 of Fig. 11-22). During

TABLE 11-6

Different stages (I–V) of ooids' ferruginization

	I	II	III	IV	V
FeO	44.63	52.92	69.27	73.82	79.26
Fe_2O_3	–	–	57.15	63.41	66.76
FeOOH	55.18	65.44	22.07	20.73	23.73
MgO	2.19	1.69	1.09	1.13	0.56
MnO	0.12	0.14	1.78	0.15	0.19
TiO_2	0.27	0.41	0.38	0.30	0.20
K_2O	0.31	0.22	–	–	–
CaO	2.76	1.85	1.34	0.56	0.42
Al_2O_3	11.26	9.51	6.57	6.60	3.98
SiO_2	27.01	20.92	8.90	5.99	3.12
P_2O_5	0.72	0.30	0.71	1.13	1.10
	99.82	100.48	100.00	100.00	100.00

The ooids consisted originally of chamosite (Rumelange, Lothringia; see also Fig. 11-23). Total Fe was determined as FeO; Fe_2O_3 and FeOOH were calculated on the basis of the subtotal = 100 (analyses III–V).

replacement ferruginization, however, the material present originally is frequently pseudomorphously replaced (Photo 4 of Fig. 11-22 and Photo 2 of Fig. 11-24). Consequently, the arrangement of the replacing mineral is determined by the location and orientation of the replaced mineral: in ooids, the replacer prefers a tangential arrangement. In cases of aggressive ferruginization, the original ooidal structure is completely destroyed (Photo 1 of Fig. 11-24). In rare cases, ferric-hydroxide is replaced by manganomelane (Photo 2 of Fig. 11-24).

Usually, in their ferruginized state, ooids, sometimes broken (Photo 6 of Fig. 11-24), have almost exclusively been reworked, redeposited, and finally embedded in a fresh groundmass (= matrix). Many authors incorrectly concluded that ooids consisting of ferric-hydroxide and/or hematite are of primary origin (e.g., Nahon et al., 1980; Schiavon, 1988; Gehring, 1989; and Williams and Owen, 1990), because the evidence for this redeposition was not recognized. For instance, in the *Green Deposits* of Haverlahwiese, Salzgitter (Germany), ferric-hydroxide ooids are cemented by glauconite. The latter is fresh and unaltered (showing green internal reflections) and contain porphyroblasts of diagenetic pyrite and siderite (Photo 3 of Fig. 11-24).

This mineral association can only be explained by redeposition of ferruginized ooids. During subsequent diagenesis, ferric-hydroxide (of the ooids) persisted in a metastable state in the younger glauconitic cement, which formed under reducing conditions.

The relative ages of older ooid and younger cement shown in Photo 4 of Fig. 11-24, are easy to establish. Iron-rich solutions obviously had penetrated into the ooid along shrinkage spaces. The difference in age is evident by the mineralized cracks failing to continue through the cement, thus indicating that ooid ferruginization did not occur in situ.

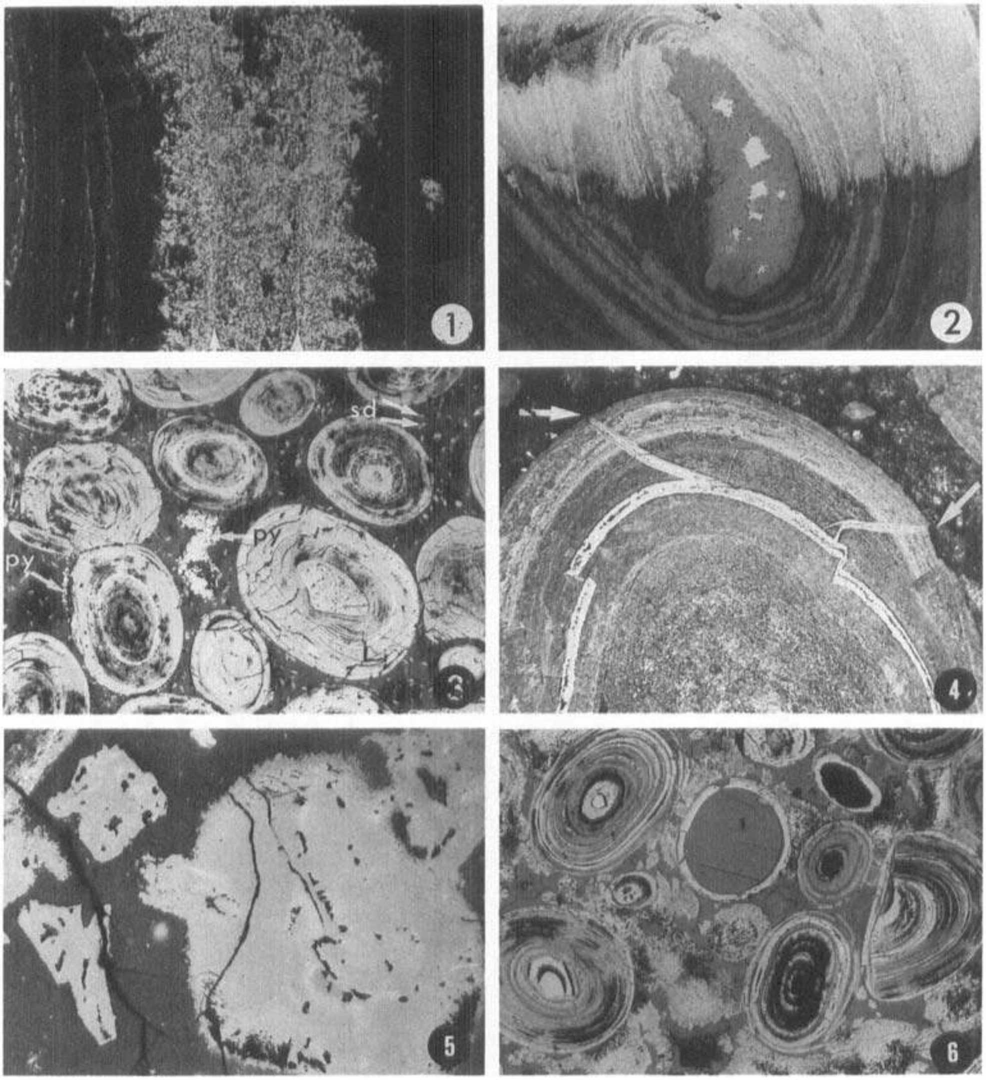

Fig. 11-24. Phanerozoic ironstones and kaolins. 1. The ferruginization (by ferric-hydroxide of the chamositic cement) penetrates the chamosite of the ooid. The original boundaries between the ooids and the cement are still visible (see arrows). Aswan, Egypt. 2. Completely ferruginized (ferric-hydroxide) ooid (originally consisting of chamosite) was partially replaced by manganomelane. The tangential arrangement of the chamosite was preserved during the two replacement stages. Bahariya Oasis, Western Desert, Egypt. 3. Ferruginized and redeposited ooids of ferric-hydroxide in glauconitic cement containing pyrite (in the center and along the boundaries of the ooids) and randomly distributed dog-tooth-shaped siderite crystals. Reflected light; normal objective; length of the longer edge of the photo is 3.2 mm. Haverlahwiese, Salzgitter, Germany. 4. The degree of ferruginization by ferric-hydroxide is controlled by tangentially arranged zones of the ooid. The small ferric-hydroxide-rich ooid layer was mineralized by infiltrating solutions; the micro-channel does not continue into the fresh cement (arrows). The latter contains pyrite and siderite. Haverlahwiese, Salzgitter, Germany. 5. Inhomogeneously ferruginized (ferric-hydroxide) kaolinitic cement. Mt. Patti, Nigeria. 6. Ferruginized (ferric-hydroxide) ooids and cement. The ooid close to the center was filled during the preparation of thin sections by the embedding material. Sokoto, Nigeria.

As has already been stated, many papers have discussed the idea of primary origin of ferric-hydroxide ooids. Two recent publications are referred to here as examples:

(1) Williams and Owen (1990) described recently-formed ooids from the Lake Malawi, Central Africa, consisting of concentric shells of hydrous Fe^{3+}-oxides surrounding siliceous nuclei. The sediments in which the ooids are embedded contain 18.70% by weight Fe, in contrast to those free of ooids with an iron concentration of 3–5% by weight. Unfortunately, Al, Si, and Mg contents were not determined by Williams and Owen (1990).

(2) Ooids of "primary" goethite have been described by Schiavon (1988) from the Billington Crossing quarry, United Kingdom. These ooids have high Al_2O_3 and SiO_2 contents (Table 11-7) which can be attributed to ooids originally composed of sheet silicates incompletely replaced by ferric-hydroxides. A comparison of the Billington samples (Table 11-7) with those of Agbaja, Nigeria (Table 11-8), and Rumelange, Luxembourg (Table 11-6), shows the following characteristics:

(a) the content of MgO in the ferruginized kaolinitic cement of Agbaja samples (Table 11-8) is very low (down to zero);
(b) the ferruginized chamositic ooids of Rumelange samples (Table 11-6) are relatively high in MgO content; and
(c) the ferruginized ooids of Billington Crossing quarry have moderate MgO contents (Table 11-7).

Based on the above considerations, the ooids of the Billington Crossing quarry most probably originated from chamosite. The lower MgO contents compared to Rumelange samples (Table 11-7) is a sign of more intensive ferruginization. On the other hand, MgO content is too high to postulate a kaolinitic precursor, as is the case for Agbaja deposits.

TABLE 11-7

Chemical composition of ooids in different stages of ferruginization (Billington Crossing quarry, Leighton Buzzard, Bedfordshire, United Kingdom)

	I	II	III
FeO	75.03	76.08	70.55
Fe_2O_3	47.84	61.59	26.10
FeOOH	39.55	25.55	58.20
Al_2O_3	6.49	6.08	6.69
SiO_2	3.92	4.67	7.08
MgO	0.47	0.44	0.54
MnO	0.11	0.10	0.13
TiO_2	0.23	0.23	–
K_2O	0.10	0.10	0.48
CaO	0.24	0.23	0.17
P_2O_5	1.05	1.01	0.61
	100.00	100.00	100.00

Total Fe was determined as FeO; Fe_2O_3 and FeOOH were calculated on the basis of the subtotal = 100.00.

TABLE 11-8

Different stages of cement ferruginization originally consisting of kaolinite (II–V)

	I	II	III	IV	V
FeO	1.71	8.77	39.34	45.87	78.83
FeOOH	2.11	10.84	48.64	56.71	97.48
MgO	0.13	–	–	0.16	–
K_2O	0.49	–	–	–	–
Al_2O_3	38.43	34.22	20.79	17.86	0.41
SiO_2	45.57	42.06	22.83	19.77	2.74
P_2O_5	–	0.17	1.14	0.29	0.32
H_2O	13.60	12.33	7.09	6.11	–
	100.33	99.62	100.49	101.00	100.95

I = fresh kaolinite (Agbaja/ Nigeria; see also Fig. 11-25).
Total Fe was determined as FeO; FeOOH was calculated from FeO; H_2O is calculated from Al_2O_3 and SiO_2, which are considered to be constituents of preserved (unreplaced) kaolinite.

Chauvel and Guerrak's (1989) explanation is similar to the ferruginization model, assuming that chamosite alteration was caused by leaching accompanied by oxidation, which resulted in relative enrichment of Fe and decrease in Al, Si, and Mg contents.

FERRUGINIZATION OF KAOLIN AND BAUXITE

Ferruginization is not merely restricted to oolitic ironstones, but may also be observed in other sediments, such as kaolins and bauxites.

Replacement of kaolinite by ferric-hydroxide has been found to be particularly striking in the Nigerian Eocene deposits of Mount Patti and Agbaja Plateau in the Niger Basin, near the town of Lokoja, Kogi State. They have been known for a long time and described as oolitic ironstones by Jones (1958) and Adeleye (1973), but owe their origin to the ferruginization of lithified kaolin, which was originally developed as fine-grained matrix with embedded kaolinitic peloids. Their combined reserve is over 300×10^6 t of Fe (Fadare, 1982).

Both the matrix and peloids have been largely replaced, and at the present time kaolinite occurs only as relics located within the newly-formed replacer ferric-hydroxide. Kaolinite ferruginization was most likely more or less a continuous process accompanied by a reduction in Si and Al contents, and enrichment in iron (Fig. 11-25 and Table 11-8; Photo 5 of Fig. 11-24).

The entire stratigraphic sequence is exposed in a road-cut at the Agbaja Plateau; it has a thickness of about 70 to 80 m, with the Basement Complex representing its lower limit. The top layer of bog iron ore (2.5 m) is underlain by ferruginized kaolin 10 to 15 m in thickness. The middle of the sequence comprises another three layers of kaolin, 1.5 to 2.0 m thick, which are interbedded with sandstones and kaolinitic sandstones. The second kaolin horizon, located some 20 m below the ferruginized

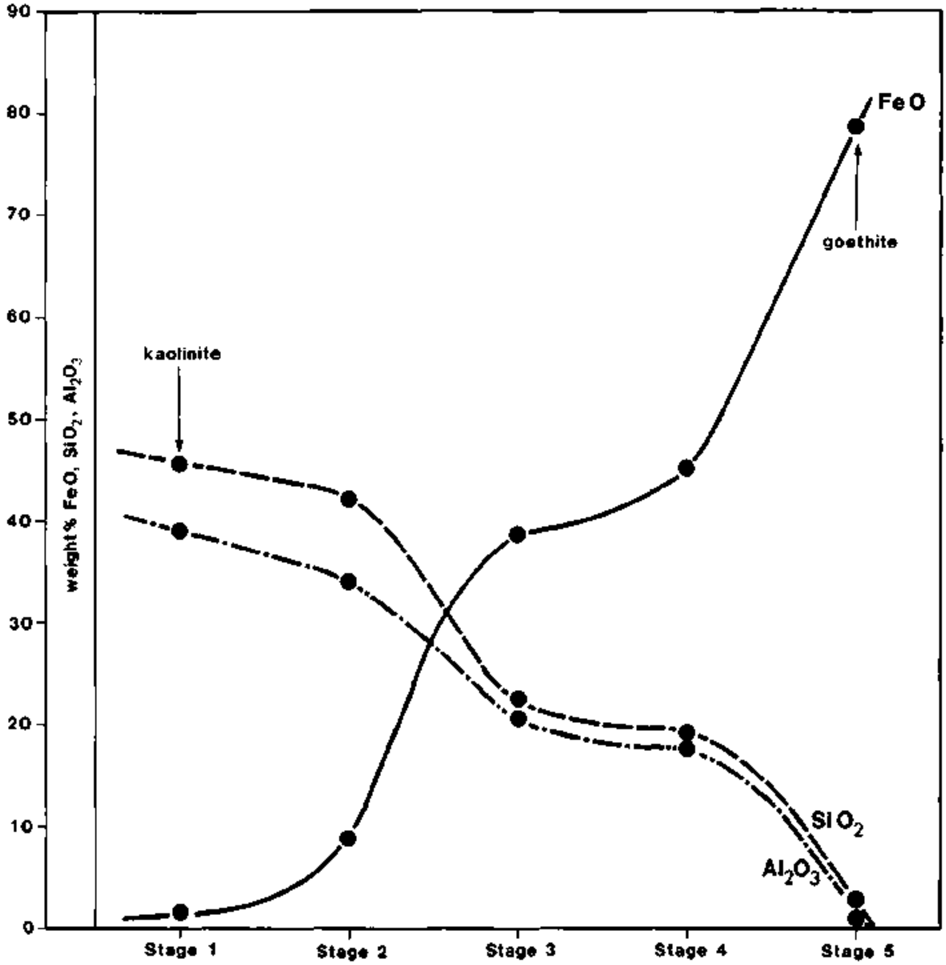

Fig. 11-25. Distribution of elements in the kaolinite cement during different stages of ferruginization (stage 1: fresh kaolinite; stage 5: final stage of replacement). Agbaja, Nigeria.

kaolin remained unaffected by the migrating Fe-solutions. Consequently, this kaolin layer and the other two in the lower section remained unaltered and white.

Another area of Nigeria where oolitic ironstone occurs lies in the Iullemmeden Basin, close to the town of Sokoto. This late Paleocene ironstone is associated with overlying crusty–concretionary laterite and ferruginous sandstones. The beds are up to 5 m in thickness. Laterite, ferruginized sandstones and oolitic ironstone outcrop over thousands of square kilometers (Kogbe, 1978). Strongly ferruginized, reworked, and redeposited ooids are embedded in a "cement" consisting of ferric-hydroxide (Photo 6 of Fig. 11-24). Analogous to Agbaja and Patti deposits, these ironstones probably also had primarily kaolinite as a pre-ferruginization precursor. The lack of MgO and the high Al_2O_3 and SiO_2 contents (especially of the "cement") is indicative

TABLE 11-9

Ferruginized kaolinite

	I	II	III	IV	V	VI
FeO	67.44	67.83	69.80	70.67	77.92	76.89
FeOOH	83.40	83.88	86.31	87.39	96.36	95.08
MnO	0.19	0.28	0.34	0.25	0.30	0.56
TiO_2	0.59	0.51	0.48	0.49	–	–
Na_2O	0.14	–	0.33	–	–	–
Al_2O_3	6.67	6.59	5.56	5.23	2.18	3.85
SiO_2	7.36	5.85	4.94	5.04	0.55	1.64
H_2O(calc.)	2.28	2.03	1.73	1.68	–	–
	100.63	99.14	99.69	100.08	99.39	101.13

I–IV = cement; V and VI = ooid (Sokoto, Nigeria).
Total Fe was determined as FeO; FeOOH was calculated from FeO, H_2O from Al_2O_3 and SiO_2, which are considered to be constituents of preserved (unreplaced) kaolinite.

of ferruginized kaolinite (Table 11-9). Moreover, the Al_2O_3/SiO_2 ratios lie in the range of 0.91–1.13 and are close to the theoretical ratio for kaolinite (0.85).

In these Nigerian occurrences, the precursor kaolinite contained abundant diagenetic FeS_2 (as idiomorphic pyrite, framboids and marcasite). Fresh pyrite has not been observed, but there are pseudomorphs of hematite after the above-mentioned primary FeS_2 minerals (Photo 1 of Fig. 11-26).

A similar development is observed at Wadi Halfa, northern Sudan, close to the Egyptian border, represented by what Fuganti et al. (1987) called an oolitic ironstone deposit. It occurs in the Nubian Formation (= Nubian Sandstone) and, according to van Houten et al. (1984), is of Cenomanian to Turonian age and originated in a coastal plain. In Wadi Halfa, a 90-m thick sedimentary sequence is exposed (Fuganti et al., 1987) in which sandstone is predominant. In addition to the two oolitic horizons, there are several intercalations of mudstones.

Microscopic comparison of the Kalabscha kaolin deposit (Said and Mansour, 1971; Fischer, 1989), located farther north of Wadi Halfa (about 100 km south of the oolitic ironstone of Aswan), with those of Wadi Halfa deposits reveals a striking similarity of the cement and peloids (Photos 2 and 3 of Fig. 11-26). Ooids are absent in both these occurrences.

They differ, however, in iron contents: strong ferruginization occurs at Wadi Halfa, whereas in Kalabscha deposits there is generally very little iron enrichment. The kaolinitic precursor of Wadi Halfa deposits can be easily demonstrated: both the "cement" and the peloids contain relics of kaolinite (Photo 4 of Fig. 11-26) as well as exhibit various stages of ferruginization (Table 11-10). The secondary ferric-hydroxide is characterized by high SiO_2 and Al_2O_3 contents (Fig. 11-27). In contrast to the MgO-bearing replacement products (having significant contents of MgO; Figs. 11-21 and 11-23), resulting from the replacement of chamosite, MgO concentration is relatively low.

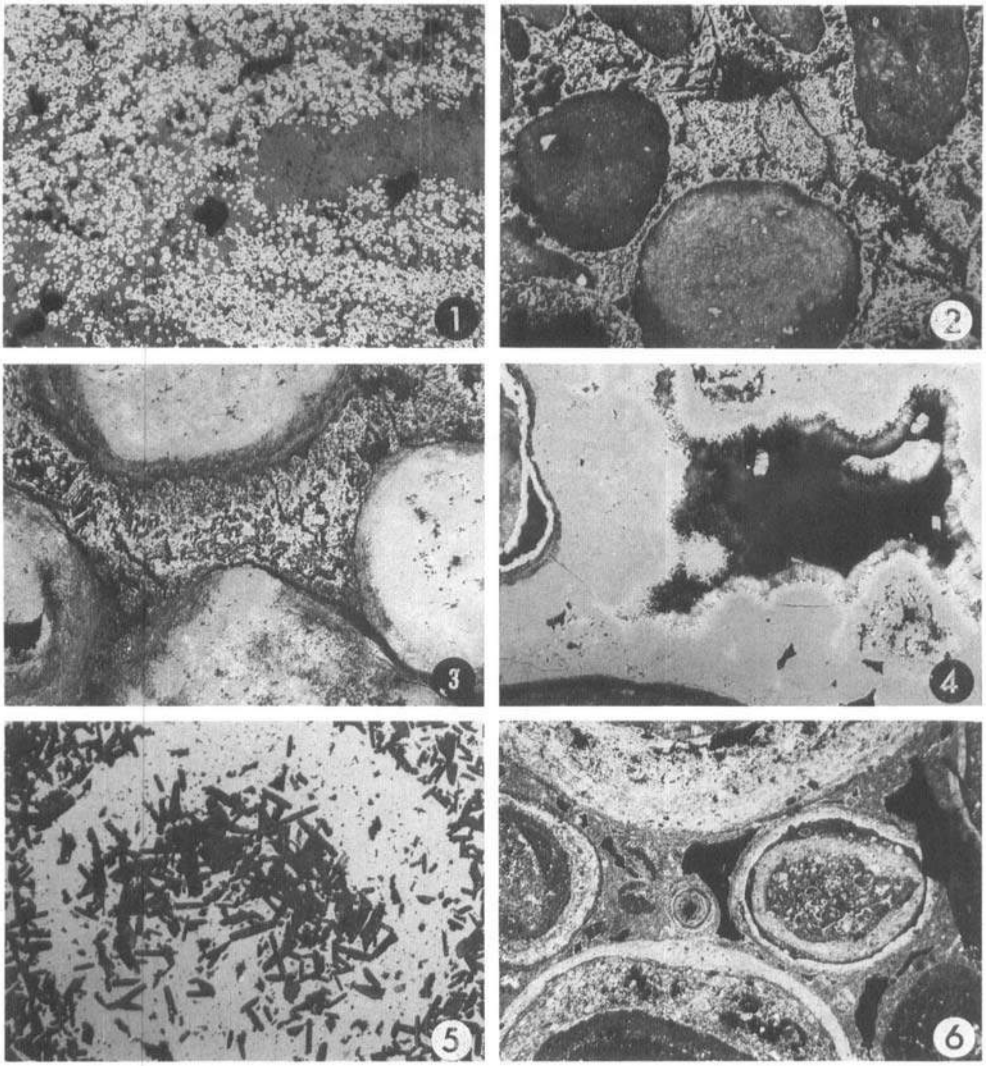

Fig. 11-26. Kaolins and bauxites. 1. Pyrite pseudomorphously replaced by hematite embedded in inhomogeneously ferruginized kaolinitic cement. Agbaja, Nigeria. 2. Kaolinitic peloids in strongly ferruginized (hematite) cement originally consisting of kaolinite. Kalabscha, Egypt. 3. Peloids and cement (both originally composed of kaolinite) are strongly ferruginized by ferric-hydroxide (peloids) and hematite (cement). Wadi Halfa, Sudan. 4. Ferruginized (ferric-hydroxide) cement with relic of kaolinite (in the center). Wadi Halfa, Sudan. 5. Diagenetically-formed porphyroblasts of boehmite in a peloid as well as in the surrounding cement. Peloid and cement are ferruginized (ferric-hydroxide). Sedisehir, Turkey 6. Inhomogeneously ferruginized bauxite. Goethite (grey) is partially transformed to hematite (white). Les Baux, France.

In bauxite, secondary ferruginization is distinctly less marked than it is in kaolinitic and chamositic sediments, because of the mineralogy of bauxite. In contrast to boehmite, diaspor resists the process of ferruginization (Photo 5 of Fig. 11-26;

TABLE 11-10

Different stages of ferruginized kaolinitic cement (II and III)

	I	II	III
FeO	1.45	53.62	74.82
Fe_2O_3	–	–	17.13
FeOOH	1.79	66.31	73.46
MgO	0.12	0.31	0.64
MnO	–	0.41	2.94
TiO_2	–	0.64	–
Na_2O	–	0.27	–
K_2O	0.17	–	–
CaO	0.50	0.45	0.43
Al_2O_3	37.51	17.60	0.82
SiO_2	44.47	8.43	4.26
P_2O_5	0.52	0.51	0.32
H_2O	13.27	5.07	–
	98.38	100.00	100.00

I = fresh kaolinite (Wadi Halfa, Sudan).
Total Fe was determined as FeO; Fe_2O_3 and FeOOH were calculated on the basis of the subtotal = 100.

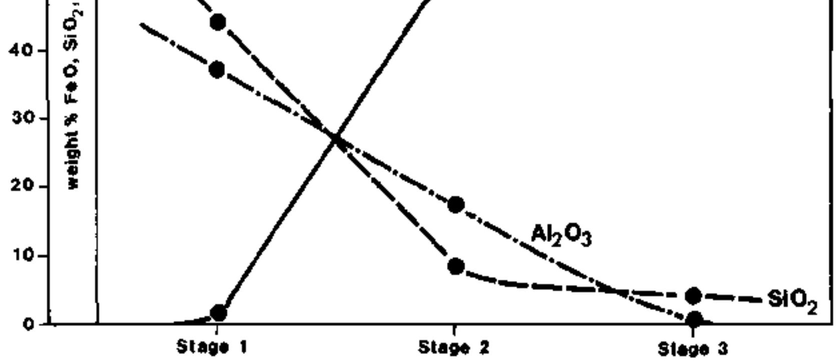

Fig. 11-27. Element distribution of kaolinitic cement in different stages of ferruginization (stage 1: unreplaced kaoline; stage 3: final stage of replacement). Wadi Halfa, Sudan.

TABLE 11-11

Different stages of ferruginization of bauxite (Sedisehir, Turkey)

	I	II	III	IV	V
FeO	2.74	9.16	25.16	45.73	61.68
Fe_2O_3	3.05	10.18	27.96	50.82	68.55
Al_2O_3	80.15	72.60	55.67	34.01	22.68
Fe_2O_3	3.05	–	–	17.34	51.59
FeOOH	–	11.32	31.11	37.25	18.87
TiO_2	1.56	2.21	1.74	3.94	1.55
BaO	–	0.17	0.14	0.27	0.09
Cr_2O_3	0.13	0.10	0.12	0.18	0.20
AlOOH	94.30	85.41	65.49	40.01	26.68
SiO_2	1.32	1.01	1.46	1.01	1.02
	98.80	100.23	100.06	100.00	100.00

Total Fe and Al were determined as FeO and Al_2O_3, respectively, from which Fe_2O_3, FeOOH and AlOOH were calculated.

Haase, 1993). The general lack of strong ferruginization may also be explained by the bauxites' greater compactness and lower porosity, and as a consequence (as at Les Baux, France) of a thick layer of overlying limestone, allowing only a limited supergene water circulation. Where local Fe-enrichments do occur, they are replacements of AlO(OH) (Photo 6 of Fig. 11-26). The brown pigmentation of the

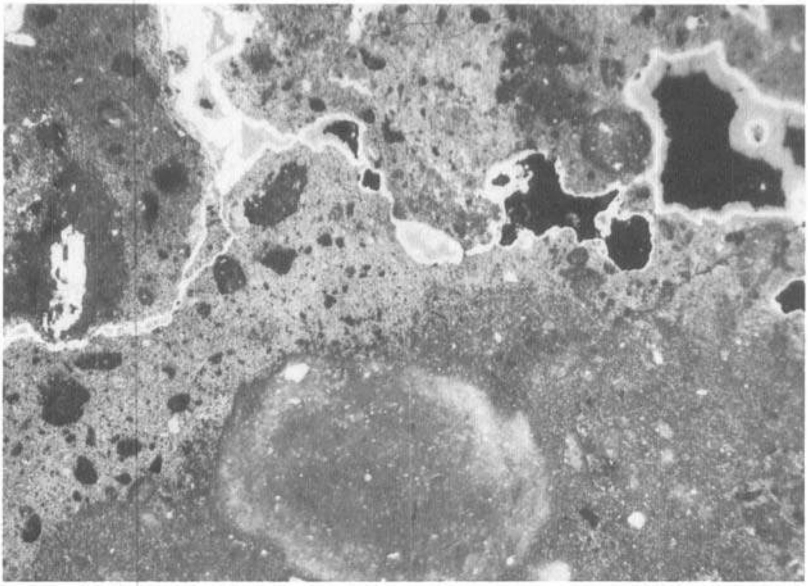

Fig. 11-28. Incomplete replacement of boehmitic peloids and boehmitic cement by ferric-hydroxide; Sedisehir, Turkey.

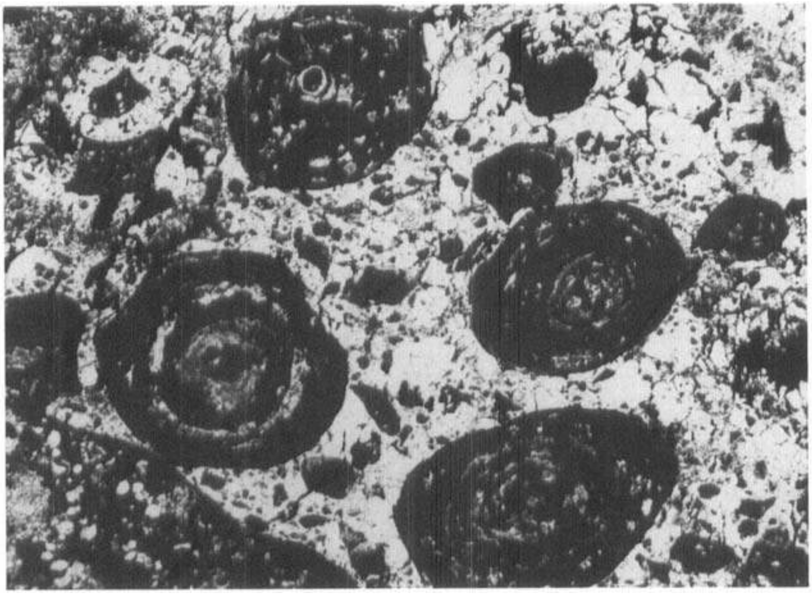

Fig. 11-29. Bauxitic peloids embedded in a pyrite-rich cement. Reflected light; normal objective; diameter of the bigger peloids is 0.8 mm; Sedisehir, Turkey.

overlying limestone indicates its impregnation by oxidizing solutions: fresh limestone is commonly bluish.

In Sedisehir, Turkey, the Fe_2O_3 of bauxite is on the average almost 20% by weight (Atabey, 1976). Ore microscopy clearly shows that the Fe-content is partially a result of ferruginization and locally may increase up to 62% by weight (Table 11-11 and Figs. 11-27 and 11-28). Some parts of the bauxite sequence at Sedisehir, which are unaffected by ferruginization, contain abundant diagenetic pyrite (Fig. 11-29).

SUMMARY AND CONCLUSIONS — IN CONTEXT WITH RED BEDS

Proof of postdiagenetic ferruginization is of particular importance in interpreting the genesis of oolitic ironstone. Earlier hypotheses proposed that all the material of the oolitic ironstones have been of syngenetic origin. As a result, both facies-analytical analyses and genetic hypotheses of the complexly-layered ooids seem to have overemphasized data and concepts that actually supported syngenesis without offering alternative interpretations. In particular, the complicated features of ooids gave rise to a large number of genetic models.

Using the ferruginization model, Caillere and Kraut's (1954) minette ore types and their arrangement in the Lorraine basin can easily be explained. Starting from the top to bottom they described *Red, Yellow, Grey, Brown, Black* and *Green Deposits*. Only deeper parts of the sediments which are either slightly exposed or not exposed to the oxidation and ferruginization processess, are grey, black (brown) or green in color. The overlying yellow deposits contain abundant postdiagenetic ferric-hydroxide, whereas close to the surface, dehydration of ferric-hydroxide gave rise to the fine-grained red hematite.

From these observations, some conclusions on red beds may also be drawn. Green deposits, occurring at the base of variegated red beds, represent those sediments which were not involved in oxidation and ferruginization. Folk (1976), Braunagel and Stanley (1977), and others interpreted these green sediments as secondarily-reduced red beds.

The comparison of ferruginization in red beds (of the Bahariya Oasis, Egypt) and in intercalated sandstone layers in oolitic ironstones (e.g., Aswan, Egypt) shows analogous mineralogy and structure: the original cement was replaced by ferric-hydroxides, and is either preserved as relics or has disappeared completely, depending on the degree of replacement (Photo 4 of Fig. 11-14 and Photo 5 of Fig. 11-18). There are, however, differences along quartz-grain boundaries: in red beds they are smooth, whereas in sandstone layers within oolitic ironstone deposits they are corroded. The reason for this is the mechanism of iron-mobilization and precipitation: in red beds a change from reducing to oxidizing conditions took place, whereas in oolitic ironstone the change was from acidic to alkaline environment.

Ferruginized sandstones (by iron-hydroxides or by hematite originating from dehydrated ferric-hydroxide) are not restricted to the deposits investigated. For example, Hunter (1970) reported: "Hematite-cemented sandstones are, next to the oolitic ironstone, the most iron-rich rocks in the Clinton Group".

The ferruginization model of oolitic ironstone presented in this chapter, recently has been supported by Yapp (1991). He analyzed goethite ooids from the Upper Ordovician Neda Formation in Wisconsin and Iowa, USA, and found uniform δ^{18}O-values of about 1‰. Yapp summarized his results as follows: The spatial uniformity of the oolitic goethite δ^{18}O-values suggests that meteoric water was present at the time of goethite formation and is consistent with formation of the oolitic goethite in a continental environment.

PHANEROZOIC IRONSTONE OR SCOS-IF?

This section deals with the classification of ore deposits, evoked by Kimberley (1989a, b). Detailed microscopic studies, however, led to a different classification of iron ore deposits than that proposed by Kimberley.

The iron deposits studied here are classified as SCOS-IF type as suggested by Kimberley (1989a, b). SCOS-IF stands for: Sandy, Clayey, and Oolitic, Shallow island-dotted sea Iron Formation, replacing the name Phanerozioc ironstone, for which the term oolitic ironstone is synonymous.

Differences between the individual deposits are lost in Kimberley's classification, which overemphasizes environmental features.

According to Kimberley's definition, Ordovician oolitic ironstones of the Prague Basin, Thüringen, and Wales also belong to the SCOS-IF type. Those deposits, however, differ compositionally (the cement is sometimes composed entirely of carbonate) and structurally from the other ironstone deposits that were investigated. In the Ordovician deposits, ferruginization was not observed, thus explaining their limited discussion in this chapter. Furthermore, it has been shown here that the deposits of Wadi Halfa (Sudan), Agbaja, Mount Patti and Sokoto (Nigeria) were originally kaolin deposits. In the sense of Kimberley (1989a, b), therefore, they do not belong to the iron formations at all.

As was stated by Kimberley, the iron ore deposits of the Bahariya Oasis, Western Desert, Egypt, also belong to the SCOS-IF. These deposits are compositionally and structurally different from the other two groups. Ooids are only of subordinate significance here, as it is a relatively quartz-rich sediment. From the genetic point of view, the Bahariya deposits are related to the Lahn-Dill type (Agthe, 1986). The latter has, however, been placed by Kimberley into another group, namely: SVOP-IF (Shallow-Volcanic-Platform Iron Formation). The well-known Kiruna type (of which the genesis is still being hotly debated and for which Kimberley only mentions the models of sedimentary origin, e.g., Parák, 1975, 1984, 1985), however, that is composed of coarse-grained magnetite, is grouped together with the Lahn-Dill type, which is predominantly composed of fine-grained hematite and/or cryptocrystalline FeOOH.

Kimberley stated that in the European usage, the Lahn-Dill type corresponds to the Algoma type iron ore deposits. The Lahn-Dill type, contrary to the Algoma type, which is sometimes interbedded with gondite, is always non-metamorphic. Minerals like grunerite, ferrosilite, and garnet (almandine–spessartite), that are closely associated with the Algoma type, are unknown in the Lahn-Dill type iron ore deposit.

In addition, there is another disadvantage of Kimberley's classification, namely, that the primary composition of sediments, in addition to the environment, is the basis of the classification. Primary material, however, occurs in many iron deposits (e.g., cherty and noncherty iron formations) as relics having survived postsedimentary alterations such as diagenesis, submarine weathering, metamorphism and postdiagenetic (-metamorphic) ferruginization.

Although one could continue the discussion of Kimberley's classification, the writers would like to offer the following constructive advice: microscopic work is still profitable today! In reflected light, the structural and mineralogical differences between the Kiruna type, the Lahn-Dill type, the Algoma type, and oolitic ironstones become easily apparent! It is certainly correct that a classification cannot be based on genetic characteristics alone as long as genetic questions are still unanswered, but it is equally correct that structural and mineralogical characteristics (that naturally depend on the genesis) are easily determinable and should not be missing in any classification. Conseqently, the classification of iron ore (and related) deposits is as yet not settled to everyones satisfaction.

ACKNOWLEDGEMENTS

The writer is particularly grateful to Dr. Th. Doering for many discussions and to Mr. Peter Meier for his display of immense initiative during scrupulous preparation of the polished sections. Johannes Haase performed the microprobe analyses (ARL, Geochemisches Institut der Universität Göttingen), and Mr. Eberhard Wartala did the drawings. The writer wishes to express his gratitude to both of them.

The writer is also grateful to Prof. G. Morteani and Dr. Grundmann (München), for the samples from Wadi Halfa, to Dr. N. Schiavon United Kingdom, who sent material from the Billington Crossing quarry, and to Prof. K. German (Berlin) for fruitful discussions on the deposits of Eastern Desert, Egypt.

For critical evaluation of the manuscript the author is indebted to Dr. T. Pick (University of California, San Diego). The writer is especially grateful to the editors of this volume, Drs. K.H. Wolf and G. Chilingarian for discussions, suggestions, and linguistic assistance.

The author would like to thank the Deutsche Forschungsgemeinschaft (DFG) for financing the field trip to Egypt (in the frame of the Sonderforschungsbereich 69 of the Technische Universität, Berlin), and particularly the Deutscher Akademischer Austauschdienst (DAAD) for supporting field trips in Nigeria.

Thanks are also due to the ETIBANK Company in Turkey and to the LARCO Company in Larymna, Greece. The writer is also grateful to Mr. Marcel Klein of Rumelange, Luxembourg, to Drs. S.O. Akande, T. Annor and K. Ladipo of the University of Ilorin, Nigeria, and Dr. Tim Young of the United Kingdom for valuable assistance during the field-work in Seydisehir (Turkey), Rumelange (Luxembourg), Agbaja and Patti (Nigeria), and Wales.

The last project (Phanerozoic Ironstones) is included in the IGCP Project 277.

REFERENCES

Adeleye, D.R., 1973. Origin of ironstone, an example from the middle Niger Valley, Nigeria. *J. Sediment. Petrol.*, 43: 709–727.

Agthe, C., 1986. Die Genese der Eisenerze von Djebl El Ghorabi, Djebl El Harra, El Gedida und der Eisenkrusten von El Heiz, Bahariya Oasis/Western Desert, Ägypten. *Berl. Geowiss. Abh., Reihe A/Bd.*, 68: 85 pp.

Atabey, M.E., 1976. Mineralogy, chemistry and origin of the Mortas bauxite deposit, Sedisehir, Konya, Turkey. In: Acad. Yougoslave des Sciences et des Arts (Editor), *Symposium on Advances in Geology, Geochemistry, and Treatment of Bauxite*, pp. 77–89.

Bafor, B. and Mücke, A., 1990. The genesis of manganese concretions in the Igarra area, southwestern Nigeria. *J. Afr. Earth Sci.*, 10: 595–601.

Ball, J. and Beadnell, H.J., 1903. *Bahariya Oasis, Its Topography and Geology*. Natl. Print. Dep., Cairo, 84 pp.

Barrell, J., 1908. Relations between climate and terrestrial deposits. *J. Geol.*, 16: 159–190, 255–295, 363–384.

Bates, R.L. and Jackson, J.A. (Editors), 1987. *Glossary of Geology*. Geological Institute, Alexandria, Va., 3rd ed., 788 pp.

Battacharyya, D.P., 1980. *Sediments of Late Cretaceous Nubia Formation at Aswan, Southeast Egypt, and Origin of the Associated Ironstone*. Ph.D. thesis, Princeton University, Princeton, N.J., 122 pp.

Battacharyya, D.P. and Kakimoto, P., 1982. Origin of ferriferrous ooids: a SEM study of ironstone ooids and bauxite pisoids. *J. Sediment. Petrol.*, 52: 849–857.

Battacharyya, D.P., 1989. Concentrated and lean ooliths: examples from the Nubia Formation at Aswan, Egypt, and their significance of the oolithe types in ironstone genesis. In: T.P. Young and W.E.G. Taylor (Editors), *Phanerozoic Ironstones. Geol. Soc. London, Spec. Publ.*, 46: 93–103.

Berg, G., 1921. Über die Struktur und Entstehung der lothringischen Minetteerze. *Z. Dtsch. Geol. Ges.*, 73: 113–136.

Berg, G., 1944. Vergleichende Petrographie oolitischer Eisenerze. *Arch. Lagerstättenforsch.*, 76: 126 pp.

Berner, R.A., 1969. Goethite stability and the origin of red beds. *Geochim. Cosmochim. Acta*, 33: 267–273.

Berner, R.A., 1991. A new geochemical classification of sedimentary environments. *J. Sediment. Petrol.*, 51: 359–365.

Borchert, H., 1952. Die Bildungsbedingungen mariner Eisenerzlagerstätten. *Chem. Erde*, 16: 49–74.

Braunagel, L.H. and Stanley, K.O., 1977. Origin of variegated red beds in the Cathedral Bluffs Tongue of the Wasatch Formation (Eocene), Wyoming. *J. Sediment. Petrol.*, 47: 1201–1219.

Bubenicek, L., 1968. Geologie des minerais de fer oolithiques. *Miner.Deposita*, 3: 89–108.

Bubenicek, L., 1971. Geologie du gisement de fer de Lorraine. *Cent. Rech. Pau Soc. Nat. Pét. Aquitaine, Bull.*, 5: 223–320.

Caillere, S. and Kraut, F., 1954. Les gisements de fer du bassin Lorraine. *Mem. Mus. Nat. Hist. Nat., Ser. C*, 4: 1–176.

Chauvel, J.-J. and Guerrak, S., 1989. Oolitization process in Paleozoic ironstone of France, Algerie and Libya. In: T.P. Young and W.G.E. Taylor (Editors), *Phanerozoic ironstones. Geol. Soc., London, Spec. Publ.*, 46: 165–173.

Crosby, W.O., 1885. The color of soils. *Boston Soc. Nat. Hist. Proc.*, 23: 219–222.

Crosby, W.O., 1891. On the contrast of color of the soils of high and low latitudes. *Am.Geol.*, 8: 72–82.

Dahannayake, K. and Krumbein, W.E., 1982. Microbial structures in oolitic iron formations. *Mineral. Deposita*, 21: 85–94.

Dapples, E.C., 1967. Diagenesis of sandstone. In: G. Larsen and G.V. Chilingar (Editors), *Diagenesis in Sediments. Developments in Sedimentology 8*. Elsevier, Amsterdam, pp. 91–125.

Dawson, J.W., 1848. On the coloring matter of red sandstones and greyish and white beds associated with them. *Q. J. Geol. Soc., London*, 5: 25–30.

Delaloye, M.F. and Odin, G.S., 1988. Chamosite, the green marine clay from Chamoson. A study of Swiss oolitic ironstones. In: G.S. Odin (Editor), *Green Marine Clays. Developments in Sedimentology 45*. Elsevier, Amsterdam, pp. 7–28.

Doering, Th., 1990. *Die Genese der oolitischen Eisenerze von Assuan in Oberägypten. Eine erzpetrographisch-mikroanalytische Untersuchung*. Ph.D. Thesis, Georg-August-Universität, 185 pp. (unpublished).

Dominik, W., 1985. Stratigraphie und Sedimentologie der Oberkreide von Bahariya und ihre Korrelation zum Dakhla-Becken, Western Desert, Ägypten. *Berl. Geowiss. Abh., Reihe A/Bd.*, 62, 173 pp.

El Akad, S. and Issawi, B., 1963. Geology and iron deposits of Bahariya Oasis. *Geol. Surv. Egypt, Cairo, Pap.*, 18, 300 pp.

El Shazly, E.M., 1962. The results of drilling in the iron deposits of Gabal Ghorabi, Bahariya Oasis, Western Desert, and report on mineralogy and the low grade iron ore of El Heiz area, Bahariya Oasis, Western Desert.*Egypt. Geol. Surv., Dep.*, Cairo, pp. 1–51.

Fadare, V.O., 1982. Precambrian iron ore formation of the OkeneAjaokuta Area of Kwara State. *Niger. Min. Geosci. Soc., Abstr.*, 18th Annu. Conf., Kaduna.

Fischer, K., 1989. Prozesse und Produkte lateritischer Verwitterung in oberkretazischen Sedimenten Oberägyptens und des Nordsudan. *Berl. Geowiss. Abh., Reihe A*, 115: 123 pp.

Folk, R.L., 1976. Reddening of desert sandstone: Simpson Desert, N. T., Australia. *J. Sediment. Petrol.*, 46: 604–615.

Foos, A., 1983. Formation of hematite ooids by alteration of chamosite ooids (abstr.). *Geol. Soc. Am., Abstracts with Programs*, 15: 575.

Franke, W. and Paul, J., 1980. Pelagic red beds in the Devonian of Germany, deposition and diagenesis. *Sediment. Geol.*, 25: 231–256.

Friend, P.F., 1966. Clay fractions and colours of some Devonian red beds in the Catskill Mountains, USA. *Q. J. Geol. Soc.*, 122: 273–292.

Fuganti, A., Morteani, G. and Grundmann, G., 1987. Oolitic iron ore deposits in the Nubian Formation of Wadi Halfa area (northern Sudan). In: G. Matheis and H. Schandelmeier (Editors), *Current Research in African Earth Sciences*. Balkema, Rotterdam, pp. 379–382.

Gehring, A.V., 1989. The formation of goethitic ooids in condensed Jurrassic deposits in northern

Switzerland. In: T.P. Young and W.E.G. Taylor (Editors), *Phanerozoic Ironstones. Geol. Soc. London, Spec. Publ.*, 46: 133–139.

Goss, J.C., 1987. The kinetics and reaction mechanism of the goethite hematite transformation. *Mineral. Mag.*, 51: 437–451.

Gygi, R.A., 1981. Oolitic iron formation: marine or not marine? *Eclogae Geol. Helv.*, 74: 233–254.

Haase, J., 1993. *Vergleichende Untersuchungen von eisenreichen oolitischen Kaolinit- und Bauxitvorkommen. Eine erzpetrographisch-mikroanalytische Untersuchung.* Ph.D. Thesis, Universität Göttingen, Göttingen, 188 pp.

Halbach, P., 1969. Zu den Bildungsprozessen bei der Genese von Brauneisenerzooiden. *Chem. Erde*, 28: 40–58.

Happel, L., 1930. Eineisenung und Vereisenung, abgegrenzt am Beispiel der devonischen Roteisenhorizonte der Eifel. *Senckenbergiana*, 12: 76–89.

Harder, H., 1951. Über den Mineralbestand und die Entstehung einiger sedimentärer Eisenerze des Lias. *Heidelb. Beitr. Mineral. Petrogr.*, 2: 455–476.

Harder, H., 1989. Mineral genesis in ironstone: a model based upon laboratory experiments and petrographic observations. In: T.P. Young and W.E.G. Taylor (Editors), *Phanerozoic Ironstones. Geol. Soc. London, Spec. Publ.*, 46: 9–18.

Hartmann, M., 1963. Einige geochemische Untersuchungen an Sandsteinen aus Perm und Trias. *Geochim. Cosmochim. Acta*, 27: 459–499.

Hemingway, J.E., 1951. Cyclic sedimentation and the deposition of ironstone in the Yorkshire Lias. *Yorksh. Geol. Soc. Proc.*, 28: 67–74.

Hubert, J.F. and Reed, A.A., 1978. Red bed diagenesis in the East Berlin Formation, Newark Group, Connecticut Valley. *J. Sediment. Petrol.*, 48: 175–184.

Hunter, R.E., 1970. Facies of iron sedimentation in the Clinton Group. In: G.W. Fisher et al. (Editors), *Studies of the Appalachian Geology, Central and Southern.* Wiley-Interscience, New York, N.Y., pp. 101–121.

Jones, H.A., 1958. The oolitic ironstones of Agbaja Plateau, Kabba Province. *Rec. Geol. Surv., Nigeria*, pp. 20–43.

Kearsley, A.T., 1989. Iron-rich ooids, their mineralogy and microfabric: clues to their origin and evolution. In: T.P. Young and W.E.G. Taylor (Editors), *Phanerozoic Ironstones. Geol. Soc. London, Spec. Publ.*, 46: 141–163.

Kessler, R.L., 1978. Diagenetic sequence in acient sandstones deposited under desert climatic conditions. *J. Geol. Soc., London*, 135: 41–49.

Kimberley, M.M., 1979. Origin of oolitic iron formations. *J. Sediment. Petrol.*, 49: 111–132.

Kimberley, M.M., 1989a. Nomenclature of iron formations. *Ore Geol.Rev.*, 5: 1–12.

Kimberley, M.M., 1989b. Exhalative origins of iron formations. *Ore Geol. Rev.*, 5: 13–145.

Kogbe, C.A., 1978. Origin and composition of the ferruginous oolites and laterites of North-Western Nigeria. *Geol.Rundsch.*, 67: 662–674.

Kolbe, H., 1970. Zur Entstehung und Charakteristik mesozoischer marin-sedimentärer Eisenerze im östlichen Niedersachsen. *Clausthaler Hefte Lagerstättenkd. Geochem. Miner. Rohst.*, 9: 161–184.

Kowalczyk, G., 1983. Das Rotliegende zwischen Taunus und Spessart. *Geol. Abh. Hessen*, 84, 99 pp.

Krynine, P.D., 1949. The origin of red beds. *Trans. N.Y. Acad. Sci.*, 11: 60–68.

Langmuir, D., 1971. Particle size effect on the reaction Goethite–Hematite + H_2O. *Am. J. Sci.*, 271: 147–156.

Langmuir, D. and Whittemore, D.O., 1971. Variations in the stability of precipitated ferric oxyhydroxides. In: J.D, Hem (Editor), *Non-Equilibrium Systems and Processes in Natural Water Chemistry, a Symposium. Advances in Chemistry.* Am. Chem. Soc., pp. 209–234.

Lemoalle, J. and Dupont, B., 1973. Iron-bearing oolites and the present conditions of iron sedimentation in Lake Chad (Africa). In: G.C. Amstutz and A.J. Bernard (Editors), *Ores in Sediments.* Springer-Verlag, Berlin, 350 pp.

Maynard, B.J., 1986. Geochemistry of oolitic iron stone, an electron microprobe study. *Econ. Geol.*, 81: 1473–1483.

McBride, E.F., 1974. Significance of color in red, green, purple, olive, brown, and grey beds of Difunta Group, northeastern Mexico. *J. Sediment. Petrol.*, 44: 760–773.

Middleton, G.V., 1960. Chemical composition of sandstones. *Geol. Soc. Am. Bull.*, 71: 1011–1026.

Mücke, A. and Agthe, Ch., 1988. Mineralization, origin and age classification of ferruginized sandstone in the Bahariya Oasis, Western Desert/Egypt: A contribution to the origin of red beds. *Lithos*, 22: 59–73.

Mücke, A. and Chaudhuri, J.N. Bhadra, 1991. The continuous alteration of ilmenite through pseudorutile to leucoxene. *Ore Geol.Rev.*, 6: 25–44.

Nahon, D., Carozzi, V.A. and Parron, C., 1980. Lateritic weathering as a mechanism for the generation of ferruginous ooids. *J. Sediment. Petrol.*, 50: 1287–1298.

Odin, G.S. (Editor), 1988. *Green Marine Clays. Developments in Sedimentology 45*. Elsevier, Amsterdam, 445 pp.

Odin, G.S., Knox, R.W., O.B., Gygi, R.A. and Guerrack, S., 1989. Green marine clays from the oolitic ironstone facies: habit, mineralogy, environments. In: T.P. Young and W.E.G. Taylor (Editors), *Phanerozoic Ironstones. Geol. Soc. London, Spec. Publ.*, 46: 29–52.

Palache, C., Berman, H. and Frondel, C., 1944. *The System of Mineralogy*, Vol. 1. John Wiley and Sons, New York, N.Y., 834 pp.

Parák, T., 1975. Kiruna iron ores are not "intrusive-magmatic ores of the Kiruna type". *Econ. Geol.*, 70: 1242–1258.

Parák, T., 1984. On the magmatic origin of the iron ores of the Kiruna type — A discussion. *Econ. Geol.*, 79: 1945–1949.

Parák, T., 1985. Phosphorus in different types of ore, sulfides in the iron deposits, and the type and origin of ores at Kiruna. *Econ. Geol.*, 80: 646–665.

Perelman, A.I., 1972. *Geochemie Epigenetischer Prozesse*. Akademie Verlag, Berlin, 400 pp.

Petranek, J., 1964. Gemeinsame Merkmale der Eisenerzlager im böhmischen und thringischen Ordovizium. *Abh. Deut. Akad. Wiss., Berlin* (F. Deubel Festband), pp. 79–95.

Petranek, J., Duremberg, D. and Melka, K., 1988. Oolitic iron deposit at Chrustenice. *Sb. Geol. Ved, Loziskova Geol., Mineral.*, 28: 9–55.

Pettijohn, F.J., 1963. *Data of Geochemistry. U.S. Geol. Surv. Prof. Pap.*, 440-5: 21.

Pfannenstiel, F., 1953. Das Quartär der Levante, Teil II: Entstehung der ägyptischen Oasendepressionen. *Abh. Math. Kl., Akad. Wiss. Mainz*, 7: 108–181.

Picard, M.D., 1965. Iron oxides and fine grained rocks of Red Peak and Crow Mountain Sandstone Members, Chugwater (Triassic) Formation, Wyoming. *J. Sediment. Petrol.*, 35: 464–479.

Rubie, D.C. and Thompson, A.B., 1985. Kinetics and metamorphic reactions at elavated temperatures and pressures: an appraisal of available experimental data. In: A.B. Thompson and D.C. Rubie (Editors), *Advances in Physical Geochemistry*, Vol. 4: *Metamorphic Reactions, Kinetics, Textures, and Deformation*. Springer-Verlag, Berlin, pp. 27–79.

Said, R. and Mansour, A.O. (Editors), 1971. *The Discovery of a New Kaolin Deposit in Wadi Kalabscha, Nubia, Egypt. Egypt. Geol. Surv. Miner. Anth.*, Cairo, 138 pp.

Schellmann, W., 1969. Die Bildungsbedingungen sedimentärer Chamosit- und Hämatit-Eisenerze am Beispiel der Lagerstätte Echte. *Neues Jahrb. Mineral., Abh.*, 111: 1–31.

Schiavon, N., 1988. Goethite ooids: growth mechanism and sandwave transport in the Lower Greensand (early Cretaceous, southern England). *Geol. Mag.*, 125: 57–62.

Schlegelmilch, V., 1968. Rotfärbungen im Thüringer Schiefergebirge. *Geologie*, 17: 136–155.

Schluger, P.R. and Roberson, H.E., 1975. Mineralogy and chemistry of the Patapsco Formation, Maryland, related to the groundwater geochemistry and flow system — A contribution to the origin of red beds. *Geol. Soc. Am. Bull.*, 86: 153–158.

Schmalz, R.F., 1968. Formation of red beds in modern and ancient deserts. Discussion. *Geol. Soc. Am. Bull.*, 79: 277–280.

Schweigart, H., 1965. Zur Bildung von Eisenooiden. *Neues Jahrb. Geol. Paläontol., Abh.*, 121: 285–292.

Schwertmann, U. and Fischer, W.R., 1974. Natural "amorphous" ferric hydroxides. *Geoderma*, 10: 237–247.

Schwertmann, U. and Taylor, R.M., 1977. Iron oxides. In: J.B. Dixon and S.B. Weed (Editors), *Minerals in Soil Environments. Soil Sci. Soc. Am.*, Madison, Wisc., pp. 145–179.

Siehl, A. and Thein, J., 1978. Geochemische Trends in der Minette (Jura, Luxemburg/Lothringen). *Geol. Rundsch.*, 67: 1052–1077.

Siehl, A. and Thein, J., 1989. Minette-type ironstone. In: T.P. Young and W.E.G. Taylor (Editors), *Phanerozoic Ironstones. Geol. Soc. London, Spec. Publ.*, 46: 175–193.

Stucki, J.W., Goodmann, B.A. and Schwertmann U. (Editors), 1985. *Iron in Soils and Clay Minerals.* A Nato Advanced Study Institute of Fe. Bad Winsheim, Germany.

Turner, P., 1974. Origin of red beds in the Ringerike Group (Silurian) of Norway. *Sediment. Geol.*, 12: 215–235.

Turner, P. (Editor), 1980. *Continental Red Beds. Developments in Sedimentology, 29.* Elsevier, Amsterdam, 562 pp.

Urban, H., 1966. Bildungsbedingungen und Faziesverhältnisse der marin-sedimentären Eisenerzlagerstätten am Kahlenberg bei Ringsheim (Baden). *Jahrb. Geol. L.A., Baden-Württ.*, 8: 125–267.

Valeton, I., 1953. Petrographie des süddeutschen Hauptbuntsandsteins. *Heidelb. Beitr. Mineral. Petrol.*, 3: 335–379.

van Houten, F.B., 1961. Climatic significance of red beds. In: A.E.M. Nairn (Editor), *Descriptive Paleoclimatology.* Interscience, New York, N.Y., pp. 89–139.

van Houten, F.B., 1964. Origin of red beds — some unresolved problems. In: A.E.M. Nairn (Editor), *Problems in Paleoclimatology.* Interscience, New York, N.Y., pp. 647–661.

van Houten, F.B., 1968. Iron oxides in red beds. *Geol. Soc. Am. Bull.*, 79: 399–416.

van Houten, F.B., 1973. Origin of red beds. A review. *Annu. Rev. Earth Planet. Sci.*, 1: 39–61.

van Houten, F.B. and Battacharryya, D.P., 1982. Phanerozoic oolitic ironstone. Geological Record and Facies Model. *Annu. Rev. Earth Planet. Sci.*, 10: 441–457.

van Houten, F.B., Battacharyya, D.P. and Mansour, S.E.I., 1984. Cretaceous Nubia Formation and correlation deposits, eastern Egypt: Major regressive–transgressive complex. *Bull. Geol. Soc. Am.*, 95: 397–405.

van Houten, F.B. and Arthur, M.A., 1989. Temporal patterns among Phanerozoic oolitic ironstones and oceanic anoxia. In: T.P. Young and W.E.G. Taylor (Editors), *Phanerozoic Ironstones. Geol. Soc. London, Spec. Publ.*, 46: 33–49.

van Houten, F.B., (1990).Palaeozoic oolitic ironstones on the North American Craton.*Palaeogr., Palaeoclimatol., Palaeoecol.*, 80: 245–254.

Walker, T.R., 1967a. Formation of Red Beds in modern and ancient desert. *Geol. Soc. Am. Bull.*, 78: 353–368.

Walker, T.R., 1967b. Colour of recent sediments in tropical Mexico: A contribution to the origin of red beds. *Geol. Soc. Am. Bull.*, 78: 917–919.

Walker, T.R., 1974. Formation of red beds in moist tropical climates: A hypothesis. *Geol. Soc. Am. Bull.*, 85: 633–638.

Walker, T.R., 1976. Diagenetic origin of continental red beds. In: H. Falke (Editor), *The Continental Permian in Central, West, and South Europe.* D. Reidel, Dordrecht, pp. 240–282.

Walker, T.R. and Honea, R.M., 1969. Iron content in modern deposits in the Sonoran Desert: A contribution to the origin of red beds. *Geol. Soc. Am. Bull.*, 80: 535–544.

Walker, T.R., Waugh, B. and Crone, A.J., 1978. Diagenesis in first-cycle desert alluvium of Cenozoic age, southwestern United States and northwestern Mexico. *Geol. Soc. Am. Bull.*, 89: 19–32.

Williams, T.M. and Owen, R.B., 1990. Authigenesis of ferric oolites in superfical sediments from Lake Malawi/Central Africa. *Chem. Geol.*, 89: 179–188.

Wopfner, H. and Schwarzmann, M., 1976. Ore deposits in the light of paleoclimatology. In: K.H. Wolf (Editor), *Handbook of Stratabound and Stratiform Ore Deposits*, Vol. 3. Elsevier, Amsterdam, pp. 43–92.

Worral, G.A., 1969. The red sands of the southern Sahara. *Bull. de Liason, Assoc. Sénégalaise pour l'Étude du Quarternaire de l'Ouest Africaine*, 21: 36–39.

Yapp, C.J., 1991. Oxygen isotopes in an oolitic ironstone and the determination of goethite δ^{18}O values by selective dissolution of impurities: The 5M NaOH method. *Geochim. Cosmochim. Acta*, 55: 2627–2634.

Young, T.P., 1989. Phanerozoic ironstone: an introduction and review. In: T.P. Young and W.E.G. Taylor (Editors), *Phanerozoic Ironstones. Geol. Soc. London, Spec. Publ.*, 46: IX–XXV.

Young, T.P. and Taylor, W.E.G. (Editors), 1989. *Phanerozoic Ironstones. Geol. Soc. London, Spec. Publ.*, 46, 251 pp.

This Page Intentionally Left Blank

Diagenesis, IV. Developments in Sedimentology 51
edited by K.H. Wolf and G.V. Chilingarian
© 1994 Elsevier Science B.V., Amsterdam. All rights reserved.

Chapter 12

DIAGENETIC PROCESSES ASSOCIATED WITH PLANT ROOTS AND MICROORGANISMS IN KARST TERRAINS OF THE CAYMAN ISLANDS, BRITISH WEST INDIES

BRIAN JONES

INTRODUCTION

Large volumes of water passing over and through karst terrains are responsible for much of the dissolution and precipitation that produce this distinctive landscape (James and Choquette, 1984). It is becoming increasingly clear, however, that lichens (Klappa, 1979a; Jones and Kahle, 1985), algae or cyanobacteria (James, 1972; Knox, 1977; Klappa, 1979b), fungi (Klappa, 1979b; Calvet, 1982; Coniglio and Harrison, 1983), bacteria (Calvet, 1982; Jones and Motyka, 1987), and actinomycete (Klappa, 1979b; Calvet, 1982) are common in these terrains and play an important role in the diagenetic development of the carbonates on which the karst terrain has developed.

On the Cayman Islands, dolostones of the Oligocene–Miocene Bluff Formation are characterized by a wide variety of karst features (Doran, 1954; Jones and Smith, 1988; Squair, 1988). Karst features on the overlying limestones of the Pleistocene Ironshore Formation are more subdued than those on the Bluff Formation. Nevertheless, examination of both successions provides information pertinent to any discussion concerning the role of microorganisms in diagenetic processes associated with karst development. In addition, experimental work using fungi cultured on calcite crystals has yielded information (Jones and Pemberton, 1987a, b) that provides a baseline against which natural processes can be compared.

This chapter discusses the results of experimental information pertaining to the role of microorganisms in carbonate diagenesis, and examines specific examples where microorganisms contributed to the diagenesis of carbonates exposed on the Cayman Islands (Fig. 12-1). With this data base, it is possible to (1) discuss the type and recognition of microorganisms involved in diagenesis in karst terrains, (2) discuss the processes that have been governed by the activity of microorganisms, and (3) detail the distribution of the different processes that are related to the activity of the microorganisms.

GEOLOGY OF THE CAYMAN ISLANDS

Each of the Cayman Islands have a core of Oligocene–Miocene Bluff Formation that is flanked and unconformably overlain by the Pleistocene Ironshore Formation (Fig. 12-1). The Bluff Formation is formed of poorly bedded, white, dense, very finely crystalline dolostone that contains an abundant, diverse fauna of corals, bivalves,

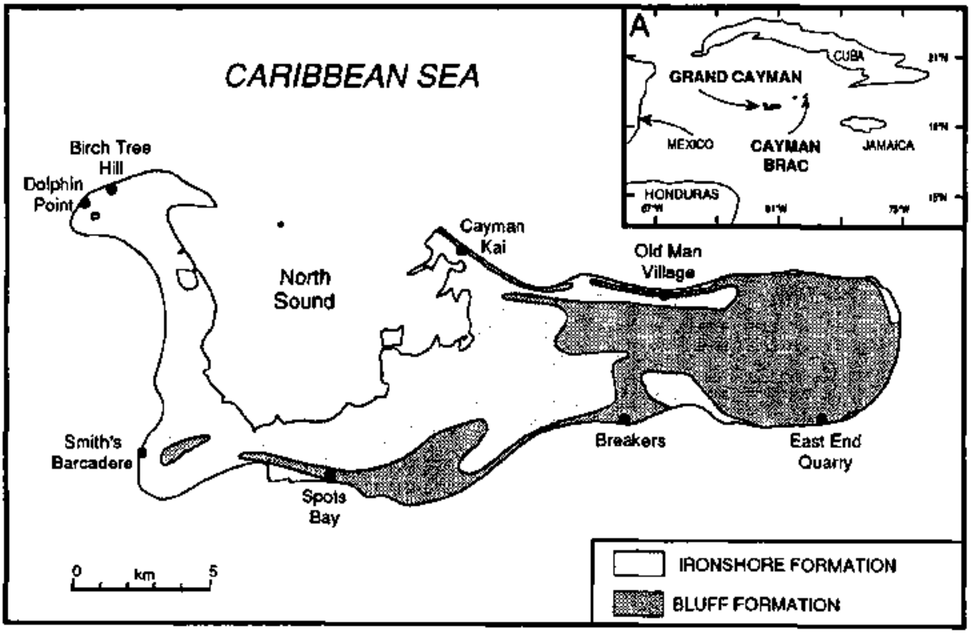

Fig. 12-1. Sketch map of Grand Cayman Island showing (A) the distribution of the Ironshore and Bluff formations, and (B) localities cited in this study.

gastropods, red algae, and foraminifera (Folk et al., 1973; Jones et al., 1984; Hunter and Jones, 1988). The Ironshore Formation is formed of limestones that contain an abundant, well preserved fauna of corals, bivalves, gastropods, and foraminifera (Brunt et al., 1976; Hunter and Jones, 1988, 1989; Cerridwen, 1989). Staining and XRD analysis shows that virtually all limestone in the Ironshore Formation and most of its skeletal material is still formed of aragonite.

GENERAL CLIMATIC CONDITIONS OF THE CAYMAN ISLANDS

The Cayman Islands enjoy a tropical climate with daily temperatures of 25 to 30°C and an annual average rainfall of 1513 mm/year during the 1920 to 1987 period (Ng, pers. commun., 1989). Rainfall amounts vary systematically across the island; for example, in 1987 the east coast of the Grand Cayman received 900 mm of precipitation, whereas the southwest corner of the island received 1600 mm (Ng, pers. commun., 1989). The rainfall is commonly in the form of torrential tropical downpours of short duration.

Except in places where sinkholes intercept the water table, there are no free-standing surface freshwater ponds or streams on the islands. Any rain is quickly channelled, via the extensive karst system, into the subsurface.

TABLE 12-1

Features produced through the action of different species of fungi on crystals of Iceland spar calcite (from Jones and Pemberton, 1987a, table 2)

Species	IE[1]	SP[1]	TB[1]	SC[1]	NC[1]
Phoma glomerata	×	×	×	×	
Epicoccum nigrum	×	×	×		×
Penicillum chrysogenum	×	×		×	
Cladosporium herbarum	×	×		×	
Alternaria tenuis	×	×	×	×	
Aspergillus ustus	×	×	×		

[1] IE = irregular etching, SP = sparmicritization, TB = trapping and binding, SC = spiky calcite, and NC = new crystal growth.

EXPERIMENTAL DATA

The role of microorganisms in carbonate diagenesis has been deduced largely from the study and interpretation of fabrics preserved in limestones. In many cases it is difficult, if not impossible, to identify a microorganism and link it to the formation of a particular structure or fabric (e.g., Phillips et al., 1987; Jones, 1988). In an effort to overcome this problem various experimental approaches have been utilized. Danielli and Edington (1983) cultured various strains of bacteria obtained from moonmilk in various Welsh caves in order to examine their effect on calcite formation. Kieft and Caldwell (1984) tested the corrosive effects of the thermophilic bacteria *Thermothrix thiopora* by periodically examining crystals of Iceland Spar calcite that had been placed in a hot spring in New Mexico. Jones and Pemberton (1987a, b) cultured known species of fungi on crystals of Iceland Spar calcite housed in glass dishes. Processes or fabrics produced during those experiments could then be ascribed to fungal action and related to a known species of fungi. Such experiments demonstrated that fungi mediate a wide array of destructive and constructive processes that can substantially modify calcareous substrates (Table 12-1). Pentecost and Bauld (1988) cultured cyanobacteria in various solutions in order to assess their role in calcification, whereas Ferrer et al. (1988) examined calcification associated with the halophilic bacteria *Deleya halophilia*.

Destructive processes

Kieft and Caldwell (1984) argued that the thermophilic bacteria *Thermothrix thiopora* was partly responsible for the dissolution of calcite crystals that had been placed in a hot spring in New Mexico. This dissolution probably occurred because of the production of sulphuric acid by the bacteria (Kieft and Caldwell, 1984). Such dissolution occurred rapidly with the first detectable dissolution being noted only 2 days after the crystals were placed in the hot springs pool.

The experiments of Jones and Pemberton (1987a, b) showed that the destructive processes mediated by fungi resulted in (1) sparmicritization due to dissolution

(Jones and Pemberton, 1987a), (2) the production of silt- and clay-sized particles of calcite by breakdown of the substrate (Jones and Pemberton, 1987a), (3) the formation of spiky calcite by dissolution (Jones and Pemberton, 1987a, b), and (4) $CaCO_3$ being placed into solution (Jones and Pemberton, 1987a). Boring, a destructive process commonly associated with fungal activity (e.g., Kendrick et al., 1982), did not occur during the experiments of Jones and Pemberton (1987a, b).

Sparmicritization describes the alteration of spar calcite to micrite by any known or inferred process (Kahle, 1977). On the basis of their experiments, Jones and Pemberton (1987a) suggested that sparmicritization resulted from (1) localized dissolution of calcite following a pattern (Fig. 12-2) controlled by the distribution of fungal hyphae and/or mucilaginous mats associated with the hyphae, (2) the formation of monticuli because of increased solution at selected sites, and (3) further solution around the bases of monticuli so that the upper part eventually becomes a loose, detached silt- or clay-sized grain (Fig. 12-3). These loose grains may be a source for vadose silt (Jones and Pemberton, 1987a).

The term spiky calcite describes a calcite crystal surface that appears to be covered with a forest of spikes like a fakir's bed (Folk et al., 1985, p. 362–364). Although Folk et al. (1985) suggested that spiky calcite may be a product of growth or dissolution, Jones and Pemberton (1987b) argued that it resulted from dissolution mediated by fungi located on the crystal surfaces (Figs. 12-4, 12-5).

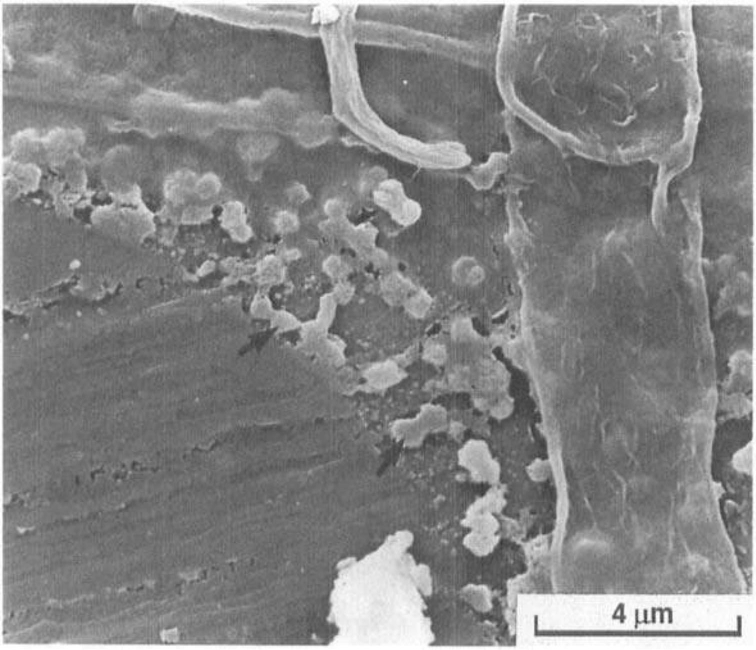

Fig. 12-2. Etching produced experimentally by culturing fungi (*Alternaria tenuis*) on a crystal of Iceland Spar calcite that was housed in a covered glass (see Jones and Pemberton, 1987a, b). Note that etching produced isolated islands of calcite (monticuli — arrows) which eventually become detached to form detrital particles.

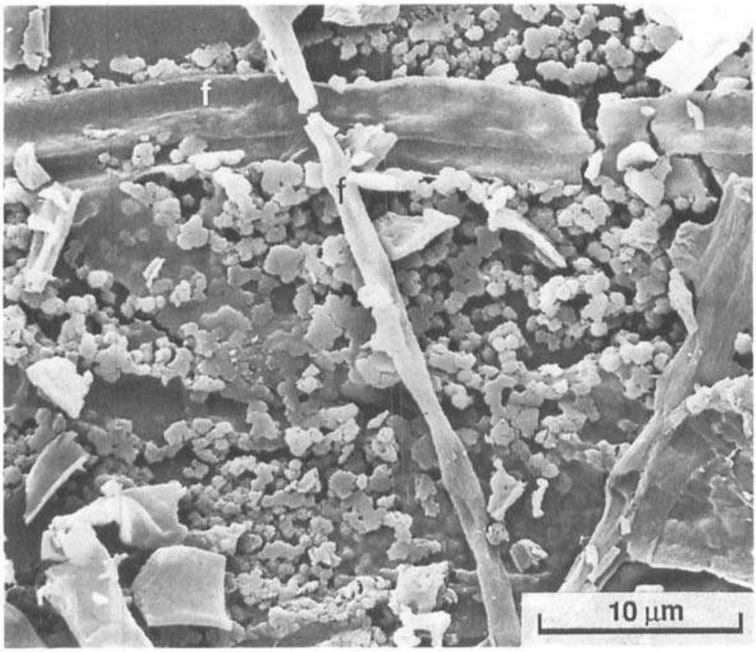

Fig. 12-3. Similar view to Fig. 12-2 but showing area that has been more extensively etched. As a result, many of the monticuli have become detached and are now loose on the surface of the crystal. Note fungal hyphae (*f*) crossing surface of crystal.

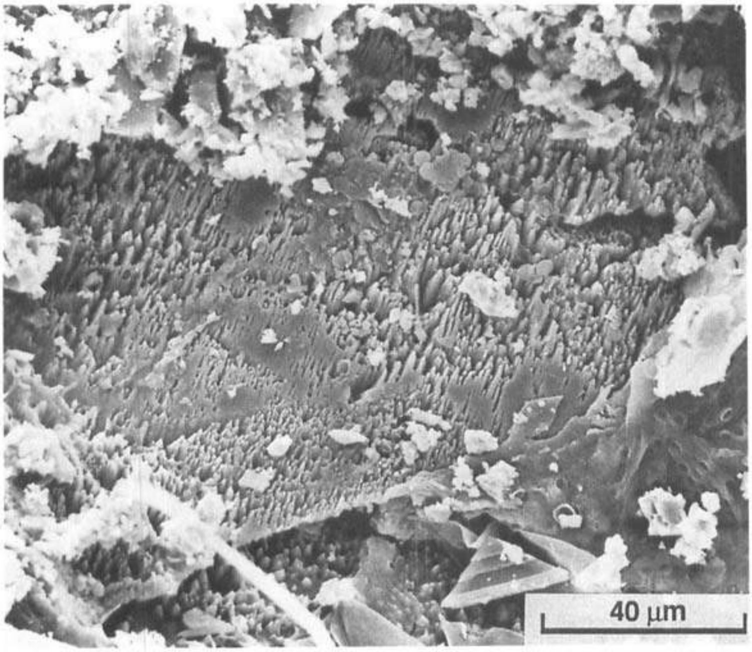

Fig. 12-4 Well developed spiky calcite produced experimentally by the etching activity of *Penicillum chrysogenum*. Note loose pieces of calcite in surrounding area.

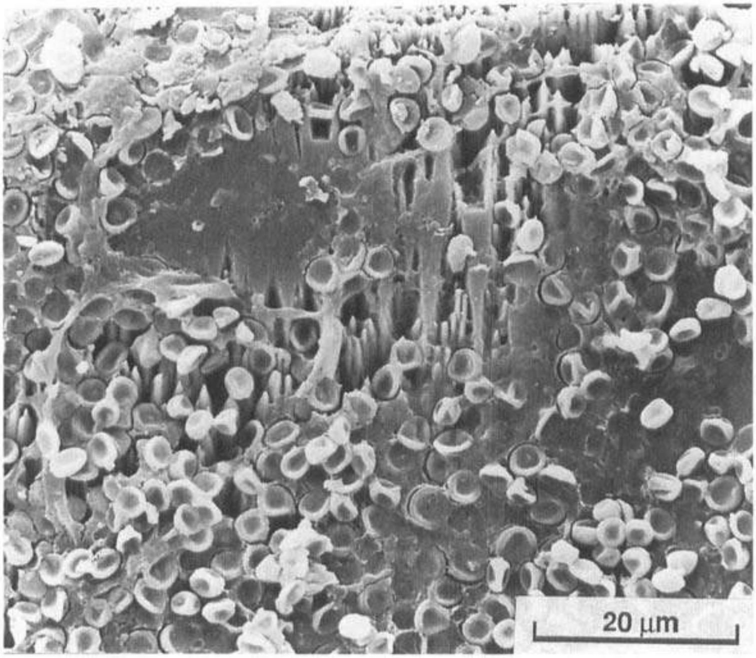

Fig. 12-5. Detailed view of surface of Iceland Spar calcite that has been partly etched by the activity of *Penicillum chrysogenum*. This texture was produced experimentally.

The experiments of Jones and Pemberton (1987a, b) were designed to obtain information on borings produced by fungi because such substrate modification has been well documented (e.g., Zebrowski, 1936; Porter and Zebrowski, 1937; Korringa, 1951; Perkins and Halsey, 1971; Rooney and Perkins, 1972; Edwards and Perkins, 1974; Kendrick et al., 1982). The experiments did not, however, provide any information about the boring activity of fungi.

Constructive processes

Bacteria cultured in solutions containing calcium carbonate commonly become coated with calcite crystals that display variable morphology (e.g., Danielli and Edington, 1983; Ferrer et al., 1988). Calcification of cultured bacteria produced spherical masses up to 400 μm in diameter that were formed of radiating calcite needles or masses of irregular-shaped rhombs (Danielli and Edington, 1983). Calcification, which occurred in 8 to 15 days (Danielli and Edington, 1983, table 3), was attributed to the bacteria dumping waste calcium after it had obtained the necessary nourishment from the organic salt that was provided. Ferrer et al. (1988) adopted a similar approach and showed that laboratory cultivation of bacteria after as little as 20 days produced "...porous aggregates with external globular to spherical form..." that are 40 to 60 μm in diameter. Some of the spherical bodies were smooth, whereas others were covered with small calcite crystals (Ferrer et al., 1988, fig. 2). The degree

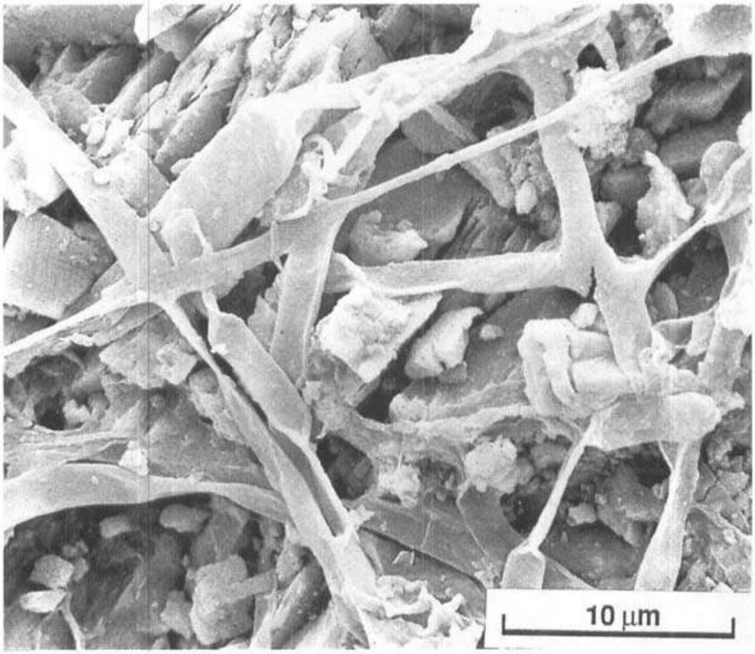

Fig. 12-6. Example of hyphae of the fungi *Aspergillus ustus* binding loose particles of calcite to the surface of the calcite crystal. Texture produced experimentally on Iceland Spar calcite crystal after 253 days.

of calcification of the bacteria was reduced by increasing the Mg content of the fluid but increased as the temperature of the fluid changed from 22°C to 32°C (Ferrer et al., 1988). Pentecost and Terry (1988) isolated bacteria from various travertines in Europe and North America but found that none were capable of nucleating calcite when placed in calcium bicarbonate solutions.

Constructive processes apparent from the experiments of Jones and Pemberton (1987a, b) were trapping and binding of detrital particles and precipitation of new crystals. Silt- and clay-sized particles formed through the destruction of calcareous substrates by fungi can be moved and deposited elsewhere by water (Jones and Pemberton, 1987a). Locally, these particles were trapped and bound in place by fungal hyphae (Fig. 12-6). Although no substantial buildups formed during the experiments which lasted 253 days, it is not unreasonable to suggest that such structures could be formed. There was no evidence of calcification of the fungal filaments.

Fungal attack on calcareous substrates commonly results in $CaCO_3$ being put into solution and transported elsewhere. If physicochemical conditions are suitable, $CaCO_3$ can be reprecipitated elsewhere as new crystals. Jones and Pemberton (1987a, figs. 5, 6) demonstrated that some $CaCO_3$ was precipitated beneath mats of fungal filaments (Fig. 12-7). It is also possible that some microorganisms may use this $CaCO_3$ in the calcification of their filaments. If so, it is possible that fungi can recycle $CaCO_3$ from the substrate to their filaments.

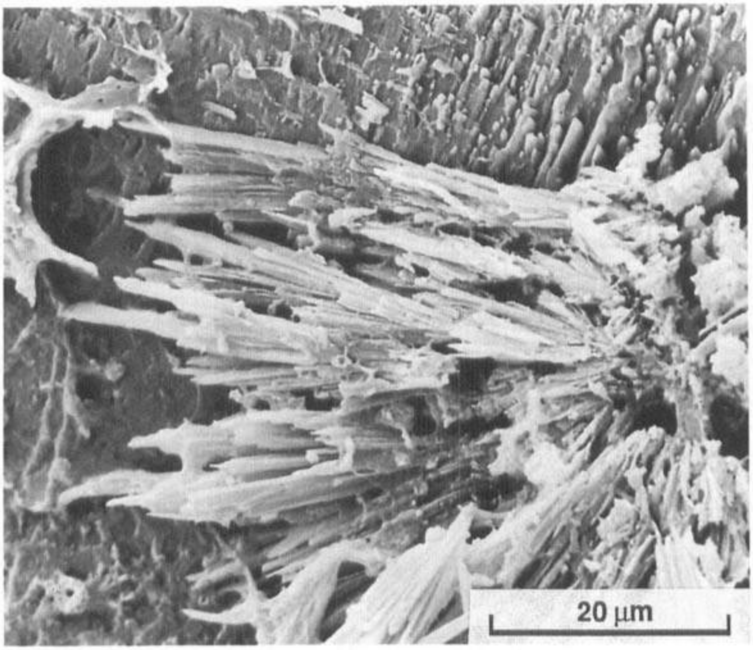

Fig. 12-7. Elongate crystals of aragonite(?) precipitated on the surface of an Iceland Spar calcite crystal. The precipitation of these crystals is attributed to the action of the fungi *Epicoccum nigrum* that was cultured on a crystal of Iceland Spar calcite. (From Jones and Pemberton, 1987, fig. 6B.)

Pentecost and Bauld (1988) found that calcite crystals developed on the filaments of the cyanobacteria *Scytonema myochrous* and *Lyngbya aestuarii* in 3 to 12 hours. Although most of the crystals formed as distinct rhombohedra, there were rare examples of anhedral crystals and clusters of crystals (Pentecost and Bauld, 1988, fig. 3).

MICROORGANISMS AND DIAGENETIC FABRICS IN THE KARST TERRAINS OF THE CAYMAN ISLANDS

Microorganisms and their associated fabrics are common throughout the surface and subsurface karst features developed on the limestones and dolostones of the Cayman Islands. This can be demonstrated by considering the microorganisms and fabrics associated with (1) surface weathering, (2) caves, (3) karst breccias, (4) rhizoliths, and (5) root borings.

Surface weathering

Surface weathering of carbonates is controlled by a complex array of mechanical, chemical, and biological processes (Trudgill, 1985). Folk et al. (1973, p. 2351), following study of exposures at Hell (Fig. 12-1), highlighted the role of plants by

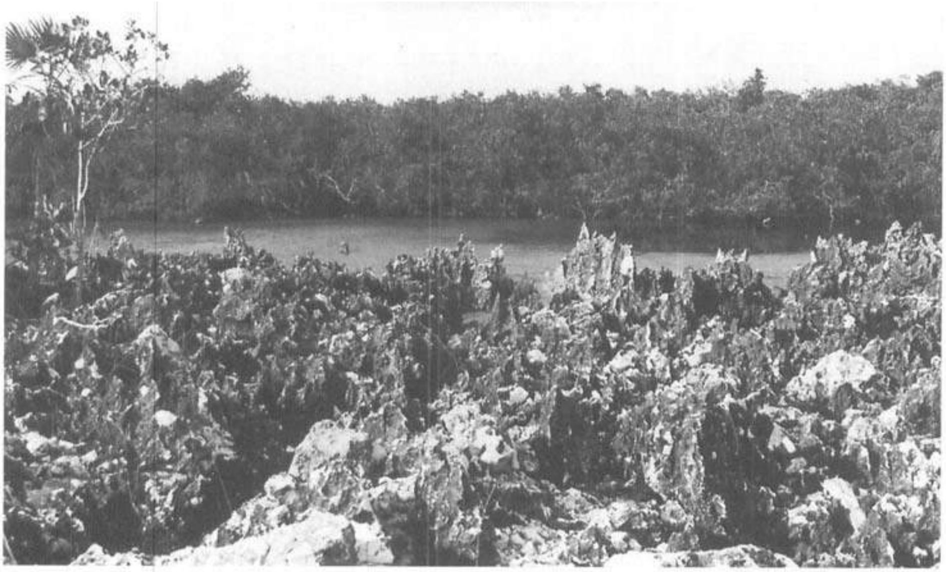

Fig. 12-8. General view of phytokarst surface developed on the dolostones of the Bluff Formation. Northwest corner of abandoned quarry at Spots Bay, Grand Cayman (Fig. 12-1).

coining the term phytokarst for "...a landform produced by rock solution in which boring plant filaments are the main agents of destruction...". The dark grey to black color of such surfaces was attributed to decaying microorganisms. Although phytokarst (Fig. 12-8) is well developed on dolostones of the Bluff Formation (Folk et al., 1973; Squair, 1988; Jones and Smith, 1988; Jones, 1989) it is more subdued on the limestones of the Ironshore Formation (Jones, 1989). The development of phytokarst can be attributed to the activity of endolithic and epilithic microorganisms (Jones, 1989). It should be noted, however, that Spencer (1981, 1985a, b), Spencer et al. (1984) and Viles and Spencer (1983) argued that microorganisms are not responsible for all the weathering seen on the limestones and dolostones of the Cayman Islands.

Endolithic microorganisms

The hard, finely crystalline dolostones of the Bluff Formation are penetrated by isodiametric unlined borings, up to 10 μm in diameter, that extend from weathered surfaces to depths of at least 200 μm (Fig. 12-9). Although most borings are perpendicular to the weathered surface, others follow a convoluted path and branch at irregular intervals (Fig. 12-9). Many borings contain unmineralized branching, nonseptate algal filaments that have the same diameter as the borings (Fig. 12-9). The borings are generally widely spaced, although they may be closely spaced on small upstanding ridges.

The soft limestones of the Ironshore Formation are penetrated by an abundant, diverse flora of endolithic microorganisms (Fig. 12-10). Samples from Dolphin Point

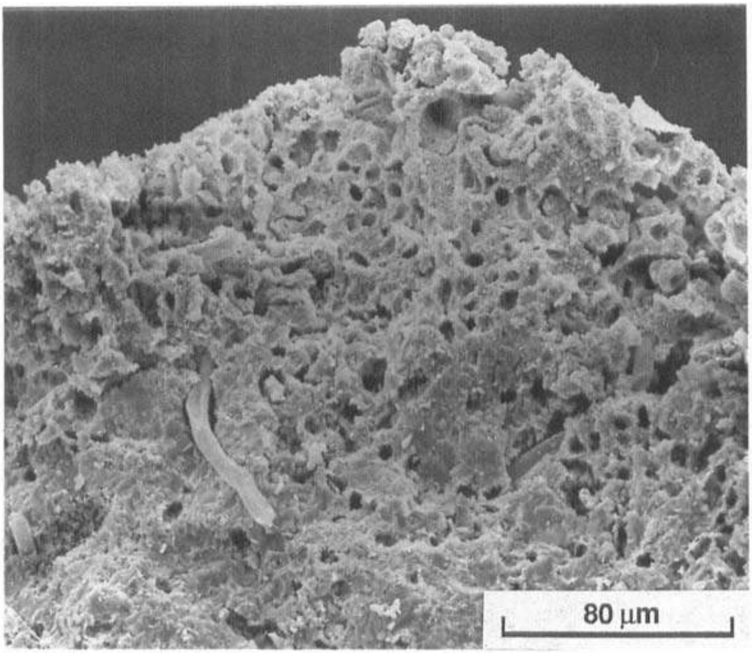

Fig. 12-9. Photomicrograph showing extensively bored zone beneath weathered surface of dolostone from the Bluff Formation at Cayman Kai (Fig. 12-1). Note filament still present in one of the borings. Dolostones from the Bluff Formation usually have fewer borings than this penetrating the substrate. (From Jones, 1989, fig. 4A.)

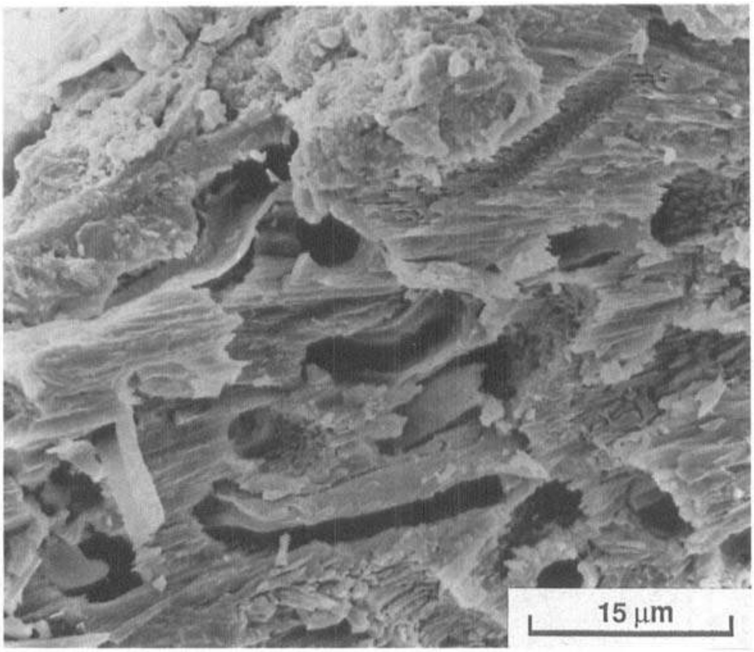

Fig. 12-10. Example of marine aragonite cements in the Ironshore Formation that have been extensively bored by algae(?). Sample from Smith's Barcadere (Fig. 12-1). (From Jones, 1989, fig. 4I.)

(DP — Fig. 12-1), Birch Tree Hill (BTH — Fig. 12-1), and Smith's Baracadere (SB — Fig. 12-1) are characterized by an extensively bored zone beneath the weathered surfaces (Fig. 12-10). Although most borings are vertical to subvertical, some are parallel to the weathered surface, stretching for distances of more than 350 μm. The filaments and borings are typically isodiametric, straight to contorted, branched or unbranched, and up to 10 μm in diameter (Fig. 12-10) and penetrate to depths of 1 cm. Most borings, however, are less than 3 mm deep. There is no evidence that boring morphology is controlled by rock texture. Although most filaments are uncalcified, some have been encased by micrite to form tubes with an external diameter of 12 μm and an internal diameter of 6 μm. Other filaments have calcite crystals up to 4 μm long scattered across their surfaces. Attached to some filaments are numerous smooth, ovate to spherical bodies, up to 1 μm long, that display varying degrees of cell division (Jones, 1989, figs. 4K, 4L). Although not calcified they have not collapsed. Their size and style of division suggest that they are bacteria.

Epilithic microorganisms

Weathered surfaces of the Bluff Formation are covered by an organic coating formed of sporangia (a sac which bears endogenous nonsexual spores; Moore-Landecker, 1982, p. 555), a diverse array of spores (a discrete sexual or nonsexual reproductive unit which is capable of being disseminated; Moore-Landecker, 1982, p. 555), rare algal and/or fungal filaments, and mucilage (Jones, 1989). Black, dome-shaped sporangia, up to 0.5 mm in diameter and 0.2 mm high, are scattered

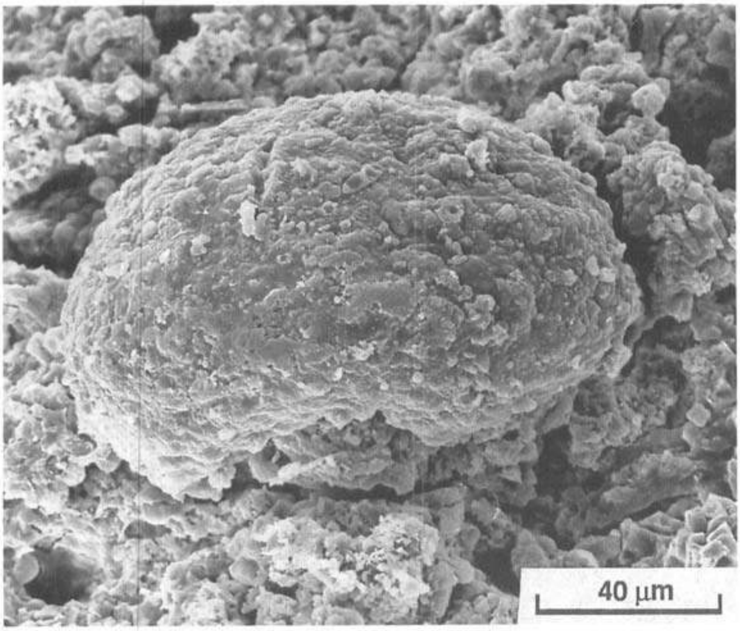

Fig. 12-11. Example of sporangia that occurs on the weathered surfaces of the Bluff Formation at Cayman Kai (Fig. 12-1). (From Jones, 1989, fig. 3D.).

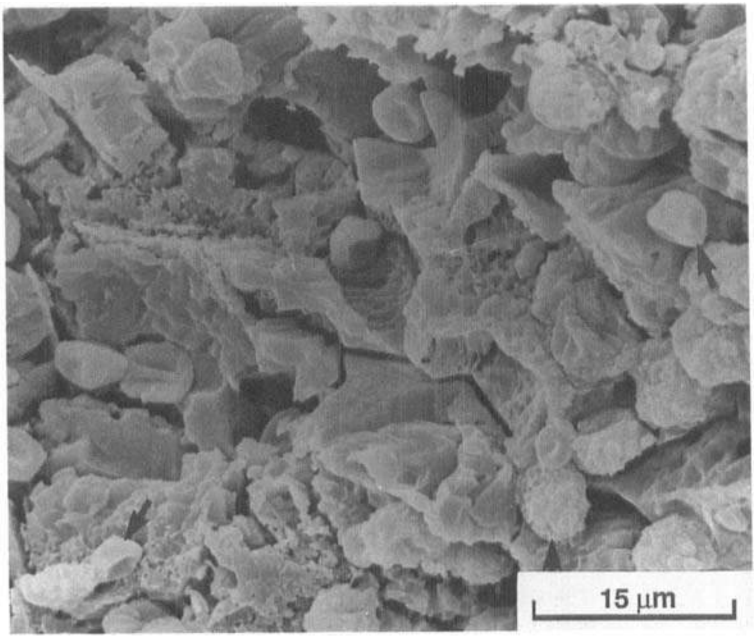

Fig. 12-12. General view of spores (arrows) on weathered surface of dolostone from the Bluff Formation at Cayman Kai (Fig. 12-1). Note abundant etch features associated with the spores. (From Jones, 1989, fig. 3F.)

across the weathered surfaces (Fig. 12-11). On the surrounding substrate there are numerous unmineralized filaments, 3 to 4 μm in diameter, that penetrate the rock thereby "rooting" the sporangia to the surface. The sporangia are probably the "black dots" which Folk et al. (1973, p. 2355) identified as the coccoid blue-green algae *Gloeocapsa alpina*.

Smooth and ornamented spores, 4 to 10 μm in diameter, are the most common elements of the organic coatings on weathered surfaces of the Bluff Formation (Fig. 12-12). Collapsing of many spores suggests that they were not extensively mineralized even though some have scattered anhedral crystals, up to 2 μm long, that contain Mg and Ca on their surfaces. The degree of mineralization is highly variable even in small areas. Thus, one spore may have only a few crystals on its surface, whereas another, only 20 to 30 μm away, may be completely coated with crystals. When viewed at high magnification, the heat of the beam on the SEM usually caused the spores to break open, suggesting that mineralization is superficial and incomplete. Filaments are rare on the weathered surface apart from those associated with the sporangia. These filaments, which include septate forms, up to 2 μm in diameter, and nonseptate forms up to 4 μm in diameter that are collapsed, display no evidence of mineralization.

The black weathered surfaces of the Ironshore Formation are characterized by coatings of filaments, mucilage, and rare spores (Jones, 1989). No sporangia were found. The surfaces of limestones from locality WBB and DP (Fig. 12-1) have dense

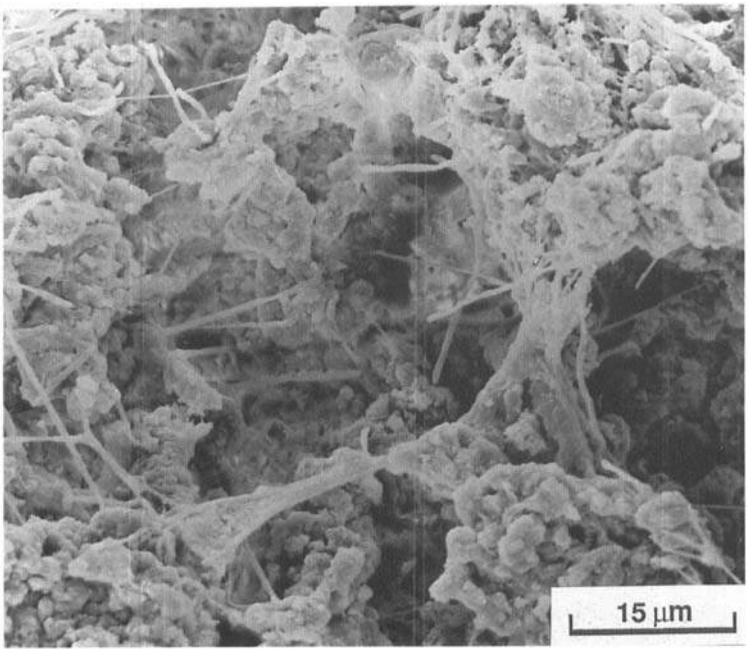

Fig. 12-13. Example of filaments and mucus that occurs on weathered surfaces of limestone from the Ironshore Formation at Dolphin Point (Fig. 12-1). (From Jones, 1989, fig. 3K.)

meshworks of uncalcified, isodiametric, branching, non-septate filaments, up to 1.5 μm in diameter, that are locally covered by mucilage (Fig. 12-13). Locally, uncalcified filaments are wrapped around calcified filaments that have an outside diameter of 7 μm and an inside diameter of 3 to 5 μm. Spores are rare on the limestones of the Ironshore Formation, being restricted to scattered, smooth, ovate to spherical bodies up to 6 μm in diameter.

Caves

Cave entrances

The "twilight zone", which occurs around cave entrances, is the transition zone between normal light conditions and the black interior of the cave (Cox, 1977a, b). Rock surfaces in the twilight zone of caves on the Cayman Islands are green, presumably because of the presence of microorganisms. Although this color is best developed in areas under the direct influence of sunlight, it is also present in areas that seem to receive little light.

Walls in the twilight zone are characterized by an abundant and diverse array of microorganisms (Figs. 12-14, 12-15, 12-16) that probably includes algae, cyanobacteria, fungi and bacteria. On a microscale, the rocks of the cave walls have been significantly modified by the microorganisms. In this setting, destructive processes are more important than constructive processes.

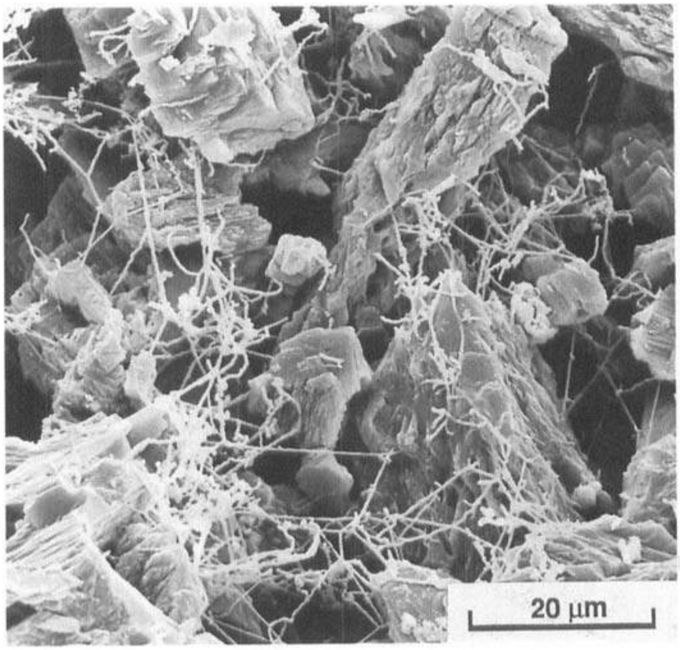

Fig. 12-14. General view of filaments covering calcite crystals that occur on a cave wall in the twilight zone. Note highly irregular topography of underlying crystals which can probably be attributed to etching that was mediated by the microorganisms. Sample from entrance to cave near Old Man Village (Fig. 12-1).

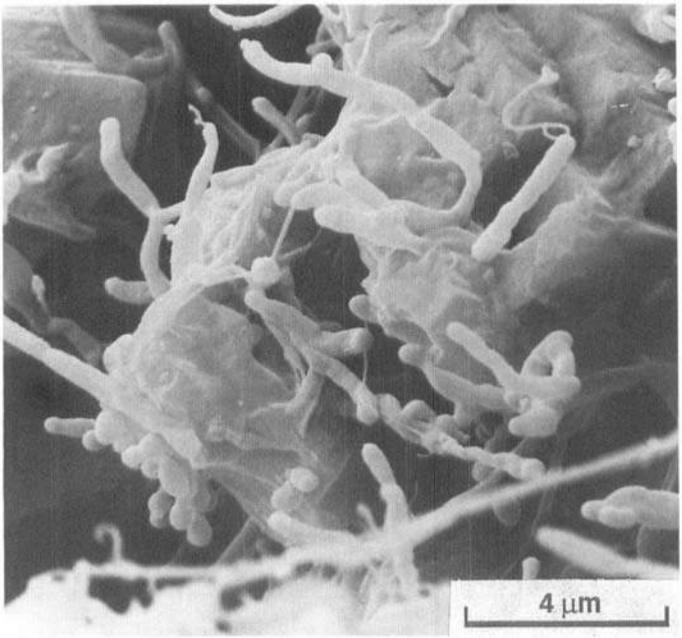

Fig. 12-15. Detailed view of filaments on calcite grains that occur on a cave wall in the twilight zone. The constrictions in the filaments suggest that they may be septate. Sample from entrance to cave near Old Man Village (Fig. 12-1).

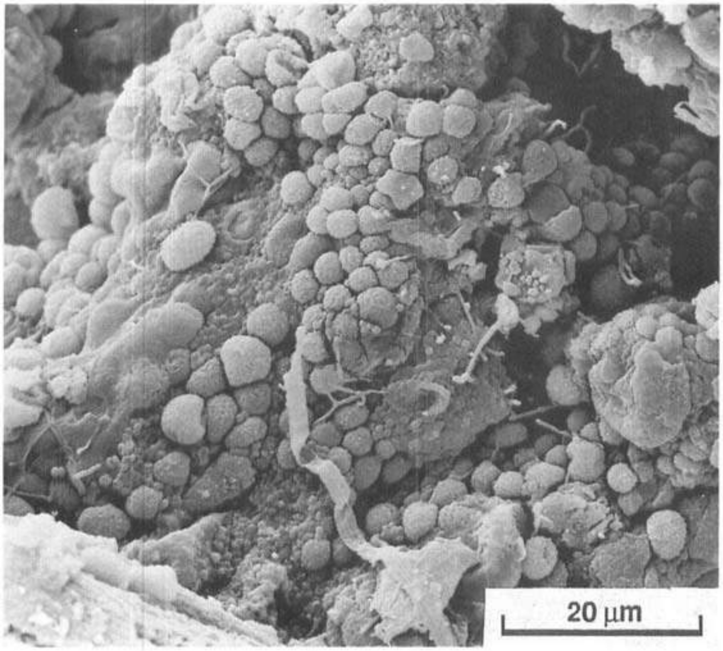

Fig. 12-16. Agglomeration of uncalcified hemispherical and spherical bodies coating calcite substrate. The affinity of these bodies is uncertain. Sample from entrance to cave near Old Man Village (Fig. 12-1).

The destructive processes operative in this area of the cave have led to micritization (Fig. 12-17), and the formation of irregular etch patterns, spiky calcite (Fig. 12-18), and "blocky topographies" (Fig. 12-19). Boring occurs locally. Conversely, constructive activity is minimal because there is no evidence of new crystal growth and calcification of microorganisms is limited. Although individual particles have been trapped and bound to the surface in a manner similar to that seen in the experiments of Jones and Pemberton (1987a, b), there are no laminated microstromatolites of the type described by Jones and Kahle (1985).

Stalactites

Stalactites are common features of caves developed in the Bluff Formation of the Cayman Islands (Jones and Smith, 1988). Jones and Motyka (1987) examined stalactites from an ancient filled cave near Breakers and an open cave near Old Man Village on Grand Cayman (Fig. 12-1). Most stalactites are characterized by a "soda-straw" surrounded by a core of micrite and an outer zone of crystalline calcite (Fig. 12-20). The core is formed of radiating, internally laminated columns, 2 to 3 mm wide at their base and 3 to 6 mm wide at their maximum expansion (Fig. 12-20). Their overall morphology and internal laminations are suggestive of stromatolitic development.

Constructive processes evident in the micrite cores of the Caymanian stalactites

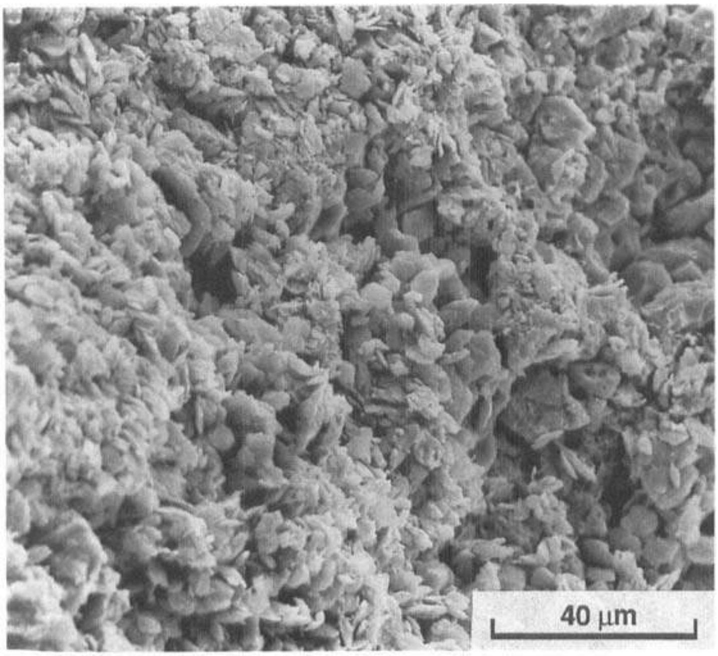

Fig. 12-17. Example of micrite which probably resulted through the breakdown of spar calcite. Sample from entrance to cave near Old Man Village (Fig. 12-1).

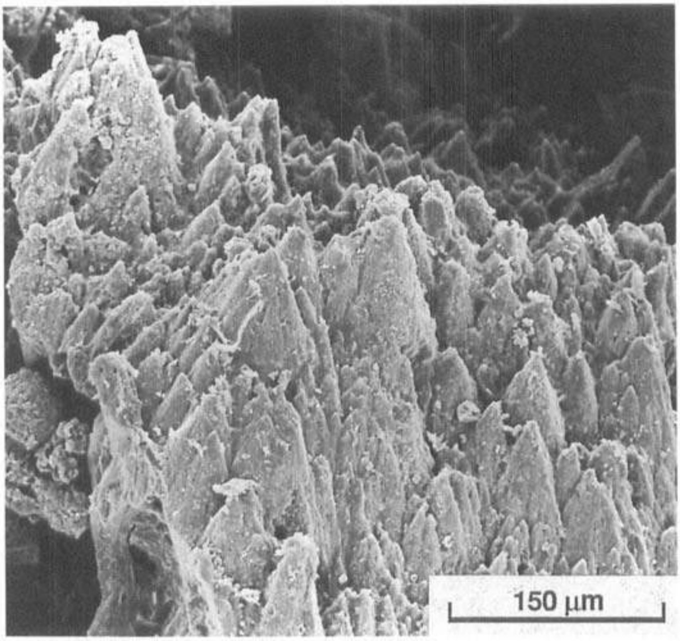

Fig. 12-18. Spiky calcite which is presumed to have developed through the etching of spar calcite. Sample from entrance to cave near Old Man Village (Fig. 12-1).

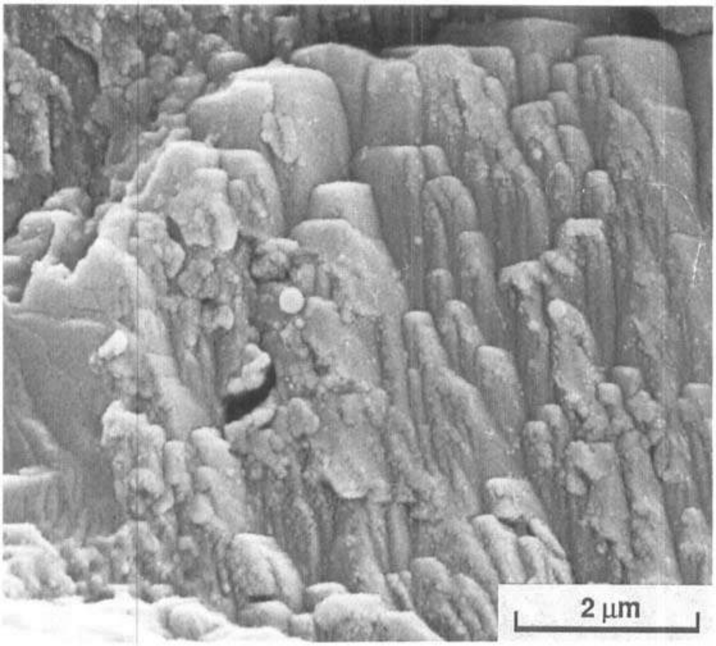

Fig. 12-19. Example of "blocky topography" which probably resulted from the etching of sparry calcite. Sample from entrance to cave near Old Man Village (Fig. 12-1).

include calcification of filaments (Figs. 12-21, 12-22), fixing of elements (e.g., Mn and Al), trapping, and binding of micrite. There is no evidence of destructive activity by boring or dissolution.

Bacteria-like structures (Figs. 12-23, 12-24) and calcified filaments (Figs. 12-21, 12-22) that may be of algal origin occur in the micrite that forms the central parts of the stalactites (Jones and Motyka, 1987). Jones and Motyka (1987) divided the opaque, bacteria-like structures into (1) Type I, 3 to 24 μm in diameter, which are formed of numerous small platelets and have a high Fe content along with lesser amounts of Ca and more rarely, Al (Fig. 12-23); and (2) Type II, 3 to 12 μm in diameter, that have a distinctive reticulate appearance (Fig. 12-24) and a high Mn content along with lesser amounts of Ca and Al but no Fe. Shrub-like masses of these bodies are similar to bacterial shrub-like masses present in travertines elsewhere in the world (e.g., Chafetz and Meredith, 1983, fig. 2A; Chafetz and Folk, 1984, fig. 22B; Folk et al., 1985, fig. 2B). These bacteria helped in the construction of the micritic masses, and selectively fixed elements such as Fe, Mn and Al.

Calcified filaments are common in many parts of the micrite. The isodiametric, unbranched filaments, which have a central tube 2 to 4 μm in diameter, are calcified by a single layer of "spike-like" crystals or irregularly shaped crystals 2 to 4 μm long. Jones and Motyka (1987) suggested that they were probably algal filaments. The calcified filaments are important because (1) they trapped and bound micrite, (2) they added mass to the stalactite through calcification, and (3) the breakdown of the

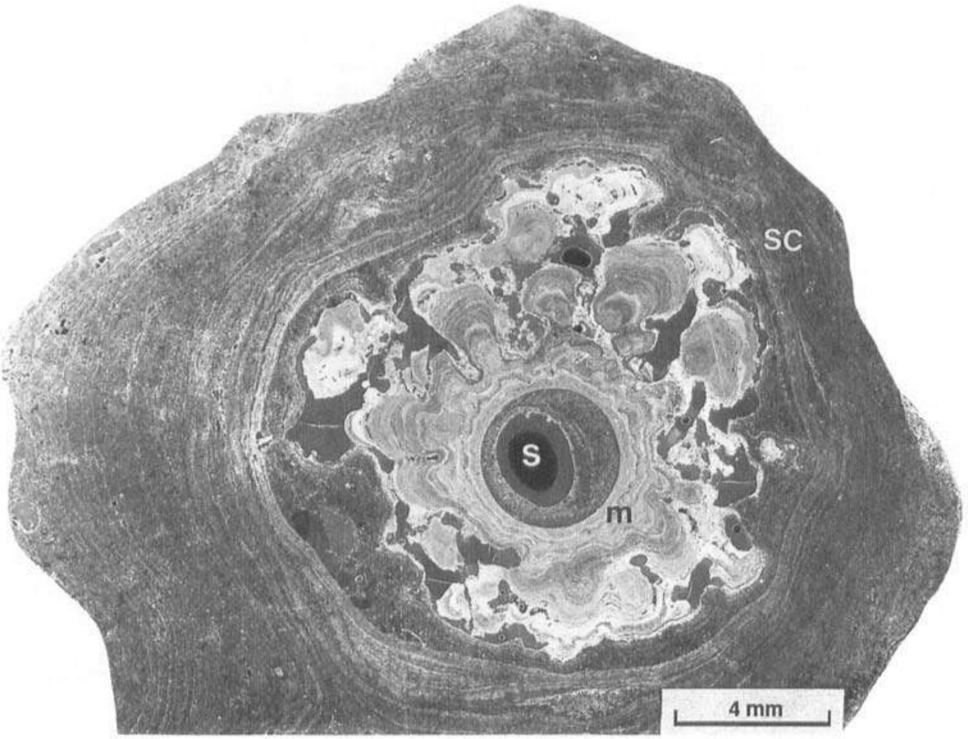

Fig. 12-20. Negative print from thin section through a stalactite showing "soda straw" (*S*) surrounded by micrite (*m*) and sparry calcite (*SC*). Note laminations in outward expanding columns of micrite. Stalactite from an old cave exposed in roadside cut near Breakers (Fig. 12-1). (From Jones and Motyka, 1987, fig. 2A.)

calcified filaments, by whatever process, acted as the source for some of the micrite (Jones and Motyka, 1987).

Cave pisoliths

The cave near Old Man Village on Grand Cayman is characterized by dry terraced pools that contain numerous cave pisoliths which are up to 8 cm long (Jones and MacDonald, 1989). Cave pisoliths (or cave pearls, as they are commonly called) are usually considered to be entirely of inorganic origin (e.g., Kirchmayer, 1987). Analysis of the Cayman cave pisoliths demonstrated, however, that microorganisms in the form of uncalcified, isodiametric, irregularly branching filaments (1 to 20 μm diameter), calcified filaments, and spherical to hemispherical bodies are common. Jones and MacDonald (1989) suggested that the microorganisms may have played an important role in the formation of the micrite layers that are an integral part of these pisoliths. These microorganisms may also have promoted calcite precipitation by modifying the microenvironment (Jones and MacDonald, 1989).

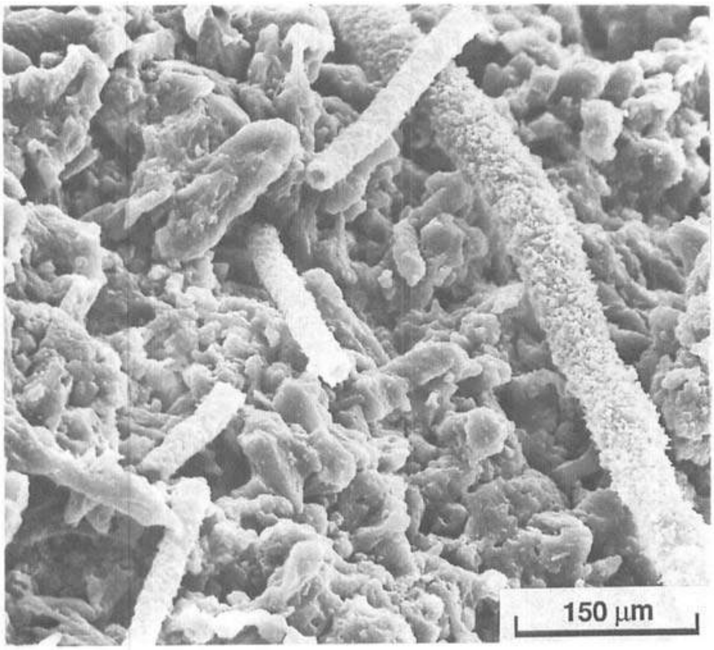

Fig. 12-21. Example of calcified algal filaments that occur in the laminated micrite masses from the central part of the stalactite shown in Fig. 12-20. (From Jones and Motyka, 1987, figs. 6B and 6C.)

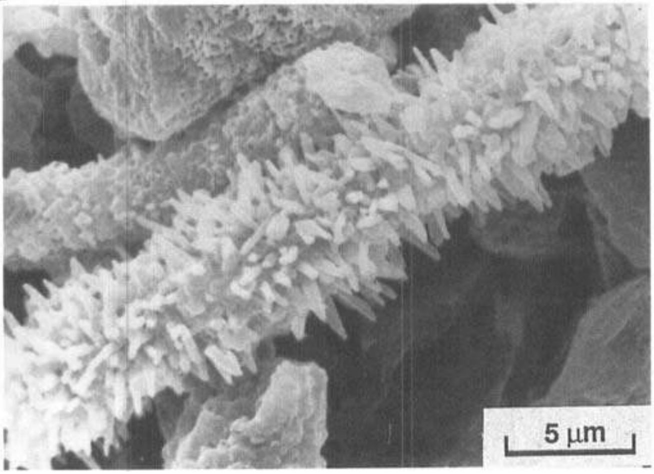

Fig. 12-22. Filament calcified with radiating acicular crystals, from laminated micrite masses of the central part of the stalactite shown in Fig. 12-20.

Karst breccia

In many areas, the Bluff Formation is characterized by numerous sinkholes up to 30 m deep (Doran, 1954; Jones and Smith, 1988) that are either open or filled with

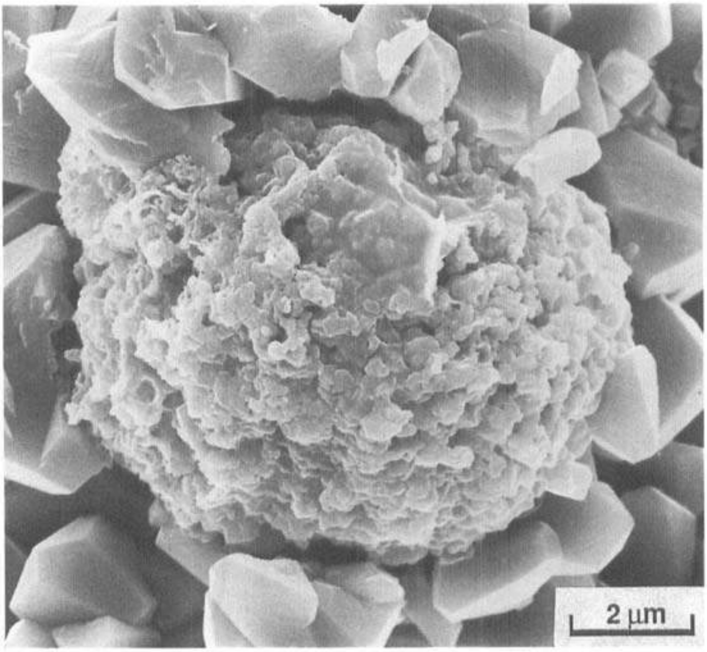

Fig. 12-23. Example of Type I bacteria-like structures from stalactite that are characterized by a high concentration of Fe along with minor amounts of Ca and Al. (From Jones and Motyka, 1987, fig. 4B.) Stalactite from an old cave exposed in roadside cut near Breakers (Fig. 12-1).

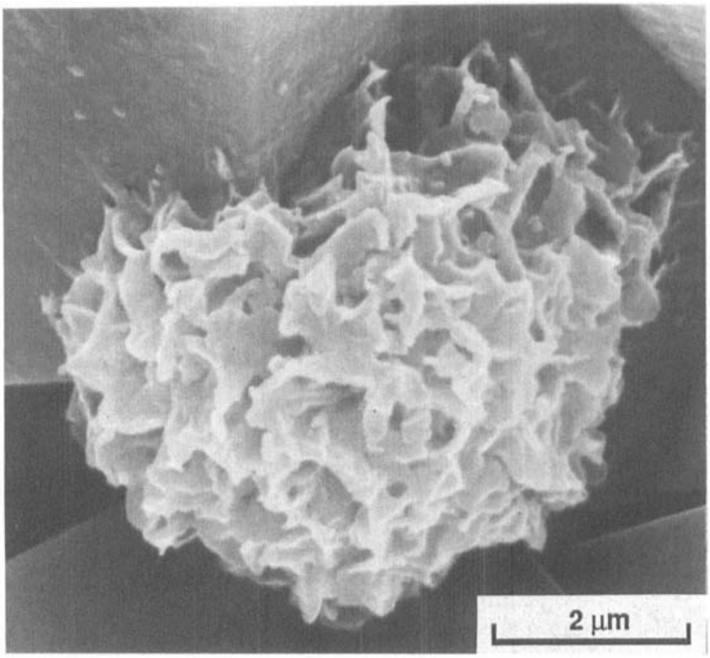

Fig. 12-24. Example of Type II bacteria-like structures from stalactite that are characterized by a high concentration of Mn and minor amounts of Ca and Al. Note distinctive reticulate pattern. (From Jones and Motyka, 1987, fig. 4C.) Stalactite from an old cave exposed in roadside cut near Breakers (Fig. 12-1).

breccia. Although developed in the dolostones of the Bluff Formation, the breccias that fill the sinkholes show no evidence of dolomitization and must, therefore, have formed after dolomitization of the host rock. Excellent exposures of numerous discordant breccia bodies occur in a small quarry near East End (Fig. 12-1). The fact that many of the breccia bodies cut across each other shows that there has been numerous episodes of sinkhole formation and filling. Indeed, the process is still ongoing because sinkholes along the southeast coast of Grand Cayman are being actively filled with irregularly-shaped clasts derived primarily from the surrounding bedrock and carbonate sands from the adjacent seafloor and brought onshore by storms and hurricanes (Jones and Kahle, 1985).

The breccias in the filled sinkholes are highly variable in terms of clast type and matrix/cement types. Jones and Kahle (1985, 1986) examined breccia formed of well cemented clasts of variable lithology, whereas Jones (1987) described a breccia formed of dolostone clasts derived from the Bluff Formation and cemented by calcite. Both breccias outcrop in a small quarry near East End, Grand Cayman (Fig. 12-1).

The clast-supported breccia described by Jones and Kahle (1985, 1986) is formed of clasts, up to 80 × 35 × 25 mm in size, that show no preferred orientation. The clasts are formed of (1) dark grey, light grey and light brown fossiliferous micrite, (2) brown pisolitic limestone, (3) light grey calcrete(?), (4) white corals, (5) dark grey to black micrite, and (6) rare clasts of white crystalline dolostone. Although the dolostone clasts are from the surrounding Bluff Formation, the origin of other clasts is unknown because there are no similar lithologies in the surrounding strata.

The irregularly-shaped interclast cavities are filled or partly filled with a complex array of detrital carbonates and cements. The detrital carbonates include skeletal sands, silts, and clays that were probably derived from the nearby seafloor and brought onshore by wave action during storms and hurricanes. Microorganisms played an integral role in the development of spar calcite and micrite cements that line many cavities. Indeed, Jones and Kahle (1985) used the term biodiagenesis to signify the role that the microorganisms played in the formation of these cementation. In many cavities, the following clast to pore sequence of cements occurs (Figs. 12-25, 12-26): (1) thin black coating with bulbous projections in a poreward direction, (2) spar calcite, (3) microstromatolites, (4) spar calcite, and (5) micrite. Microorganisms played an important role in the development of zones 1, 3 and 5.

Zone 1, 0.1 to 0.3 mm thick, is characterized by (1) its black color, (2) its high Mn content along with lesser amounts of Al and Ca, (3) a poorly defined and gradational contact with the clast which it coats, (4) bulbous projections in a poreward direction (Fig. 12-27) that are especially well developed on projecting parts of the clasts, and (5) distinct, straight tubes (0.01 mm in diameter and up to 0.1 mm long) that extend from the coating into the clast. Based on comparisons with Hale (1974) and Klappa (1979a), Jones and Kahle (1985, p. 454) suggested that these coatings are crustose lichens. Comparison with the element-fixing capabilities of lichen (e.g., Lawrey and Rudolph, 1975) led Jones and Kahle (1985) to conclude that concentration of Mn in this zone along with lesser amounts of Al was due to the activity of lichen.

Zone 3, termed a microstromatolitic cement by Jones and Kahle (1985, p. 454), is formed of bulbous, laminated masses of micrite that are up to 1 mm high and

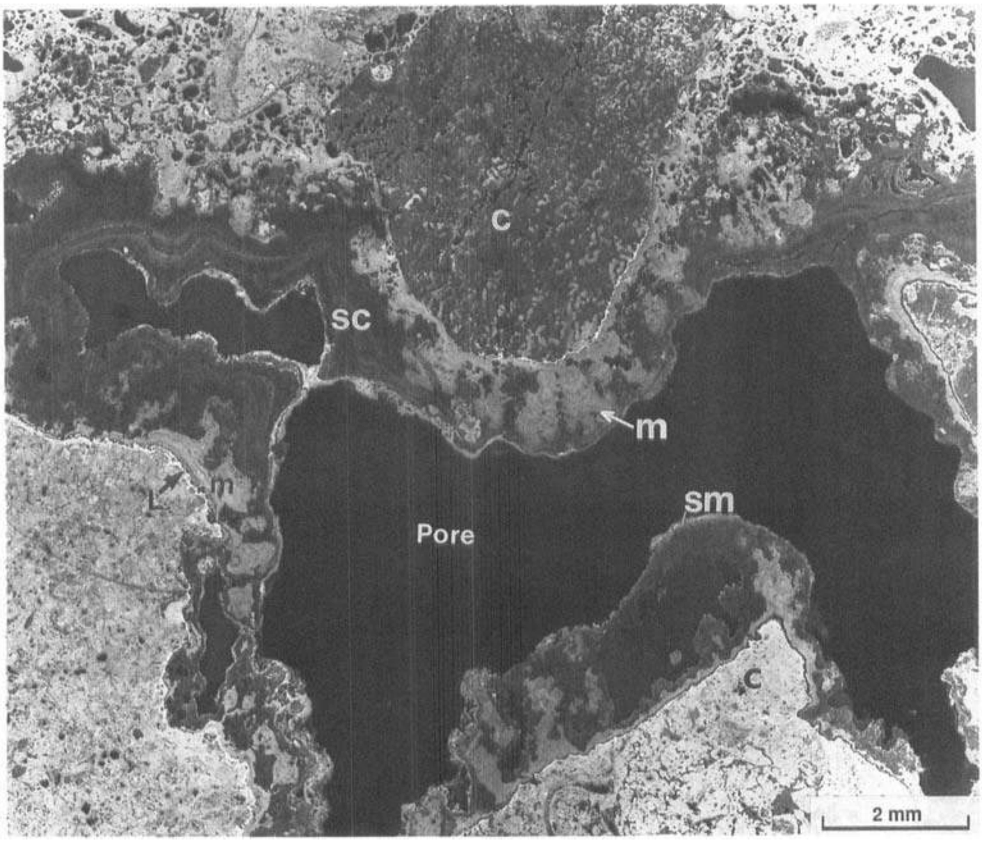

Fig. 12-25. Negative photograph of thin section showing complex cements associated with a karst breccia from East End Quarry, Grand Cayman Island (Fig. 12-1). The clasts (*c*) are coated with black manganese, coated successively by lichens (*L*), microstromatolites (*m*), spar calcite (*sc*), and, locally, sparmicrite (*sm*).

0.5 mm wide (Figs. 12-25, 12-26, 12-27). Jones and Kahle (1985, p. 454) termed these structures stromatolites because (1) of their external morphology, (2) of their internal laminations which mimics the external form of the structures, (3) they contain sediment-binding microorganisms, and (4) except for size, they are identical in appearance to known algal stromatolites. The micrite in the microstromatolites is bound by filaments up to 120 μm long and 3 μm in diameter. Where the microstromatolites are visible on cavity walls, their surfaces have a distinct green color which suggests that microorganisms, such as algae, are present. Their outer surfaces are covered with dense, interwoven mats of filaments. Moults of insects bound onto the surface of the microstromatolite by the filaments attests to the terrestrial origin of these structures (Jones and Kahle, 1985, fig. 8). With respect to the microstromatolites, Jones and Kahle (1985, p. 454–455) argued that the microorganisms were important because they (1) trapped and bound micrite on the cavity walls, (2) made a direct contribution to the cement via filament calcification,

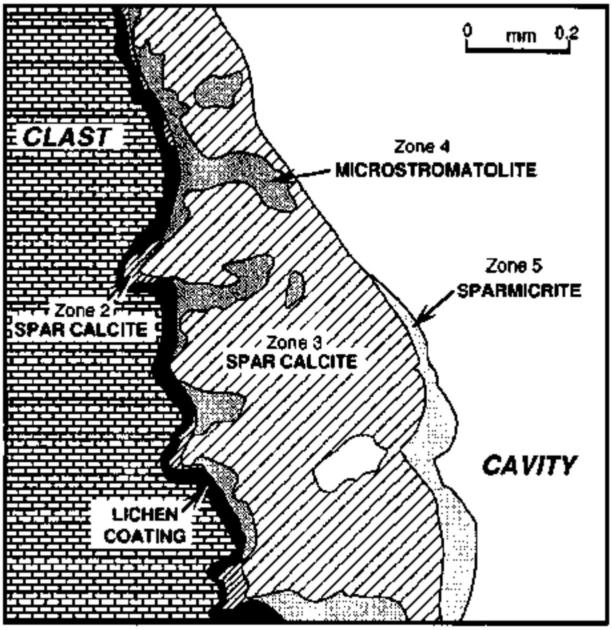

Fig. 12-26. Line diagram showing cement zones associated with karst breccia shown in Fig. 12-25.

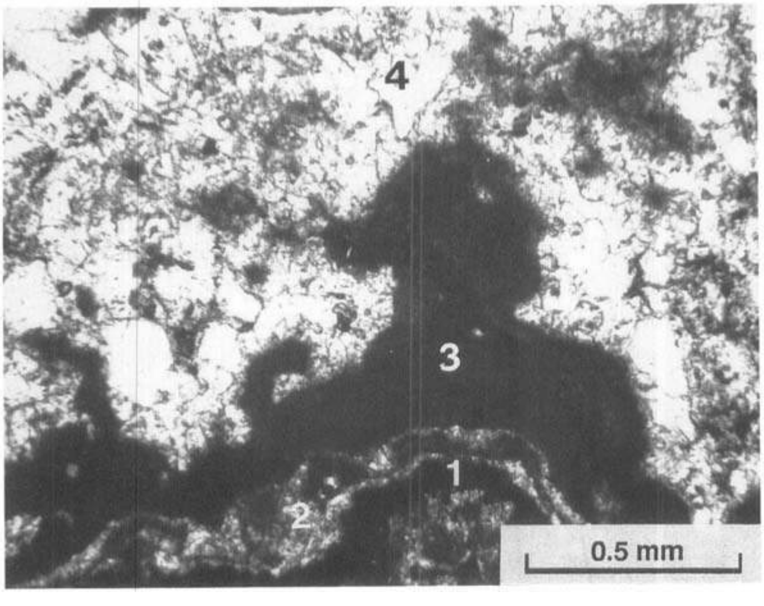

Fig. 12-27. Photomicrograph showing cements lining clasts in breccia from the East End quarry (Fig. 12-1). *1* = lichen coating, *2* = spar calcite, *3* = microstromatolites, and *4* = spar calcite. (From Jones and Kahle, 1985, fig. 3D.)

Fig. 12-28. Photomicrograph of sparmicrite in zone 5 (Fig. 12-26) showing algal and/or fungal filaments penetrating the micrite.

and (3) may have promoted precipitation of calcium carbonate by modifying the microenvironment in the cavities. The formation of these microstromatolites is important because they cemented the clasts and thereby reduced interclast porosity and permeability.

Zone 5, the poreward most zone in many cavities (Fig. 12-26), is formed of micrite that does not display any internal laminations or bulbous structures like the microstromatolites of zone 3. The micrite contains numerous borings, up to 8 μm diameter, that still contain filaments (Fig. 12-28). The boundary between this zone and the underlying spar calcite of zone 4 is irregular because of the borings which penetrate the spar calcite (Fig. 12-29). This zone of micrite probably formed by sparmicritization. In most cavities, the micrites of zones 3 and 5 are only 1 to 2 mm apart. Despite this, the micrite originated through two diametrically opposed processes even though similar microorganisms were probably involved in both cases. The micrite of zone 3 originated through constructive processes, whereas that in zone 5 is formed by destructive processes. This example clearly illustrates the complexity of microbial activity.

The dolostone breccia documented by Jones (1987) outcrops in the floor of the quarry approximately 3 m below the breccia described by Jones and Kahle (1985, 1986). It is formed of poorly sorted, angular dolostone clasts cemented by two generations of brown-colored calcite cement that has been altered by the activity of endolithic, epilithic and chasmolithic microorganisms that are rarely calcified

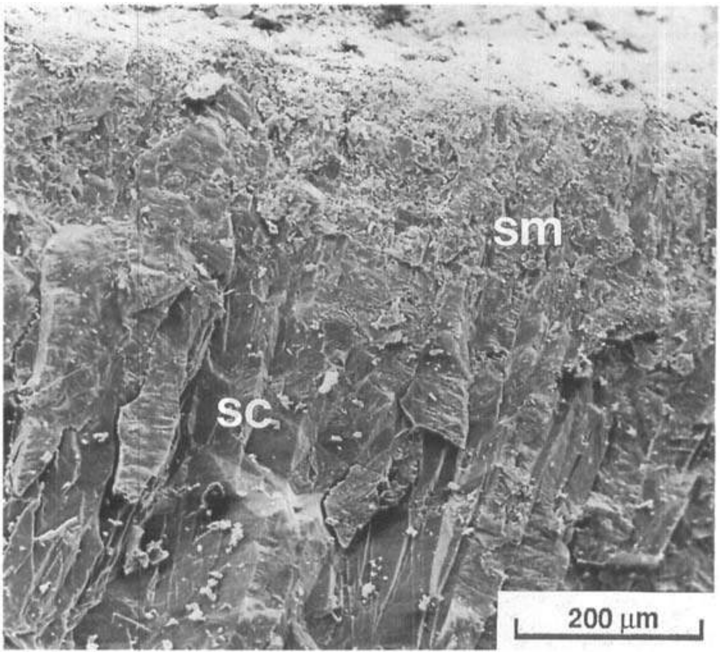

Fig. 12-29. SEM photomicrograph sparmicrite (*sm* — zone 5, Fig. 12-26) replacing outer part of spar calcite crystals (*sc*). (From Jones and Kahle, 1986, fig. 6B.)

(Jones, 1987). Calcified spherical and hemispherical bodies associated with these filaments may be fruiting bodies of microorganisms or bacteria. Collectively, the microorganisms modified the calcite crystals (Fig. 12-30) by (1) boring (Fig. 12-31), (2) forming spiky calcite (Fig. 12-32), (3) mediating surface etching (Fig. 12-33), (4) etching surfaces to produce a "blocky topography" (Fig. 12-34), and (5) highlighting spiral growth patterns of the calcite crystals through etching, and (6) forming constructive micrite envelopes (Fig. 12-35). The constructive micrite envelopes probably formed in a manner similar to that described by Kobluk and Risk (1977). Etch pits in these calcite crystals are similar to those found in weathered crystals of hypersthene, augite (Berner et al., 1980, figs. 1a, 1b), feldspar (Wilson, 1975, fig. 1; Keller, 1976, fig. 24; Berner and Holdren, 1977, figs. 2, 3; 1979, figs. 3, 4, 7; Berner, 1978, plate 2B; 1981, fig. 4b) and hornblende (Berner, 1981, fig. 8).

Rhizoliths

Rhizoliths are cylindrical organosedimentary structures (Klappa, 1980) composed of well-cemented material that forms around plant roots. Rhizoliths, common in many parts of the world, can form around small wetland plants, coastal mangroves or large trees (Bown, 1982). Rhizoliths are common in many parts of the Caribbean (e.g., Ward, 1985; Jones and Ng, 1988; Curran and White, 1987).

Jones and Ng (1988) described rhizoliths that occur in friable limestones of the

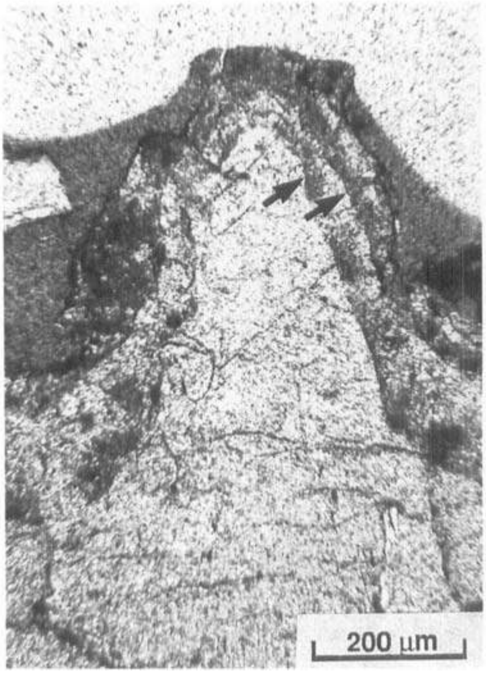

Fig. 12-30. Photomicrograph showing calcite crystal that lines cavity walls in a breccia formed of dolostone clasts cemented by brown-colored calcite. From East End Quarry, Grand Cayman Island (Fig. 12-1). Note that outer parts of the crystal have laminae of micrite (arrows) that probably formed through sparmicritization. (From Jones, 1987, fig. 2C.)

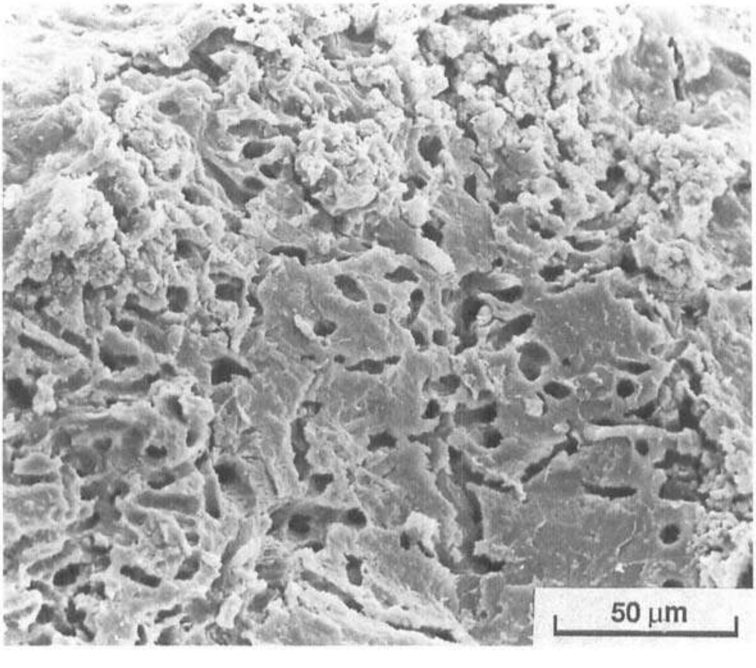

Fig. 12-31. Photomicrograph showing extensively bored calcite crystal from dolostone breccia in the East End quarry.

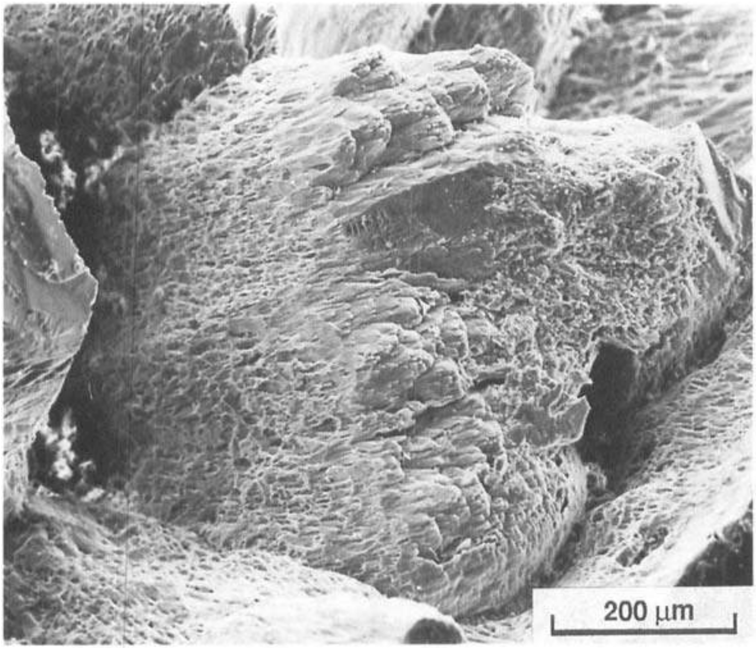

Fig. 12-32. Photomicrograph of calcite crystals from dolostone breccia in the East End Quarry, Grand Cayman Island that have been extensively etched.

Ironshore Formation on Cayman Brac. These rhizoliths, 3 to 25 mm in diameter and at least 0.5 m long, branch downwards with 2nd, 3rd, and 4th order branches. The outer parts of the rhizoliths are cemented by grain-coating calcite needle mats, isolated calcite rhombs, calcite rhomb chains (Fig. 12-36), calcified filaments (types I and II; Fig. 12-37), and calcified spherical bodies (Jones and Ng, 1988). In contrast, the sediment around the rhizoliths contained much less cement. Although the sediment contains many of the same cements as in the rhizolith, it does not contain grain coating mats of calcite needles or type II calcified filaments (Table 12-2).

Determining the origin of any given cement in subaerial exposed limestones is difficult because they may be related to either inorganic or organic processes. Jones and Ng (1988), however, attributed the differences in the amount and types of cement between the rhizoliths and the surrounding sediment (Table 12-2) to the influences of the plant roots and their associated microorganisms. Furthermore, this example demonstrates the profound influence that plant roots and their associated microorganisms can have on carbonate diagenesis.

There is no universal scheme to cementation in rhizoliths, because the precipitation of various minerals in these structures is controlled by many variables. For example, halophytic and xerophytic plants can selectively concentrate sulfates in their fluids that may lead to the formation of anhydrite (Glennie and Evamy, 1968). Elsewhere, however, plants concentrate Fe in the rhizoliths (Pilkey and Gorsline, 1961; Claxton, 1969).

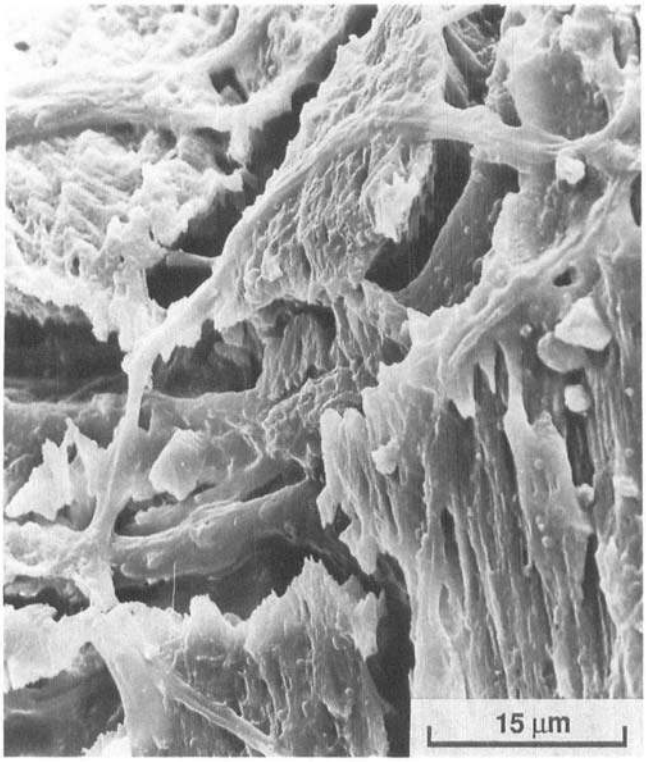

Fig. 12-33. Photomicrograph of extensively etched calcite crystal from dolostone breccia in the East End quarry.

TABLE 12-2

Comparison of cements in rhizoliths and surrounding sediment (adapted from Jones and Ng, 1988, table 1)

Cement	Rhizolith	Sediment
Rhomb chain	3	P
Isolated rhombs	2	P
Calcified spherical bodies	6	P
Calcified filaments		
Type I (blocky crystals)	5	P
Type II (needles)	4	A
Grain-coating mats	1	A
Needles	A	P
Cryptocrystalline cement	A	P

Note: For the rhizoliths the cements are ranked in order of abundance (1–6). In the sediment, the cements are rare and are recorded as being present (P) or absent (A).

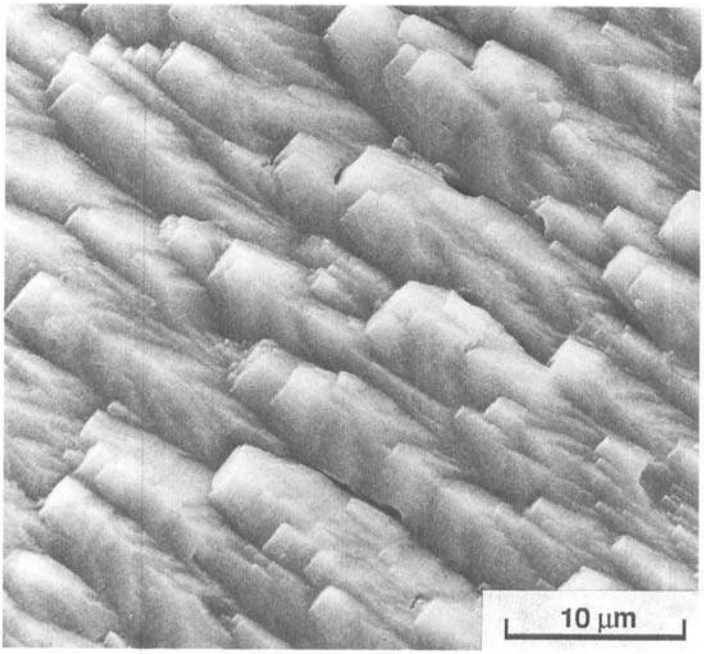

Fig. 12-34. Example of "blocky topography" produced by the etching of a calcite crystal from dolostone breccia in the East End quarry.

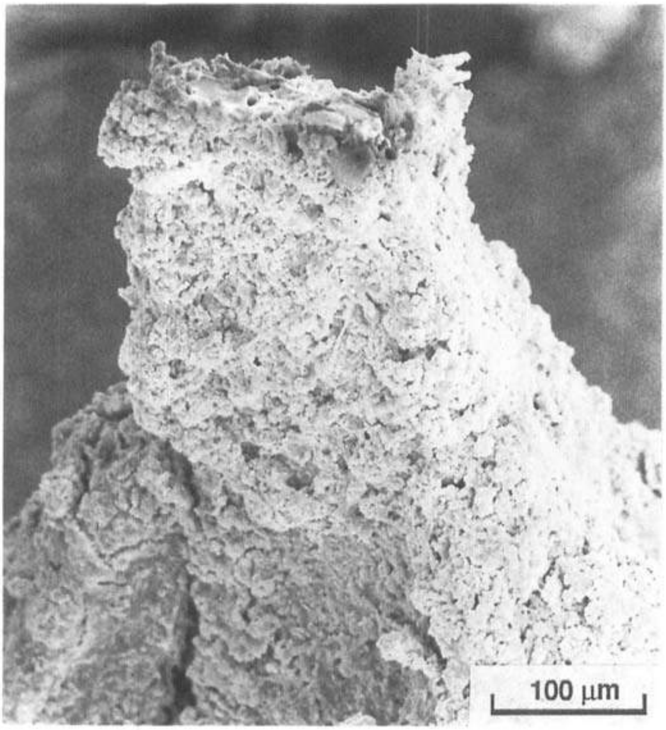

Fig. 12-35. Calcite crystal from dolostone breccia in the East End quarry that has been completely encased by a constructive micrite envelope.

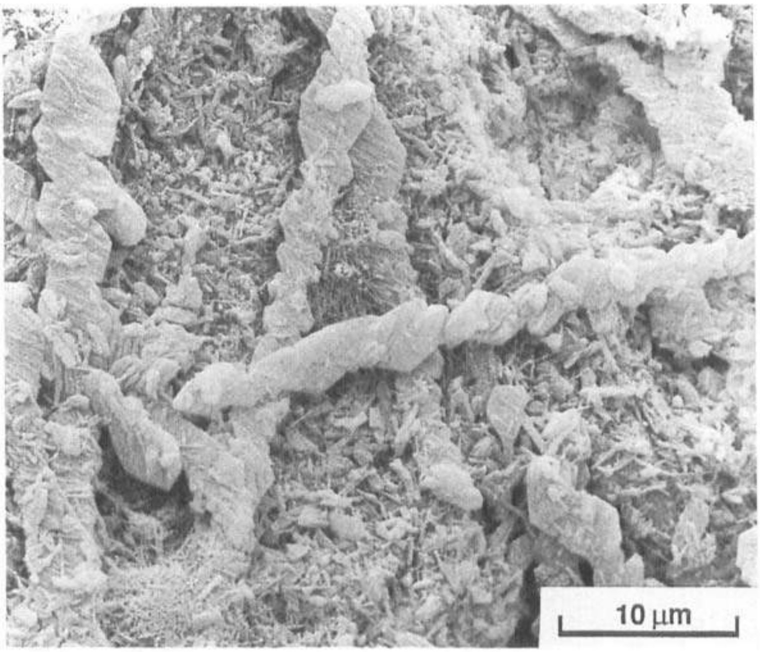

Fig. 12-36. Examples of calcite rhomb chains from a rhizolith that occur in the Ironshore Formation of Cayman Brac. (From Jones and Ng, 1988, fig. 6A.)

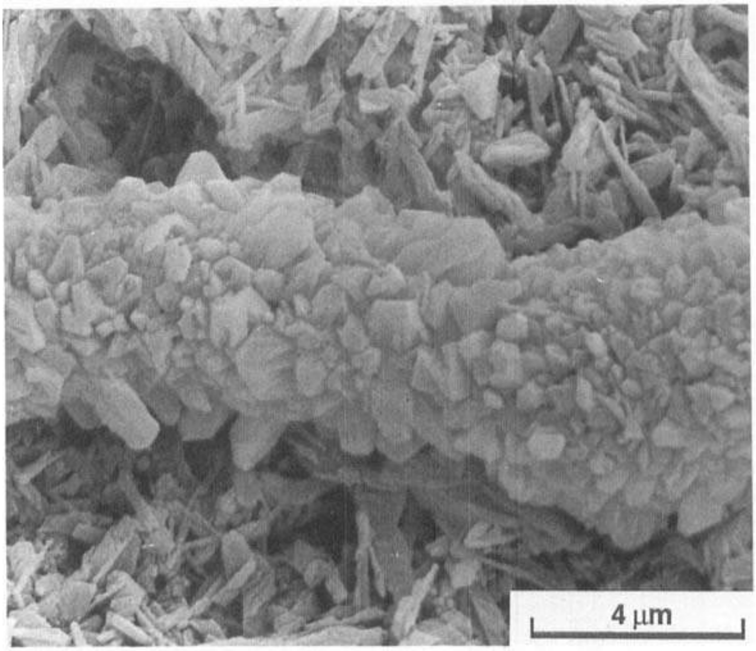

Fig. 12-37. Example of calcified filament from a rhizolith that occurs in the Ironshore Formation of Cayman Brac. (From Jones and Ng, 1988, fig. 7A.)

Root borings

There is little surface soil on the Bluff Formation of the Cayman Islands because most is washed away by torrential tropical rainfalls. Despite this, there is a dense vegetation dominated by large trees (e.g., mahogany), bushes and grasses that root directly into the dolostones of the Bluff Formation (Squair, 1988). Tree roots, which penetrate to depths of at least 10 m, probably extend down to the water table. Although some roots follow pre-existing planes of weakness (e.g., joints) most bore into the dolostone by using substances which they secrete. Penetration of the dolostone by tree roots is important because it (1) increases porosity and permeability, (2) introduces organic acids into the system, and (3) allows microorganisms to access the subsurface rock (Jones, 1988).

A calcrete layer capping the Ironshore Formation near the airport on Cayman Brac provides the best example of diagenetic processes associated with tree roots (Jones, 1988). Microorganisms associated with these root borings are uncalcified filaments, calcified filaments (Fig. 12-38), uncalcified spherical and hemispherical bodies, and calcified spherical and hemispherical bodies (Fig. 12-39).

Uncalcified filaments commonly form mats that cover the walls of the borings. Mucilagenous sheets similar to those figured from marine oncolites by Jones and Goodbody (1985, fig. 5) and the fungal mats illustrated by Jones and Pemberton (1987a, b) are commonly associated with the filaments. Branched and unbranched

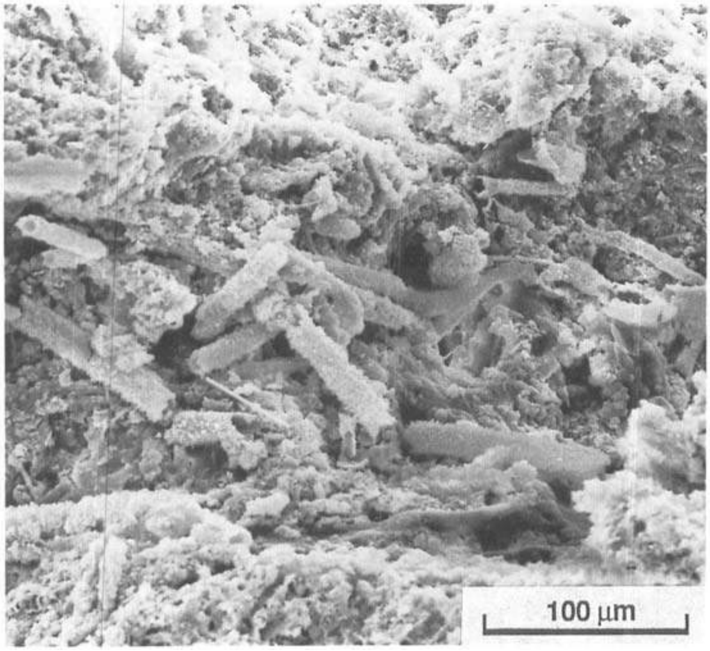

Fig. 12-38. Example of calcified root hairs and/or algae coating wall of rootlet boring in a caliche unit that caps the Ironshore Formation on Cayman Brac. (From Jones, 1988, fig. 6B.)

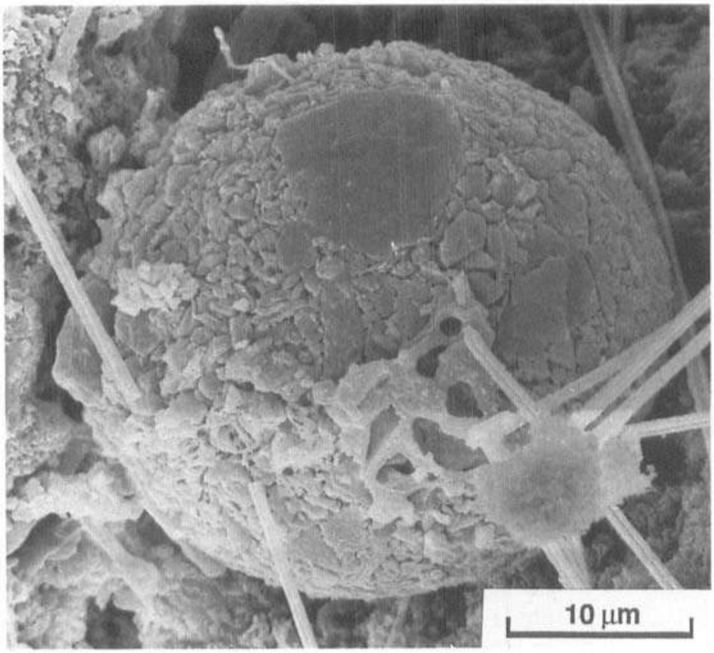

Fig. 12-39. Example of calcified spherical body associated with root borings from a caliche unit that caps the Ironshore Formation of Cayman Brac. (From Jones, 1988, fig. 7B.)

filaments (0.5 to 3.0 μm in diameter) have (1) no ornamentation, (2) small, smooth, spherical bodies (fruiting bodies?) attached at irregular intervals along the length of the filaments, or (3) small spherical, highly ornate fruiting bodies at their ends.

Isodiametric calcified filaments, which occur with the uncalcified filaments, have an open central tube, 1 to 1.5 μm in diameter surrounded by a calcified wall up to 4 μm thick. Calcification involves either irregularly shaped crystals, 0.3 to 1.8 μm long, or needle-shaped crystals, 0.5 to 1.5 μm long and about 0.1 μm wide. Some filaments have little or no calcification, whereas others have been fully encased with calcite. In some examples, the degree of calcification varies along the length of a filament.

Uncalcified spherical and hemispherical bodies, common in many parts of the root borings, are 3 to 4 μm in diameter and usually associated with calcified and uncalcified filaments. Some are collapsed, suggesting that little or no mineralization has occurred. The complex ornamentation of the uncalcified spherical and hemispherical bodies is similar to that on the fruiting bodies that are attached to the uncalcified filaments, suggesting that they are genetically related. Locally, there are chains formed of spherical bodies (0.5 μm in diameter) connected by smaller spherical bodies (0.2 to 0.3 μm in diameter). Other strings have spheres 0.3 μm in diameter connected by a filament that is 0.1 μm in diameter.

Calcified hemispherical and spherical bodies, 5 to 67 μm in diameter and up to 55 μm high, occur with the other microorganisms in the root borings (Fig. 12-39). Calcification has hidden all internal features and original ornamentation.

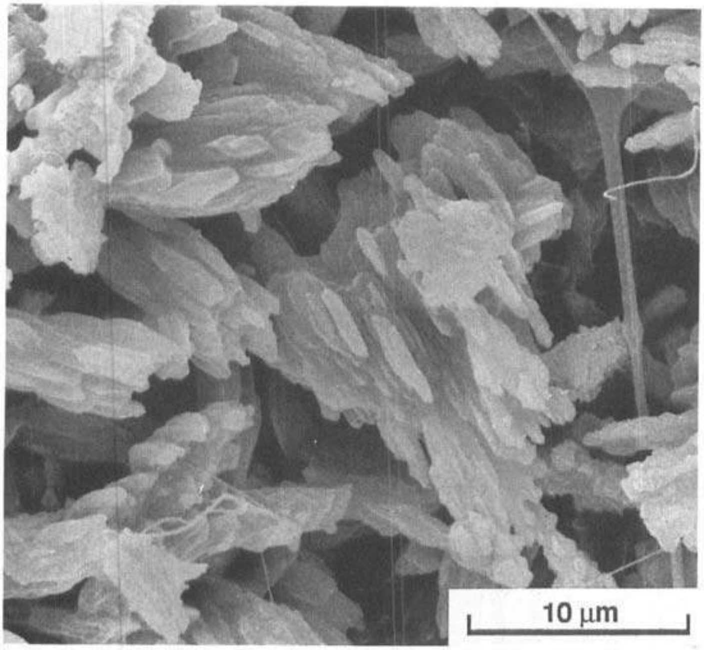

Fig. 12-40. Example of etched calcite crystals that occur along the walls of a root boring from a caliche unit that caps the Ironshore Formation on Cayman Brac. The etching was probably mediated by the abundant microorganisms that occur in these borings. (From Jones, 1988, fig. 6F.)

Throughout the root borings, there is evidence of filamentous microorganisms trapping and binding loose calcite grains to the walls of the borings. Calcite crystals, which occur as a cement lining the walls of some borings, commonly have an irregular topography because of etching (Fig. 12-40).

The diverse array of filaments associated in root borings is important because (1) the endolithic microorganisms promote substrate destruction, (2) the microorganisms may promote dissolution of the substrate, (3) calcification of the microorganisms make a direct contribution to the development of cements in the root borings, and (4) it is possible that the microorganisms may have promoted precipitation of $CaCO_3$ by influencing the microenvironment.

IDENTIFICATION OF MICROORGANISMS

General comments

Algae, blue-green algae or cyanobacteria (James, 1972; Knox, 1977; Klappa, 1979b), root hairs (Ward, 1973, 1978, 1985; Knox, 1977; Klappa, 1979b; McKee and Ward, 1983; Coniglio and Harrison, 1983), fungi (Klappa, 1979b; Calvet, 1982; Coniglio and Harrison, 1983), actinomycete (Klappa, 1979b; Calvet, 1982), and bacteria (Calvet, 1982) are common in surface and near-surface exposures of carbonates.

Identification of microorganisms is difficult because there are few morphological characters that are diagnostic of a particular microorganism. Although mineralization (mostly by calcification), preserves the microorganisms, it destroys or hides the taxonomically valuable features (Riding, 1977; Klappa, 1979b).

Klappa (1979b, table 1) suggested that fungi could be separated from algae by using a combination of filament size, branching style, branching angle, and shape. In many cases, however, the distinction between algae and fungi has commonly been based on size, particularly where calcification has occurred. Thus, small-diameter filaments or borings (typically <4 μm) have been treated as fungi (e.g., Perkins and Halsey, 1971; Rooney and Perkins, 1972; Ward, 1985), whereas large-diameter filaments or borings (>4 μm) have been regarded as algae (e.g., Kendrick et al., 1982). The rationale of using this dimension to separate fungi from algae is not clear because there is no natural break. For example, fungal hyphae illustrated by Brown and Brotzman (1979) have diameters ranging from 2 μm to 10 μm with many in the 4 to 7 μm range. Similarly, fungal hyphae illustrated by Tsuneda (1983) have diameters ranging from 0.9 μm to 5.2 μm with many in the 4 to 5 μm range. Thus, it seems advisable to follow Edwards and Perkins (1974) who suggested that 1 to 4 μm filaments/borings should be considered fungal only if sporangia or conidia occur with them.

There are numerous recorded examples of algae, fungi and bacteria associated with caves (e.g., Coase and Judson, 1977; Danielli and Edington, 1983). Høeg (1946, p. 100) described bacteria, fungi and cyanophycea from cave walls in Nord Rana, Norway. Likewise, Palik (1960) noted bacteria and algae on cave walls, roofs, stalactites, stalagmites and water-filled depressions in various Hungarian caves. Nagy (1965) recognized seven species of algae from cave walls, stalactites and stalagmites in Crystal Cave, Kentucky, whereas Jones (1965) identified 27 taxa of algae from Mammoth Cave. Green algae, blue-green algae, bacteria and diatoms occur in Welsh caves (Mason-Williams, 1967, tables 3, 4, 5, 6). Fungal hyphae were common on all cave walls, stalactites and other limestone structures in the Lehman Caves of Nevada (Went, 1969). Lefevre and Laporte (1969) demonstrated that the "Maladie Verte", which was destroying cave paintings in the Lascaux Cave in France, was caused by bacteria, fungi and algae growing over the paintings. Cubbon (1966) suggested that the black-colored deposits on ancient bones in the Mendip Caves of England was probably due to bacterial action. Draganov (1977) showed that blue-green algae accounted for 48.5% of the 627 taxa of cave algae that had been documented up to 1977. Gracia Alonso (1974), and Friedmann (1955, 1979) noted that the calcified filaments of *Geitleria* occur in caves all over the world.

Included in the cave fauna/flora are filamentous microorganisms that have been identified as blue-green algae (e.g., Høeg, 1946; Palik, 1960; Nagy, 1965; Jones, 1965; Mason-Williams, 1967; Lefevre and Laporte, 1969; Rippka, 1972; Bourrelly and Dupuy, 1973; Gracia Alonso, 1974; Draganov, 1977; Friedmann, 1979; Jones and Motyka, 1987; Couté, 1982; Jones and MacDonald, 1989). Given that algae are generally considered to be photosynthetic, the problem became one of explaining how these algae could survive in an environment where light is absent. This apparent dichotomy was largely resolved with the realization that blue-green algae are really procaryotes that should be classified as blue-green bacteria (e.g., Stanier et al., 1976) or cyanobacteria (e.g., Stanier, 1977, 1982). Cyanobacteria are a diverse group of gram negative bacteria (Stanier et al., 1976; Stanier, 1977; Rippka et al., 1979) that are distinguished from other bacteria by the nature of their pigment system and their performance of aerobic photosynthesis (Stanier et al., 1971). Cyanobacteria inhabit in a diverse range of marine, freshwater and terrestrial environments (e.g., Stanier, 1977). For example, thermophilic cyanobacteria are common in hot springs, whereas other cyanobacteria are common in desert settings where large diurnal ranges in temperatures are common (Stanier et al., 1976). Although many cyanobacteria are obligate phototrophs (e.g., Rippka, 1972; Stanier et al., 1976), others are known to grow in the dark (e.g., Kiyohara et al., 1962; Hoare et al., 1971; Stanier et al., 1976) or where light is dim (van Baalen et al., 1971). Cyanobacteria, which include unicellular rods or cocci as well as filamentous forms (Stanier, 1977), are capable of producing compounds that contain glycogen (Stanier, 1982) and large amounts of mucilage. The structure and composition of cyanobacteria are well known from studies, such as those by Stanier et al. (1976), Stanier (1977), Rippka et al. (1979), Herdman et al. (1979), and Drews and Weckesser (1982). Unfortunately, many of the standard biological criteria used to recognize cyanobacteria cannot be used in situations encountered by geologists. This is especially the case where calcification has disguised the microorganisms and the filaments are no longer visible. Thus, despite inherent disadvantages, identification of microorganisms involved with carbonate diagenesis must rely on identification keys, such as that provided by Klappa (1979b, table 1) or comparison with previously identified forms.

In near-surface and surface vadose settings, the identification of microorganisms is even more difficult, because algae, cyanobacteria, and fungi are commonly associated with plant roots, rootlets, and root hairs (Jones, 1988, 1989). Plant roots and rootlets usually have a larger diameter and are, thus, easy to identify. Conversely, roots hairs can be difficult (if not impossible) to recognize, especially if mineralization has occurred (Jones, 1988, 1989). Ward (1970) described root hair sheaths from Pleistocene eolianites on the Yucatan Peninsula that were 5 to 15 μm in diameter with walls 1 to 2 μm thick. Conversely, James (1972, p. 827) attributed similar calcified tubules in calcrete on Barbados to algae. Klappa (1979b) argued that root hairs "...are 5–17 μm in diameter, straight or curved and unbranched", whereas green and blue-green algae (= cyanobacteria) are 0.5 to 20 μm in diameter and "... show false ramifications, variable angles of branching and irregular shapes." Where root hairs and algae occur together, such criteria are difficult to apply, especially where only small segments of the filaments are visible.

Little attention has been paid to bacteria (other than cyanobacteria), despite their occurrence in nearly all environments (Friedman and Sanders, 1978). The importance of bacteria in the formation of travertines has been well demonstrated by Chafetz and Meredith (1983), Chafetz and Folk (1984) and Folk et al. (1985). Although bacteria are morphologically variable, they are usually less than 1 μm long and commonly occur as small rods or chains of spherical bodies. As with other groups, there are problems with confidently identifying bacteria.

Microorganisms in Cayman samples

Determining the identity of microorganisms involved in the diagenesis of carbonates on the Cayman Islands in surface or near-surface settings may be unnecessary, because it is the collective effect of the microbial community that is important (Jones, 1989). Nevertheless, care must be taken because the identification of a microorganism commonly dictates the interpretation of the environment in which the microorganisms lived. For example, the identification of algae carries the implication of photosynthesis and invariably leads to the conclusion that they must have been exposed to daylight.

Many borings in the Cayman rocks can be easily attributed to the action of plants because the roots and rootlets are still in the borings. In most settings, however, there is a diverse array of algae, cyanobacteria, fungi and bacteria associated with the tree roots and rootlets. Thus, in many cases it is difficult to decide if calcified tubules are related to root hairs, algal filaments, fungal hyphae, or cyanobacteria.

In many modern settings, the presence of microorganisms is indicated by a distinct green coloration that presumably reflects the presence of algae or cyanobacteria. Although a detailed examination of the sample usually confirms such an assessment, it also becomes apparent that other microorganisms, such as fungi and bacteria, are commonly associated with them. Thus, it becomes necessary to use either identification keys, such as the template provided by Klappa (1979b, table 1), or comparisons with microorganisms identified and illustrated by other workers. Implicit to the last procedure is the assumption that those microorganisms have been correctly identified. Many of the microorganisms from the Cayman karst terrains can be compared with previously described and illustrated microorganisms. For example, many small-diameter filaments in the Cayman examples are comparable to calcified fungal filaments described and illustrated by Kahle (1977, fig. 4a), Rooney and Perkins (1972, figs. 3, 4), Perkins and Halsey (1971, figs. 2, 3, 4, 5) and Edwards and Perkins (1974, fig. 2). The small-diameter (1 to 4 μm) fruiting bodies associated with uncalcified filaments tend to substantiate this suggestion. Likewise, the small bead-like filaments associated with plant roots are comparable to bacteria described by Calvet (1982, p. 171).

Isolated calcified and uncalcified hemispherical and spherical bodies, 2 μm to 67 μm in diameter, are common in samples from karst terrains on the Cayman Islands. Specific identification is difficult, because spherical and hemispherical bodies of this general architecture can be derived from algae, cyanobacteria, fungi, or bacteria. For example, algal mats from a desert lake in the Gulf of Aqaba contain smooth *Aphanocapsa* colonies, 15 to 35 μm in diameter, that are commonly covered with monohydrocalcite or other carbonates (Krumbein, 1975). Spores or fruiting bodies with a spherical to hemispherical form commonly occur as clusters in fungal meshworks (Perkins and Halsey, 1971, p. 845). Some fungi, such as *Penicillum chrysogenum,* are characterized by few filaments but numerous spores and sporangia (e.g., fig. 8 of Jones and Pemberton, 1987a). Although cyanobacteria are commonly filamentous, some can either produce large, heavy-walled resting cells (akinetes) or heterocysts which play a role in nitrogen fixation (e.g., Stanier et al., 1976). In situations where mineralization of the cells has occurred, it becomes almost impossible to assign the structures to a particular group of microorganisms. Consequently, they are herein simply referred to as spherical and hemispherical bodies.

The microbial accumulations that occur in the karst terrains of the Cayman Islands include a diverse array of root hairs, algae, fungi, cyanobacteria, and bacteria. In most cases, however, it is difficult to identify an individual filament or body, especially where extensive mineralization has occurred. Although such identifications may be desirable, they may be of little consequence. From viewpoint of carbonate diagenesis, it is perhaps more important to recognize and determine the presence of the microorganisms and acknowledge the influence that they can have on precipitation and dissolution.

CALCIFICATION OF MICROORGANISMS

Specificity of calcification

The suggestion that calcification or the style of calcification might be species- or genus-specific (e.g., Desikachary, 1959; Starmach, 1966; Bourrelly, 1970; Riding, 1977; Krumbein and Giele, 1979; Round, 1981; Jones and Kahle, 1986) has been based on the variable calcification patterns of microorganisms and the fact that calcified and non-calcified filaments commonly occur together. Pentecost and Riding (1986) noted that many cyanobacteria exhibit specificity for calcification even though none are known to be obligate calcifiers. Friedmann (1979), however, showed that the cyanobacteria *Geitleria*, a common inhabitant of caves, has a characteristic calcareous sheath. Furthermore, Friedmann (1979) noted that *Geitleria floridana* has a calcareous sheath, the shape of a quadratic prism with an obliquely truncated apex, that is formed of acicular crystals that are arranged so as to form a rhombic-lattice. The sheath appears to act as a single optical unit (Friedmann, 1979), implying that the calcification of the filament can give rise to a single calcite crystal.

Riding and Voronova (1982) suggested that although calcification appears to be specific to certain taxa, it must also be a function of the environmental setting. Golubic (1973, p. 445) also argued against species- or genus-specific calcification by noting that environmental factors unrelated to the microorganisms may control the calcification process, and that the calcification process may be governed by associated bacteria rather than the algae and fungi themselves (Pautard, 1970).

Sites of calcification

A calcified filament may be defined as a biogenic structure in which $CaCO_3$ has replaced the filament or has been precipitated on (encrustation) or within (impregnation) a filament (Kahle, 1977, p. 415; Riding, 1977; Klappa, 1979b, p. 956). This reflects the fact that calcification of microorganisms can occur at various sites on and in the sheath (Wallner, 1934; Gleason, 1972; Golubic, 1973; Pentecost, 1978; Casanova and Tiercelin, 1982; Wood, 1984). Pentecost and Riding (1986) suggested that calcite can contact and grow on the sheaths of cyanobacteria through (1) the attraction of positively charged Ca^{2+} ions by the various acids (mainly ionizable uronic acid) that occur in the polysaccharides of the sheath, (2) nucleation on attached bacteria, or (3) nucleation on bacteria or other particles in suspension which subsequently become attached to the filaments.

Timing of calcification

Calcification can occur while the filaments are alive, shortly after their death or at some considerable time after their death (Jones and Kahle, 1986, pp. 222–223). The isodiametric uncollapsed form of many calcified filaments indicates that calcification must have taken place before filament decay and collapse began. In this respect, filaments with variable degrees of calcification along their length are important. Fully calcified portions of such filaments are isodiametric with no evidence of collapse, whereas other uncalcified parts of the same filaments are collapsed and broken. Partly-calcified filaments show a lesser degree of collapse and breakage. Variation in the amount of calcification over short lengths of the filaments illustrates the complex nature of the calcification process. Furthermore, it argues against calcification being species- or genus-specific unless it is suggested that the chemical composition of the filament rather than the life processes controlled calcification.

Calcification patterns

Calcification patterns on filaments from the karst terrains of the Cayman Islands are variable (e.g., Jones and Kahle, 1985; Jones and Motyka, 1987), probably because they are controlled by a complex array of organic and inorganic processes. Understanding the factors responsible for calcification is difficult, because of the inherent problems of examining and monitoring microorganisms, and the microenvironments in which they live. Although experiments like those of Jones and Pemberton (1987a, b) can help, many questions remain unanswered. In natural settings, the factors controlling the calcification process must be based on the interpretation of calcification patterns and speculation.

Crystal morphology involved in the calcification of microorganisms varies from rhomb-like crystals (Gleason, 1972), to acicular crystals (Gleason, 1972; Friedmann, 1979; Riding, 1977), to thin platy crystals (Gleason, 1972), to dendrite crystals (Gleason, 1972; Friedmann, 1979; Couté, 1982; Jones and Kahle, 1986). Irrespective of the crystal morphology involved in calcification, there is a basic dichotomy between those filaments which have clear crystallographic orientation of crystals relative to the sheath and those that do not (Pentecost and Riding, 1986). For example, Pentecost (1978, 1985) found no evidence of crystal orientation in *Phorimidium*, *Rivularia*, or *Schizothrix*. Conversely, other filaments show clear evidence of preferred crystal orientation (e.g., Couté, 1982; Riding, 1977; Jones and Kahle, 1986; Jones and Motyka, 1987). In some cases, the individual crystals are arranged so that they seem to be forming the framework of a single larger crystal. For example, Friedmann (1979) demonstrated that the acicular crystals on *Geitleria floridana* are arranged so as to form a rhombic-lattice that appears to conform to the basic crystallographic properties of a single calcite rhomb. Indeed, Friedmann (1979) noted that the calcareous sheaths behaved optically as a single crystal. Similarly, Jones and Kahle (1986) noted that dendritic calcite crystals on filaments from a karst breccia on Grand Cayman appear to be crystallographically orientated according to the shape of a standard calcite rhomb. Factors affecting the orientation of crystals in the Cayman examples are not known.

On a broad scale, the calcified filaments from Cayman Islands can be divided into the single-wall type (e.g., Jones and Motyka, 1987, fig. 6D) and the double-wall type (e.g., Jones and Kahle, 1985, fig. 4B). Both have an open central tube that was originally occupied by the filament. The single-wall type is formed of one layer of calcite or aragonite crystals. The double-wall type is formed of an inner wall and an outer wall. The inner wall, which has a smooth inner surface, is usually formed of homogeneous, cryptocrystalline calcite. The outer wall is formed of calcite and/or aragonite crystals like those in the single-wall type. In the Cayman examples, this involves (1) dentritic calcite crystals (Jones and Kahle, 1986, figs. 3, 4, 5, 6; Figs. 12-41, 12-42), (2) needle-shaped calcite crystals that radiate from the filament (Jones and Motyka, 1987, figs. 6E, 6F; figs. 12E, 12F, 12G; Fig. 12-22), and (3) irregularly-shaped calcite crystals less than 4 μm long (Jones and Kahle, 1985, fig. 6I; Jones and Motyka, 1987, fig. 7; figs. 12H, 12I). There are also rare examples of filaments coated with euhedral dolomite crystals (Pleydell, 1987, plate 11E, 11F; Fig. 12-43).

Conclusions regarding the factors that control calcification patterns of filaments are also difficult to interpret, because the factor(s) controlling calcite crystal morphology are poorly understood. In this context, Jones and Kahle (1985) examined dendritic calcite crystals on calcified algal filaments from a karst breccia on Grand

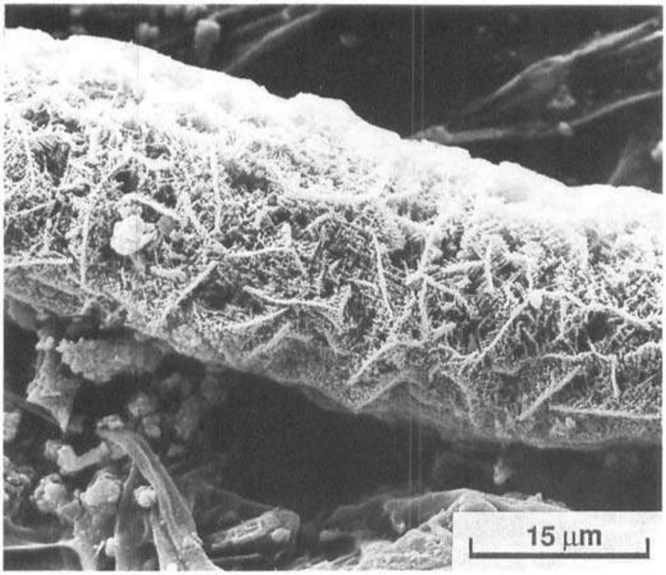

Fig. 12-41. Algal filament calcified with dendritic calcite crystals. This algae, which is probably *Geitleria*, occurs on cavity walls in a karst breccia from the East End quarry on Grand Cayman.

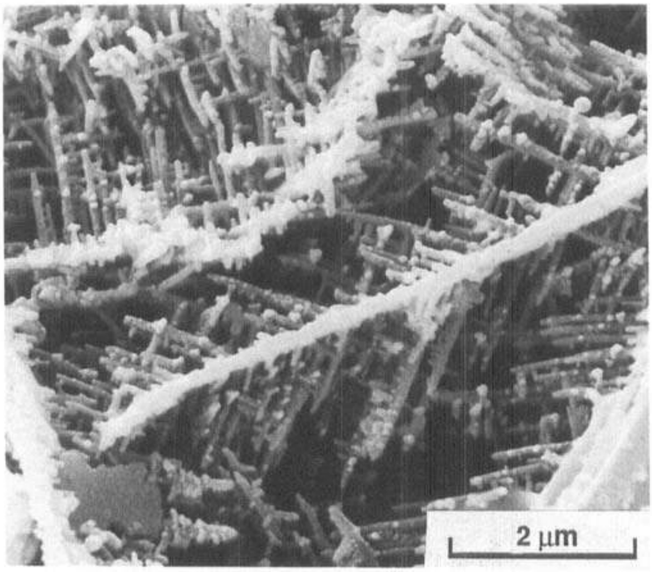

Fig. 12-42. Detailed view of dendritic calcite crystals that occur on wall of *Geitleria*. (From Jones and Kahle, 1986, fig. 5D.)

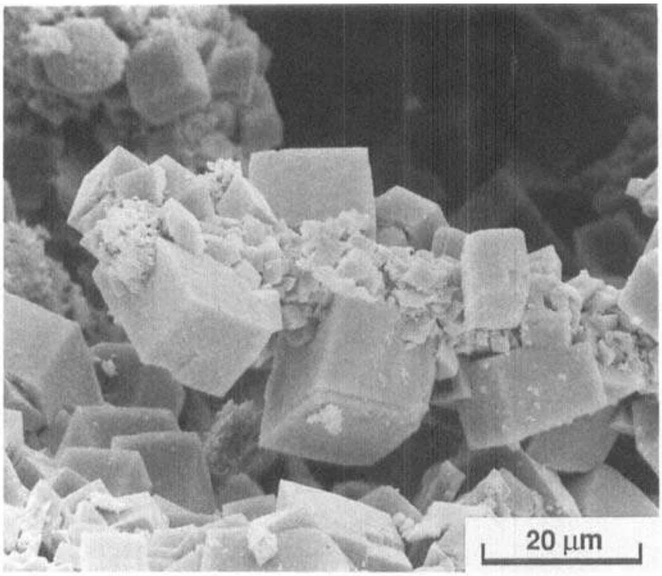

Fig. 12-43. Example of chasmolithic filament that has been coated with two generations of dolomite crystals. Sample from cavity in the Bluff Formation on Grand Cayman. (From Jones et al., 1989, fig. 1D.)

Cayman. Similarly, Friedmann (1979) noted that some of the acicular crystals in the calcareous sheath of *Geitleria floridana* have a dendritic growth pattern with short, lateral branches. After comparing them with crystal development in ice and metals, Jones and Kahle (1986) argued that the dendrite crystals probably formed because of impurities in the precipitating fluids. Such impurities may have been related to the algal filaments themselves (Jones and Kahle, 1985). Kirchmayer (1987), however, attributed dendritic calcite crystals in cave pearls to inorganic processes because of the supposed absence of microorganisms in caves. Conversely, Jones and MacDonald (1989) demonstrated that dendritic calcite crystals occurred in cave pisoliths (= cave pearls of Kirchmayer, 1987) along with calcified microorganisms.

Crystal composition

Pentecost and Riding (1986) suggested that the composition of crystals involved in the calcification of cyanobacteria may be controlled by the type of water that the microorganisms are living in. Thus, cyanobacteria living in freshwater contain or are encrusted by low-magnesium calcite (Gleason, 1972), whereas seawater induces the formation of aragonite and/or Mg-calcite (Golubic and Campbell, 1981). In rare examples from Grand Cayman, chasmolithic filaments are encrusted with euhedral limpid dolomite crystals (Pleydell, 1987; Jones et al., 1989). Most filaments from the Cayman Islands, however, appear to have been calcified by low-magnesium calcite. This assessment must be treated with caution, because it is commonly difficult to establish the true mineralogy of the minute crystals that are involved in the calcification of microorganisms. The practice of using crystal morphology as an indication of mineralogy is dangerous, because it has been demonstrated that the same mineral (i.e., low- or high-magnesium calcite) can exist in many different forms.

Microorganisms from the karst terrains of the Cayman Islands are also responsible for the fixing of other elements. For example, elements such as Mn, Fe and Al are commonly associated with the spherical and hemispherical bodies that occur in stalactites (Jones and Motyka, 1987). This may be a selective process because some microorganisms have only Mn in them, whereas others contain only Fe (Fig. 12-5). Although the mineralization makes identification difficult, Jones and Motyka (1987), following comparison with bacterial structures illustrated by Chafetz and Meredith (1983), Chafetz and Folk (1984) and Folk et al. (1985), suggested that they were of bacterial origin. The ability of microorganisms to selectively fix elements other than Ca is also known from other studies. For example, Schulz-Baldes and Lewin (1974) documented algal zygotes that selectively fixed manganese in brown plaques around their bodies. Similarly, Lawrey and Rudolph (1975) showed that lichen can accumulate P, K, Ca, Mg, Mn, Fe, Cu, Zn, Al, and Mo many times the concentration present in the substrate on which they occur.

DESTRUCTION OF SUBSTRATES BY ETCHING

Etching crystal surfaces of calcite can produce either (1) rounded surfaces with little evidence of crystallographic control (e.g., Berner and Morse, 1974, plate 1B;

Berner, 1978, plate 1A, 1981, figs. 4a; Morse, 1983, fig. 11a) if transport-controlled kinetic processes are operative; or (2) surfaces with crystallographically-controlled angular etch pits, ledges, and corners (e.g., Berner and Morse, 1974, plate 1C; Berner, 1978, plate 1B, 1981, figs. 4b; Morse, 1983, fig. 11b) if surface-controlled kinetic processes are operative (Berner, 1978, 1981). To a large extent the style of dissolution is controlled by the amount of fluid that passes across the crystal surfaces.

Dissolution by surface-reaction-controlled kinetics is usually associated with situations where there is little water passing over the crystal surfaces. As a result dissolution is highly selective in its action with low energy, defect-free areas of the crystals escaping dissolution (Berner, 1978, 1981). Conversely, areas of excess energy located at growth dislocations (Stanley, 1959; Watts, 1959), dislocations along twin boundaries (Berner and Holdren, 1979), or cleavage planes are preferentially attacked. In this situation, ions are detached slowly from the crystal surface, because of the limited quantity of water that is involved. The lack of turbulence in the water means that the detached ions tend to stay close to the crystal surface, thereby causing the water to become progressively saturated with respect to $CaCO_3$. This leads to a relatively slow rate of selective dissolution.

Transport-controlled kinetics produces rounded surface features where large volumes of water are involved. Ions detached from the crystal surface are moved away quickly because of the turbulence in the water. As a result, the water near the crystal surface maintains its undersaturated state and rapid dissolution can occur. The speed of dissolution means that the entire crystal surface is subjected to dissolution without much regard for the crystallographic structure of the crystal.

In vadose settings, it can be difficult to maintain fluids on cavity walls because any water introduced into the cavity will either drain away because of gravity or be evaporated because of the elevated temperatures that are common on and in the surface rocks of the Cayman Islands. Microbial accumulations of algae, fungi, cyanobacteria, and bacteria, which commonly coat cavity walls, however, are capable of retaining moisture in the cavity, usually close to the rock surface. In this respect, cyanobacteria are important, because they can produce copious amounts of mucilage (Stanier, 1982). Thus, the carbonate substrate may be covered with mucilage that contains water as well as elements and body fluids excreted by the cyanobacteria. In general, the effect of mucilage on substrate destruction has been underestimated and largely ignored.

Mucilage appears to be ideally suited for the slow dissolution processes associated with surface-controlled kinetics (Jones and Pemberton, 1987a, b; Jones, 1987). The experiments of Jones and Pemberton (1987a, b) demonstrated that mucilage can mediate substantial amounts of dissolution in as little as 253 days. Thus, it is relatively easy to envisage how much dissolution could be achieved over the millions of years that the carbonate rocks have been exposed to weathering on the Cayman Islands. Indeed, Jones and Pemberton (1987b, p. 693–694) estimated that fungi might be responsible for the destruction and loss of at least 15 mm of substrate over a period of one million years.

Calcium carbonate obtained from the substrate by the action of the microorganisms then becomes available for calcification of filaments, spores or fruiting bodies, or the formation of new crystals beneath the filamentous mats (e.g., Jones and Pemberton, 1987b). In effect, the microorganisms can recycle $CaCO_3$ on a microscopic scale.

RELATIONSHIPS BETWEEN CONSTRUCTIVE AND DESTRUCTIVE PROCESSES

The activity of microorganisms is commonly considered only in terms of their destructive or constructive capabilities. For example, discussion may focus on the trapping and binding of particles by algae and fungi but ignore other aspects, such as substrate dissolution which may be just as important. Jones and Pemberton (1987a, fig. 7), however, argued that processes mediated by microorganisms are interrelated. Study of microbial accumulations in the karst terrains of the Cayman Islands tends to support this concept.

The cumulative evidence available from the experimental data of Jones and Pemberton (1987a, b) and natural examples (e.g., Jones and Kahle, 1985, 1986; Jones, 1987, 1988) suggests that the destructive and constructive processes are intimately related and can be related in a single model. Destructive processes include sparmicritization (Figs. 12-2, 12-3, 12-29) or the formation of irregularly etched surfaces (Figs. 12-32, 12-40), spiky calcite (Figs. 12-4, 12-5, 12-18, 12-33), or blocky topographies (Figs. 12-19, 12-24) by etching. Loose clay- and silt-sized grains of calcite produced during sparmicritization may be transported by water passing through the system. Such particles may subsequently be trapped and bound to form microstromatolites, or form vadose silt that contributes to the internal sediment that may be deposited in any cavities that are available. As substrates destruction proceeds, dissolved $CaCO_3$ enters the pore fluids and may eventually be reprecipitated as new crystals, utilized by microorganisms for calcification of their filaments, or removed from the system. This model suggests that microorganisms mediate a wide array of related processes that have important consequences for diagenesis in karst terrains.

FACTORS CONTROLLING BEHAVIOR OF MICROORGANISMS

The occurrence of microorganisms throughout the karst terrains of the Cayman Islands demonstrates that they are capable of inhabiting numerous different settings (Fig. 12-44), which are under the influence of many different environmental parameters. It is also apparent that the microorganisms are responsible for the formation of different features in different settings (Fig. 12-44). Thus, it is necessary to determine if any intrinsic or extrinsic controls are responsible for the destructive and constructive processes mediated by the microorganisms.

The reason why microorganisms, such as algae, cyanobacteria and fungi employ an endolithic rather than epilithic or chasmolithic mode of life has been the subject of considerable debate. Microorganisms may assume an endolithic mode of life in order to (1) avoid the physical stresses of wave activity in coastal zones (Ercegoviç,

	FEATURE	CAVES			KARST BRECCIA		ROOTS	
		Twilight zone	Cave Pisoliths	Stalactites	Type 1	Type 2	Rhizoliths	Borings
Micro-organism	Uncalcified filaments	▨	▨		▨	▨	▨	▨
	Calcified filaments	▨	▨	▨	▨		▨	▨
	Mucilagenous mats	▨				▨	▨	▨
	Spherical/hemispherical bodies	▨	▨	▨		▨	▨	▨
Substrate feature	Irregular etching	▨				▨		▨
	Spiky calcite	▨				▨		▨
	Blocky topography	▨				▨		▨
	Sparmicritization	▨			▨			
	Micrite envelope					▨		
	Trapping and binding*	▨	▨	▨	▨		▨	
	Microstromatolites			?	▨			
	Fixing of Mn, Fe, Al			▨				
	Boring	▨			▨	▨		▨
	$CaCO_3$ precipitation	▨	▨	?	▨		▨	▨

Note: Type I karst breccia is that described by Jones and Kahle (1985)
Type II karst breccia is that described by Jones (1987)

* trapping and binding of grains without formation of microstromatolites

Fig. 12-44. Summary diagram showing occurrence of microorganisms and substrate features in different settings of the karst terrain on Grand Cayman. Shaded box indicates that feature is present; open box indicates that feature is absent.

1934), (2) escape from grazing pressures (Perkins and Halsey, 1971; Kobluk and Kahle, 1978), (3) obtain nutrients (Kobluk and Kahle, 1978), (4) obtain moisture from the substrate (Kobluk and Kahle, 1978), or (5) provide a holdfast or protection against moving water (Boekschoten, 1966, 1967; Perkins and Halsey, 1971). Kobluk and Kahle (1978) suggested that there was little evidence to support Ercegoviç's (1934) contention that wave activity caused microorganisms to assume an endolithic mode of life. The presence of endolithic microorganisms in the karst terrains of the Cayman Islands also suggests that Ercegoviç's (1934) idea is not universally applicable. The fact that algae bore into glass fragments argues against the possibility that the microorganisms are assuming an endolithic mode of life in order to find nutrients or moisture (Jones and Goodbody, 1982).

The experiments of Jones and Pemberton (1987a, b) provided some information that is pertinent to the discussion concerning the life modes of fungi. In their experiments, fungi were cultured on crystals of Iceland Spar calcite housed in covered glass dishes. The system was kept damp by pouring small quantities of distilled water into the dish at regular intervals. No nourishment was supplied. Although the fungi mediated a wide array of constructive and destructive processes, they did not bore into the substrate. The lack of boring might be attributed to the lack of (1) physical stresses or grazing pressures, (2) nutrients in the substrate, or (3) moisture in the substrate. It is also possible that the experiments were too short (253 days) to allow boring to become established.

In many cases, it is assumed that large-scale environment parameters control the life style of the microorganisms. For example, the life style(s) of microorganisms in the intertidal zone is commonly attributed to the physical stresses imposed by the breaking waves and periodic exposure to the atmosphere (e.g., Ercegoviç, 1934). Furthermore, in coastal settings, the distribution of species, the number of species, and depth of boring by endolithic cyanobacteria has been attributed to the amount of wave action, the degree of exposure to the atmosphere, and the amount of desiccation (Whitton and Potts, 1980). For coastal settings, Lechampion-Alsumard (1970) suggested that the shallowest borings by endolithic cyanobacteria occurred in the upper littoral zone where there was little moisture. Although the large-scale environmental setting must play some role, it is also apparent that the microenvironments must also play a critical role. This was well demonstrated by the experiments of Jones and Pemberton (1987a, b) and the natural examples documented by Jones (1987, 1988, 1989), where trapping and binding may occur within microns of areas that are being etched by microorganisms. Similarly, epilithic and chasmolithic microorganisms commonly occur close to endolithic microorganisms. These observations suggest that the environment of the cavities in which the microorganisms live is far more important than the large-scale environment in determining the mode of life of the microorganisms.

The complex cements in the breccia described by Jones and Kahle (1985, 1986) also suggest that the microenvironment must play some role in controlling the life style and processes of the microorganisms. Thus, one zone of micrite was formed by microorganisms trapping and binding micrite to form microstromatolites, whereas another zone of micrite less than 2 mm away was formed by sparmicritization that was related to the destructive activity of microorganisms. Furthermore, the spar calcite crystals in the breccia described by Jones (1987), which come from the same quarry, have been extensively bored but show no evidence of sparmicritization. Thus, in samples that occur in very close proximity there are examples of microorganisms, which appear to be of the same type, trapping and binding micrite, boring with the formation of sparmicrite and boring without the formation of sparmicrite. The factors controlling these different life styles and processes are not readily apparent because they all occur in settings that seem to be identical.

CONCLUSIONS

Plant roots and microorganisms play an important role in the diagenesis of carbonates that form the karst terrains of the Cayman Islands (Fig. 12-44). Detailed analysis of the microorganisms from many different settings in these terrains permits the following conclusions:

(1) The assemblages of microorganisms in the karst terrains of the Cayman Islands include a diverse array of root hairs, algae, fungi, cyanobacteria, actinomycete, and bacteria.

(2) Identification of the microorganisms is difficult, especially where mineralization has occurred.

(3) Microorganisms mediate numerous destructive processes, including (a) irregular etching leading to sparmicritization, (b) etching to produce angular to almond-shaped etch pits, (c) etching to produce spiky calcite, and (d) boring which may lead to sparmicritization. These processes cause substrate modification or destruction and results in the liberation of $CaCO_3$ into the surrounding pore fluids.

(4) Microorganisms mediate constructive processes, including (a) trapping and binding of loose sediment particles to form microstromatolites, (b) calcification of filaments and fruiting bodies, (c) selective fixing of elements such as Mn, Fe and Al, and (d) precipitation of calcite or aragonite cements by modifying the physicochemical properties of the pore waters.

5) Calcification of filaments and bodies occurs while the organism is alive, shortly after its death, or at some considerable time after its death.

(6) Calcification of filaments can involve crystals that show a preferred orientation relative to the filament or crystals that are randomly orientated.

(7) Calcification of filaments can involve dendrite crystals, needle-like crystals, or small irregular, anhedral crystals. Rare examples of filaments coated with dolomite crystals also occur.

ACKNOWLEDGEMENTS

The field work and preparation work on which this paper is based would have been impossible without a grant from the Natural Sciences and Engineering Research Council of Canada (grant No. A6090) and the logistical support supplied by Mr. Richard Beswick who is the director of the Cayman Islands Water Authority. The writer is also indebted to numerous colleagues, and in particular Dr. C. F. Kahle, who have helped him to formulate some of the ideas contained in this paper by their active discussion.

The writer is also indebted to Kwok-Choi Ng and Ian Hunter who assisted him in the field on many occasions, and Elsie Tsang who helped in the preparation of the manuscript. Editorial assistance of Drs. G.V. Chilingarian and K.H. Wolf is also greatly appreciated.

REFERENCES

Berner, R.A., 1978. Rate control on mineral dissolution under earth surface conditions. *Am. J. Sci.*, 278: 1235–1252.

Berner, R.A., 1981. Kinetics of weathering and diagenesis, In: A.C. Lasaga and R.J. Kirkpatrick (Editors), *Kinetics of Geochemical Processes. Am. Mineral. Soc. Rev. Mineral.*, 8: 111–134.

Berner, R.A. and Holdren, G.R., 1977. Mechanisms of feldspar weathering: some observational evidence. *Geology*, 5: 369–372.

Berner, R.A. and Holdren, G.R., 1979. Mechanism of feldspar weathering — II. Observations of feldspars from soils. *Geochim. Cosmochim. Acta*, 43: 1173–1186.

Berner, R.A. and Morse, J.W., 1974. Dissolution kinetics of calcium carbonate in sea water, IV. Theory of calcite dissolution. *Am. J. Sci.*, 274: 108–134.

Berner, R.A., Sjöberg, E.L., Velbel, M.A. and Krom, M.D., 1980. Dissolution of pyroxenes and amphiboles during weathering. *Science*, 207: 1205–1206.

Boekschoten, G.J., 1966. Shell borings of sessile epibiontic organisms as paleoecological guides (with examples from the Dutch coast). *Palaeogeogr., Palaeoclimatol., Palaeoecol.*, 2: 333–379

Boekschoten, G.J., 1967. Paleoecology of some mollusca from the Tielrode Sands (Pliocene, Belgium). *Palaeogeogr., Palaeoclimatol., Palaeoecol.*, 3: 311–362.

Bourrelly, P., 1970. *Les Algues d'Eau Douce. III: Les Algues Bleues et Rouges, les Eugléniens, Peridiniens et Cryptomonadines.* N. Boubée & Cie, Paris, 512 pp.

Bourrelly, P. and Dupuy, P., 1973. Quelques stations françaises de *Geitleria calcarea*, Cyanophycée cavernicole. *Rev. Suisse Hydrol., Schweiz. Z. Hydrol.*, 35: 136–140.

Bown, T.M., 1982. Ichnofossils and rhizoliths of the nearshore fluvial Jebel Qatrani Formation (Oligocene), Fayum Province, Egypt. *Palaeogeogr., Palaeoclimatol., Palaeoecol.*, 40: 255–309.

Brown, M.F. and Brotzman, H.G., 1979. *Phythopathogenic Fungi. A Scanning Electron Stereoscope Survey.* University of Missouri Columbia Extension Division, 355 pp.

Brunt, M.A., Giglioli, M.E.C., Mather, J.D., Piper, D.J.W. and Richards, H.G., 1976. The Pleistocene rocks of the Cayman Islands. *Geol. Mag.*, 110: 209–221.

Calvet, F., 1982. Constructive micrite envelope developed in vadose continental environment in Pleistocene eolianites of Mallorca (Spain). *Acta Geol. Hisp.*, 17: 169–178.

Casanova, J. and Tiercelin, J.J., 1982. Constructions stromatolitique en mileau carbonaté sodique: les oncolites des plains incondables du lac Magadi. *C.R. Acad. Sci., Paris, Sér. II*, 295: 1139–44.

Cerridwen, S.A., 1989. *Paleoecology of Pleistocene Mollusca from the Ironshore Formation, Grand Cayman, B.W.I.* M.Sc. Thesis, University of Alberta, Edmonton, Alta., 270 pp. (unpublished).

Chafetz, H.S. and Folk, R.L., 1984. Travertines: depositional morphology and the bacterially constructed constituents. *J. Sediment. Petrol.*, 54: 289–316.

Chafetz, H.S. and Meredith, J.S., 1983. Recent travertine pisoliths (pisoids) from southeastern Idaho, U.S.A. In: T.M. Peryt (Editor), *Coated Grains.* Springer-Verlag, Berlin, pp. 450–455.

Claxton, C.W., 1969. Cylindrical tapering structures in the alluvial sands of the Trent Valley. *Mercian Geol.*, 3: 265–267.

Coase, A. and Judson, D., 1977. Dan Yr Ogof and its associate caves. *Trans. Br. Cave Res. Assoc.*, 4: 332–342.

Coniglio, M. and Harrison, R.S., 1983. Facies and diagenesis of Late Pleistocene carbonates from Big Pine Key, Florida. *Bull. Can. Pet. Geol.*, 31: 135–147.

Couté, A., 1982. Ultrastructure d'une Cyanophycée aérienne calcifiée cavernicole: *Geitleria calcarea* Friedman. *Hydrobiologia*, 97: 255–274.

Cox, G., 1977a. A "living fossil" in the twilight zone: a cave-wall bacterium of unique ultrastructure. In: T.D. Ford (Editor), *Proc. 7th Int. Speleological Congr., Sheffield.* Br. Cave Res. Assoc., Bridgewater, pp. 129–131.

Cox, G., 1977b. Photosynthesis in the deep twilight zone: micro-organisms with extreme structural adaptations to low light. In: T.D. Ford (Editor), *Proc. 7th Int. Speleological Congr., Sheffield.* Br. Cave Res. Assoc., Bridgewater, pp. 131–133.

Cubbon, B.D., 1966. Cave Flora. In: T.D. Ford (Editor), *Proc. 7th Int. Speleological Congr., Sheffield.* Br. Cave Res. Assoc., Bridgewater, pp. 155–156.

Curran, H.A. and White, B., 1987. Trace fossils in carbonate upper beach rocks and eolianites: recognition of the backshore to dune transition. In: H.A. Curran (Editor), *Proc. Third Symp. Geology Bahamas.* Fort Lauderdale, Florida, CCFL Bahamian Field Station, pp. 243–254.

Danielli, H.M.C. and Edington, M.A., 1983. Bacterial calcification in limestone caves. *Geomicrobiol. J.*, 3: 1–16.

Desikachary, T.V., 1959. *Cyanophyta.* Indian Council of Agriculture Research, New Delhi, 686 pp.

Doran, E., 1954. Landforms of Grand Cayman Island, British West Indies. *Tex. J. Sci.*, 6: 360–377.

Draganov, S.J., 1977. Taxonomic structure of cave algal flora. In: T.D. Ford (Editor), *Proc. 7th Int. Speleological Congr., Sheffield.* Br. Cave Res. Assoc., Bridgewater, pp. 155–156.

Drews, G. and Weckesser, J., 1982. Function, structure and composition of cell walls and external layers. In: N.G. Carr and B.A. Whitton, B.A. (Editors), *The Biology of Cyanobacteria. Bot. Monogr.*, 10: 333–357.

Edwards, B.D. and Perkins, R.D., 1974. Distribution of microborings within continental margin sediments of southeastern United States. *J. Sediment. Petrol.*, 44: 1122–1135.

Ercegoviç A., 1934. Wellengang und Lithophytenzone on der Ostadriatischen Kuste. *Acta Adriat.*, 1: 1–20.

Ferrer, M.R., Quevedo-Sarmiento, J., Bejar, V., Delgado, R., Ramos-Cormenzana, A. and Rivadeneyra, M.A., 1988. Calcium carbonate formation by Deleya halophila: effect of salt concentration and incubation temperature. *Geomicrobiol. J.*, 6: 49–57.

Folk, R.L., Chafetz, H.S. and Tiezzi, P.A., 1985. Bizarre forms of depositional and diagnetic calcite in hot-spring travertines, central Italy. In: N. Schneidermann and P.M. Harris (Editors), *Carbonate Cements. Soc. Econ. Paleontol. Mineral., Spec. Publ.*, 36: 349–369.

Folk, R.L., Roberts, H.H. and Moore, C.H., 1973. Black phytokarst from Hell, Cayman Islands, British West Indies. *Geol. Soc. Am. Bull.*, 84: 2351–2360.

Friedmann, E.I., 1955. *Geitleria calcarea* n. gen. n. sp. A new atmophytic lime-incrusting blue-green alga. *Bot. Not.*, 108: 439–445.

Friedmann, E.I., 1979. The genus *Geitleria* (Cyanophyceae or Cyanobacteria): Distribution of *G. calcarea* and *G. floridana* n. sp. *Plant Systematics and Evolution*, 131: 169–178.

Friedman, G.M. and Sanders, J.E., 1978. *Principles of Sedimentology*. John Wiley and Sons, New York, N.Y., 792 pp.

Gleason, P.J., 1972. *The origin, sedimentation and stratigraphy of a calcitic mud located in the southern fresh-water Everglades*. Thesis, Pennsylvania State University, University Park, Pa. (unpublished).

Golubic, S., 1973. The relationship between blue-green algae and carbonate deposits. In: N.B. Carr and B.A. Whitton (Editors), *The Biology of the Blue-Green Algae. Bot. Monogr.*, No. 9. Blackwell Scientific Publications, Oxford, pp. 434–474.

Golubic, S. and Campbell, S.E., 1981. Biogenically formed aragonite concretions in marine Rivularia. In: C. Monty (Editor), *Phanerozoic Stromatolites*. Springer-Verlag, Berlin, pp. 209–229.

Gracia Alonso, C.A., 1974. *Geitleria calcarea* Friedmann nueva alga cavernicola para España. *Speleon.*, 21: 133–136.

Glennie, K.W. and Evamy, B.D., 1968. Dikata: plants and plant root structures associated with aeolian sand. *Palaeogeogr., Palaeoclimatol., Palaeoecol.*, 4: 77–87.

Hale, M.E., 1974. *The Biology of Lichens*. Elsevier, Amsterdam, 181 pp.

Herdman, M., Janvier, M., Waterbury, J.B., Rippka, R. and Stanier, R.Y., 1979. Deoxyribonucleic acid base composition of Cyanobacteria. *J. Gen. Microbiol.*, 111: 63–71.

Hoare, D.S., Ingram, L.O., Thurston, E.L. and Walkup, R., 1971. Dark heterotrophic growth of an endophytic blue-green alga. *Arch. Mikrobiol.*, 78: 310–321.

Høeg, O.A., 1946. Cyanophyceae and bacteria in calcareous sediments in the interior of Limestone Caves in Nord-Rana, Norway. *Nyatt Magasine for Naturvidenskapene*, 85: 99–104.

Hunter, I.G. and Jones, B., 1988. Corals and paleogeography of the Pleistocene Ironshore Formation on Grand Cayman, B.W.I. In: *Proc. Sixth Int. Coral Reef Symp.*, Townsville, Queensland, 3: 431–435.

Hunter, I.G. and Jones, B., 1989. Sedimentology of the Late Pleistocene Ironshore Formation on Grand Cayman. *12th Caribbean Geol. Conf., Abstr.*, p. 78.

James, N.P., 1972. Holocene and Pleistocene calcareous crust (caliche) profiles: criteria for subaerial exposure. *J. Sediment. Petrol.*, 42: 817–836.

James, N.P. and Choquette, P.W., 1984. Diagenesis — 9. Limestones — the Meteoric Diagenetic Environment. *Geosci. Can.*, 11: 161–194.

Jones, B., 1987. The alteration of sparry calcite crystals in a vadose setting, Grand Cayman Island. *Can. J. Earth Sci.*, 24: 2292–2304.

Jones, B., 1988. The influence of plants and micro-organisms on diagenesis in caliche: example from the Pleistocene Ironshore Formation on Cayman Brac, British West Indies. *Bull. Can. Pet. Geol.*, 36: 191–201.

Jones, B., 1989. The role of micro-organisms in phytokarst development on dolostones and limestones, Grand Cayman, British West Indies. *Can. J. Earth Sci.*, 26: 2204–2213.

Jones, B. and Goodbody, Q.H., 1982. The geological significance of endolithic algae in glass. *Can. J. Earth Sci.*, 19: 671–678.

Jones, B. and Goodbody, Q.H., 1985. Oncolites from a shallow lagoon, Grand Cayman Island. *Bull. Can. Pet. Geol.*, 32: 254–260.

Jones, B. and Kahle, C.F., 1985. Lichen and algae: agents of biodiagenesis in karst breccia from Grand Cayman Island. *Bull. Can. Pet. Geol.*, 33: 446–461.

Jones, B. and Kahle, C.F., 1986. Dendritic calcite crystals formed by calcification of algal filaments in a vadose environment. *J. Sediment. Petrol.*, 56: 217–227.

Jones, B. and Motyka, A., 1987. Biogenic structures and micrite in stalactites from Grand Cayman Island, British West Indies. *Can. J. Earth Sci.*, 24: 1402–1411.

Jones, B. and MacDonald, R.W., 1989. Micro-organisms and crystal fabrics in cave pisoliths from Grand Cayman, British West Indies. *J. Sediment. Petrol.*, 59: 387–396.

Jones, B. and Ng, K.C., 1988. The structure and diagenesis of rhizoliths from Cayman Brac, British West Indies. *J. Sediment. Petrol.*, 58: 457–467.

Jones, B. and Pemberton, S.G., 1987a. The role of fungi in the diagenetic alteration of spar calcite. *Can. J. Earth Sci.*, 24: 903–914.

Jones, B. and Pemberton, S.G., 1987b. Experimental formation of spiky calcite through organically mediated dissolution. *J. Sediment. Petrol.*, 57: 687–694.

Jones, B. and Smith, D.S., 1988. Open and filled karst features on the Cayman Islands: implications for the recognition of paleokarst. *Can. J. Earth Sci.*, 25: 1277–1291.

Jones, B., Lockhart, E.B. and Squair, C., 1984. Phreatic and vadose cements in the Tertiary Bluff Formation of Grand Cayman Island, British West Indies. *Bull. Can. Pet. Geol.*, 32: 382–397.

Jones, B., Pleydell, S.A., Ng, K.C. and Longstaffe, F.J., 1989. Formation of poikilotopic calcite–dolomite fabrics in the Oligocene–Miocene Bluff Formation of Grand Cayman, British West Indies. *Bull. Can. Pet. Geol.*, 37: 255–265.

Jones, H.J., 1965. Algological investigations in Mammoth Cave, Kentucky. *Speleology*, 1: 491–516.

Kahle, C.F., 1977. Origin of subaerial Holocene calcareous crusts: role of algae, fungi and sparmicritization. *Sedimentology*, 24: 413–435.

Keller, W.D., 1976. Scan electron micrographs of kaolins collected from diverse environments of origin — I. *Clays Clay Miner.*, 24: 107–113.

Kendrick, B., Risk, M.J., Michaelides, J. and Bergman, K., 1982. Amphibious microborers; bioeroding fungi isolated from live corals. *Bull. Mar. Sci.*, 32: 862–867.

Kieft, T.L. and Caldwell, D.E., 1984. Weathering of calcite, pyrite, and sulfur by *Thermothrix thiopora* in a thermal spring. *Geomicrobiol. J.*, 3: 201–216.

Kirchmayer, M., 1987. Universal stage grain fabrics statistics on dendrites of mine cave pearls. *Carbonates and Evaporites*, 2: 59–65.

Kiyohara, T., Fujita, Y., Hattori, A. and Watenabe, A., 1962. Heterotrophic growth of a blue-green alga *Tolypothrix tenuis*. *J. Gen. Appl. Microbiol.*, 6: 176–182.

Klappa, C.F. 1979a. Lichen stromatolites: criteria for subaerial exposure and a mechanism for the formation of laminar calcretes (caliche). *J. Sediment. Petrol.*, 49: 378–400.

Klappa, C.F., 1979b. Calcified filaments in Quaternary calcretes: organo-mineral interactions in the subaerial vadose environment. *J. Sediment. Petrol.*, 49: 955–968.

Klappa, C.F., 1980. Rhizoliths in terrestrial carbonates, classification, recognition, genesis and significance. *Sedimentology*, 27: 613–629.

Knox, G.J., 1977. Caliche profile formation, Saldanha Bay (South Africa). *Sedimentology*, 24: 657–674.

Kobluk, D.R. and Risk, M.J. 1977. Calcification of exposed filaments of endolithic algae, micrite envelope formation, and sediment production. *J. Sediment. Petrol.*, 47: 517–528.

Kobluk, D.R. and Kahle, C.F. 1978. Geologic significance of boring and cavity-dwelling marine algae. *Bull. Can. Pet. Geol.*, 26: 362–379.

Korringa, P., 1951. Investigations on shell-disease in the oyster *Ostrea edulis* L. Rapp. *Conseil Permanent International d'Exploration, Mer.*, 128: 50–54.

Krumbein, W.E., 1975. Calcification of bacteria and algae. In: P.A. Trudinger and D.J. Swaine (Editors), *Biogeochemical Cycling of Mineral-Forming Elements. Studies in Environmental Science 3.* Amsterdam, Elsevier, pp. 47–63.

Krumbein, W.E. and Giele, C., 1979. Calcification in a coccoid cyanobacterium associated with the formation of desert stromatolites. *Sedimentology*, 26: 593–604.

Lawrey, J.D. and Rudolph, E.D., 1975. Lichen accumulation of some heavy metals from acidic substrates of coal mine ecosystems in southeastern Ohio. *Ohio J. Sci.*, 75: 114–117.

Lechampion-Alsumard, T., 1970. Cyanophycées marines endolithes colonisant les surfaces rocheuses dénudées (Étages Supralittoral et Médiolittoral de la région de Marseille). *Rev. Suisse Hydrol.*, 32: 552–558.

Lefevre, M. and Laporte, G.S., 1969. The "Maladie Verte" of Lascaux. *Studies in Speleology*. William Pengelly Cave Studies Trust Ltd., 2: 34–44.

Mason-Williams, M.A., 1967. Further investigations into bacterial and algal populations of caves in South Wales. *Speleology*, II: 389–395.

McKee, E.D. and Ward, W.C., 1983. Eolian environment. In: P.A. Scholle, D.G. Bebout and C.H. Moore (Editors), *Carbonate Depositional Environments. Am. Assoc. Pet. Geol., Mem.*, 33: 131–170.

Moore-Landecker, E., 1982. *Fundamentals of the Fungi*. Prentice-Hall Inc., Englewood Cliffs, N.J., 578 pp.

Morse, J.W., 1983. The kinetics of calcium carbonate dissolution and precipitation. In: R.J. Reeder (Editor), *Carbonates: Mineralogy and Chemistry. Am. Mineral. Soc. Rev. Mineral.*, 11: 227–264.

Nagy, J.P., 1965. Preliminary notes on the algae of Crystal Cave, Kentucky. *Speleology*, I: 479–490.

Palik, P., 1960. Study into the algal flora of caves. *Hidrologiani Kozlony*, 5: 417–422.

Pautard, F.G.E., 1970. Calcification in unicellular organisms. In: H. Schraer (Editor), *Biological Calcification: Cellular and Molecular Aspects*. Appleton-Crofts, New York, N.Y., pp. 105–201.

Pentecost, A., 1978. Blue-green algae and freshwater carbonate deposits. *Proc. R. Soc. London*, 200: 43–61.

Pentecost, A., 1985. Association of cyanobacteria with tufa deposits: identity, enumeration and nature of the sheath material revealed by histochemistry. *Geomicrobiol. J.*, 4: 285–298.

Pentecost, A. and Bauld, J., 1988. Nucleation of calcite on the sheaths of cyanobacteria using a simple diffusion cell. *Geomicrobiol. J.*, 6: 129–135.

Pentecost, A. and Riding, R., 1986. Calcification in cyanobacteria. In: B.S.C. Leadbeater and R. Riding (Editor), *Biomineralization in Lower Plants and Animals. The Systematics Association Spec. Vol.*, 30: 73–90.

Pentecost, A. and Terry, C., 1988. Inability to demonstrate calcite precipitation by bacteria isolates from travertine. *Geomicrobiol. J.*, 6: 185–194.

Perkins, R.D. and Halsey, S.D., 1971. Geologic significance of microboring fungi and algae in Carolina Shelf sediments. *J. Sediment. Petrol.*, 41: 843–853.

Phillips, S.E., Milnes, A.R. and Foster, R.C., 1987. Calcified filaments: an example of biological influences in the formation of calcrete in south Australia. *Aust. J. Soil Res.*, 25: 405–428.

Pilkey, O.H. and Gorsline, D.S., 1961. Recent root casts in sediments of the Applachian Delta, Florida. *Southeast. Geol.*, 3: 37–47.

Pleydell, S.M., 1987. *Aspects of Diagenesis and Ichnology in the Oligocene–Miocene Bluff Formation of Grand Cayman Island, British West Indies*. M.Sc. Thesis, University of Alberta, Edmonton, Alta., 209 pp. (unpublished).

Porter, C.L. and Zebrowski, G., 1937. Lime-loving molds from Australian sands. *Mycologia*, 29: 252–257.

Riding, R., 1977. Calcified *Plectonema* (blue-green algae), a Recent example of *Girvanella* from Aldabra Atoll. *Palaeontology*, 20: 33–46.

Riding, R. and Voronova, L., 1982. Recent freshwater oscillatoriacean analogue of the Lower Paleozoic calcareous algae *Angulocellularia*. *Lethaia*, 15: 105–114.

Rippka, R., 1972. Photoheterotrophy and chemoheterotrophy among unicellular blue-green algae. *Arch. Mikrobiol.*, 87: 93–98.

Rippka, R., Deruelles, J., Waterbury, J.B., Herdman, M. and Stanier, R.Y., 1979. Generic assignments, strain histories and properties of pure cultures of cyanobacteria. *J. Gen. Microbiol.*, 111: 1–61.

Rooney, W.S. and Perkins, R.D., 1972. Distribution and geologic significance of microboring organisms within sediments of the Arlington Reef Complex, Australia. *Geol. Soc. Am. Bull.*, 83: 1139–1150.

Round, F.E., 1981. *The Ecology of Algae*. Cambridge University Press, Cambridge, 653 pp.

Schulz-Baldes, M. and Lewin, R.A., 1974. Manganese encrustation of zygospores of a Chamydomonas (Chlorophyta: Volvocales). *Science*, 188: 1119–1120.

Spencer, T., 1981. Micro-topographic change on calcarenites, Grand Cayman Island, East Indies. *Earth Surface Processes and Landforms*, 6: 85–94.

Spencer, T., 1985a. Weathering rates on a Caribbean reef limestone: results and implications. *Mar. Geol.*, 69: 195–201.

Spencer, T., 1985b. Marine erosion rates and coastal morphology of reef limestones on Grand Cayman Island, West Indies. *Coral Reefs*, 4: 59–70.

Spencer, T., Woodroffe, C.D. and Stoddart, D.R., 1984. Calcareous crusts and contemporary weathering on raised reef limestones, Grand Cayman Island, West Indies. *Advances in Reef Science*, Miami, Abstracts of Papers, p. 117.

Squair, C.A., 1988. *Surface Karst on Grand Cayman Island, British West Indies.* M.Sc. Thesis, University of Alberta, Edmonton, Alta., 107 pp. (unpublished).

Stanier, R.Y., 1977. The position of cyanobacteria in the world of phototrophs. *Carlsberg Res. Commun.*, 42: 77–98.

Stanier, R.Y., 1982. Foreword. In: N.G. Carr and B.A. Whitton (Editors), *The Biology of Cyanobacteria. Bot. Monogr.*, 19: ix–x.

Stanier, R.Y., Kunisawa, R., Mandel, M. and Cohen-Bazire, G., 1971. Purification and properties of unicellular blue-green algae (order *Chroococcales*). *Bacteriol. Rev.*, 35: 171–205.

Stanier, R.Y., Adelberg, E.A. and Ingraham, J. L., 1976. *The Microbial World.* Prentice-Hall Inc., Englewood Cliffs, N.J., 4th ed., 871 pp.

Stanley, R. C., 1959. Etch pits on calcite cleavage faces. *Nature*, 183: 1548.

Starmach, K., 1966. Cyanophyta–Sinice, Glaucophyta–Glaukofity. Flora slodkowodna Polski. *Polish Acad. Sci.*, 2: 1–807.

Trudgill, S. T., 1985. *Limestone Geomorphology.* Longman Inc., New York, N.Y., 196 pp.

Tsuneda, A., 1983. *Fungal Morphology and Ecology. Mostly Scanning Electron Microscopy.* Tokyo Press, Tokyo, 320 pp.

Van Baalen, C., Hoare, D. S. and Brandt, E., 1971. Heterotrophic growth of blue-green algae in dim light. *J. Bacteriol.*, 105: 685–689.

Viles, H. A. and Spencer, T., 1983. "Phytokarst", blue-green algae and limestone weathering. In: K. Paterson and M. M. Sweeting (Editors), *New Directions in Karst. Proc. Anglo-French Karst Symp.*, pp. 115–140.

Wallner, J., 1934. Über der Beteiligung Kalkablagender Pflanze bei der Bildung südbayerischer Tuffe. *Bibliotheca Botany*, 111: 1–30.

Ward, W. C., 1970. *Diagenesis of Quaternary Eolianites of N. E. Quintana Roo, Mexico.* Ph.D. Thesis, Rice University, 206 pp. (unpublished).

Ward, W.C., 1973. Influence of climate on the early diagenesis of carbonate eolianites. *Geology*, 1: 171–174.

Ward, W.C., 1978. Indicators of climate in carbonate dune rocks. In: W.C. Ward and A.E. Weidie (Editors), *Geology and Hydrogeology of Northeastern Yucatan. New Orleans Geol. Soc.*, pp. 191–208.

Ward, W.C., 1985. Quaternary Geology of northeastern Yucatan Peninsula. In: W.C. Ward, A.E. Weidie and W. Back (Editors), *Geology and Hydrogeology of the Yucatan and Quaternary Geology of Northeastern Yucatan Peninsula. New Orleans Geol. Soc.*, pp. 23–95.

Watts, H., 1959. Etch pits on calcite cleavage faces. *Nature*, 183: 314.

Went, F.W., 1969. Fungi associated with stalactite growth. *Science*, 166: 386–387.

Whitton, B.A. and Potts, M., 1980. Blue-green algae (Cyano-bacteria) of the oceanic coast of Aldabra. *Atoll Res. Bull.*, 238: 1–8.

Wilson, M.J., 1975. Chemical weathering of some primary rock-forming minerals. *Soil Sci.*, 119: 349–355.

Wood, P., 1984. *Structural and Physiological Studies of the Effects of Mineral Deficiencies on the Rivulariaceae (Cyanobacteria).* Ph.D. Thesis, University of Durham and Sutherland Polytechnic (unpublished).

Zebrowski, G., 1936. New genera of Cladochytriaceae. *Ann. Mo. Bot. Gard.*, 23: 553–564.

This Page Intentionally Left Blank

Diagenesis, IV. Developments in Sedimentology 51
edited by K.H. Wolf and G.V. Chilingarian
© 1994 Elsevier Science B.V., Amsterdam. All rights reserved.

Chapter 13

PALEOKARST (DISSOLUTION DIAGENESIS): ITS OCCURRENCE AND HYDROCARBON EXPLORATION SIGNIFICANCE

V.P. WRIGHT and P.L. SMART

INTRODUCTION

Paleokarst refers to karstic (dissolution-related) features formed in the past, related to an earlier hydrological system or landsurface (modified from Wright, 1982). Karst is a term used to describe distinctive terrains whose landforms and hydrology result from a combination of high rock solubility and well-developed secondary porosity (Ford and Williams, 1989). From a diagenetic point of view, karstification can be considered as one of the range of processes affecting sediments, especially carbonates and evaporites. Esteban and Klappa (1983) have regarded karst as a "diagenetic facies" and the importance of paleokarstic processes in the developments of porosity is becoming increasingly widely appreciated.

Karst systems have been intensively studied and the hydrological principles of their formation are well understood. Thus, in studying paleokarsts it is possible to employ the knowledge of present-day systems to understand ancient ones. Indeed this is one of the few occasions when "diagenesis" can be related to hydrology and hydrogeology, allowing some predictive element.

There are two main drawbacks encountered in studying paleokarsts which frustrate attempts to apply karst-science to interpret them. Firstly, many paleokarsts are encountered in the subsurface, particularly during hydrocarbon exploration, and interpreting paleokarst style from limited seismic or borehole data is very difficult. At outcrop, the task can be easier, but the second major problem is that many major paleokarsts are polyphase and are difficult to interpret for this reason. Major paleokarsts are either associated with unconformities or high amplitude sea-level falls. In both cases, long exposure periods and complex base-level changes result in multiple phases of development making formulating simple paleohydrological models difficult.

The majority of paleokarsts, however, are of minor development (but can create significant porosity). They are associated with small-scale sea-level changes (e.g., fourth- and fifth-order changes) and should be regarded as an integral part of the diagenetic spectrum for shallow-marine limestones. After all, most limestones were deposited in very shallow water (less than 10 m) and were as such, vulnerable to even small-scale changes in sea level and related meteoric diagenesis.

Important as meteoric processes are to karst and paleokarst formation in near-surface zones, dissolution diagenesis occurs in other settings, including marine-meteoric mixing zones, and in deeper burial sites. This chapter will also cover these other settings.

The current interest in paleokarsts is evidenced by the recent appearance of two books on the subject. James and Choquette (1988) have compiled a series of reviews and case studies on karstic processes and paleokarsts which is essential reading. Bosák et al. (1990) have provided a global review of paleokarst occurrence.

This chapter aims at presenting a review of paleokarst occurrence which will be of use in subsurface exploration. It is not intended as a review of karstic processes and geomorphology, and Ford and Williams (1989) have recently provided a detailed synthesis of these topics. Shorter reviews on karst systems and hydrogeochemistry written for geologists, have been given by Ford (1988) and Lohmann (1988). A general introduction to karst and paleokarst has been provided by Choquette and James (1988), who have also given a very useful review of meteoric diagenesis in carbonates (James and Choquette, 1984). In order to concentrate on aspects relevant to hydrocarbon exploration, topics such as evaporite dissolution and paleokarst-hosted mineralization are not covered.

SITES OF MAJOR DISSOLUTION DIAGENESIS

Karstic processes have traditionally been regarded as being related to near-surface meteoric (rain-sourced) waters. Most paleokarsts encountered in the geological record are directly attributable to such waters, but it is becoming increasingly clear that significant dissolution of carbonates can also take place in other settings, related to other fluids besides meteoric-sourced groundwaters.

Figure 13-1 shows the major sites of dissolution diagenesis. Each is associated with its own fluid type and dissolution processes, but considerable overlap can occur between each. The chemical processes involved are not reviewed here, but

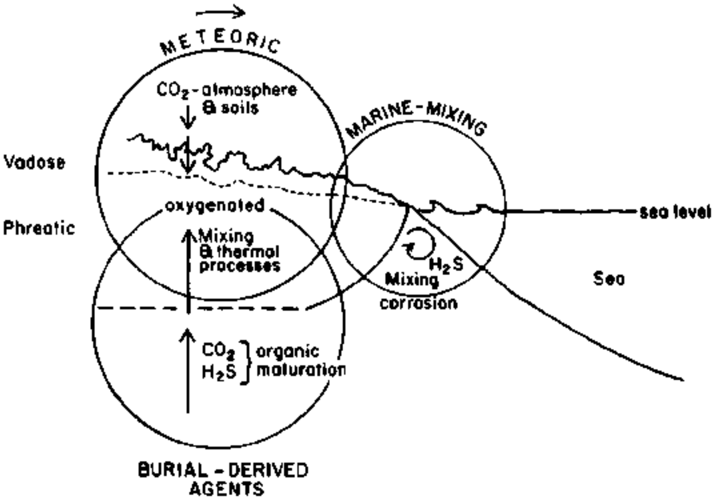

Fig. 13-1. Occurrence of extensive carbonate dissolution diagenesis and main processes and agents responsible for the dissolution.

the distribution and styles of each type are the aspects relevant for hydrocarbon exploration and these are the themes covered below.

Meteoric system

The most familiar karst products are those associated with meteoric water and most paleokarsts are attributable to such origins. Surface and subsurface karst features develop: surface features vary from millimeter-scale dissolution "scars" to large tower karsts, and fossil examples of many of these are known. Subsurface karst refers to cave systems and other conduits.

The main agent of dissolution is carbonic acid. Small amounts of carbon dioxide are absorbed from the atmosphere, but most is derived from the soil as the rainfall percolates into the limestone aquifer. The thickness of the soil and its vegetation cover are critical factors influencing the CO_2 concentration. The CO_2 is derived from respiration, but the oxidation of organic matter, abundant in near-surface waters, also results in carbonic acid production. Mixing corrosion can also occur in this setting but is a more important process in the marine–meteoric system (see below).

Most meteoric paleokarsts have originated where shallow-marine limestones have become subaerially exposed by a fall in relative sea level. The carbonate body is thus open to the atmosphere at its surface, forming an unconfined reservoir. Confined reservoirs are where the aquifer is confined by some overlying impermeable or poorly permeable layer.

A series of hydrologic zones can be defined (Fig. 13-2). The vadose zone is the unsaturated zone above the water-table through which water drains. The soil zone is underlain by the subcutaneous (or epikarst) zone which is highly weathered. Beneath

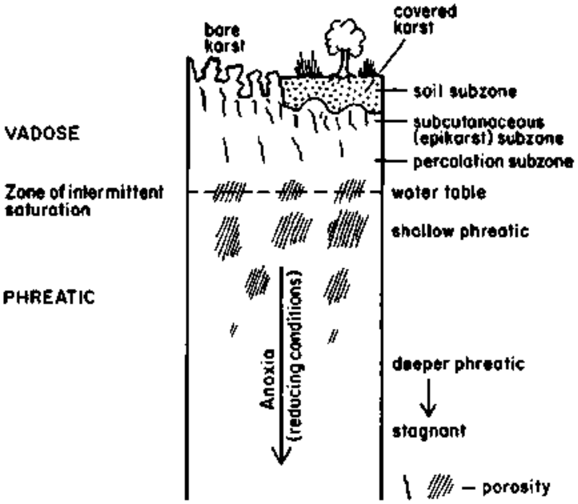

Fig. 13-2. Hydrological zones in karst. Note contrast between the irregular "bare" and smoother, soil-covered karst surfaces. Dissolution porosity formation is greatest in the more active upper part of the phreatic zone and also where mixing corrosion occurs.

is a less weathered free-draining zone. The water-table (or piezometric surface) is the surface where hydrostatic and atmospheric pressures are equal. It is mobile and, thus, a zone of intermittent saturation exists. Below is the phreatic zone, where all pores are saturated with water and within which broad subzones may be recognized related to the flow activities. Caves can develop in any of these zones, a cave being defined as any solution conduit larger than 5–15 mm (Ford, 1988). The hydrologic characteristics of such channels are very similar despite their size variations.

The nature and extent of such cave systems has been extensively documented in many published works (e.g., Ford, 1988; Ford and Williams, 1989), and differences occur between those developed in vadose, unconfined phreatic and confined phreatic systems. The enormous amount of information on such cave system styles and on their porosity and permeability characteristics, available from studies of karst systems, appears at first ideal to apply to paleokarsts. Indeed the sophisticated hydrological models might seem directly applicable to reservoir modelling. There are many problems, however, particularly because many paleokarsts have had complex, polyphase histories. It might be instructive to consider the stages of development that an uplifted carbonate terrain would undergo during prolonged karstification to illustrate this point.

The newly emerged sediments would both be unconsolidated and contain a variety of carbonate forms of different solubilities (low- and high-magnesian calcite, aragonite and possibly dolomite). The exposed surface would undergo dissolution, the degree of which would ultimately depend on the climate (see below). Initially, meteoric water would pass through bare sediment, or a thin soil cover and flow would be intergranular and intragranular (diffuse flow). With time cementation would take place, especially in the phreatic zone, and flow will become "channelized" in conduits (conduit flow of White, 1969). The product of synchronous lithification and karstification is referred to as syngenetic karst (Jennings, 1971). Thus, primary porosity is reduced, whereas secondary porosity increases. Depending on the climate and length of exposure, a wide range of porosities can result (Fig. 13-3).

While these processes are taking place, the carbonates are also becoming progressively stabilized to a low-magnesian calcite mineralogy (James and Choquette, 1984). Even with complete stabilization, high primary porosities remain (Schmoker and Hester, 1986); only 15–20% of the original porosity being lost. Thus, for extensive cementation to have occurred there must have been either net loss of sediment by dissolution or by the addition of material from elsewhere. As conduit flow develops, caves result and the high flow rates in the shallow phreatic zone creates greater local dissolution. Such high-porosity zones have even been recognized in paleokarst reservoirs (Craig, 1988).

Recently, Budd and Vacher (1991) have offered a predictive model for phreatic lenses beneath carbonate paleoislands, based on the Dupuis-Ghyben-Herzberg relationship. The thickness of the freshwater lens (H) will be a function of the island's width (a), hydraulic conductivity (K) and the amount of recharge (R). The ratio of R/K in Holocene and Pleistocene sediments and rocks is in the range 10^{-4} to 10^{-6} and, ideally, H should be 1–3% of the magnitude of the island width, but values 0.2–2% are more typical with 1% being representative. Budd and Vacher used this

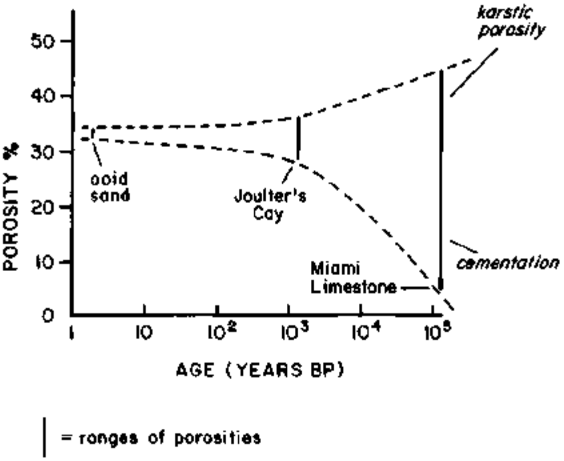

Fig. 13-3. Porosity versus time plot for three oolitic sands. The Joulter's Cay oolite has been exposed for 1000 years where as the Miami Oolite is Pleistocene in age. The upper curve represents the development of karstic porosity, whereas the lower one represents porosity loss by cementation. (Based on Halley and Evans, 1983; Evans and Ginsburg, 1987.)

approach on two reservoir intervals, the Upper Jurassic Smackover Oaks Field of Louisiana and the Late Permian Yates Field of Texas, which has a paleocave system.

The flow rates through the conduit systems are much greater than through the host rock where diffuse flow operates. In the former, the rate is both rapid and turbulent, enhancing dissolution, whereas in the latter it is much slower and is laminar (White, 1977). This is a property which explains the complex behaviors of some paleokarstic reservoirs where both cave and matrix porosity occur.

The development of caves can be very rapid if a large source of water is available from outside the immediate catchment area (allogenic input), such as a nearby land area. An understanding of the regional paleogeography could be critical in assessing the potential for paleokarst development in any sequence. If areas of localized authogenic recharge occur, such as dolines, flow rates and dissolution rates will be higher near them (Williams, 1985). Such features have been detected using 3-D seismic data (Brown, 1985), but the relatively small "catchments" of dolines are such that the actual amount of increased dissolution associated with them will be low compared with that of allogenic recharge areas. Paleodolines associated with collapse features may also have enhanced porosities reflecting brecciated zones where collapse has occurred.

Flow, as stated above, is greatest in the upper phreatic zone and the less active zones may become stagnant. The upper phreatic zone is also oxic, although microbial activity can reduce this and the stagnant areas are typically suboxic to anoxic. This trend is also seen laterally when unconfined aquifers become confined down dip (Edmunds and Walton, 1983). This trend towards reducing conditions has commonly been found in studies of paleoaquifer systems using cathodoluminescence behavior as a guide to the redox conditions (Choquette and James, 1988).

Recognizing a paleokarst in the geological record as of meteoric origin will depend on being able to relate its distribution to a particular exposure surface or unconformity. If the paleokarst is a single-phase system, i.e., it is not the product of more than one overlapping hydrological system, it may be possible to crudely predict aspects of the dissolution porosity zones. Cave porosity will be highest near the paleo-watertable and will decrease with depth. Zones of preferentially higher porosity and permeability may be present near large authogenic drainage recharges, such as dolines, and may also be higher near allogenic recharge zones. However, not only does the system evolve from diffuse flow to conduit flow (with more complex porosity–permeability characteristics), but as base-levels change (due to tectonic, eustatic or even to geomorphic changes), karst zones will be overprinted. These aspects are further discussed below.

Marine mixing system

In the last few years, the importance of the marine–meteoric mixing zone has become widely appreciated. It is not only in such "brackish" mixing zones that extensive dolomitization occurs (see review in Tucker, 1990), but it is a zone where very high levels of dissolution can also occur.

The main process creating karstic porosity is mixing corrosion. The chemistry and geological implications of this process have been succinctly reviewed by James and Choquettte (1984). Basically, it occurs when two solutions, saturated with respect to a given mineral phase, are mixed with resulting undersaturation or supersaturation. This will result when waters with different P_{CO_2}, temperatures, salinities, calcite saturations, and pH mix (Bogli, 1964; Runnels, 1969). Such mixing corrosion may take place where vadose and phreatic waters mix or at the base of the phreatic lens between marine and meteoric phreatic waters. In the former case, high porosities may occur at the water-table and paleokarst examples of this have been recorded (Wright, 1982).

Besides mixing corrosion other processes can operate. Recently Smart et al. (1988b) have suggested that microbial oxidation of organic matter, producing CO_2, is also an important process leading to undersaturation in marine-meteoric mixing zones. An additional process in the mixing zones may be dissolution related to bacterial reduction of sulphate, present in the seawater.

Mixing zone waters can be especially aggressive and result in spectacular degrees of corrosion particularly in unstabilized carbonate sediments. The result is a distinctive "Swiss-cheese" style of dissolution illustrated by Back et al. (1986) and Smart et al. (1988a). Extensive cave development can also take place (Vernon, 1969; Leve, 1984; Mylroie, 1988; Smart et al., 1988a) and subsequent collapse can even control coastline shapes and sediment distributions (Hanshaw and Back, 1980; Back et al., 1984; Hine et al., 1988). The mixing zone is also one of dolomitization, and highly vuggy and porous Quaternary dolomites, which reflect such settings, have been described (Ward and Halley, 1985).

Whereas mixing corrosion can take place in other settings besides marine–meteoric ones, it is these which are best documented and arguably of most relevance to hydrocarbon exploration. As stated above, most limestones were deposited in shallow water and were especially prone to subaerial exposure as a result of sea-level changes. This point has been dramatically shown in the study of Matthews and Frohlich (1987), who have computer-modelled shelf margin diagenesis. As their work shows, the opportunities for mixing-zone alteration of shallow-water limestones, using Quaternary sea-level changes as a guide, is considerable. It is likely that more examples of ancient mixing–corrosion zones will be discovered.

In general such zones will have developed in the coastal areas around carbonate terrains which were subaerially exposed and possessed a meteoric lens. Undersaturation can occur at a wide range of seawater–meteoric water mixtures (Back et al., 1986), even as high as 90% seawater for calcite (Stoessell et al., 1989). These coastal mixing zones will occur around the edges of carbonate shelves and carbonate ramps and also around and under isolated carbonate buildups such as isolated platforms and atolls (see later section). Sandford and Konikow (1989), using models, have discussed the positions of mixing corrosion zones in relation to groundwater zones. They noted that calcite dissolution and porosity formation occur primarily on the "fresh" side of the mixing zone and in two distinct areas: one near the base, and one near the top where flow velocities are highest. The major control on such dissolution is the fresh-water flux, whereby much greater dissolution is associated with carbonates bordering large land areas than with small islands. Their models also show how rapidly such porosity could form, even over geologically short periods.

Mixing zones can also develop well offshore, where, if the hydrostatic head is sufficient, freshwater springs can emerge at the sea floor kilometers or even tens of kilometers offshore (Johnson, 1983; Chafetz et al., 1988).

Mazzullo et al. (1990) have described extensive small-scale dissolution porosity from the Upper Triassic Steinplatte and basal Liassic Hirlatz carbonates of the Northern Calcareous Alps of Austria which may represent mixing-zone karstification. The cavity systems are highly complex, sub-meter scale, from vertically disposed to anastomosing networks with more near horizontal orientations. These cavity systems occur over a vertical thickness of 180 m and are cross-cut by neptunean fractures.

The importance of mixing zone dissolution in hydrocarbon reservoirs has been noted by Craig (1988) from the Permian Yates Field of West Texas, and Bouvier et al. (1990) from the Amposta Marino Field, offshore northeast Spain. It is still rather "early days" in the study of paleokarst facies to define the characteristics of a paleo-mixing zone reservoir, but some general points may be relevant. The zones will probably be highly porous with irregular vuggy, earthy porosities associated with dolomite in some cases. The, probably, penecontemporaneous dissolution of calcite (or aragonite) and precipitation of dolomite will create an unusually complex porosity distribution. The individual zones will probably be relatively thin up to perhaps ten meters, but circumstances could have developed allowing thicker ones to have formed. In shelf or ramp settings they will probably thicken seaward, whereas on low relief isolated buildups they may be very extensive laterally (e.g., Andros Island, see below). The extensive breccia-fracture reservoirs of the Ordovician Ellenberger Group of west Texas may be a candidate for such a platform-wide mixing zone system (Kerans, 1988).

Deep burial fluid karstification

Dissolution can occur in deeper burial settings, but will not create large-scale porosity (caves) because of the high lithostatic pressures. Its effects are commonly seen in many diagenetic sequences where "late" burial secondary porosities develop, often associated with hydrocarbons and mineralization.

Several processes operate to cause the undersaturation of calcium carbonate, and these operate over a wide depth range. They are related to burial processes, especially the maturation of organic matter, and the migration of oil field gases and fluids and other thermal fluids. Extensive dissolution porosity, however, may develop in shallower settings where cooling or mixing with oxygenated, cooler meteoric waters takes place.

The two main agents of dissolution are CO_2 and H_2S. The former is typically derived from the decarboxylation of organic matter during hydrocarbon maturation. Thus, extensive dissolution porosity can be created in association with migrating oil (Druckman and Moore, 1985).

Whatever the exact source of the CO_2, thermal waters enriched in it can migrate into shallower burial settings and create significant dissolution porosity as the waters cool and mix with meteoric water. Whereas mixing corrosion may also occur, it is the cooling of the waters which is probably the major cause of dissolution. The solubility of calcite is greater at low temperatures and as the fluids migrate they cool and cause dissolution (Wood, 1986). This possible role of CO_2-enriched thermal fluids has been discussed by Ford and Williams (1989) and spectacular examples occur in the Jewel and Wind caves of South Dakota (Bakalowicz et al., 1987) and in eastern Europe. Ford and Williams have suggested diagnostic features for thermal CO_2 systems such as the development of highly complex, multi-storey, maze-like cavern architecture. These systems lack typical "meteoric" cave sediments, but are associated in many cases with hydrothermal mineralization and extensive brecciation.

Hydrogen sulphide (H_2S) is also an agent of dissolution when it reacts with water to form sulphuric acid. This occurs by mixing with shallow, oxygenated meteoric waters. The acid reacts with the limestone forming gypsum which can then later dissolve to form larger caves. Both simple (e.g., Egemeier, 1981) and highly complex systems may develop; the latter are exemplified by the caves found in the Guadalupe Mountains of New Mexico and West Texas (Fig. 13-4) (Hill, 1987). In this area, H_2S and CO_2 are derived from oil fields in an adjacent basin. These migrated up into shelf margin reefal limestones (Capitan reef complex) and reacted with oxygenated meteoric waters. The thick, evaporitic Castile Formation (Fig. 13-4) having acted as a seal, preventing the simple upward migration of the gases. The resulting dissolution has created huge caves associated with gypsum, which has a distinctive sulphur isotopic signature, enriched in the light isotope similar to the H_2S gas derived from the basin. Details of this system are to be found in Davis (1980), Hill (1987, 1989), and DuChene and McLean (1989).

These karst systems may be genetically linked to maturing hydrocarbons in the same basin, but many such systems are also associated with Mississippi Valley type mineralization (Dzulynski and Sass-Gutkiewicz, 1989).

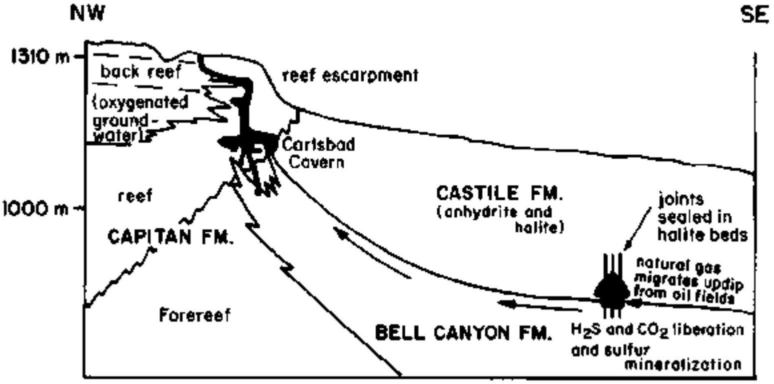

Fig. 13-4. Karst development in the Guadalupe Mountains of New Mexico and West Texas. Hydrogen sulphide gas mixes with oxygenated ground waters, the former derived from adjacent oil fields. (After Hill, 1987.)

PALEOKARST — TERMINOLOGY AND CONCEPTS

At the simplest level, two simple divisions of paleokarst can be made, as in the case of karst, between surface paleokarst (formed at an ancient landsurface) and subsurface paleokarst (formed beneath the ancient landsurface). A special case exists, of subjacent karst which is a form of subsurface dissolution which can mimic surface dissolution.

Broadly speaking, three types of paleokarst can be recognized (Wright, 1982): relict, buried and exhumed.

(1) Relict paleokarst represents karst that developed under different climatic conditions from which it is now found. It relates mainly to Cenozoic karst and is of no significance in an exploration context.

(2) Buried paleokarst is ancient karst overlain by younger sediments. Karstification took place prior to burial (cf. interstratal-karst).

(3) Exhumed paleokarst refers to paleokarst which although once buried, is now being exhumed and exposed to further karstification. This is also termed fossil karst (fossilis = dug up).

The most important category for hydrocarbon exploration is buried subsurface paleokarst, but surface paleokarsts can, when detected, provide subtle clues to paleoclimates and porosity evolution (see below).

Subjacent paleokarst

Interstratal karst traditionally refers to the development of dissolution features on a soluble host rock at its upper contact with a cover of permeable (and usually siliciclastic) material. The term has been used synonymously with subjacent or subadjacent karst. Slight confusion over terminology can arise because the term interstratal has been used in, for example, sandstone diagenetic studies to refer to any subsurface dissolution. It is proposed here that its use be modified and used to

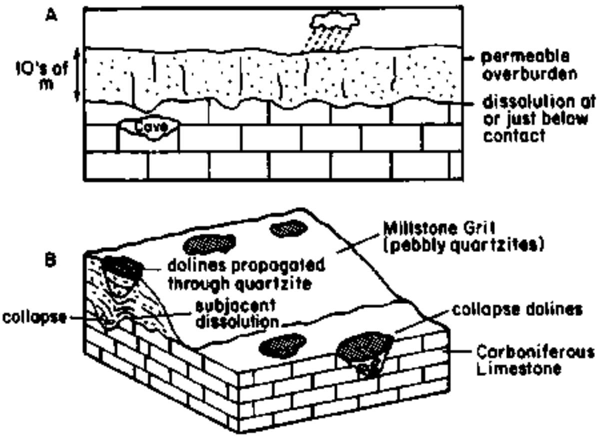

Fig. 13-5. A. Formation of subjacent karst. Dissolution occurs beneath impermeable cover. B. Example on Carboniferous of South Wales (see text).

refer to wholesale dissolution of rocks, in the subsurface. The dissolution of evaporite beds is the simplest case.

Subjacent karst should refer to karst features developed at the contact between overlying permeable, typically siliciclastic deposits and underlying lithologies. For subjacent karst, the simplest case to imagine is where porous sediment (e.g., sands or sandstones) overlay limestones. Water may move down through the upper unit (depending on the water-table level) and corrode the top of the underlying limestone (Fig. 13-5). In some cases this leads to the formation of cavities at the contact, followed by collapse of the overlying unit to form karstic (doline) features on the non-carbonate unit (Fig. 13-5B). The best-known example is the Millstone Grit (Namurian)–Carboniferous Limestone (Dinantian) contact in South Wales. As a result of collapse at depth (over 40 m in places), the surface of the Namurian pebbly quartzites is pock-marked with large "doline" structures. This dissolution of the Carboniferous Limestone is believed to have been controlled by the positions of earlier (pre-Namurian) paleokarstic topography (legacy karst, see below). This example (see Wright, 1986, for details and references) has wider implications for the Mississippian-Pennsylvanian contact in many areas (U.S., Europe), which is an unconformity between carbonates and overlying siliciclastics.

The main problem for exploration is that subjacent karstification can produce features resembling paleokarstic surfaces. For example, a shallow-marine limestone overlain by sandstones, may later undergo interstratal dissolution, either early or late in its history, to form a karst horizon at its upper contact which could be misinterpreted as a true surface paleokarst. Virtually nothing is known of the styles of karst associated with this type of dissolution. Criteria for differentiating subjacent from buried surface paleokarsts have been discussed by Wright (1982). Extensive subjacent dissolution will result in the collapse of overlying beds which may be a signature for subsurface recognition.

To summarize, subjacent and interstratal karst are special cases of subsurface karst. Subjacent karst refers to dissolution at a lithological discontinuity between overlying permeable strata and underlying soluble lithologies. Interstratal karst refers to wholesale dissolution of a soluble unit such as buried evaporites.

Polyphase karstification and paleokarsts

Many carbonate sequences exhibit multiple phases of karstification and an appreciation of this should prove useful in interpreting complex paleokarst systems. Such phases may be multiple, and result in discrete paleokarst features, whereas others overprint earlier phases.

The simplest case is where multiple changes in sea level result in stacked karst systems. Under Andros Island (Fig. 13-6), on the Great Bahama Bank, there is a major cavern system related to the last low-stand mixing zone (Smart et al., 1988a) and other systems may exist below this one related to other mixing zones.

Stacked surface paleokarsts have been documented from the early Carboniferous of Britain. Walkden and Davies (1983) have described a large number of paleokarst surfaces and associated fluvial intercalations from the Asbian and Brigantian (late Dinantian) of North Wales. The ability to recognize such paleokarstic surfaces in outcrop or subcrop is clearly important, but the preservation potentials of such surfaces is a critical factor to consider. Rasmussen and Neumann (1988) have discussed this aspect in relation to exposure surfaces in the Pleistocene of the Bight of Abaco, Bahamas. They found that the final record of exposure within the platform deposits was controlled by a variety of factors, such as topography, sea-level flooding history and the position of the surface within the flooded platform. Whether the platform is silled or open is critical. In the case of the former, the exposure surfaces are best preserved in the deeper, interior areas of the platform lagoon, while they are being modified or destroyed by bioerosion around the elevated platform margins.

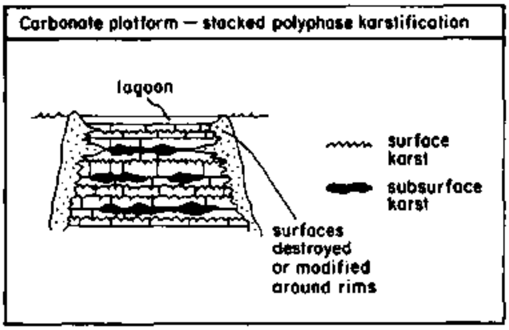

Fig. 13-6. Polyphase stacked paleokarsts on a carbonate platform. Similar subsurface karst systems probably occur on the Bahamian platforms related to various Pleistocene low-stand mixing zones. The preservation of paleokarstic surfaces depends on the configuration of the platform and on its sea-level flooding history. On silled platforms the surfaces have generally been strongly modified or destroyed around the margins as a result of physical and biological erosion. The late Mississippian platform sequences of Britain contain large numbers of stacked paleokarstic surfaces (see text).

In more open platform settings, both physical erosion and bioerosion reduces the preservation potential of the surface during sea-level rise. On ramps such surfaces may be preserved if buried by low-energy back-barrier deposit during transgressions associated with barrier shorelines (Riding and Wright, 1981).

It is common for later phases of karstification to overprint earlier ones. One case was noted earlier in the Carboniferous of South Wales, where paleokarst (developed at the top Dinantian unconformity) may have influenced later (Quaternary or Tertiary) subjacent karstification. The term legacy karst might be appropriate for such a situation. Legacy karstification refers to dissolution which is occurring at the present or has occurred in the past, the distribution of which is controlled by an earlier (paleo-)karst system (Fig. 13-7A). In such a case, the overlying units will show signs of collapse and not simply passive infilling on a non-active dissolution surface or zone.

Another simple case occurs where a landscape is undergoing erosion and earlier phreatic subsurface karst is emplaced in the vadose zone (Fig. 13-7B). Such an example has been described from Precambrian paleokarst from the North West Territory of Canada by Kerans and Donaldson (1988). In this case a broad carbonate platform of Middle Proterozoic age was subaerially exposed. Initially karstification took place in clearly-defined vadose and phreatic settings, the latter associated with caves. Subsequently, as a result of falling base-level and erosion, the phreatic caves were modified in the vadose zone and had a variety of sediments deposited in them by free-flowing streams. It may be more realistic to envisage the reverse situation for many ancient carbonate sequences, where phreatic, subsurface karst may overprint earlier vadose karst. In the Amposta Marino field, offshore northeast Spain, the karstified lower Cretaceous Montsia Limestone is sealed by Miocene shales at a "buried-hill" trap. The main high-porosity zone is strikingly continuous and subhorizontal, quite unlike a simple fracture-controlled phreatic karst system. Wigley et al. (1988) and Bouvier et al. (1990) have interpreted this as a marine-mixing corrosion zone, overprinting the original phreatic system as a result of a net sea-level rise (Fig. 13-8). Again this serves to illustrate the common occurrence of polyphase karstification.

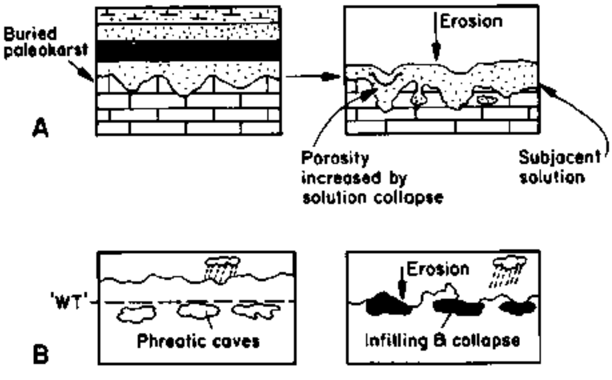

Fig. 13-7. Polyphase karst. A. Buried paleokarst influences later subjacent dissolution (e.g., Carboniferous Limestone of South Wales; see text). B. Phreatic karst later overprinted by vadose processes (see text for details).

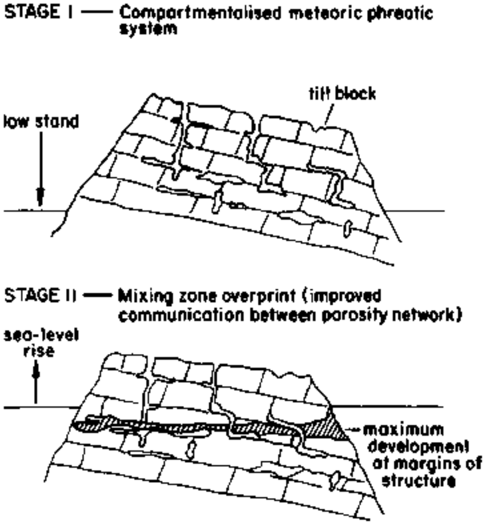

Fig. 13-8. Schematic diagram of polyphase development of tilt-block paleokarst. Based on Amposta-Marino Field, offshore north east Spain (see text).

The situation can be even more complex in carbonate sequences exposed either to prolonged, continuous exposure or to complex burial histories. Two examples have been documented which illustrate long-term polyphase karstification: the Turonian limestones of Israel, and the Carboniferous Limestone of South Wales.

Turonian to Neogene paleokarst of Israel

The extensive karstic systems found today in the Cretaceous carbonates in central and northern Israel have been developing for over 80 Ma (since late Turonian times; Buchbinder et al., 1983). In late Turonian times exposure resulted in the formation of small dolines (20–100 m in diameter) within the upper Turonian limestones. During the Senonian, two subsequent phases occurred in Coniacian and Santonian times. These resulted in the development of larger dolines, filled by contemporaneous sediment. Another phase of pre-Middle Eocene doline development occurred followed by an extensive phase of Neogene karstification. This was characterised by deep subsurface dissolution.

Not all phases occur in all areas; this partial absence is a common feature of regional polyphase karstification. This reflects areal variations in emergence. Whereas much of the study material described by Buchbinder et al. was seen at outcrop, deep boreholes have encountered Turonian-hosted paleokarst in the subsurface of the Israeli coastal plain.

Carboniferous limestone of South Wales

The Dinantian (Mississippian) limestones of South Wales also illustrate the problems of multiple exposure to karstic system development. The limestones, over 1500 m thick in places, were deposited during the ramp to shelf evolution of a developing foreland basin fill. The sequence contains a number of paleokarsts (Wright, 1986) which are strongly areally differentiated. This resulted from the differentiation of the province during foreland basin evolution with the emergence of the present northern outcrop areas as a foreland bulge in late Visean times. In contrast, the present southern outcrops subsided very rapidly at the end of the Dinantian and were only unroofed in the Mesozoic (see later section on foreland basin paleokarst).

Both the northern and southern outcrops underwent numerous phases of exposure during deposition. The northern area was affected by local phases of uplift related to active strike-slip faults and has slightly more exposure surfaces than the southern sequences (Figs. 13-9 and 13-10).

The uplift of the northern areas as a foreland bulge at the end of Dinantian times led to extensive erosion. Here, the top Dinantian unconformity is a paleokarstic surface, later modified by interstratal dissolution (Fig. 13-5), acting along the limestone unconformity surface, apparently following and enhancing relief on that

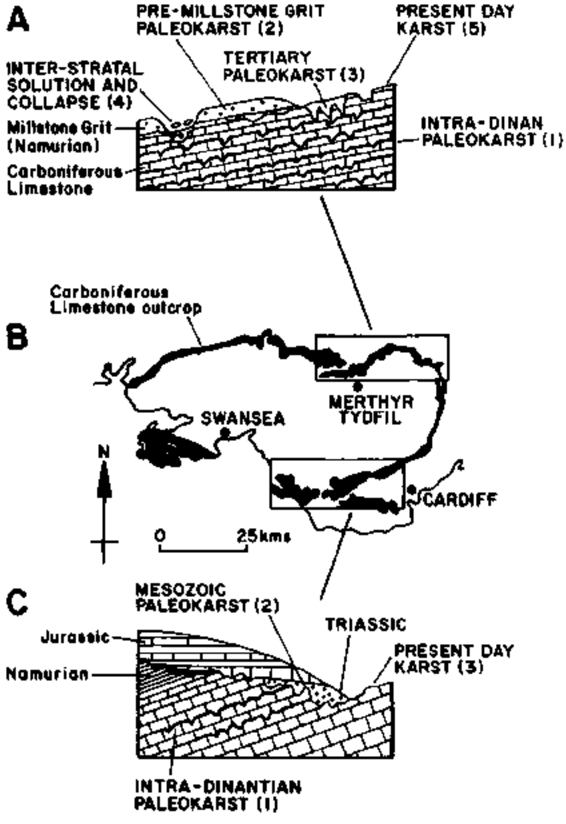

Fig. 13-9. Polyphase karstification of the Carboniferous Limestone (Dinantian Mississippian) of South Wales. A. Karst history of northern outcrops. B. Locality map. C. Karst history of southern outcrops. See Fig. 13-10. (Modified from Wright, 1986.)

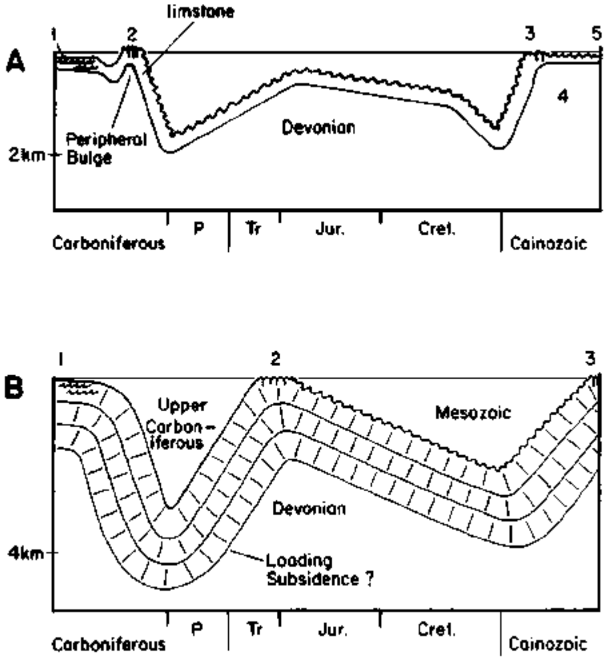

Fig. 13-10. Contrasting subsidence and karst histories of the Carboniferous Limestone in South Wales. A. Northern outcrops. B. Southern outcrops. Numbers refer to those in Fig. 13-9A, B.

surface (legacy karst). As a result of subsurface cavern collapse at the top of the limestone, the overlying Namurian quartzites collapsed locally and presently exhibit a doline-like morphology at the surface. However, an alternative explanation has been offered by Battiau-Queney (1986) who interpreted the quartzite doline terrain as reflecting tropical silicate weathering during the early Tertiary. She also recognized tropical karst features in the local limestones. Thus a Tertiary phase of karsting may also have occurred (Fig. 13-9A).

In the southern outcrops (Fig. 13-9C) the limestones were deeply buried in a developing fore-deep and were apparently not exposed at the end of the Dinantian. They were not exhumed until the Triassic or Jurassic and cave fills of these ages are known. A probably Cretaceous cover was not removed until after early Tertiary tropical weathering which is not evident in the region, only along the northern outcrops (Fig. 13-9).

SUBSURFACE RECOGNITION

The various techniques which have been used to detect paleokarst zones, are briefly reviewed here, but few studies have been published. Often such zones are indicated by a loss of circulation or the dropping of a drill bit when a large cavity is breached.

Paleokarsts have been detected by wire-line techniques. For example, gamma-ray logs may show progressive up-hole peaks reflecting terra-rossa deposits (clay-filled karstic cavities). Sonic logs have also shown up-hole gradients related to the degree of fissuring and brecciation (Del Olmo and Esteban, 1983). In both cases, vertical trends are useful for recognition. Dip-meter data can also indicate drape over paleo-(karstic)-topography (Vandenberghe et al., 1986). Density log, caliper log and bulk-density porosity logs can also show karstic porosity, down to small caverns with heights of 0.3 m (Craig, 1988).

There are several methods whereby paleokarst has been detected by seismic techniques (Fontaine et al., 1987):

(1) Erosional truncation of reflectors at an unconformity will suggest the possibility of paleokarst on limestone sequences (Del Olmo and Esteban, 1983).

(2) Topography on limestones and unconformities and, hence, the possibility of paleokarsts, can be revealed by onlap of reflectors onto the unconformity (Fig. 13-11).

(3) Collapse zones may be revealed by abundant irregularities affecting the seismic marker (Jenyon, 1984).

(4) 3-D seismics have been used to identify karstic depressions (Brown, 1985) and even paleo-mixing corrosion zones (Wigley et al., 1988; Bouvier et al., 1990).

(5) Amplitude analyses (offset-seismic) has proved a useful tool (Vandenberghe et al., 1983, 1986). In simple terms, it is a technique which reflects the density of the limestone, and is useful for detecting highly fissured zones. Vandenberghe and co-workers tested this technique on the major sub-Namurian paleokarst in northern Belgium. It has also been used in the offshore paleokarst reservoirs of northeastern Spain (Fontaine et al., 1987). Bouvier et al. (1990) have used amplitude differences to map paleokarstic porosity distribution on the Amposta Marino oil field offshore Sapin. Areas of high amplitudes corresponded to highly cavernous zones around the buried "hill" (Fig. 13-8) where cavern collapse had occurred, with porosity/permeability later enhanced in zones of mixing corrosion dissolution. Areas of low

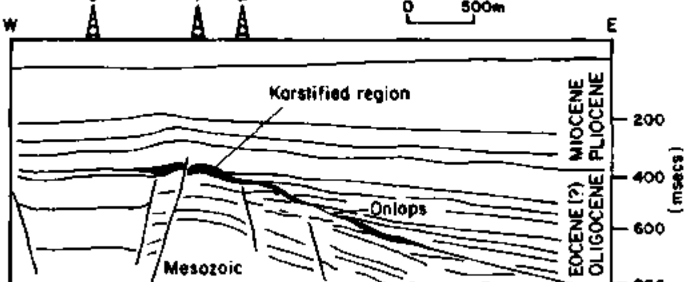

Fig. 13-11. Simplified seismic section through the Bresse Basin (France) showing Eocene–Oligocene onlap on a Jurassic paleokarstic high. Well No. 3 encountered unkarsted Mesozoic limestone. The paleokarst is limited to the high. (Based on Fontaine et al., 1987.)

amplitude occur around the crest of the field where less significant fissure porosity occurs.

Cores have particular limitations for evaluating paleokarstic features, because of the often large size (relative to core width) and irregular orientations of karstic features. Such porosity would be classified as vuggy, channel, and cavern porosity; but many "fractured" reservoirs are also probably paleokarstic in origin. The Ordovician Ellenberger Group reservoirs of west Texas are a striking example of such a system (Kerans, 1988). This extensive reservoir interval had previously been interpreted as a tectonically fractured dolomite, whereas detailed subsurface studies showed that the fracturing was clearly related to an overlying unconformity. The fracture-breccia porosities appears to have resulted from the collapse of large-scale cavern systems developed by an extensive mixing zone under a carbonate platform (Kerans, 1988). Clues to the paleokarstic origin of irregular porosity would include large non-fabric selective solutional pores, which may be open or partially filled with internal sediments or cements. Speleothems (commonly coarsely crystalline calcite cements) are an obvious feature but are not always found associated with paleokarsts. Argillaceous materials, often red, are a common feature, and are generally referred to as "terra-rossa". Such material occurs near the top of a karstic profile but may be washed down to considerable depths below an unconformity. It may have been derived from dissolution of limestone as residual insolubles, or it may be aeolian in origin.

Other exposure related features may provide clues to the nature of the irregular porosity zone, such as paleosols including calcretes. Esteban and Klappa (1983) have reviewed many of these criteria.

CONTROLLING FACTORS ON KARST DEVELOPMENT

Paleokarst and paleoclimates

Whereas the style of meteoric diagenesis and karstification a carbonate unit undergoes will, in part, be controlled by whether the material is unconsolidated (diffuse flow) or lithified, bedded or fractured (free or conduit flow), the main controls will be climate, composition, relief (in relation to sea-level changes) and time.

In this section the influence of climate is discussed both with respect to karst morphology and also in relation to general porosity evolution during meteoric diagenesis. Climate is important not only in its influence on the availability of meteoric water and its flux, but also for temperature and related factors such as soil cover and vegetation (Ford and Williams, 1989).

The effects of climate on the rates of karst denudation have been discussed in detail by White (1984) and the rates are highest in regions of high effective rainfall (precipitation minus evapotranspiration) and high CO_2 levels in the soil.

Under arid conditions, low rainfall will result in relatively slow rates of meteoric alteration (dissolution, cementation and mineralogical stabilization), and little water will reach the aquifer through the vadose zone. Secondary carbonates will accumulate slowly in the upper part of the vadose zone, typically as calcrete, and the water-table will be deep. Low rates of groundwater movement will result in little phreatic cementation. Under wetter conditions net dissolution may occur with extensive mouldic and karstic porosity formation, with little secondary carbonate accumulation in the vadose zone (no calcrete). As a consequence of high rates of dissolution and a high flux, however, extensive cementation occurs in the upper phreatic zone. These two scenarios are end-members and most subtropical carbonates undergo meteoric diagenesis in an intermediate setting.

The influence of climate on the whole evolution of porosity in subaerially-exposed carbonate sediments has been documented from several Quaternary and pre-Quaternary sequences. A comparison of Pleistocene and Holocene carbonate eolianites of northeast Yucatan is particularly instructive in this sense (Ward, 1978; McKee and Ward, 1983). In the region, in late Pleistocene times the eolianites were subaerially exposed under an arid climate. Whereas unconsolidated carbonate sands underwent little secondary porosity formation and little cementation, they exhibit pedogenic (calcrete) features, such as finely crystalline calcite cements, rhizocretions, needle-fiber calcite, and calcrete crusts. In the younger Holocene eolianites, secondary porosity is more extensive and coarse calcite cements are common, including even some of the youngest deposits being locally totally cemented. However, rhizocretions, needle-fibre calcite and calcrete crusts are absent. The present-day climate is humid. During the late Pleistocene the more arid climate resulted in a lower flux of meteoric waters and less dissolution and less cementation. Similar climatic controls on porosity evolution have been documented from the Pleistocene of Mallorca (Calvet et al., 1980) and Barbados (Harrison, 1975).

Similar climatic controls on subaerial diagenesis have been recorded from the Carboniferous oolitic grainstones and peritidal limestones of South Wales. These examples suggest a possible means of predicting the porosity evolution of subaerially-exposed carbonates based on assessing the paleoclimate during exposure from the nature of the exposure surface itself, and this should be possible even from core material. Within the various oolitic sand bodies comprising the early Carboniferous succession in South Wales, two styles of meteoric diagenesis can be recognised: semi-arid, and humid (Hird and Tucker, 1988; Wright, 1988). The oolites exposed under semi-arid conditions exhibit minor karstic surfaces of the mammillated type (Fig. 13-12), which are veneered by thin calcrete crusts with abundant rhizocretions and needle-fibre calcite. The associated oolitic grainstones show virtually no evidence of significant pre-compaction (pre-burial) cementation. A younger oolite exhibits, locally, total early phreatic cementation. The exposure surface is characterized by an intense zone of solution piping (a form of Kavornossen karren, see below), which is a style more typical of humid climates. Calcrete crusts, rhizocretions, and needle-fiber calcite are absent.

The diagenesis of the weakly karsted oolite can be compared with the late Pleistocene of Yucatan, whereas that of the other resembles the present-day situation. These differences are shown diagrammatically in Fig. 13-12. Other formations occur in the succession also referable to semi-arid or humid phases (Wright, 1988).

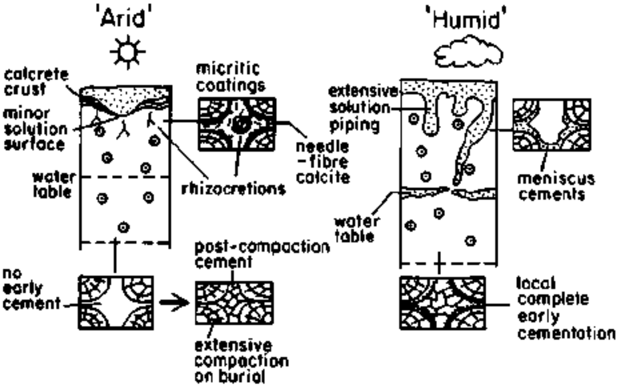

Fig. 13-12. Contrasting styles of karstification seen in the early Carboniferous oolites of South Wales. (Based on Wright, 1990.)

Secondary porosity and temporal changes in carbonate mineralogy

Diagenesis in carbonates is driven by the instabilities of carbonate sediments and rocks. During burial diagenesis the driving forces are enhanced temperatures and pressures, whereas many of the important changes during diagenesis occur very early on in the burial history because of the mineralogical instability of carbonate sediments in the near-surface meteoric conditions. This instability is the driving force for much of "early diagenesis" and is especially important as it influences the degree of dissolution diagenesis. Marine carbonate sediments in today's oceans consist of calcite and aragonite. The calcite is in two forms: low-magnesium (or magnesian) calcite (LMC) (<4 mole% Mg) and high-magnesium calcite (HMC) (>4 mole% Mg). Both aragonite and HMC are replaced during diagenesis by LMC. Aragonite is replaced, usually, via a dissolution void stage (HMC is replaced by very fine-scale dissolution/precipitation, which does not result in porosity formation). Sediments rich in aragonite (e.g., some oolites, most post-Paleozoic shallow-water bioclastic limestones) will undergo considerable dissolution, and mouldic porosity will form, commonly later occluded by cement. Calcitic material can, of course, also undergo dissolution.

Clearly, mouldic porosity will be greater in originally aragonite-dominated limestones than in non-aragonitic ones. Indeed, overall solution rates will be greater in aragonitic host rocks. Thus, one can refer to a sediment's "diagenetic potential" in relation to its susceptibility to dissolution diagenesis.

The diagenetic potential of marine limestones has varied through geologic time because of two factors:

(1) As a consequence of biological evolution, bioclastic limestones have had different bulk compositions through time. For example, in broad terms, shallow-marine bioclastic and reefal limestones in the Paleozoic were calcite dominated. Since the early Mesozoic times, with the diversification of molluscs and the appearance of scleractinian corals (both aragonitic), the diagenetic potential of bioclastic limestones has increased.

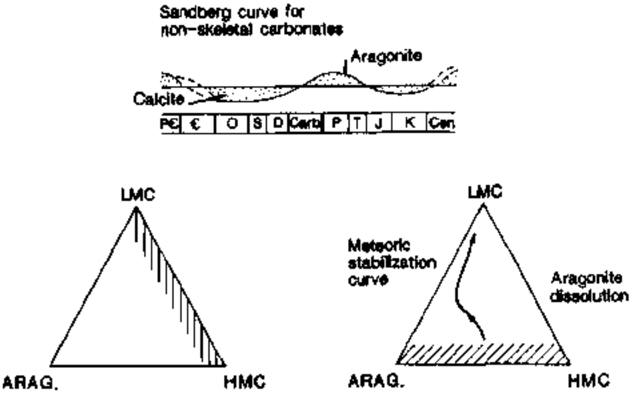

Calcitic sediments

Low diagenetic potential during 'calcite' phases (calcitic ooids) or lower Palaeozoic skeletal limestones.

Recent sediments

High diagenetic potential for aragonite dissolution (and cementation) during aragonite phases and aragonite skeletal biotas.

Fig. 13-13. Diagenetic potential of limestones through geologic time. The Sandberg curve indicates phases of different mineralogies of abiogenic carbonates. Aragonite phases have the greatest potential for secondary porosity development. However, long term changes in the skeletal composition of bioclastic material also needs to be considered. Lower Paleozoic shallow-marine limestones contain mainly calcitic bioclasts, whereas Mesozoic and Tertiary bioclasts were dominantly aragonitic.

(2) The mineralogy of non-skeletal marine carbonates is controlled by a number of factors, especially Mg/Ca ratio and P_{CO_2}. These have varied through geologic time with the result that the mineralogy of non-skeletal precipitates (e.g., ooids, lime muds and cements) has also varied. These variations, of calcite or aragonitic phases, have been plotted to produce what is known as the Sandberg curve (Sandberg, 1983; Figs. 13-13 and 13-14). For example, during the Ordovican to early Carboniferous, ooids were calcitic, with a low diagenetic potential for mouldic porosity. Mid Carboniferous to Triassic ooids, however, were aragonitic and had a high potential for mouldic porosity formation. Local environmental effects can overprint this general trend and exceptions are known.

In addition, other factors have varied through geologic time, e.g., the P_{CO_2} of the atmosphere (greenhouse phases; Fischer, 1981; Fig. 13-14) and the degree of biological activity on the land surface (affecting soil cover). Both of these inter-related factors have influenced paleokarst development. Even though broad speculations can be made about atmospheric composition changes through geologic time, and the biofunction of soils, a more striking relationship is emerging between carbonate mineralogy and sea-level changes (see below).

Sea-level changes and paleokarsts

Relative sea-level falls are, of course, a pre-requisite for the subaerial exposure of subaqueously deposited carbonates. In relation to this, two aspects require consideration. Firstly, the actual amount of fall, or base-level change, is critical in controlling

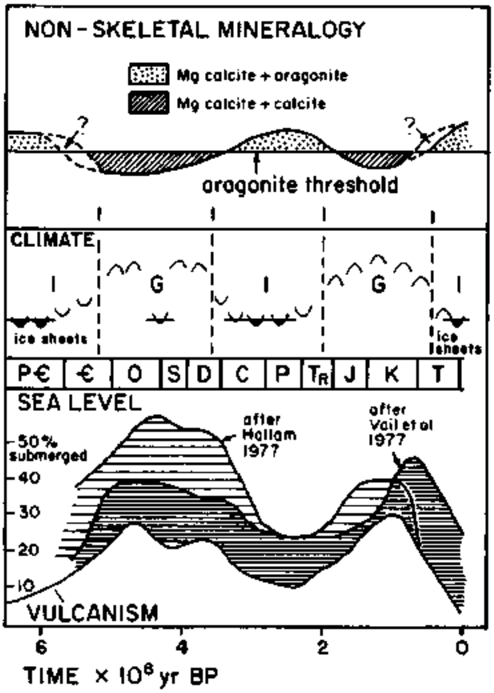

Fig. 13-14. Upper diagram shows Sandberg curve for aragonite–calcite marine precipitates (see Fig. 13-13). The midpart shows phases of high P_{CO_2} ("greenhouse effect", *G*) and low P_{CO_2} ("ice house phases", *I*).

the style of karstification. Secondly, there is a general relationship between global sea level and carbonate mineralogy (Wilkinson et al., 1985; James and Choquette, 1984).

In the latter case it has been found that during major high stands calcite was the predominant marine precipitate, and aragonite during low stands. The nature of the relationship is believed to be controlled by geotectonics. High stands reflect periods of major plate movements, when hydrothermal weathering of basalts causes Mg depletion (lowering Mg/Ca and so promoting calcite, not aragonite, formation). In addition, high plate activity affects P_{CO_2}, for it is believed that much of this is produced at subduction zones during metamorphism. High P_{CO_2} and high sea levels will create "greenhouse global climates" and enhanced karstification (James and Choquette, 1984).

It is possible to make the general statement that during high stands (e.g., Cambrian–early Carboniferous, and Jurassic–Cretaceous) rates of karstification were probably high (high P_{CO_2}), whereas during the Jurassic–Cretaceous the overall diagenetic potential was higher because of abundant aragonitic biotas. During the low-stand phases (Permian–Jurassic and Tertiary to present day) more limestones may have been exposed but under lower P_{CO_2}. However, the overall diagenetic potential was higher, because of the greater amounts of aragonite in the sediments.

Thus any attempt to predict the abundance of paleokarst through time needs to consider a number of conflicting factors: sea level, skeletal composition, non-skeletal carbonate composition, P_{CO_2}. Ideally, a combination of low stand (hence widespread exposure), high aragonite skeletal composition, high aragonite non-skeletal composition and high P_{CO_2} would be required. A study of Fig. 13-14, taking the Vail et al. curve, reveals a phase of low stand through the late Triassic to early Cretaceous, corresponding with a greenhouse phase and with a high diagenetic potential because of the abundance of aragonite skeletal components. However, to date no compilation of paleokarst abundance in the Phanerozoic is available to test this idea, although Mesozoic bauxites associated with paleokarst are well documented. It remains to be shown if the late Triassic to early Cretaceous was a time of enhanced karstification.

The other influence on sea level is on the hydrological development of karst, controlled by the amplitude of the changes. This factor will be most clearly seen if one considers the effects of different orders of sea-level change (Fig. 13-15). During small, fourth- or fifth-order changes, the residence time of the carbonate sediments in the meteoric zone will be relatively short, perhaps only a few thousand years. Such small-scale falls will create little topographic relief and the flux of meteoric waters will probably be small. As a result, relatively little dissolution and cementation will occur. Most flow will be of the diffuse-type, and the opportunities for karst development will be minor.

During progressively greater amplitude changes (third- and even second-order sea-level cycles) such effects will be much greater, reflecting longer residence times, increased relief and deeper flow. As flow passes to conduit type, larger-scale karstic features, including caverns, will develop.

Most paleokarstic zones encountered in the geologic record are those representing the higher frequency "Milankovitch", orbitally-forced cycles and it is worth considering how changes in the magnitude of the cycles through the Phanerozoic may

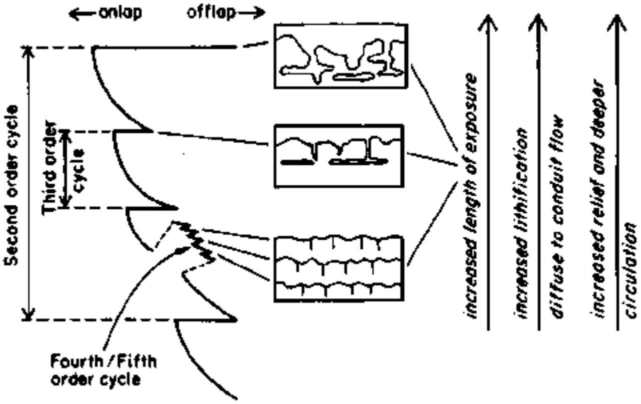

Fig. 13-15. Schematic relationship between orders of sea-level cycles (coastal onlap curves) and paleokarst development. (Modified from Kerans, 1989.)

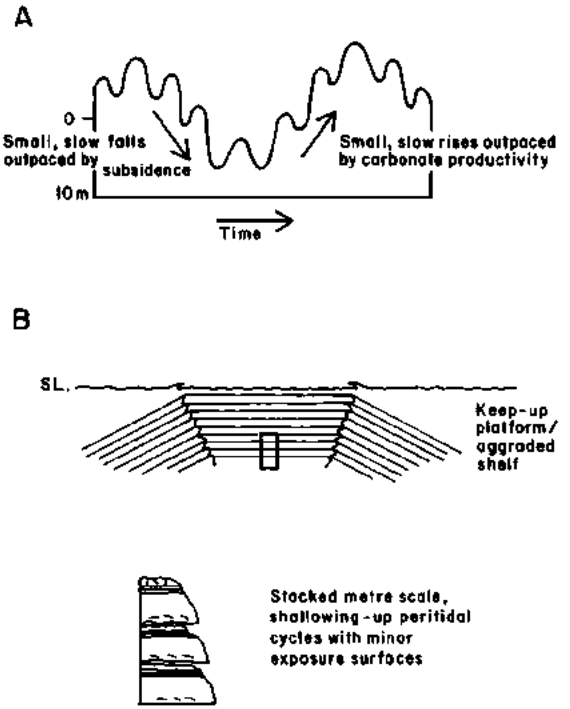

Fig. 13-16. A. Fourth- and fifth-order sea-level curves during "no-ice" phase. B. Depositional and early diagenetic styles seen in carbonate sequences deposited during high-frequency sea-level changes without significant continental ice-buildups, e.g., Triassic (Ladinian) of northern Italy (see text).

have controlled not only the styles of paleokarsts, but also the architectures and compositions of the host carbonates (Fig. 13-16).

The precession, obliquity and eccentricity cycles are now known to be very important in controlling carbonate deposition in the geological record (Koerschner and Read, 1989; Goldhammer et al., 1987). These former two cycles have varied in length during the Phanerozoic as a result of the evolution of the earth/moon system but a more significant factor relating to the potential of all these to affect both carbonate deposition and karstification has been the changed degree of continental ice buildup, itself dependant on both global paleogeography and climatic change. We contend here that the propensity for ice buildup is an important factor in controlling the types of paleokarsts developed in carbonate buildups.

During periods when these high-frequency sea-level changes occur without significant ice buildups, the amplitudes of the sea-level changes are very small, in the order of a few meters (Koerschner and Read, 1989). These small sea-level falls may occur at slower rates than the ones driven by ice buildup, and are outstripped by regional subsidence. The later, small, relatively slow sea-level rises are outpaced by carbonate productivity. As a result, the carbonate platform is essentially one exhibiting "keep-up" characteristics resulting in thick sequences of stacked, small-scale peritidal cycles.

In such cases carbonate ramps rapidly evolve into aggradational shelves in the sense of Koerschner and Read (1989).

In summary, the carbonate buildup will consist, architecturally, of stacked, shallowing-up cycles representing precession cycles, perhaps arranged in penta-cycles representing the eccentricity changes (Goldhammer et al., 1987). Exposure events will be both short lived and the small sea-level falls will have created little relief on the platform. The effects of any eccentricity-related changes will be smothered by subsidence and productivity factors. Opportunities for karst development will be very minor, but under suitably arid climates extensive sabkhas, evaporites, and dolomites may form. The reservoir potential of such aggraded platforms will reflect the generally low permeabilities of the peritidal sequences (unless dolomitized) although the likelihood of stratigraphic trapping, associated with evaporites, may be high. Paleokarstic plays may be unimportant, but intraplatformal basins may have developed, with their high source-trap potential, as well as peritidal/sabkha plays. Ancient platforms exhibiting this aggradational style include the Proterozoic Rockness platform of Canada (Grotzinger, 1986), the Cambro-Ordovician of the eastern U.S. (Koerschner and Read, 1989) and the Triassic of Italy (Goldhammer et al., 1987).

If major ice buildups occur, the facies and diagenetic style is changed radically to one, potentially, favoring major meteoric alteration and karst development. This situation is clearly exhibited in the late Quaternary record of the Great Bahama Banks (Fig. 13-17). As a consequence of ice buildups the amplitude of both the falls and rises is large. Major falls, typically rapid, result in prolonged exposure and relatively deep meteoric circulation. As a consequence karst development occurs, including significant mixing-zone dissolution (Smart et al., 1988a). The rapid "ice-melt" seal-level rises cause initial platform drowning and typically only reef growth around the margins of the platform is capable of keeping-up with such rises, creating steep rimmed margins. The platform interior will contain predominantly subtidal deposits and patch reefs with minor peritidal facies (Beach and Ginsburg, 1982; Koerschner and Read, 1989). Under such conditions carbonate ramps will show less aggradation and may be dominated by grainstone wedges capped by exposure surfaces, onlapped by offshore ramp deposits.

Paleokarstic hydrocarbon plays will be major targets in such carbonate buildups. Architecturally, the platforms may consist of subtidal, low- to high-energy carbonates, and both meteoric and mixing-related porosity formation will be likely to be significant. Under more arid conditions, evaporites may form during sea-level down-draw. The steep, reefal platform margins may act to enhance circulation (and diagenesis) within the platform related to such factors as geothermal gradients (Whitaker and Smart, 1990).

The Bahama Banks might provide a present day analogue, and the Mississippian of Britain provides a very striking, ancient one. During late Mississippian times (Asbian and Brigantian stages) Britain (as well as northern France, Belgium and southern Germany) was covered by a series of carbonate shelves and isolated platforms. As a consequence of asymmetric sea-level changes, with both a rapid sea-level rises and relatively rapid falls, the sequence throughout the area is characterized

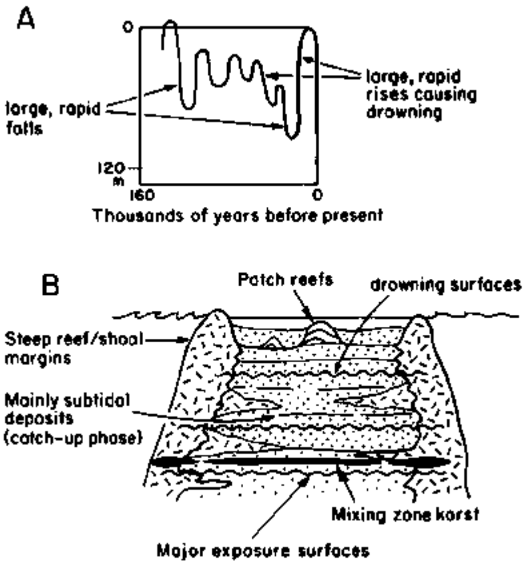

Fig. 13-17. A. Example of ice-enhanced sea-level curves — Pleistocene sea-level fluctuations. B. Paleokarst-platform architecture during periods of significant continental ice buildup and melt. Relatively rapid falls and rapid rises result in a sequence of predominantly subtidal (catch-up) deposits and major exposure surfaces (based on late Mississippian of Britain).

by cycles of shallow, subtidal carbonates capped by prominent paleokarstic surfaces (Fig. 13-22; Walkden, 1974; Walkden and Walkden, 1990). Horbury (1989) has described the styles of Asbian cycles in detail and has argued that they reflect a 100,000-year-style sea-level oscillation of 30–50 m with similar maxima for each subsequent rise. These oscillations are interpreted as glacio-eustatic in origin, related to fluctuations in southern Gondwanaland continental ice sheets, but of a much smaller size than ice sheets formed in the Pleistocene. These late Mississippian successions provide an example of multiple paleokarsts separated by predominantly subtidal deposits, reflecting ice-enhanced, eccentricity-generated eustatic cycles.

In summary paleokarst development can be crudely related to sequence (and seismic) stratigraphic boundaries, but it can also be related to higher frequency sea-level changes. In the latter case, the role of major continental ice buildups is a crucial factor in controlling not only the degree of karstification, but also the architecture and regional diagenesis of the carbonate platform. Recently, Esteban (1991) has provided a detailed analysis of paleokarst occurrence in relation to sequence stratigraphy.

PALEOKARST ASSOCIATIONS

Rather than simply reviewing the paleokarst case studies, it might be instructive to chose some distinctive associations with direct relevance to general exploration in carbonate terrains. To this end, paleokarst associated with three typical play associations are discussed: reefs, evaporite basins and platform margins. In addition, aspects of paleokarst development in foreland and extensional basins are also reviewed.

Reefs and karst

The importance of karstic processes and reefs has been noted by Purdy (1974a,b), who argued that such processes are important, during low stands, in generating relief used for later reef growth during rising sea levels. The karst relief acted as antecedent topography, where preferential reef growth occurs. As a result, reef growth can be localized on original karst features, especially around the margins of isolated platforms or shelves to create barrier reefs or atolls.

Isolated reef atolls and also any isolated carbonate buildup, such as a small platform, have the potential to develop distinctive groundwater geometries. On such isolated settings, following subaerial exposure, the meteoric lens will float on the denser, marine phreatic lens beneath and under the island. In unconfined aquifers, the meteoric phreatic lens extends below sea level approximately forty times the height of the water-table above sea level, known as the Ghyben-Herzberg relationship (Todd, 1980). This is an important effect by which a deep meteoric phreatic lens can develop following relatively small sea-level falls. This simple relationship assumes no mixing of the marine and meteoric waters which does take place. The relationship does apply to lenses bounded by the 50% isochlor surface (Vacher, 1978), but in strongly heterogeneous aquifers such as reefs, the lens has a more complex geometry (Buddemeier and Oberdorfer, 1986). The small catchment areas and low relief on such islands will not result in extensive karst development, but meteoric diagenesis can be significant.

A more unusual relationship between karst and reefs may exist because some types of karst features resemble pinnacle reefs. Mogotes (tower karst) are large, isolated pinnacles of limestone often with considerable relief, and some striking examples have been documented from Paleozoic paleokarsts. Bless et al. (1980) and Poty (1980) have described Devonian tower karst from Belgium, which was progressively drowned during the early Carboniferous. Locally, the mogotes even acted as a substrate for coral growth. Mogotes associated with extensive mineralization have also been described from Colorado by Maslyn (1977) and De Voto (1988). In this example, Devonian and Mississippian shallow-water limestones were heavily karsted to form tower karst with 30 m of relief, and also as ridges 120 m long. These were buried by Pennsylvanian organic-rich shales. Similar karst has been recorded from Ordovician sequences of Quebec by Desrochers and James (1988).

In all these cases of ancient mogotes, one is left wondering if, given greater relief, such structures might not be interpreted, on seismic profiles, as reefs and not paleokarst. It is reasonable to ask if some reefs, recognized from purely seismic data, may not actually be mogote karst, perhaps developed on non-reefal limestone?

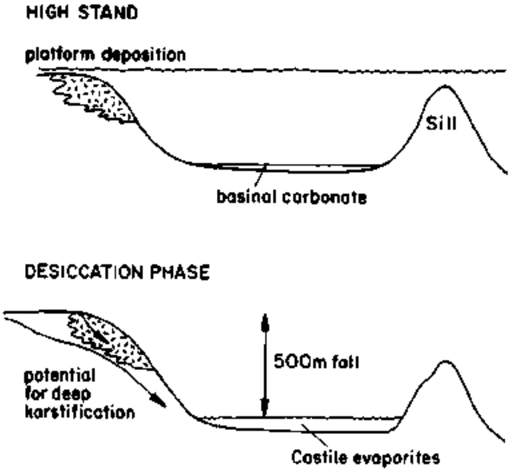

Fig. 13-18. Effects of desiccation on karst development in a salt basin, e.g., Delaware Basin. (Modified from Kendall and Harwood 1989.)

Paleokarst and evaporites

Whereas the occurrence of dissolved evaporites and interstratal karst has been recorded on many occasions, there is another association between karst and evaporite basins which requires consideration. During the desiccation of large salt basins the down-draw of saline brines causes a regional lowering of the groundwaters. For example, during the Messinian desiccation of the Mediterranean the fall in the base-level was over 2000 m and lasted for as long as one million years. As a result, major valleys and gorges were cut and deep cave systems formed (Corra, 1986).

Recently Kendall and Harwood (1989) have suggested that some of the Castile evaporites of the Delaware Basin (Fig. 13-4) formed in very shallow brine pools and not in a deep saline basin as had been previously thought. Such an interpretation requires a drop in sea level in the basin of probably over 500 m, and raises the possibility that deep karstification could have taken place in the surrounding platform sequences (Fig. 13-18). The extent of karstification will have depended on the climate (which must have been one of low rainfall) and length of exposure. It is possible that deep paleokarst systems may develop around salt basins during their desiccation, but as yet little work has been carried out on such systems. In as much as many major hydrocarbon provinces are associated with saline basins (Devonian of Alberta, Williston Basin, Zechstein of Europe, Infra-cambrian of Oman), the possibility of major karstic porosity formation around the basin margins should be considered.

Paleokarst at platform/shelf margins

Whereas, broadly speaking, paleokarst evolution under a given set of circumstances develops along similar pathways in its earliest stages, regardless of platform configuration (ramp, shelf), there is a particular style of karstification associated with steep (aggrading or stationary) escarpment margins that is worthy of special consideration in as much as such fossil margins are traditionally targets for exploration because of their association with grainstones or reefs.

The steep margins of some platforms and shelves, typically a function of high rates of sea-level rise or structural control, are modified by large-scale collapse. Basically the margins spall-off, because of lateral unloading (Freeman-Lynde et al., 1981; Mullins and Neumann, 1979), and this manifests itself on the margins as a series of fractures. Along the margins of the present-day Great Bahama Bank, these fractures are often multiple and complex, sometimes curvilinear and near vertical, but showing no displacement (Smart et al., 1988a). Many can be traced laterally for tens of kilometers, both on the submarine banks and across land (e.g., Andros Island; Dougherty et al., 1986). Major perpendicular joint sets are also present. On land, both sets of fractures are enlarged by dissolution processes giving straight but irregular rifts up to half a meter wide and up to several meters deep. Some fractures, paralleling the bank margin, have been greatly enlarged and constitute major cavities, averaging 2–5 m wide (but up to 30 m), in excess of 90 m deep and running for hundreds of meters (Smart et al., 1988a). The development of the fractures, in the case of the Bahamian platforms today, appears to be due to lateral unloading. In other examples, the margins may be directly tectonically defined and the fractures reflect the regional tectonics (Vera et al., 1988), although again lateral unloading is important. In other cases, differential compaction of the basin and platform has created stresses along the margins (Playford, 1984).

Similar fracture systems have been widely documented from ancient platform sequences. Many of these ancient fractures have been filled with marine sediment to give "neptunean dykes". Some of these fractures also show evidence of karstification. Platform fracture systems have been described from the Devonian Canning Basin (Playford, 1984), and the Tafilait platforms of Morocco (Wendte et al., 1984). They are especially well documented from the Tethyan break-up sequences of southern Europe. Vera et al. (1988) provided a detailed description of Jurassic platform margin paleokarsts in southern Spain (Fig. 13-16). Smart et al. (1988a) have reviewed the terminology for such fracture systems and their deposits.

The exploration significance for this type of paleokarst is clear. At high-relief platform margins, extensive fracture systems, with or without paleokarst, should be very common. Many platform margins in the Tethyan sequences are defined by listric or normal faults and footwall uplift is a common process at such zones, resulting in subaerial exposure and karstification (discussed in the next section).

There are other implications for this model. The fracture systems in the Bahamas connect with interior platform cavity systems related to mixing zone dissolution (Smart et al., 1988b). Indeed, a situation could be envisaged where platform margin fracture systems may connect with earlier "stacked karst" within the platform interior providing a large interconnected reservoir (Fig. 13-19).

The model offered here (Fig. 13-19) recognizes two major controls on karst development: the platform parallel fracture system and the development of mixing zones. The karst hydrological system is effectively an authogenic one. In the case

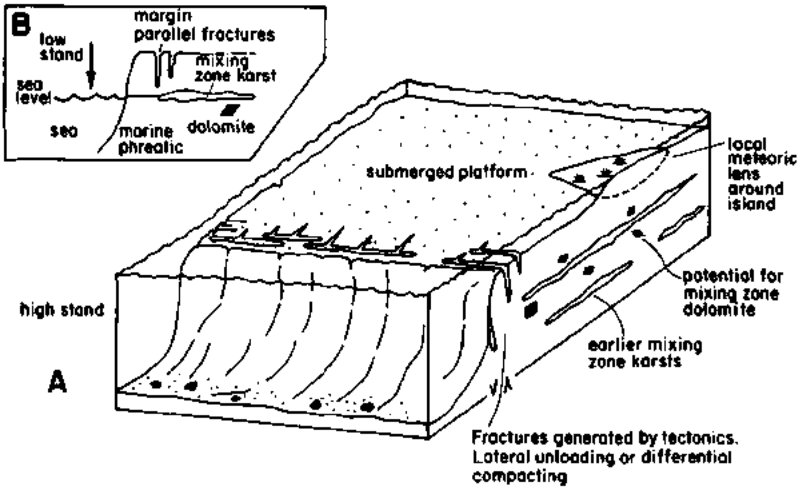

Fig. 13-19. Schematic representation of a typical platform margin fracture system. During low stands karstification will take place. During high stands marine sediments are deposited in the fractures. The fractures may connect both interior mixing zone karst systems and other porosity zones within the platform.

of shelves bordering land masses, or carbonate ramps, however, allogenic hydrologic systems are likely to arise with more complex karst development (e.g., see Ford and Williams, 1989, section 10.5). In such cases, very extensive karstification may result including mixing zone dissolution evolution (Hanshaw and Back, 1980; Back et al., 1984).

Paleokarsts in extensional tectonic regimes

Recent studies of Triassic extensional tectonic systems in Europe have revealed distinctive paleokarst developments. These studies may serve as a useful guide to exploration in similar tectonic settings.

The external Subbetics of southern Spain contain a sequence of classic Tethyan break-up sequences in the Granada–Jaen area (Molina et al., 1985). Extensive shallow-water, Lower and Middle Jurassic platforms were dissected by listric faults and subsequently rapidly subsided so that platform sequences are capped by pelagic limestones. Initially subaerial exposure of the platforms occurred killing off carbonate production and extensive fracture systems formed along the faulted tilt-block margins, as described in the previous section. These were locally karstified and were later filled by speleothems and various pelagic sediments (Vera et al., 1988). By detailed mapping of the region, it has been possible to recognize differences in the degrees of karstification across the various tilted blocks (Fig. 13-20). The footwall zones of each block were preferentially karsted, with the degree of dissolution decreasing down the adjacent hanging wall (Fig. 13-20). This is interpreted as reflecting footwall uplift. Some blocks were never subaerially exposed, whereas others were exposed for short periods of time and relatively lightly karstified. Some blocks remained exposed

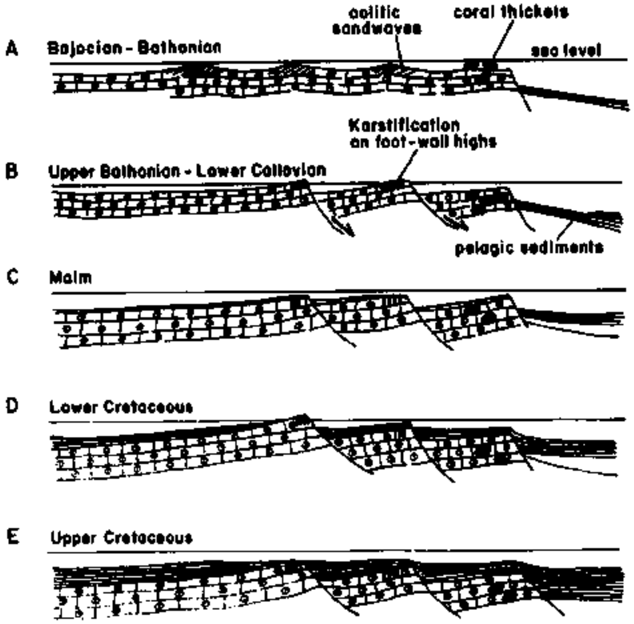

Fig. 13-20. Schematic reconstruction of the evolution of the carbonate platform of the External Subbetic region of southern Spain. Note the preferential karstification on the crests of the hanging walls. (Based on Molina et al., 1985.)

until the Upper Cretaceous. In these latter examples, extensive cavern development and collapse took place (Vera et al., 1988). More, as yet unpublished examples of this style of karstification also occur in the Mesozoic Lusitanian Basin of Portugal, associated with Atlantic opening.

As a general rule, such paleokarst systems should be relatively small, capping individual tilt-blocks. Nearby blocks may lack such karsts. Such a setting would result in buried-hill-type traps and should be readily recognizable from seismic data. The adjacent half-graben basins may well have been the sites of organic-rich sediment accumulation with anoxia, as was the case with many of the Tethyan and the Lower-Middle Jurassic systems.

In the examples noted above, the karst developed as rift-onset unconformities early in passive margin growth. More extensive exposure, however, occurs later in passive margin development with regional "break-up" unconformities.

Paleokarst and foreland basins

Paleokarsts are also a typical feature of many foreland basin sequences. They occur, in carbonate sequences, related to the formation of peripheral bulges (Fig. 13-21). As a consequence of flexural downwarp due to thrust emplacement and loading, uplift occurs in the foreland with subaerial exposure (Quinlan and Beaumont, 1984).

Such peripheral bulge paleokarsts have been recorded from the Ordovician of the Canadian Appalachians by Desrocher and James (1988) and James et al. (1989).

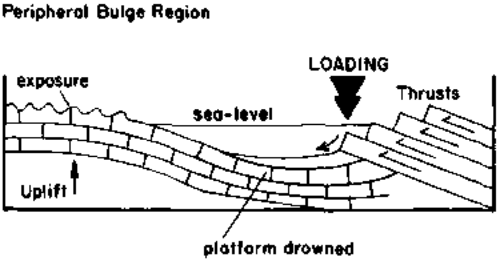

Fig. 13-21. Schematic diagram showing the paleokarst development in foreland basins.

Similar associations have also been noted in the Tethyan sequences of the northern Mediterranean by Bosellini (1989). One example has already been noted, that of the Carboniferous Limestones of South Wales (Figs. 13-9 and 13-10). In this example, the northern limb of the synclinorium represents the peripheral bulge region, where uplift and karstification occurred in pre-Namurian (pre-Pensylvanian) times. To the south, rapid subsidence occurred taking the limestones down to 7 km locally. The most northern areas have not matured, whereas thick shales developed and matured in the foredeep area.

The significance of such settings is that paleokarst might be regarded as an integral part of foreland basin development. With propagation of the bulge ahead of the migrating thrust front, extensive karsted areas may form.

PROBLEMATIC PALEOKARSTS

Documentation of paleokarsts is improving rapidly (e.g., see papers in James and Choquette, 1988), but there are some paleokarsts which present particular problems. Two of these are common in early Carboniferous (Mississippian/Dinantian) limestones of Europe and North America: mammillated surfaces and rubble-and-fissure paleokarst.

"Mammillated" paleokarstic surfaces

A very widespread "mammillated" paleokarst was first described by Walkden (1974) from the late Dinantian platformal limestones of northern England. Within these sequences a large number of such horizons occur, but they have also been found widely in north and south Wales (Wright, 1982) and the Bristol Mendip area of western England, Belgium and northern France. They are also likely to occur in late Mississippian limestones in North America.

The paleokarstic surfaces consist of large "potholes" up to 1 m in diameter and 1.5 m deep. These potholes are roughly circular in plan and have rounded areas between (Fig. 13-22). They are filled by volcanic-derived clays and locally by thin coals, and represent solution pits arising initially from kamenitza basins on flat carbonate surfaces (usually grainstones or packstones). Soil would have accumulated in these depressions and with vegetation preferentially colonizing these areas, a feedback

Fig. 13-22. Exposed mammillated paleokarstic surface from late Dinantian limestones, Grangemill, Derbyshire, England. (For details see Walkden, 1974.)

between plant cover and dissolution would have occurred. As a result the pits would have deepened.

The surfaces of many are veneered with calcrete crusts having abundant rhizocretions and needle-fiber calcite (Walkden, 1974; Wright, 1982). The presence of such crusts is unusual. Surprisingly, this type of karst form has not been described by karst geomorphologists. Exact analogues, however, do occur in the Quaternary eolianite and beach sequences of southern Australia (Fig. 13-23). The association of dissolution features and secondary carbonate precipitation is odd, unless a change in the soil moisture budget has occurred. Such surfaces may prove to be useful indicators of paleoclimates and vegetation types, and their sheer abundance in the Carboniferous limestones of Europe warrants further study.

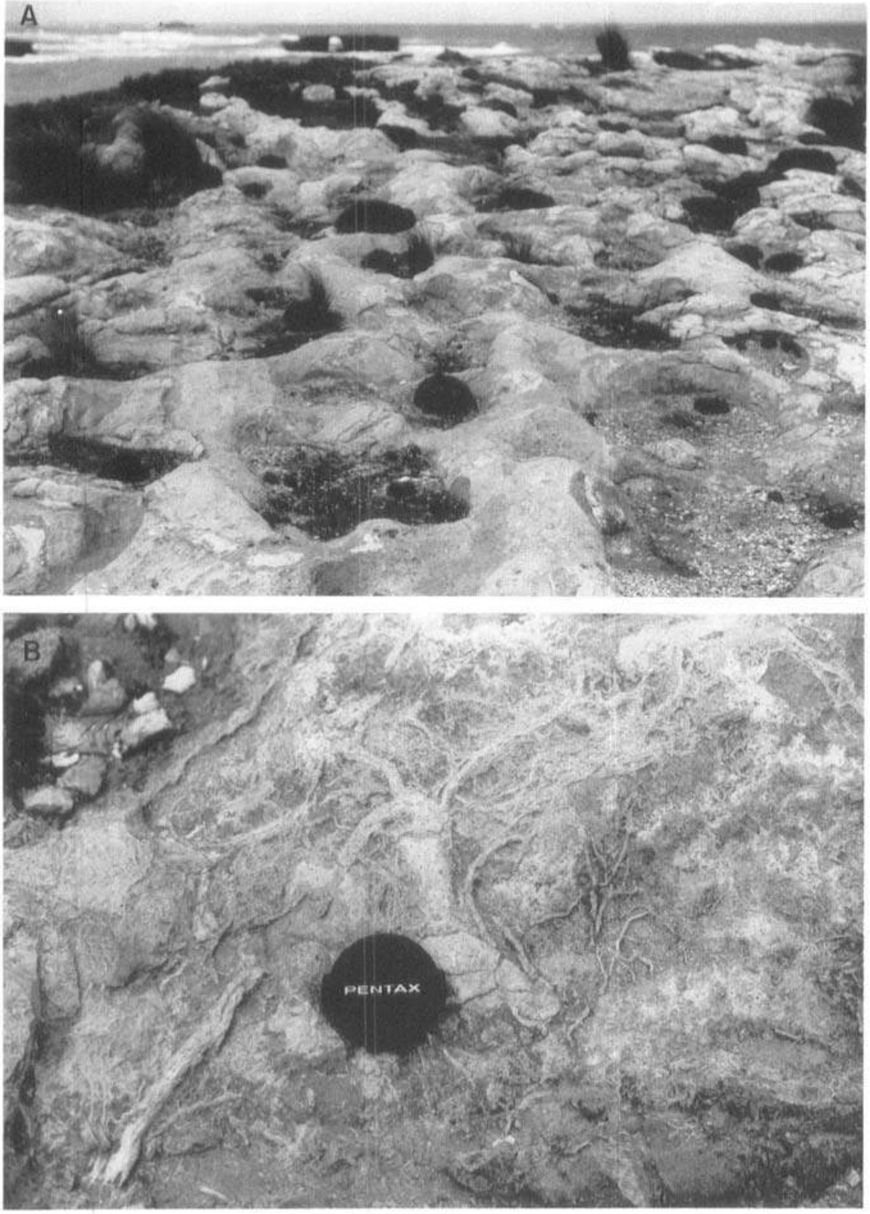

Fig. 13-23. A. Mammillated karstic surface; soil cover has been eroded off. The depressions are 0.2–0.5 m in diameter. B. Rhizocretions which veneer the karstic surface. Both A and B from Robe area, South Australia.

Rubble and fissure paleokarst

Another striking style of paleokarst occurs, although less commonly, in early Carboniferous limestones in South Wales and also widely in the southwest U.S. (Meyers, 1988; Wright, 1982).

In South Wales, it occurs as rubble horizons up to 6 m thick, which exhibit variable degrees of solution piping, fissuring and local collapse (Fig. 13-24). The basic components are highly irregular masses of oolitic grainstone and clay-filled solution pipes and fissures. These may occur as discrete features, but more commonly form dense rubble zones in which local collapse appears to have occurred resulting often in loose blocks of oolite surrounded by irregular clay seams. The pipes and fissures are up to tens of centimeters wide, but because of their sinuous form, their individual vertical extent is difficult to assess. In many sections, the piped horizon is underlain by a prominent fissure parallel to the top of the paleokarst zone. Similar "fissures" occur at the water-table on some present-day Caribbean Islands and probably result from mixing corrosion at the water-table (Wright, 1982).

An exact modern analogue has not been found for this type of paleokarst, but Wright (1982) compared these features to a poorly described type of tropical karst called Kavornossen karren. These are highly solution-altered horizons, riddled with small pipes and fissures, such that the horizon looks like a jumbled mass of boulders. Wright (1982) interpreted this style of karstification as indicating that a humid climate prevailed at that time. Even though extensive dissolution occurred, the ooids were calcitic and mouldic porosity only developed immediately around the fissured zone. Locally, very extensive sparry calcite cementation took place, however, occluding the primary intergranular porosity (Wright, 1988). If such humid paleokarst horizons are encountered in the subsurface, they might be misinterpreted as conglomerates or breccias. It appears that this type of paleokarst is an indicator for humid conditions and for extensive early cementation, especially in the upper phreatic zone.

This type of paleokarst also occurs beneath the sub-Pennsylvanian unconformity in the southwest United States, as an horizon a few tens of meters thick, throughout several tens of thousands of square kilometers in New Mexico and central Arizona (Meyers, 1988). In this case, the paleokarst developed at a major regional unconformity and appears to be much more developed than the South Wales example. Meyers has recognized a distinct karst sequence in this horizon (Fig. 13-25). Rather like the South Wales example, much of the karstic porosity was plugged by clays and siltstones. The degree of associated cementation is difficult to assess but the paleokarst developed on limestone already partially cemented. Of significance is the abundance of microspars, some of which may be analogous to the cements associated with "microporosity" chalkification. If this proposal is correct, Kavornossen karren (or "rubble and fissure" karst of Meyers) may be a distinctive karst facies typified by a rubble zone of variable thickness underlain by a chalky zone of microporosity.

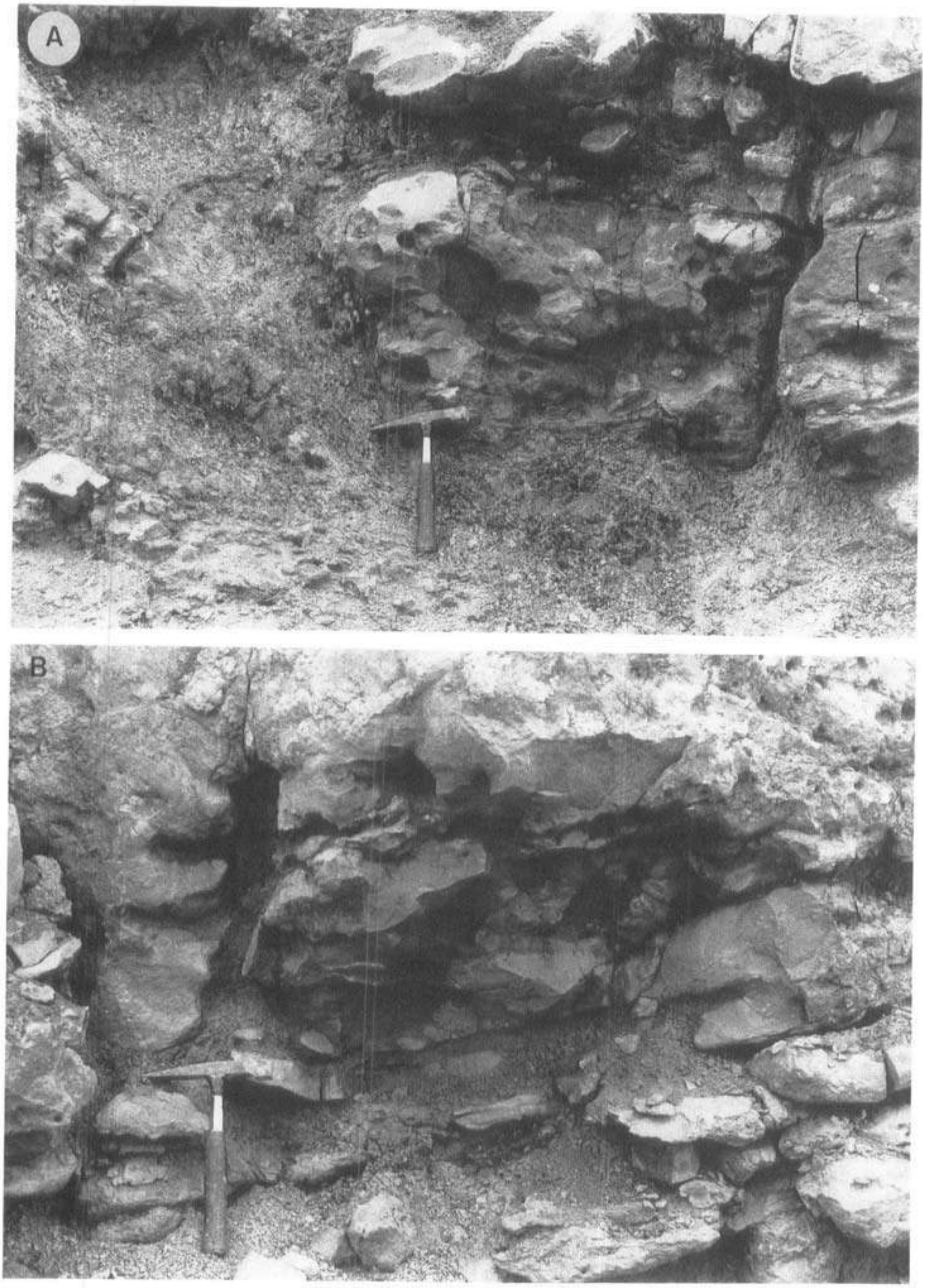

Fig. 13-24. Rubble and fissure paleokarst capping the early Carboniferous Oolite Group, South Wales (see Wright, 1982). Both photographs are taken from 2.5 m below the top of the paleokarst profile. A. Large clay-filled pipe to the left of the hammer, which is overlain by heavily solution-pocked oolite block. Note narrow vertical pipe to the right of photo. B. Rubble and fissure features. These irregular pipes are filled with clays. Note the rubbly nature of the oolitic limestones. Blaen Onneu Quarry, near Crickhowell, Powys.

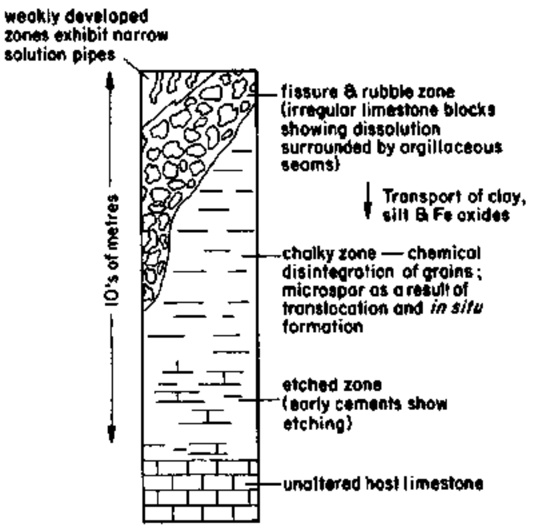

Fig. 13-25. Schematic of paleokarst from the top Mississippian of southern central New Mexico (from Meyers, 1988). The paleokarst developed on crinoidal calcarenites of the Lake Valley and Kelley formations. It developed at a major regional unconformity and is probably a more evolved version of the South Wales example described above.

SUMMARY

Most limestones are deposited in very shallow water and are susceptible to exposure during sea-level changes. Both meteoric and mixing zone dissolution diagenesis should be common features in such limestones. During burial diagenesis and partial exhumation, limestones may be affected by dissolution related to aggressive fluids derived from deeper settings.

Whereas there have been relatively few studies of paleokarst systems, some broad patterns are emerging, and distinctive paleokarst facies and paleokarst associations can be recognized, which should provide useful guides in hydrocarbon exploration.

The present-day situation is not necessarily a reasonable guide to karst development in the past. Changes in limestone composition and in global climate may have reduced or enhanced the potential for karst formation at various times in the past. Some Carboniferous paleokarsts, for example, do not have well-documented modern analogues.

It is already clear that many major paleokarsts are polyphase in origin. The possibility of similar situations must be born in mind when attempts are made to interpret any paleokarst system.

Recognizing and interpreting paleokarsts in the subsurface is difficult but a variety of techniques can be applied. Modelling a paleokarstic reservoir is particularly difficult and it is likely that some fractured reservoirs may be paleokarstic in origin.

ACKNOWLEDGEMENTS

The writers wish to thank Royal Dutch Shell and Amoco for support for the research on karst and paleokarsts. Many people have stimulated the ideas on paleokarst and we wish to especially thank Fiona Whitaker. Alan Cross and James Watkins are also thanked for technical assistance. This paper is based on Postgraduate Research Institute for Sedimentology short course notes.

REFERENCES

Back, W., Hanshaw, B.B. and Van Driel, J.J., 1984. Role of groundwater in shaping the eastern coastline of the Yucatan Peninsula, Mexico. In: R.G. LaFleur (Editor), *Groundwater as a Geomorphic Agent*. Allen and Unwin, Boston, Mass., pp. 157–172.

Back, W., Hanshaw, B.B., Herman, J.S. and Van Driel, J.J., 1986. Differential dissolution of a Pleistocene reef in the ground-water mixing zone of costal Yucatan, Mexico. *Geology*, 14: 137–140.

Bakalowicz, M.J., Ford, D.C., Miller, T.E., Palmer, A.N. and Palmer, M.V., 1987. Thermal genesis of dissolution caves in the Black Hills, South Dakota. *Bull. Geol. Soc. Am.*, 99: 729–738.

Battiau-Queney, Y., 1986. Buried palaeokarstic features in South Wales: examples from Vaynor and Cwar yr Ystrad quarries, near Merthyr Tydfil. In: K. Paterson and M.M. Sweeting (Editors), *New Directions in Karst*. Geo Abstracts, Norwich, pp. 551–567.

Beach, D.K. and Ginsburg, R.N., 1982. Facies succession of Plio-Pleistocene carbonates, northwestern Great Bahama Bank. *Bull. Am. Assoc. Pet. Geol.*, 66: 106–108.

Bless, M.J.M., Bouckaert, J. and Paproth, E., 1980. Environmental aspects of some pre-Permain deposits in N.W. Europe. *Meded. Rijks Geol. Dienst.*, 32: 3–13.

Bogli, A., 1964. Mischungskorrosion — Ein Beitrag zum Verkarstungsproblem. *Erdkunde*, 18: 83–92.

Bosák, P., Ford, D.C., Glazek, J. and Horácek, I., 1989. *Paleokarst — a Systematic and Regional Review*. Acad. Praha/Elsevier, Prague and Amsterdam.

Bosellini, A. 1989, Dynamics of Tethyan carbonate platforms. *Soc. Econ. Paleontol. Mineral., Spec. Publ.*, 44: 3–13.

Bouvier, J.D., Gevers, E.C.A. and Wigley, P.L., 1990. 3-D seismic interpretation and lateral prediction of the Amposta Marino field (Spanish Mediterranean Sea). *Geol. Mijnbouw*, 69, 105–120.

Brown, A.R., 1985. The role of horizontal seismic sections in stratigraphic interpretations. *Am. Assoc. Pet. Geol., Mem.*, 39: 37–47.

Buchbinder, B., Margaritz, M. and Buchbinder, L.A., 1983. Turonian to Neogene palaeokarst in Israel. *Palaeogeogr., Palaeoclimatol., Palaeoecol.*, 43: 329–350.

Budd, D.A. and Vacher, H.L., 1991. Predicting the thickness of fresh-water lenses in carbonate paleo-islands. *J. Sediment. Petrol.*, 61: 43–53.

Buddemeier, R.W. and Oberdorfer, J.A., 1986. Internal hydrology and geochemistry of coral reef and atoll islands: key to diagenetic variations. In: J.H. Schroeder and B.H. Purser (Editors), *Reef Diagenesis*. Springer-Verlag, Heidelberg, pp. 91–111.

Calvet, F., Plana, F. and Traveria, A., 1980. La tendencia mineralogica de las eolianites de Pleistocene de Mallorca, mediante la aplicacion del metodo de Chung. *Acta Geol. Hisp.*, 15: 39–44.

Chafetz, H.S, McIntosh, A.G. and Rush, P.F., 1988. Freshwater phreatic diagenesis in the marine realm of Recent Arabian Gulf carbonates. *Sediment. Petrol.*, 58: 433–440.

Choquette, P.W. and James, N.P., 1988. Introduction. In: N.P. James and P.W Choquette (Editors), *Paleokarst*. Springer-Verlag, New York, N.Y., pp. 3–21.

Corra, G., 1986. La régression Messinienne dans la Méditerranée et les consequences pour les phénomènes karstiques. In: K. Paterson and M.M. Sweeting (Editors), *New Directions in Karst*. Geo Abstracts, Norwich, pp. 581–589.

Craig, D.H., 1988. Caves and other features of Permian karst in San Andres Dolomite, Yates Field Reservoir, West Texas. In: James, N.P. and Choquette, P.W. (Editors), *Paleokarst*. Springer-Verlag, New York, N.Y., pp. 342–363.

Davis, G.D., 1980. Cavern development in the Guadalupe Mountains: a critical review of recent hypotheses. *Nat. Speleol. Soc. Bull.*, 42: 42–48.

Del Olmo, W.M. and Esteban, M., 1983. Paleokarst development. *Am. Assoc. Pet. Geol., Mem.*, 33:93–95.

Desrochers, A. and James, N.P., 1988. Early Paleozoic surface and subsurface paleokarst: Middle Ordovician carbonates, Mingan Islands, Quebec. In: N.P. James and P.W. Choquette (Editors), *Paleokarst*. Springer-Verlag, New York, N.Y., pp. 183–210.

De Voto, R.H., 1988. Late Mississippian paleokarst and related mineral deposits, Leadville Formation, central Colorado. In: N.P. James and P.W. Choquette (Editors), *Paleokarst*. Springer-Verlag, New York, N.Y., pp. 278–305.

Dougherty, D.R., Boardman, M.R. and Metzler C.V., 1986. Characteristics and origins of joints and sedimentary dikes of the Bahama Islands. In: *Proc. 3rd Symp. Geology Bahamas*, pp. 45–56.

Druckman, Y. and Moore, C.H., 1985. Late subsurface secondary porosity in a Jurassic grainstone reservoir, Smackover Formation, Mt. Vernon Field, southern Arkansas. In: P.O. Roehl and P.W. Choquette (Editors), *Carbonate Petroleum Reservoirs*. Springer-Verlag, New York, N.Y., pp. 369–384.

DuChene, H.R. and McLean, J.S., 1989. The role of hydrogen sulphide in the evolution of caves in the Guadalupe Mountains of south eastern New Mexico. *Soc. Econ. Mineral. Paleontol. Core Workshop*, 13: 475–481.

Dzulynski, S. and Sass-Gutkiewicz, M.,1989. Lead–zinc ores. In: P. Bosak, D.C. Ford, J. Glazek and I. Horácek (Editors), *Paleokarst — A Systematic and Regional Review*. Acad. Praha/Elsevier, Prague and Amsterdam.

Edmunds, W.M. and Walton, N.R.G., 1983. The Lincolnshire Limestone — hydrochemical evaluation over a ten year period. *J. Hydrol.*, 61: 201–211.

Egemeier, S.J., 1981. Cavern development by thermal waters. *Nat. Speleol. Soc. Bull.*, 43: 31–51.

Esteban, M., 1991. Palaeokarst: practical applications. In: V.P. Wright, M. Esteban and P.L. Smart (Editors), *Palaeokarsts and Palaeokarstic Reservoirs*. Univ. of Reading, Reading, pp. 89–119.

Esteban, M. and Klappa, C.F., 1983. Subaerial exposure environment. *Am. Assoc. Pet. Geol., Mem.*, 33: 1–54.

Evans, C.G. and Ginsburg, R.N., 1987. Fabric-selective diagenesis in the late Pleistocene Miami Limestone. *J. Sediment. Petrol.*, 57: 311–318.

Fischer, A.G., 1981. Climatic oscillations in the biosphere. In: M. Nitecki (Editor), *Biotic Crises in Ecological and Evolutionary Time*. Academic Press, New York, N.Y., pp. 103–131.

Fontaine, J.M., Cussey, R., Lacaze, J., Lanaud, R. and Yapaudjian, L., 1987. Seismic interpretation of carbonate depositional environments. *Bull. Am. Assoc. Pet. Geol.*, 71: 281–297.

Freeman-Lynde, R.P., Cita, M.B., Jadoul, F., Miller, E.L. and Ryan, W.B.F., 1984. Marine geology of the Bahama escarpment. *Mar. Geol.*, 44: 119–156.

Ford, D.C., 1988. Characteristics of dissolution cave systems in carbonate rocks. In: N.P. James and P.W. Choquette (Editors), *Paloeokarst*. Springer-Verlag, New York, N.Y., pp. 25–57.

Ford, D.C. and Williams, P.W., 1989. *Karst Geomorphology and Hydrology*. Unwin Hyman, Boston, Mass., 601 pp.

Goldhammer, R.K., Dunn, P.A. and Hardie, L.A., 1987. High frequency glacio-eustatic sea-level oscillations with Milankovitch characteristics recorded in Middle Triassic platform carbonates in N. Italy. *Am. J. Sci.*, 287: 853–892.

Grotzinger, J.P., 1986. Cyclicity and paleoenvironmental dynamics, Rocknest platform, northwest Canada. *Bull. Geol. Soc. Am.*, 97: 1208–1231.

Hallam, A., 1977. Secular changes in marine inundation of USSR and North America through the Phanerozoic. *Nature*, 269: 762–772.

Halley, R.B. and Evans, C.C., 1983. The Miami Limestone: a guide to selected outcrops and their interpretation. *Miami Geol. Soc.*, 67 pp.

Hanshaw, B.B. and Back, W., 1980. Chemical mass wasting of the northern Yucatan peninsula by groundwater dissolution. *Geology*, 8: 222–224.

Harrison, R.S., 1975. Porosity in Pleistocene grainstones from Barbados: some preliminary observations. *Bull. Can. Pet. Geol.*, 23: 383–392.

Hill, C.A., 1987. Geology of Carlsbad Cavern and other caves in the Guadalupe Mountains, New Mexico and Texas. *N.M. Bur. Mines Miner. Resour., Bull.*, 117: 150 pp.

Hill, C.A., 1989. The evolution of the Delaware Basin — preliminary results. *Soc. Econ. Paleontol. Mineral., Core Workshop*, 13: 467–473.

Hine, A.C. Belknap, D.F., Hutton, J.G., Osking, E.B. and Evans, M.W., 1988. Recent geological history and modern sedimentary processes along an incipient, low energy, epicontinental sea coastline, northwest Florida. *J. Sediment. Petrol.*, 58: 567–579.

Hird, K. and Tucker, M.E., 1988. Contrasting diagenesis of two Carboniferous oolites from South Wales: a tale of climatic influence. *Sedimentology*, 35: 587–602.

Horbury, A.D., 1989. The relative roles of tectonism and eustacy in the deposition of the Urswick Limestone in south Cumbria and north Lancashire. In: R.S. Arthurton, P. Gutteridge and S.C. Nolan (Editors), *The Role of Tectonics in Devonian and Carboniferous Sedimentation in the British Isles.Occas. Publ. Yorksh. Geol. Soc.*, 6: 153–169.

James N.P. and Choquette, P.W., 1984. Diagenesis 9. Limestones — the meteoric diagenetic environment. *Geosci. Can.*, 11: 161–194.

James, N.P. and Choquette, P.W. (Editors), 1988. *Paleokarst*. Springer-Verlag, New York, N.Y., 416 pp.

James, N.P. Stevens, R.K. Barnes, C.R. and Knight, I., 1989. Evolution of a Lower Paleozoic continental-margin carbonate platform, northern Canadian Appalachians. *Soc. Econ. Paleontol. Mineral., Spec. Publ.*, 44: 123–146.

Jennings, J.N., 1971. *Karst*. MIT Press, Cambridge, Mass.

Jenyon, M.K., 1984. Seismic response to collapse structures in the southern North Sea. *Mar. Petrol. Geol.*, 1: 27–36.

Johnson, R.H., 1983. The saltwater–freshwater interface in the Tertiary limestone aquifer, southeastern Atlantic continental shelf of the USA. *J. Hydrol.*, 61: 239–251.

Kendall, A.C. and Harwood, G.M., 1989. Shallow gypsum in the Castile Formation — signficance and implications. *Soc. Econ. Paleontol. Mineral., Core Workshop*, 13: 451–457.

Kerans, C., 1988. Karst-controlled reservoir heterogeneity in Ellenburger Group carbonates, West Texas. *Bull. Am. Assoc. Pet. Geol.*, 72: 2133–2141.

Kerans, C., 1989. Karst-controlled reservoir heterogeneity and an example from the Ellenburger Group (Lower Ordovician) of West Texas. *Bureau Econ. Geol., Univ. of Texas at Austin, Rep. Invest.*, 186: 40 pp.

Kerans, C. and Donaldson, J.A., 1988. Proterozoic paleokarst profile, Dismal Lakes Group, North West Territory, Canada. In: N.P. James and P.W. Choquette (Editors), *Paleokarst*. Springer-Verlag, New York, N.Y., pp. 167–182.

Koerschner, W.F. and Read, J.F., 1989. Field and modelling of Cambrian carbonate cycles, Virginia Appalachians. *J. Sediment. Petrol.*, 59: 654–687.

Leve, G.W., 1984. Relation of concealed faults to water quality and the formation of solution features in the Floridan aquifer, northeastern Florida, USA. *J. Hydrol.*, 61: 251–266.

Lohmann, K.C., 1988. Geochemical patterns of meteoric diagenetic systems and their application to studies of paleokarst. In: N.P. James and P.W. Choquette (Editors), *Paleokarst*. Springer-Verlag, New York, N.Y., pp. 59–80.

Maslyn, R.M., 1977. Fossil tower karst near Molas Lake, Colorado. *Mountain Geol.*, 14: 17–25.

Matthews, R.K. and Frohlich, C., 1987. Forward modelling of bank-margin carbonate diagenesis. *Geology*, 15: 673–676.

Mazzullo, S.J., Bischoff, W.D. and Lobitzer, H., 1990. Diagenesis of radial fibrous calcites in a subconformity, shallow burial setting: Upper Triassic and Liassic, Northern Calcareous Alps, Austria. *Sedimentology*, 37: 407–425.

McKee, E.D. and Ward, W.C., 1983. Eolian environment. *Am. Assoc. Pet. Geol., Mem.*, 33: 132–170.

Meyers, W.J., 1988. Paleokarstic features in Mississippian limestones, New Mexico. In: N.P. James and P.W. Choquette (Editors), *Paleokarst*. Springer-Verlag, New York, N.Y., pp. 306–328.

Molina, J.M., Ruiz-Ortiz, P.A. and Vera, J.A., 1985. Sedimentación marina somera entre sedimentos pelagicos en el Dogger del Subbetico externo (Sierras de Corbra y Puente Genil, Provincia de Cordoba). *Trabajos de Geología de Universidad de Oviedo*, 15: 127–146.

Mullins, H.T. and Neumann, A.C., 1979. Deep carbonate bank structure and sedimentation in the northern Bahamas. *Soc. Econ. Paleontol. Mineral., Spec. Publ.*, 27: 165–192.

Mylroie, J.E. (Editor), 1988. *Field Guide to the Karst Geology of San Salvador Island*. College Center of the Finger Lakes, San Salvador, Bahamas, pp. 17–43

Playford, P.E., 1984. Platform-margin and marginal slope relationships in Devonian reef complexes of the Canning Basin. In: *Proc. Geol. Soc. Austr. Symp., Perth, W.A.*, pp. 189–214.

Poty, E., 1980. Evolution and drowning of paleokarst in Frasnian carbonates onto Vise, Belgium. *Meded. Rijks Geol. Dienst*, 32: 53–55.

Purdy, E.G., 1974a. Reef configurations: cause and effect. *Soc. Econ. Paleontol. Mineral., Spec. Publ.*, 18: 9–76.

Purdy, E.G., 1974b. Karst-determined facies patterns in British Honduras: Holocene carbonate sedimentation model. *Bull. Am. Assoc. Pet. Geol.*, 58: 825–855.

Quinlan, G.M. and Beaumont, C., 1984. Appalachian thrusting, lithospheric flexture and the Paleozoic stratigraphy of the Eastern Interior of North America. *Can. J. Earth Sci.*, 21: 973–996.

Rasmussen, K.A. and Neumann A.C., 1988. Holocene overprints of Pleistocene paleokarst Bight of Abaco, Bahamas. In: N.P. James and P.W. Choquette (Editors), *Paleokarst*. Springer-Verlag, New York, N.Y., pp. 132–148.

Riding, R. and Wright, V.P., 1981. Paleosols and tidal flat lagoon sequences on a Carboniferous carbonate shelf. *J. Sediment. Petrol.*, 51: 1323–1339.

Runnels, D.D., 1969. Diagenesis, chemical sediments, and the mixing of natural waters. *J. Sediment. Petrol.*, 39: 1188–1201.

Sandberg, P.A., 1983. An oscillating trend in Phanerozoic non skeletal carbonate mineralogy. *Nature*, 305: 19–22.

Sandford, W.E. and Konikow, L.F., 1989. Porosity development in coastal carbonate aquifers. *Geology*, 17: 249–252.

Schmoker, J.W. and Hester, T.C., 1986. Porosity of the Miami Limestone (late Pleistocene), lower Florida Keys. *J. Sediment. Petrol.*, 56: 629–634.

Scoffin, T.P., 1987. *An Introduction to Carbonate Sediments and Rocks*. Blackie, Glasgow, 274 pp.

Smart, P.L., Palmer, R.J., Whitaker, F. and Wright, V.P., 1988a. Neptunian dike and fissure fills: an overview and account of some modern examples. In: N.P. James and P.W. Choquette (Editors), *Paleokarst*. Springer-Verlag, New York, N.Y., pp. 149–163.

Smart, P.L., Dawans, J.M. and Whitaker, F.F., 1988b. Carbonate dissolution in a modern mixing zone, south Andros, Bahamas. *Nature*, 335: 811–813.

Stoessell, R.K., Ward, W.C., Ford, B..H. and Schuffert, J.D., 1989. Water chemistry and $CaCO_3$ dissolution in the saline part of an open-flow mixing zone, coastal Yucatan Peninsula, Mexico. *Bull. Geol. Soc. Am.*, 101: 159–169.

Todd, D.K., 1980. *Groundwater Hyrdrology*. John Wiley and Sons, London, 535 pp.

Tucker, M.E., 1990. Dolomites and dolomitization. In: M.E. Tucker and V.P. Wright (Editors), *Carbonate Sedimentology*. Blackwell Scientific Publications, Oxford, pp. 370–406.

Vacher, H.L., 1978. Hyrology of Bermuda — significance of an across-the-island variation in permeability. *J. Hydrol.*, 39: 207–226.

Vail, P.R., Mitchum, R.M. and Thompson, III S., 1977. Seismic stratigraphy and global changes in sea-level. Part 4: Global cycles of relative changes in sea-level. *Am. Assoc. Pet. Geol., Mem.*, 26: 83–97.

Vandenberghe, N., Poggiagliomi, E. and Watts, G., 1986. Offset dependent seismic amplitudes from Karst limestones in northern Belgium. *First Break*, 4: 9–27.

Vandenberghe, N., Poggiagliomi, E. and Schwarz, E., 1983. Analysis of reflection seismic data for the detection of karstified limestones at depth. *European Geothermal Update: Extended Summaries*, 1.7. European Patent Office, pp. 122–133.

Vera, J.A., Ruiz-Ortiz, P.A., Garcia-Hernandez, M. and Molina, J.M., 1988. Paleokarst and related pelagic sediments in the Jurassic of the Subbetic Zone, southern Spain. In: N.P. James and P.W. Choquette (Editors), *Paleokarst*. Springer-Verlag, New York, N.Y., pp. 364–384.

Vernon, R.O., 1969. The geology and hydrology associated with a zone of high permeability (Boulder Zone) in Florida. *Soc. Min. Eng., Preprint*, 69-AG-12.

Walkden, G.M., 1974. Paleokarstic surfaces in the Upper Visean (Carboniferous) limestones of the Derbyshire Block, England. *J. Sediment. Petrol.*, 44: 1234–1247.

Walkden, G.M. and Davies, J., 1983. Polyphase erosion of subaerial omission surfaces in the late Dinantian of Anglesey, North Wales. *Sedimentology*, 30: 860–878.

Walkden, G.M. and Walkden, G.D., 1990. Cyclic sedimentation in carbonate and mixed carbonate–clastic environments: four simulation programs for a desktop computer. In: M.E. Tucker et al. (Editors), *Carbonate Platforms: Facies, Sequences and Evolution. I.A.S. Spec. Publ.*, 9: 55–78.

Ward, W.C., 1978. Indication of climate in carbonate dune rocks In: W.C. Ward and A.E. Weide (Editors), *Geology and Hydrogeology of North Eastern Yucatan*. New Orleans Geol. Soc., New Orleans, La., pp. 191–208.

Ward, W.C. and Halley, R.B., 1985. Dolomitization in a mixing zone of near-seawater composition, late Pleistocene, northeastern Yucatan Peninsula. *J. Sediment. Petrol.*, 55: 407–420.

Wendte, J., Aigner, T. and Neugebauer, J., 1984. Cephalopod limestone deposition on a shallow pelagic ridge: The Tafilait Platform (Upper Devonian), eastern Anti-Atlas, Morocco. *Sedimentology*, 31: 601–625.

Whitaker, F.F. and Smart, P.L., 1990. Active circulation of saline ground waters in carbonate platforms: evidence from the Great Bahama Bank. *Geology*, 18: 200–203.

White, W.B., 1969. Conceptual models for carbonate aquifers. *Ground Water*, 7: 15–21.

White, W.B., 1977. Conceptual models for carbonate aquifers: revisited. In: R.R. Dilamarter and S.C. Csallany (Editors), *Hydrologic Problems in Karst Regions*. Western Kentucky University, Bowling Green, Ky., pp. 176–187.

White, W.B., 1984. Rate processes: chemical kinetics and karst landform development. In: R.G. La Fleur (Editor), *Groundwater as a Geomorphic Agent*. Oxford Univ. Press, Oxford, pp. 227–248.

Wigley, P.L., Bouvier, J.D. and Dawans, J.M., 1988. Karst and mixing zone porosity in the Amposta Marino Field, offshore Spain. *Bull. Am. Assoc. Pet. Geol.*, 72: 1031 (abstract).

Wilkinson, B.H., Owen, R.M. and Carroll, A.R., 1985. Submarine hydrothermal weathering, global eustacy and carbonate polymorphism in Phanerozoic marine oolites. *J. Sediment. Petrol.*, 55: 171–1833.

Williams, P.W., 1985. Subcutaneous hydrology and the development of doline and cockpit karst. *Z. Geomorphol.*, 29: 463–482.

Wood, J.R., 1986. Thermal mass transfer systems containing quartz and calcite. *Soc. Econ. Paleontol. Mineral., Spec. Publ.*, 38: 169–187.

Wright, V.P., 1982. The recognition and interpretation of paleokarsts: two examples from the Lower Carboniferous of South Wales. *J. Sediment. Petrol.*, 52: 83–94.

Wright, V.P., 1986. The polyphase karstification of the Carboniferous Limestone of South Wales. In: K. Paterson and M.M. Sweeting (Editors), *New Directions in Karst*. Geo Abstracts, Norwich, pp. 569–580.

Wright, V.P., 1988. Paleokarst and paleosols as indicators of paleoclimate and porosity evolution: a case study from the Carboniferous Limestone of South Wales. In: N.P. James and P.W. Choquette (Editors), *Paleokarst*. Springer-Verlag, New York, N.Y., pp. 329–341.

Wright, V.P., 1990. Meteoric Diagenesis. In: M.E. Tucker and V.P. Wright (Editors), *Carbonate Sedimentology*. Blackwell Scientific Publications, Oxford, pp. 336–348.

This Page Intentionally Left Blank

SUBJECT INDEX *

---

* Prepared by the editors.

This Page Intentionally Left Blank